UNIVERSITY *of the*
WESTERN CAPE

INTEGRATION OF PETROGRAPHIC AND PETROPHYSICAL LOGS ANALYSES TO CHARACTERIZE AND ASSESS RESERVOIR QUALITY OF THE LOWER CRETACEOUS SEDIMENTS IN THE ORANGE BASIN, OFFSHORE SOUTH AFRICA

A Thesis in Applied Geology

By

MURENDENI HADLEY MUGIVHI

Submitted in Fulfillment of the Requirements for the Degree of Magister Scientiae in the Department of Earth Sciences,
University of the Western Cape,
Cape town, South Africa.

Supervised by: Dr Mimonitu Opuwari

June, 2017

DECLARATION

I declare that my research work titled **"Integration of petrographic and petrophysical logs analyses to characterize and assess reservoir quality of the lower cretaceous sediments in the Orange Basin, Offshore South Africa.**" is my own work, that it has not been submitted before for any degree or examination in any other university, and that all the sources I have used or quoted have been indicated and acknowledged by means of complete references.

Murendeni H. Mugivhi June, 2017.

……..

Signature

DEDICATION

This project is dedicated

to

The

memory

of

my late uncle

Captain Tshammbenga Tomas Mugivhi (1949 -2016).

ACKNOWLEDGEMENT

Albert Einstein said “Education is not the learning of facts, but the training of the mind to think”. I take this opportunity to honour several people who contributed during this project until its completion. Their unconquerable strength deserves special attention with praises to the most high.

To my supervisor, Dr. Opuwari Mimonitu, without you this research would have not been possible. You introduce me to the petrophysics and developed my knowledge of Interactive Petrophysics (IP). I am deeply grateful for your time, your support and your care. You motivated me during critical stages of this study and I thank you.

My gratitude goes to the Petroleum Agency of South Africa for financial support and releasing of the data to complete this study. Special thanks to my colleagues who contributed towards achieving this work: Viljoen Storm, Jimmy Jansen, Chantell Van Bloemenstein, Jonathan Salomo, Selwyn Adams, Anthony Fielies, Iyani Nedzamba, Thembani Munengwane, David Aphane and Dovhani Mahumele.

I extends my appreciation to my friends, Sedzani Nethenzheni, Hakundwi Mandende, Stephane Tsako for their encouragement, and most importantly, Moses Mogoba for his sleepless nights and endless efforts. Your support and courage yielded this achievement.

I am particularly grateful to my family, my mother (Ms. Vhulahani Netshitanini) My grandmother (Ms. Masindi Netshitanini) and my three younger brothers (Lutendo, Thendo and Mutshidzi) for all their prayers. To Lingedzani Mukhawa, there is no one like you.

KEY WORDS

Reservoir quality

Petrophysical logs

Petrographic analyses

Detrital components

Authigenic components

Diagenesis

Porosity (φ)

Permeability (k)

Economic cut-offs

Storage capacity

Flow capacity

ABBREVIATIONS

XRD	X-ray diffraction
SEM	Scanning electron microscope
PASA	Petroleum Agency of South Africa
EDX	Energy dispersive analyses
SRF	Sedimentary rock fragments
VRF	Volcanic rock fragments
MRF	Metamorphic rock fragments
LWD	Logging While Drilling
GR	Gamma ray

ABSTRACT

Commercial hydrocarbon production relies on porosity and permeability that defines the storage capacity and flow capacity of the resevoir. To assess these parameters, petrographic and petrophysical log analyses has been found as one of the most powerful approach. The approach has become ideal in determining reservoir quality of uncored reservoirs following regression technique. It is upon this background that a need arises to integrate petrographic and petrophysical well data from the study area. Thus, this project gives first hand information about the reservoir quality for hydrocarbon producibility.

Five wells (A-J1, A-D1, A-H1, A-K1 and K-A2) were studied within the Orange Basin, Offshore South Africa and thirty five (35) reservoirs were defined on gamma ray log where sandstone thickness is greater than 10m. Eighty three (83) sandstone samples were gathered from these reservoirs for petrographic analyses within Hauterevian to Cenomanian sequences. Thin section analyses of these sediments revealed pore restriction by quartz and feldspar overgrowths and pore filling by siderite, pyrite, kaolinite, illite, chlorite and calcite. These diagenetic minerals occurrence has distructed intergranular pore space to almost no point count porosity in well K-A2 whilst in A-J1, A-D1, A-H1 and A-K1 wells porosity increases at some zones due to secondary porosity.

Volume of clay, porosity, permeability, water saturation, storage capacity, flow capacity and hydrocarbon volume were calculated within the pay sand interval. The average volume of clay ranged from 6% to 70.5%. The estimated average effective porosity ranged from 10% to 20%. The average water saturation ranged from 21.7% to 53.4%. Permeability ranged from a negligible value to 411.05mD. Storage capacity ranged from 6.56 scf to 2228.17 scf. Flow capacity ranged from 1.70 mD-ft to 31615.82 mD-ft. Hydrocarbon volume varied from 2397.7 cubic feet to 6215.4 cubic feet. Good to very good reservoir qualities were observed in some zones of well A-J1, A-K1 and A-H1 whereas well A-D1 and K-A2 presented poor qualities.

TABLE OF CONTENTS

LIST OF FIGURES

CHAPTER 1: INTRODUCTION

CHAPTER 2: LITERATURE REVIEW

CHAPTER 3: DATA AND METHODS

CHAPTER 4: CORE DESCRIPTION AND PETROGRAPHIC ANALYSIS

CHAPTER 5: WELL LOG ANALYSES AND INTEPRETATION

LIST OF TABLES

CHAPTER 2: LITERATURE REVIEW

CHAPTER 4: CORE DESCRIPTION AND PETROGRAPHIC ANALYSES

CHAPTER 5: WELL LOG ANALYSES AND INTERPRETATION

CHAPTER ONE: INTRODUCTION

1. Introduction

1.1. Background of the study

Security of energy supply has global effect on economy. Sufficient energy supply at affordable price maintains the balance of socio-economic development. Recently the demand of primary energy and liquid fuels has increased rapidly and were predicted to go higher with 36% between 2008 and 2035 globally (Figure 1.1) (International Energy Agency, 2013). In South Africa lack of primary energy has been witnessed through recurring loadshedding and increase in electricity and fuel prices. In June 2013, Eskom declared that the country electricity demand has exceeded available supply which consequently retains the community living under stressed energy capacity (https://www.esi-africa.com/news/south-africa-s-electricity-demand-exceeds-available-supply/).

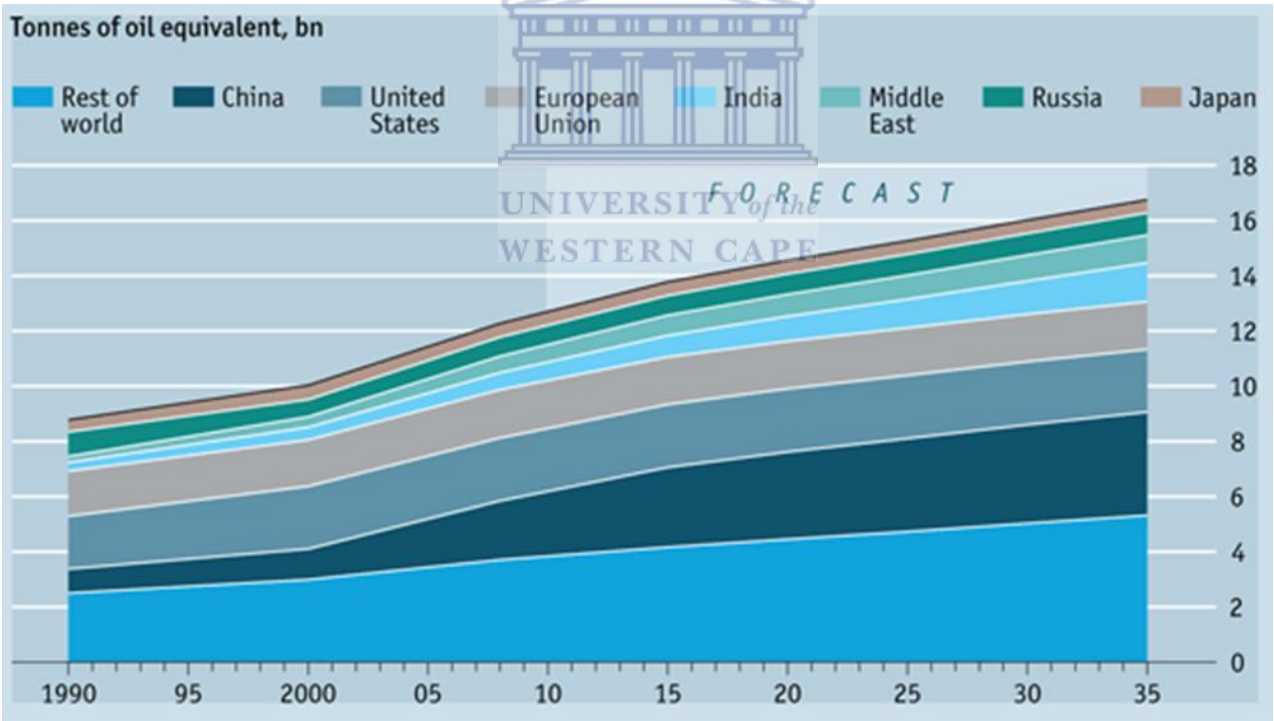

Figure 1.1: Global primary energy demand curve forecasting the current capacity demand with 36% from 2008 to 2035 (International Energy Agency, 2013).

This demand has shifted the focus from high air pollution coal fired and diesel powered stations to less air pollution gas powered station. The focus aims to deliver gas from offshore petroleum resources in the Orange Basin to exchange Ankerlig Power

Station from diesel powered station to gas powered station (http://www.southafrica.info/business/investing/energy-190315.htm#.V6SJivl97mE). This interchange will help to sustain and boasts security of energy supply and reduces obnoxious regular increase in energy prices. The basin is already regarded as prolific for hydrocarbon generation and accumulation (Jungslagger, 1999; Van der Spuy, 2003) and postulated siliciclastic and carbonate bearing reservoirs in frontier areas (Mello et al., 2012).

The current study assesses reservoir rock properties (such as mineralogy, porosity, permeability and saturation) of the Lower Cretaceous sediments to predict reservoir quality, estimate storage, flow capacity and estimates hydrocarbon reserves. This work was encouraged by Hill and James-Rutledge (2005) who observed that Cretaceous reservoir properties are poor and can inhibit hydrocarbons flow capacity due to quartz overgrowth and illite cementation that occurred during diagenesis with increasing burial depth of the sediments. To unravel these sedimentological effects this work engage petrographic quantitative approach to characterize rock physical properties; and lastly petrophysically estimates reservoir parameters such as resistivity of formation water, water and hydrocarbon saturations for selected reservoir intervals in all the wells. These petrophysical properties will be used further to identify productive zones, pay zone thickness; and distinguish between oil, gas or water in the reservoir and lastly to estimate the hydrocarbon reserves to solve energy crises.

1.2. Statement of the research problem

Sunbird Energy (Pty) Ltd and Thombo Petroleum (Pty) Ltd are in the process of infrastructure development in the Orange Basin, West Coast of South Africa. The process aims to deliver oil and gas petroleum resources from offshore to onshore for commercial development. This can be achieved if hydrocarbon reservoirs can support commercial flow capacity suitable for liquids and gaseous hydrocarbons at 10% porosity and 1 md permeability and 7% porosity and 0.1 md permeability respectively. To understand these reservoir quality economic cut-offs suitable for hydrocarbon producibility an integrated approach was designed involving petrographic and petrophysical log analyses.

The use of petrographic and petrophysical log analyses has been found one of the most powerful approach in reservoir studies at development stage. The approach has

become ideal in determining reservoir quality of uncored reservoir in a well. It is upon this background that a need arises to integrate petrographic and petrophysical well data from the study area. Thus, this project is intended to give first hand information about the reservoir quality for hydrocarbon producibility.

1.3. Outline of the thesis structure

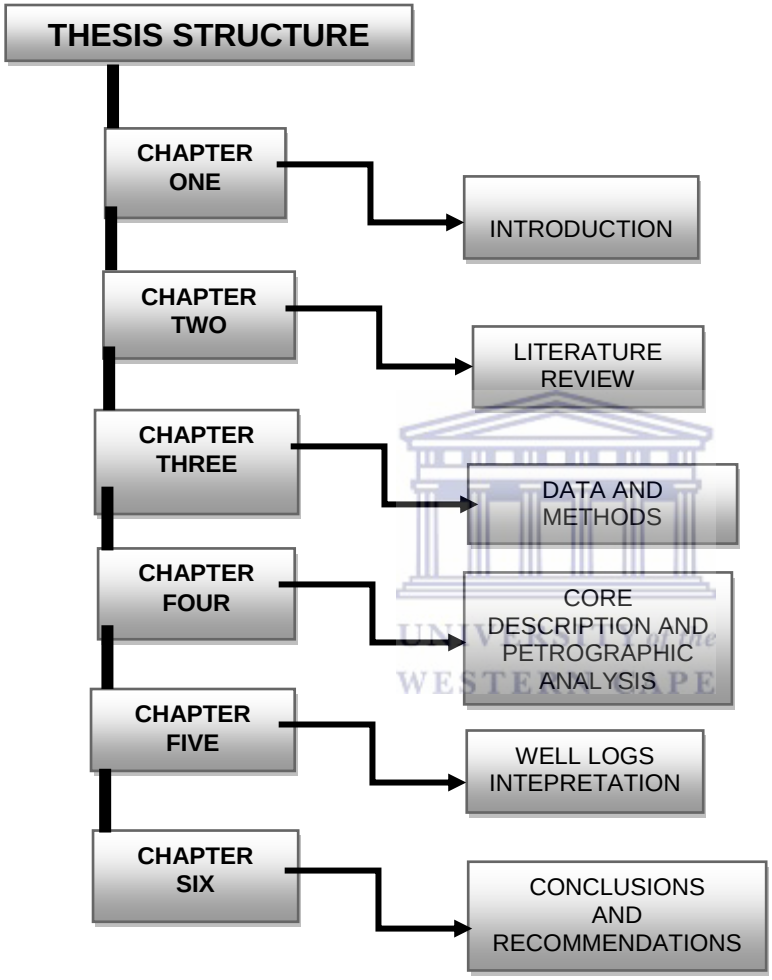

Figure 1.2: Flow chart of the thesis structure

1.4. Geographical location of the study area

The project area is situated in the West Coast of South Africa. It is geographically centered between 32°00'00'' and 31°00'00'' latitudes (S) and 13°00'00'' and 17°05'00'' longitude (E). In this vicinity water depth varies from 175m to 2300m in the deep locality (Figure 1.3). Thombo Petroleum (Blocks 2B), PetroSA (Blocks 2A) and Sungu-Sungu Petroleum (Mid Orange Basin) blocks are within the study area. In the Orange Basin forty one exploration wells have been drilled and only two were successful; the oil discovery of

A-J1 and the Ibhubesi gas fields. The area is underexplored and no infrastructures for commercial development exist to date. This study focuses on A-D1, A-J1, K-A2, A-K1 and A-H1 wells (Figure 1.3) for reservoir quality assessment.

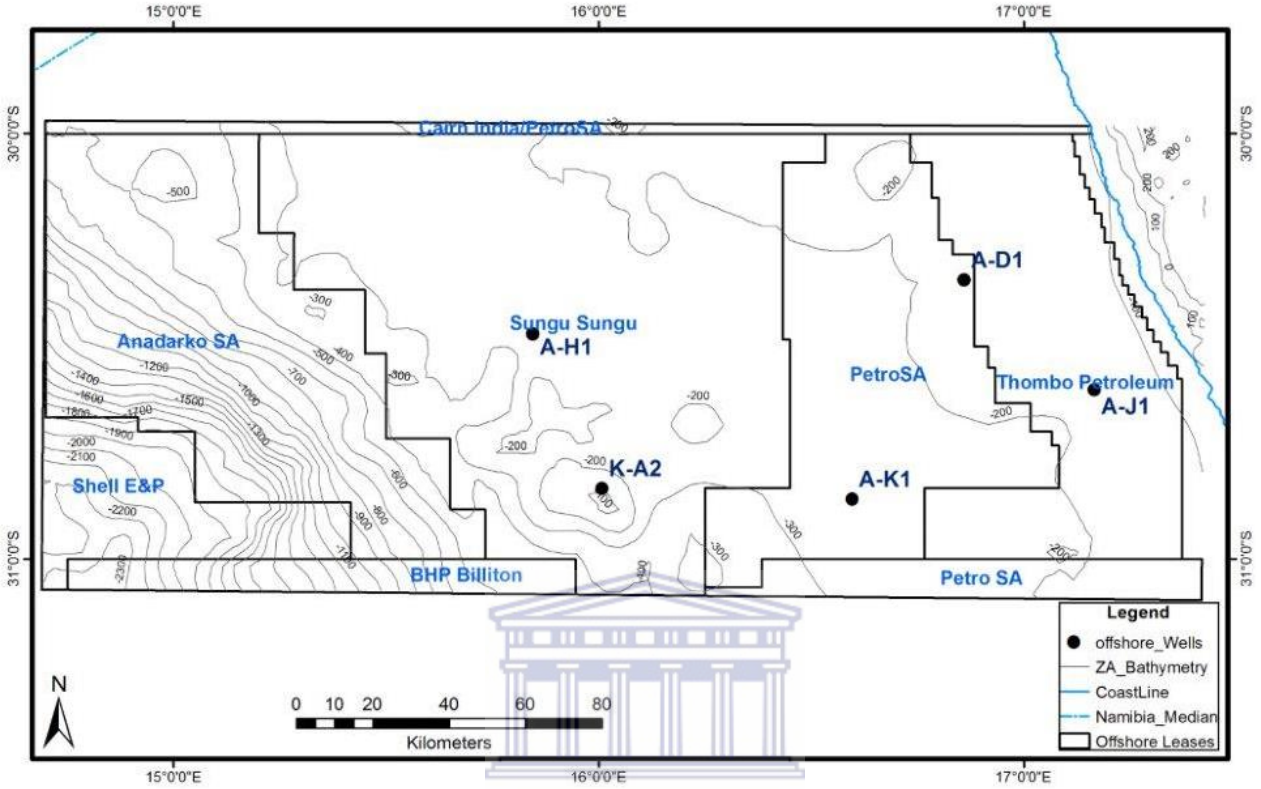

Figure 1.3: Maps showing the location of the study area with the wells selected for this study.

1.5. Research aims and objectives

The general aim of this thesis is to contribute towards the understanding of Lower Cretaceous reservoir evolution in the Orange Basin whilst providing insights about its economic potential. Most importantly identify potential reservoirs using well logs (gamma ray) and assess their qualities using core data for hydrocarbon producibility. To achieve this work intended outcome of this study includes:

- Selecting potential reservoirs and distinguish possible fluids saturation using combination of gamma ray, deep and shallow resistivities, sonic, neutron and density logs.
- Evaluating detrital and authigenic mineralogical components that contributed to reservoir properties using thin sections, XRD and SEM petrographic analyses for selected cored reservoir intervals.

- Estimating porosity of the selected reservoirs using point count modal analyses and compare the results with the legacy ambient helium porosity recorded in the well completion reports.
- Using point count porosity, legacy ambient helium porosity and single phase gas permeability to evaluate economic cut-offs for both oil and gas potential producibility over selected reservoirs.
- Integrating porosity and permeability of the cored reservoir interval with petrophysical log to predict porosity and permeability of the uncored reservoir intervals.
- Calculating reservoir storage and flow capacity of the selected reservoir intervals; and estimate their recoverable using petrophysical analysis over selected intervals.

1.6. Geological framework

The Orange Basin is a typical passive margin and owes its origin to breakup of the African craton from Gondwana land, followed by rifting and drifting of the African and South American plates that resulted in the opening of the South Atlantic Ocean during Jurassic / Early Cretaceous and the generation of oceanic basement (Brown et al., 1995) (Figure 1.4). The basin in the northern part is bordered by the Lüderitz Transfer Zone (LTZ) and contains a thickness of about 7km of sediments whilst to the south it meets with Agulhas Falkland Fractured Zone (AFFZ) and contains about 3km of sediments (Paton et al., 2008) (Figure 1.5b).

These sediments resulted from weathering and erosion processes of the African continent entering the basin in the southern part by Olifants River, established between 117.5 (6At1) and 103Ma (14At1) and in the northern part by Orange River, established some 103Ma (14At1) and lasting up to about 60 to 70Ma (22At1) (Figures 1.6 & 1.7) as the basin opens up (Figure 1.5a) (Brown et al., 1995; Van der spur, 1999 and Tinker et al., 2008). This basin contains no record for evaporitic deposits which has been discovered to be the primary sealing component in the coasts of South America and other West Africa basins (Ala and Selley, 1997).

Hirsch et al., 2007 observed that the stratigraphic record in the basin ranges from the lithospheric extension and rift tectonics throughout a fully evolved post-break-up setting. The stratigraphy comprises a pre-rift successions (older than Late Jurassic, >~130Ma), that is overlain by syn-rift deposits of Late Jurassic to Hauterivian age (~121 to

~117.5Ma), and in turn by sediments of early drift stages up to Aptian age (~113 to ~103Ma) (Figures 1.6 & 1.7) (Hirsch et al., 2007).

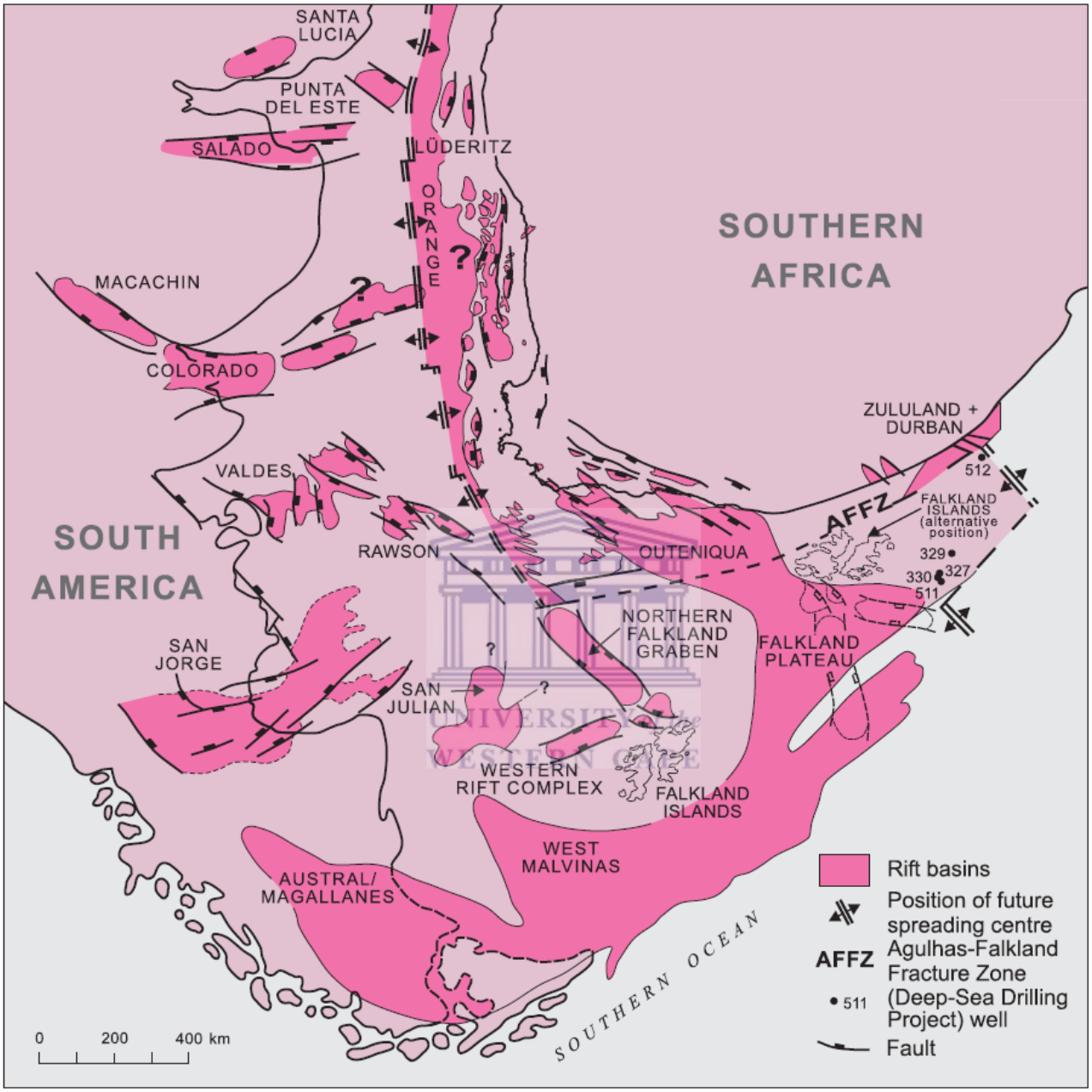

Figure 1.4: Plate tectonic reconstruction illustrating the likely pre-break-up configuration of Late Jurassic to Early Cretaceous rift basins within southwest Gondwana. An alternative inverted northeast position of the Falkland Islands illustrates the possibility that the Falklands microplate may have undergone clockwise rotation of 180° during continental separation (after Jungslager, 1999a).

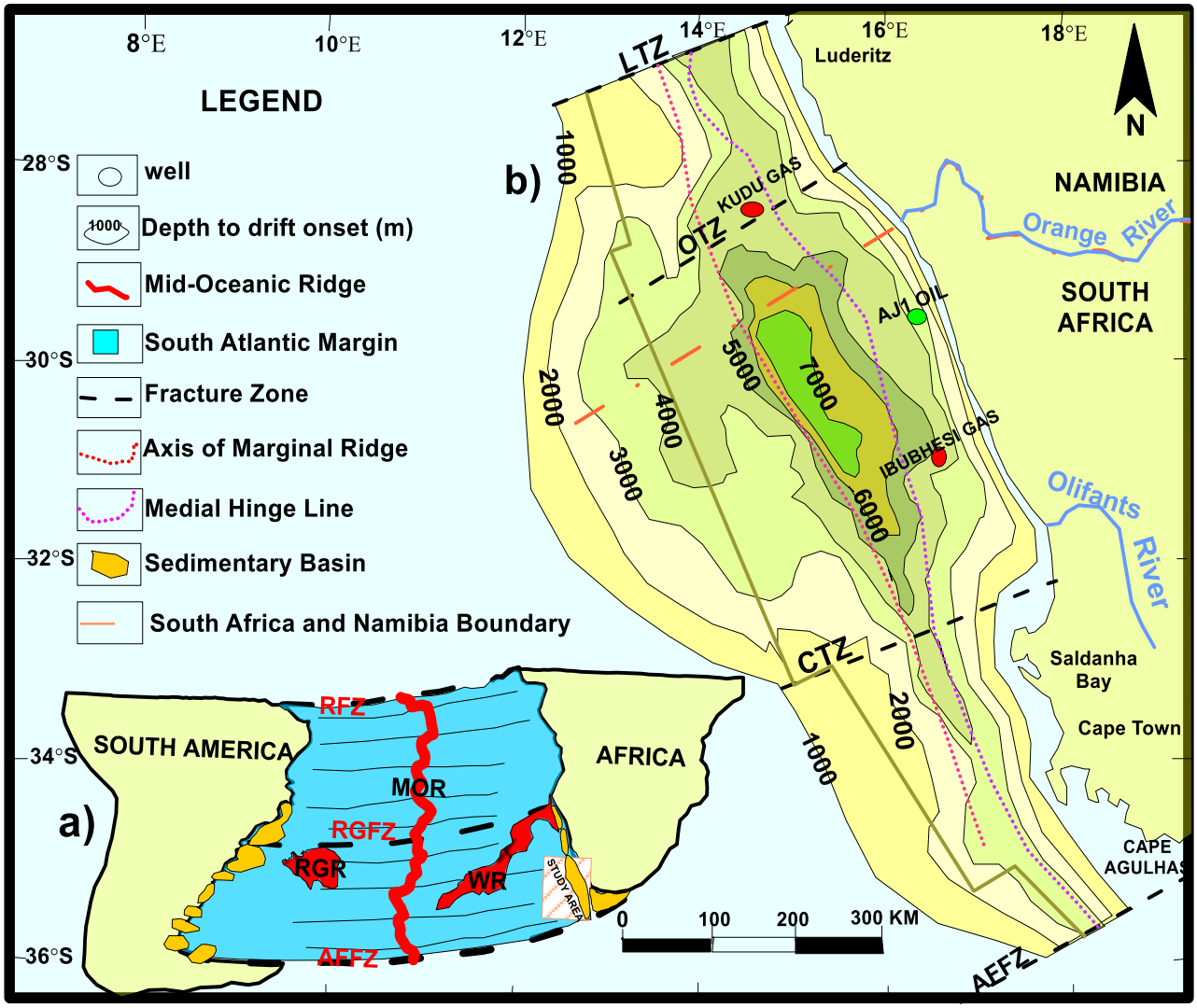

Figure 1.5: A) Regional map of the South Atlantic. B) Structural framework and the main depocentre of the west coast Orange Basin (modified from PASA, 2015).

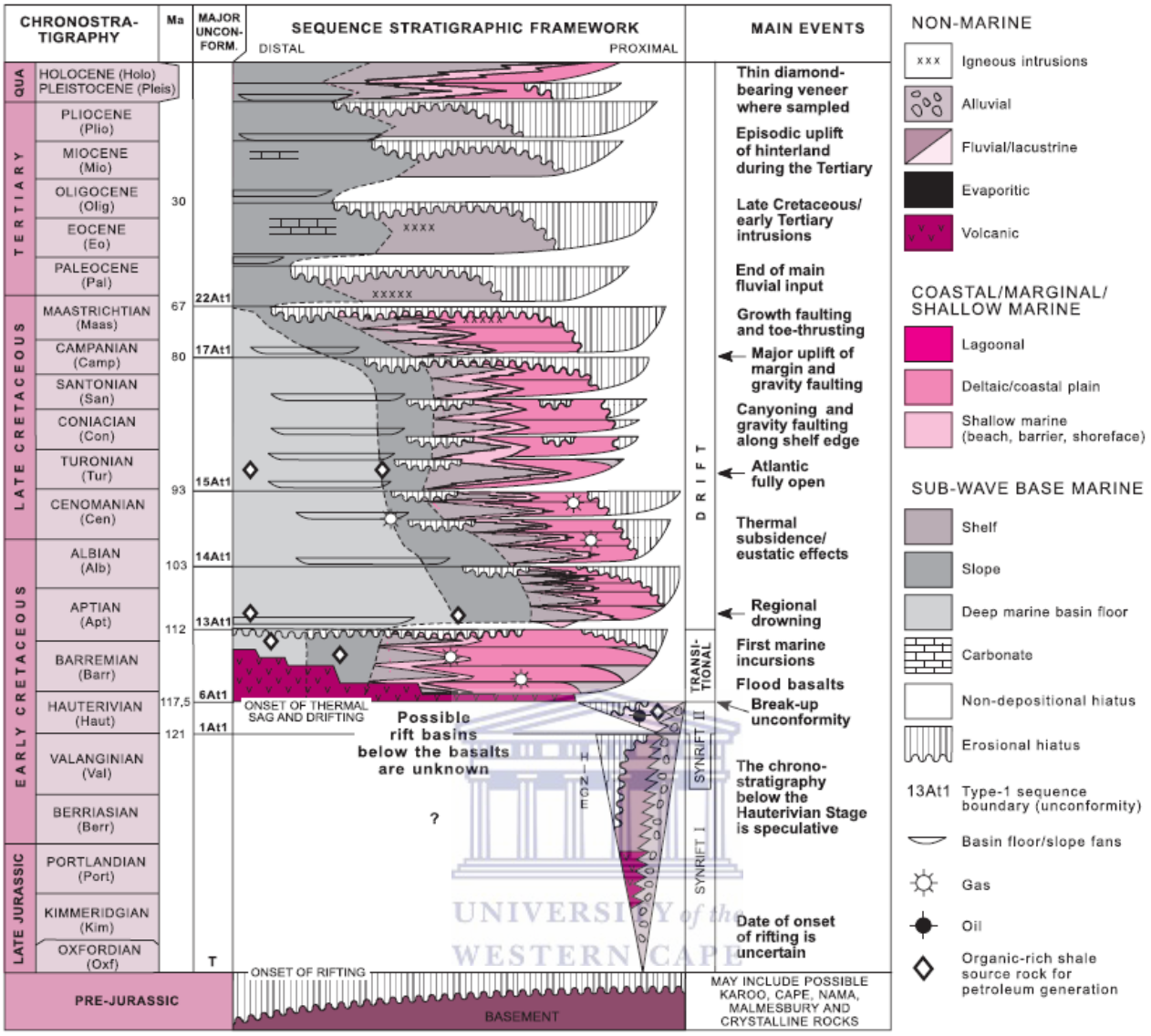

Figure 1.6: Generalised chronostratigraphy of the South African offshore Mesozoic basins, based on the results of sequence stratigraphic studies. No vertical or horizontal scale or thickness is implied (after Brown et al., 1995; Jungslager, 1996, Soekor, 1994a,b). USM, upper shallow marine; UF, upper fluvial; LSM, lower shallow marine; LF, lower fluvial; BUSM, unconformity at base of upper shallow marine; Ma, age in millions of years using the time scale of Haq et al. (1988).

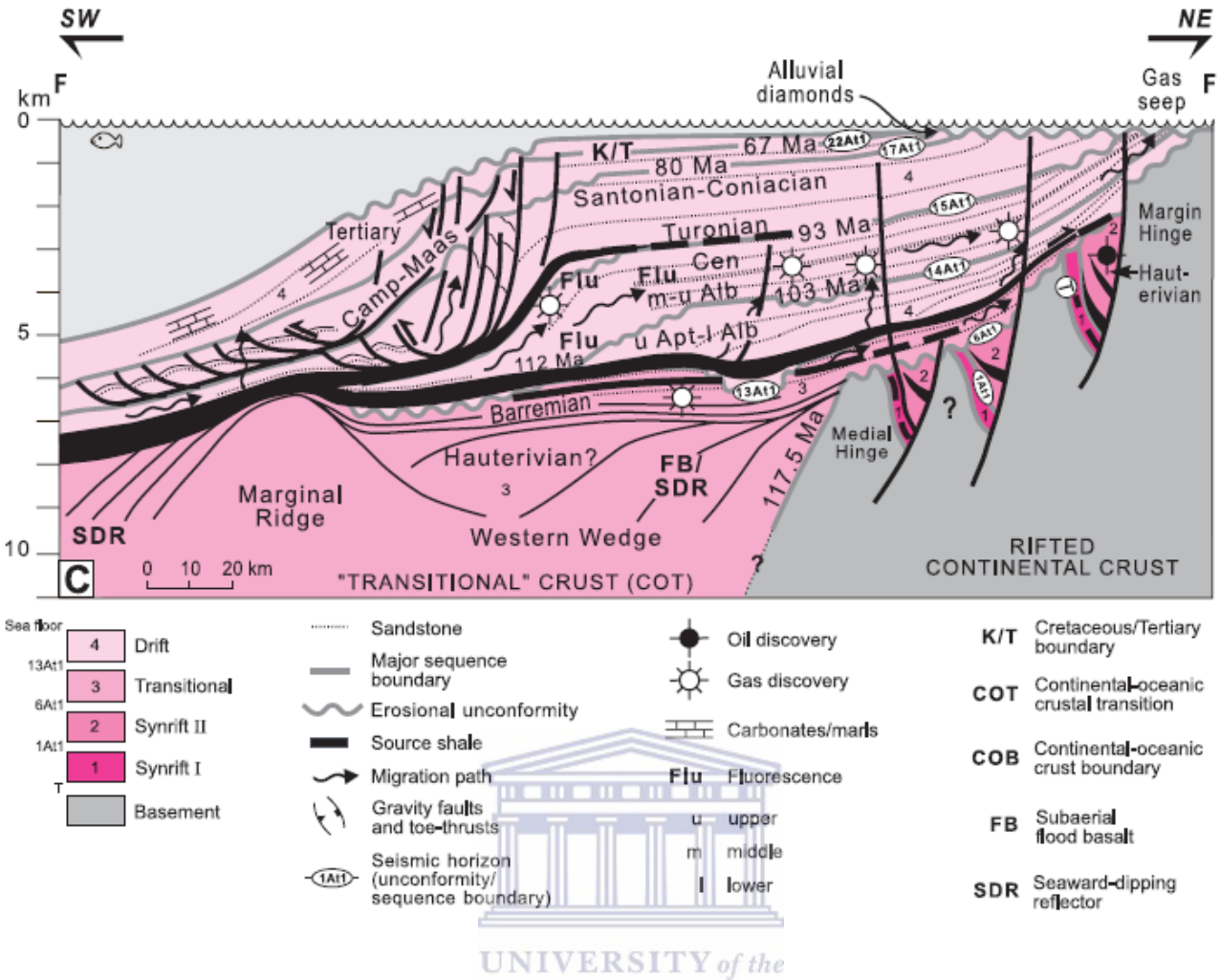

Figure 1.7: Regional geology of South Africa's western margin displaying F-F schematic geological profile across the central Orange Basin to illustrate the structural style, the main sedimentary sequences and their ages, and the main petroleum elements (after Broad et al., 2005). Projected locations of inner and outer margin are shown.

Interpretation of the regional seismic profiles calibrated by well data indicates that syn-rift sediments are confined to localized half grabens trending sub parallel to the coastline and are overlain by aggrading shelf margin sediments with little or no deformation. The sediments are sourced from margin tilting during the elastic rebound phase of rifting. The second spate of sedimentation during tertiary was characterized by margin instability resulting in development of a coupled growth fault and toe thrust system. The extensional domain of the toe thrust is characterized by basinward dipping listric faults rooted at an Aptian decollement level and have been identified between 500 to 1500m of present day bathymetry (Granado et al., 2009). The compressional domain

accommodates the up-dip extension that is observed on the lower slope and is characterized by landward dipping faults (Figure 1.8) (Granado et al., 2009).

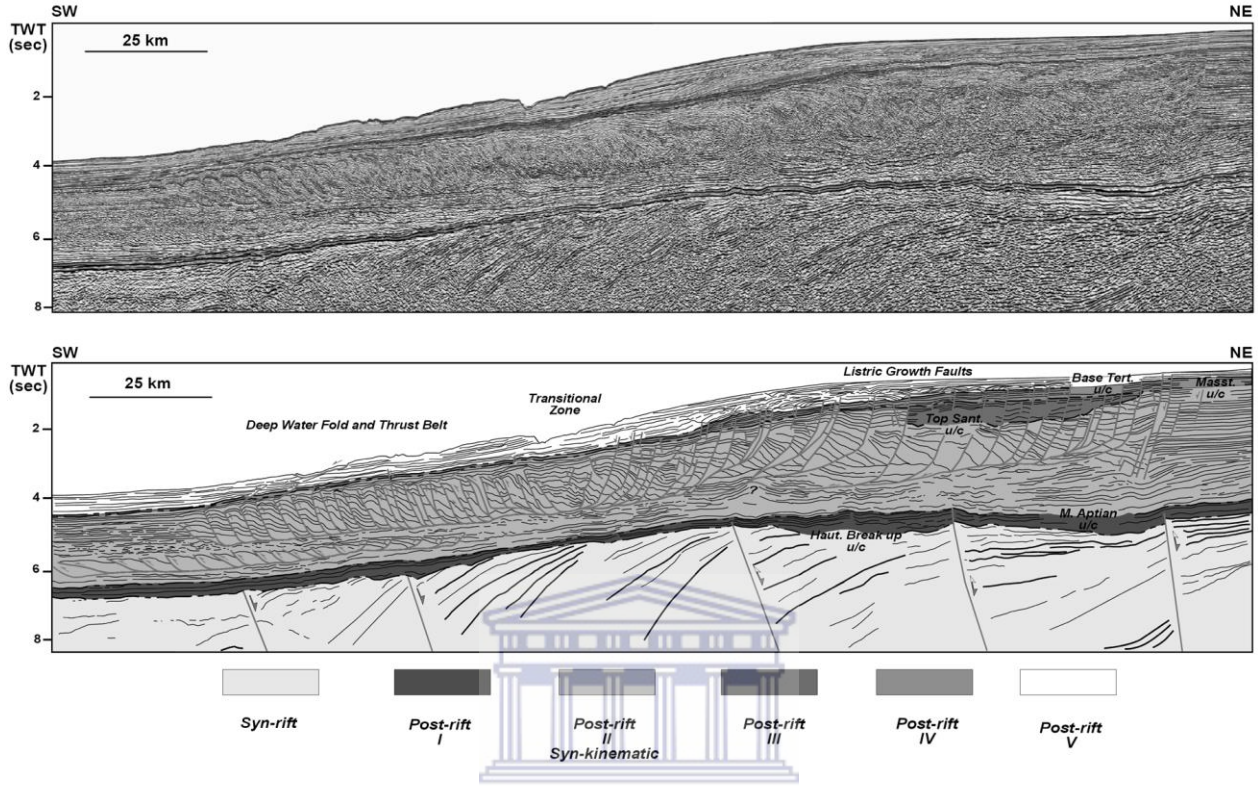

Figure 1.8: Regional seismic line vernab_03_063a and tectonostratigraphic interpretation (copied from Granado et al., 2009).

1.7. Exploration history of the Orange Basin

Exploration of hydrocarbon in the Orange Basin began with SOEKOR (PASA) in 1974 (Gerrard and Smith, 1982) after unsuccessful exploration in the Karoo Basin (Rowsell and Swaedt, 1976). This exploration resulted with the discovery of the Kudu gas field in the South Namibia through detailed regional geological interpretation, stratigraphic analyses and petroleum system evaluation of geologic and seismic data (Austin and Uchupi, 1982). Similar data strategy and petroleum system derivation was applied in South African part to evaluate the prospectivity of the basin (Muntingh and Brown, 1993). The concept was applied to define stratigraphic overview from syn-rift to post-rift sequences and analyse petroleum system to support wildcat exploration drilling (Muntingh, 1993). Only two wells showed encouraging potential flow rate of gas and condensate within the post-rift sediments; one well encountered oil in the syn-rift sequence whilst fifteen had gas shows (Muntingh and Brown, 1993; Muntingh, 1993).

From 2010 to date, oil and gas explorers have extensively acquired 2D and 3D seismic data to maximize chances of finding new hydrocarbon reservoirs. These data are currently under interpretation (PASA, 2015).

CHAPTER TWO: LITERATURE REVIEW

2. Literature review

2.1. Introduction

This chapter review and address how reservoir quality prediction was achieved from other international and local basins through integration of core samples and well logs. The discussion on core data focuses on how detrital and authigenic compositions affect reservoir quality with burial depth. Whilst well log analyses focuses on integrating cored depth to predict the quality of uncored depth following regression analysis.

2.2. Evolution of sediments widely known for hydrocarbon reservoir

Globally literature reveal that hydrocarbons where mainly produced from terrigenous clastic material, such as Cretaceous marine turbidites sandstone, e.g. Santos Basin (Moraes, 1989) and from carbonates, e.g. Mississippian Madison Group, Willson Basin (Brown, 1997). This review concentrates on sandstones as potential reservoir. Sandstone is a sedimentary rock that is formed from combination of loose grains that were lithified into a rock. Its grain size ranges between 2mm to 1/16mm (62.5 microns). Sand grains that forms sandstone are formed by the breakdown of pre-existing rocks through weathering and erosion, and from material that forms within the depositional environment. These materials that break down from this process can be grouped into derital mineral grains (eroded from pre-existing rocks) and sand-sized pieces of rock (or lithic fragments)**.** These products are subjected to lithification and diagenesis processes that precipitate authigenic chemicals coating around the grains and cementing them into a rock.

2.2.1. Parameters that control reservoir quality for hydrocarbon producibility

The quality of the reservoir rock for hydrocarbon flow is a function of its porosity and permeability. In sandstone, these two parameters are controlled by initial sediments composition and succeeding alteration resulting from burial temperature and lithification process. Compactions from overlying rocks during burial induces stress that act on sands reducing porosity and constricting pore throats. Pore structure are also affected by dissolution and precipitation of minerals in response to changes in formation temperature. Extreme temperature causes quartz and feldspar cementations that can also lead to compartmentalization of the reservoir rock (Prosser et al., 1993).

2.2.2. Why assess reservoir quality?

Porosity and permeability need to be assessed to understand how a reservoir will perform from exploration to production phases. According to Sneider (1990) precise estimate of reservoir quality is required throughout the entire “life cycle” of a reservoir. Accurate evaluation of reservoir quality must be continually refined, throughtout all phase ranging from prior to exploratory drilling, to discovery, during appraisal and development drilling, and throughout reservoir management.

At exploration phase the key challenge is to assess and predict the geometry and distribution of reservoir facies. Furthermore, it is important to know reservoir quality parameters (porosity and permeability) to estimate hydrocarbon in-place. Seismic attributes might help to understand rock qualities. At this phase, the limit of economic basement is a key datum to define; the depth at which sediments are insufficiently permeable to sustain economic production is difficult to define.

At the development phase (or appraisal), it is of paramount important to understand and predict reservoir porosity, permeability, and reservoir distribution to determine the location and optimal number of development wells, as well as to estimate economic production cutoff values, hydrocarbon pore volumes, recoverable reserves, and production rates (Sneider, 1990).

At the reservoir management phase, it is important to predict porosity and permeability variations in three-dimensions for better hydrocarbon production and possible fluid injection.

2.2.3. Predicting diagenetic styling in assessing sandstone reservoir quality

Sandstones that constitute sediment composition, depositional environment, facies associations, and burial history of similar geological histories undergo similar styles of diagenesis. Even though alteration caused by diagenetic cement reduces porosity on a simple volume-for-volume basis, it is crucial to establish a style containing different cements with distinct habits and distributions at the pore scale (e.g., thin pore lining or blocky pore blocking). The same volumetric content of different cements can have different effects on permeability. For example, Pallatt et al. (1984) express the inconsistent effect that small quantities of authigenic illite can have on permeability. Clear

establishment of a “style” of diagenetic process can help provide a framework in which modification of reservoir quality by post-depositional processes can be predicted more quantitatively.

Primmer et al. (1997) documented world-wide database from various petroleum fields and show how sediment composition, depositional environment, and burial temperature combine to institute particular styles of diagenesis. Such diagenetic styling has improved the perceptive used to predict likely changes in the porosity and permeability of sandstones during burial. Data used for this observations dominated fluvial, deltaic, and shallow marine sandstones while aeolian, deep-marine and lacustrine environments sandstones reflects poor preservation and lack good diagenetic description. In addition, even though the selected data are drawn from the most widespread studies available, data on maximum burial temperature are sparse and often poorly constrained. Their estimates of maximum burial temperature were available for just over 60% of the cases studied and range from 25° to 300°C. In trying to estimate the effect of burial temperature, fluid inclusion, stable isotope, and organic maturation data have been analysed where appropriate.

Review of these documented historic data has outlined five styles of diagenesis in sandstone (Figure 2.1) of which each has a distinctive diagenetic mineral assemblage and their characteristics are:

a. Detrital quartz dominated, which often occurs in association with smaller quantities of neoformed clays (e.g., kaolinite and/or illite) and late-stage, high temperature, ferroan carbonate.
b. Authigenic clay minerals dominated such illite or kaolinite with smaller quantities of quartz or zeolite and late-diagenetic carbonate.
c. Early diagenetic (low-temperature) grain-coating clay mineral cements, such as chlorite cements. These may prevent or restrict subsequent quartz cementation during burial to higher temperatures. This can, with help from overpressuring, maintain higher porosity than might be expected when buried to considerable depths (>3.5 km).
d. Early diagenetic carbonate accreation or evaporite cement dominated, often localized, which rigorously reduces porosity and net pay from very shallow burial depths.

e. Zeolite dominated, which accreate over a wide range in burial temperatures, often in association with abundant clay (usually smectite or chlorite) and late-diagenetic nonferroan carbonates.

Table 2.1: Schematic illustration of the relationship between commonly occurring diagenetic cements (shown in order of decreasing abundance) and their associated styles Primmer et al. (1997).

Common diagenetic minerals	Common styles of diagenesis
Quartz	Quartz dominated + late clays & carbonate
Carbonates	Clay dominated + late carbonate & quartz or zeolite
Zeolites	Early grain coating clays wholly/ partially inhibiting later quartz + late carbonate
Clays	Early carbonate or evaporate dominated
Evaporates	Zeolite + clays, late carbonate, opal or quartz

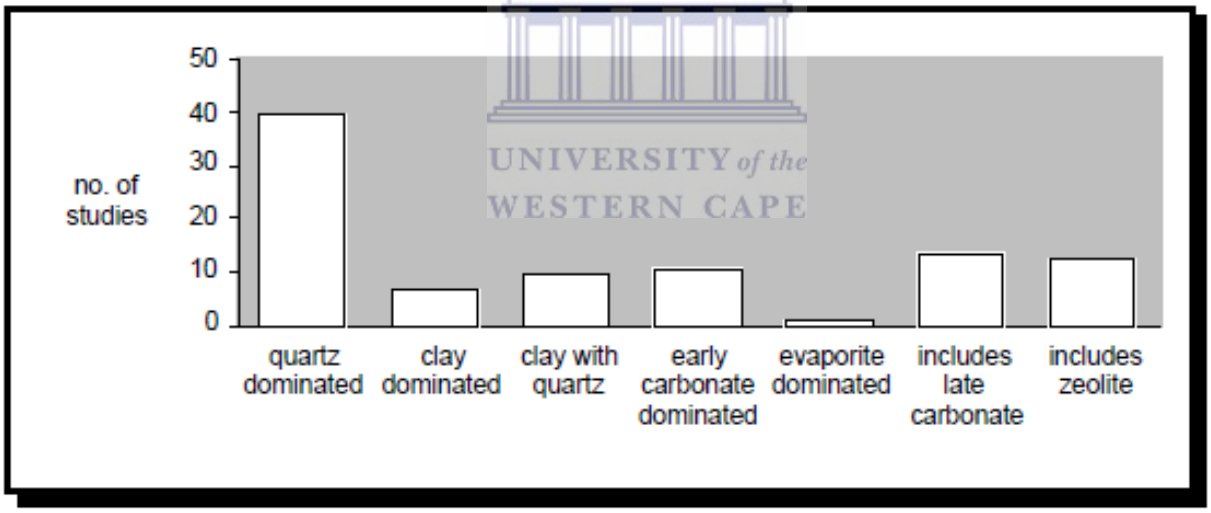

Figure 2.1: Occurrence of different styles of diagenesis (from Primmer et al. (1997))

This study shows that quartz-dominated diagenesis (representing 40% of the total) is the most common diagenetic style seen in the selected studies (Figure 2.1). It is also noted that the specific association of early diagenetic grain-coating clay with inhibition of later quartz cement is more common than diagenesis dominated by clay minerals alone. In ~10% of cases, early or late diagenetic carbonates were the major cements, and a similar number of cases contained significant quantities of zeolite. However, evaporite minerals were significant cements in <1% of the examples investigated.

Figure 2.2 shows the frequency of occurrence of particular clay minerals in the clay-dominated and early grain-coating clay with quartz styles of diagenesis. Chlorite is the most commonly occurring clay mineral, mainly as a result of its frequent occurrence as early grain-coating clay. Both kaolinite and illite are less important; they most commonly occur in subordinate quantities with quartz in quartz-dominated diagenesis. Where carbonates occur as significant cements, Fe-calcite and Fe-dolomite are the more common late-diagenetic cements, whereas siderite and dolomite are more common as early cements (Figure 2.3). Calcite is common both as early cement and as late stage cement.

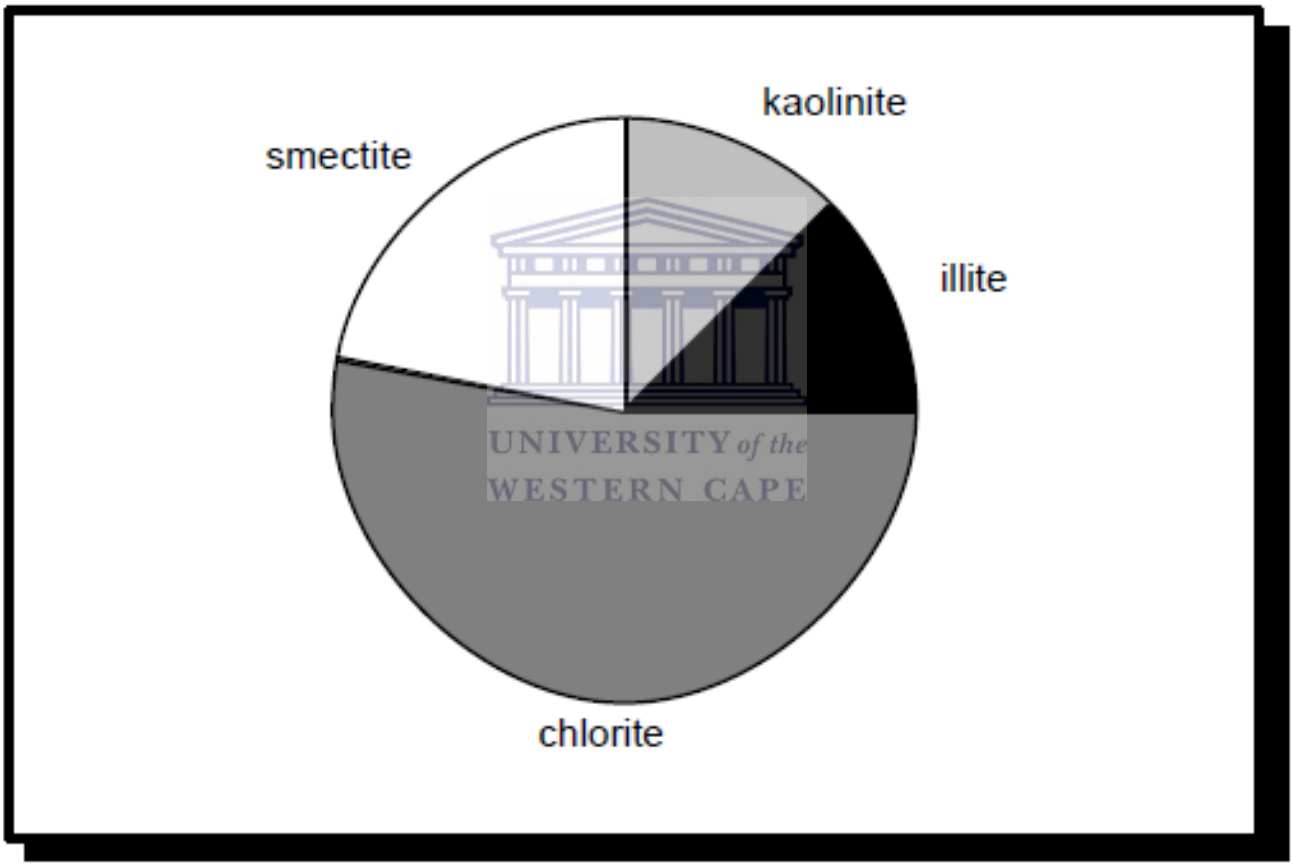

Figure 2.2: Occurrence of different clay minerals in clay-dominated or clay with quartz styles of diagenesis (from Primmer et al. (1997)).

A

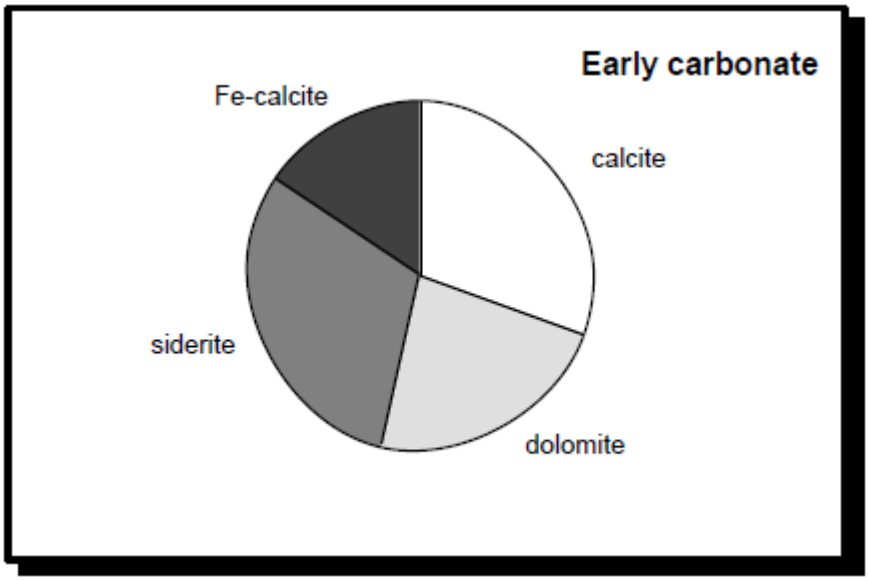

B

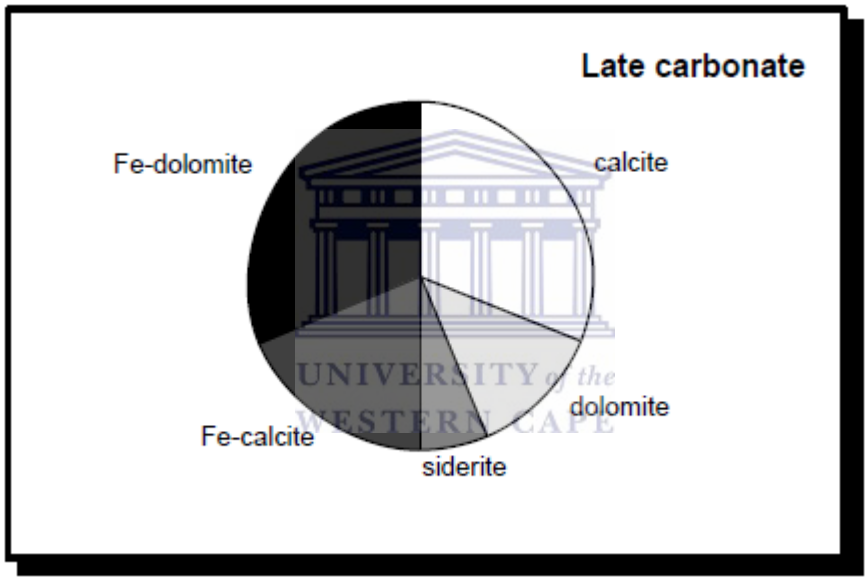

Figure 2.3: Occurrence of different carbonates in situations where early carbonate cement is dominant (A) or where significant late carbonate occurs (B) (from Primmer et al. (1997)).

2.2.4. Contribution of compaction in porosity and permeability reduction

Besides authigenic cements, the main factor that influences porosity and permeability in sedimentary rocks is compaction. Compaction curves determined from laboratory experiments enable porosity to be estimated as a function of burial depth, overpressure, and ductile grain/clay content (Kurkjy, 1988). These estimates can be further refined by taking into account the most likely diagenetic cement predicted at the given depth/temperature of burial for a particular style of diagenesis in the formation of

interest. Simulations from sphere-pack models (Bryant et al., 1993) have indicated that permeability can be calculated directly as a function of porosity, grain size, sorting, and the type of cement present (Cade et al., 1994; Evans et al., 1994).

With porosity-depth trends established, analysis of the effect of different styles of diagenesis on permeability can be made in terms of a series of characteristic porosity-permeability curves for a given sand grain size and sorting. Two hypothetical examples are shown in Figure 2.4, in which clean, compositionally mature quartz-cemented sandstone buried to 3000m is compared to a less mature, subarkosic quartz-kaoliniteillite–cemented sand of similar grain size buried to the same depth/temperatures of burial. Permeability in the subarkosic quartz-kaolinite-illite–cemented sand is consistently lower than the compositionally more mature quartz-cemented sand at any given porosity. Graphical representations such as in Figure 2.4 can be used as “maps” during exploration to predict modifications in porosity and permeability relationships as a result of a specific style of the cementation. Predictions of overall reservoir effectiveness at any given depth of burial can be made, allowing a porosity threshold (and, hence, a depth threshold) to be estimated from the porosity permeability relationship established.

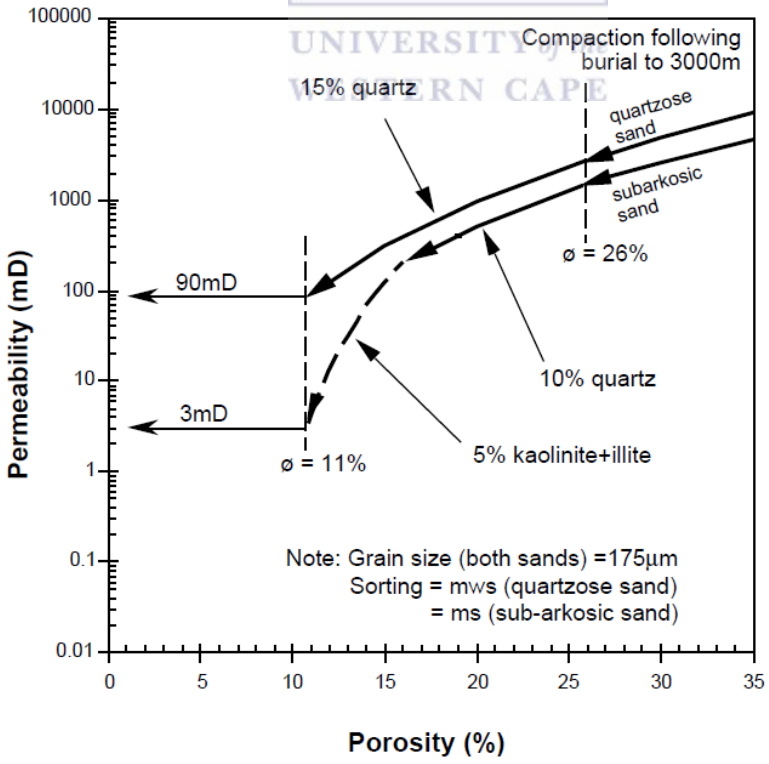

Figure 2.4: Example porosity – permeability trends contracted using the principles outlined by Code et al., 1994 for two sands of similar grain size but different detrital

composition that have experienced similar burial histories (from Primmer et al. (1997)).

2.3. Integration of exploration techniques and analytical approach

Reservoir geometry and its in-situ properties discussed in section 2.2 above can be studied from core samples; the fluid contents within reservoir interstitial space can be evaluated from well logs data (Emery et al., 1990; Cobrera-Garzon et al., 1997; Ketzer, 2002). The section below discusses each exploration techniques and their use in combination.

2.3.1. Core sample analysis

Core samples recovered from the reservoir interval provides compleling information which plays an important role in reservoir facies analyses, well completion and work over operations and reservoir evaluations (Adams et al., 1984). Analyses of core samples provide compeling evidence of hydrocarbons presence, reservoir porosity (for fluid storage capacity), and reservoir permeability (for fluid flow capacity and distribution) expected (Tyler et al., 1984; Ebanks, 1990; Kerans et al, 1994; Stoudt and Harris, 1995). Residual fluid contents allow interpretation of probable production of oil, gas or water (Bennion et al., 1996).

Core studies, supported by supplementary test information gained from well test, provide insight into reservoir performance and unusual response to well treatment yields a sound basis for reserves estimates and reservoir modelling enhances log interpretation, and supplies guidance in secondary and tertiary recovery programs (Bennion et al., 1996). There are two types of core analysis namely conventional and sidewall cores; Conventional or plug-type core analysis is the logging, sampling, and analysis of core wherein a portion of each interval to be analyzed is selected to represent the interval. Three to four inches of each foot of core are commonly used. This type of analysis is performed on reasonably homogeneous formation especially sandstone as reservoir rock whereas sidewall core analysis is the type of analysis performed on percussion sidewall samples. The equipment and techniques used are particularly suitable for the small size of the samples. The procedures are closely related to conventional core analysis.

Core data retrieved through these sampling techniques are studied on thin-section of the rock (Welton, 2003). The study allows the nature of the individual grains and the relationship between these grains and the material between them best observed in a thin-section of the rock (Halley and Beach, 1979; Scholle and Halley, 1985; Budd et al., 1993; Saller et al., 1994; Bloch, 1994).

2.3.2. Well log analysis

Reservoir structure discussed above can be investigated of their porosity, permeability and fluid content properties using well logs (Amigun and Odole, 2013). Well logs are record versus depth of some physical property of the rock in the subsurface. These logs can be recorded while drilling the well using electronic equipment that is part of the drilling referred to as Logging While Drilling (LWD). The data are stored in downhole memory for retrieval after the equipment has been pulled out of the borehole. The measurements can also be made after the drilled string has been pulled out of the hole using electronic equipment carried at the end of a cable (electric line). The line is used to transmit measurement at high data rate from downhole sensor to the surface recording system. This option is called wireline logging.

Several logging tools are usually hooked together to acquire many different measurements during a single descent in the borehole. A typical combination includes gamma ray, resistivity, neutron porosity and density logs. Such measurements records characteristics of the rock material penetrated during drilling. Throughout the world these measurements has become the most universal documents available for the description of well drilled for oil and gas. These measurements are regarded geophysical in nature as they indirectly record the rock physical properties which inversely interpreted in geology. It is well understood that well logging does not measure the geological characteristics directly but records the physical properties of rock material. Well log interpretation involves the derivation of descriptive geological parameters from the measured properties. The main properties of interest in this interpretation are porosity, fluid saturation and permeability. These parameters are also needed to estimate the amount of hydrocarbon present in a well.

Information gathered from geophysical logs are calibrated using core or chip sampled during drilling to match the geological formations. Geological sampling during

drilling provide a very imprecise record of geological layers encountered. This is mainly attributed the type of drilling chosen for sampling either chips or coring sampling. For an example, core sampling is very expensive and consume a lot of rig time but provide detailed geological information whereas chips sampling is quick with missing geological information for the interval not sampled. These information retrieved play an important role in matching petrophysical logs for concise geological interpretation and modelling though petrophysical properties obtained from sampling may not always be directly comparable. In uncored intervals petrophysical logs helps to fill the gaps as its measurement is continuous over a large interval of a well. Considered core for reservoir analyses should be matched precisely with petrophysical logs for proper integration of uncored interval.

Petrophysical logging and core sampling can be performed simultaneously as drilling continues but the data obtained differs and measurements retrieved from these two components also differ. Well logging measures formation properties of the rock that requires interpretation for geological consideration in petrophysical analysis. Wireline logging tools in the hole can be affected by formation temperature, overburden stress and casings used to maintain well integrity (Rider, 1996). Core sample at the lab for reservoir analysis it is no longer representing the reservoir condition fully because is no longer sitting at its formation temperature and pressure as it is brought to surface. Some of these challenges can be dealt with and important information can be retrieved for reservoir assessment and management by integrating well logs and core data.

In most cases the use of these two techniques is mainly in correcting the depth of core data against the recorded depth by well logs. For example the comparison of lithology defined by neutron-density log with the detailed gained from core description. In addition, reservoir properties obtained from core sample in the lab is used to calibrate well logs to use confidently to predict reservoir properties of uncored reservoir intervals. Core data provide with detail geological information such as mineralogical properties, porosity and permeability, fluid saturation and can be used effectively to manage the reservoir interval whilst integrating with well logs data.

2.3.2.1. Classification of geophysical wireline logs

Well logs can be classified on the bases of usage or on the operational principle. On operational practice well logs can be classified as electrical logs (resistivity and spontaneous potential (SP)), radioactive or nuclear logs (density, neutron and gamma) and acoustic logs (sonic). On usage well logs are classified as porosity logs (neutron, density and sonic), lithology logs (SP and gamma), Auxiliary logs (bit size and calliper) and resistivity logs (deep resistivity, laterolog and induction).

2.3.2.2. Characteristics of selected wireline logs

2.3.2.2.1. Gamma ray (GR) logs

The gamma ray logging tool measures natural radioactivity of the formation in a wellbore. All rocks have some radioactivity. The natural radiation is due to the disintegration of nuclei in the subsurface. Three main elements that are radioactive include Potassium (K^{40}), Thorium (Th^{232}) and Uranium (U^{238}). K^{40} decays in a single step positron emission. Th^{232} and U^{238} decay to their final state through a series of intermediate steps, emitting apha and beta particles and gamma rays in the process. They are found in various proportions in crystalline rocks. During deposition these elements tend to concentrate in shale, therefore shale is more radioactive than sands.

In general, sandstones, carbonates and evaporates have very little radioactive content. This is due to that clean sands may contain feldspars and mica which contain valuable amount of these radioactive elements whereas clean carbonates may contain uranium salts and these radioactive salts get deposited near the wellbore over perforated intervals. Gamma ray units are measured in American Petroleum Institute (API). High gamma ray values of about 100 API are mostly encountered in shales. Organic shales may have much higher gamma ray values. Clean reservoirs (without shale) normally have low gamma ray values (15 to 25 API units).

The measurements obtained helps to estimate the amount shale content in the formation as a function of depth. The vertical resolution of the tool is approximately 0.6m with a depth of investigation of 0.15 – 0.3m depending on the density of the rock. The gamma ray log is used for basic lithology analysis, quantitative estimation of clay content, correlation of formations, and the depth matching of multiple tool runs. The simple gamma ray log is usually recorded in track one and scales chosen locally, but 0 – 100 and 0 – 150

API are common. A deflection of GR log to the right demonstrates shales, where continuous increase or constant natural radioactivity to the right indicate shale line whereas a deflection to the left demonstrate sandstone, where a continuous decrease or constant in the left indicates sandstone line as indicated in Figure 2.5.

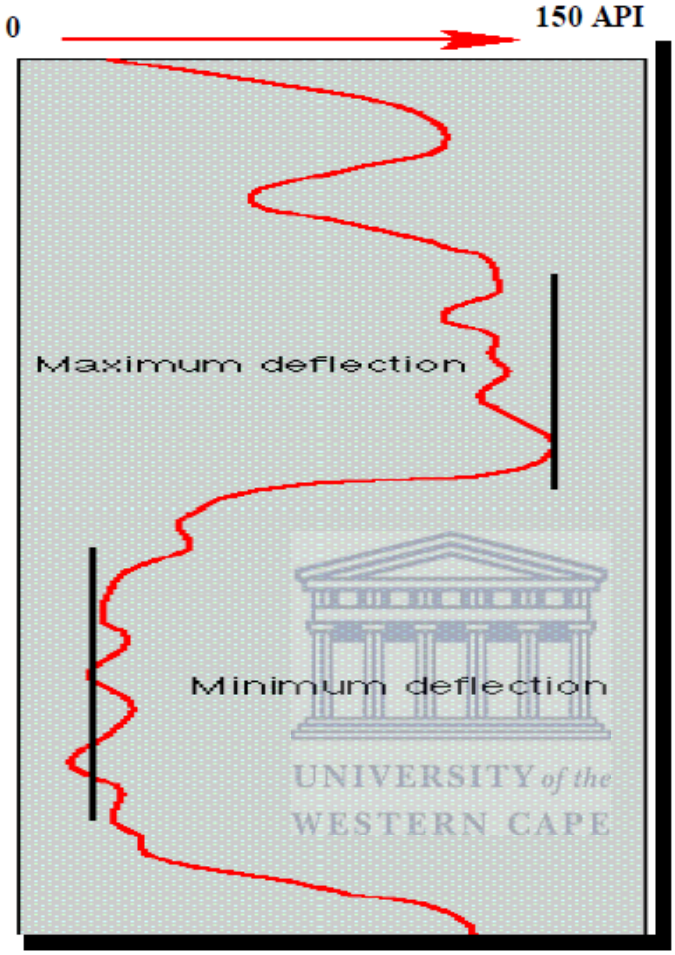

Figure 2.5: Diagram of GR log (Modified after Russel, 1944).

2.3.2.2.2. Density logs

The density logging tool measures the electron density of the formation (number of electron per unit volume). The electron density is converted to actual density of the formation (mass per unit volume). Its geological interpretation is primarily used to determine hydrocarbon density, detect-gas zones, identify evaporates minerals, evaluate shaly sand reservoirs and complex lithology. The porosity of the formation can be derived from density log if formation pore fluid and lithology are known. Logging tool used for density is a contact device which consists of a medium-energy gamma rays source that emits gamma rays into a formation. The gamma rays source is either Cobalt-60 or ceisium-137. Gamma rays collide with electrons in the formation; the collision results in

energy loss from gamma ray particle. Tittman and Wahl, 1965 define the interaction between incoming gamma rays particles and electrons in the formation as Compton Scattering. Scattered gamma rays which reach the detector located at a fix distance from the gamma ray source are countered as an indicator of formation density. The number of Compton Scattering collisions is a direct function of the number of electrons in a formation (electron density). Consequently, electron density can be related to bulk density (ρ_b) of a formation in gm/cc. Formation bulk density (ρ_b) is a function of matrix density, porosity, and density of the fluid in the pores (salt mud, fresh mud, or hydrocarbon).

2.3.2.2.3. Neutron log

Neutron porosity logging tool measures the concentration of hydrogen ion in a formation. In clean reservoirs (that are free shale), their pore spaces are filled with fluids such as water or oil. The neutron logging device measures liquid that filled such pore spaces. Neutrons are created from a chemical source in the neutron logging tool. The chemical source maybe a mixture of americium and beryllium which will continuously emits neutrons. These neutrons collides with the nuclei of the formation material and results in a neutron losing some of its energy. Because the hydrogen atom is almost equal in mass to the neutron, maximum energy loss occurs when the neutron collides with the hydrogen atom. Therefore, the maximum amount of energy loss is a function of formation's hydrogen concentration. Because hydrogen in a porous formation is concentrated in the fluid-filled pores, energy loss can be related to the formation's porosity. Whenever pores are filled with gas rather than oil or water, neutron porosity will be lowered. This occurs because there is less concentration of hydrogen in gas compared to oil or water. A lowering of neutron porosity by gas is called gas effect. Neutron log responses vary depending on differences in the detector types, spacing between source and detector and lastly lithology e.g. sandstone, limestone and dolomite. These variations in response can be compensated for by using the appropriate chart. Neutron logs are interpreted from the specific chart designed for a specific log. The reason for this is that while other logs are calibrated in basic physical units, neutrons are not.

The first modern neutron log was the Sidewall Neutron Log. The Sidewall Neutron Log has both the source and the detector in a pad which is pushed against the side of the borehole. The most modern of the neutron log is a Compensated Neutron Log which has a neutron source and two detectors. The advantage of Compensated Neutron Logs over

Sidewall Neutron Logs is that they are less affected by borehole irregularities. Both Sidewall and Compensated Neutron logs can be recorded in apparent limestone, sandstone or dolomite porosity units. If a formation is sandstone, and the neutron log is recorded in apparent limestone porosity units, apparent porosity is equal to true porosity. However, when the lithology of a formation is sandstone or dolomite apparent limestone porosity must be corrected to true porosity.

2.3.2.2.4. Combination of Neutron-Density

This is the combination of the porosity logs. It is mainly used porosity determination but it is also used to determine lithology and to detect gas-bearing zones. Both the neutron and density curves are generally logged in limestone porosity units with each division equal to either two percent or three percent porosity; however, sandstone and dolomite porosity units can also be recorded.

True porosity can be known by first reading apparent limestone porosities from the neutron and density curves. Then, these values are crossplotted on a neutron-density porosity chart to find true porosity. Examination of the neutron-density porosity chart reveals that the porosity values are only slightly affected by changes in lithology. Therefore, porosity from a Neutron-Density Log can be calculated mathematically. The alternate method of determining neutron-density porosity is to use the root mean square formula. Change in neutron - density response between an oil- or water –bearing sand and a gas-bearing sand. The oil-or water – bearing sand has a density log reading of four porosity units more than the neutron log. In contrast, the gas – bearing sand has a density reading of up to 10 porosity units more than the neutron log.

A combination of neutron-density logs, where an increase in density porosity occurs along with a decrease in neutron porosity in a gas – bearing zone such occurance is called gas effect. Gas effect is created by gas in the pores. Gas in the pores causes the density log to record too high a porosity (i.e. gas is lighter than oil or water), and causes the neutron log of record too low a porosity (i.e. gas has a lower concentration of hydrogen atoms than oil or water). The effect of gas on the Neutron-Density log is a very important log response because it helps a geologist to detect gas-bearing zones.

2.3.2.2.5. Sonic log

The sonic log is a porosity log that measures interval transit time (Δt) of a compressional sound wave travelling through one foot of formation. The sonic log device consists of one or more sound transmitter, and two or more receivers. Modern sonic logs are borehole compensated device. These devices greatly reduce the spurious effects of borehole size variations (Kobesh and Blizard, 1959), as well as errors due to tilt of the sonic tools (Schlumberger, 1972). Interval transit time (Δt) in microsecond per foot is the reciprocal of the velocity of a compressional sound wave in feet per second. Interval transit time (Δt) is dependent upon both lithology and porosity. Therefore, a formation's matrix velocity must be known to device sonic porosity. The sonic log is used in combination with other logs (e.g. density and neutron logs for porosity, shaliness and lithology interpretation. Integrating transit time is also helpful in interpreting seismic records.

2.3.2.2.6. Resistivity logs

Resistivity logs are electric logs which are used to determine hydrocarbon versus water-bearing zones, indicate permeable zones, and determine resistivity porosity. Most importantly resistivity log is used to determine hydrocarbon versus water-bearing zones. Because the rock's matrix or grains are non-conductive the ability of the rock to transmit a current is almost entirely a function of water in the pores. Hydrocarbons like the rock's matrix are non-conductive. Therefore, as the hydrocarbon saturation of the pores increases the rock's resistivity also increases.

2.3.2.2.7. Calliper logs

Mechanical Calliper measures the varieties in borehole diameter with depth. Calliper log accomplish the measurements by utilizing two enunciated arms that are pushed against the borehole wall. The arms are interfaced to the cursor along the resistance. Parallel development of the arms is deciphered into the movements of the cursor along the resistance, and henceforth varieties in electrical yield. The contrasts in yield are deciphered into diameter varieties after a simple calibration. Calliper log is usually equipped with frequently used logging tools such as micrologs and density and neutron where it is used to apply the measuring head of the tool to the borehole wall.

2.3.3. The importance of core samples and well log in reservoir assessment

This section review the traditional methods applied to estimates fluids saturation within the reservoir. Bennion et al., 1998 noted that initial fluid saturations, the fraction of the interstitial space in a pore system occupied by oil, water and gas, are key factors in determination of initial reserves and dominate reservoir flow properties due to the influence they exhibit on relative permeability. Improper saturation measurements can lead to the bypassing of potentially productive pay zones result in significant lost reserves, or the erroneous completion of ineffective pay resulting in lost revenue. If initial fluid saturation is improperly measured it can lead to gross over or under estimation of oil or gas reserves in place (Bennion et al., 1998). For the development plans deemed important for the Orange Basin, improper determination of the initial oil, water or gas saturations which exist in porous media may often lead to expensive mistakes during field development that may lead to commercial development that could not last the expected life time or may lead to non-development at all.

Investigation by Bennion et al., 1998 discovered that hazards involved with an inadequate understanding of initial saturation conditions can generally be grouped into three categories:

2.3.3.1. Poor initial reserves evaluation.

Oil and gas accumulated in a reservoir are based on a simple volumetric calculation of hydrocarbon volume present in the effective porosity of the system. This is achived following the usual assumed equation of 1-Swi. Bennion et al., 1996 noted that under or overestimation of the initial water saturation (Swi) can grossly affect the observed amount of oil or gas in place in the reservoir. An underestimation of Swi could result in expensive development of a field which has much less oil or gas in place than predicted, resulting in partial or negative return on ultimate investment. Equally, if Swi is overestimated, a potentially viable and highly productive pay zone may be abandoned.

2.3.3.2. Poor completion zone selection.

Figure 2.6 demonstrates a typical set of water-oil or gas-water relative permeability curves. With the aid of this figure Bennion et al., 1996 illustrated that underestimation of the initial water saturation may result in completion of zones with high potential water phase relative permeability which will result in immediate high water cuts and poor oil or

gas production rates (i.e. the water saturation was believed to be at point “A", when, in fact, it is actually at point "B" on Figure 2.6).

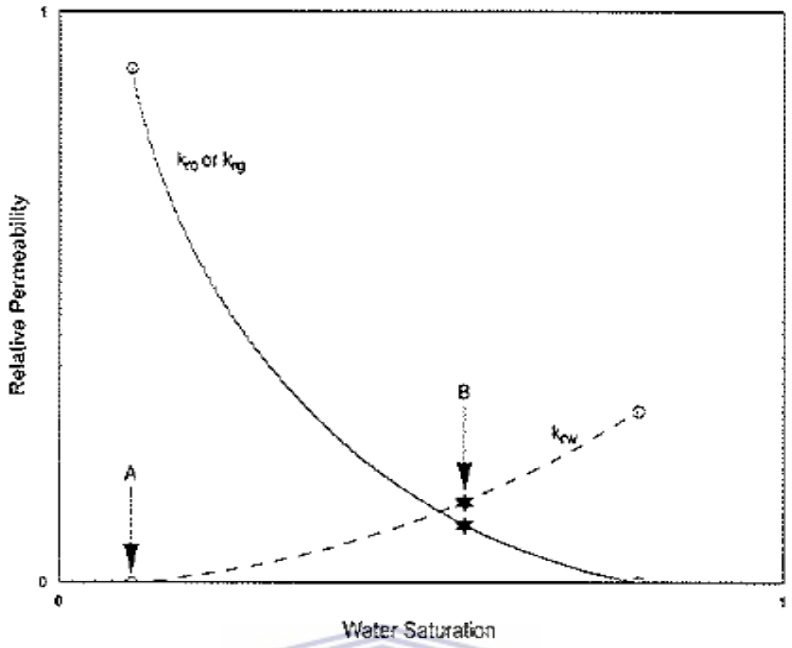

Figure 2.6 water-oil or gas-water relative permeability curves (Bennion et al., 1996).

Conversely, Bennion et al., 1996 also demonstrated that over estimation of initial water saturation may result in the decision to not complete a zone which could conceivably produce at economic rates, resulting in lost opportunities and revenue (i.e. the water saturation was thought to be at point "B" on Figure 2.6 in this case when it was actually at point “A”).

2.3.3.3. Flow mechanics.

Multiphase flow is governed by the relative permeability which exists between the individual phases. Relative permeability is in turn governed directly by the respective saturations of the individual fluid phases which are present in the porous media. Proper knowledge of both the relative permeability characteristics of the porous media and the initial saturation conditions will allow inflow calculations to determine if, in the presence of mobile or immobile water or gas saturations, economic production rates of oil or gas will be feasible.

2.3.3.3.1. Saturation determination techniques

Initial saturations are commonly determined using the following techniques; Log based saturation evaluations or direct saturation measurements on in-situ samples

2.3.3.3.1.1. Log based saturation evaluations

Water saturation determinations in clean (non-shaley) formations are based on Archie's equation.

$$S_w^n = (FR_w)/R_t \quad \text{.....(1)}$$

where

S_w = Fraction of pore space occupied by water

n = Saturation exponent

R_w = Formation water resistivity

R_t = True water resistivity

F = Formation factor

The formation factor is given by the equation:

$$F = \alpha/\phi^m \quad \text{.....(2)}$$

Where

a = Archie constant

m = cementation exponent

ϕ = Porosity fraction

Therefore, combining equation 1 and 2 yields:

$$S_w^n = (aR_w)/(\phi^m R_t) \quad \text{.....(3)}$$

2.3.3.3.1.2. Direct saturation determination

It is well observed from the previous discussion that, although log techniques are commonly used to evaluate initial water saturations, there may be substantial uncertainty with respect to the complete validity of the numbers obtained, particularly in the absence of any precise actual measurements of the electrical properties of the rock under consideration.

Other, possibly less vague and more precise technique is acquired by a direct measurement of fluid saturations from core samples obtained from the formation during the initial drilling process. This data, if appropriately acquired, can offer representative fluid saturation measurements which are regularly used to rectify field logs and then apply the corrected log calibration constants to other wells in the same field (which may not have been cored).

CHAPTER THREE: DATA AND METHODS

3. Data and methods

3.1. Introduction

This chapter presents methodology and various analytical procedures used to conduct this study. The diagram in Figure 3.1 presents the flow chart that outlines steps that were followed to complete this study. The data set was obtained from Petroleum Agency SA (PASA).

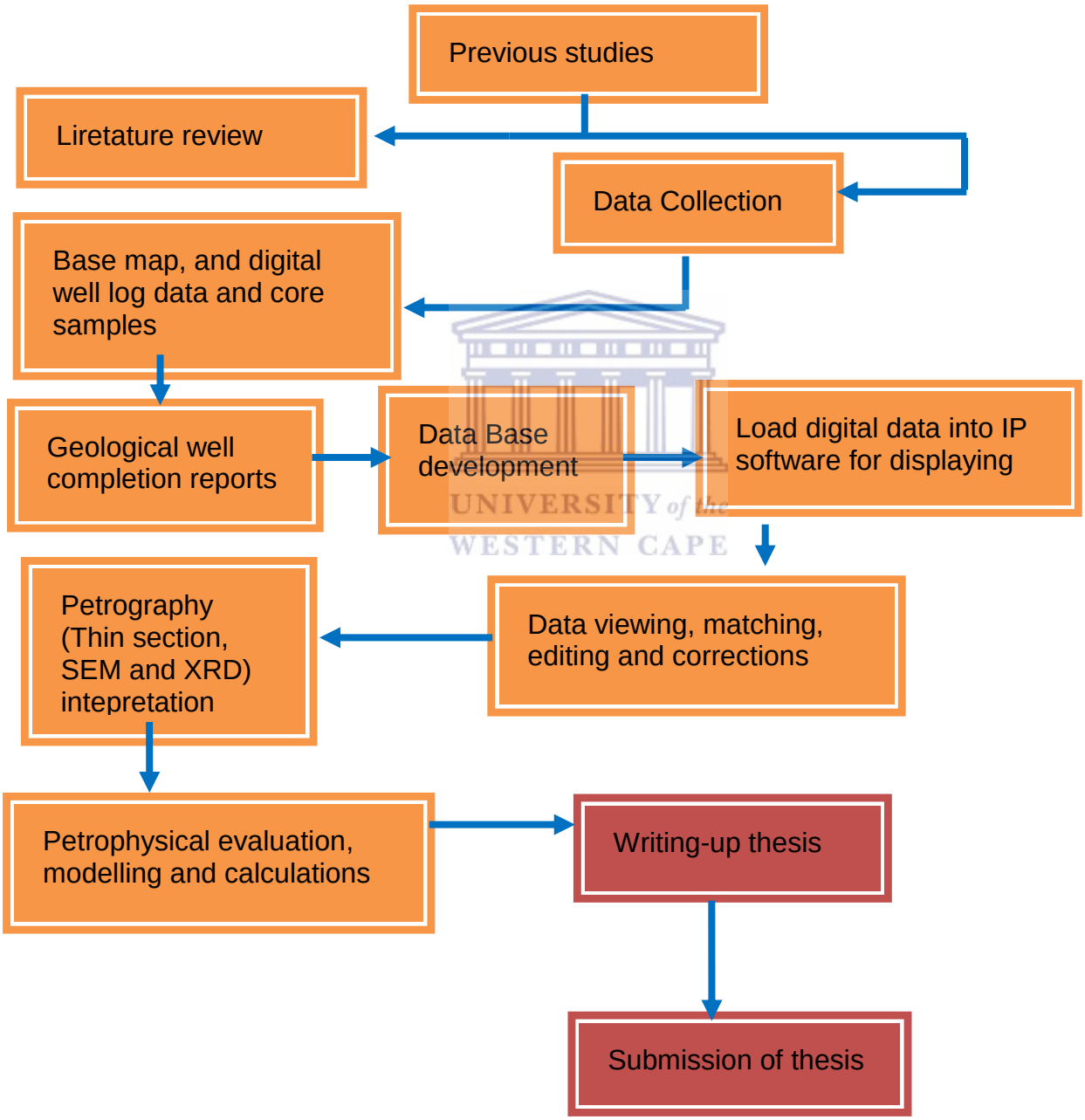

Figure 3.1: The flow chart of the research methodology.

3.2. Well data

Five (A-D1, A-J1, K-A2, A-K1 and A-H1) wells were provided by PASA for this study. These wells were selected to understand reservoir properties from the shelf to deep water. The deepest were drilled to the depth of more than 5500m having some intersecting oil and gas prospects. All of these wells are located in the continental shelf. Well data provided for this study include:

- Electrical logs in paper and digital (LAS) formats;
- Side wall cores and full sets of cutting sample;
- Petrography reports;
- Well recommendation reports;
- Well completion report;
- Composite logs;
- Engineering reports;
- Geological evaluation reports;

3.3. Methods

3.3.1. Core description procedure

All wells in the study area were cored and the following present cored depth of each well;

- A-J1 cored interval
  - Core 1 from 1617-1635m
  - Core 2 – 6 from 3191-3259.30m
- A-D1 cored interval
  - Core 1 from 2661.8-2666.4m
- A-K1 Cored interval
  - Core 1 from 3236-3249m
  - Core 2 from 3283-3296m
- A-H1 Cored interval
  - Core 1 from 3022.4 to 3039m
- K-A2 Cored interval
  - Core 1 from 3982.1 - 3991.85m
  - Core 2 from 4076.1-4083.1m

Description of core embraces a combination of quantitative and qualitative data, which needs to be briefly documented. The quantitative information differs incessantly down hole and greatly demonstrated in a graphic plot. In reservoir assessment and evaluation core description processes starts with identifying the depth of interest and then assemble tray and layout of cores. The tools used for actual description of core are itemised below:

- Digital Camera
- Tape rule
- Log sheet
- Microscope
- Hammer
- Water bottle and foam
- Small Clip board
- Hand lens
- Grain size standard chart

The cores were laidout and depth of drilling was established together with the log format. Core trays with sample were assembled and laidout per tray to allow a sequence of four to twelve samples to be perceived in a single tray. All core samples used were laid in a pile of five-cell trays with their sequential depths marked on the side of the trays. Five metres of the samples were perused to observe the lithologic “breaks”. The samples were then reviewed for thorough study to identify other reservoir properties. Soaking samples in the water was achived to clean the dirt off and other unwanted contaminants, and also to bring out clear the properties rock. Attention was paid to the following factors: rock type, sedimentary structures and grain size variation, packing pattern, fossils assemblages, colour, textures, cement/matrix and the effect of HCL on the samples. In core description, the rock type was first identified, followed by the colour with the aid of the standard geologic colour chart, then an appropriate scrutiny was achived to describe the grain size, texture and degree of sorting.

3.3.2. Petrographic procedures

3.3.2.1. Thin section analysis

Thin sections were made from plug trims for the sampled zones in all cored intervals. The rock material in the plug was impregnated with blue-dyed epoxy resin to highlight porosity. The plug was stained for calcite, dolomite (Alizarin-Red S Solution and Potassium Ferricyanide) and feldspars. Sedimentological description of the reprentative plugs detailed depositional texture including sorting, grain-size, compaction, lamination together with mineralogy of detrital minerals and cements, fractures and visible pore types. Point count modal analysis involves the counting of 300 mineral counts, to obtain a semiquantitative assessment of bulk composition and visible porosity were used. The results were presented by four colour photomicrographs per sample.

3.3.2.2. X-ray diffraction analysis

Samples are hand-crushed and homogenized before splitting by cone and quartering to give approximately 5 gms for whole-rock analysis. The samples are then prepared by micronizing under acetone for six minutes. After drying the mixture is homogenized in a vibratory ball mill before back loading into aluminium sample holders. A single scan from 5 to 70 degrees two theta, at a rate of 0.6 degrees/minute is run for each sample. Quantification of the whole rock composition is based upon calibration curves and comparison of the sample traces with those of artificial mixtures.

Clay fractions are prepared by repeated centrifuging of suspensions, using an ultrasonic probe to aid dispersion of the sample material. Samples were mounted by suction onto porous teflon membranes and mounted in turn onto glass discs and aluminium sample holders. Two scans are made of each sample: one from 3 to 16 degrees two theta with the sample in the air dried state, and one from 3 to 35 degrees two theta after saturation of the sample with ethylene glycol. The scan rate for these runs is 0.48 degrees two theta/minute. Quantification of the clay fractions is based on measurements of the intensities of characteristic basal reflections. These measurements are compared to intensities obtained from standard clay minerals. XRD results are presented as summary histograms on the SEM plates.

3.3.2.3. Scanning electron microscopy analysis

For scanning electron microscopy, plug trims are mounted on standard aluminium stubs using colloidal graphite, and coated with gold using a sputter coater. SEM descriptions include a summary of depositional textures, fracture types, pore types and the composition and morphology of pore-occluding minerals. Mineral identification is supplemented by EDX (energy dispersive X-ray) analysis. Descriptions are illustrated by four photomicrographs per sample.

The plug samples were analysed by thin section petrography, scanning electron microscopy and X-ray diffraction. Thin section petrography was performed to determine the detrital and authigenic mineralogy and texture of the samples and to determine the major controls on reservoir quality. Scanning electron microscopy was performed to determine the types, morphology and distribution of authigenic and clay minerals present in the pore network, and to characterize porosity and pore interconnectivity. X-ray diffraction analyses were performed to determine bulk mineralogy and relative proportions of clay minerals present in the samples.

3.3.3. Wireline logs loading

Interactive Petrophysics (IP) software were used for the loading and displaying log curves, the data were received in LAS format and were loaded directly into the IP workstation where depth shifting was done based on the core description along with necessary environmental corrections. Proper quality control was achieved and reservoir zones were identified using the appropriate well logs. A database was created on petrel for well correlation based formation tops. Another database was generated in Interactive Petrophysics on the basis of different information including conventional core analysis and well description to complete this project. This allowed evaluation of sandstone reservoirs and also calculation of porosity, permeability, water saturation, clay volume, flow capacity and storage capacity. Once the petrophysical evaluation was completed hydrocarbon generation potential and its volumetrics was estimated. This work was achieved as follows:

3.3.3.1. Identification of possible sandstone reservoir

The first step in a log interpretation is to categorize zones of interest or potential sandstone reservoirs and define a clean and shale baseline on the gamma ray (GR) logs

(Figure 3.2). This is achieved by detecting the behavior of the gamma ray log, maximum deflection to the right indicate a shale formation and maximum deflection to the left indicate clean sandstone (Jensen et al., 2013).

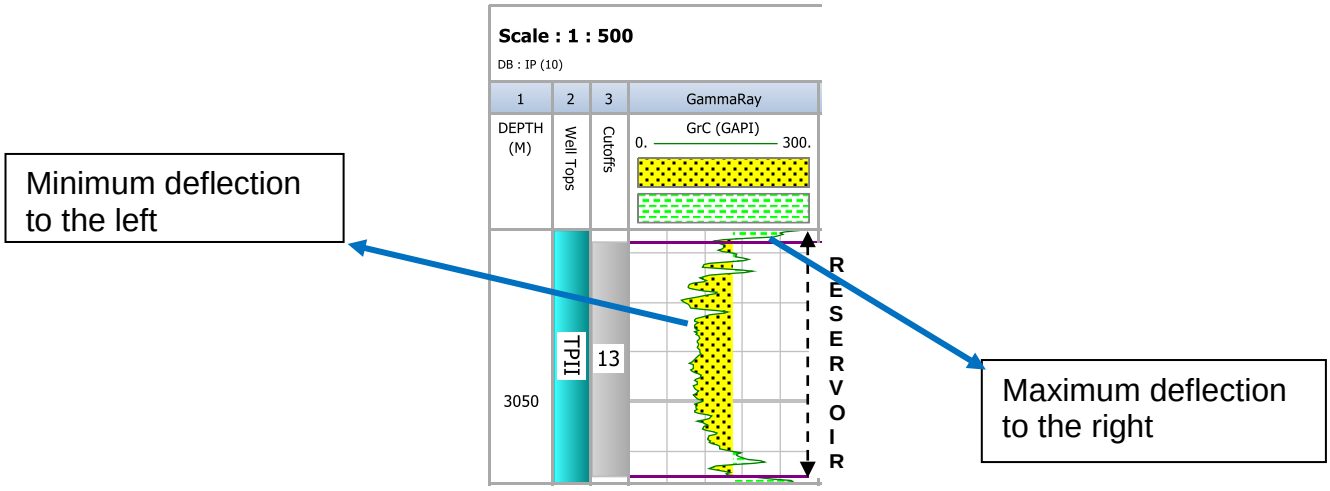

Figure 3.2: Example of the selected potential sandstone reservoir.

3.3.3.2. Determination of m, a, n and Rw parameters from standalone picket plots

Determination of tortuosity factor (a), cementation factor (m), water saturation factor (n) and water resistivity factor (Rw) play an important role in log interpretation. To determine these parameters, resistivity and porosity was plotted against each in water bearing interval using a standalone picket plot. Figure 3.3 below shows a typical example of A-J1 well standalone picket plot for the determination of these values in a water bearing zone between 1448.6 – 1540.6m. The straight lines in the cross-plot represent the amount of water saturation; the red line represents 100% water saturation, 0.5 line represents 50%, 0.3 line represents 30% and line 0.2 represents 20% water saturation.

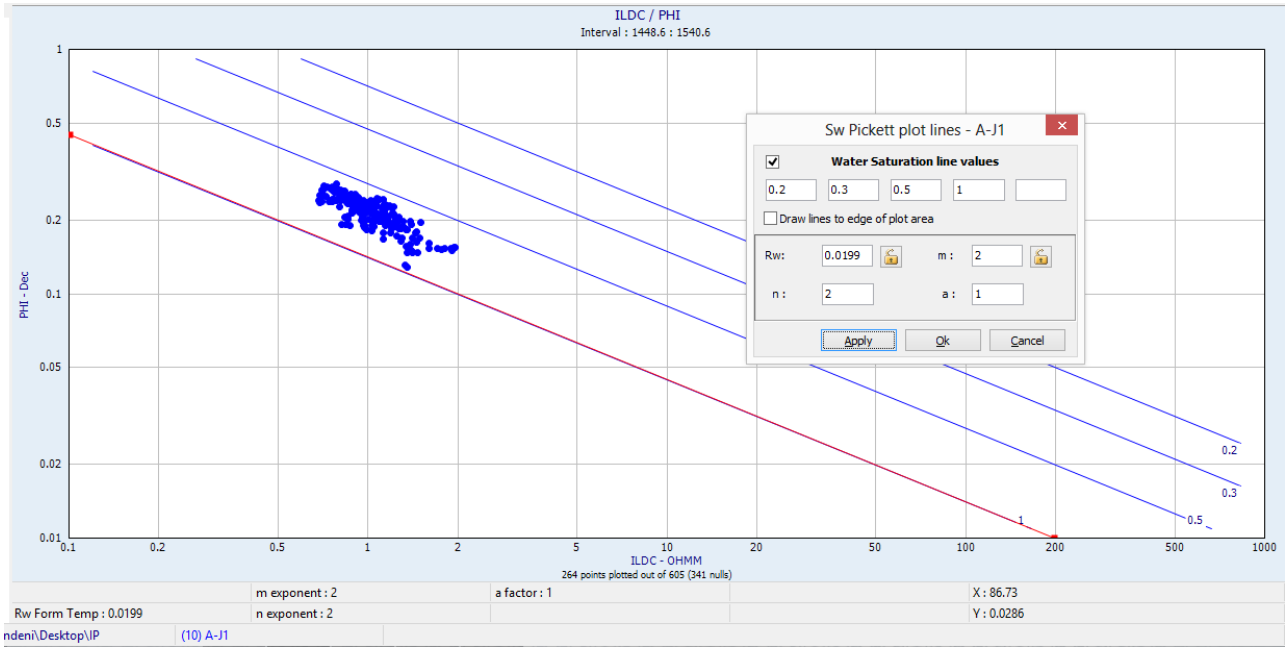

Figure 3.3: Standalone picket plot used to determine the above mentioned parameters (A-J1 well).

3.3.3.3. Determination of initial fluid saturation parameters

Fluid saturation parameters were determined in a water bearing zones of the studied wells.

3.3.3.3.1. Water saturation exponent (n)

The water saturation exponent value is a function of both pore geometry and formation wettability (Bennion et al., 1996). The water saturation exponent is generally thought to be 2.0 however this varies relying upon the formation and may bring about overestimation and underestimation of water saturation in many situations (Bennion et al., 1996. The "n" value measurement is generally conducted from samples from the range of permeability, porosity and lithology which may be available in the formation; this is because of the way that the "n" values contrast with both lithology and wettability. The standard "n" value of 2.0 is utilized so generally in the oil and gas industry. In this study the saturation exponents of each of the five wells (A-D1, A-J1, K-A2, A-K1 and A-H1) were measured to be 2 from the standalone picket plots in which porosity is plotted against the resistivity in a water bearing zone (Figure 3.3).

3.3.3.3.2. Tortuosity factor (a)

Tortuosity values are measured experimentally for a sequence of formation factors that are determined on a range of porosity value samples for a given lithology that is expected to exist in a specific formation (Bennion et al., 1996). The degree of consolidation controls the Archie constant because generally the lower the degree of consolidation the lower the value of the tortuosity constant and vice versa. The value of 1.0 is found for compacted sands, and a value as low as 0.62 for poorly consolidated sands and it may exceed 1.0 as the degree of compaction becomes extreme (Bennion et al., 1996). The tortuosity constant value was calculated to be 1.0 for all five wells from the standalone pickets plot. The 1.0 value shows that the sands for all five wells are compacted.

3.3.3.3.3. Cementation exponent (m)

The value of the cementation exponent depends on the degree of cementation and the type of cementation in the pore system. Generally a value of 2.0 is used, but this value can vary depending on the degree of cementation (Bennion et al., 1996). For example, for a poorly cemented rock “m” value may be less than 2.0 and for a highly cemented or ooliclastic rock “m” values may be as high as 3. The cementation values of 2 were measured for well A-D1, A-J1, K-A2, A-K1 and A-H1 from the standalone picket plot respectively. All well are highly cemented with carbonates minerals (carbonates and dolomites).

3.3.3.3.4. Formation water resistivity

Formation water resistivity is a very important factor in the initial water saturation calculation due to the fact that the ionic composition of the water affects its overall conductivity and hence resistivity. This factor is controlled by the type of water that is present in the formation. Fresh water exhibit high resistivity while saline brine exhibit low resistivity. Standalone picket plots were used to calculate the water resistivity (Rw).

3.3.4. Petrophysical calculation procedures

The methodological approach used in arriving at the petrophysical results was as follows:

3.3.4.1. Volume of shale (V_{sh})

The volume of shale (V_{sh}) quantity is defined as the volume of the wetted shale per unit volume of reservoir rock. The volume of shale can be expressed as decimal fraction or percentage. To determine the volume of shale in all selected reservoirs a gamma ray log was used. This is because shale is more radioactive than sand or carbonate. The first step is to calculate the gamma ray index. Schlumberger (1974) devoted the following formula which was adopted in this study.

$I_{GR} = (GR_{log} – GR_{min}) / (GR_{max} – GR_{min})$ …….(1)

Where:

I_{GR} = Gamma ray index

GR_{log} = Gamma ray reading of formation

GR_{min} = Minimum gamma ray (Clean sands)

GR_{max} = Maximum gamma ray (Shale)

The minimum and maximum values used in the equation were obtained from the gamma ray histogram plots. The value of (V_{sh}) obtained have to be corrected by valid formula to obtain the optimum value usable for interpretation (Jensen et al., 2013). The volume of clay readings for each zone is obtained from the volume of clay log curves derived from the gamma ray log. Various non-linear (correction) equations and models used to calculate the volume of shale is presented below:

Older rocks, consolidated:

$V_{sh} = 0.33 (2^{(2 \times I_{GR})} – 1.0)$ …….(2)

Where:

V_{sh} = Volume of shale

I_{GR} = Gamma ray index

Larinov (1969) for tertiary rocks

Vsh= 0.083(23.7IGR-1)……..…….... (2)

Steiber (1970) Vsh = IGR 3−2∗ IGR…….. (3)

Clavier (1971) Vsh= 1.7-[(3.38-(IGR+0.7)2]1/2……(4)

Larinov for older rocks Vsh= 0.33*(22IGR-1)…….…… (5)

3.3.4.2. Porosity and water saturation determination

The porosity curves were derived from the density, neutron and sonic logs. Neutron-density combination logs were used to calculate the porosity and water saturation of the wells under study. The following formula was used to derive the density porosity log curve:

$\Phi = (\rho_{ma} - \rho_b) / (\rho_{ma} - \rho_f)$……..... (6)

Where:

Φ = density derived porosity (g/cc)

ρ_{ma} = matrix density (g/cc)

ρ_b = formation bulk density (g/cc)

ρ_f = fluid density of the mud filtrate (g/cc); salt mud=1 and fresh water= 1

And the formula used to derive the neutron porosity log curve was as follows:

PHIN = PHIe x Sxo x PHINw…….. (7)

Where:

PHIN = log reading

PHIe = effective porosity

Sxo = water saturation in invaded zone

PHINw = log reading in 100% water

The porosity from the sonic slowness is different than that from the density or neutron tool. It reacts to primary porosity only (it does not react to fractures or vugs). The basic equation for sonic porosity is the Wyllie Time Average:

$\Phi = (\Delta t_{log} - \Delta t_{ma}) / (\Delta t_f - \Delta t_{ma})$ …… (8)

Where:

Φ = Sonic derived porosity

Δt_{ma} = Interval transit time of the matrix

Δt_{log} = Interval transit time of formation

Δt_f = Interval transit time of the fluid in the well bore

A cluster of different porosity and water saturation curves were plotted from the database development so as to obtain the correct curves for water saturation and

porosity, the curves derived from the IP software had to be calibrated with the core data and then select the best curves that best fit the trend set by the core data. Modified Simandoux water saturation (SwModSim), Simandoux (SwSim) water saturation and Modified Indonesian water saturation (SwModind) curves were found to be the best fit curves when calibrated with the core data of well A-D1, A-J1, K-A2, A-K1 and A-H1.

The water saturation of these reservoir rocks has been determined from the calibration of core data with the wireline logs (log derived water saturation model). The determination of water saturation from log curves can be grouped into two models namely, clean sand (shale free) and shaly sand models. The reservoir rocks in this study are shaly-sand reservoir; therefore shaly-sand water saturation model has been used to determine the water saturation. The water saturation models used were simandoux, modified simandoux and Indonesia models. The models used the effective porosity as the input porosity in the water saturation model.

Simandoux (1963) proposed the following relationship:

$Sw = aRw / 2\Phi m - Vsh/Rsh + \sqrt{(Vsh/Rsh)^2 + 4/F * Rw * Rt}$ …….…….. (9)

Where:

Sw	=	Water Saturation
a	=	Equation Coefficient
Rw	=	Resistivity of water
Rsh	=	Resistivity of shale
Vsh	=	Volume of shale
F	=	Formation Resistivity factor
Rt	=	True formation resistivity from corrected deep resistivity log.
Φ	=	Effective Porosity, fraction
M	=	Cementation exponent

And the Indonesian formula was proposed in 1971 by Puopon and Leveaux. The relationship can be written as follows:

$1/\sqrt{Rt} = \sqrt{\Phi em}/ a*Rw + Vcl (1-Vcl/2/\sqrt{Rcl}) * Swn1/2$…….(10)

Where:

Rt = Resistivity curve from deep log reading

Rcl = Resistivity of wet clay

Φe = Effective porosity

Sw = Water saturation, fraction

Vcl = Volume of shale, fraction

Rw = Formation water resistivity

m = Cementation exponent

a = Tortuosity factor

n = Saturation exponent

3.3.4.3. Permeability determination from well logs

Permeability is the ease with which fluids flow (oil, gas or oil) through a medium in response to a fluid pressure gradient. It is the most essential rock property when calculating the flow capacity of the fluids in the reservoir. It is not measured directly, but calculated from other physical measurements with various theoretical and empirical relationships. Different methods are used to predict permeability to understand reservoir quality. Bloch (1991) described two approaches fundamentally used in predicting reservoir quality in sub-surface sandstones which are empirical techniques and 'process-oriented' techniques. An empirical techniques use a calibration data set and multiple regression analysis to determine the relationship between rock property variables and reservoir quality. This approach is frequently used where relationships between measured porosity and permeability were investigated. Similarly to the current study this approach was adopted. The empirical models were based on the correlation between porosity, permeability and irreducible water saturation under through models, namely: Tixier, Timur, Coates and Dumanoir, and Coates (Mohaghegh et at., 1997). Three of these models (Tixier, Timur and Coates) assume values of cementation (m) and saturation exponent (n) and can be applied to clean sand formation where residual water saturation exists. These methods use core and log data to calculate common exponent w for both n and m. However, they may not work if the reservoir is heterogeneous (Mohaghegh et, at. 1997). The second method is called multiple variable regressions; this is the method that was used to predict permeability in this study. However, permeability (predicted K) was estimated from the regression equation obtained from the porosity versus permeability cross plots (Figures 3.4). Regression equation on figure 3.3 was used to predict the permeability of the respective wells.

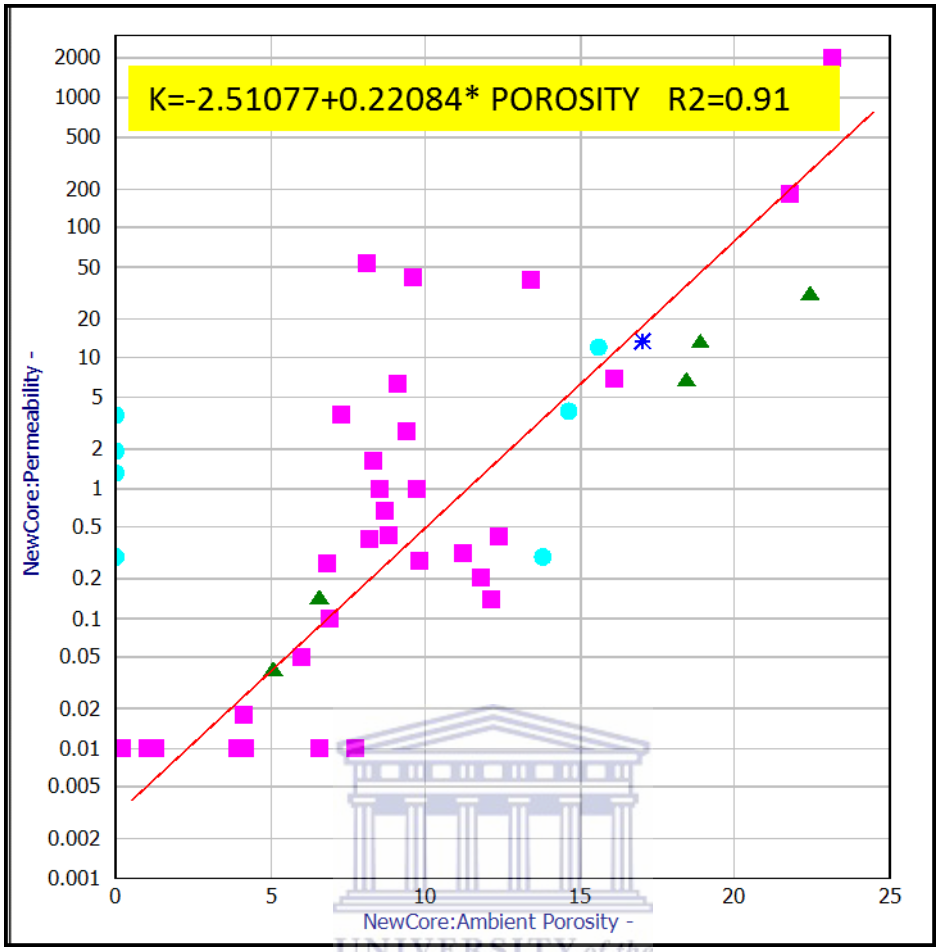

Figure 3.4: Core porosity versus permeability cross plot for multi-wells under study

CHAPTER FOUR: CORE DESCRIPTION AND PETROGRAPHIC ANALYSIS

4. Core description and petrographic analyses: interpretation and results

4.1. Introduction

This chapter presents the core description and petrographic analyses of five wells: A-J1, A-D1, A-H1, A-K1 and K-A2. The investigation of rock properties that contributes to the quality of the reservoir concentrates only on the cored intervals. General core descriptions were obtained from well completion reports provided by PASA. Petrographic analyses were performed on selected interval from each cored sample to determine mineralogy, texture, porosity and permeability of the reservoir at Corelabs in United Kingdom. Cored zones of these well are presented in table 4.1.

Table 4.1: well cored reservoir interval

ERA	SEQUENCE	AGE	A-J1	A-D 1	A-K1	K-A2	A-H1
Lower Cretaceous	Drifting	Albian			14Jt1	14Jt1	14Jt1
			14Ht1		14Ht1	14Ht1	14Ht1
			14At1	14At1			
		Aptian		13At1		13At1	
	Transitional	Barremian	6At1				
	Syn-rifting	Hauterevian	T				

4.2. Cored intervals

All cored intervals are divided into lithofacies as described below:

4.2.1. Well A-J1 cored interval (Appendix 1)

Two sets of cores were sampled on A-J1. The first set (Core #1) was cut for stratigraphic purposes and the second set (Core #2 - #6) were cut in order to evaluate reservoir sandstones and associated hydrocarbon shows.

Core #1, in Figure 1 – 3 were cut from 1617 - 1635m with a full 18m of core being recovered. The core consists of interbedded sandstones and claystone deposited in a marginal marine environment. The sandstones in the interval are clean, poorly sorted,

coarse grained, and commonly pebbly. They are very lithic, (with metamorphic, granitic and volcanic clasts), very feldspathic, and micaceous. This sandstone interval is divided into three lithofacies due to clay interbeds namely; lithofacies A (clayey sandstone), lithofacies B (wackestone) and Lithofacies C (clean sandstone) (Table 4.3).

Cores #2 to #6, in Figure 4 – 10 were cut back-to-back from 3191 to 3259.30m to evaluate good hydrocarbon shows. The core consists of thin oil-bearing lacustrine sandstones, conglomerates and breccias, intercalated with oil shales. Grain size and sorting are widely variable ranging from fine grained and well sorted, to conglomeratic and very poorly sorted. The core consists of non-marine fluvio-deltaic and lacustrine turbidite sediments. This interval is divided into five lithofacies (Table 4.3) following interbedding layers. The lithofacies include lithofacies C (clean sandstone), lithofacies D (silty/ sandy marlstone), lithofacies E (pebbly sandstone), lithofacies F (dolomitic claystone), and lithofacies G (granular sandstone).

4.2.2. Well A-D1 cored interval (Appendix 1)

One core was cut from 2661.8 to 2666.4m in Figure 11 – 12 with 100% recovery in sequence 13At1. The core has two distinct lithofacies (Table 4.3); lithofacies C is a massive fine to medium grained marginal marine sandstone with 2m thickness. Lithofacies B is wackestone.

4.2.3. Well A-H1 cored interval (Appendix 1)

A single 18 metre core in Figure 13 – 16 were cut from 3022.4 to 3039m with 100% recovery. The core consists of sandstone interbedding with siltstones and claystones. It is clean and tight with the presence of lignitic lenses, limestone nodules and shell lineation that regressive shallowing upward sequence. This core is divided into four lithofacies (Table 4.3) namely; lithofacies C (clean sandstone), lithofacies H (sandy ironstone), lithofacies I (sandy siltstone), and lithofacies B (wackestone).

4.2.4. Well A-K1 cored interval (Appendix 1)

Two sets of conventional cores were cut in sandstones associated with hydrocarbon shows.

Core #1, in Figure 17 – 19 were cut from 3236-3249m, and consists of light grey

sandstone characterized by immature components such as lithoclasts, feldspar, muscovite flakes and humic material mainly in the form of sand-sized coal fragments. The sandstone is slightly calcitic. Sorting is good, the grain size ranging from fine to medium, with an upward fining trend. The grains are subrounded to rounded. Bedding varies from low angled cross-bedding to horizontal and is seemingly absent in places. The cross-bedding displays varying dip directions suggesting trough cross-bedding. Bedding is underlined by laminae, mostly by subtle grain size variations and only rarely by carbon fragments and silty drapes. This core consists of three lithofacies (Table 4.3) namely; lithofacies C (clean sandstone), lithofacies I (sandy siltstone) and lithofacies B (wackestone).

Core #2, in Figure 20 were cut from 3283-3296m and is predominantly of sandstone intebedding with claystone rip-up clasts floating in the sandstone occur within two intervals. The first interval (3283.51-3283.58m) occurs immediately above an erosional contact. The second interval (3285.78-3286m) occurs 1,66m above the erosional base of the sandstone. The clasts are angular and delicate, mostly flat or slightly curved and the largest clast is 7cm long. The core is divided into two lithofacies (Table 4.3) namely; lithofacies C (clean sandstone), and lithofacies I (sandy siltstone).

4.2.5. Well K-A2 cored interval (Appendix 1)

Two sets of cores were cut using 9m core barrel. These cores were sampled for facies analysis and to investigate porosity and permeability.

Core #1, in Figure 21 – 22 were cut from 3982.1 to 3991.85m (99% recovery) and consist of tight to slightly porous silty sandstones lithofacies with interlaminated siltstone and shales. The core consists of one lithofacies, lithofacies I (sandy siltstone) (Table 4.3).

Core #2, in Figure 22 – 23 were cut from 4076,1 to 4083,1m (79% recovery). The core consists of tight sandstone lithofacies interbedded with siltstone and shale. This core also consists of one lithofacies, lithofacies I (sandy siltstone) (Table 4.3).

4.3. Petrographic analyses

A total of eighty three (83) sandstone samples were collected for petrographic analyses at different intervals of the cored sections in each well as demonstrated in

section 4.2. Of these eighty three (83) samples, seventy six (76) samples were subjected to thin section examination whilst seven were examined through scanning electron microscope. The use of these petrographic techniques in these terrigenous clastic materials was used to investigate the nature of the individual grains, their relationship and materials that settled between them to understand reservoir quality. It is known that diagenesis affects initial porosity and permeability of the rock with increasing depth (Sombra and Chang, 1997). Diagenetic processes are controlled by different parameters, such as framework composition, early and late cementation, clay coatings, dissolution, pore fluid composition, pressure (Nagtegaal, 1980), geothermal gradient (Galloway, 1974), time temperature exposure (Schmoker and Gautier, 1988), and duration of burial (Scherer, 1987; Bruhn et al., 1988).

Detailed modal (point-count) analyses were performed on seventy six (76) samples to obtain quantitative estimates of detrital and authigenic mineralogies and visible porosity. The samples were stained for calcite, dolomite (Alizarin-Red S Solution and Potassium Ferricyanide) and feldspars; and also impregnated with blue-dyed epoxy resin to highlight porosity. Identification of sandstone constituents includes a detailed description of depositional texture including sorting, grain-size, compaction, lamination together with mineralogy of detrital minerals and cements, fractures and visible pore types. Point count porosity results were compared with ambient helium porosity obtained from well completion reports. After comparing porosities values, these values and single phase gas permeability results from well completion reports were tabled in Table 4.3 and qualitative evaluated based on Rider (1986) (Table 4.2). Depth of which porosity and permeability are negligible they are presented as dash (-) in Table 4.3. Porosity and permeability values in Table 4.3 were plotted in a logarithmic scale to determine their controlling factor following Glover (2009) (Figure 4.1). The descriptions are illustrated by means of colour photomicrographs, column chart, pie chart, scatter plots and ternary diagrams. The remainder seven (7) samples were also examined with a scanning electron microscope (SEM) to aid in the identification of authigenic components, particularly clay minerals, and to better visualize pore geometries. SEM descriptions include a summary of depositional textures, fracture types, pore types and the composition and morphology of pore-occluding minerals. Mineral identification is supplemented by EDX (energy dispersive X-ray) analysis. Descriptions are illustrated by photomicrographs.

Table 4.2: Porosity and permeability values for reservoirs qualitative description (adapted from Rider, 1986).

Qualitative Evaluation of Porosity	
Percentage Porosity (%)	***Qualitative Description***
0 - 5	Negligible
5 - 10	Poor
15 - 20	Good
20 – 30	Very good
> 30	Excellent
Qualitative Evaluation of Permeability	
Average K_Value (md)	***Qualitative Description***
< 10.5	Poor to fair
15 – 50	Moderate
50 – 250	Good
250 – 1000	Very good
> 1000	Excellent

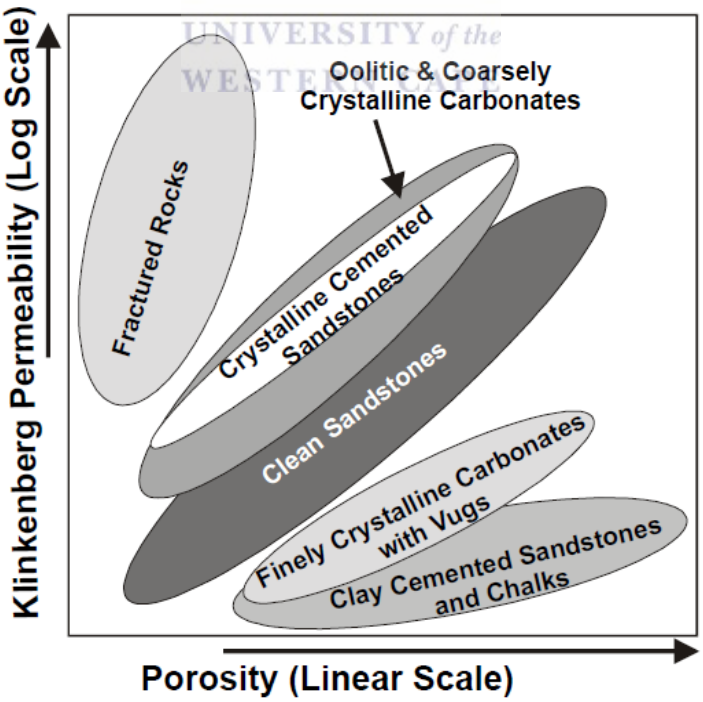

Figure 4.1: Porosity – permeability relationship (after Glover 2009)

Table 4.3: Wells sampled depth for petrographic analyses

Well ID	Lithology	Lithofacies	Code	Sampled Depth (M)	Point count porosity	Ambient helium Porosity (%)	Single phase gas Permeability (mD)	Ternary composition
A-J1 Core1	Clayey Sandstone	Lithofacies A	1	1617.27	0	11.2	0.32	Feldspathic arenite/wacke
	Wacke	Lithofacies B	2	1619.42	0	1.3	0.01	Feldspathic wacke
	Sandstone	Lithofacies C	3	1619.84	5	8.8	0.44	Feldspathic arenite
	Sandstone	Lithofacies C	3	1621.81	0	0	0	Feldspathic arenite
	Sandstone	Lithofacies C	3	1623.04	0	21.3	1289	Sub-feldspathic arenite
	Sandstone	Lithofacies C	3	1625.68	0	23.1	2039	Sub-feldspathic arenite
	Clayey Sandstone	Lithofacies A	1	1627.87	0	0	0	Feldspathic arenite/wacke
	Sandstone	Lithofacies C	3	1629.02	14.3	12.4	0.42	Feldspathic arenite
	Clayey Sandstone	Lithofacies A	1	1630.54	0	11.8	0.21	Feldspathic arenite/wacke
	Sandstone	Lithofacies C	3	1632.72	0	8.7	0.67	Feldspathic arenite
	Sandstone	Lithofacies C	3	1633.1	0	21.8	183	Sub-feldspathic arenite
	Sandstone	Lithofacies C	3	1634.46	0	16.1	6.9	Sub-feldspathic arenite
A-J1 Core 2 - 6	Sandstone	Lithofacies C	3	3191.23	0	0.2	0.01	Sub-feldspathic arenite
	Silty/sandy marlstone	Lithofacies D	4	3191.61	0	0	0	Dolo-marlstone
	Sandstone	Lithofacies C	3	3192.59	0	0	0	Feldspathic arenite
	Pebbly Sandstone	Lithofacies E	5	3193.5	0	8.3	1.6	Feldspathic arenite
	Sandstone	Lithofacies C	3	3195.35	0	0	0	Feldspathic arenite
	Sandstone	Lithofacies C	3	3195.35	0	0	0	Feldspathic arenite
	Sandstone	Lithofacies C	3	3198.67	0	6.6	0.01	Feldspathic arenite
	Pebbly Sandstone	Lithofacies E	5	3199.81	0	9.4	2.7	Feldspathic arenite
	Dolomitic claystone	Lithofacies F	6	3200.9	0	0	0	Silty/sandy dolomitic claystone
	Sandstone	Lithofacies C	3	3201.6	7	9.6	41	Feldspathic arenite

	Sandstone	Lithofacies C	3	3205.42	0	12.1	0.141	Feldspathic arenite
	Sandstone	Lithofacies C	3	3210.2	5.7	9.1	6.3	Feldspathic arenite
	Pebbly Sandstone	Lithofacies E	5	3213.47	0	6	0.05	Feldspathic arenite
	Sandstone	Lithofacies C	3	3213.88	0	9.7	0.98	Feldspathic arenite
	Pebbly Sandstone	Lithofacies E	5	3215.37	0	0	0	Feldspathic arenite
	Granular Sandstone	Lithofacies G	6	3217.96	0	4.1	0.018	Feldspathic arenite
	Sandstone	Lithofacies C	3	3219.62	0	7.7	0.01	Feldspathic arenite
	Sandstone	Lithofacies C	3	3220.72	0	3.9	0.01	Calcite/ dolomite cemented Feldspathic arenite
	Sandstone	Lithofacies C	3	3222.15	0	8.2	0.4	Feldspathic arenite
	Granular Sandstone	Lithofacies G	6	3222.88	0	6.8	0.27	Feldspathic arenite
	Sandstone	Lithofacies C	3	3232.25	14	13.4	40	Feldspathic arenite
	Pebbly Sandstone	Lithofacies E	5	3235.42	0	11.3	0.29	Feldspathic arenite
	Pebbly Sandstone	Lithofacies E	5	3238.54	0	8.5	1	Feldspathic arenite
	Sandstone	Lithofacies C	3	3235.42	0	1	0.01	Feldspathic arenite
	Sandstone	Lithofacies C	3	3245.03	0	7.3	3.6	Feldspathic arenite
	Sandstone	Lithofacies C	3	3248.95	0	0	0	Feldspathic arenite
	Sandstone	Lithofacies C	3	3251.1	0	4.2	0.01	Feldspathic arenite
	Sandstone	Lithofacies C	3	3252.73	7	6.9	0.1	Feldspathic arenite
	Pebbly Sandstone	Lithofacies E	5	3254.19	0	0	0	Feldspathic arenite
	Sandstone	Lithofacies C	3	3255.42	0	9.8	0.28	Feldspathic arenite
	Sandstone	Lithofacies C	3	3256	6	8.1	54	Feldspathic arenite
A-D1	Sandstone	Lithofacies C	3	2662.49	0	0	0	Feldspathic arenite
	Sandstone	Lithofacies C	3	2663.39	11.7	17	13.5	Feldspathic arenite
	Wacke	Lithofacies B	2	2665.88	0	0	0	Feldspathic wacke
A-H1	sandstone	Lithofacies C	3	3022.6	0	14.6	3.9	Subfeldspathic-sublithic arenite

	sandstone	Lithofacies C	3	3023.75	9	0	3.6	Subfeldspathic-sublithic arenite
	Ironstone	Lithofacies H	7	3024.2	10	0	3.6	Sideritic Wackestone
	Wackes	Lithofacies B	2	3026.4	0	15.6	12	Quartz-feldspathic wacke
	Sandy siltstone	Lithofacies I	8	3029.32	0	0	0	Feldspathic sandy siltstone
	sandstone	Lithofacies C	3	3030.77	0	0	0.3	Subfeldspathic sublithic arenite
	sandstone	Lithofacies C	3	3032.64	0	0	1.3	Subfeldspathic sublithic arenite
	sandstone	Lithofacies C	3	3033.26	0	0	0	Subfeldspathic sublithic arenite
	sandstone	Lithofacies C	3	3033.26	0	0	0	Subfeldspathic sublithic arenite
	sandstone	Lithofacies C	3	3035.5	0	13.8	0.3	Subfeldspathic sublithic arenite
	sandstone	Lithofacies C	3	3035.62	0	0	1.9	Subfeldspathic sublithic arenite
	Sideritic wacke	Lithofacies B	2	3037.8	0	0	0	Lithic wacke
	Sandy ironstone	Lithofacies H	7	3038	0	0	0	Sandy sideritic wackestone
	Sandy ironstone	Lithofacies H	7	3038.7	0	0	0	Sandy sideritic wackestone
A-K1 Core 1	sandstone	Lithofacies C	3	3236.46	10.9	0	0	Sublithic arenite
	sandstone	Lithofacies C	3	3238.57	0	6.6	0.14	Sublithic arenite
	Sandy siltstone	Lithofacies I	8	3239.2	0	5.1	0.04	Argillaceous/ Organic matter-rich siltstone
	Wackes	Lithofacies B	2	3241.2	0	0	0	Feldspathic/ lithic wacke
	sandstone	Lithofacies C	3	3243.58	0	0	0	Sublithic arenite
A-K1 Core 2	sandstone	Lithofacies C	3	3284.41	15	22.4	30	Sublithic arenite
	sandstone	Lithofacies C	3	3285.9	0	18.4	6.6	Sublithic arenite
	sandstone	Lithofacies C	3	3285.9	0	18.4	6.6	Sublithic arenite
	Sandy siltstone	Lithofacies I	8	3287.33	0	18.9	13	feldspathic
K-A2 Core 1	Silty sandstone	Lithofacies J	9	3982.77	0	0	0	Sub-feldspathic arenite
	Sandy siltstone	Lithofacies I	8	3982.77	0	0	0	Sandy feldspathic siltstone
	Sandy siltstone	Lithofacies I	8	3984.64	0	0	0	Dolomitic & bioclastic sandysiltsone
	Sandy siltstone	Lithofacies I	8	3986.72	0	0	0	Argillaceous feldspathic

								siltstone
	Silty sandstone	Lithofacies I	8	3987.63	0	0	0	Sub-feldspathic arenite
	Sandy siltstone	Lithofacies I	8	3989.7	0	0	0	Dolomitic & bioclastic sandysiltsone
	Sandy siltstone	Lithofacies I	8	3991.4	0	0	0	Dolomitic & bioclastic sandysiltsone
K-A2 Core 2	Silty sandstone	Lithofacies I	8	4076.6	0	0	0	Sub-feldspathic arenite
	Silty sandstone	Lithofacies I	8	4078.4	0	0	0	Sub-feldspathic arenite
	Silty sandstone	Lithofacies I	8	4078.4	0	0	0	Sub-feldspathic arenite
	Silty sandstone	Lithofacies I	8	4079.42	0	0	0	Sub-feldspathic arenite

4.3.1. Well A-J1 cored intervals

4.3.1.1. Core #1: Thin Section Petrography

On this core, twelve thin section samples were collected at different depth (Table 4.3). Representative samples at 1619.84m at the top and 1629.02m at the bottom were selected for detailed discussion on this core. Interpretation and analyses of other samples are presented in Appendix II, A-J1 well – Petrographic Analyses.

At 1619.84m depth, thin section petrographic analysis (Figure 4.2), reveals the majority of 74% detrital components (Figure 4.3D) of total rock constituents dominated by quartz and feldspars with minor contribution of plagioclase, lithic grains (sedimentary and igneous) mica, detrital chlorite, organic material, accessory grains (mainly zircon), and sparsely distributed detrital clay matrix (Figure 4.3A). Dominated grains are fine grained, moderately sorted, point to point to long grain contact, angular to rounded grain shape (Figure 4.2B & C) with moderate compaction that reduced the initial porosity and permeability of the rock. Occurrence of authigenic minerals contributed 21% of total rock constituents (Figure 4.3B & D) dominated by siderite filling pore throats between quartz and feldspar grains (Figures 4.3D). Pore filling continued with minor occurrence of kaolinite, chlorite and grain replacive illite minerals (Figure 4.3B). Quartz and feldspar overgrowths are

also dominant with effective pore restriction. These diagenetic mineral occurrence has reduced integranular pore space to 1.7% (Figure 4.3C), lately expanded by 3.3% of secondary porosity that occurred from mineral dissolution (Figure 4.3C) resulting to the total rock point count porosity of 5% (Figure 4.3D). Laboratory test of ambient helium porosity and single phase gas permeability recorded in the well completion report revealed 8.8% porosity with 0.44md permeability. Sandstone reservoir quality at this depth is very poor due to strongly downgraded pore throats by siderite and clays.

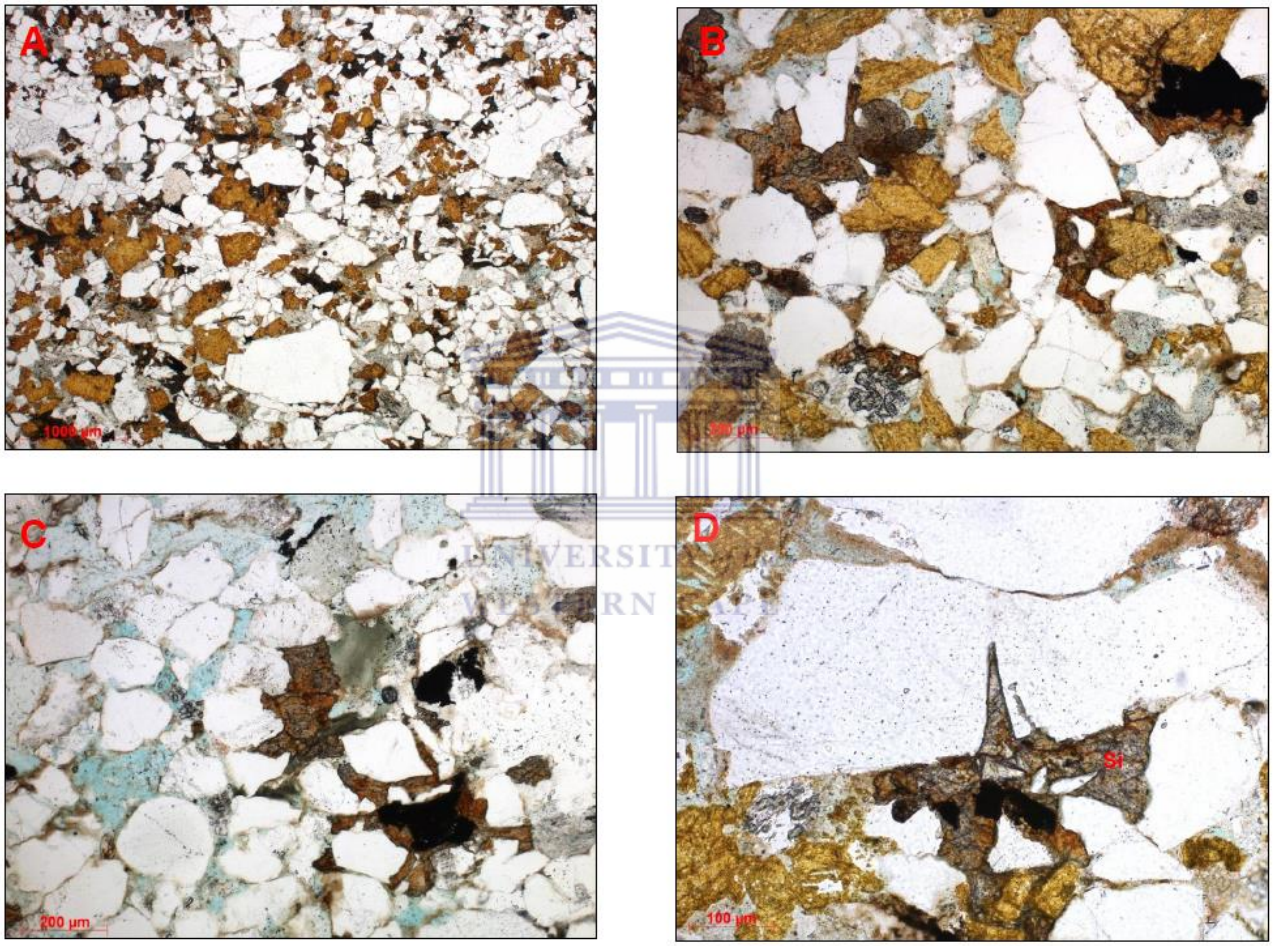

Figure 4.2: Thin-Section micrographs of AJ-1 sandstone at 1619.84m showing: (A) generalized composition of the rock sample; (B) common pore restricting quartz overgrowth with clear clay-induced dissolution contact; (C) sparsely distributed feldspar overgrowths); (D) common pore filling to grain replacive siderite. φ = 8.8%, k = 0.44 md. Sandstone reservoir quality is poor.

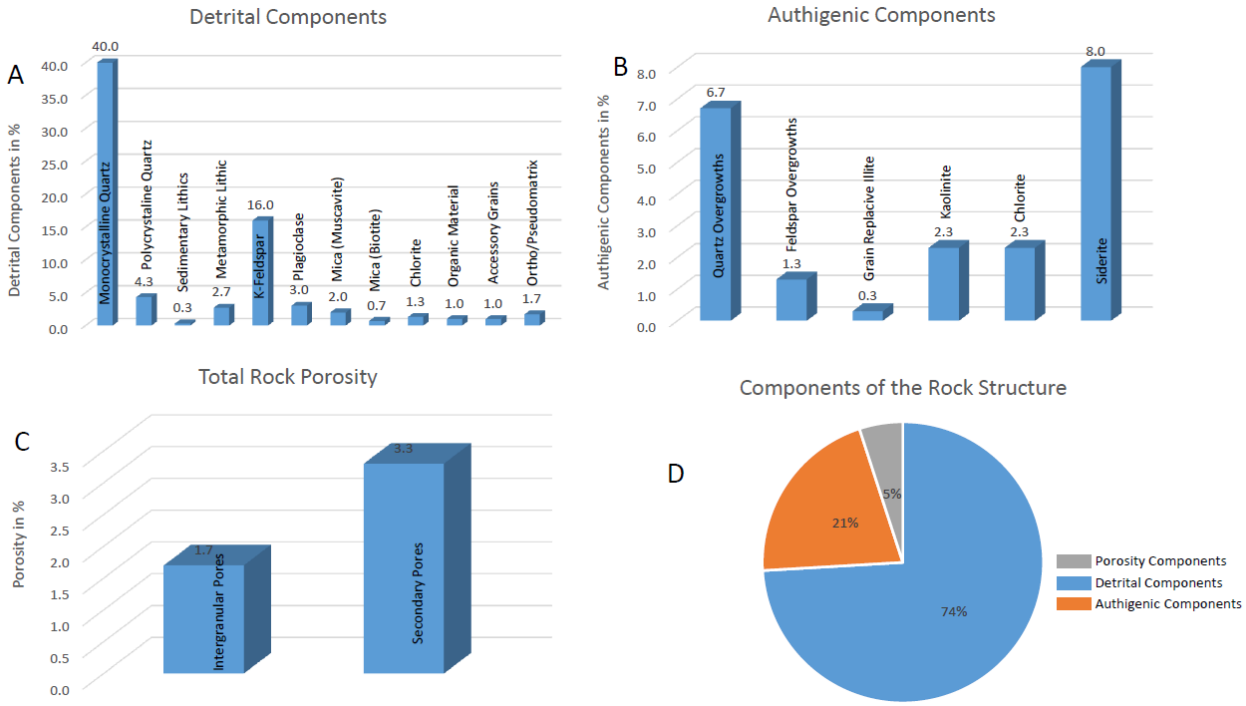

Figure 4.3: AJ-1 sandstone at 1619.84m, total rock constituents composed of (A) detrital components, (B) authigenic components, (C) rock porosity and (D) aggregate of total rock structure.

At 1629.02m depth, thin section petrographic analysis (Figure 4.4), reveals the majority of 74% detrital components (Figure 4.5D) of total rock constituents dominated by quartz and feldspars with minor contribution of plagioclase, mica, organic material, lithic grains (sedimentary and igneous), accessory grains (mainly zircon), and sparsely distributed detrital clay matrix (Figure 4.5A). Dominated grains are fine grained, moderately to well sorted, point to point to long grain contact, angular to rounded grain shape with moderate compaction. Occurrence of authigenic minerals is less contributed with 12% of total rock constituents (Figure 4.5B&D). Sparsely pore restriction by quartz and feldspar overgrowths is noted with less effect to pore throats (Figure 4.4B,C&D). Scattered pore filling by minor occurrence of kaolinite, chlorite, grain replacive illite, dolomite, calcite and pyrite minerals is also noted (Figure 4.4D & 4.5B). Porosity at this depth is moderately good having intergranular pore space of 3% and secondary porosity of 11.3% linked to the dissolution of feldspar grains (Figure 4.5C&D). Laboratory test of ambient helium porosity and single phase gas permeability recorded in the well completion report revealed 12.4% porosity with 0.42md permeability. Sandstone reservoir quality at this depth is very poor.

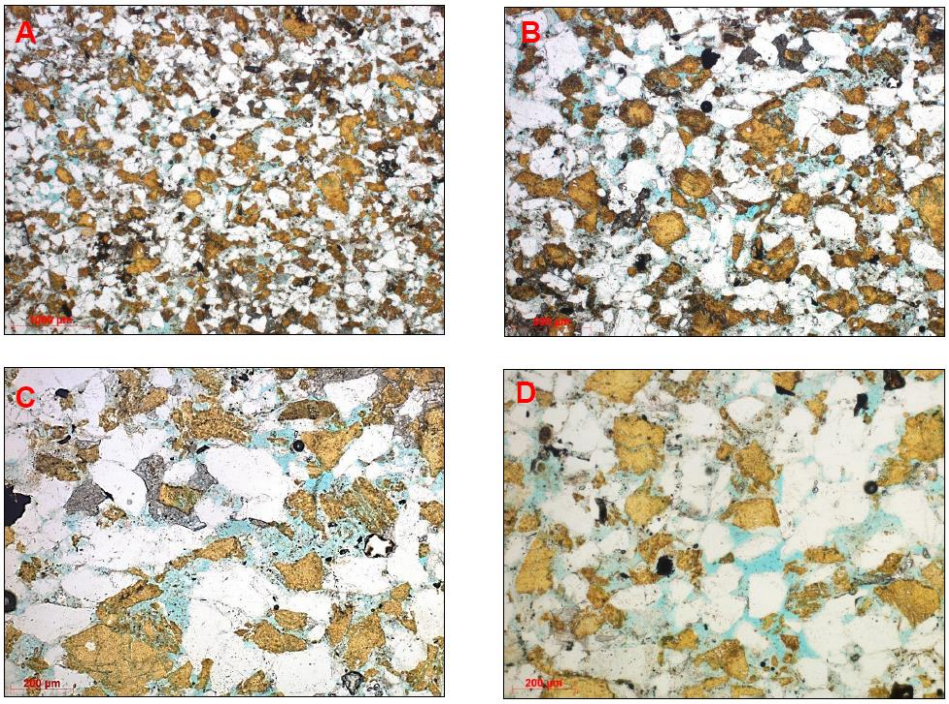

Figure 4.4: Thin-Section micrographs of AJ-1 sandstone at 1629.02m showing: (A) generalized composition of the rock sample; (B) common pore restricting quartz overgrowth with clear clay-induced dissolution contact; (C) sparsely distributed quartz and feldspar overgrowths); (D) common pore filling to grain replacive siderite/ dolomite. φ = 12.4%, k = 0.42 md. Sandstone reservoir quality is poor

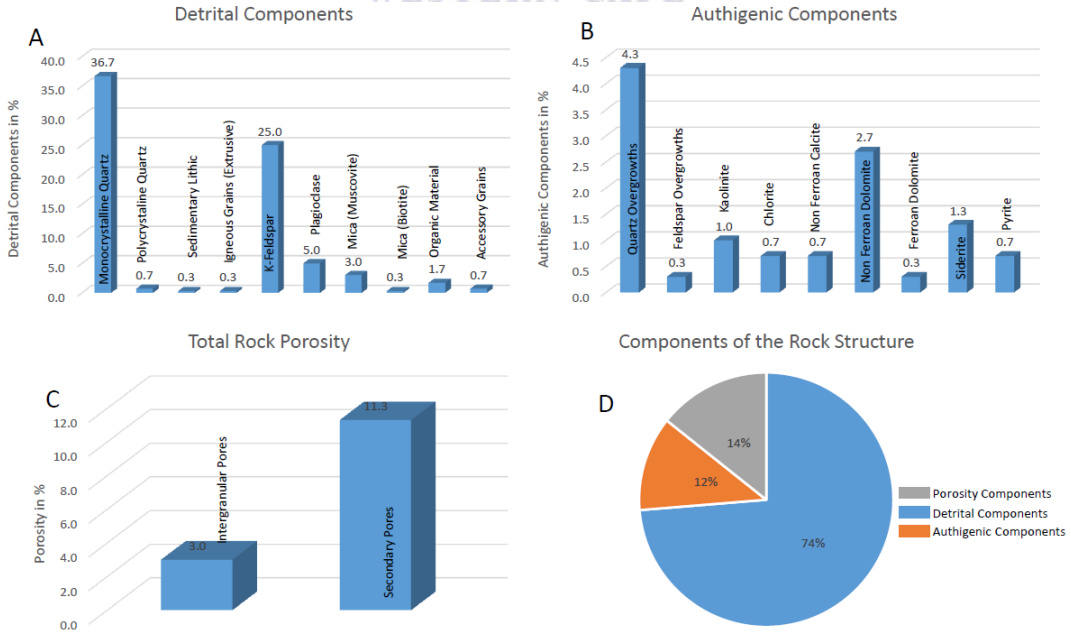

Figure 4.5: AJ-1 sandstone at 1629.02m, total rock constituents composed of (A) detrital components, (B) authigenic components, (C) rock porosity and (D) aggregate of rock structure, all in percentage.

4.3.1.2. Core #1: Scanning Electron Microscope

One SEM and XRD sample was collected at 1627.87m depth (Figure 4.6). Analysis of this sample presents a poorly sorted fine grained sandstone that appears massive at the scale of SEM (A). The sample is well compacted with long to weakly concavo-convex grain contacts observed. Detrital grains are dominated by K-feldspar with abundant quartz. K-feldspar grains vary in preservation from fresh in appearance to weakly or highly leached (D). Accessory grains include Ti-minerals (A, C) and 'exotics' (A inset, Ca+Ce+Nd+La mineral).

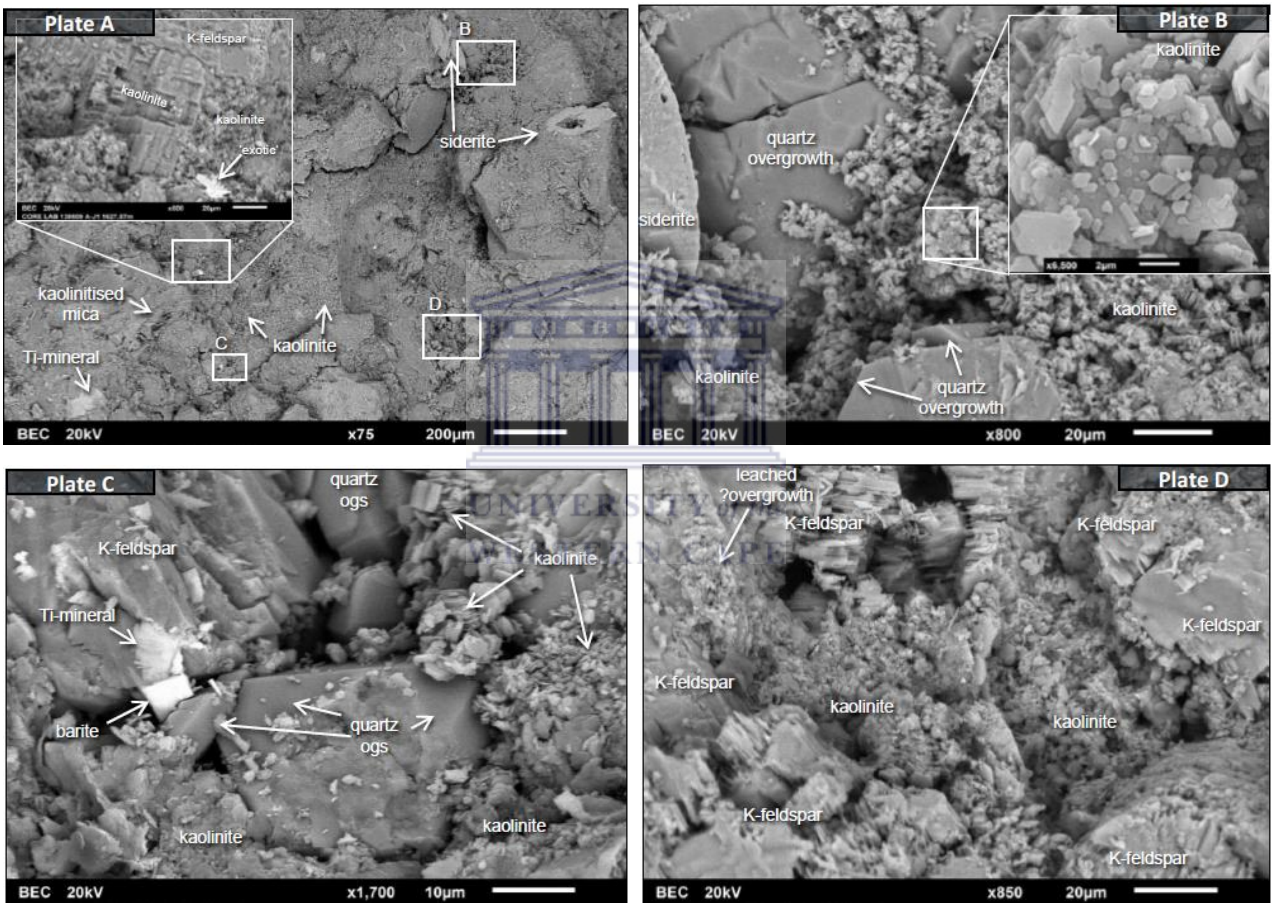

Figure 4.6: SEM micrographs of AJ-1 sandstone at 1627.87m showing authigenic minerals occurrences: Abundant kaolinite which is pore lining, pore filling and grain-replacive (A); strong reflective siderite filling pore (A, B); Assessory grains (Ti-minerals and barite) (A, C); quartz and feldspar overgrowths (B, D).

The sample is characterised by abundant kaolinite, which is pore-lining, pore-filling and commonly grain-replacive. The kaolinite is very variable in form, observed mainly as

very fine platy to blocky books and short verms, and in places is pseudomorphic after precursor grains (A, mica; and inset possibly after feldspar grain).

Quartz overgrowths are common, typically as thin developments (B, D). Possible overgrowths of K-feldspar are highly leached (D). Minor siderite (A, B) takes the form of fine lozenges, locally with leached cores visible (A). The siderite has a strong Mg component, with very low Ca and Mn detected by EDX analysis. A trace of barite was also observed (C).

Porosity appears moderate, and is dominated by microporosity associated with kaolinite and leached K-feldspar grains. Intergranular pores are typically small and lined with kaolinite or overgrowths. Pore throats are commonly constricted and pore connectivity appears to be commonly restricted to microporous networks. Permeability is poor.

4.3.1.3. Core #2 - #6: Thin Section Petrography

On these cores, thirty two petrographic samples were collected at different depth (Table 4.3), thirty for thin sections and two for scanning electron microscope (SEM). For presentation of these data only 3201.60m, 3210.20m, 3232.25m, 3252.73m and 3256m depth were selected. Interpretation and analyses of other samples are presented in Appendix II, A-J1 well – Petrographic Analyses.

At 3201.60m depth, thin section petrographic analysis (Figure 4.7), reveals the majority of 72% detrital components (Figure 4.8D) of total rock constituents dominated by quartz, feldspars and plagioclase with minor contribution of mica, lithic grains (sedimentary and igneous), organic material, accessory grains (mainly zircon), and sparsely distributed detrital clay matrix (Figure 4.8A). Quartz and feldspar grains are medium grained, moderately to well sorted, long to sutured grain contact, angular to rounded grain shape with moderate strong compaction. Occurrence of authigenic minerals contributed 21% of total rock constituents (Figure 4.8B&D) dominated by quartz and feldspar overgrowths with effective pore restriction (Figures 4.7). Scattered pore filling by minor occurrence of siderite, chlorite, calcite, pyrite, and kaolinite is also noted (Figure 4.7D & 4.8B). Mechanical compaction and diagenetic mineral occurrence has downgraded porosity effectively. Micro fractures are noted (Figure 4.7C) with 2.7%

porosity contribution (Figure 4.8C). Intergranular pore space contributes 4% with little secondary porosity of 0.3% that occurred from mineral dissolution resulting to the total rock point count porosity of 7% (Figure 4.8D). Laboratory test of ambient helium porosity and single phase gas permeability recorded in the well completion report revealed 9.6% porosity with 41md permeability. Sandstone reservoir quality at this depth is moderate.

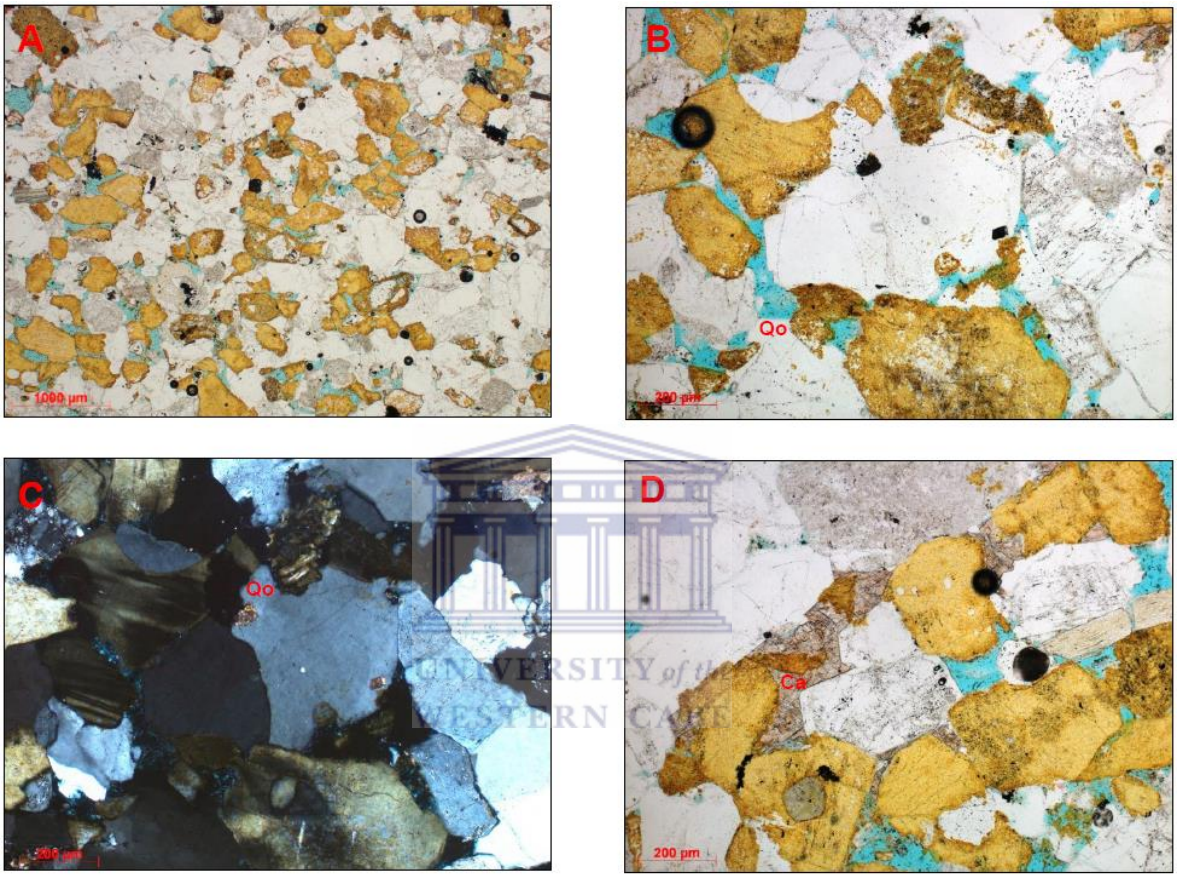

Figure 4.7: Thin-Section micrographs of AJ-1 sandstone at 3201.60m (A: 1000µm, B: 500µm, C: 200µm and D: 200µm), φ = 9.6%, k = 41 md.

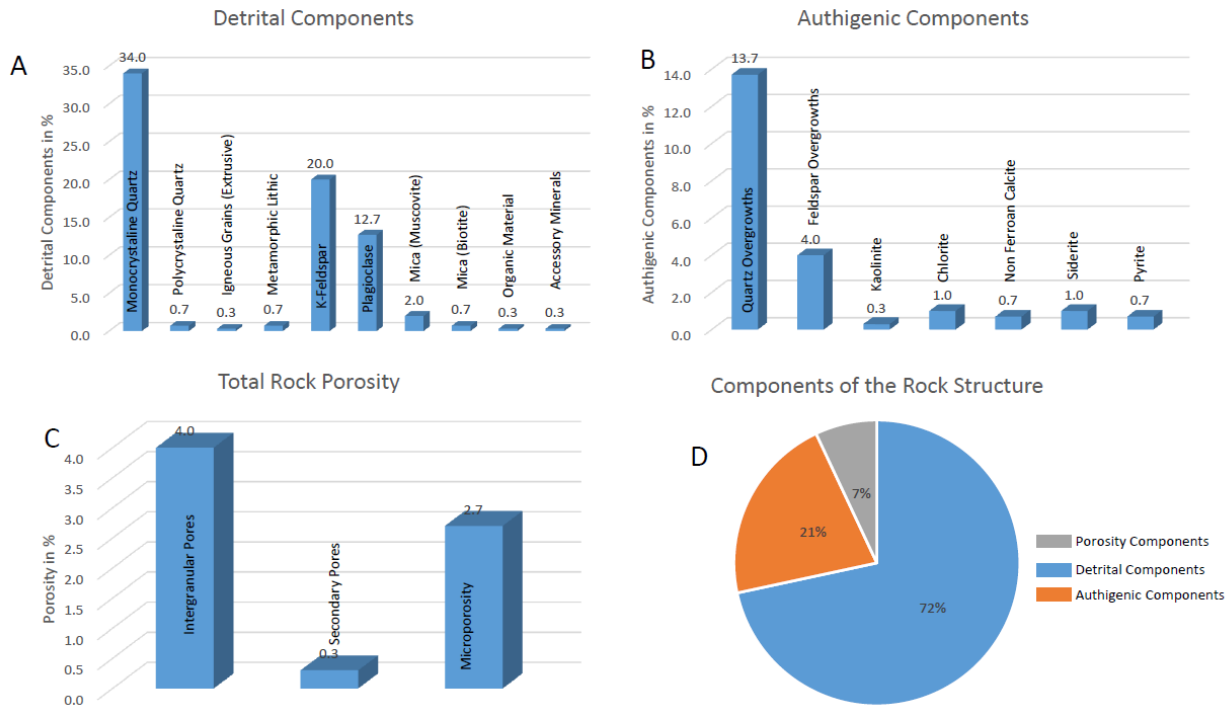

Figure 4.8: AJ-1 sandstone at 3201.60m, total rock constituents composed of (A) detrital components, (B) authigenic components, (C) rock porosity and (D) aggregate of rock structure.

At 3210.20m depth, thin section petrographic analysis (Figure 4.9), reveals the majority of 77% detrital components (Figure 4.10D) of total rock constituents dominated by quartz, feldspars and plagioclase with minor contribution of mica, organic material, lithic grains (sedimentary and igneous), chlorite, accessory grains (mainly zircon), and sparsely distributed detrital clay matrix (Figure 4.10A). Dominated grains are very fine grained, poorly sorting (Figure 4.9A), mainly long to convcavo-convex grain contact (Figure 4.9B& C), subangular to rounded grain shape with moderate strong compaction. Occurrence of authigenic minerals contributed 17% of total rock constituents (Figure 4.10B & D) with quartz and feldspar restricting pore throats (Figure 4.9B). Pore filling by chlorite, calcite, pyrite and siderite dominate at this depth (Figure 4.9B, C & D). Porosity at this depth is poor with intergranular pore space of 3.7% and secondary porosity of 2% linked to the dissolution of feldspar grains (Figure 4.9D). Laboratory test of ambient helium porosity and single phase gas permeability recorded in the well completion report revealed 9.1% porosity with low permeability of 6.3md. Sandstone reservoir quality at this depth is poor with some local moderation enhanced by feldspar dissolution.

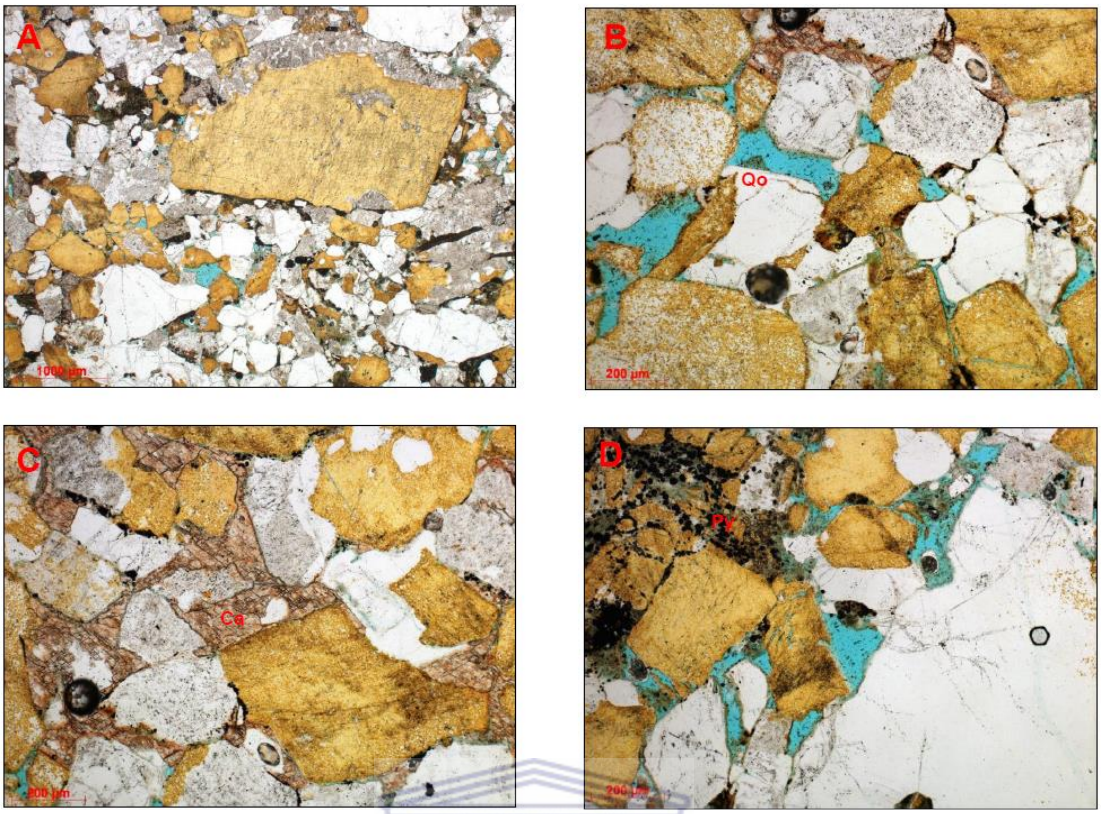

Figure 4.9: Thin-Section micrographs of AJ-1 sandstone at 3210.20m (A: 1000µm, B: 500µm, C: 200µm and D: 200µm), φ = 9.1%, k = 6.3 md.

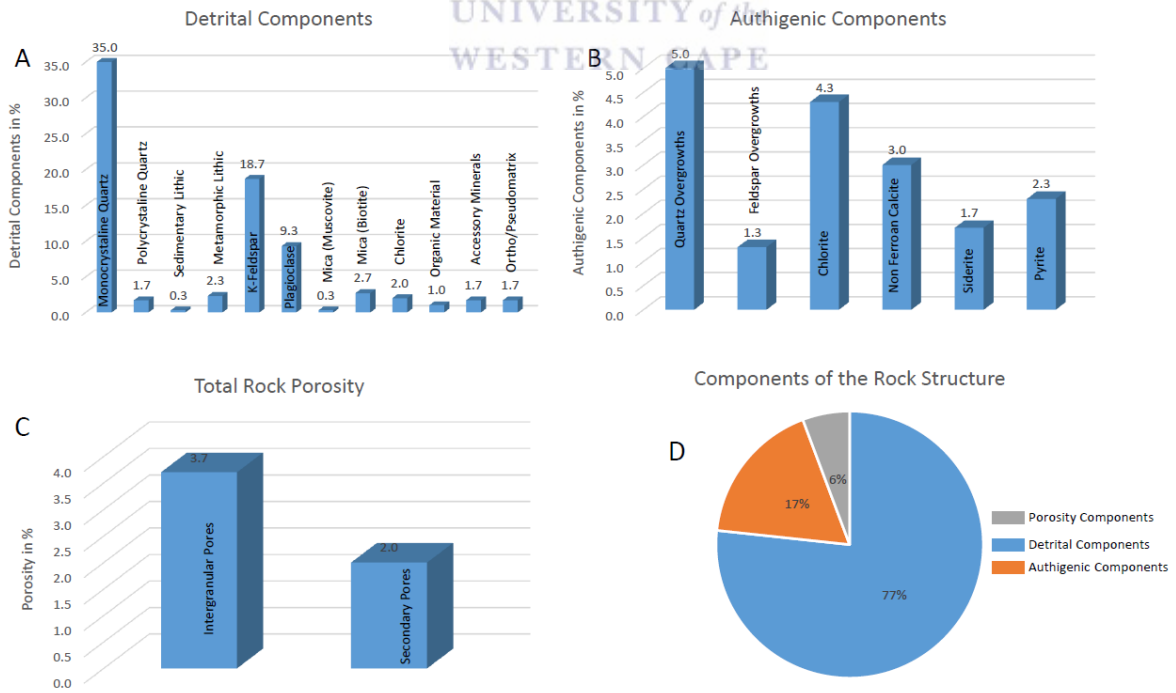

Figure 4.10: AJ-1 sandstone at 3210.20m, total rock constituents composed of (A) detrital components, (B) authigenic components, (C) rock porosity and (D) aggregate of rock structure.

At 3232.25m depth, thin section petrographic analysis (Figure 4.11), reveals the majority of 70% detrital components (Figure 4.12D) of total rock constituents dominated by quartz and feldspars with minor contribution of plagioclase, lithic grains (sedimentary and igneous), mica, chlorite, organic material, accessory grains (mainly zircon), and sparsely distributed detrital clay matrix (Figure 4.12A). Dominated grains are medium grained, moderately sorted, long grain contact, subangular to rounded grain shape with moderate compaction. Occurrence of authigenic minerals contributed 16% of total rock constituents (Figure 4.12B & D). Sparsely pore restriction by quartz and feldspar overgrowths is noted with less effect to pore throats (Figure 4.11B, C &D). Scattered pore filling by minor occurrence of chlorite, calcite, siderite and pyrite minerals is noted (Figure 4.11D & 4.12B). Porosity at this depth is moderately good having intergranular pore space of 10.7% and secondary porosity of 3.3% linked to the dissolution of feldspar grains (Figure 4.11C & D). Laboratory test of ambient helium porosity and single phase gas permeability recorded in the well completion report revealed 13.4% porosity with moderate permeability of 40md. Sandstone reservoir quality at this depth is moderate due to slightly intergranular porosity.

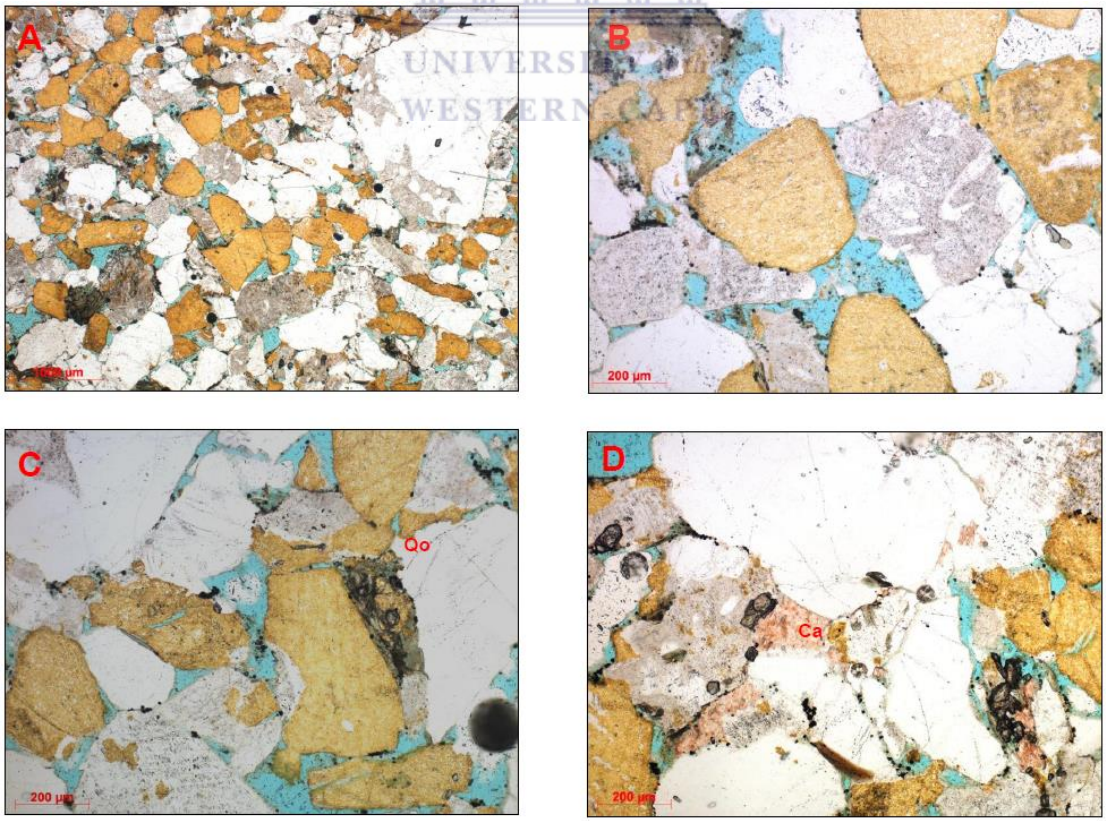

Figure 4.11: Thin-Section micrographs of AJ-1 sandstone at 3232.25m (A: 1000µm, B: 500µm, C: 200µm and D: 200µm), φ = 13.4%, k = 40 md.

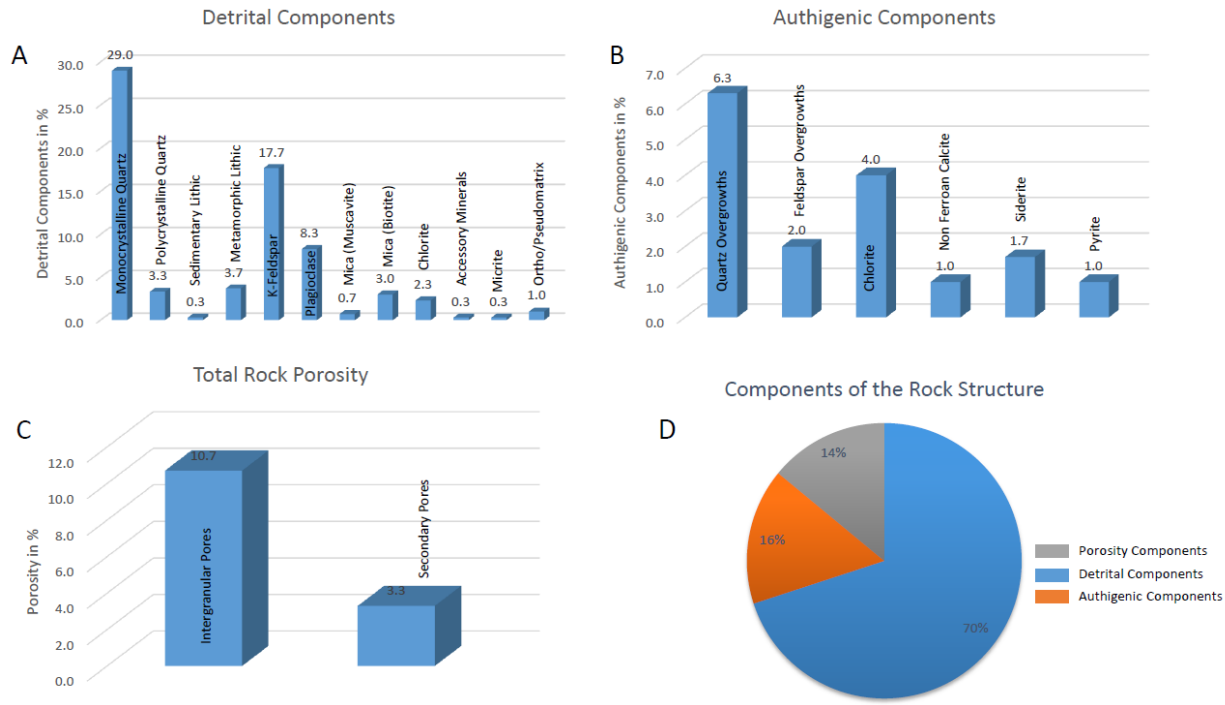

Figure 4.12: AJ-1 sandstone at 3232.25m, total rock constituents composed of (A) detrital components, (B) authigenic components, (C) rock porosity and (D) aggregate of rock structure.

At 3252.73m depth, thin section petrographic analysis (Figure 4.13), reveals the majority of 72% detrital components (Figure 4.14D) of total rock constituents dominated by quartz, feldspars and plagioclase with minor contribution of mica, accessory grains (mainly zircon), Chlorite, lithic grains (sedimentary and igneous) and sparsely distributed detrital clay matrix (Figure 4.14A). Dominated grains are medium grained, poorly sorted, long to concavo-convex grain contact, subangular to rounded grain shape with moderately strong compaction. Occurrence of authigenic minerals contributed 21% of total rock constituents (Figure 4.14B & D) dominated by chlorite (Figure 4.14B) filling pore throats between quartz, feldspar and plagioclase grains (Figure 5.17). Pore filling continued with minor occurrence of calcite, siderite, kaolinite and grain replacive illite minerals (Figure 4.14B). Relatively common pore restriction by quartz and feldspar overgrowths is also noted. These diagenetic mineral occurrence has reduced intergranular pore space to 4% (Figure 4.14C), lately expanded by 3% of secondary porosity that occurred from mineral dissolution resulting to the total rock point count porosity of 7% (Figure 4.14D). Laboratory test of ambient helium porosity and single phase gas permeability recorded in the well completion report revealed 6.9% porosity with poor permeability of 0.1md. Sandstone reservoir quality at this depth is very poor largely due to pore filling minerals.

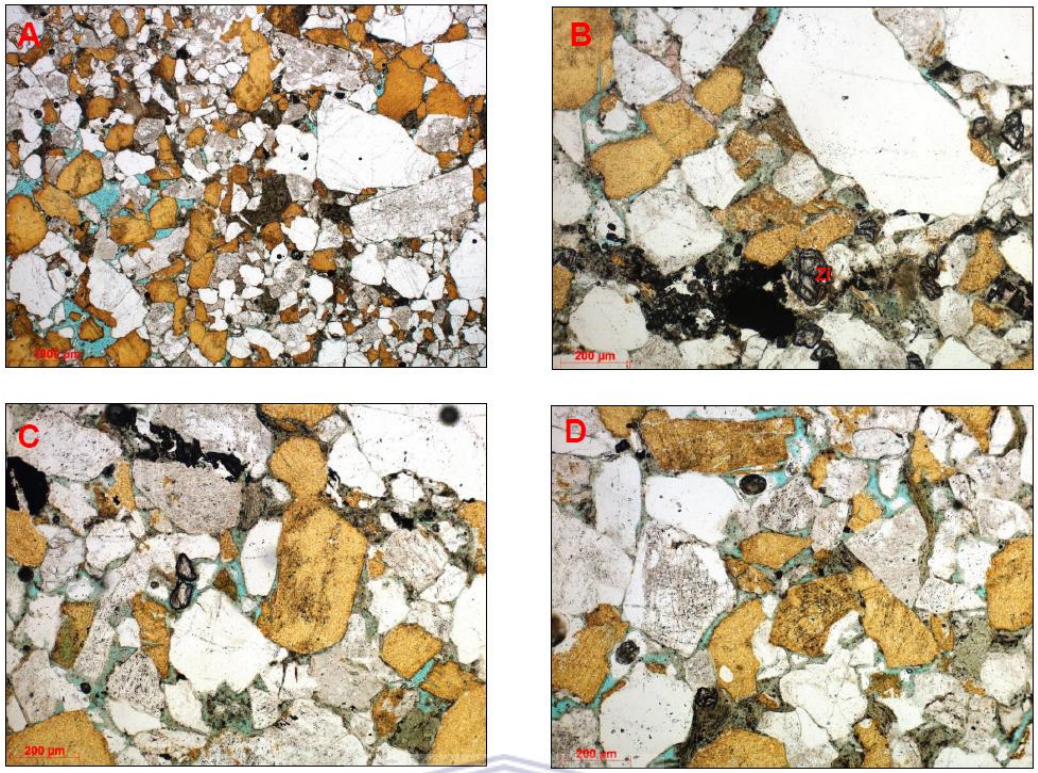

Figure 4.13: Thin-Section micrographs of AJ-1 sandstone at 3252.73m (A: 1000µm, B: 500µm, C: 200µm and D: 200µm), φ = 6.9%, k = 0.1 md.

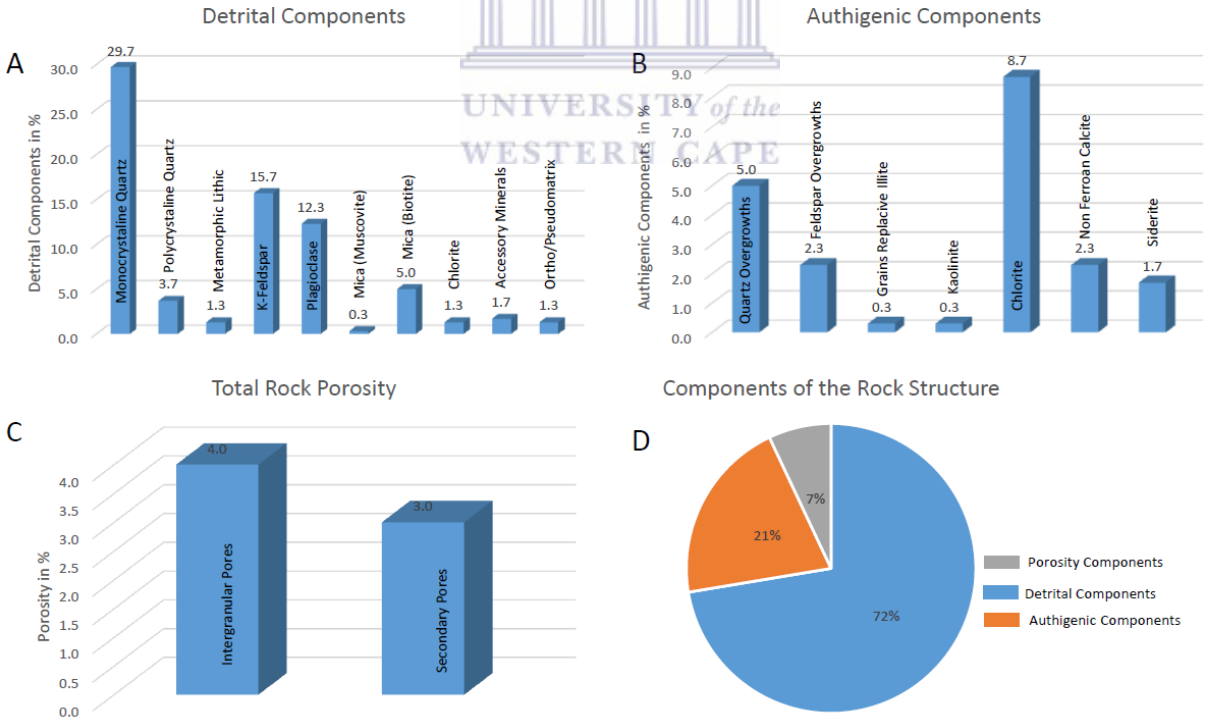

Figure 4.14: AJ-1 sandstone at 3252.73m, total rock constituents composed of (A) detrital components, (B) authigenic components, (C) rock porosity and (D) aggregate of rock structure.

At 3256.00m depth, thin section petrographic analysis (Figure 4.15), reveals the majority of 81% detrital components (Figure 4.16D) of total rock constituents dominated by quartz, feldspars and plagioclase with minor contribution of lithic grains (metamorphic), mica, chlorite, and sparsely distributed detrital clay matrix (Figure 4.16A). Dominated grains are course grained, moderate sorted, long to concavo-convex grain contact, subangular to well-rounded grain shape with moderately strong compaction. Occurrence of authigenic minerals is less contributed with 13% of total rock constituents (Figure 4.16B & D). Common pore restriction by quartz overgrowths and sparse feldspar overgrowth is noted (4.15B, C &D). Pores are also filled by occurrence of scattered chlorite, calcite, dolomite, siderite and pyrite (Figure 4.15 & 4.16B). Intergranular pore space contributed 4.7% and secondary porosity of 1.3 % with the total porosity of 6% (Figure 4.16D). Laboratory test of ambient helium porosity and single phase gas permeability recorded in the well completion report revealed 8.1% porosity with good permeability of 54md. Sandstone reservoir quality at this depth is moderately good.

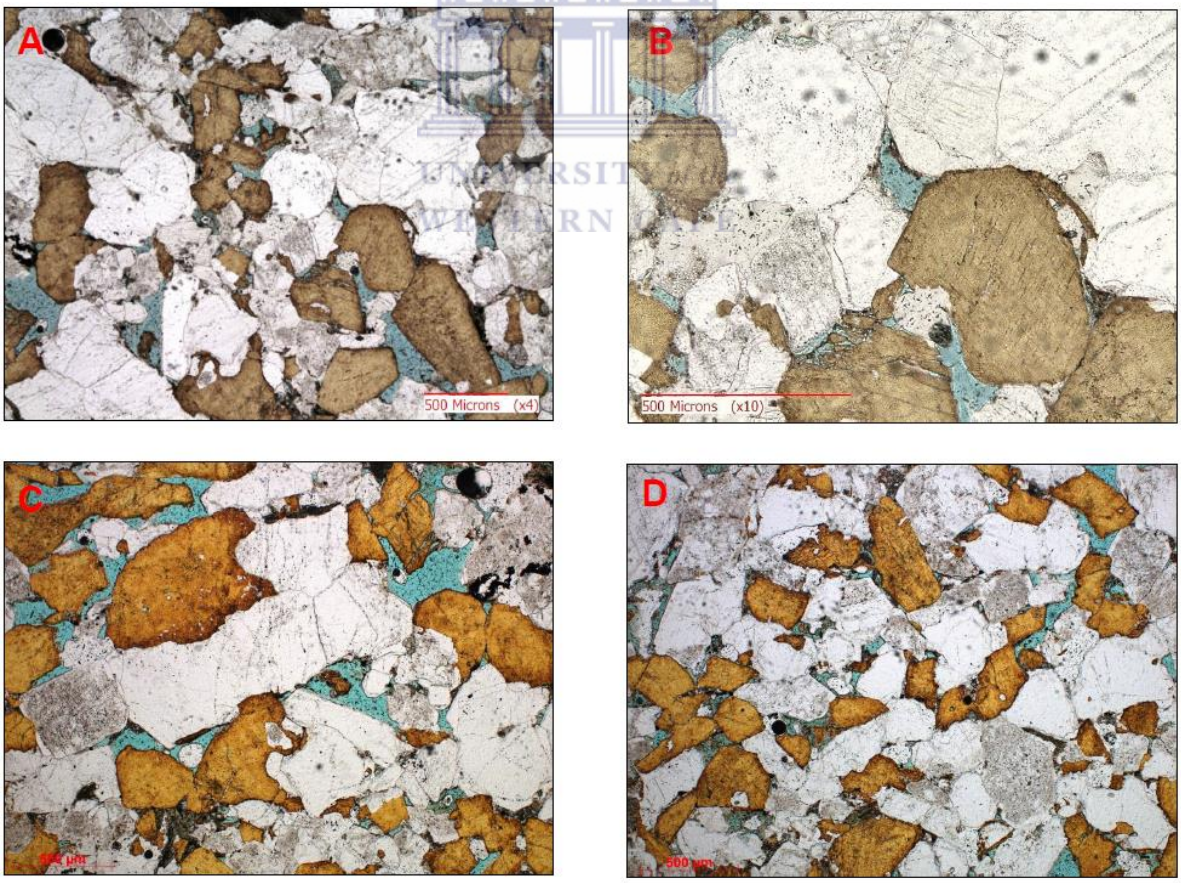

Figure 4.15: Thin-Section micrographs of AJ-1 sandstone at 3256.00m (A: 1000µm, B: 500µm, C: 200µm and D: 200µm), φ = 8.1%, k = 54 md.

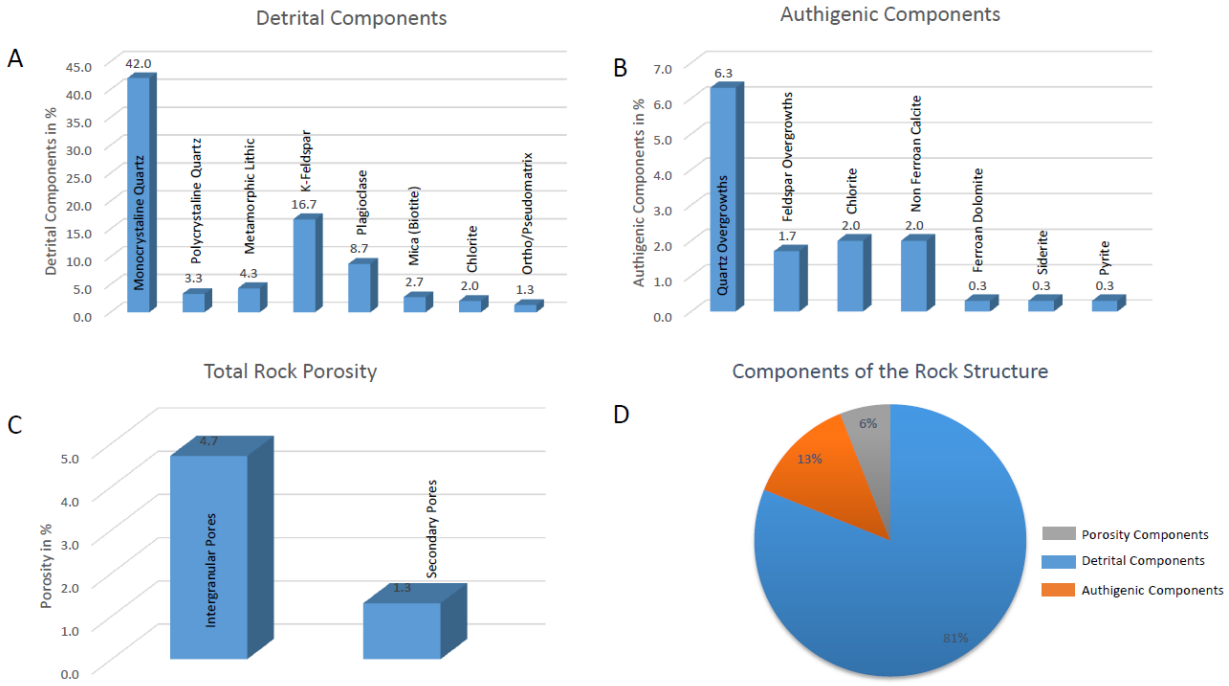

Figure 4.16: AJ-1 sandstone at 3256.00m, total rock constituents composed of (A) detrital components, (B) authigenic components, (C) rock porosity and (D) aggregate of rock structure.

4.3.1.4. Core #2 - #6: Scanning Electron Microscope

On these cores, two samples for SEM and XRD were collected at 3191.23m and 3195.35m depths (Table 4.3) to investigate diagenetic control on total rock porosity.

At 3191.23m depth, SEM and XRD petrographic analysis (Figure 4.17) revealed detrital grains that comprise a mix of quartz, K-feldspar, plagioclase and chlorite. Abundant chlorite appears to be mainly in the form of compacted detrital flakes, but may include matrix clays that could not be differentiated under SEM. EDX analysis locally detected Ca associated with the chlorite. It is unclear if this is due to underlying calcite or is a component of chlorite (possibly smectitic). Accessory grains include scattered Ti-minerals and zircon (D). These grains are moderately poorly sorted, fine to locally medium grained that appears massively at the scale of SEM (A). The sample appears highly compacted with long to concavo-convex grain contacts abundant.

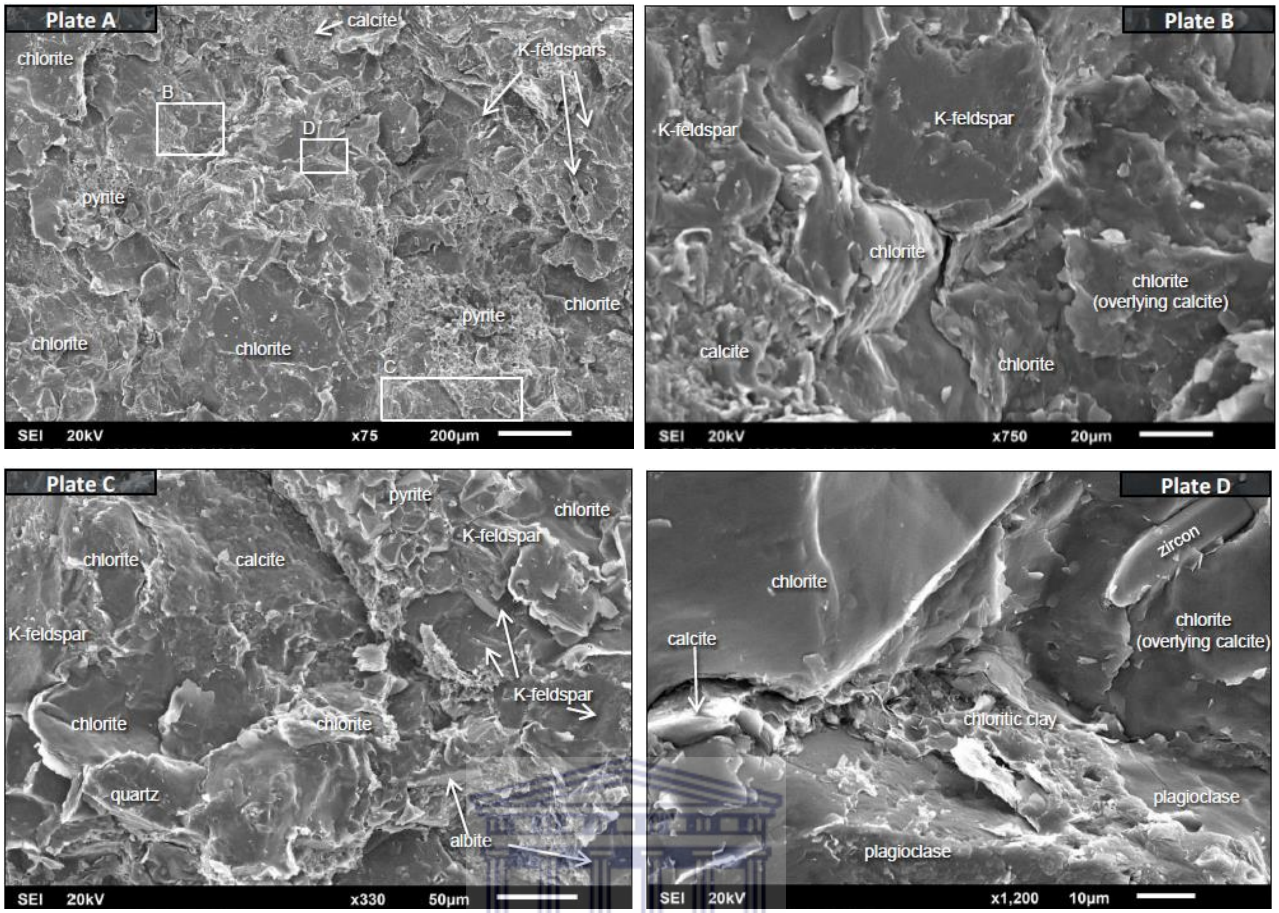

Figure 4.17: SEM micrographs of AJ-1 sandstone at 3191.23m showing detrital and authigenic minerals occurrences: Chlorite and Albite pore lining, pore filling and grain-replacive (A,B); strong reflective pyrite filling pore (A, B); Assessory grains (Zircon) (D); feldspar overgrowths (C).

Authigenic cements are dominated by common calcite, which forms fine, patchy anhedral developments (B, C). Moderate patchy pyrite forms finely crystalline aggregates of cubes and octahedral (A, C). No overgrowths were identified. Straight and angular forms within K-feldspars (A, C) are thought to be due to breakage along cleavages, but could possibly include overgrowths. Minor chloritic clays were identified as an intergranular phase (D). These are matted to weakly webbed, with K and Ca detected by EDX analysis indicating a probable smectitic composition.

Porosity appears to be very poor, consisting entirely of tight micropores within clays / micas and at grain / clay / cement interfaces. Due to the lack of any visible pore network permeability is negligible.

At 3195.35m depth, SEM and XRD petrographic analysis (Figure 4.18) revealed detrital grains that are dominated by K-feldspar with abundant quartz and plagioclase. Detrital chlorite takes the form of fine flakes (C). Common Ti-minerals, concentrated within silt grade lamination are dominated by sphene (C, sph). Accessory grains include zircon, apatite and 'exotics' (A, 'exotic' is a Ca+La+Ce+Nd mineral). At this depth sandstone is laminated by variations in grain size (A). The sample is mainly fine grained, with rare grains up to course; with very fine and silt dominated (C) laminae. The sample is well compacted with common long grain contacts observed.

Authigenic chlorite is abundant as a well-developed authigenic phase within sand grade laminae. The chlorite is both grain-coating (B) and pore-filling (D). Intergranular chlorite also commonly takes the form of poorly developed matted to weakly platy matrix clays. Overall porosity appears moderate to moderately poor, and is dominated by microporosity associated with clays and silt grade phases. Pore connectivity appears to be largely restricted to microporous pathways, so permeability is expected to be poor.

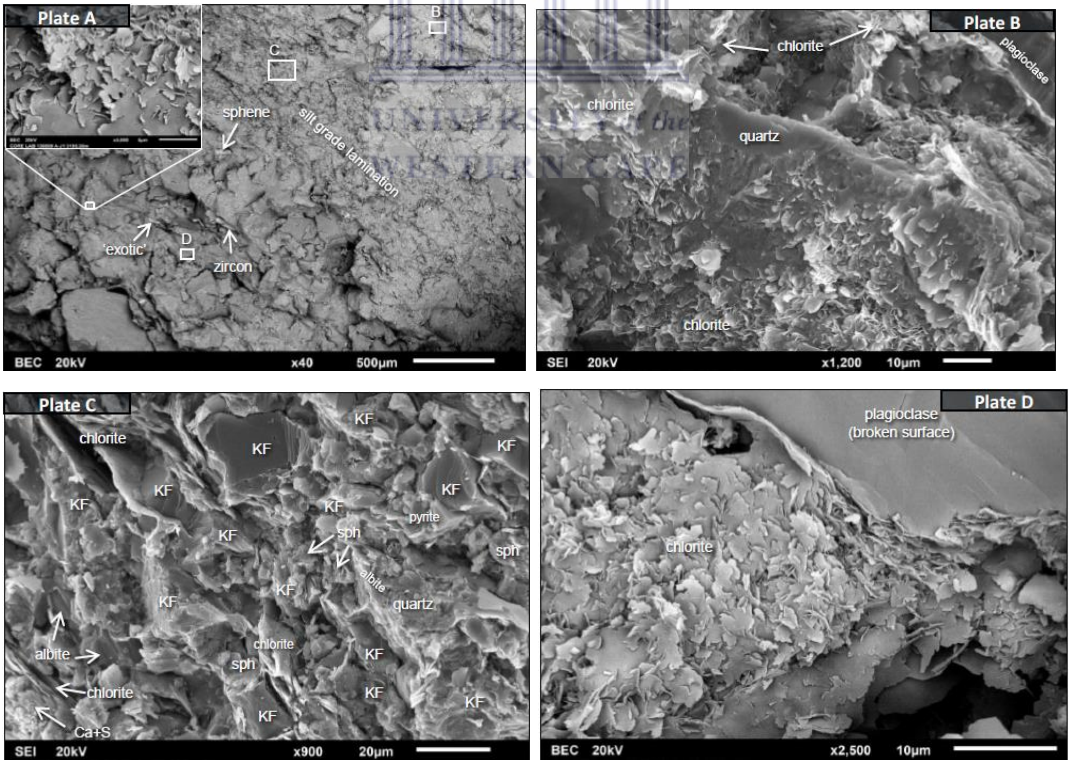

Figure 4.18: SEM micrographs of AJ-1 sandstone at 3195.35m showing detrital and authigenic minerals occurrences: Quartz and plagioclase (B,D), Chlorite pore filling (B,D); feldspar overgrowths (C). Zircon occurrence (A).

4.3.2. Well A-D1 cored interval

4.3.2.1. Core #1: Thin Section Petrography

On this core, three thin section samples were collected at different depth (Table 5.5). One representative sample at 2663.39m depth was selected for detailed discussion on this core. Interpretation and analyses of other samples are presented in Appendix II, A-D1 well – Petrographic Analyses.

At 2663.39m depth, thin section petrographic analysis (Figure 4.19), revealed the majority of 70% detrital components (Figure 4.20D) of total rock constituents dominated by quartz, feldspars and plagioclase with minor contribution of mica, lithic grains (sedimentary, metamorphic and igneous), organic material and no detrital clay matrix noted (Figure 4.20A). Dominated grains are medium grained, moderately sorted, long to sutured grain contact, sub-angular to sub-rounded grain shape with strong compaction. Occurrence of authigenic minerals contributed 18% of total rock constituents (Figure 4.20B & D) dominated by kaolinite filling pore throats between quartz, feldspar and plagioclase grains (Figures 4.19D). Pore filling continued with minor occurrence of grain replacive illite, pyrite, chlorite, calcite and anhydrate (Figure 4.19B). Quartz and feldspar overgrowths are noted with little pore restriction. These diagenetic minerals occurrence has reduced intergranular pore space to 1% (Figure 4.20C), lately expanded by 10% of secondary porosity that occurred from feldspar dissolution and 0.7% of micropores resulting to the total rock point count porosity of 12% (Figure 4.20D). Laboratory test of ambient helium porosity and single phase gas permeability recorded in the well completion report revealed 17% porosity with moderate permeability of 13.5md. Overall sandstone reservoir quality at this depth is moderate due to dissolution of unstable feldspars.

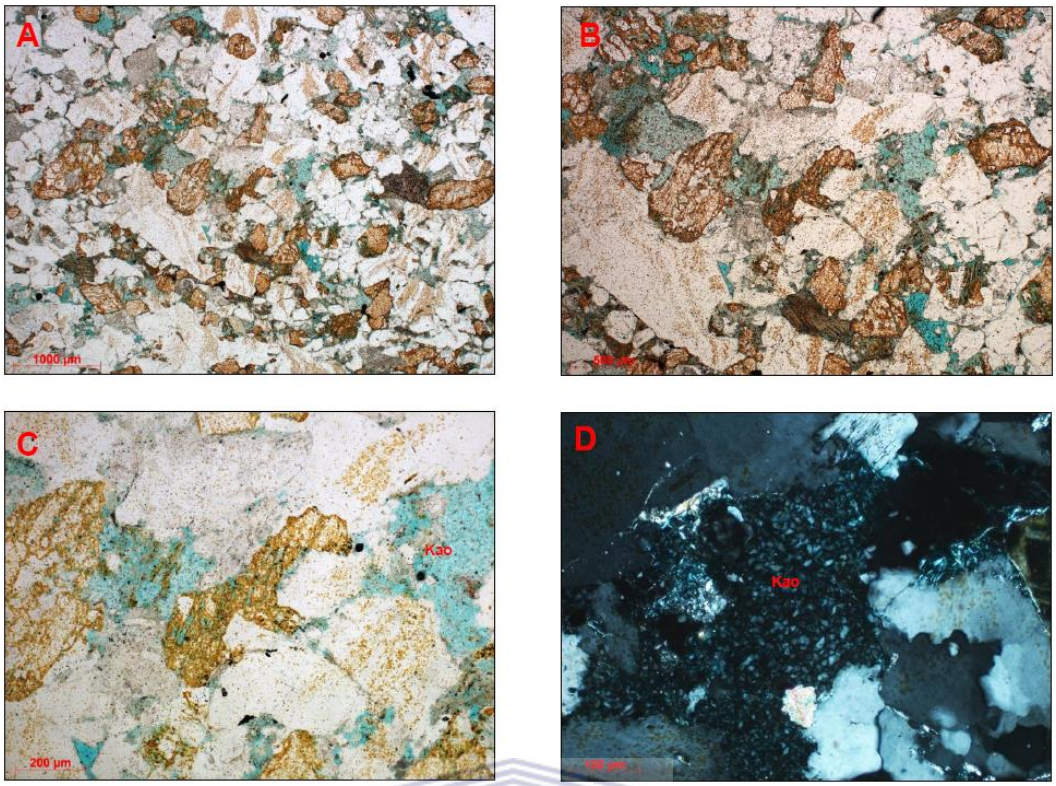

Figure 4.19: Thin-Section micrographs of AD-1 sandstone at 2663.39m (A: 1000µm, B: 500µm, C: 200µm and D: 200µm), φ = 17%, k = 13.5 md.

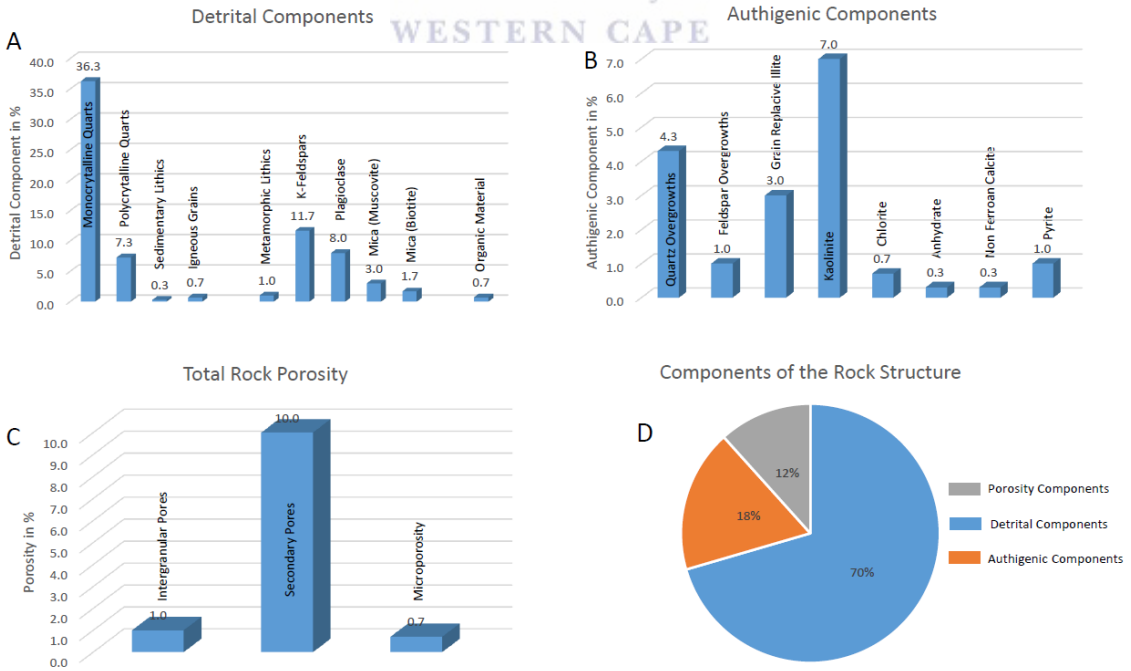

Figure 4.20: A-D1 sandstone at 2663.39m rock constituents composed of (A) detrital components, (B) authigenic components, (C) rock porosity and (D) aggregate of rock structure.

4.3.3. Well A-H1 cored interval

4.3.3.1. Core #1: Thin Section Petrography

On this core, fourteen thin section samples were collected at different depth (Table 5.6). One representative sample at 3024.20m depth was selected for detailed discussion on this core. Interpretation and analyses of other samples are presented in Appendix II, A-H1 well – Petrographic Analyses.

At 3024.20m depth, thin section petrographic analysis (Figure 4.21), revealed the majority of 70% detrital components (Figure 4.22D) of total rock constituents dominated by quartz only with minor contribution of lithic grains (sedimentary, metamorphic and igneous), feldspars, plagioclase, mica, detrital chlorite, organic material, accessory grains (mainly zircon), and widely distributed detrital clay matrix (Figure 4.21A). Dominated grains are fine grained, moderately well sorted, long to sutured grain contact, subangular to rounded grain shape with strong compaction. Occurrence of authigenic minerals contributed 20% of total rock constituents (Figure 4.22B & D) dominated by siderite filling pore throats between quartz and feldspar grains (Figures 4.21D). Pore filling continued with minor occurrence of grain replacive illite, chlorite, pyrite, kaolinite, and ferroan dolomite minerals (Figure 4.22B). Quartz overgrowths are dominant with effective pore restriction. These diagenetic mineral occurrence has reduced intergranular pore space 4% (Figure 4.22C), lately expanded by 6% of secondary porosity that occurred from feldspar dissolution resulting to the total rock point count porosity of 10% (Figure 4.22C). Laboratory test of ambient helium porosity and single phase gas permeability recorded in the well completion report revealed 15.6% porosity with moderate permeability of 12md. Sandstone reservoir quality at this depth is poor to locally moderate due to feldspar dissolution.

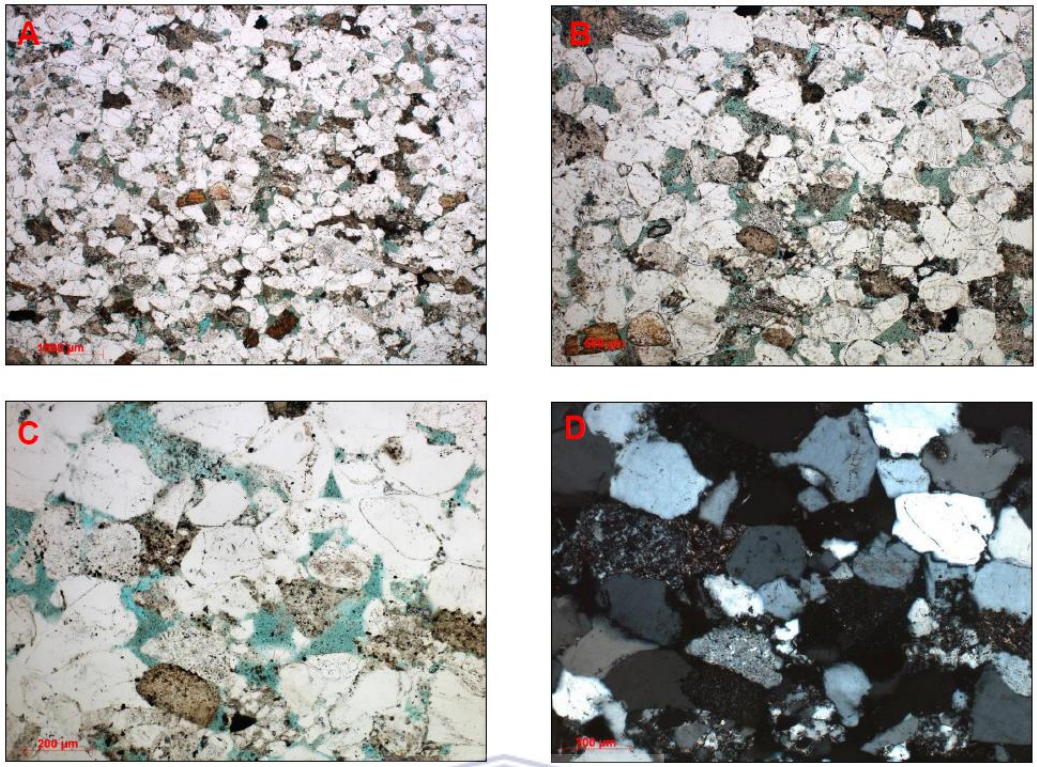

Figure 4.21: Thin-Section micrographs of AH-1 sandstone at 3024.20m (A: 1000µm, B: 500µm, C: 200µm and D: 200µm), φ = 0%, k = 3.6 md.

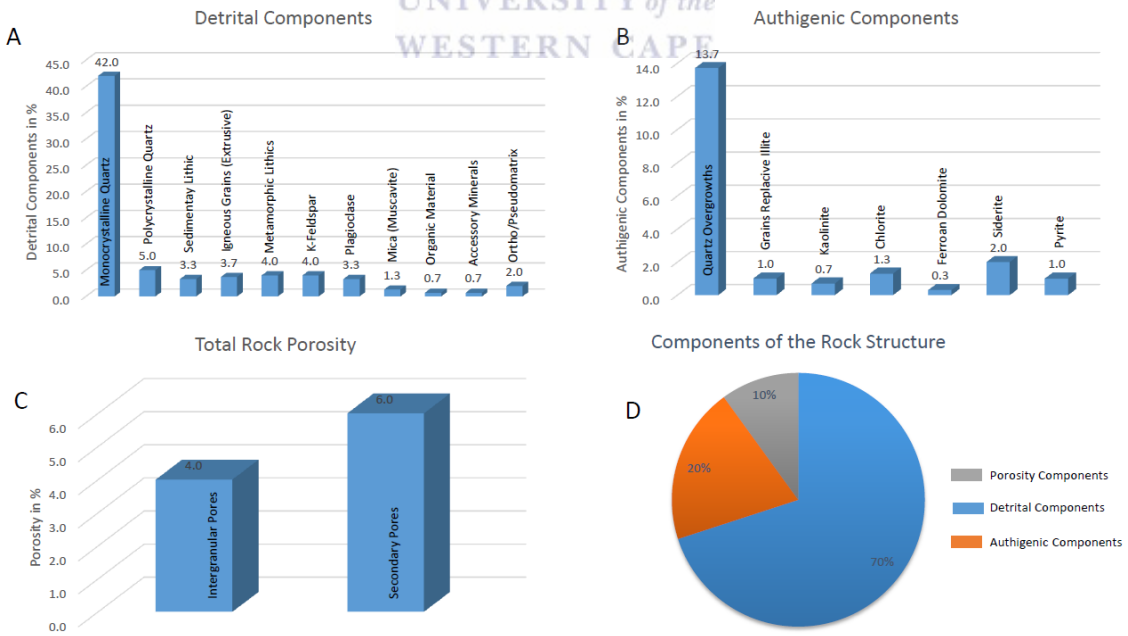

Figure 4.22: A-H1 sandstone at 3024.20m, total rock constituents composed of (A) detrital components, (B) authigenic components, (C) rock porosity and (D) aggregate of rock structure.

4.3.3.2. Core #1: Scanning Electron Microscope

On this core one sample for SEM and XRD was collected at 3033.26m depth (Table 4.3) to investigate diagenetic control on total rock porosity.

At 3033.26m depth, SEM and XRD petrographic analysis (Figure 5.32) revealed detrital grains that include quartz (micro-quartz, C); common feldspars (plagioclase with rare K-feldspar, locally leached or albitised). Some indeterminate grains are leached to leave dissolution pores (A). These grains are very fine, moderately well sorted and appears massively on the scale of SEM (A). The sample is well compacted, with common long grain contacts observed.

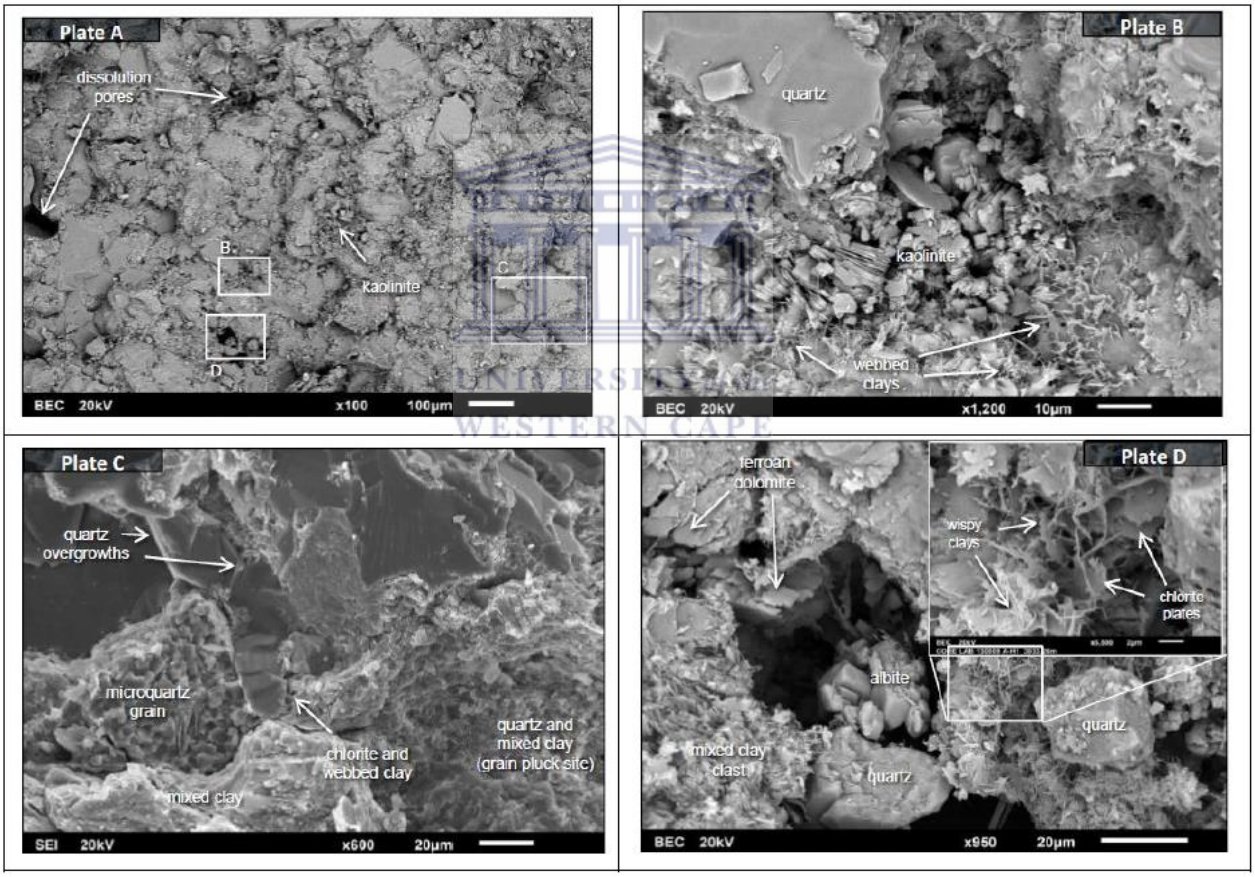

Figure 4.23: SEM micrographs of A-H1 sandstone at 3195.35m showing detrital and authigenic minerals occurrences: Abundant kaolinite which is pore lining, pore filling and grain-replacive (A,C); quartz overgrowths (C); Clear pore space resulted from mineral dissolution (A,D).

Pore-lining clay matrix appear to be widespread, and of mixed composition. Matted clays are observed adjacent to grain contact areas. Authigenic grain-coating clays comprise a mix of platy chlorite and very finely webbed to wispy clays (illite / illite-smectite) (B, D). Kaolinite is a common patchy phase that appears to be an intergranular as well as a replacive phase, typically forming short blocky verms (B). Quartz overgrowths were observed as mainly isolated projections, and are rarely interlocking (C). Rare authigenic albite is present with in dissolution pores / replacive of leached feldspar grains (D). Traces of ferroan dolomite were also observed within dissolution pores (D).

Porosity appears to be moderate to moderately poor. Small intergranular and scattered dissolution pores appear largely isolated. Overall porosity may be dominated by micro porosity mainly associated with clay mineral aggregates. Pore connectivity appears to be largely restricted to micro porous networks. Permeability is poor.

4.3.4. Well A-K1 cored interval

4.3.4.1. Core #1: Thin Section Petrography

On this core, five thin section samples were collected at different depth (Table 4.3). One representative sample at 3236.46m depth was selected for detailed discussion on this core. Interpretation and analyses of other samples are presented in Appendix II, A-K1 well – Petrographic Analyses.

At 3236.46m depth, thin section petrographic analysis (Figure 4.24), revealed the majority of 65% detrital components (Figure 4.25D) of total rock constituents dominated by quartz only with minor contribution of lithic grains (sedimentary, metamorphic and igneous), plagioclase, mica, organic material, accessory grains (mainly zircon), and sparsely distributed detrital clay matrix (Figure 4.25A). Dominated quartz grains are fine grained, well sorted, long grain contact, subangular to subrounded grain shape with moderate compaction. Occurrence of authigenic minerals contributed 24% of total rock constituents (Figure 4.25B & D) dominated by chlorite (Figure 4.24D) and siderite filling pore throats between quartz and feldspar grains (Figures 4.24D). Pore filling continued with minor occurrence of grain dolomite, calcite, pyrite, kaolinite, and illite minerals (Figure 4.25B). Quartz overgrowths are fairly distributed with effective pore restriction. These diagenetic minerals occurrence has reduced intergranular pore space 4.3% (Figure 4.25C), lately expanded by 6.3% of secondary porosity and 0.3% of micro-porosity

resulting to the total rock point count porosity of 11% (Figure 4.25D). This porosity did not yield any permeability. Sandstone reservoir quality at this depth is very poor due to chlorite grain rimming, dolomite pore filling and quartz overgrowth.

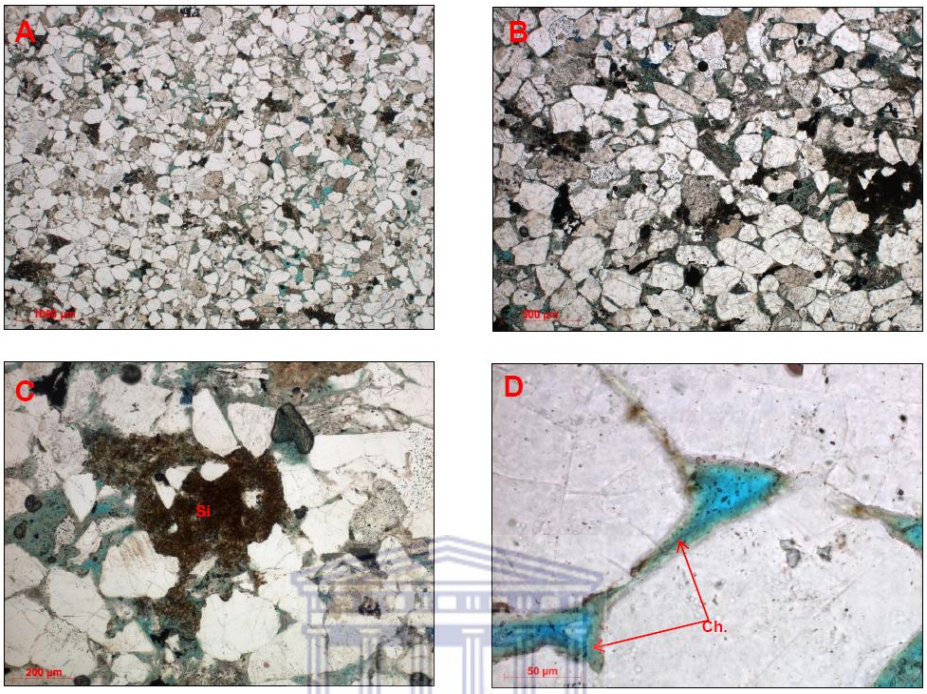

Figure 4.24: Thin-Section micrographs of A-K1 sandstone at 3236.46m (A: 1000µm, B: 500µm, C: 200µm and D: 200µm), φ = 11%, k =0 md.

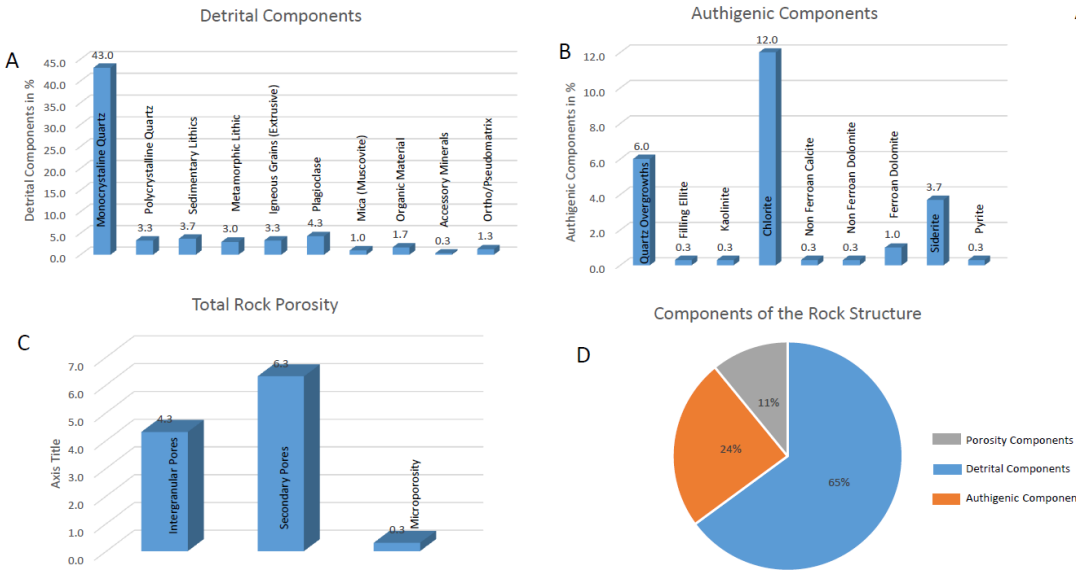

Figure 4.25: A-K1 sandstone at 3236.46m, total rock constituents composed of (A) detrital components, (B) authigenic components, (C) rock porosity and (D) aggregate of rock structure.

4.3.4.2. Core #2: Thin Section Petrography

On this core, five thin section samples were collected at different depth (Table 4.3). One representative sample at 3284.41m depth was selected for detailed discussion on this core. Interpretation and analyses of other samples are presented in Appendix II, A-H1 well – Petrographic Analyses.

At 3284.41m depth, thin section petrographic analysis (Figure 4.26), revealed the majority of 66% detrital components (Figure 4.27D) of total rock constituents dominated by quartz only with minor contribution of lithic grains (sedimentary, metamorphic and igneous), feldspars, plagioclase, mica, detrital chlorite, organic material, accessory grains (mainly zircon), and sparsely distributed detrital shaly matrix (Figure 4.27A). Dominated quartz grains are fine grained, well sorted, long to point to point grain contact, angular to rounded grain shape with moderate compaction. Occurrence of authigenic minerals contributed 19% of total rock constituents (Figure 4.27B & D) dominated by chlorite and siderite filling pore throats between quartz grains (Figures 4.26D). Pore filling continued with minor occurrence of ferroan dolomite and hematite minerals (Figure 4.27B). Quartz overgrowths are sparsely distributed with effective pore restriction. These diagenetic mineral occurrence has reduced intergranular pore space 8.3% (Figure 4.27C), lately expanded by 6.7% of secondary porosity resulting to the total rock point count porosity of 15% (Figure 4.27D). Laboratory test of ambient helium porosity and single phase gas permeability recorded in the well completion report revealed 22.4% porosity with moderate permeability of 30md. Sandstone reservoir quality at this depth is good.

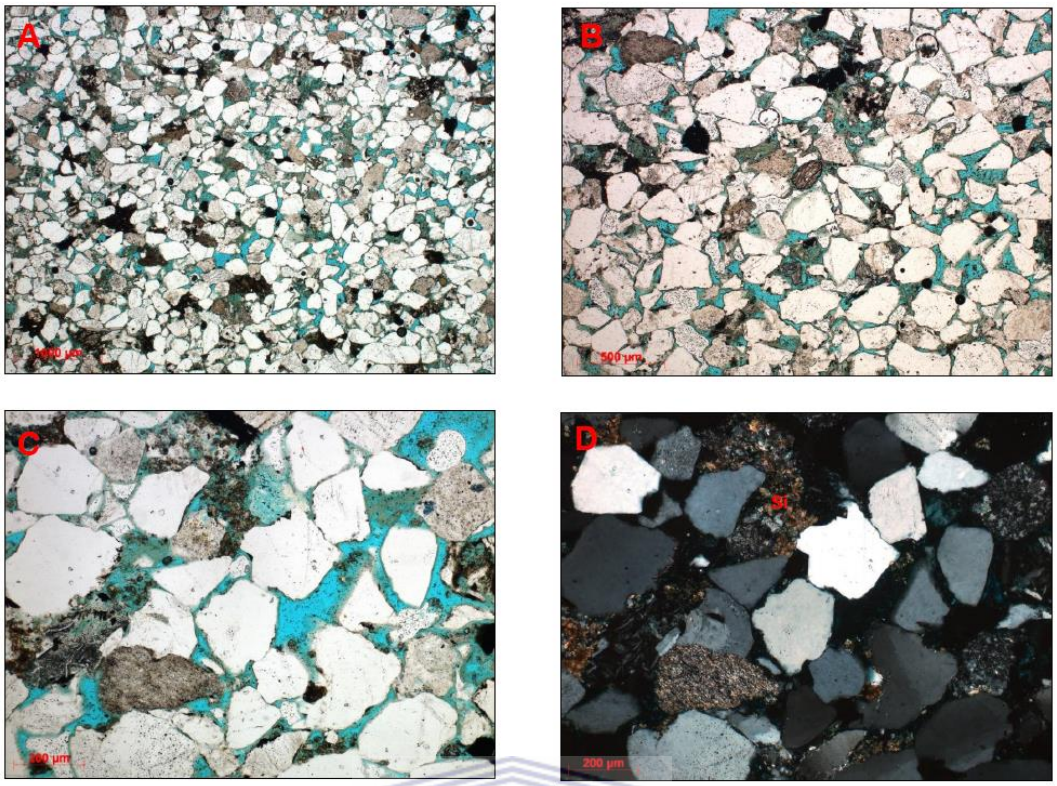

Figure 4.26: Thin-Section micrographs of A-K1 sandstone at 3284.41m (A: 1000µm, B: 500µm, C: 200µm and D: 200µm), φ = 22%, k = 30 md.

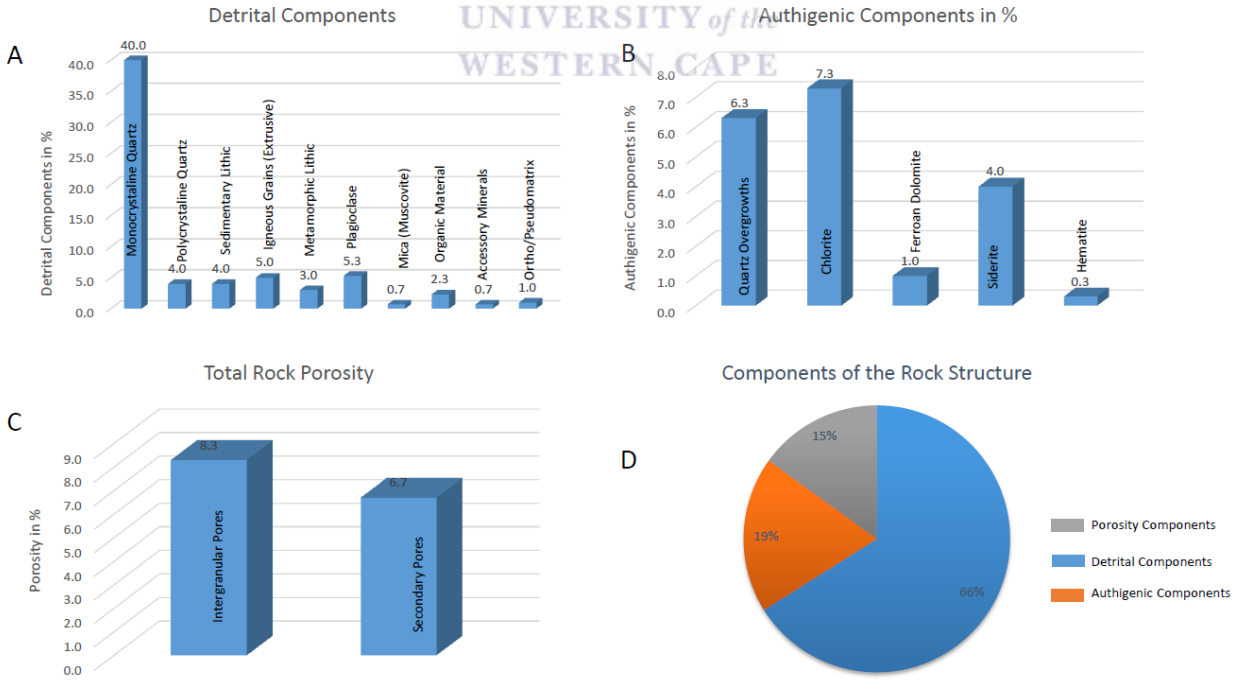

Figure 4.27: A-K1 sandstone at 3284.41m, total rock constituents composed of (A) detrital components, (B) authigenic components, (C) rock porosity and (D) aggregate of rock structure.

4.3.4.3. Core #2: Scanning Electron Microscope

On this core one sample for SEM and XRD was collected at 3285.90m depth (Table 5.5) to investigate diagenetic control on total rock porosity.

At 3085.90m depth, SEM and XRD petrographic analysis (Figure 2.28) revealed detrital grains dominated by quartz. Common feldspar grains (plagioclase and minor K-feldspar) are locally leached or albitised (B). Lithic grains include clay-rich, quartz-mica and Ti-rich varieties. Scattered Ti-minerals are typically corroded (B). Traces of apatite are also present. A moderately well sorted very fine to fine grained sandstone that appears mainly massive at the scale of SEM, with some alignment of elongate grains (A). The sample is well compacted and long grain contacts are common (C, D).

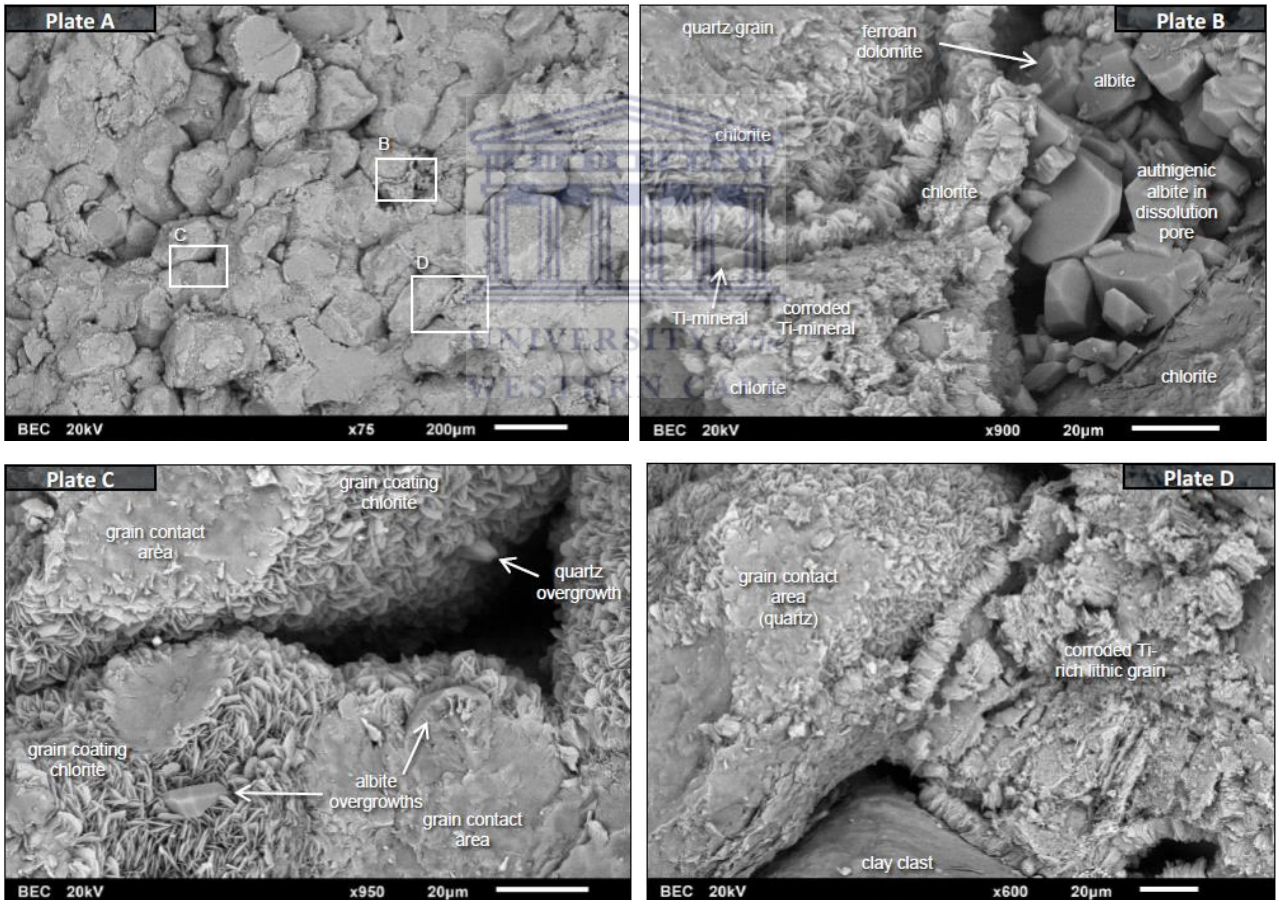

Figure 4.28: SEM micrographs of A-K1 sandstone at 3085.90m showing detrital and authigenic minerals occurrences. Chlorite and dolomite pore filling (B, C) quartz and feldspar overgrowths (B, C & D). Mineral dissolution (B).

The authigenic mineralogy is dominated by abundant grain-coating chlorite, which form is opachous platy rims on grains (B, C, D). The development of overgrowths has been inhibited by the chloritic clays. Rare small isolated quartz and albite overgrowths were observed (C). Authigenic albite more commonly forms fine blocky developments associated with leached feldspar grains / dissolution pores (B). Traces of ferroan dolomite were observed with in dissolution pores (B, possibly? pre-dating authigenic albite).

Porosity appears to be moderately good, comprising a mix of intergranular pores, dissolution pores and microporosity associated with chloritic clays and leached framework grains. Abundant grain-coating chlorite means pore walls typically have very high surface areas, and pore throats are constricted / made tortuous. Overall pore connectivity and permeability are moderate.

4.3.5. Well K-A2 cored interval

4.3.5.1. Core #1: Thin Section Petrography

On this core, seven thin section samples were collected at different depth (Table 4.3). One representative sample at 3982.77m depth was selected for detailed discussion on this core. Interpretation and analyses of other samples are presented in Appendix II, K-A2 well – Petrographic Analyses.

At 3982.77m depth, thin section petrographic analysis (Figure 4.29), revealed the majority of quartz, feldspar and plagioclase with minor occurrence of lithic (mudclasts, volcanic and metamorphic) grains, mica, zircon, organic matter and sparsely distributed detrital clay matrix of detrital components in the total rock constituents. Quartz, feldspar and plagioclase are very fine grained, well sorted, long to concavo-convex grain contact, angular to well-rounded grain shape with moderately strong compaction. Occurrence of authigenic minerals to total rock constituents is dominated by chlorite and smectite filling pore throats between the detrital grains. Pore filling continued with minor occurrence of ferroan dolomite and pyrites minerals. Poorly developed quartz overgrowths are sparsely distributed with effective pore restriction. These diagenetic minerals occurrence has completely reduced intergranular pore space. No point count porosity observed. Sandstone reservoir quality at this depth is very poor.

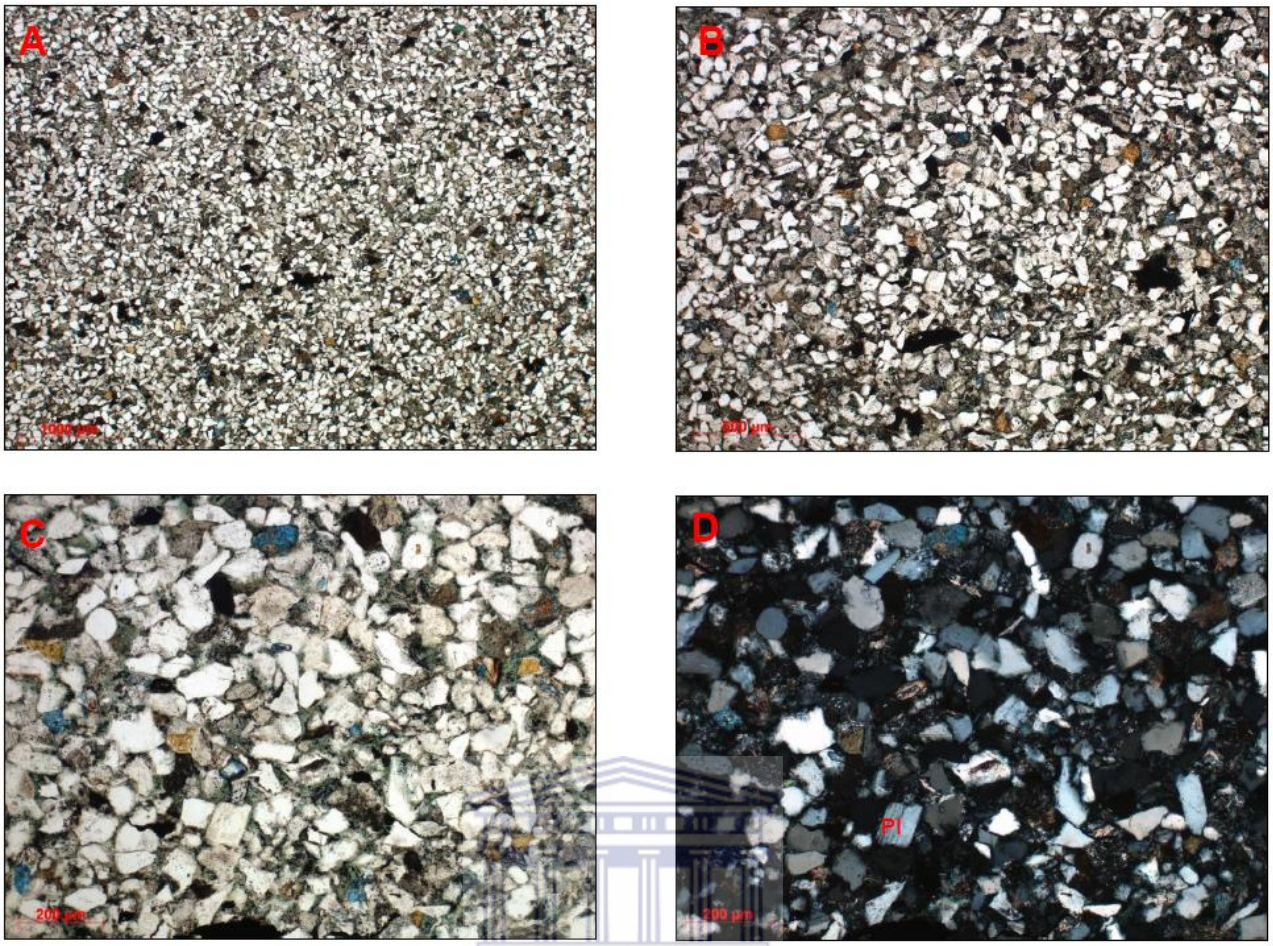

Figure 4.29: Thin-Section micrographs of K-A2 sandstone at 3982.77m showing (A: 1000µm, B: 500µm, C: 200µm and D: 200µm), φ = 0%, k = 0 md.

4.3.5.2. Core #1: Scanning Electron Microscope

On this core one sample for SEM and XRD was collected at 3982.77m depth (Table 5.7) to investigate diagenetic control on total rock porosity.

At 3982.77m depth, SEM and XRD petrographic analysis (Figure 4.30) reveal detrital grains that include quartz, abundant feldspars (plagioclase with rare K-feldspar) that are commonly leached with lithic grains that are mainly clay-rich with microquartz-rich varieties, micaceous minerals (including biotite and chlorite), and minor scattered Ti-minerals. These sandstone grains are well sorted, very fine (upper) grained sandstone and appears massive at the scale of SEM (A). The sample present well compacted sandstone with the dominance of long grain contacts (B).

The authigenic mineralogy is dominated by abundant grain-coating chlorite, which forms isopachous platy rims on grains (B,C,D). Platy aggregates of chlorite also appear to be intergranular matrix-replacive in places (difficult to clearly differentiate potential pore-filling clays from compacted clay-rich lithic grains). The development of overgrowths has been inhibited by the chloritic clays. Rare small isolated quartz overgrowths were observed (C). Authigenic albite forms very fine blocky developments associated with leached feldspar grains(C). Moderate calcite (C) forms fine subhedral developments that may be replacive as well as pore-filling. Rare ferroan dolomite takes the form of fine rhombic developments (A,C), and is a microcrystalline replacive phase within some clay-richlithics.

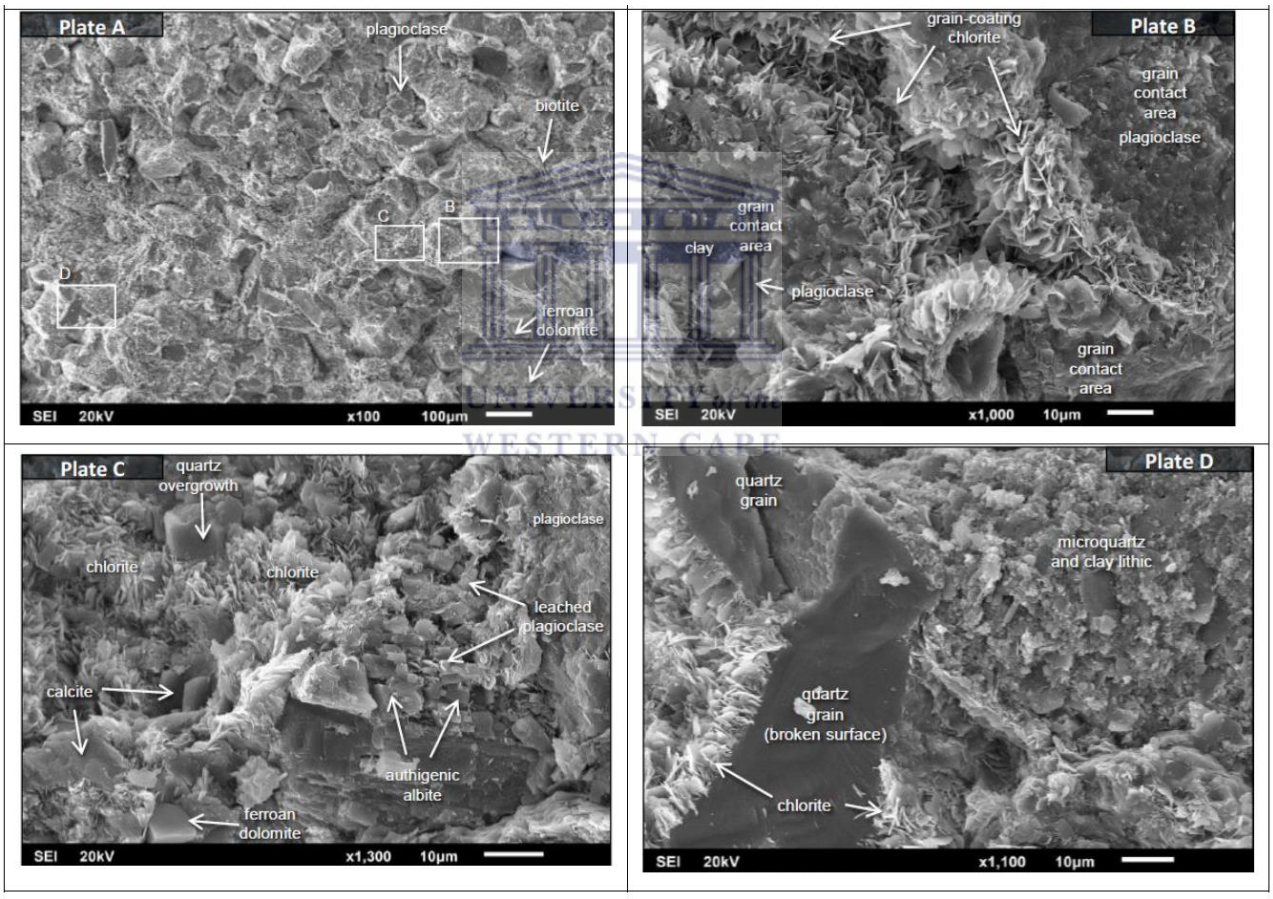

Figure 4.30: SEM micrographs of K-A2 sandstone at 3982.77m showing detrital and authigenic minerals occurrences: Detrital quartz and plagioclase (A, B, C & D); Abundant albite which is pore lining, pore filling and grain-replacive (A); strong reflective chlorite & dolomite filling pore (A, B & D); quartz overgrowths (C).

Traces of NaCl are thought to be a drying precipitate. Porosity appears to be moderately poor, dominated by microporosity associated with clays and leached frame work grains. Intergranular pores (B) are small, having been significantly reduced by compaction and grain-coating clay development. Pore connectivity appears to be restricted to microporous / highly tortuous pathways. Permeability is expected to be poor to very poor.

4.3.5.3. Core Description of Core #2

On this core, three thin section samples were collected at different depth (Table 5.1). A representative sample at 4078.40 was selected for detailed discussion on this core. Interpretation and analyses of other samples are presented in Appendix II, K-A2 well – Petrographic Analyses.

At 4078.40m depth, thin section petrographic analysis (Figure 4.31), revealed the majority of quartz and feldspar with minor occurrence of lithic (mudclasts, volcanic and metamorphic) grains, organic matter and grain rimming to pore filling clay matrix of detrital components in the total rock constituents. This sample is laminitic; it is composed of laminae with predominant silt and relatively more abundant very fine grained sand. Grains are angular to sub-rounded, locally rounded with strong compaction. Occurrence of authigenic minerals to total rock constituents is dominated by ferroan dolomite, hematite and pyrite pore throats between the detrital grains. Poorly developed quartz overgrowths are sparsely distributed with effective pore restriction. These diagenetic minerals occurrence has completely reduced intergranular pore space. No point count porosity observed. Sandstone reservoir quality at this depth is negligible.

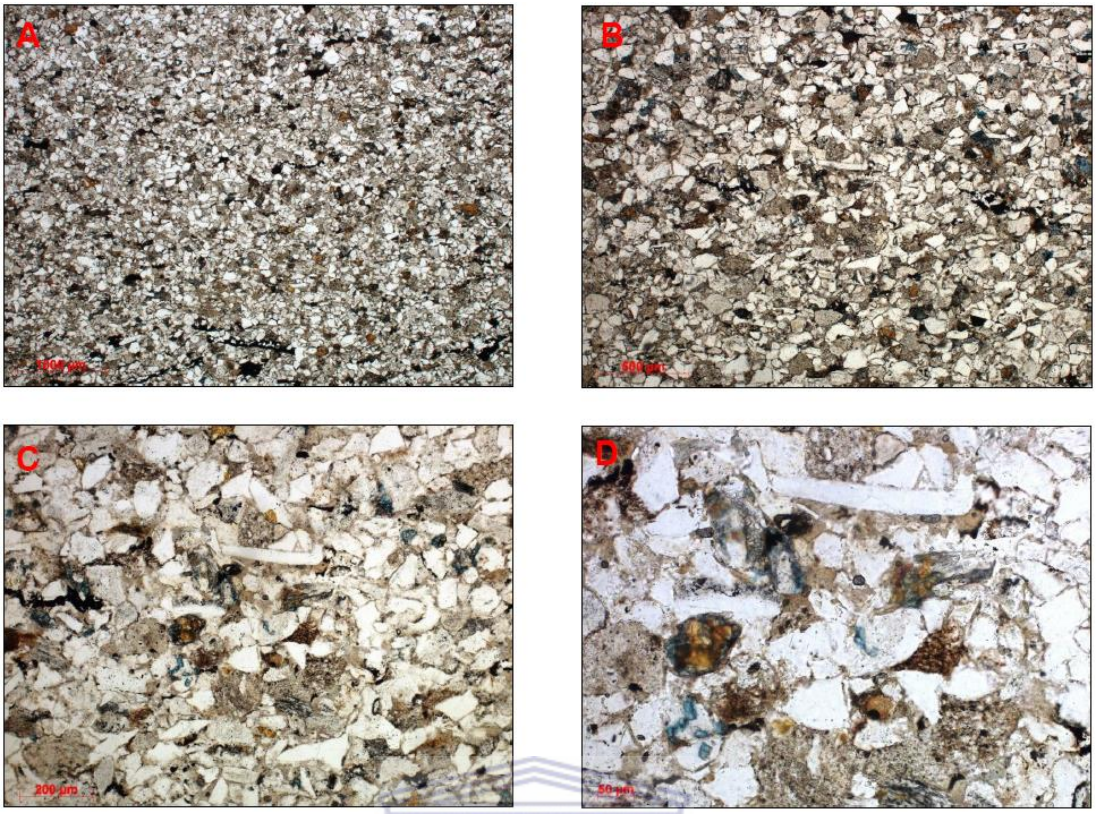

Figure 4.31: Thin-Section micrographs of K-A2 sandstone at 4078.40m showing (A: 1000µm, B: 500µm, C: 200µm and D: 200µm), φ = 0%, k = 0 md.

4.3.5.4. Core #1: Scanning Electron Microscope

On this core one sample for SEM and XRD was collected at 3982.77m depth (Table 5.7) to investigate diagenetic control on total rock porosity.

At 4078.40m depth, SEM and XRD petrographic analysis (Figure 4.32) revealed detrital grains that include quartz, abundant feldspars (plagioclase with rare K-feldspar) that are locally leached, lithic grains (mainly clay-rich, with quartz-mica varieties), micaceous minerals (including biotite and muscovite); and accessory grains (Ti-minerals and traces of apatite). It is difficult to fully differentiate some compacted lithic grains from matrix material. A well sorted very fine (lower-upper) grained sandstone that appears mainly massive, with some alignment of elongate grains (A). The sample appears well compacted, with long grain contacts observed (B), although grain contacts are commonly obscured by matrix clays.

Matrix clays are abundant. EDX analysis indicates these are likely to be dominated by chlorite, with some mixed compositions. Matrix clays are matted / morphologically indeterminate in form. Well-developed platy chlorite is locally common, coating grains and lining pores, associated mainly with small open intergranular pores (B) and probable altered lithic grains, and appears to also be partially matrix replacive.

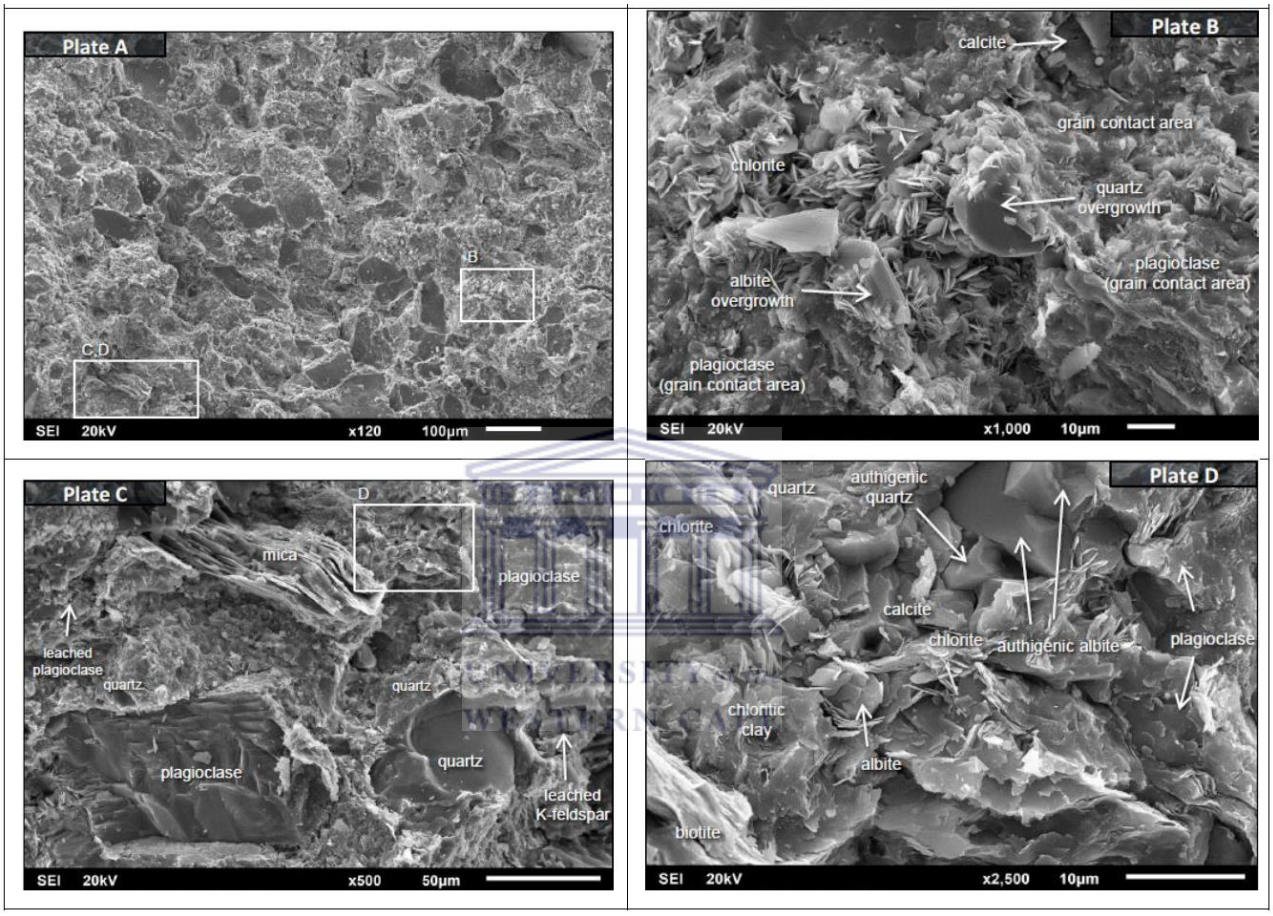

Figure 4.32: SEM micrographs of K-A2 sandstone at 3982.77m showing detrital and authigenic minerals occurrences. Plagioclase and quartz detrital grains (B, C & D); Abundant chlorite which is pore lining, pore filling and grain-replacive (A); calcite, albite and mica filling pore (D); Assessory grains (Ti-minerals and barite) (A, C); quartz and feldspar overgrowths (B, D).

Due to the abundance of clays, authigenic mineral cements are present in minor amounts only. Small isolated overgrowths of quartz and plagioclase are rare (B). Very fine / microcrystalline developments of quartz and albite that may be associated with altered lithic grains (D). Minor to moderate patchy calcite (D) forms finely crystalline developments that are possibly replacive as well as pore-filling. EDX analysis indicates

the calcite has minor Fe and Mn components. Rare ferroan dolomite forms very finely crystalline rhombs and subhedral. Porosity appears to be poor. Rare, small intergranular pores appear effectively isolated (B). Overall porosity is dominated by microporosity associated with matrix and authigenic clays and leached framework grains. Pore connectivity is restricted to microporous networks. Permeability is very poor.

4.4. Porosity and permeability analysis

Detrital sediments deposited in the lower cretaceous of the Orange Basin are dominated by quartz grains followed by feldspars with minor lithics framework compositions (Figure 4.33). Initial depositonal porosity and permeability of these sediments were moderately reduced by gravitational loading during burial. These modifications is due to mechanical compaction observed to be moderate to strongly compacted reducing pore volume of the reservoir sediments. Burial continuation increases with temperature (reaching 90°C) that allowed diagenetic authigenic mineral occurrences that have extremely altered porosity and permeability (Figures 4.34 & 4.35). In these figures between 3000 3300m depths porosity and permeability is much more variable and does not follow a simple depth trend. This reflects the onset of significant quartz and feldspars cemetations (temperature >~ 90°C at ≥ 3000m depth) and, greater porosity and permeability lost was also witnessed by mechanical compaction. This probably reflects the onset of significant quartz and feldspar cementations to shallower depth as observed in Figures 4.34 & 4.35 at 3000m depth. This geothernal heat is associated with the tertiary uplift in the Orange Basin as observed by Granado et al., 2009.

Occurrence of quartz and feldspars cemetations creates concentric rims on the surfaces of the detrital quartz and feldspars grains reducing pore volume of the rock (Figure 4.2 - 4.32) in all wells. Pore restriction was expanded by microporous grain-radially around quartz and feldspars detrital grains. These crystal growths are dominant in well K-A2 preveting permeability between the interparticle pore-space. Other minerals such as calcite, dolomite, siderite, pyrite and kaolinite precipitate filling the pore-throat between the grains. Occurrence of these authegenic minerals blocked connected throats reducing flow mechanism in A-J1, A-D1, A-K1, A-H2 and K-A2 wells.

Porosity and permeability curve plotted in Figure 4.36 following Glover (2009) in Figure 4.1 confirms lower cretaceous reservoir rock to be clean sandstones. Studied rock

samples from Figure 4.2 - 4.32 prevailed reduction in reservoir porosity and permeability by mechanical campaction and diagenetic mineral occurrence. These two factors have major effect in hydrocarbon production. Porosity of the reservoir control hydrocarbon storage capacity whereas permeability controls hydrocarbons production flow capacity. Sufficient porosity and permeability to support commercial development has a cutoff of 10% porosity and 1 md permeability (suitable for liquid hydrocarbons) and 7% porosity and 0.1 md permeability (suitable for gaseous hydrocarbons) respectively.

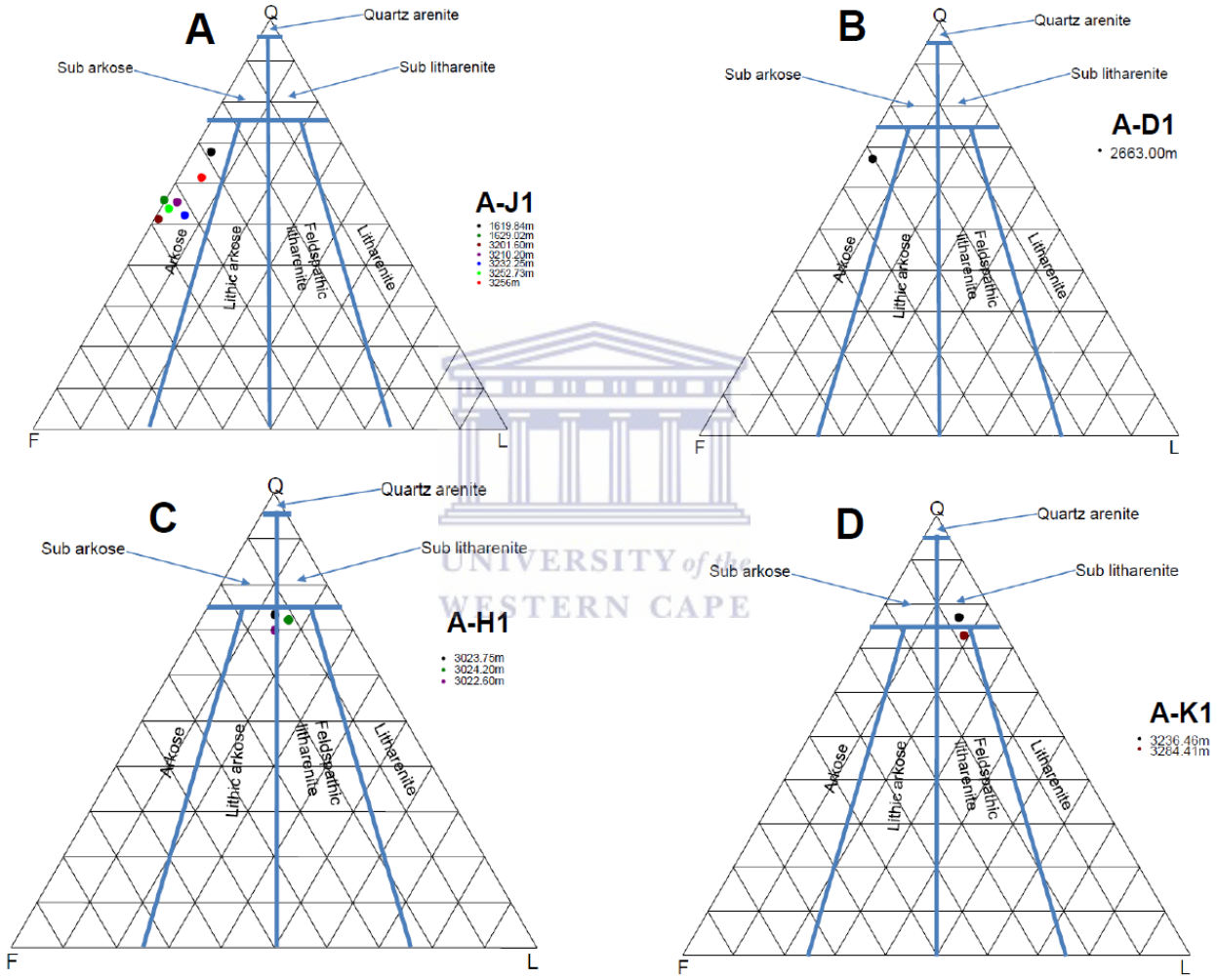

Figure 4.33: QFL (Quartz-Feldspar-Lithics) ternary diagram showing composition of detrital grains comprising the rock framework. These sandstones have less than 1% detrital clay. Sandstone samples presented in Figure 4.33A are; Quartz 50-70%, Feldspar 25-50%, Lithics <10%; in Figure 4.33B is; Quartz 65-70%, Feldspar = 30%, Lithics <10%, in Figure 4.33C are; Quartz 65-75%, Feldspar 10-20%, Lithics 10-20%; and in Figure 4.33D are; Quartz 70-80%, Feldspar <10%, Lithics 10-20%.

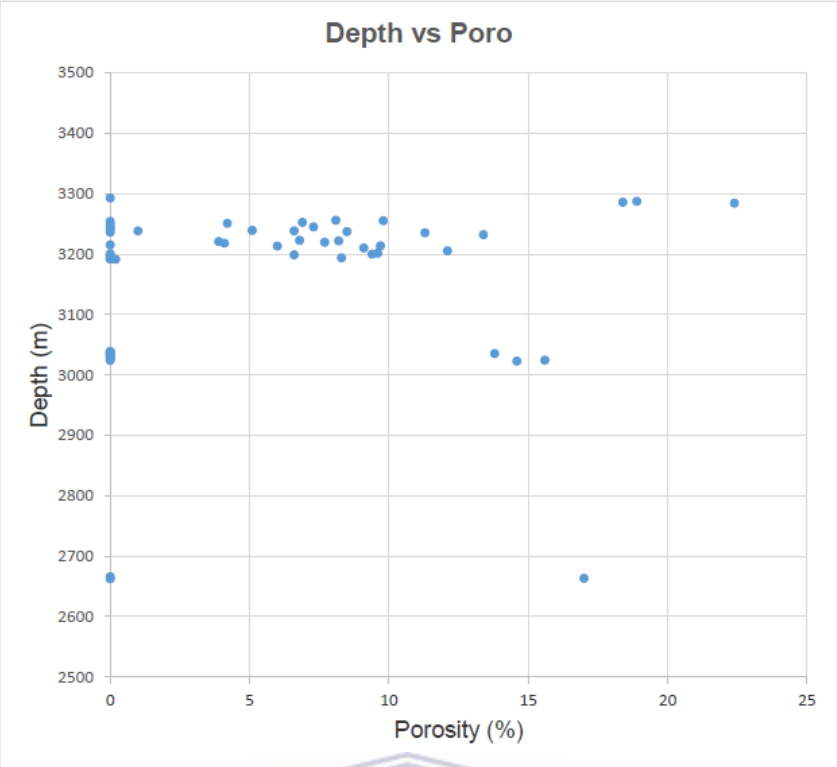

Figure 4.34: Depth-porosity relationship curve for reservoir quality analyses of the well under study.

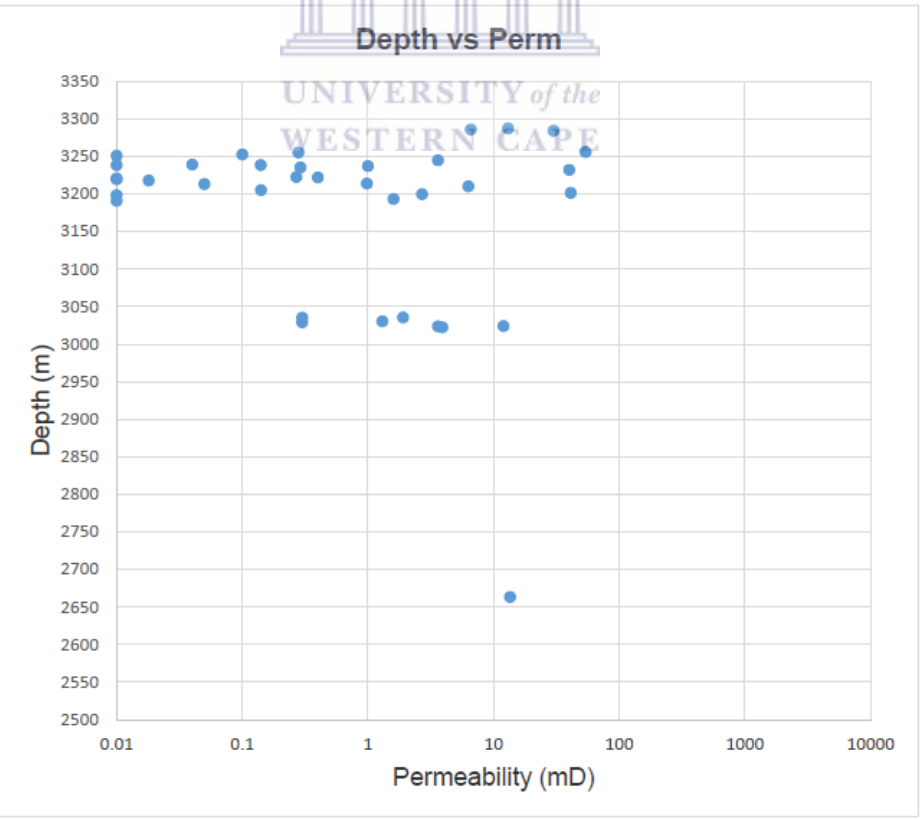

Figure 4.35: Depth-permeability relationship curve for reservoir quality analyses of the well under study.

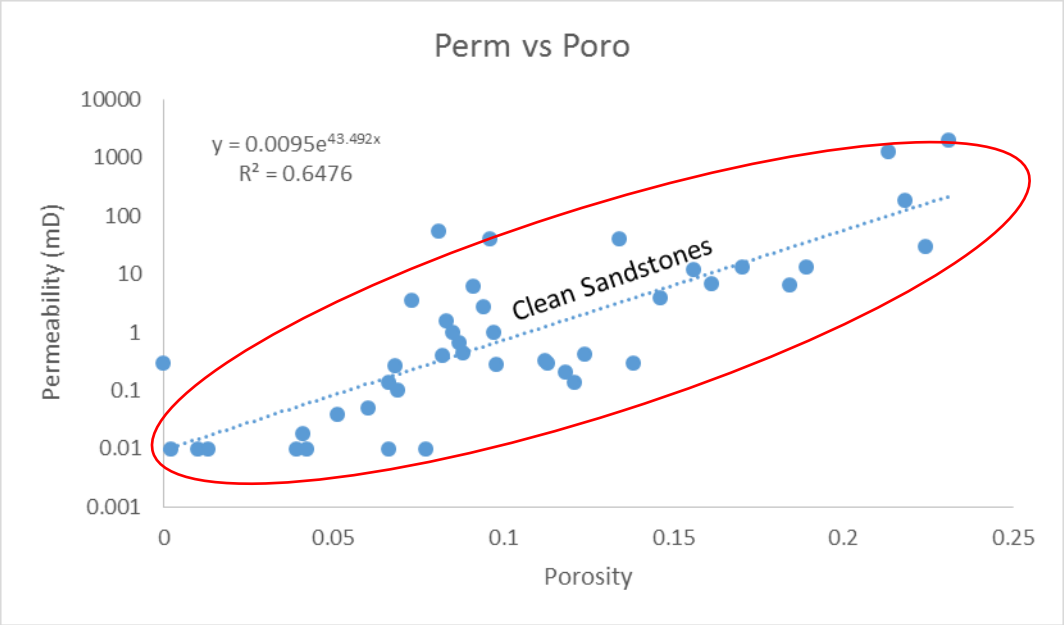

Figure 4.36: Permeability-porosity relationship curve for reservoir quality analyses of the well under study.

In well A-J1, reservoir quality of core #1 presented in Table 4.3 vary from excellent (φ > 20%, k > 100 md) to poor (φ < 10%, k < 1 md) whereas cores #2 - #6 has moderate porosity (φ) of 13.4% and permeability (k) of 52 md only at 3232.25 m and 3256 m depth. All other sampled intervals are dominated by very poor porosity φ < 10%, and permeability (k) < 1 md. Using an economic cutoff of 10% porosity and 1 md permeability (suitable for liquid hydrocarbons), the majority of sampled intervals in core #1 could be effective hydrocarbon reservoirs whereas in cores #2 - #6 almost all sampled interval could not produce. Using lower φ-k cutoffs of 7% porosity and 0.1 md permeability (for gas reservoirs) in cores #2 - #6, few additional sampled intervals could be effective due to the presence of few micro-fracture networks.

In well A-D1, reservoir quality of the cored zone in this well is presented in Table 4.3 and is poor to moderate. The quality at 2663.39m depth is 17% porosity (φ) and 13.5md permeability (k) whereas other sampled are extremely poor (φ < 10%, k < 1 md). Using an economic cutoff of 10% porosity and 1 md permeability (suitable for liquid hydrocarbons), only zone around 2663.39m could be effective hydrocarbon reservoirs. Even applying lower φ-k cutoffs of 7% porosity and 0.1 md permeability, only the zone

around 2663.39m could be effective gas reservoirs, supplement by the presence of thin artificial fractures.

In well A-H1, reservoir quality of the cored zone in this well is presented in Table 4.3 and its average porosity (φ) and permeability (k) is fairly distributed. At 3026.40 m depth the reservoir presents 15.6 % porosity (φ) and 12 md permeability (k) maximum. The reservoir is dominated by φ < 0.1% and k < 2 md. Using an economic cutoff of 10% porosity and 1 md permeability (suitable for liquid hydrocarbons); and 7% porosity and 0.1 md permeability (suitable for gaseous hydrocarbons), this cored zone could be effective hydrocarbon reservoirs.

In well A-K1, reservoir quality of the cored zones in these well is presented in Table 4.3 and varies from moderate (φ = 22.4%, k = 30 md) to poor (φ < 10%, k < 1 md). The average porosity (φ) and permeability (k) is fairly distributed. Using an economic cutoff of 10% porosity and 1 md permeability (suitable for liquid hydrocarbons); and 7% porosity and 0.1 md permeability (suitable for gaseous hydrocarbons), this cored zone could be effective hydrocarbon reservoirs.

In well K-A2, reservoir quality of the cored zones in these well is presented in Table 4.3 and they all plot at poor distribution indicating φ < 0.5%, k < 0.5 md. Application of an economic cutoff of 10% porosity and 1 md permeability suitable for liquid hydrocarbons; and a lower cutoff of 7% porosity and 0.1 md permeability suitable for gas hydrocarbons could not be possible in this reservoir. Production of either liquid or gaseous hydrocarbons will require reservoir stimulation to enhance flow capacity.

CHAPTER FIVE: WELL LOG ANALYSIS

5. Well Log Analysis: interpretation and results

5.1. Introduction to well log analysis

Petrophysical log interpretation play a pivotal role in the geological decision-making process in petroleum development cycle. Its interpretation helps to understand rock porosity, fluid saturation and permeability of which they're parameters needed to quantify the amount of hydrocarbon present in a well. These parameters are inversely calculated from well logs as they're not direct measure of the rock. Core analysis is only reservoir assessment tool that directly measure rock formation properties. The analysis determines porosity, permeability, grain-size distribution, grain density, mineral composition, sensitivity of fluids, and effect of overburden stress. Calibration of the well logs with core analyses provides a valuable basis for reservoir quality studies and enhances both field development and exploration drilling. Hence, the need for integrating core analyses results in chapter 4 with well logs interpretation in this chapter. The chapter will calculate reservoir storage and flow capacity of the hydrocarbon producing intervals; and estimate their recoverable.

5.2. Integration of core analyses results with well log analyses

Integration of well information both petrographic and petrophysical analysis plays an integral role in reservoir quality evaluation. This integration also helps in the evaluation of initial water saturation for reserves estimation. Initial water saturation can be determined from electrical log resistivity measurements or measured directly from in-situ core samples. In addition to water saturation, porosity and permeability are reservoir properties that can be determined from both core and well log analyses. These reservoir properties are parameters that are needed for evaluation of hydrocarbon potential in the selected reservoir intervals. Integration of reservoir properties of the cored intervals with the well logs helps to understand the reservoir properties of the selected reservoir intervals in uncored zones. Reservoir intervals selected for this study that are covered by well logs (both cored and uncored) are presented in table 5.1 whereas reservoir intervals that are cored are presented in table 4.1 in chapter 4. Integration of core data and well log is presented in Annexture III.

5.3. Interpretation of well logs

One of the most important definitive rock physical characteristic from well logs evaluation is lithology. In terrigenous rock studies, well logs interpretation helps to identify thick sandy layers with shale layers below and above it. If sandstone identified is ≥ 10m thick with oil and gas in the pore throats, such layer is referred to as a potential hydrocarbon reservoir. In this chapter, petrophysical evaluations of hydrocarbon potential were conducted over five wells (A-J1, A-D1, A-H1, A-K1 and K-A2) in the study area. These wells were available with a suite of logs including gamma ray (GR), resistivity (LLD and LLS/ SFLU), Bulk density (DRHO and RHOB), neutron (NPHI), Sonic (DT) and caliper (CALI) among others logs (e.g. Figure 5.1) that are used to identify hydrocarbon potential. Potential reservoirs identified with these logs extends from syn-rift Hauterevian (119.5 Ma) to post-rift Cenomanian (94) ages in the lower cretaceous stage (Figure 5.2). As explained in chapter 3, the first step in a log interpretation is to identify potential sandstone reservoirs and define a clean sand and shale baseline on the gamma ray (GR) logs. This was achieved by observing the behaviour of the gamma ray log, maximum deflection to the right indicate a shale formation and maximum deflection to the left indicate clean sandstone. Identified reservoirs demarcated by blue dotted lines above and below. Deep true resistivity log was used to measure the presence of hydrocarbons in the reservoir whereas gas-effect from neutron and density porosity logs was used to confirm the presence of hydrocarbon.

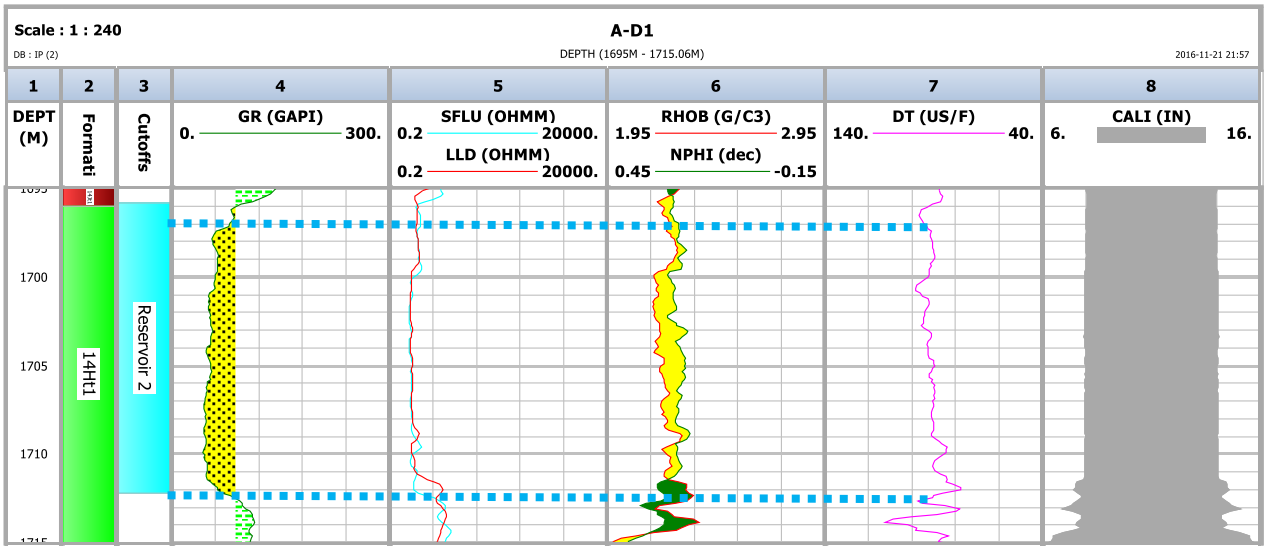

Figure 5.1: Log plot showing different log curves of well A-D1 in different tracks with track 5 indicating deep and shallow resistivity used for the determination of hydrocarbons presence in the resevoir.

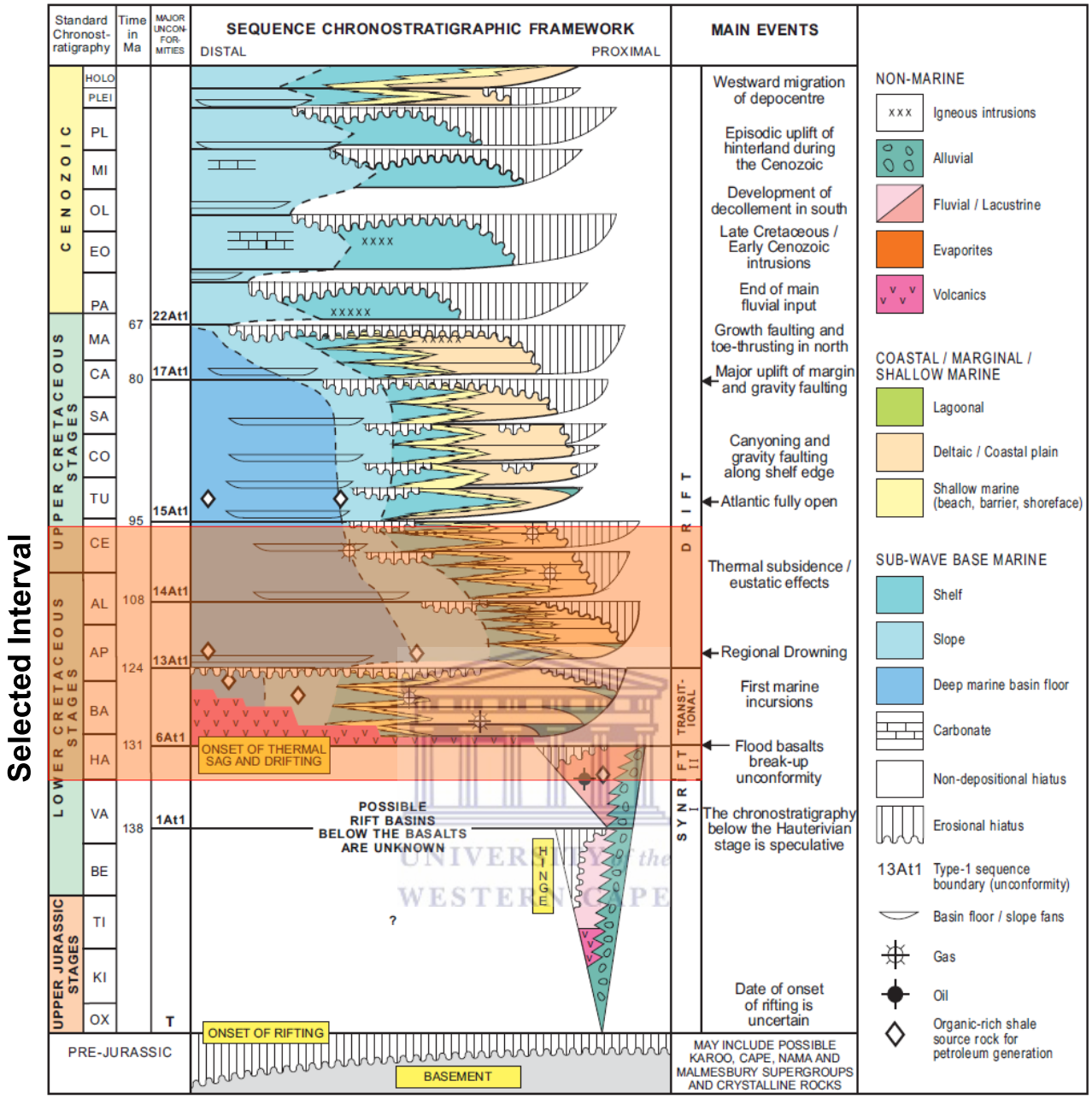

Figure 5.2: Generalised chronostratigraphy of the South African offshore Mesozoic basins (Broad et al., 2005), with the indication of target interval in this study

5.3.1. Well A-J1 wireline log Interpretation

In this well potential reservoirs were selected from post-rift (Albian) to syn-rift (Hauterevian - Barremian) sequences using gamma ray log (Gr). In the post-rift (Albian) sequence three reservoirs were identified which are Reservoir 4, 1618 – 1651m (Figure 6.3); Reservoir 5, 1755 – 1810m and Reservoir 6, 1827 – 1867m (Annexure IV, Figure 1-2. Track 5 in these annexured figures shows shallow (SFLC) and deep (ILDC) resistivity logs were deep resistivity log was used to measure the presence of hydrocarbon in

Reservoir 3, 5 and 6. Deep (ILDC) resistivity log presents very low resistivity in these resevoirs indicating water saturation.

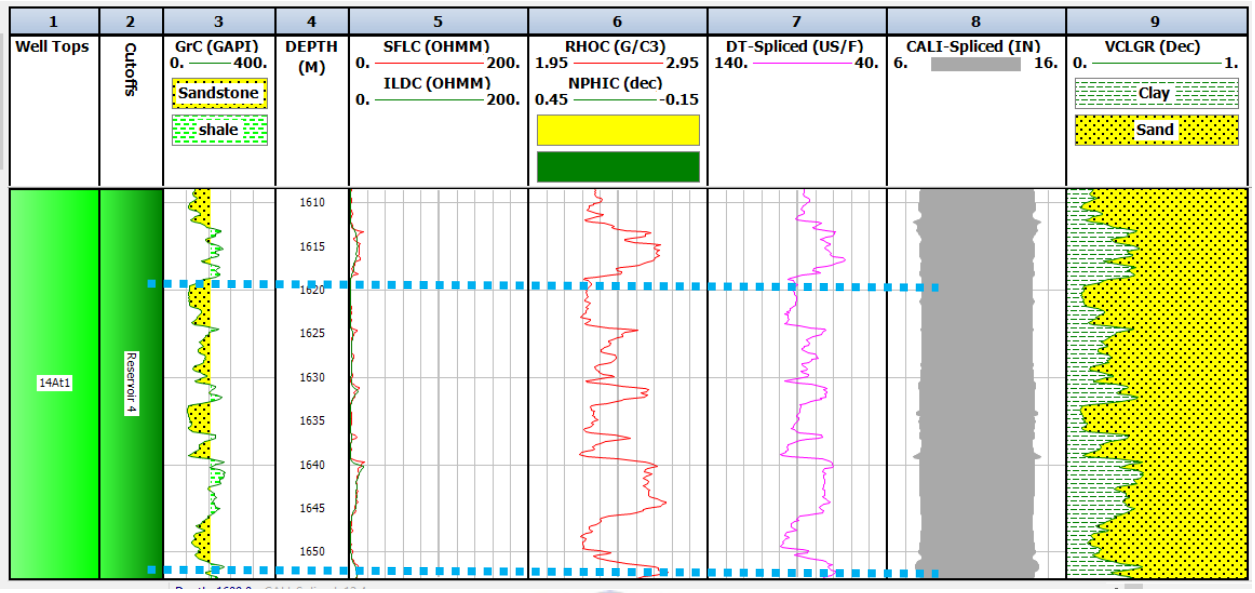

Figure 5.3: A-J1, Reservoir 4 selected reservoir interval between 1618 – 1651 m (33m) in the post-rift (Albian age) sequence.

Reservoir 7, 2047 – 2078m; Reservoir 12, 2987 – 3030m; Reservoir 13, 3035 – 3055m; Reservoir 14, 3065 – 3160m and Reservoir 15, 3188 – 3235m were selected from the syn-rift (Hauterevian - Barremian) sequence (Annexure IV, Figure 3 - 7). Reservoir 7, 12, 13, 14 and 15 assessment of hydrocarbon potential using deep (ILDC) resistivity log in Track 5 presents very low resistivity indicating water saturation. Deep (ILDC) resistivity log in Reservoir 14 presents generally low resistivity but with some increases at 3087m, 3105m, 3127m, 3140m and 3153m depth range correlating with thin claystone beds in gamma ray (GrC) log (Track 3). In Reservoir 15, this increase is between 3215 – 3225m intervals indicating the possibility of hydrocarbon accumulation. Gas effect assessment to confirm the presence of hydrocarbon was not performed.

5.3.2. Well A-D1 wireline log Interpretation

Six potential reservoirs were identified on post-rift (Aptian – Albian) sequence. These reservoirs are Reservoir 2, 1696 – 1712m; Reservoir 3, 1734 – 1774m; Reservoir 4, 1837 – 1865m; Reservoir 5, 2907 – 2921m; Reservoir 8, 2907 – 2921m; and Reservoir 9, 2907 – 2921m (Annexure IV, Figure 8 - 13). Track 5 in these annexured figures present shallow and deep resistivities (e.g. Figure 6.4) which measured the salinity of the mud and

hydrocarbon presence in the reservoir. Track 6 display density and neutron porosity logs. Assessment of hydrocarbon potential using resistivity logs and a combination of density and neutron porosity logs in Reservoir 2, 3, 4, 5, 8 and 9, presents water saturated reservoirs.

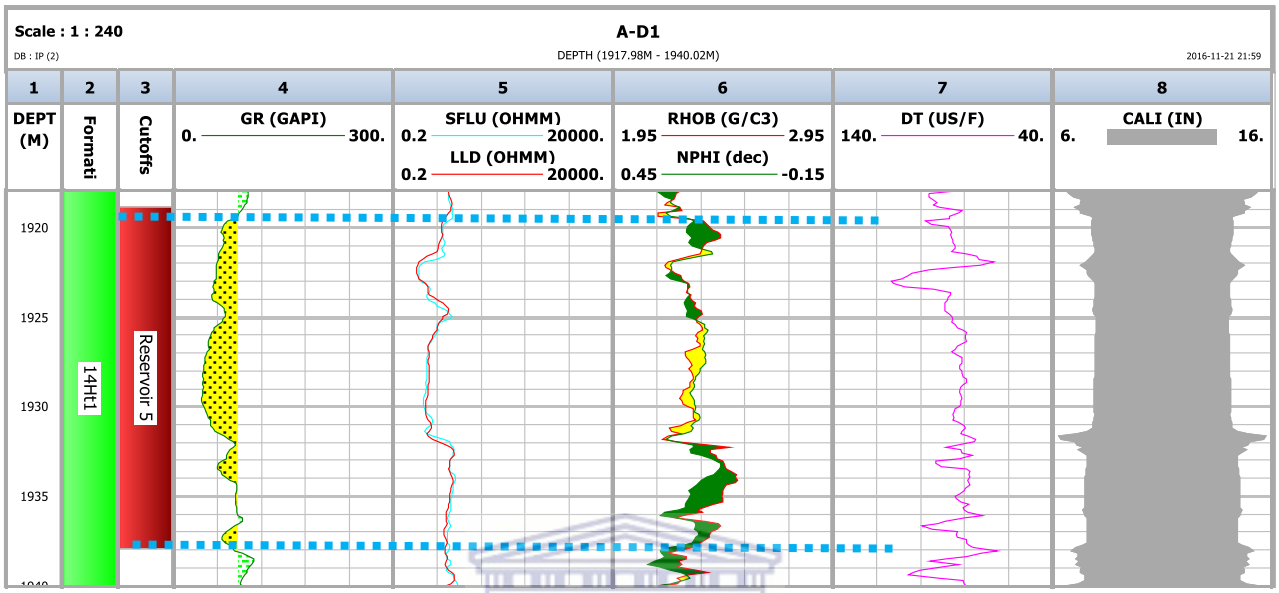

Figure 5.4: A-D1 selected reservoir interval between 1917 – 1940 m in the post-rift (Albian age) sequence.

5.3.3. Well A-H1 wireline log Interpretation

Eight potential reservoirs were identified on post-rift (Aptian – Albian) sequence in this well. Identified reservoir include Reservoir 3 & 4, 2790 – 2900m; Reservoir 5, 2905 – 3066m; Reservoir 6, 3074 – 3096; Reservoir 7, 3159 – 3221m; Reservoir 11, 3400 – 3413; Reservoir 15 & 16, 3711 – 3768m (Annexure IV, Figure 14 - 19). Hydrocarbon potential assessment of Reservoir 3, 4, 5, 6, 7 in Track 6 using deep resistivity in annxured Figure 14 – 17 present low resistivity indicating water saturated reservoirs whereas Reservoir 11, 15 & 16 in Figure 18 – 19 present high resistivity indicating hydrocarbon saturated reservoirs. The presence of hydrocarbon in Reservoir 11, 15 & 16 is supported by Neutron (NPHI_Spliced) - density (RHOB_Spliced) porosity logs cross-over (gas-effect) in Track 12 that confirms the presence of hydrocarbon.

5.3.4. Well A-K1 wireline log Interpretation

Five potential reservoir were identified on post-rift (Albian) sequence using in this well. Identified reservoirs are Reservoir 8, 3219 – 3241m; Reservoir 9, 3276 – 3288m;

Reservoir 10, 3355 – 3371m; Reservoir 11 & 12, 3460 – 3545m; Reservoir 13 & 14, 3556 – 3635m (Annexure IV, Figure 20 - 24). Assessment of hydrocarbon potential in these reservoirs using deep resistivity log in Track 5 of the annexured figures present high resistivity indicating hydrocarbon saturated reservoirs. The presence of hydrocarbon in reservoirs is supported by Neutron (NPHI_Spliced) - density (RHOB_Spliced) porosity logs cross-over (gas-effect) in Track 6 that confirms the presence of hydrocarbon.

5.3.5. Well K-A2 wireline log Interpretation

In this well eight potential reservoirs were identified on post-rift (Aptian – Albian) sequence. Identified reservoirs are Reservoir 2, 3084 – 3097m; Reservoir 3, 3010 – 3117m; Reservoir 4, 3182 – 3247m; Reservoir 6, 3765 – 3815m; Reservoir 7, 4505 – 4580m; Reservoir 8, 4829 – 4890m; Reservoir 9 & 10, 5340 – 5395m (Annexure IV, Figure 25 - 31). Reservoir 2, 3, and 4 hydrocarbon assessment using deep resitivity in Track 5 of the annexured figures present low resistivity indicating water saturated reservoir whereas Reservoir 6, 7, 8, 9 & 10 present high resistivity indicating hydrocarbon saturated reservoirs. The presence of hydrocarbon in Reservoir 6, 7, 8, 9 & 10 is supported by neutron (NPHI) - density (RHOB porosity logs cross-over (gas-effect) in Track 6 that confirms the presence of hydrocarbon.

5.4. Cut-off determination

Selected reservoir intervals evaluated for hydrocarbon potential in section 4.3 above are also evaluated for their hydrocarbon saturation, storage and flow capacity. Due to detrital clay matrix and authigenic clay occurrence during diagenesis selected reservoir interval has zones that inhibit flow capacity. Such non contributing zones of the reservoir can be determined petrophysically using the cut-off concept as explained by Worthington, 2008. The cut-off concept enables determination of the effective petrophysical properties of a rock in the presence of such poor zones. Cut-off parameters can be determined by identifying reference parameters that allow us to differentiate between the intervals that have the reservoir potential and those that do not have. There is no specific or single approach to determine the cut-off parameters (Worthington and Caseation, 2005). Magoba, 2014 noted that cut-off is normally applied to each calculated result to eliminate poor quality or non-productive zone. Non-productive zones/ non-reservoir rock may have the porosity and permeability that is too low and no hydrocarbon saturation (Opuwari, 2010). Rocks with sufficient permeability to flow hydrocarbons at commercially significant

rates are classified as net sandstone or net reservoir. If they produce hydrocarbon at commercially acceptable hydrocarbon/ water ratio, they are classified as pay reservoir (Suzanne and Robert, 2004).

To separate pay sand from non-pay sand there are typical cut-off values for formation parameters that are used, where maximum volume of shale is between 0.25 and 0.40, minimum porosity between 0.03 and 0.16, maximum water saturation between 0.30 and 0.70 and also the permeability between 0.1mD and 5.0mD. Commonly applied worldwide cut-off range of commercial producibility sandstone is usually set for both oil and gas. As applied in chapter 4 (on rock base analyses) under porosity and permeability analyses of the selected reservoirs; an economic cut-off of 10% porosity and 1md permeability was used specifically for A-J1 as it has tested oil; and a cut-off of 7% porosity and 0.1 md permeability for A-D1, A-K1, A-H1 and K-A2 wells for gas. Similar cut-offs are also applied on uncored reservoir intervals using petrophysical simulations. Permeability values of the uncored reservoirs were derived from regression equation. Reservoir intervals with porosity and permeability of less than the cut-off defined are regarded as a non-reservoir and any interval with values above the cut off is regarded as a potential reservoir. Cut-offs was applied to shale volume, porosity, water saturation and permeability respectively.

Thirty five reservoir intervals from five wells in this study were petrophysical evaluated for cut-offs and net-pay determination. Calculated results are presented in Table 6.2, the discussion of the cut-offs and net-pay values are further explained below.

Table 5.1: Petrophysical reservoir average report for cut-off and net-pay determinations

Well ID	Zone Name	Top (m)	Bottom (m)	Gross (m)	Net (m)	N/G (m)	Φ	K (mD)	S_w (%)	V_{Cl} (%)	S_{hc} (%)
A-J1	Reservoir 4	1448.40	1718.00	269.60	6.55	0.024	0.140	791.65	0.419	0.356	0.581
	Reservoir 5	1755.30	1813.30	58.00	5.94	0.102	0.132	45.811	0.465	0.350	0.535
	Reservoir 6	1826.70	1868.10	41.40	11.28	0.272	0.205	854.3	0.427	0.320	0.573
	Reservoir 7	1944.90	1966.70	21.80	7.93	0.364	0.242	41.319	0.411	0.306	0.589
	Reservoir 8	2037.40	2074.90	37.50	12.24	0.326	0.158	7.3024	0.460	0.277	0.540
	Reservoir 14	3034.00	3057.60	23.60	5.01	0.212	0.140	78.5	0.391	0.269	0.609
	Reservoir 15	3064.60	3173.40	108.80	48.86	0.449	0.139	8.3847	0.304	0.257	0.696
	Reservoir 16	3188.80	3201.00	12.20	5.64	0.462	0.141	6.35	0.221	0.283	0.779
A-D1	Reservoir 2	1695.80	1712.20	16.40	0.00	0.000	-	411.05	-	-	-
	Reservoir 3	1734.40	1712.20	35.70	0.00	0.000	-	49.728	-	-	-
	Reservoir 4	1838.00	1712.20	22.70	0.00	0.000	-	99.897	-	-	-
	Reservoir 5	1918.90	1937.90	19.00	0.00	0.000	-	43.632	-	-	-
	Reservoir 8	2906.70	2920.40	13.70	0.88	0.064	0.208	0.3138	0.424	0.314	0.686
	Reservoir 9	3082.90	3096.60	13.70	0.00	0.000	-	12.055	-	-	-
A-H1	Reservoir 3	2790.60	2872.80	82.20	2.28	0.028	0.240	2.3754	0.448	0.299	0.552
	Reservoir 5	2905.20	3066.00	160.80	5.93	0.037	0.185	1.2864	0.450	0.303	0.550
	Reservoir 6	3074.20	3094.70	20.50	3.50	0.171	0.208	1.6633	0.400	0.293	0.600
	Reservoir 7	3158.90	3220.60	61.70	2.13	0.034	0.142	0.83043	0.444	0.304	0.556
	Reservoir 11	3400.40	3412.70	12.30	1.98	0.161	0.134	0.48696	0.493	0.290	0.507
	Reservoir 15	3400.40	3728.70	17.00	1.52	0.089	0.133	0.34253	0.278	0.290	0.722
	Reservoir 16	3752.10	3767.80	15.70	4.10	0.261	0.184	1.3612	0.460	0.245	0.540
A-K1	Reservoir 9	3275.20	3287.80	12.60	7.20	0.571	0.146	165.06	0.217	0.705	0.783
	Reservoir 10	3354.20	3370.80	16.60	10.80	0.651	0.180	222.05	0.387	0.156	0.613
	Reservoir 11	3459.00	3489.60	30.60	0.80	0.026	0.103	55.474	0.278	0.378	0.722
	Reservoir 12	3494.00	3547.20	53.20	0.00	0.000	-	-	-	-	-
	Reservoir 13	3552.60	3576.00	23.40	0.20	0.009	0.101	64.839	0.455	0.060	0.545
	Reservoir 14	3581.60	3635.20	53.60	0.00	0.000	-	-	-	-	-
K-A2	Reservoir 2	2799.00	2980.00	181.00	10.00	0.055	0.144	-	0.448	0.288	0.552
	Reservoir 3	3010.00	3117.00	107.00	19.50	0.182	0.122	-	0.534	0.244	0.466
	Reservoir 4	3181.00	3117.00	66.00	19.00	0.288	0.136	-	0.431	0.277	0.569
	Reservoir 6	3766.00	3816.00	50.00	12.50	0.250	0.128	-	0.434	0.221	0.566
	Reservoir 7	4505.00	4580.00	75.00	39.00	0.520	0.143	-	0.385	0.221	0.615
	Reservoir 8	4829.00	4889.00	60.00	24.50	0.408	0.136	-	0.408	0.314	0.592
	Reservoir 9	5341.00	5368.00	27.00	0.00	0.000	-	-	-	-	-
	Reservoir 10	5378.00	5394.00	16.00	0.00	0.000	-	-	-	-	-

5.4.1. Porosity and permeability cut-off determination

A cut-off of 10% porosity and 1md permeability is applicable to oil reservoirs; and a cut-off of 7% porosity and 0.1md permeability is applicable to gas reservoirs. Any reservoir interval with the average values below the oil and gas cut-offs will be considered not a reservoir rock (low quality reservoir for hydrocarbon producibility). Average porosity and predicted permeability of the selected reservoirs are presented in Table 6.2 above. The quality of the reservoir in A-J1 well for oil producibility demonstrate fair (φ = 14.1%, k = 6.35 md at reservoir 14) to excellent (φ = 20.5%, k = 854.3 md at reservoir 6) variance of porosity and permeability. Application of the economic economic cutoff to these reservoirs presents good oil reservoir. A-D1 for gas producibility demonstrate fair reservoir quality (φ = 20.8%, k = 0.3 md at reservoir 08). Other reservoir zones couldn't be intepreted as they did not meet the cut-off requirement of the petrophysical model. A-H1 for gas producibility demonstrate fair reservoir quality with the minimum of φ = 13.3%, k = 0.34 md at reservoir 15; and maximum of φ = 24%, k = 2.37 md at reservoir 3. Average reservoir porosities and permeabilities of the selected reservoirs intervals are fair for gas production. A-K1 for gas producibility demonstrate good reservoir quality with the minimum of φ = 10.1%, k = 64.8 md at reservoir 13; and maximum of φ = 18%, k = 222md at reservoir 10. Average reservoir porosities and permeabilities of the selected reservoirs intervals are good for commercial gas production. K-A2, calculated results for this well are presented in Table 6.2 and all selected reservoirs couldn't meet the requiremet for the prediction of the permeability.

5.4.2. Volume of shale cut-off determination

The volume of shale cut-off is used to discriminate between reservoir interval and non-reservoir interval by allowing all rocks that have a volume of shale of equal or less than a certain value of the total reservoir volume. Using a cut-off of 40% as applied by Opuwari, 2010 and Magoba 2014, a reservoir rock with the volume of shale above this cut off will be regarded as non-reservoir whereas those with a volume of shale of 40% or less were classified as a reservoir. The average volume of shale was obtained from the volume of clay log curves calculated using gamma ray. The obtained results are presented in Table 6.2. Application of 40% cutoff to A-J1 reservoirs were all classified as good reservoirs. In well A-D1, only reservoir 8 was classified as a good quality reservoir. In well A-H1, reservoirs were all classified as good reservoirs as well. In well A-K2, Reservoir 9 presents the volume of clay of 70.5% making it non-resevoir; whereas

resevoirs 10, 11 and 13 are 15.6%, 37.8 and 06% resepectively, and classified as potential reservoir. In well A-K2 reservoirs, volume of clay are below 40% but were not classified as good because their permeability is negligible.

5.4.3. Water saturation cut-off determination

The discrimination between hydrocarbon bearing sandstones (pay) and water (wet) bearing intervals is established by defining the water saturation cut-off of 65%. Intervals that have a water saturation of 65% or less were assumed to be hydrocarbon bearing sandstones and those that have a water saturation of greater than 65% were assumed to be wet or non-productive intervals. The average volume of water saturation in the reservoirs were calculated and presented in Table 6.2 above. Application of the 65% cut-off to A-J1 reservoir intervals indicate hydrocarbon bearing sandstones as they all range below 65%. In well A-D2, only reservoir 8 indicates hydrocarbon bearing sandstone with 42.4% water saturation. Other reservoirs couldn't give the results for intepretation as they didn't meet the cut off requrement. In well A-H1, A-K1 and K-A2, all reservoirs are hydrocarbon bearing sandstones.

5.4.4. Hydrocarbon saturation determination

Using $S_h = 1 - S_w$ formula, hydrocarbon saturation was calculated using water saturation presented in Table 6.2 above. Hydrocarbon saturation results are also presented in Table 6.2. Well A-J1, have the minimum saturation value of 53.5% at reservoir 6 and a maximum saturation value of 77.9% at reservoir 16. Well A-D1, reservoir 8 has hydrocarbon saturation of 68.6%. Other reservoirs couldn't meet the cut-off requirement. Well A-H1, have the minimum saturaton value of 50.7% at reservoir 11 and a maximum saturation value of 72.2.9% at reservoir 15. Well A-K1, have the minimum saturation value of 54.5% at reservoir 13 and a maximum saturation value of 78.3% at reservoir 09. Well K-A2, Reservoir 9 & 10 couldn't meet the cut-off requirement for hydrocarbon saturation calculation whereas other reservoirs are hydrocarbon saturated.

5.4.5. Net-pay determination

As explained earlier, a net pay is defined as the interval of the rock that produce hydrocarbon at commercially acceptable hydrocarbon/water ratio and the gross is regarded as the reservoir interval that contains zone of which hydrocarbon can be produced and zones which does not favour the production of hydrocarbon. The

determination of the net pay is required to calculate the hydrocarbon pore feet, FHCP at the wellbore and also to calculate the overall reservoir original in place (OOIP) or (OGIP) original gas in place (Cobb et al., 1998). The net to gross ratio (N/G) is the total amount of pay footage divided by the total thickness of the reservoir interval (in simplicity the well is assumed to be vertical) (Cobb et al., 1998). N/G ratio of 1 means that the whole reservoir interval is pay footage (Cobb et al., 1998) and any interval that is considered as non-pay contributes nothing to the calculations of OOIP or OGIP reserves. The differences between gross and net pay is achieved by applying cut-off values in the petrophysical analysis. Here, cut-off values of porosity (≥ 0.1), volume of shale (≤ 0.4) and water saturation (≤ 0.65) were used to identify pay interval. That is reservoir interval with effective porosity equal or greater that 10%, shale volume of less or equal to 40 and water saturation of less or equal to 65 were regarded as the net pay interval. For A-J1, flag curves were created in the database by using cut-off limits. Net reservoir interval was defined by red colour and gross reservoir by green colour (Annexure V, Figure 1 – 5). The minimum net of these reservoirs is 5.01m at reservoir 14, with 14% porosity, 78.5 Permeability, 39.1% water saturation, 26.9% volume of clay and 60.9% hydrocarbon saturation. The maximum net of these reservoirs is 48.86m at reservoir 15, 13.9% porosity, 8.39 permeability, 30.4% water saturation, 25.7% volume of clay and 69.9% hydrocarbon saturation. For A-D1, net reservoir intervals are presented in Annexure V, Figure 6), most reservoir intervals in this well couldn't meet the cut-off requirement for petrophysical calculation of the net pay. The reservoir quality of this well is very poor. For A-H1, net reservoir intervals are presented in Annexure V, Figure 7 - 11). The minimum net of these reservoirs is 1.25m at reservoir 15, with 13.3% porosity, 0.34 permeability, 27.8% water saturation, 29% volume of clay and 72.2% hydrocarbon saturation. The maximum net of these reservoirs is 5.93m at reservoir 5, with 18.5% porosity, 1.28mD permeability, 45% water saturation, 30.3% volume of clay and 55% hydrocarbon saturation. The reservoir quality of this well is fairly good for starage, flow capacity for production of hydrocarbons. For A-K1, net reservoir intervals are presented in Annexure V, Figure 12 - 16). The minimum net of these reservoirs is 0.2m at reservoir 13, with 10.1% porosity, 64.8mD permeability, 45.5% water saturation, 06% volume of clay and 54.5% hydrocarbon saturation. The maximum net of these reservoirs is 10.8m at reservoir 10, with 18% porosity, 222mD permeability, 38.7% water saturation, 15.6% volume of clay and 61.3%% hydrocarbon saturation. The reservoir quality of this well is fairly good for starage, flow capacity for production of hydrocarbons except for reservoirs 12 and 14 that

did not meet the cit-off requirement. In K-A2 well eight reservoir intervals were petrophysical evaluated for cut-offs and net-pay determination. Calculated results are presented in Table 5.2 and all selected reservoirs couldn't meet the requiremet for the prediction of the permeability. These results fairly support the rock based results in chapter 4. Though the reservoir has stored some hydrocarbons, production will be challenging as the reservoirs do not have permeability. Discussion for cut-offs and net pay determination is not necessary as the reservoirs do not have permeabilities.

5.5. Storage capacity, flow capacity and reservoir hydrocarbon volume calculations

5.5.1. Storage and flow capacity calculations

The calculations of the storage capacity help to give an idea of how much the producing interval is able to store the hydrocarbons. This is simply obtained by multiplying the net thickness with the porosity whereas the flow capacity is used to determine how well the hydrocarbon can flow within the reservoir, by simply multiplying the net thickness with the permeability. The calculated flow and storage capacity results are presented in Table 6.3.

Of these thirty five reservoirs, only twenty six reservoir proved to be producing hydrocarbons. The evaluated intervals of A-J1 proved to have a high storage capacity with reservoir 15 showing the highest storage capacity of 2228.17 scf. Reservoir 6 of A-J1 proved to have a highest flow rate (capacity) of 31615.82mD-ft as compared to the rest. The significant variation in the flow rate (capacity) and storage capacity between the evaluated reservoirs is the results of different porosities, permeability and net thickness measured within the hydrocarbon producing intervals. The highest flow rate (capacity) is caused by the high permeability measured within reservoir 6 of A-J1 and highest storage capacity is due to high porosity and net thickness of reservoir 16 of A-J1.

Table 5.2: Summary results of the calculated flow and storage capacity

Well	Reservoir Name	Net (m)	Net (ft)	Φ (%)	Storage Capacity (scf)	K (mD)	Flow capacity (mD-ft)
A-J1	Reservoir 4	6.55	21.48	14	300.72	791.65	17012.16
A-J1	Reservoir 5	5.94	19.48	13.2	257.13	45.811	892.77
A-J1	Reservoir 6	11.28	37.00	20.5	758.50	854.3	31615.82
A-J1	Reservoir 7	7.93	26.01	24.2	629.44	41.319	1074.99
A-J1	Reservoir 8	12.24	40.15	15.8	634.37	7.3024	293.24
A-J1	Reservoir 14	5.01	16.43	14	230.02	78.5	1290.30
A-J1	Reservoir 15	48.86	160.30	13.9	2228.17	8.3847	1344.08
A-J1	Reservoir 16	5.64	18.50	14.1	260.85	6.35	117.50
A-D1	Reservoir 2	0	0	-	-	411.05	0
A-D1	Reservoir 3	0	0	-	-	49.728	0
A-D1	Reservoir 4	0	0	-	-	99.897	0
A-D1	Reservoir 5	0	0	-	-	43.632	0
A-D1	Reservoir 8	0.88	2.88	20.8	60	0.3138	0.90
A-D1	Reservoir 9	0	0	-	-	12.055	0
A-H1	Reservoir 3	2.28	7.48	24	179.52	2.3754	17.76
A-H1	Reservoir 5	5.93	19.45	18.5	359.82	1.2864	25.02
A-H1	Reservoir 6	3.5	11.48	20.8	238.78	1.6633	19.09
A-H1	Reservoir 7	2.13	6.98	14.2	99.11	0.83043	5.80
A-H1	Reservoir 11	1.98	6.49	13.4	86.96	0.48696	3.16
A-H1	Reservoir 15	1.52	4.98	13.3	66.23	0.34253	1.70
A-H1	Reservoir 16	4.1	13.45	18.4	247.48	1.3612	18.31
A-K1	Reservoir 9	7.2	23.62	14.6	344.85	165.06	3899.05
A-K1	Reservoir 10	10.8	35.43	18	637.74	222.05	7867.91
A-K1	Reservoir 11	0.8	2.62	10.3	27	55.474	145.60
A-K1	Reservoir 12	0	0	-	-	-	-
A-K1	Reservoir 13	0.2	0.65	10.1	6.56	64.839	42.54
A-K1	Reservoir 14	0	0	-	-	-	-
K-A2	Reservoir 2	10	32.80	14.4	472.32	-	-
K-A2	Reservoir 3	19.5	63.97	12.2	780.43	-	-
K-A2	Reservoir 4	19	62.33	13.6	847.68	-	-
K-A2	Reservoir 6	12.5	41.01	12.8	524.92	-	-
K-A2	Reservoir 7	39	127.95	14.3	1829.68	-	-
K-A2	Reservoir 8	24.5	80.38	13.6	1093.16	-	-
K-A2	Reservoir 9	0	0	-	-	-	-
K-A2	Reservoir 10	0	0	-	-	-	-

5.5.2. Recoverable hydrocarbon volume

Rzasa and Katz (1945) proposed a method which provides a means to calculate the gas in place volume in the absence of the area and thickness on which calculations are based on one acre of reservoir volume. The calculations and the Table of the hydrocarbon volumes for all reservoirs are shown below.

The formula used is: 43560* Φ*(1-Sw) where, Φ = Porosity, Sw = Water saturation and 43560 = Unit conversion factor.

Table 5.3: Calculated reservoir hydrocarbon volume of each reservoir

Well	Reservoir Name	Unit conversion factor	Porosity (Φ)	Hydrocarbon Saturation (Sw)	Volume (Cubic feet)
A-J1	Reservoir 4	43560	0.14	0.581	3543.1704
A-J1	Reservoir 5	43560	0.132	0.535	3076.2072
A-J1	Reservoir 6	43560	0.205	0.573	5116.7754
A-J1	Reservoir 7	43560	0.242	0.589	6208.95528
A-J1	Reservoir 8	43560	0.158	0.54	3716.5392
A-J1	Reservoir 14	43560	0.14	0.609	3713.9256
A-J1	Reservoir 15	43560	0.139	0.696	4214.16864
A-J1	Reservoir 16	43560	0.141	0.779	4784.58684
A-D1	Reservoir 2	43560	---	---	
A-D1	Reservoir 3	43560	---	---	
A-D1	Reservoir 4	43560	---	---	
A-D1	Reservoir 5	43560	---	---	
A-D1	Reservoir 8	43560	0.208	0.686	6215.48928
A-D1	Reservoir 9	43560	---	---	
A-H1	Reservoir 3	43560	0.24	0.552	5770.8288
A-H1	Reservoir 5	43560	0.185	0.55	4432.23
A-H1	Reservoir 6	43560	0.208	0.6	5436.288
A-H1	Reservoir 7	43560	0.142	0.556	3439.14912
A-H1	Reservoir 11	43560	0.134	0.507	2959.37928
A-H1	Reservoir 15	43560	0.133	0.722	4182.89256
A-H1	Reservoir 16	43560	0.184	0.54	4328.1216
A-K1	Reservoir 9	43560	0.146	0.783	4979.69208
A-K1	Reservoir 10	43560	0.18	0.613	4806.4104
A-K1	Reservoir 11	43560	0.103	0.722	3239.38296
A-K1	Reservoir 12	43560	---	---	
A-K1	Reservoir 13	43560	0.101	0.545	2397.7602
A-K1	Reservoir 14	43560	---	---	
K-A2	Reservoir 2	43560	0.144	0.552	3462.49728
K-A2	Reservoir 3	43560	0.122	0.466	2476.47312
K-A2	Reservoir 4	43560	0.136	0.569	3370.84704

K-A2	Reservoir 6	43560	0.128	0.566	3155.83488
K-A2	Reservoir 7	43560	0.143	0.615	3830.8842
K-A2	Reservoir 8	43560	0.136	0.592	3507.10272
K-A2	Reservoir 9	43560	---	---	
K-A2	Reservoir 10	43560	---	---	

The productivity calculations were performed for all hydrocarbons producing intervals. Table 5.4 above present the calculated results in cubic feet for each interval. Reservoir 8 of A-D1 shows the highest volume of hydrocarbons of 6215.4 whereas reservoir 13 of A-K1 showed the lowest volume of 2397.7 cubic feet. The volume of reservoir 8 of A-D1 was always expected to be higher because of the highest net pay thickness and porosity and the opposite applies to reservoir 13 of A-K1. On average, well A-J1 and A-H1 proved to be the best producing well whereas A-D1 and A-K1 are less producing wells.

CHAPTER SIX: CONCLUSIONS AND RECOMMENDATIONS

6. Conclusions and recommendations

6.1. Introduction

Sediments under the study were deposited during rifting to drifting stage that occured during late Jurassic to Cenomanian age. Studied reservoirs within rifting and drifting sequences were delineated from five wells through an integration of petrophysical and petropraphic approach. Core description provided good indication of facies for reservoir assessment whilist integrated with well logs.

6.2. Conclusions

- Well log interpretation identified a total of thirty five (35) reservoirs in uncored and cored intervals from all five wells (A-J1, A-D1, A-H1, A-K1 and K-A2) in both rifting and rifting sequences.
- Core description and petrographic analysis of the cored reservoirs identified nine lithofacies (clayey sandstone, wackestone, sandstone, sandy marlstone, pebbly sandstone, domomitic claystone, granular sandstone, sandy siltstone and sandy ironstone) that were deposited on fluvial, lacustrine, shallow and deep marine environments.
- Thin section analysis of these cored resevoirs revealed 60 – 80% major contributions of detrital mineralogy that constitutes quartz (monocrystalline and polycrystalline), lithics (Igneous, metamorphic and sedimentary), mica (muscovite and biotite), feldspar, plagioclase, organic materal, Accessory grains (such as zircon) and detrital clay. These minerals grains are mostly medium grained, moderately sorted, long grain contact, subangular to angular rounded grain shape, with moderate to strong compaction. Porosity and permeability reduction of these reservoir rocks was caused by diagenetic mineral occurrence that accounted 13 – 24 % to the total rock.
- Accreation of these authigenic minerals resulted from increased temperature following continual sediments compaction and geothermal flow heat. The minerals include overgrowth of quartz and feldspars, illite, kaolinite, chlorite, gluconite, siderite, pyrite, dolomite and calcite. Infill of these minerals has reduced intergranular pore space completely to zero at some reservoir zones whereas some were left with maximum of 11%.

- The presence of secondary porosity from fractures and mineral dissolution increased porosity to maximum of 21.8% and permeability to 183mD. Porosity and permeability of the overall reservoirs is dominated by negligible to poor porosity with the permeability averaging to moderate. The reservoirs of Albian and Cenomanian ages in the deep part of the basin were completely reduced to zero with no economic potential production of gas. Reservoir quality of Albian and Cenomanian ages at the continental shelf can support gas production but reservoirs at Hauterevian and Barremian was reduced to the level that cannot support oil production efficiently.
- An economic cut-off of 10% porosity and 1md permeability was used specifically for A-J1 as it has tested oil; and a cut-off of 7% porosity and 0.1 md permeability for A-D1, A-K1, A-H1 and K-A2 wells for gas. The quality of the reservoir in A-J1 well for oil producibility demonstrate fair (φ = 14.1%, k = 6.35 md at reservoir 14) to excellent (φ = 20.5%, k = 854.3 md at reservoir 6) variance of porosity and permeability. Application of the economic economic cutoff to these reservoirs presents good oil reservoir. A-D1 for gas producibility demonstrate fair reservoir quality (φ = 20.8%, k = 0.3 md at reservoir 08). Other reservoir zones couldn't be intepreted as they did not meet the cut-off requirement of the petrophysical model. A-H1 for gas producibility demonstrate fair reservoir quality with the minimum of φ = 13.3%, k = 0.34 md at reservoir 15; and maximum of φ = 24%, k = 2.37 md at reservoir 3. Average reservoir porosities and permeabilities of the selected reservoirs intervals are fair for gas production. A-K1 for gas producibility demonstrate good reservoir quality with the minimum of φ = 10.1%, k = 64.8 md at reservoir 13; and maximum of φ = 18%, k = 222md at reservoir 10. Average reservoir porosities and permeabilities of the selected reservoirs intervals are good for commercial gas production. K-A2, calculated results couldn't meet the requiremet for the prediction of the permeability.
- Fluids saturation assessed by deep resistivity and density-neutron logs identified the presence of hydrocarbons in only fourteen (14) reservoirs (A-J1, reservoir 15; A-D1, reservoir 8; A-H1, reservoir 11, 15 & 16; A-K1, reservoir 8, 9, 11, 12, 13 & 14; and K-A2, reservoir 6, 9 & 10) and the remainder charged with water. Calculation of hydrocarbon saturation in all 35 reservoirs revealed the maximum of 77.9% in A-J1, 68.6% in A-D1, 72.2% in A-H1, 78.3% in A-K1 and 61.5% in K-A2 on reservoir.
- The storage and flow capacity was calculated for the producing (pay sand) interval of the respective wells. Storage capacity shows how much the reservoir rock was able to store hydrocarbons whereas flow capacity indicated how much the rock was able to

allow fluid to flow through its pore spaces. Well A-J1 recorded an excellent total storage capacity of 5299.2 square cubic feet (scf) and an excellent total flow capacity of 53640.86 mD-ft, A-D1 recorded poor storage capacity of 60 scf and poor flow capacity of 0.9 mD-ft, A-H1 recorded moderate storage capacity of 1277.9 scf and a poor flow capacity of 90 mD-ft, A-K1 recorded an good storage capacity of 1016.15 scf and an excellent flow capacity of 11955.1 mD-ft and K-A2 recorded excellent storage capacity of 5548.19 with no flow capacity.

- Integrated approach applied to uncored zones revealed good ecomonic flow of hydrocarbons producibility from well A-J1, A-D1, A-K1 and A-H1 whereas K-A2 presented poor economic flow. Hydrocarbons flow capacity supports pipeline development in well A-J1, A-D1, A-K1 and A-H1 with poor support in K-A2.

6.3. Recommendations

This study recommends the following further investigation:

- Possibilities of building a diagenetic porosity model for the study area, in order to gain a more insight into 3-D porosity distribution of the block
- Reservoir stimulation study to determine possibilities of increase permeability that will support economic flow of hydrocarbons.

REFERENCES

Adams, A. E., MacKenzie, W. S., and Guilford, C. 1984: Atlas of sedimentary rocks under the microscope. New York: John Wiley.

Ala, M.A. and Selley, R.C., 1997: The West African Coastal Basins. In: African Basins. Sedimentary Basins of the world, 3 edited by R.C Selley, Elsevier Science B.V., Amsterdam, 173-186.

Amigun, J.O. and Odole, O.A. 2013: Petrophysical Properties Evaluation for Reservoir Characterisation of SEYI Oil Field (Niger-Delta). International Journal of Innovation and Applied Studies. Vol. 3, p. 765-773.

Austin, J. A., Jr., and Uchupi, E., 1982: Continental-oceanic crustal transition off Southwest Africa. Am. Assoc. Petrol. Geol. Bull., 66, 1328 - 1347.

Bennion, D.B., Thomas, F.B. and Bietz, R.F., 1996: Determination of initial fluid saturations- A key factor in By-passed pay determination, 3-5.

Brown, A., 1997: Porosity variation in carbonates as a function of depth: Mississippian Madison Group, Williston Basin, in J.A. Kupecz, J. Gluyas, and S. Bloch, eds., Reservoir quality prediction in sandstones and carbonates: AAPG Memoir 69, p. 29–46.

Brown, L.F. Jr, Benson, J.M. & Brink, G.J. 1995: Sequence Stratigraphy in Offshore South Africa Divergent Basins. American Association of Petroleum Geologists, Studies in Geology, 41.

Bryant S.L., Cade C.A. and Mellor D.W. 1993a: Permeability prediction from geological models. AAPG Bull. 77, 1338-1350.

Broad, D.S., Jungslager, E.H.A., McLachlan, I.R. and Roux, J., 2005: Offshore Mesozoic Basins. In: M.R. Johnson, C. R. Anhaeusser and R. J. Thomas (Editors), The Geology of South Africa. Geological Society of South Africa/Council for Geosciences, 553–571.

Bruhn, C.H.L., Cainelli, C. and Matos, R.M.D. 1988: Habitat do petróleo e fronteiras exploratórias nos rifts Brasileiros: Boletim de Geociências da Petrobrás, v. 2, p. 217–254.

Budd A.F, Stemann T.A., and Johnson K.G., 1993: Late Cenozoic turnover in the Caribbean reef coral fauna. Abstr Prog, Paleont Soc Spec Publ 6: 43 pp.

Cabrera-Garzón, R., J.F. Arestad, K. Dagdelen, and T.L. Davis, 1997: Geostatistical simulation of reservoir porosity distribution from 3-D, 3-C seismic reflection and core data in the Lower Nisku Formation at Joffre Field, Alberta, in J.A. Kupecz, J. Gluyas, and S. Bloch, eds., Reservoir quality prediction in sandstones and carbonates: AAPG Memoir 69, p. 115–125.

Code, C.A., I.J. Evans, and Bryant, S.L., 1994: Analysis of permeability controls—a new approach: Clay Minerals, v. 29, p. 491–501.

Cobb, M.W and Marek, F.J., 1998: Net pay determination and waterflood depletion mechanisms, SPE 48952, in the Annual Technical Conference and Exhibition; 14.

Ebanks, W.J., 1990: Geology of the San Andres reservoir, Mallet lease, Slaughter field, Hockley County, Texas: implications for reservoir engineering projects, in D.G. Bebout and P.M. Harris, eds., Geologic and engineering approaches in evaluation of San Andres/Grayburg hydrocarbon reservoirs - Permian Basin: University of Texas Bureau of Economic Geology Publication, p. 75–85.

Emery, D., Myers, K.J., and Young, R., 1990: Ancient subaerial exposure and freshwater leaching in sandstones: Geology **18,** 1178 - 1181.

Evans, J., Cade, C., and Bryant, S., 1994: A geological approach to permeability prediction in clastic reservoirs, in J.A. Kupecz, J. Gluyas, and S. Bloch, eds., Reservoir quality prediction in sandstones and carbonates: AAPG Memoir 69, p. 91–101.

Galloway, W.E., 1974: Deposition and diagenetic alteration of sandstone in a Northeast Pacific arc-related basin: implications for graywacke genesis: Geological Society of America Bulletin, v. 85, p. 379–390.

Gerrard, I. and Smith, G.C., 1982: The post-Palaeozoic succession and structure of the south-western African continental margin. In: Watkins, J.S. and Drake, C.L. (Eds.), Studies in Continental Margin Geology. Mem. Am. Assoc. Petrol. Geol., 34, 49–74.

Glover, P, 2009: Petrophysics M.Sc. Course notes, University of the Aberdeen, Scotland.

Granado, P., De Vera, J., and McClay, K. R. 2009: Tectonostratigraphic evolution of the Orange Basin, SW Africa. Trabajos de Geología, Universidad de Oviedo, 29: 321-328.

Haq, B.U., Hardenbol, J. and Vail, P.R. 1988: Mesozoic and Cenozoic chronostratigraphy and eustatic cycles of sealevel change. *In:* Wilgus, C.K. *et al.* (Eds*.), Sea Level Change: an Integrated Approach*. Spec. Publ. Soc. Econ. Paleontol. Mineral, 42, 71–108.

Halley, R.B., and Beach, D.K., 1979: Porosity preservation and early freshwater diagenesis of marine carbonate sands (abs.): AAPG Bull., v.63, p. 460.

Hill, S and James-Rutledge, N., 2005: Distribution and Reservoir Quality of Cretaceous Sandstones in the Southern Orange Basin, Offshore West Coast South Africa. Prepared For BHP Billiton. Integrated Reservoir Solutions. Project No. J1164. 1 - 49.

Hirsch, K.K., Scheck-Wenderoth, M., Paton, D.A., Bauer, K., 2007: Crustal structure beneath the Orange Basin, South Africa. South African Journal of Geology 110 (2-3), 249–260.

International Energy Agency (IEA), 2013: World Energy Outlook

Jungslager, E.H.A., 1996: Geological evaluation of theremaining prospectivity for oil and gas of the pre-1At1 “synrift” succession in Block 9, Republic of South Africa.
Unpubl. SOEKOR Rep., 63 pp.

Jungslager, E. H. A., 1999: Petroleum habitats of the Atlantic margin of South Africa, in N. R. Cameron, R.M. Bate, and V. S. Clure, eds., the oil and gas habitats of the South Atlantic: Geological Society (London) Special Publication 153, p. 153– 168.

Jungslager, E.H.A., 1999a: Petroleum habitats of the Atlantic margin of South Africa. In: Cameron, N.R., Bate, R.H. and Clure, V.S. (Eds.), the Oil and Gas Habitats of the South Atlantic. Spec. Publ. Geol. Soc. London, 153, 153–168.

Jungslager, E.H.A., 1999b: New geological and petroleum insights gained from geophysical imaging along South Africa's western margin. Paper 14.4., S. Afr. Geophys. Assoc., 6th Bienn. Conf., 9 pp.

Ketzer, J.M.M. 2002: Diagenesis and sequence stratigraphy: An integrated Approach and Constrain Evolution of Reservoir Quality in Sandstone. Dissertation for the Doctor of Philosophy in Mineral Chemistry, Petrology and Tectonics at the Department of Earth Sciences, Uppsala University Sweden.

Kobesh, F.P., and Blizard, R.B., 1959: Geometric factors in sonic logging: Geophysics, v, 24, p. 64 – 76.

Kurkjy, K.A., 1988: Experimental compaction studies of lithic sands: Master's thesis, University of Miami, Miami, Florida.

Magoba, M., 2014: Petrophysical evaluation of sandstone reservoir of well E-AH1, E-BW1 and E-L1 central Bredasdorp Basin, Offshore South Africa. Msc thesis. University of the Western Cape, South Africa.

Mello, M.R., De Azambuja Filho, N.C., Bender, A.A., Barbanti, S.M., Mohriak, W., Schmitt, P., De Jesus, C.L., 2012: The Namibian and Brazilian southern South Atlantic petroleum systems: are they comparable analogues? Geological Society, London, Special Publications published. Doi: 10.1144/SP369.18

Mohaghegh, S., Balan, B. and Ameri, S., 1997: "Permeability determination from well log data", Paper SPE 30978 first presented at the 1995 exhibition in Morgantown, West Virginia, 17-21 September.

Moraes, M.S., 1989: Diagenetic evolution of Cretaceous–Tertiary turbidite reservoirs, Campos Basin, Brazil: AAPG Bulletin, v. 73, p. 598–612.

Muntingh, A., 1993: Geology, prospects in Orange Basin offshore western South Africa. Oil and Gas Journal 106–109.

Muntingh, A., and Brown Jr., L.F., 1993: Sequence stratigraphy of petroleum plays, postrift Cretaceous rocks (Lower Aptian to Upper Maastrichtian), Orange Basin, Western Offshore, South Africa. Siliciclastic Sequence Stratigraphy, Recent Developments and Applications. : In: Weimar, P., Posamentier, H. (Eds.), AAPG Memoir, 58. The American Association of Petroleum Geologists, Tulsa, Oklahoma, U.S.A., pp. 71–98.

Nagtegaal, P.J.C., 1980: Diagenetic models for predicting clastic reservoir quality: Barcelona, Revista del Instituto de Investigaciones Geologicas, v. 34, p. 5–19.

Opuwari, M. 2010: Petrophysical evaluation of the albian age gas bearing sandstone reservoir of the O-M field, Orange Basin, South Africa, Ph.D. thesis, University of the Western Cape, South Africa.

Pallatt, N., M.J. Wilson, and W.J. McHardy, 1984: The relationship between permeability and the morphology of diagenetic illite in reservoir rocks: Journal of Petroleum Technology, v. 36, p. 2225–2227.

Paton, D. A., Van der Spuy, D., di Primio, R. and Horsfield, B. 2008: Insights into the hydrocarbon system evolution of the Southern Orange Basin: Journal of South African Geology, v. 110, p. 261– 274.

Primmer, T.P., C.A. Cade, I.J. Evans, J.G. Gluyas, M.S Hopkins, N.H. Oxtoby, P.C. Smalley, E.A. Warren, and R.H. Worden, 1997: Global patterns in sandstone diagenesis: their application to reservoir quality prediction for petroleum exploration, in J. Kupecz, J.G. Gluyas, and S. Bloch, eds., Reservoir quality prediction in sandstones and carbonates: AAPG Memoir 69, p. 61–78.

Prosser, D.J., Dawes, J.A., Fallick, A.E. and Williams, B.P.J., 1993: Geochemistry and diagenesis of stratabound calcite cement layers within the Rannoch Formation of the Brent Group, Murchison Field, North Viking Graben (Northern North Sea): Sedimentary Geology, v. 87, p. 139–164.

Rider, M.H., 1996: The geological interpretation of well logs. Petroleum Exploration consultant Rider-French consultant Ltd Cambridge and Sutherland. Halsted press, a division of John Wiley and Sons, New York. pp. 147 - 167.

Rider, M.H., 2002: The Geological interpretation of well logs. Second edition, p1.

Rowsell, D.M. and De Swardt, A.M.J., 1976: Diagenesis in Cape and Karoo sediments, South Africa, and its bearing on their hydrocarbon potential. Transactions of the Geological Society of South Africa 79 (1), 81-133.

Russel W.L., 1944: The Total Gamma- Ray Activity of Sedimentary Rocks as indicated by Geiger-Counter Determinations. Geophysics, April 1944.

Rzasa, M.J. and Katz, D.L., 1945: Calculations of static pressure gradients in gas wells: Transaction AIME, 160, p. 100.

Saller, A. H., Budd, D. A. and Harris, P. M., 1994: Unconformities and porosity development in carbonate strata: ideas from a Hedberg conference: AAPG Bulletin, v. 78, p. 857–871.

Scherer, M., 1987: Parameters influencing porosity in sandstones: a model for sandstone porosity prediction: AAPG Bulletin, v. 71, p. 485–491.

Schlumberger, 1972: The essentials of log interpretation, practice, Schlumberger Ltd, Paris, France.

Schmoker, J., and Gautier D.L., 1988: Sandstone porosity as a function of thermal maturity: Geology, v. 16, p. 1007–1010.

Scholle, P.A. and Halley, R.B., 1985: Burial diagenesis: out of sight, out of mind, Schneidermann, N. and Harris, P.M., eds., Carbonate cements. Society of Economic Paleontologists and Mineralogists, Special Publication, no. 36, p. 309–334.

Simandoux, P., 1963: Dielectric Measurements on Porous Media: Application to measurement of water saturation. Study of the behaviour of argillaceous formation. SPWLA, Houston, vol; 97-124.

Sneider, R.M., 1990: Introduction: reservoir description of sandstones, in J.H. Barwis, J.G. McPherson, and J.R.J. Studlick, eds., Sandstone petroleum reservoirs: New York, Springer-Verlag, p. 1–3.

Sombra, C.L., and Chang, H.K., 1997: Burial history and porosity evolution of Brazilian Upper Jurassic to Tertiary sandstone reservoirs, in J.A. Kupecz, J. Gluyas, and S. Bloch, eds., Reservoir quality prediction in sandstones and carbonates: AAPG Memoir 69, p. 79–89.

Soekor, 1994a: Orange Basin. *Rep. S. Afr. Licensing Round Inf. Brochure,* 18 pp.

Soekor, 1994b: Outeniqua Basin. *Rep. S. Afr. Licensing Round Inf. Brochure,* 52 pp.

Stoudt, E.L., and Harris, P.M., 1995: Hydrocarbon reservoir characterization: geologic framework and flow unit modeling: SEPM Short Course 34, 357 p.

Suzanne, G.C. and Robert, M.C., 2004: Petrophysics of the Lance Sandstone Reservoirs in Jonah Field, Sublette County, Wyoming. AAPG Studies in Geology 52 and Rocky Mountain Association of Geologists 2004 Guidebook; 226-227.

Tinker, T., de Wit, M. and Brown, R., 2008: Linking source and sink: Evaluating the balance between onshore erosion and offshore sediment accumulation since Gondwana break-up, South Africa. Tectonophysics, 455, 94–103.

Tittman, J., and Wahl, J.S., 1965: The physical foundations of formation density logging (Gamma-Gamma): Geophysics, v. 30, p. 284-294.

Tyler, N., Galloway, W.E., Garrett, C.M., and Ewing, T.E., 1984: Oil accumulation, production characteristics, and targets for additional oil recovery in major oil reservoirs of Texas: University of Texas Bureau of Economic Geology Circular 84-2, 31 p.

Van der Spuy, D., 2003: Aptian source rocks in some South African Cretaceous basins. In: Arthur, T.J., MacGregor, D.S. and Cameron, N.R. (Eds.) Petroleum Geology of Africa: New Themes and Developing Technologies. Spec. Pub. Geol. Soc. London, 207, 185–202.

Welton J.E., 2003*:* SEM Petrology Atlas*,* 2nd Edition*.* Methods in Exploration Series, Am Assoc Petrol Geol Method Explor Ser 237.

INTERNET REFERENCES

https://www.esi-africa.com/news/south-africa-s-electricity-demand-exceeds-available-supply/

http://www.southafrica.info/business/investing/energy-190315.htm#.V6SJivl97mE

APPENDIX I – CORE PHOTOGRAPHS

A-J1 Core Photographs

Core #1

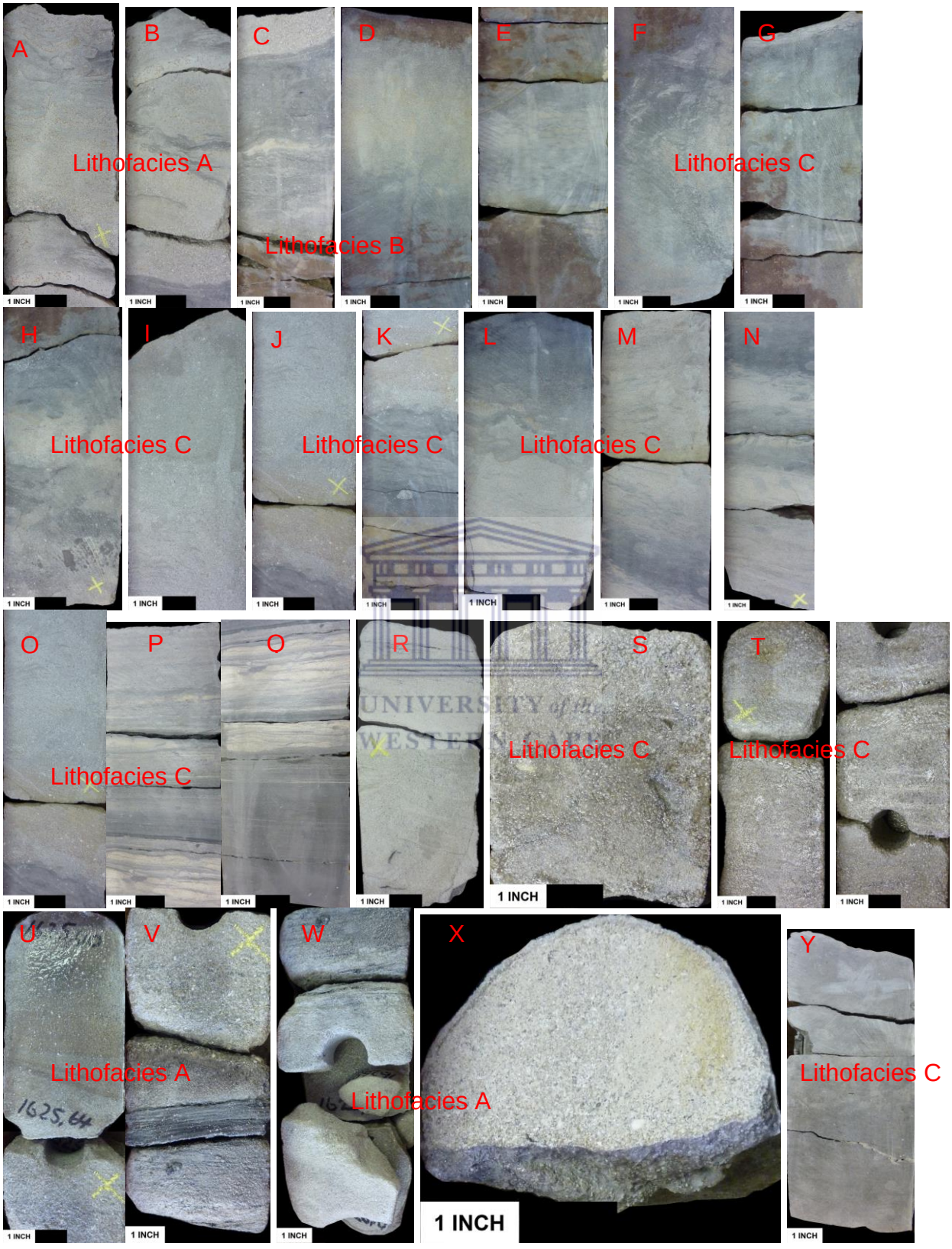

Figure 1: Core Photographs of A-J1 displaying samples (A, B, C, B, E, F, G, H, I, J, K, L, M, N, P, Q, R, S, R, U, V, W, X and Z) cored from 1617.08m – 1627.30m.

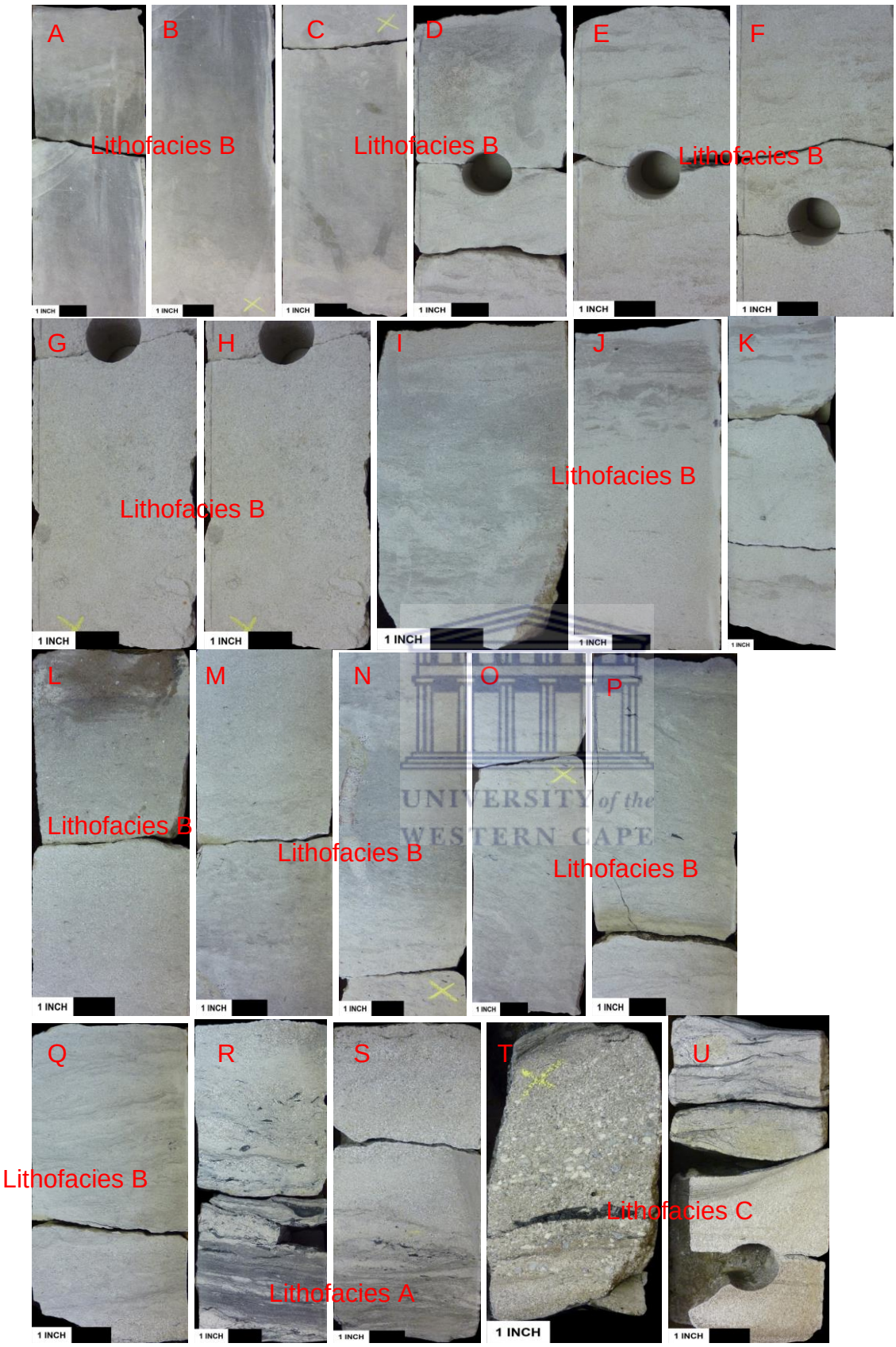

Figure 2: Core Photographs of A-J1 displaying samples (A, B, C, B, E, F, G, H, I, J, K, L, M, N, O, P, Q, R, S, R, and U) cored from 1627.39m – 1632.50m.

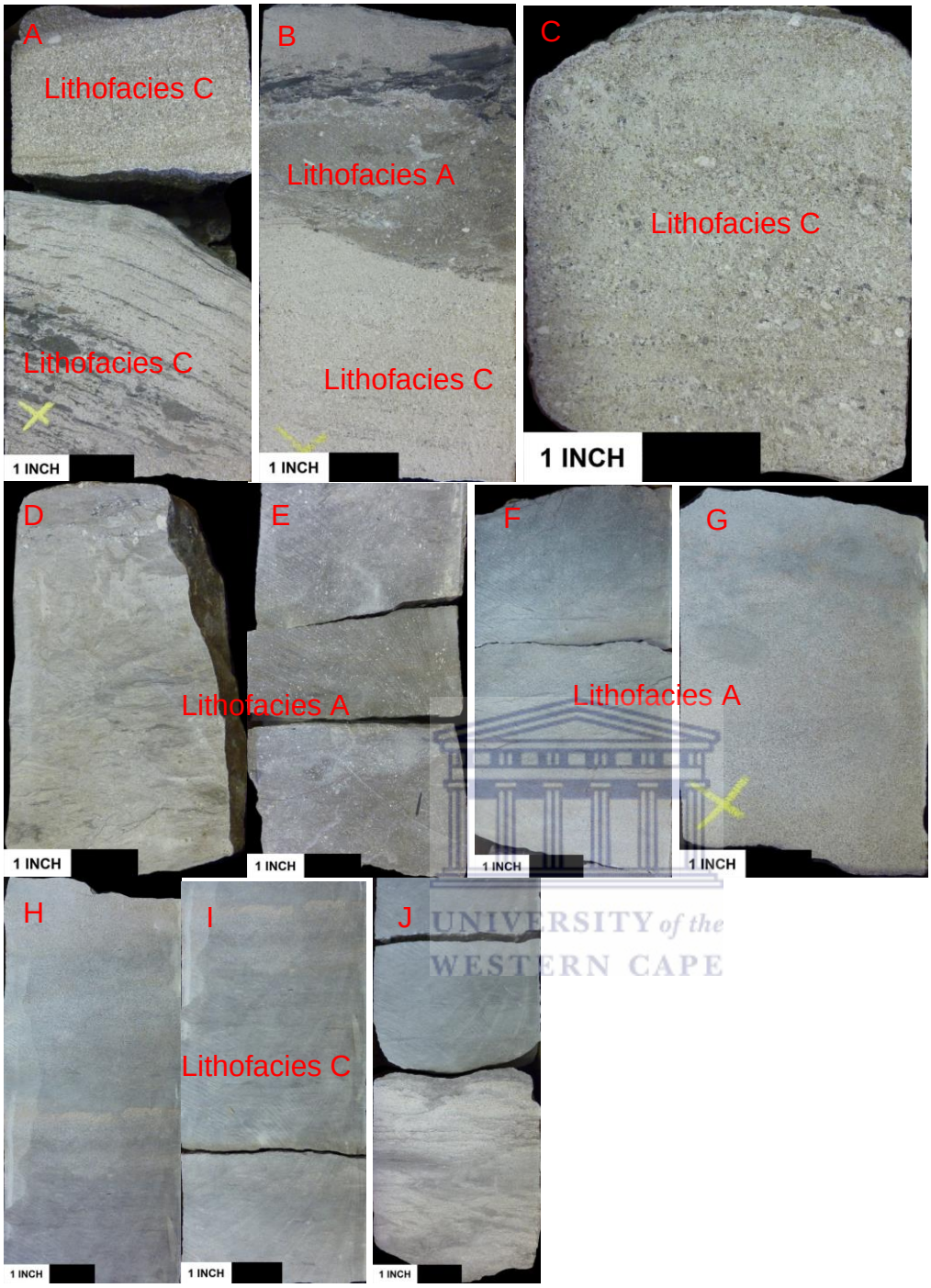

Figure 3: Core Photographs of A-J1 displaying samples (A, B, C, B, E, F, G, H, I, and J) cored from 1632.55m – 1635.10m.

Core #2

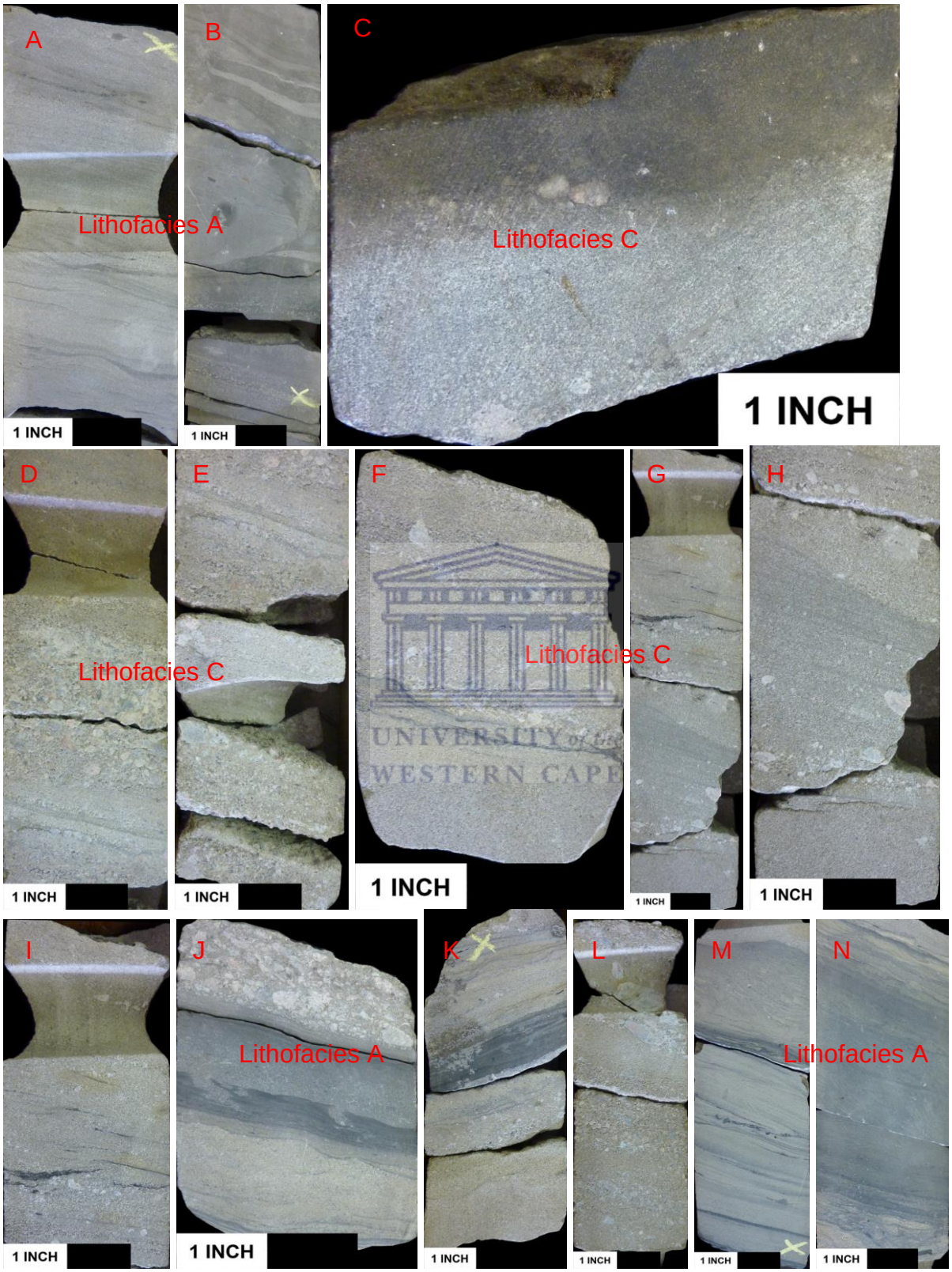

Figure 4: Core Photographs of A-J1 displaying samples (A, B, C, B, E, F, G, H, I, J, K, L, M and N) cored from 3191.20m – 3197.36m.

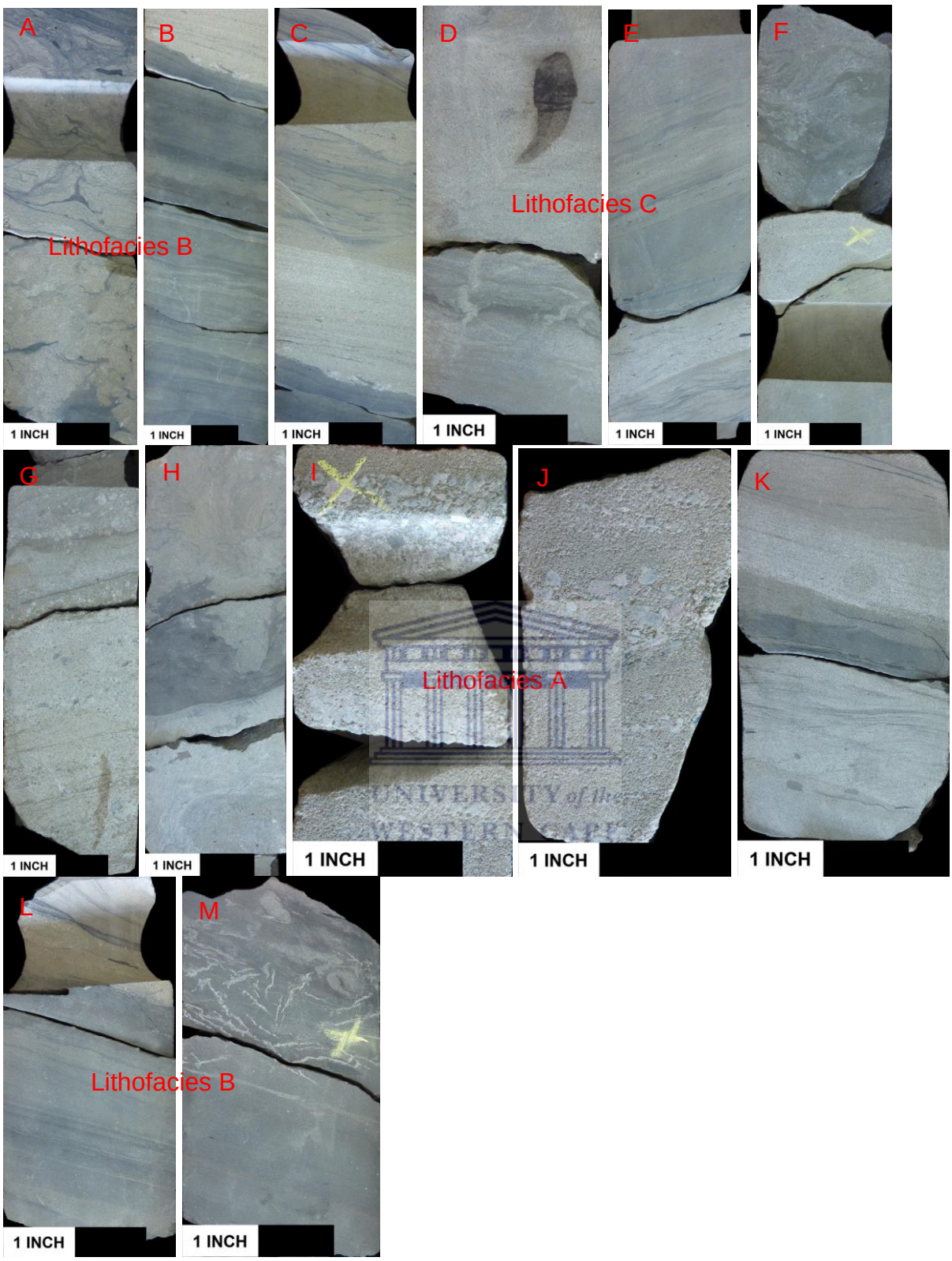

Figure 5: Core Photographs of A-J1 displaying samples (A, B, C, B, E, F, G, H, I, J, K, L and M) cored from 3196.68m – 3200.98m.

Core #3

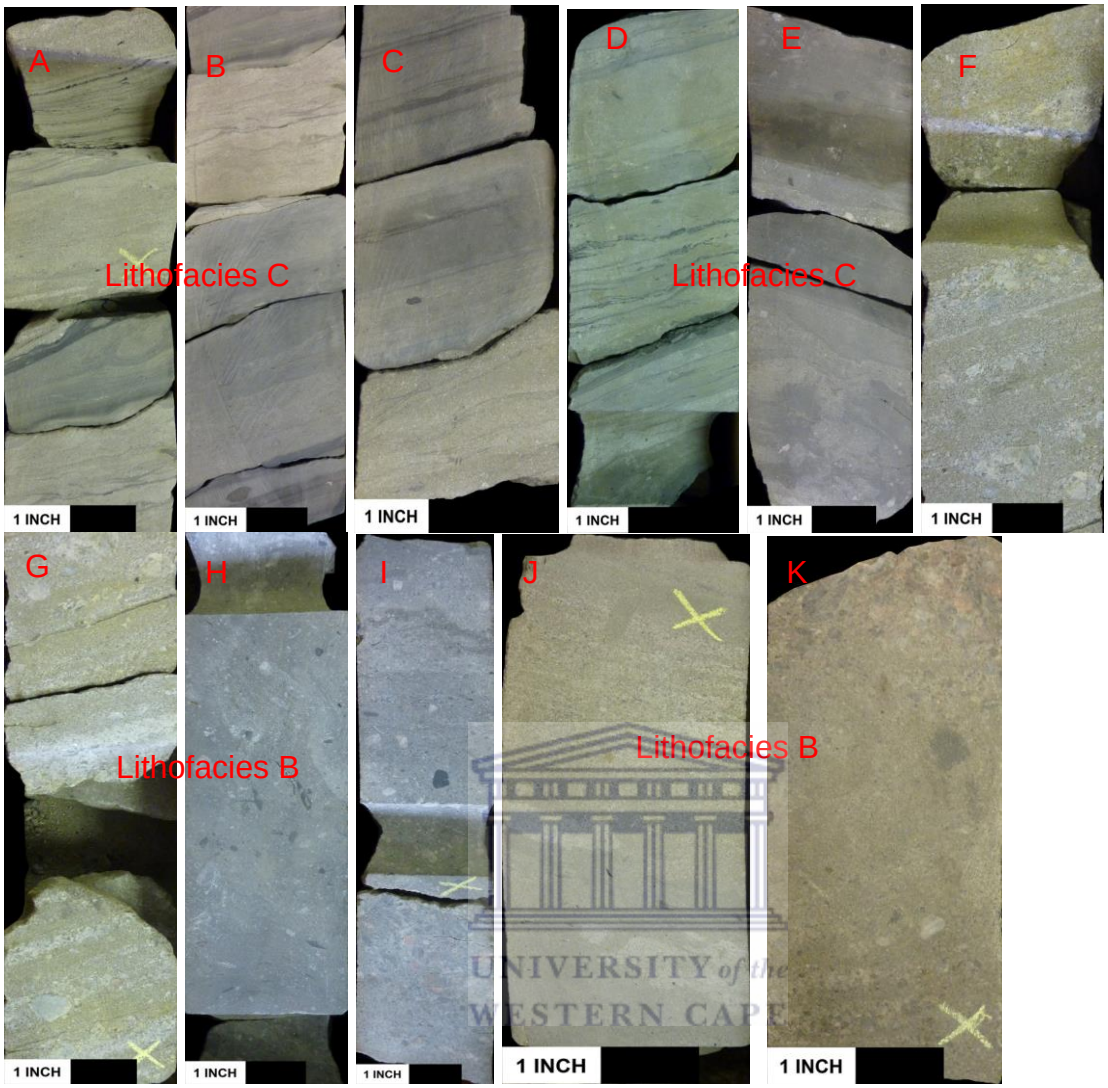

Figure 6: Core Photographs of A-J1 displaying samples (A, B, C, B, E, F, G, H, I, J and K) cored from 3205.31 – 3215.40m.

Core #4

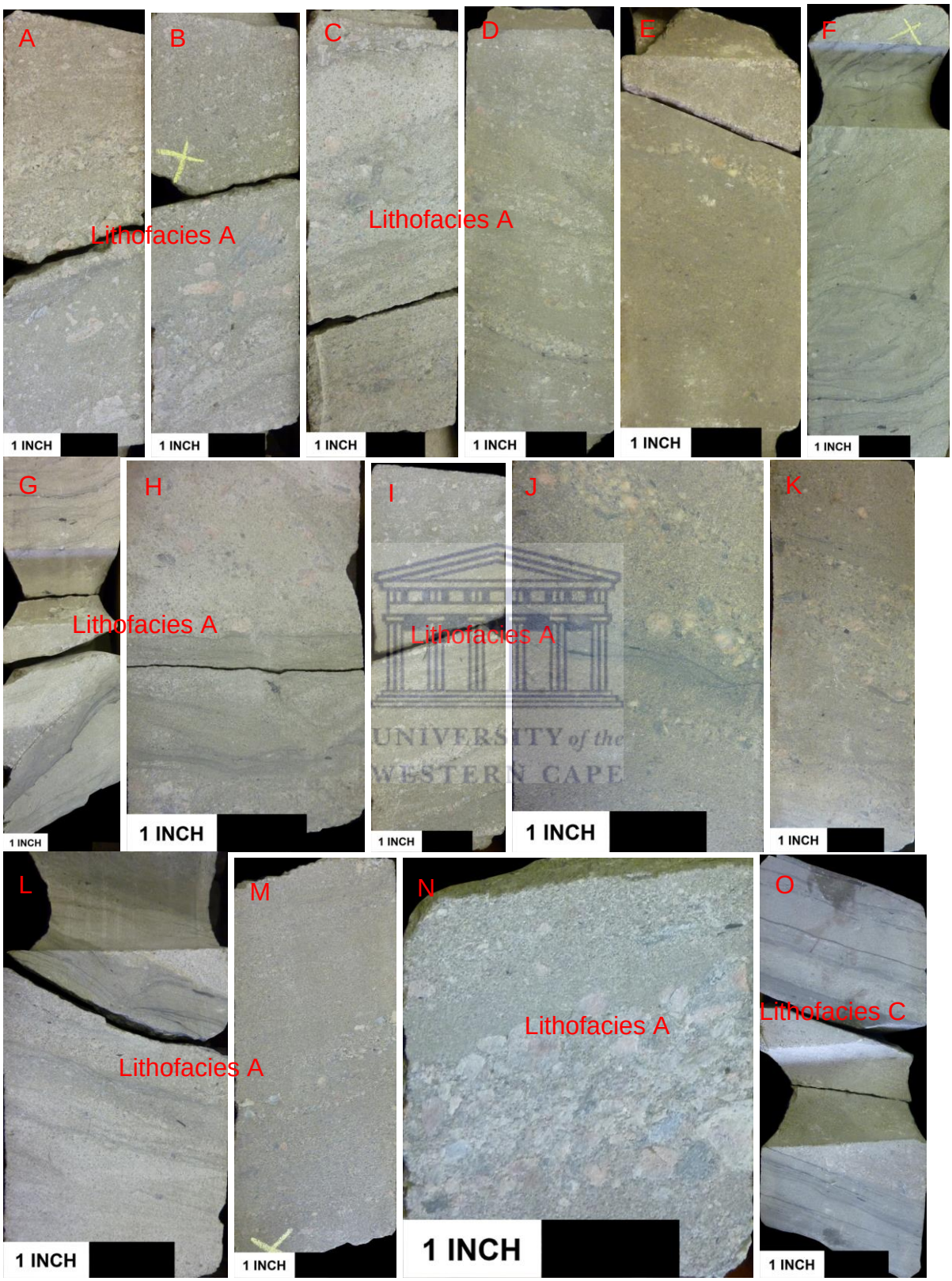

Figure 7: Core Photographs of A-J1 displaying samples (A, B, C, B, E, F, G, H, I, J, K, L, M, N and O) cored from 3217.63m – 3222.18m.

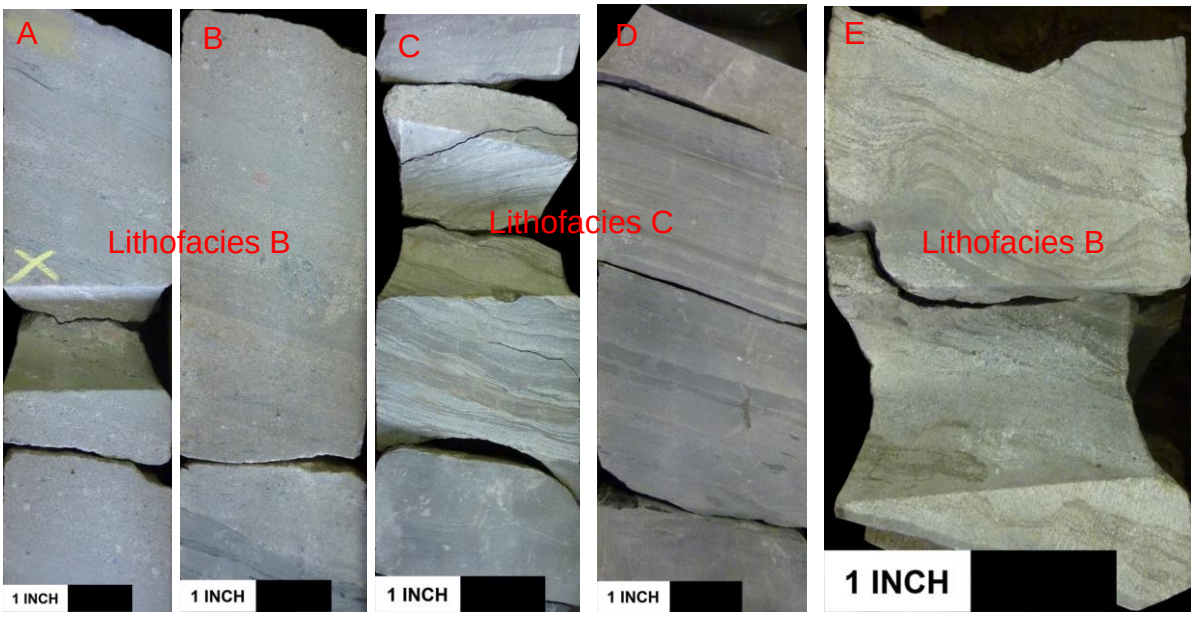

Figure 8: Core Photographs of A-J1 displaying samples (A, B, C, B and E) cored from 3222.77m - 3227.26m.

Core #5

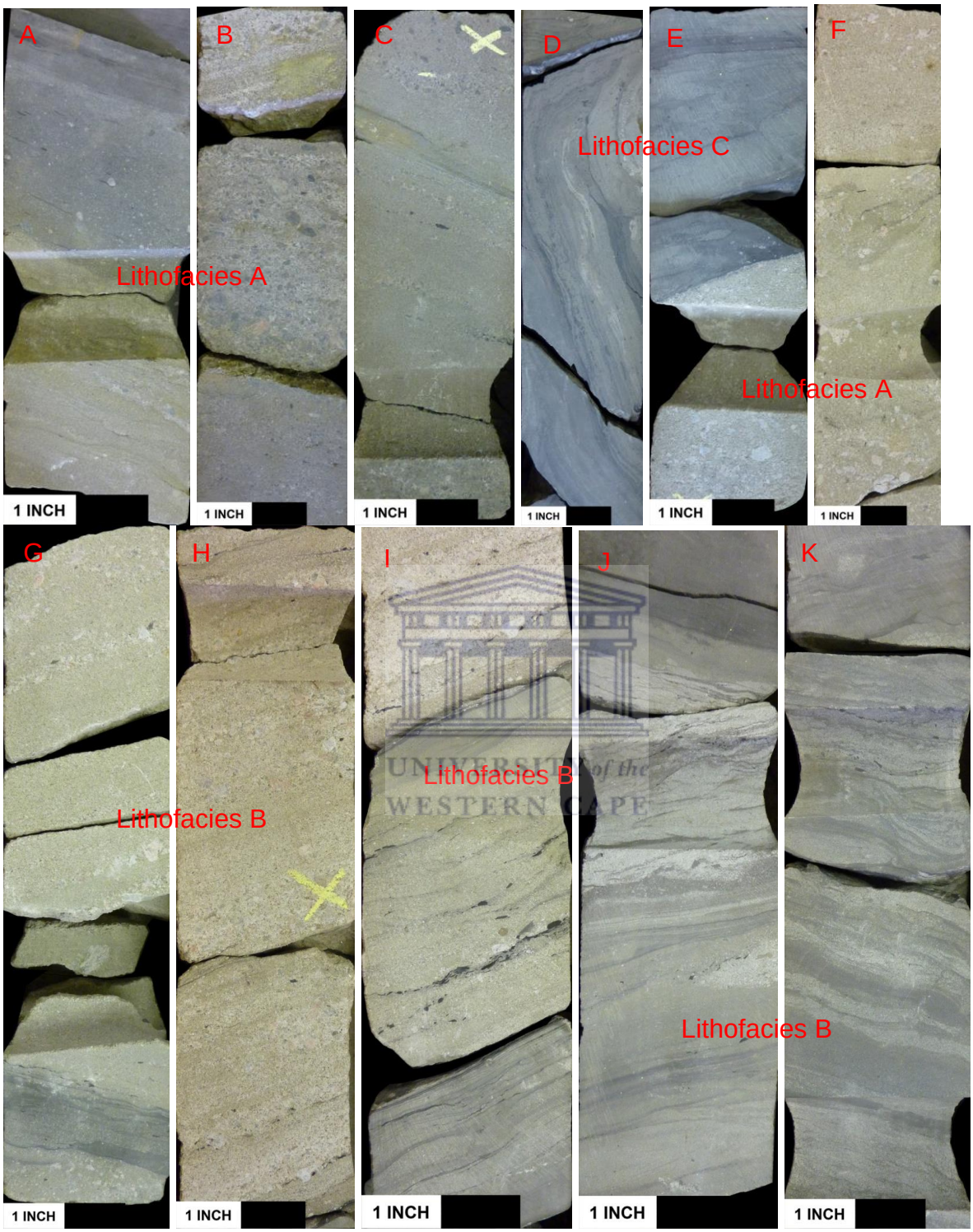

Figure 9: Core Photographs of A-J1 displaying samples (A, B, C, B, E, F, G, H, I, J and K) cored from 3231.27m – 3240.42m.

Core #6

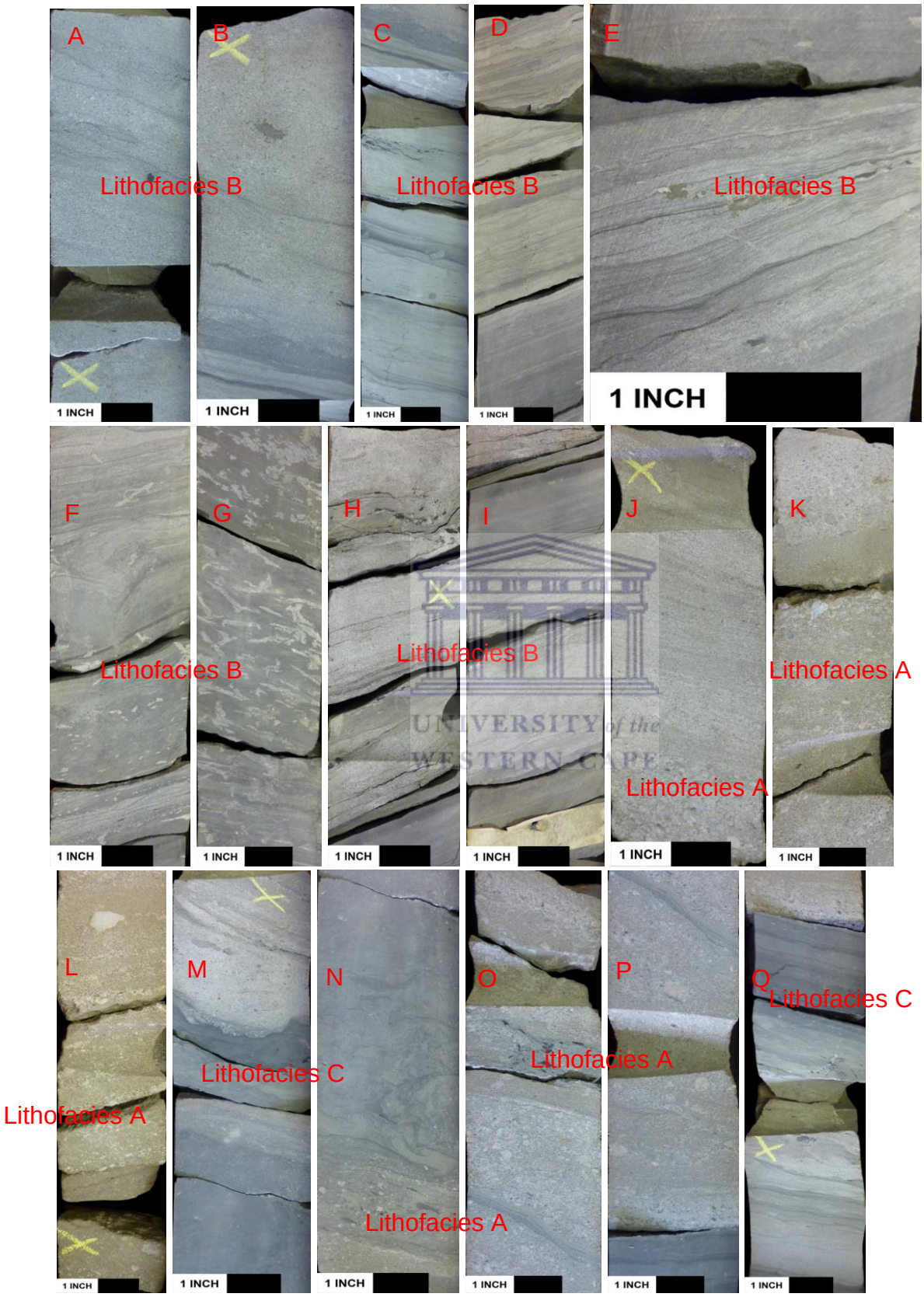

Figure 10: Core Photographs of A-J1 displaying samples (A, B, C, B, E, F, G, H, I, J, K, L, M, N, O, P and Q) cored from 3244.79m – 3255.52m.

A-D1 Core Photographs

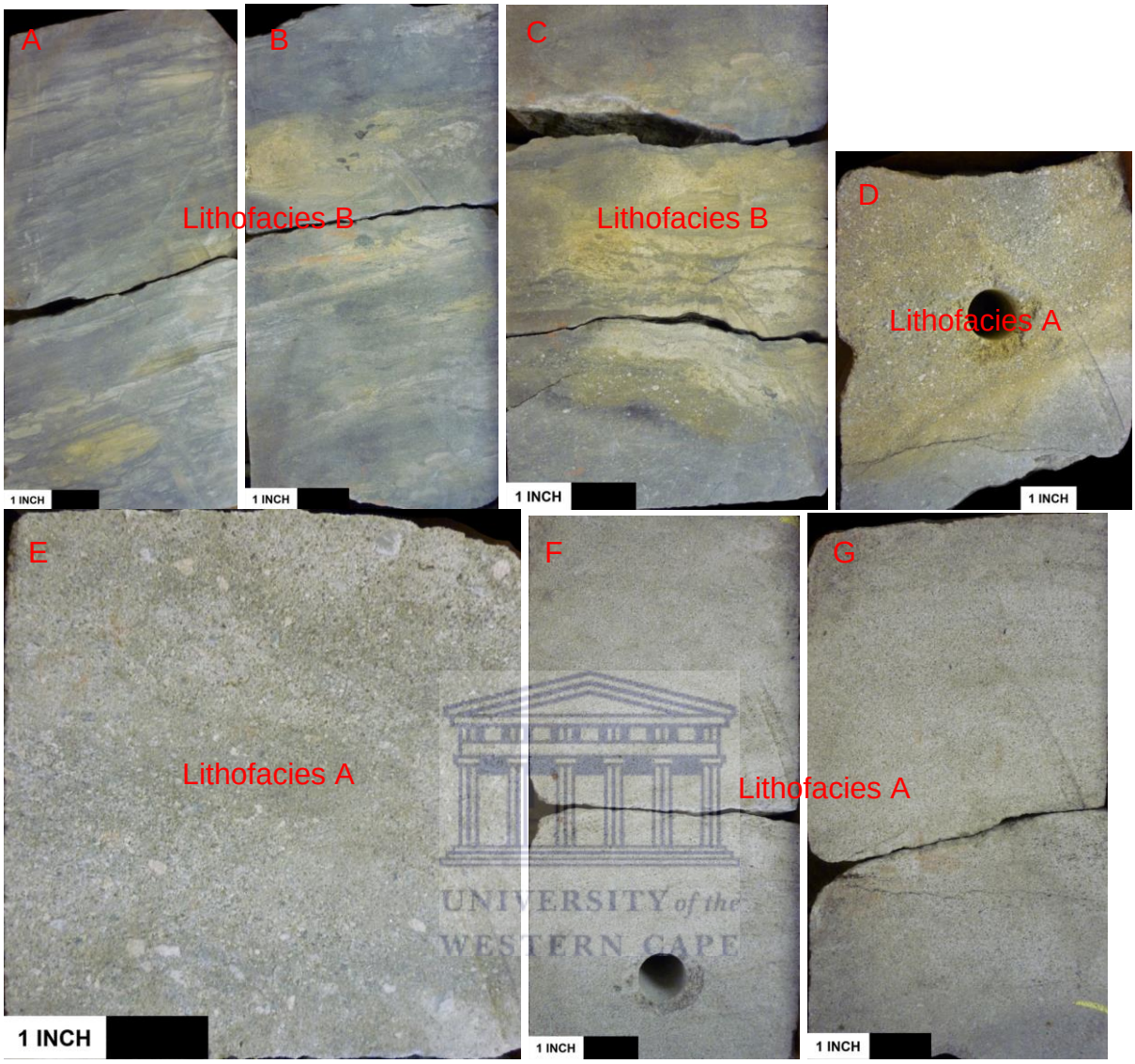

Figure 11: Core Photographs of A-D1 displaying samples (A, B, C, B, E, F and G) cored from 2661.80m – 2668.80m.

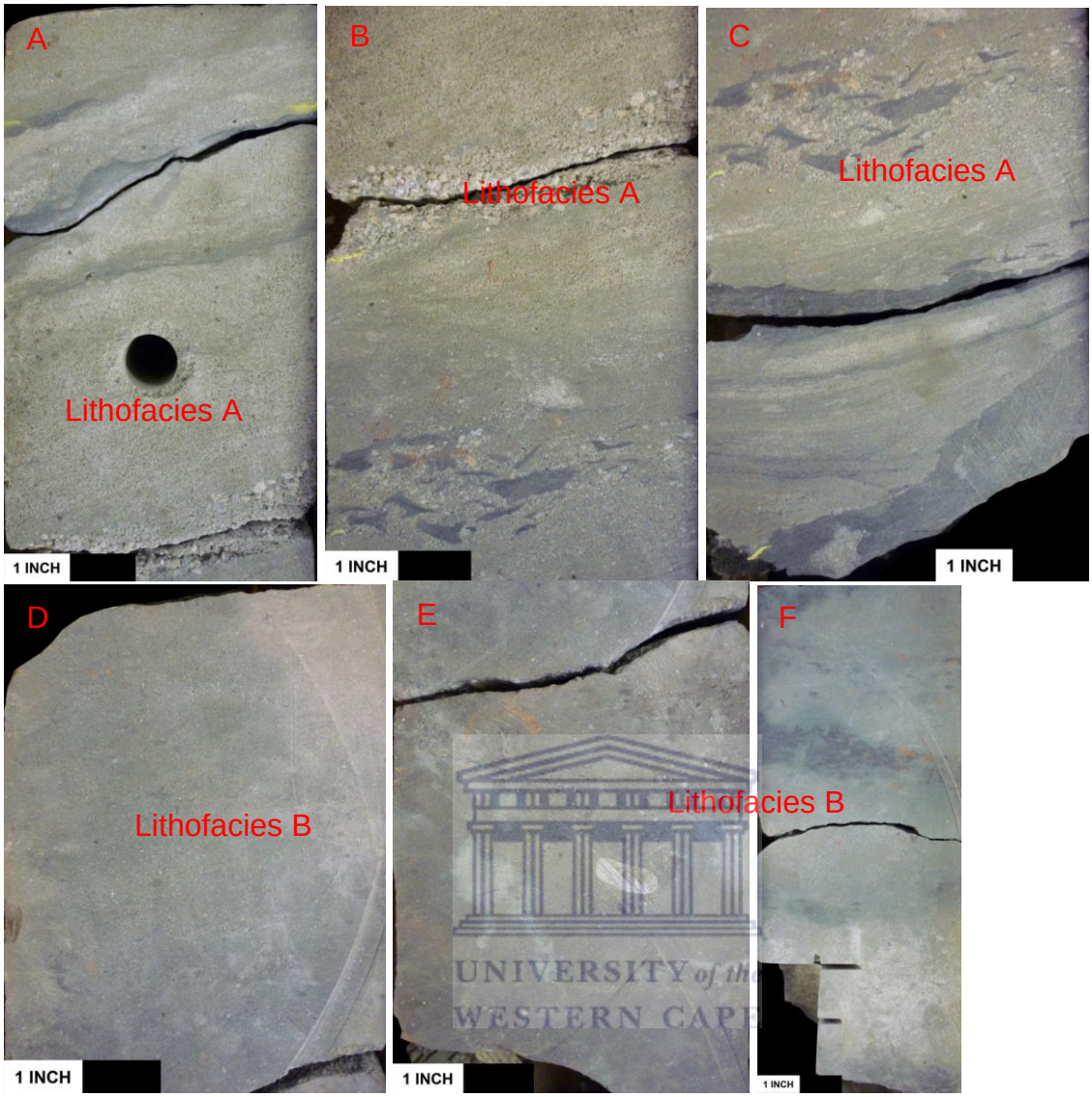

Figure 12: Core Photographs of A-D1 displaying samples (A, B, C, B, E and F) cored from 2662.80m – 2663.56m.

A-H1 core Photographs

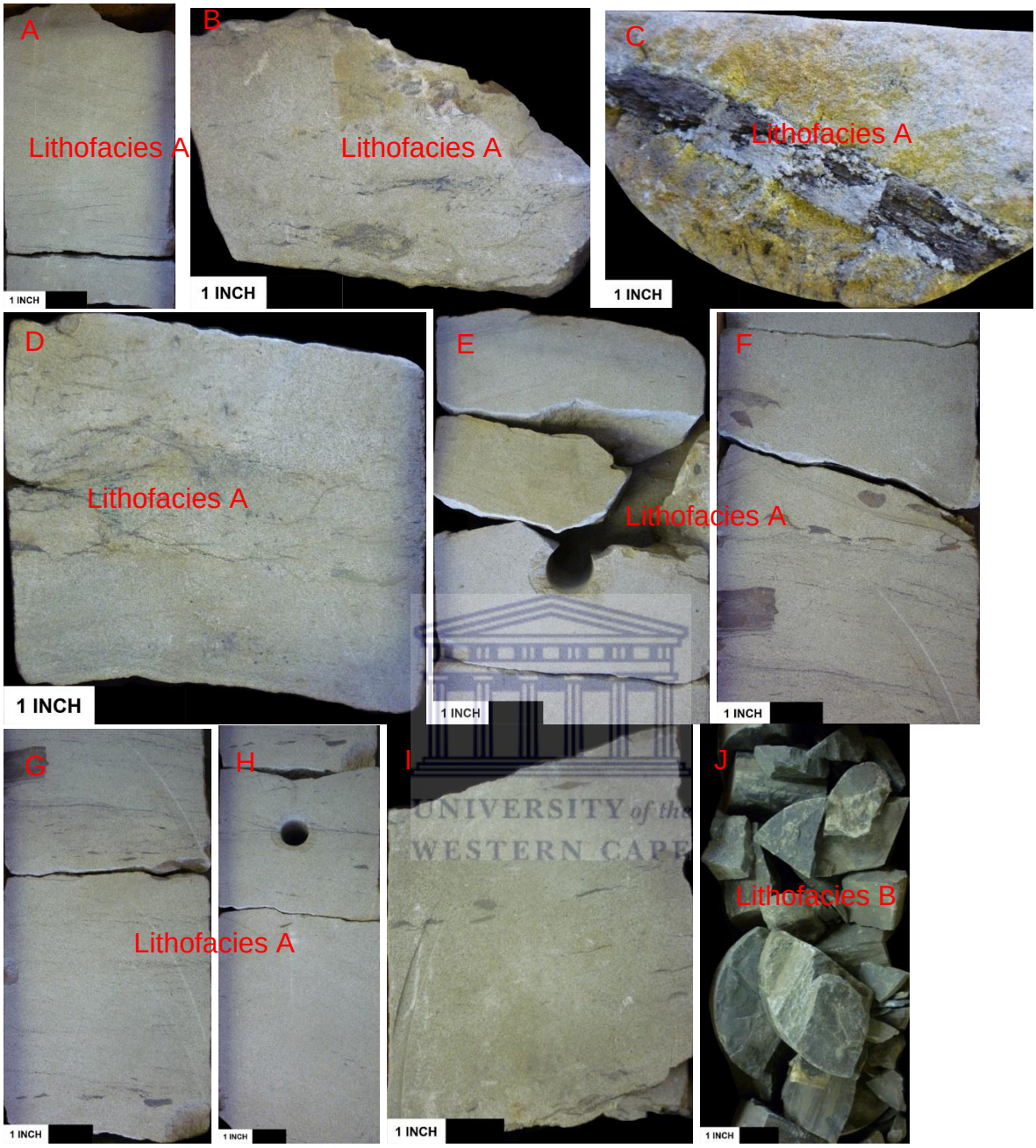

Figure 13: Core Photographs of A-H1 displaying samples (A, B, C, B, E, F, G, H, I and J) cored from 3022.50m – 3024.80m.

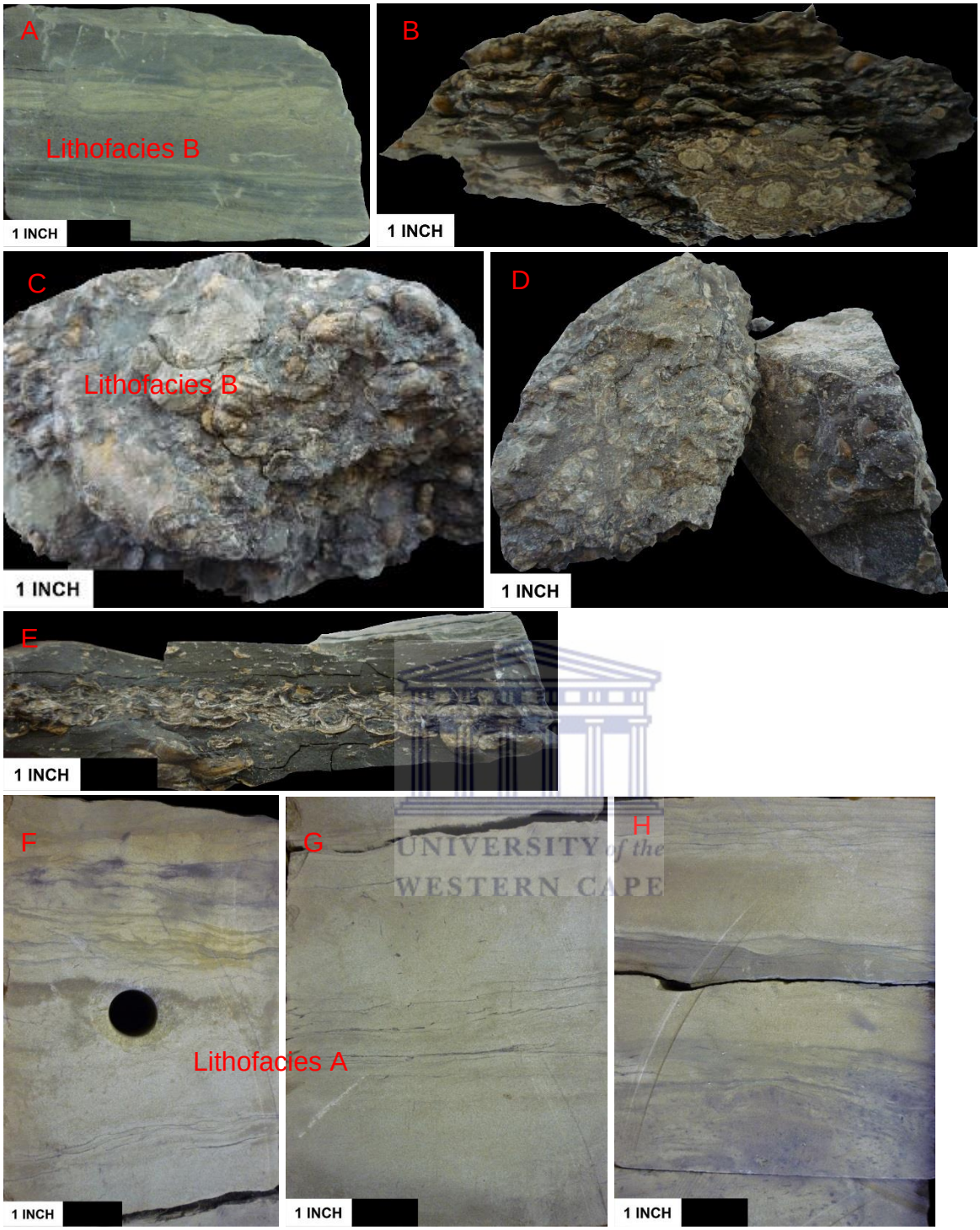

Figure 14: Core Photographs of A-H1 displaying samples (A, B, C, B, E, F, G and H) cored from 3025.25m – 3031.23m.

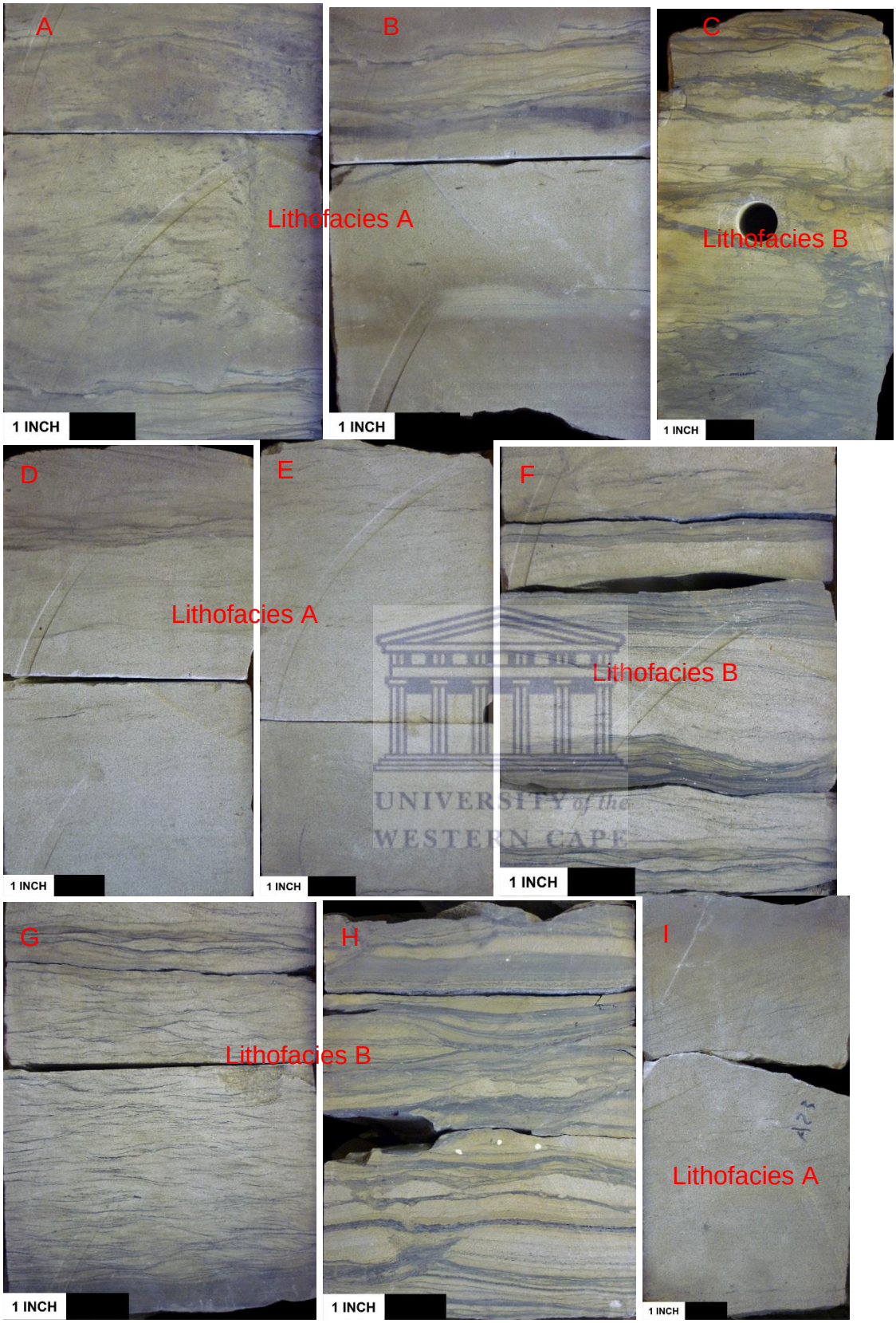

Figure 15: Core Photographs of A-H1 displaying samples (A, B, C, B, E, F, G, H and I) cored from 3031.24m – 3034.82m.

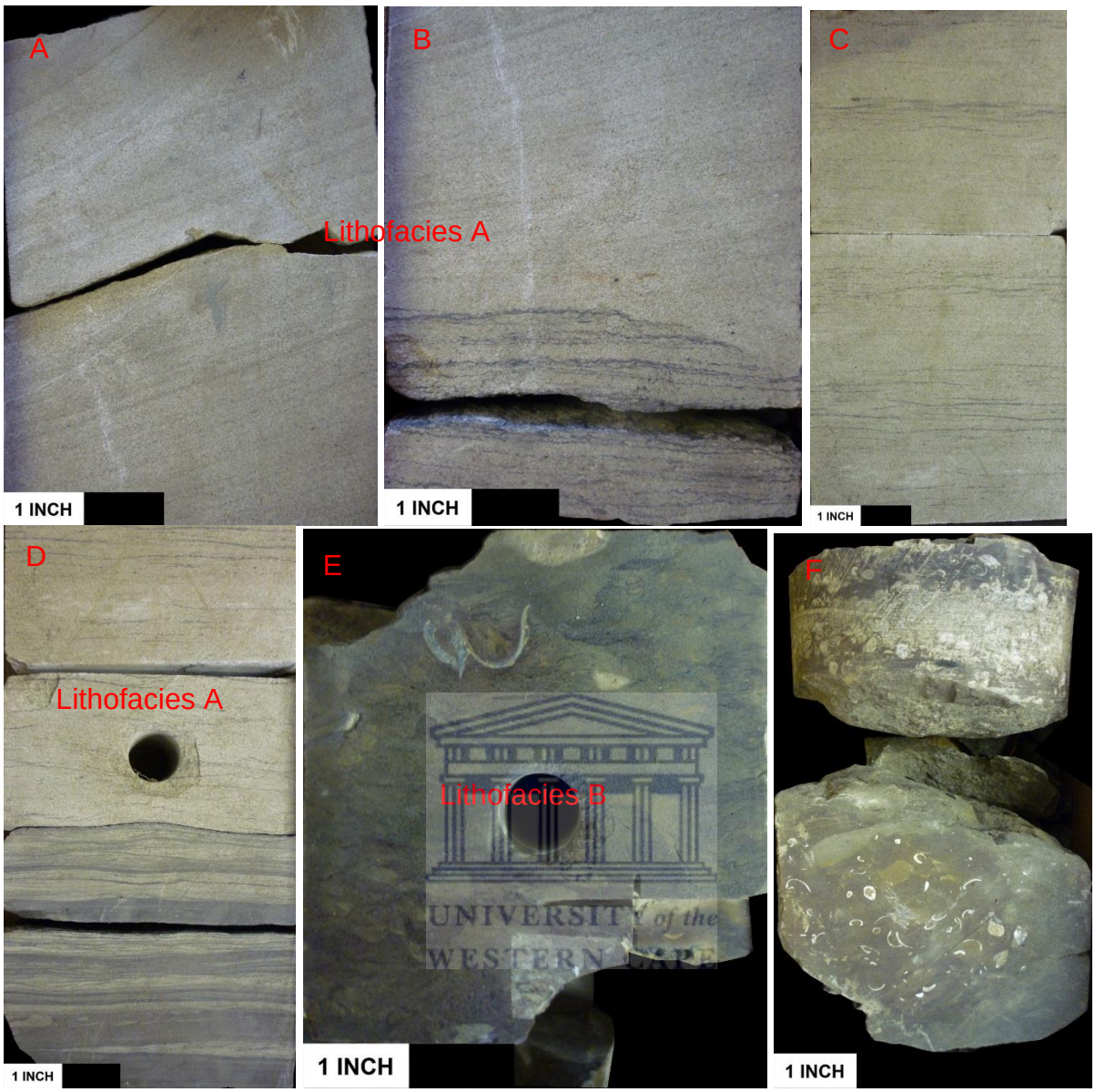

Figure 16: Core Photographs of A-H1 displaying samples (A, B, C, B, E and F) cored from 3034.92m – 3038.00m.

A-K1 Core Photographs

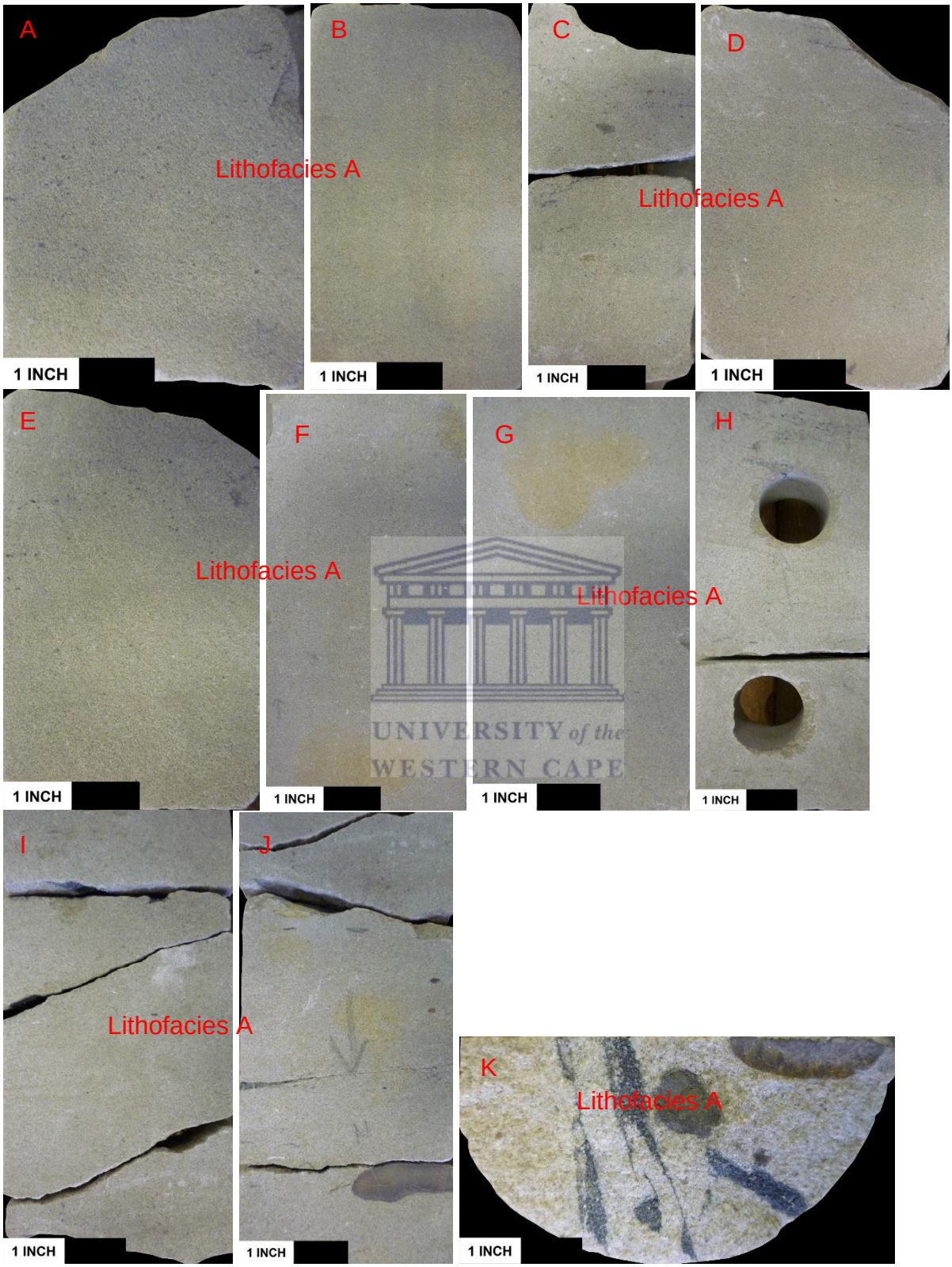

Figure 17: Core Photographs of A-K1 displaying samples (A, B, C, B, E, F, G, H, I, J and K) cored from 3236.48m – 3238.65m.

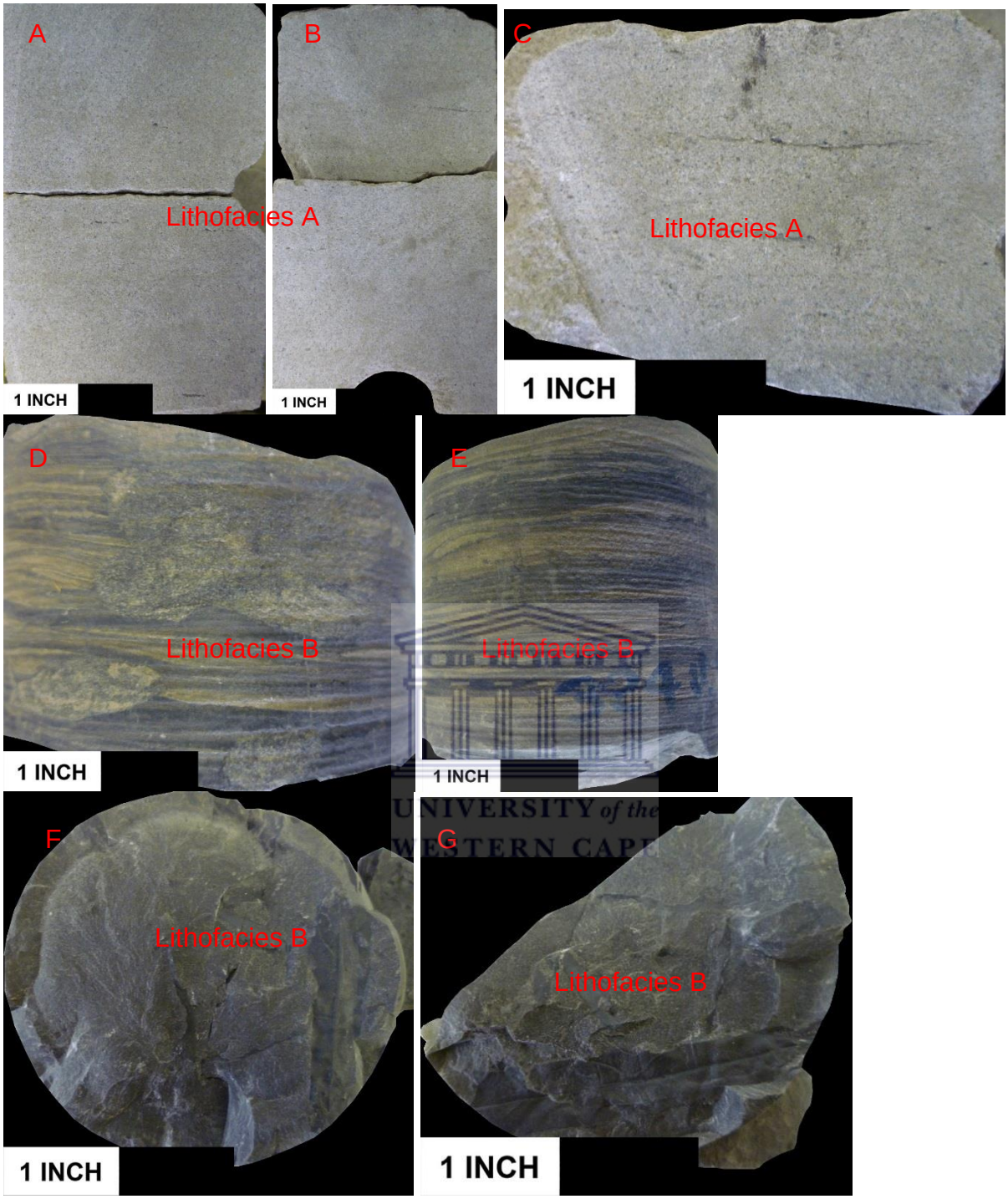

Figure 18: Core Photographs of A-K1 displaying samples (A, B, C, B, E, F and G) cored from 3238.80m – 3241.10m.

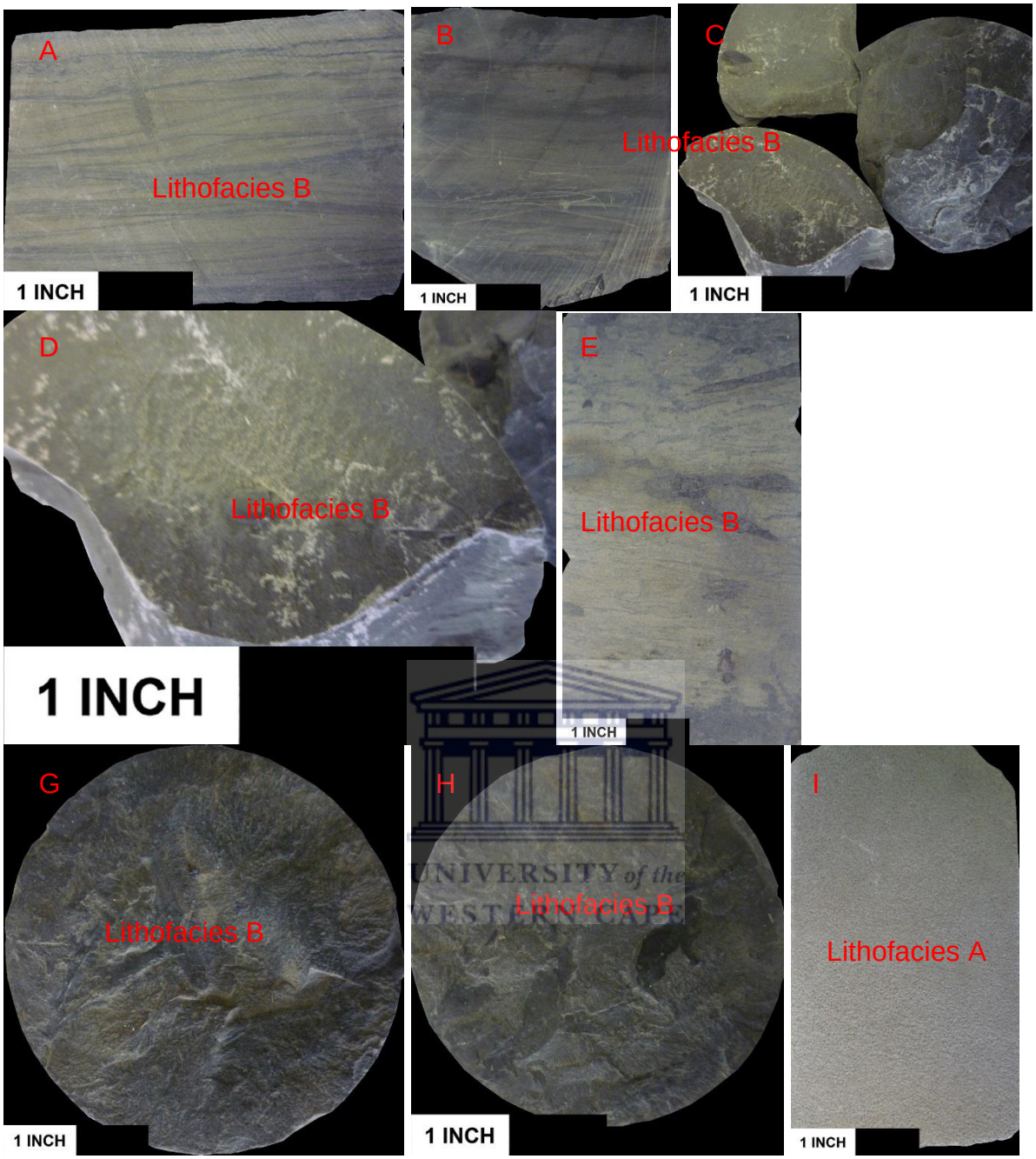

Figure 19: Core Photographs of A-K1 displaying samples (A, B, C, B, E, F, G, H, I, J and K) cored from 3236.48m – 3238.65m.

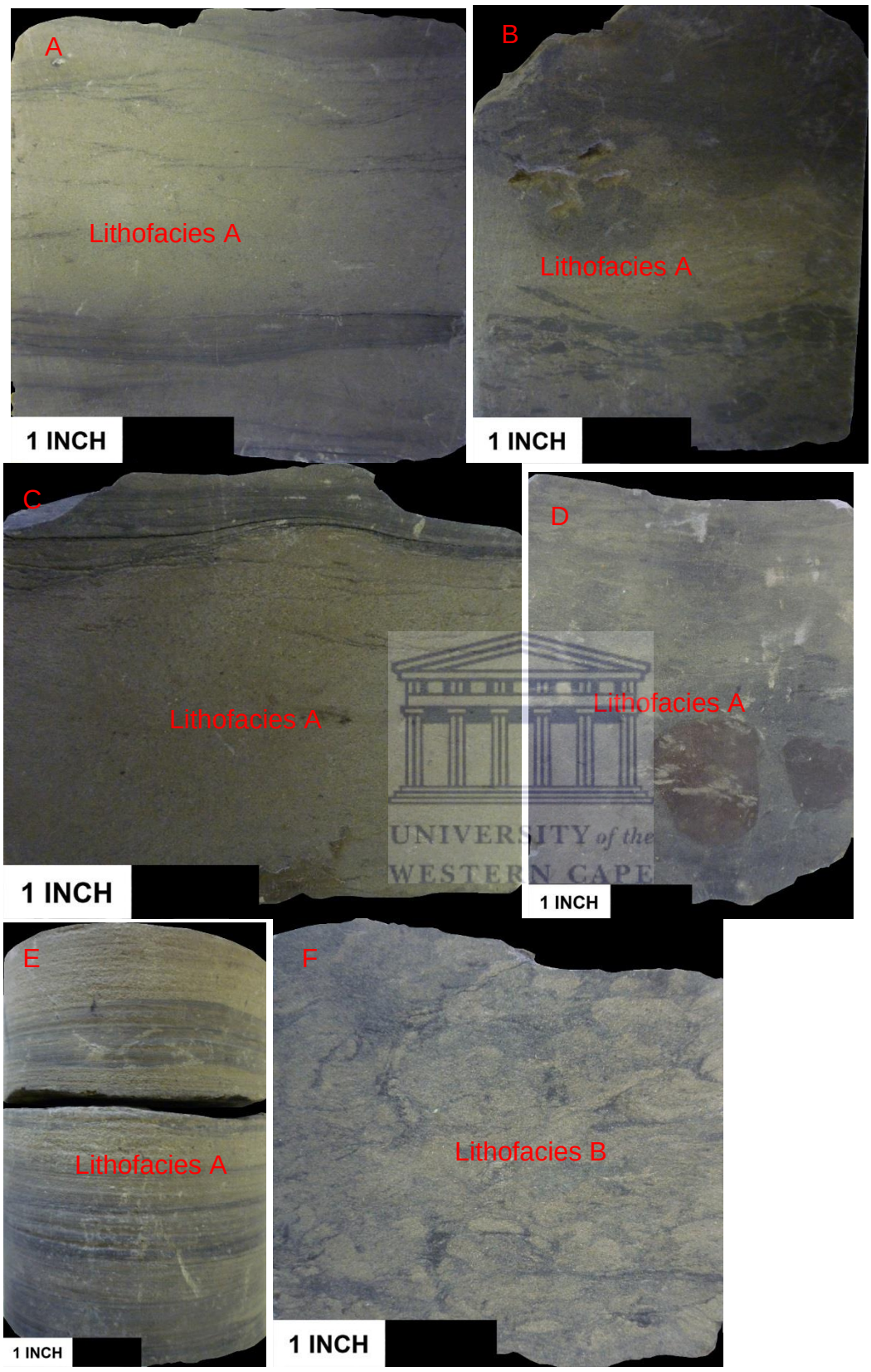

Figure 20: Core Photographs of A-K1 displaying samples (A, B, C, B, E and F) cored from 3287.30m – 3296.00m.

K-A2 Core Photographs

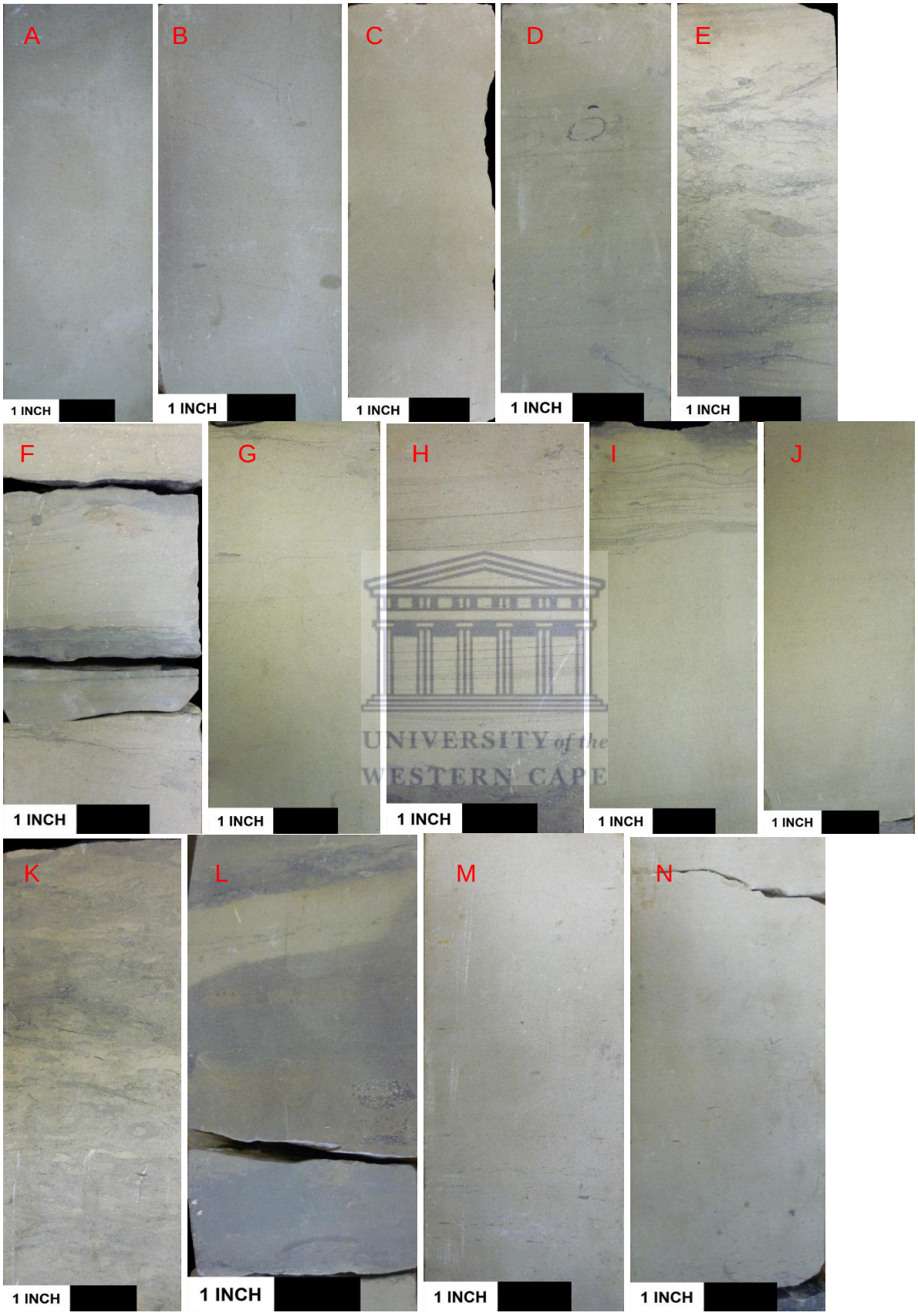

Figure 21: Core Photographs of K-A2 displaying silty sandstones lithofacies samples (from A, B, C, B, E, F, G, H, I, J, K, L, M, and N) cored from 3982.25m – 3986.75m.

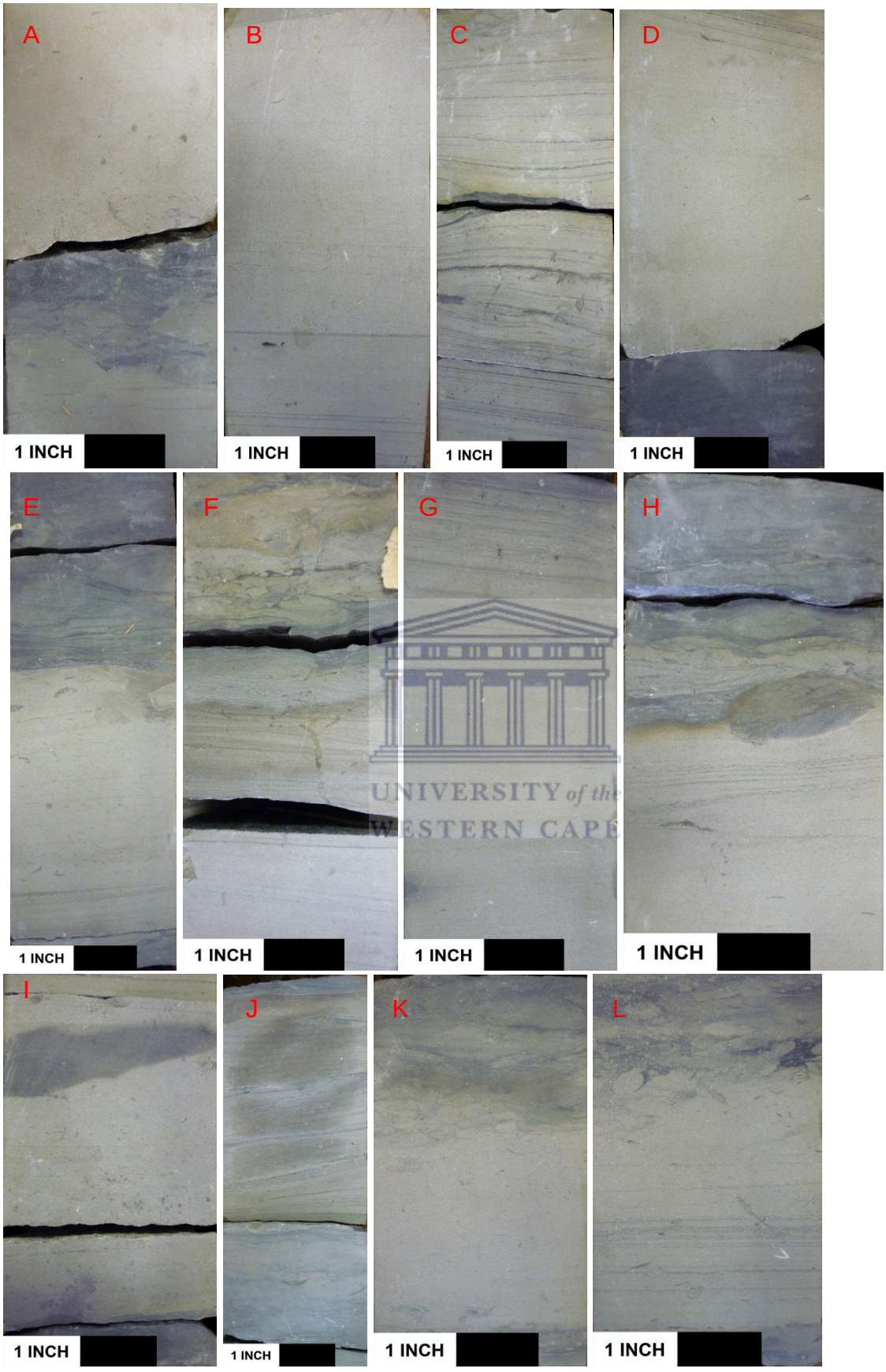

Figure 22: Core Photographs of K-A2 displaying silty sandstones lithofacies samples (from A, B, C, B, E, F, G, H, I, J, K and L) cored from 3986.75m – 3988.66m.

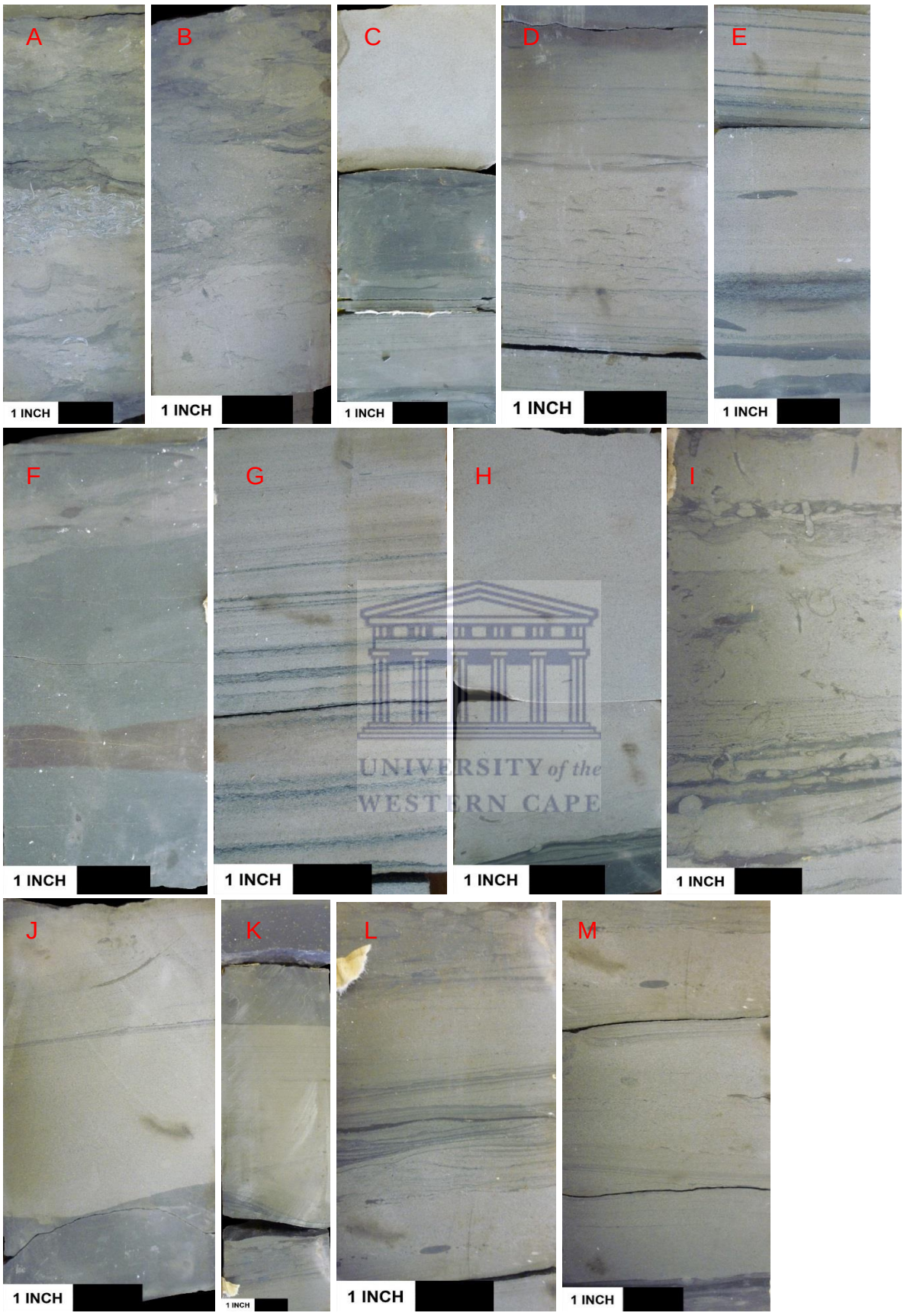

Figure 23: Core Photographs of K-A2 displaying silty sandstones lithofacies samples (from A, B, C, B, E, F, G, H, I, J, K, L and M) cored from 3989.90m – 4080.25m.

APPENDIX II – THIN SECTION PETROGRAPHIC ANALYSIS

Well: A-D1 – Petrographic Analyses
Depth: 2662.49m

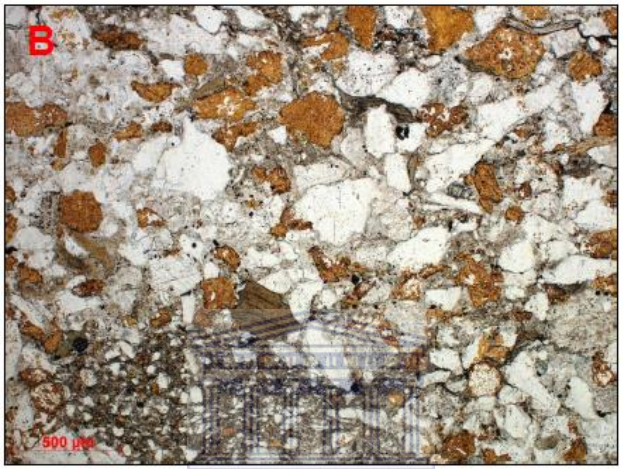

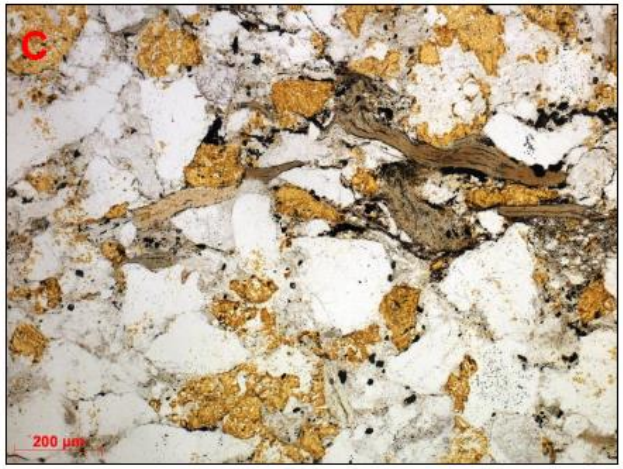

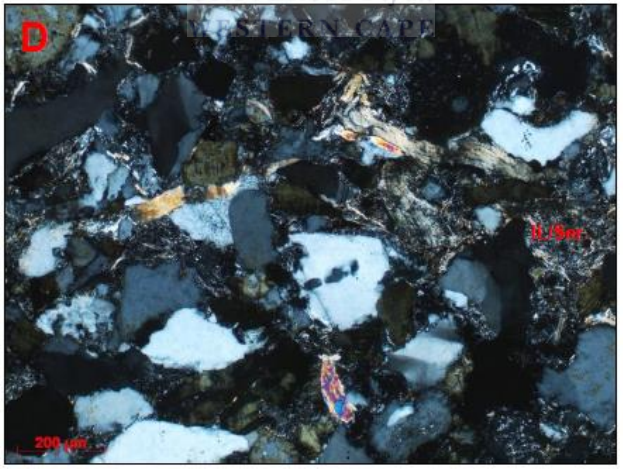

Lithology: Sandstone

Classification: Feldspathic arenite*

Texture:
Grain size: Fine (upper).
Sorting: Moderate overall.
Grain contacts: Concavo-convex & sutured.
Grain shape: Angular to subrounded.
Compaction: Strong (micro-stylolites are present).

Detrital components:
- Abundant monocrystalline quartz, K-feldspar and plagioclase;
- Relatively common polycrystalline quartz and biotite flakes, sedimentary and metamorphic lithics, sparse heavy minerals (zircon and tourmaline) and organic matter.

Matrix:
- Detrital clays (locally common) and also associated with ?burrows.

Authigenic clays:
- Common quartz and feldspar overgrowths, with lesser amounts of grain replacive illite/sericite (IL/Ser., Image D, XPL) and chlorite. Grain replacive pyrite is scattered.

Pore system: Porosity is rare (isolated secondary pores). Artificial fractures are present.

Reservoir quality: Very poor

LEGACY CORE ANALYSIS DATA
Porosity: n/a
Permeability: n/a

Point Count Porosity: n/a

**Rock classification is based on visual estimation of mineralogical components.*

Well: A-D1

Depth: 2663.39m

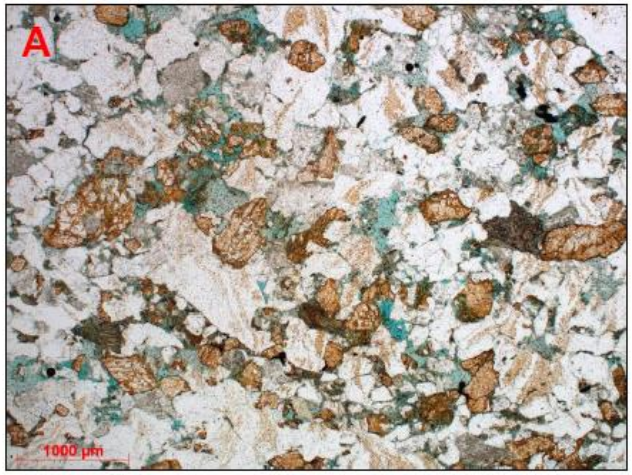

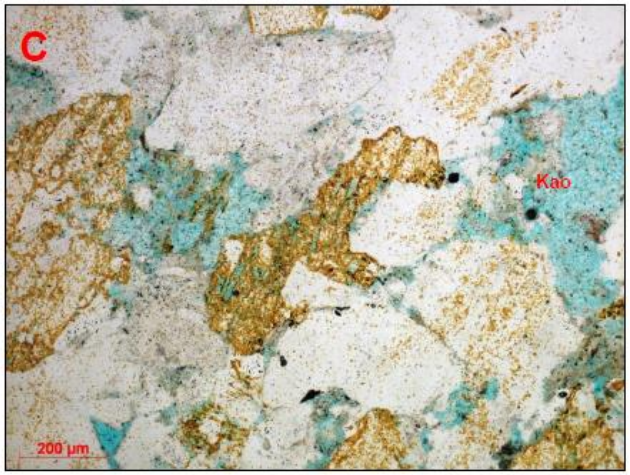

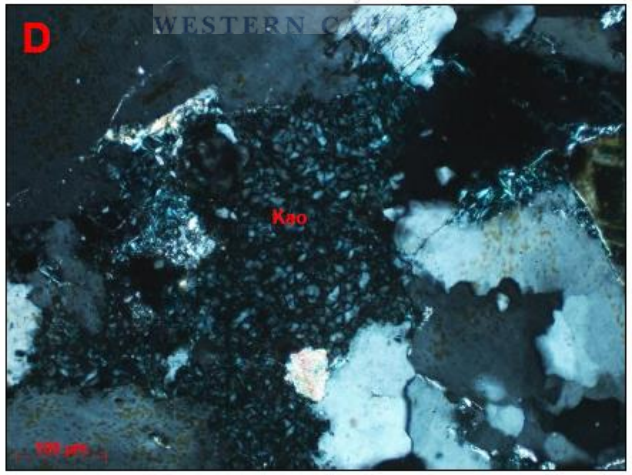

Lithology: Sandstone

Classification: Feldspathic arenite

Texture:
Grain size: Medium (upper).
Sorting: Moderately sorted overall.
Grain contacts: Long to sutured
Grain shape: Subangular to subrounded.
Compaction: Strong overall.

Detrital components:
- Abundant monocrystalline quartz, K-feldspar and plagioclase, the latter altered by sericite;
- Common polycrystalline quartz and mica flakes (altered/replaced by chlorite), with lesser amounts of lithics and organic matter.

Matrix:
- Detrital clays are not noted.

Authigenic clays:
- Common pore filling to grain replacive kaolinite (Kao, Images C-D) and quartz and feldspar overgrowths;
- Sparse grain replacive to grain rimming illite/sericite & chlorite;
- Scattered grain replacive pyrite, siderite, non ferroan calcite and possible anhydrite.

Pore system: Porosity is moderate overall. Poorly to locally moderately connected macropores are mainly secondary, being linked to the dissolution of unstable feldspars. Visible micropores (~10µm) between coarse kaolinite booklets are present.

Reservoir quality: Poor to locally moderate.

LEGACY CORE ANALYSIS DATA
Porosity: 17% (at 2663.29m)
Permeability: 13.5mD (at 2663.29m)

Point Count Porosity: 11.7%

Well: A-D1

Depth: 2665.88m

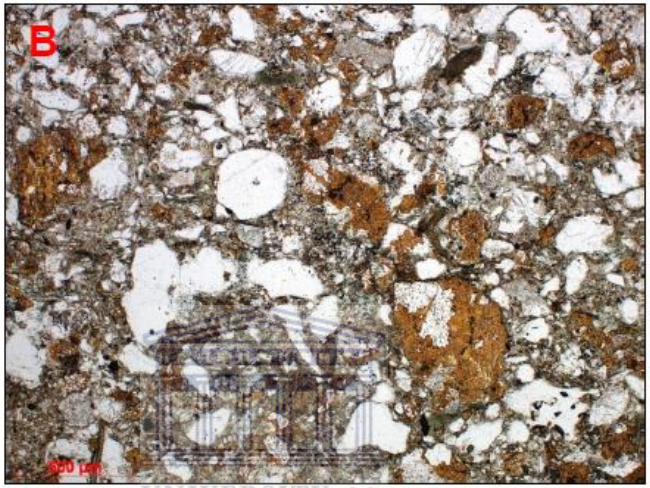

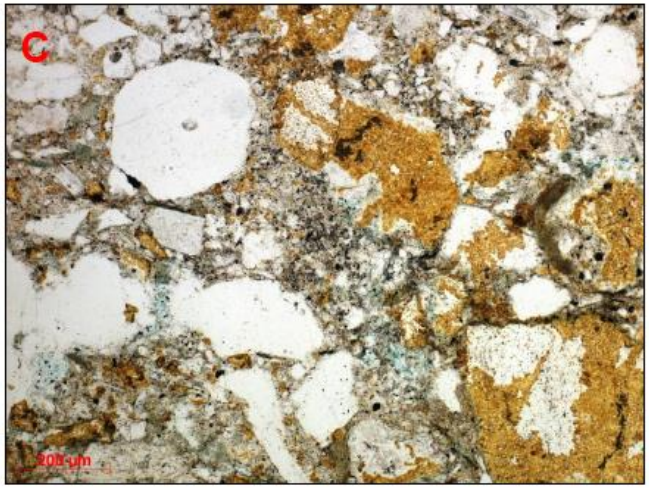

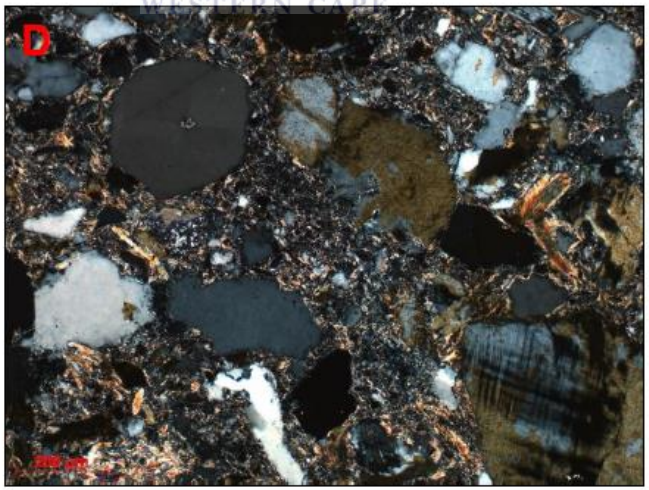

Lithology: Wackes

Classification: Feldspathic wacke*

Texture:
Quartz and feldspar grains are commonly embedded into a clayey-rich matrix. Grains are angular to rounded. Some laminae less rich in detrital clays might be classified as argillaceous feldspathic arenite. Compaction of such more grain supported laminae is strong.

Detrital components:
- Abundant monocrystalline quartz & feldspars;
- Common polycrystalline quartz, muscovite and biotite, lithics (sedimentary, metamorphic and ?igneous) and organic matter.

Matrix:
- Abundant detrital clays (orthomatrix).

Authigenic clays:
- Common illite/sericite and chlorite (replacement phases);
- Sparse quartz and feldspar overgrowths;
- Scattered grain replacive calcite and pyrite.

Pore system: Porosity is not noted, except for the presence of thin artificial fractures.

Reservoir quality: Negligible.

LEGACY CORE ANALYSIS DATA
Porosity: n/a
Permeability: n/a

Point Count Porosity: n/a

**Rock classification is based on visual estimation of mineralogical components.*

Well: A-J1 – Petrographic Analyses
Depth: 1617.27m

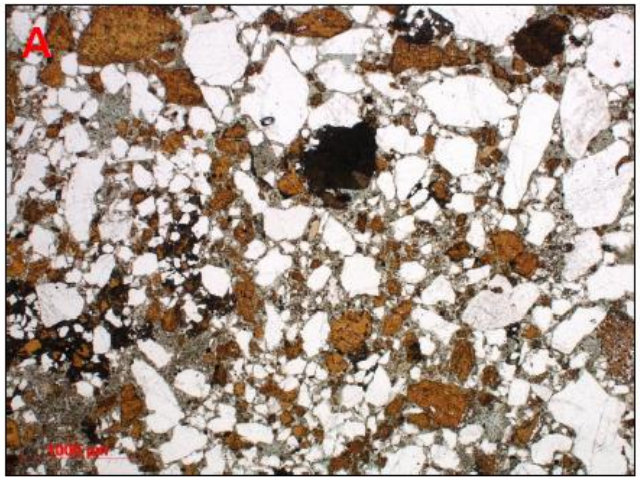

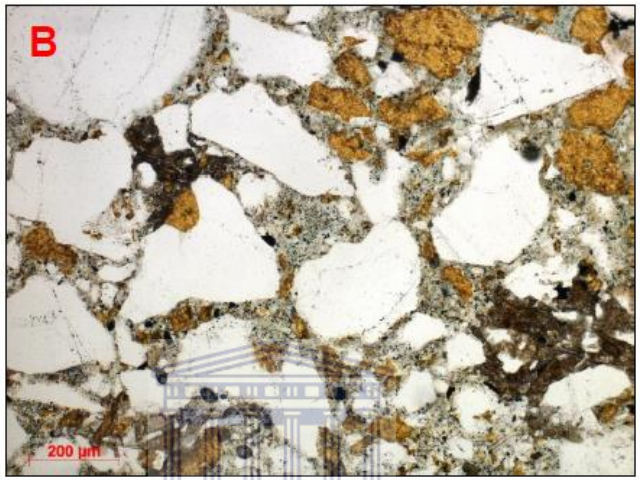

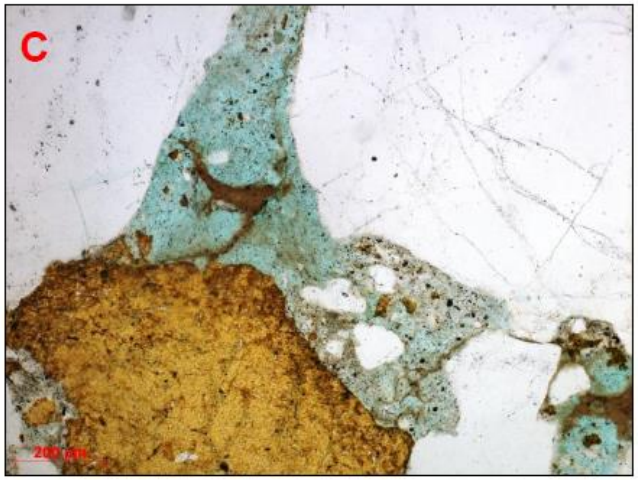

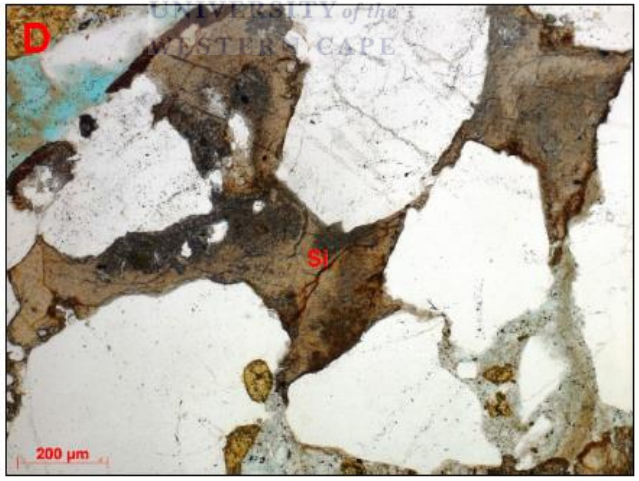

Lithology: Clayey sandstone/wackes

Classification: Feldspathic arenite/wacke*

Texture:
Grain size: Very fine to very coarse
Sorting: Poorly sorted.
Grain contacts: Floating to point to point.
Grain shape: Angular to subrounded.
Compaction: Moderately weak overall.

Detrital components:
- Predominant monocrystalline quartz and abundant feldspars (mainly K-feldspar);
- Common polycrystalline quartz and minor amounts of mudclasts, mica flakes, organic matter and heavy minerals (zircon).

Matrix:
- Detrital clays are common overall.

Authigenic phases:
- Common pore filling kaolinite reduce macropores into tortuous microporosity.
- Common pore filling to grain replacive siderite (Si, Image D, also poikilotopic) likely formed during mesodiagenesis.
- Lesser amounts of pore restricting quartz and feldspar overgrowths are also present.
- Grain replacive pyrite is scattered.

Pore system: Macroporosity is poor. Micropores between clay platelets are optically irresolvable.

Reservoir quality: Very poor

LEGACY CORE ANALYSIS DATA
Porosity: 11.2% at 1617.28m
Permeability: 0.32mD at 1617.28m

Point Count Porosity: n/a

**Rock classification is based on visual estimation of mineralogical components.*

Well: A-J1

Depth: 1619.42m

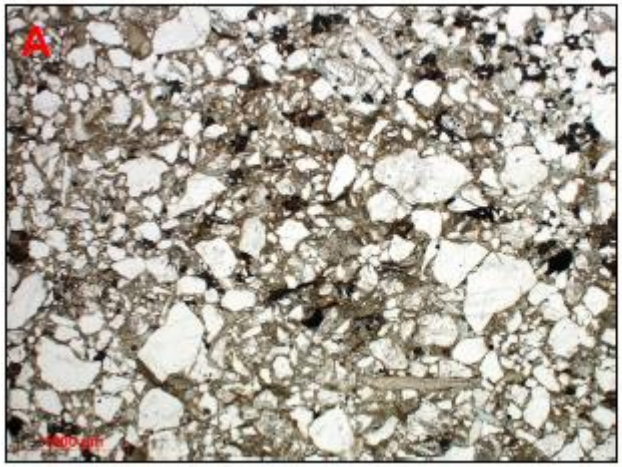

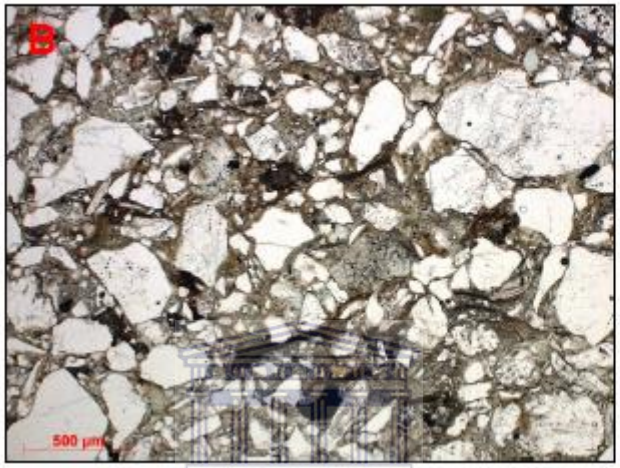

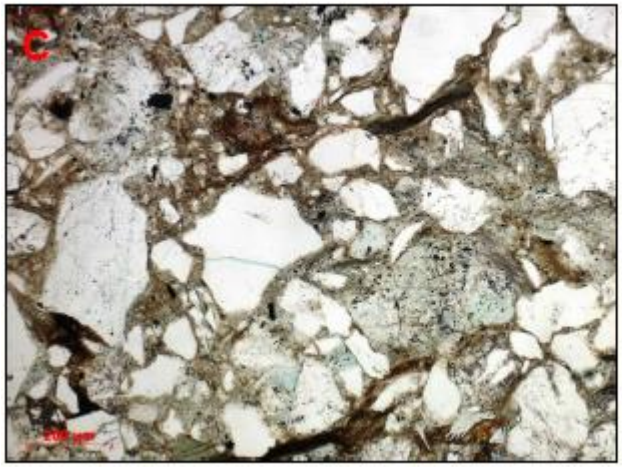

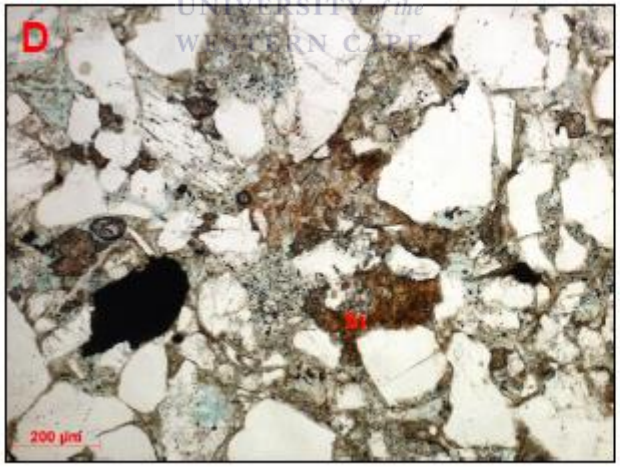

Lithology: Wackes

Classification: Feldspathic wacke*

Texture:
Grain size: Very fine to very coarse
Sorting: Poorly sorted.
Grain contacts: Floating.
Grain shape: Angular to subrounded.
Compaction: Moderately weak overall.

Detrital components:
- Predominant monocrystalline quartz with abundant K-feldspar and relatively lesser amounts of mica flakes, lithics (e.g. schistose metamorphic grains), organic matter and heavy minerals (e.g. zircon).

Matrix:
- Sample is shaly.

Authigenic phases:
- Common kaolinite is very finely crystalline in structure and noted to fill pores and replace grains. Illite/sericite is also likely common.
- Common pore filling to grain replacive siderite is present (Si, Image D).
- Minor pore restricting quartz and feldspar overgrowths and pyrite framboids are also noted.

Pore system: Macroporosity is rare. Micropores between clay platelets are optically irresolvable.

Reservoir quality: Very poor

LEGACY CORE ANALYSIS DATA
Porosity: 1.3%
Permeability: 0.01mD

Point Count Porosity: n/a

**Rock classification is based on visual estimation of mineralogical components.*

Well: A-J1

Depth: 1619.84m

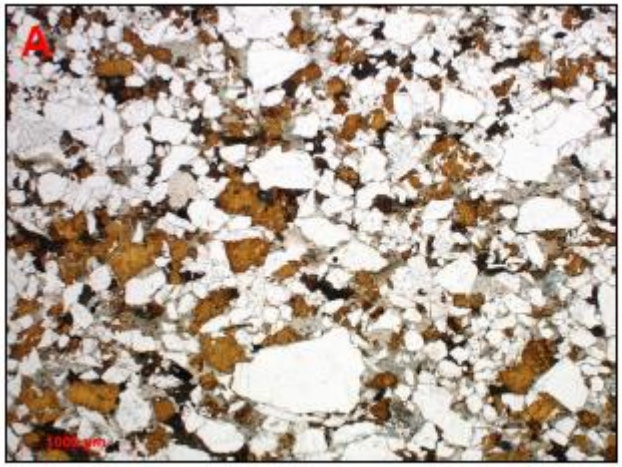

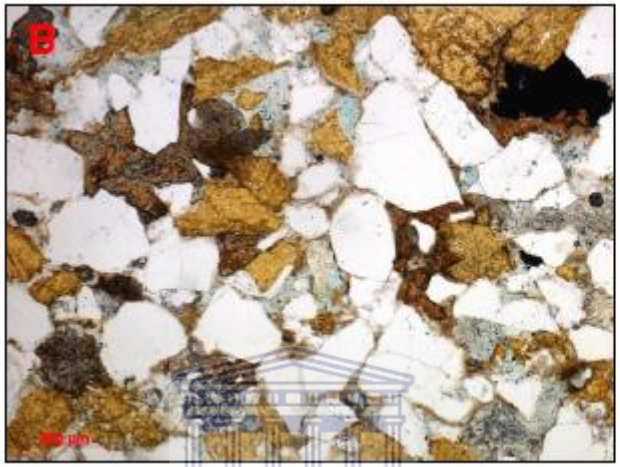

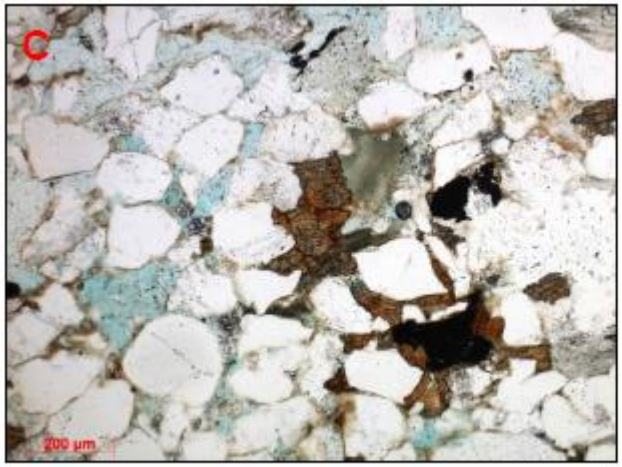

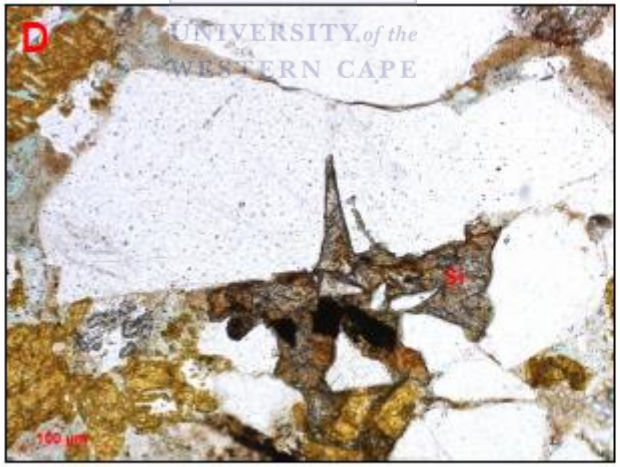

Lithology: Sandstone

Classification: Feldspathic arenite

Texture:
Grain size: Fine (upper) sand is dominant.
Sorting: Moderately sorted overall.
Grain contacts: Point to point to long.
Grain shape: Angular to rounded.
Compaction: Moderate.

Detrital components:
- Predominant monocrystalline quartz and abundant feldspars (mainly K-feldspar);
- Relatively common polycrystalline quartz and minor amounts of mudclasts, metamorphic grains, mica flakes, detrital chlorite, organic matter and heavy minerals (mainly zircon).

Matrix:
- Detrital clays are sparse.

Authigenic phases:
- Common pore filling to grain replacive siderite (Si, Image D);
- Common pore restricting quartz overgrowths and sparse feldspar overgrowths;
- Sparse pore filling kaolinite, grain replacive chlorite and ?illite/sericite are also noted;
- Grain replacive pyrite is also noted.

Pore system: Macroporosity is poor. Pore effectiveness has been strongly downgraded by siderite and clays.

Reservoir quality: Very poor

LEGACY CORE ANALYSIS DATA
Porosity: 8.8% at 1619.90m
Permeability: 0.44mD at 1619.90m

Point Count Porosity: 5%

Well: A-J1

Depth: 1621.81m

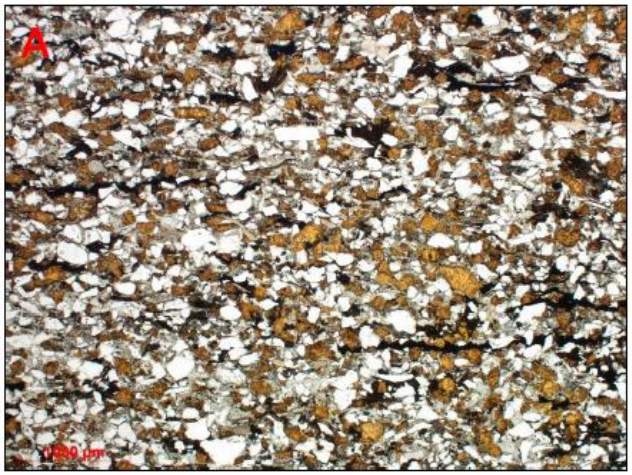

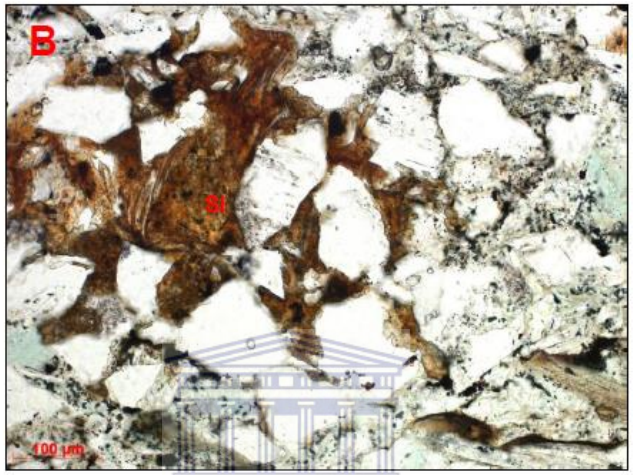

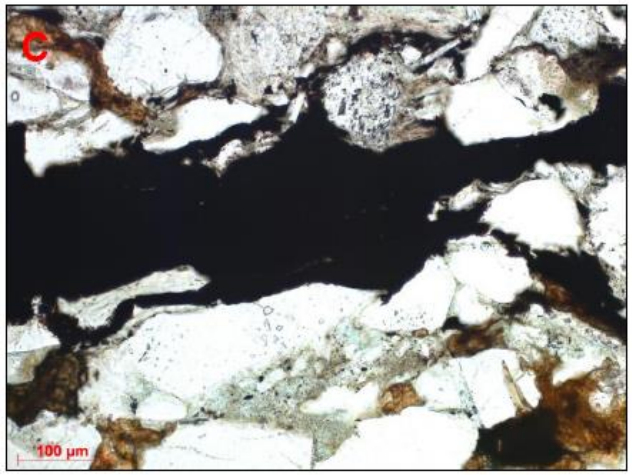

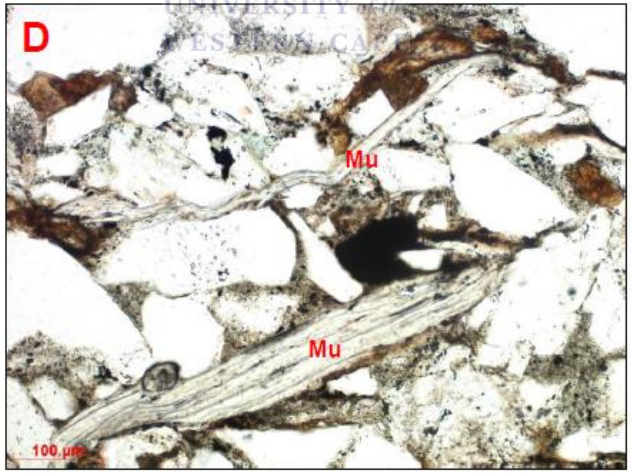

**Rock classification is based on visual estimation of mineralogical components.*

Lithology: Sandstone

Classification: (Micaceous) feldspathic arenite*

Texture:
Grain size: Very fine (upper).
Sorting: Moderately sorted overall.
Grain contacts: Long to point to point.
Grain shape: Angular to rounded.
Compaction: Moderate.

Detrital components:
- Predominant monocrystalline quartz with abundant K-feldspar and mica flakes (mainly muscovite, Mu, Image D), common organic matter/carbonaceous material and lesser amounts of lithics (e.g. metamorphic) and heavy minerals (e.g. tourmaline and zircon).

Matrix:
- Brownish to greenish clays are common.

Authigenic phases:
- Common clays (mostly optically irresolvable, also ?greenish smectite) and pore filling to grain replacive siderite (Si, Image B).
- Possible bitumen (centre of Image C), pyrite framboids and minor quartz/feldspar overgrowths are also noted.

Pore system: Macroporosity is poor. The pore system has been strongly downgraded by clays and siderite.

Reservoir quality: Poor

LEGACY CORE ANALYSIS DATA
Porosity: n/a
Permeability: n/a

Point Count Porosity: n/a

Well: A-J1

Depth: 1623.04m

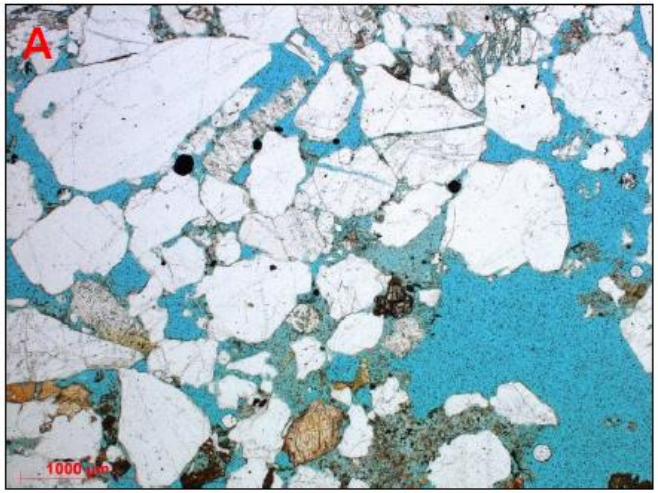

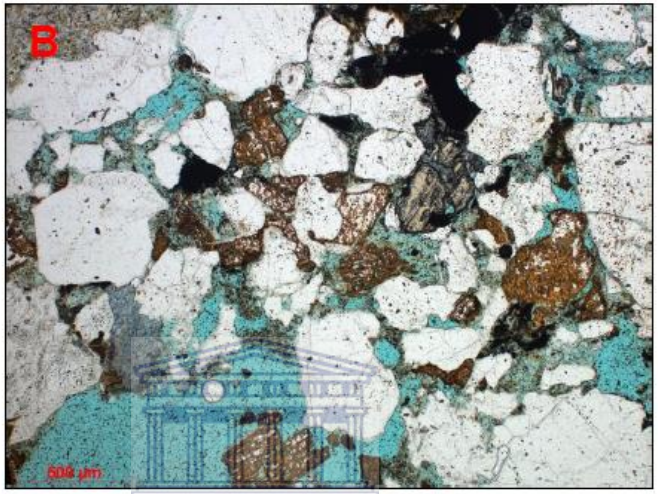

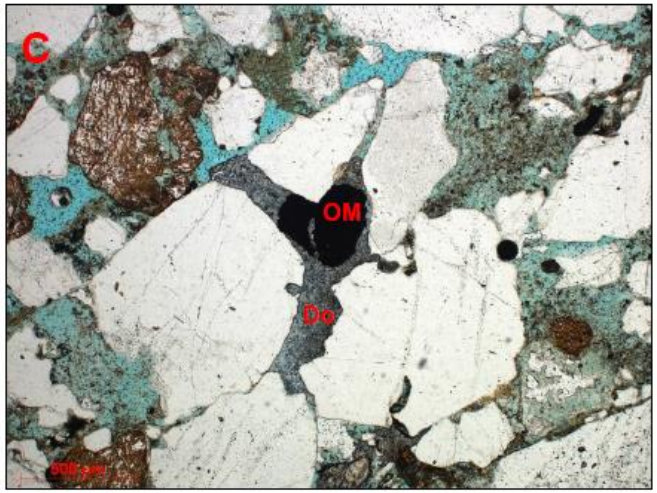

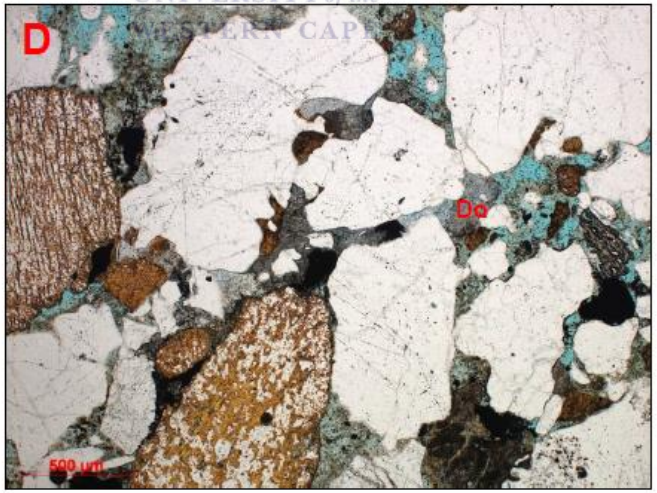

Lithology: Sandstone

Classification: Subfeldspathic arenite*

Texture:
Sample is poorly consolidated, although some areas contain a few grains cemented by carbonates (see Image A vs. Images C-D). Coarse grained sand is dominant.

Detrital components:
- Predominant monocrystalline and polycrystalline quartz, with common K-feldspar and lesser amounts of mica flakes, organic matter (OM, Image C) and heavy minerals (zircon and also ?pyroxenes).

Matrix:
- Clays are scattered.

Authigenic phases:
- Scattered pore filling ferroan dolomite (Do, Images C-D), minor pyrite and possible poorly developed quartz/feldspar overgrowths.

Pore system: Porosity is visually excellent, except for a few well consolidated/carbonate cemented areas of this sample. Note that artificial pores are common.

Reservoir quality: Excellent by legacy core analysis data**

LEGACY CORE ANALYSIS DATA
Porosity: 21.3% at 1623.01m
Permeability: 1289mD at 1623.01m

Point Count Porosity: n/a

**Rock classification is based on visual estimation of mineralogical components.*

***It is suggested that legacy core analysis data be assessed with caution for this sample.*

Well: A-J1

Depth: 1625.68m

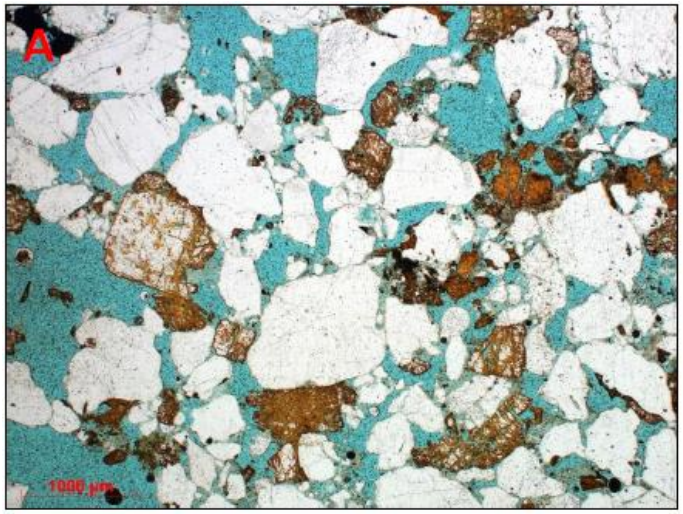

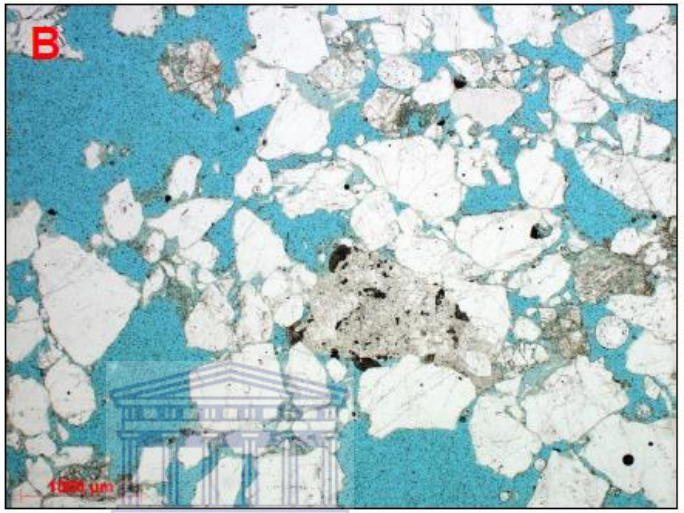

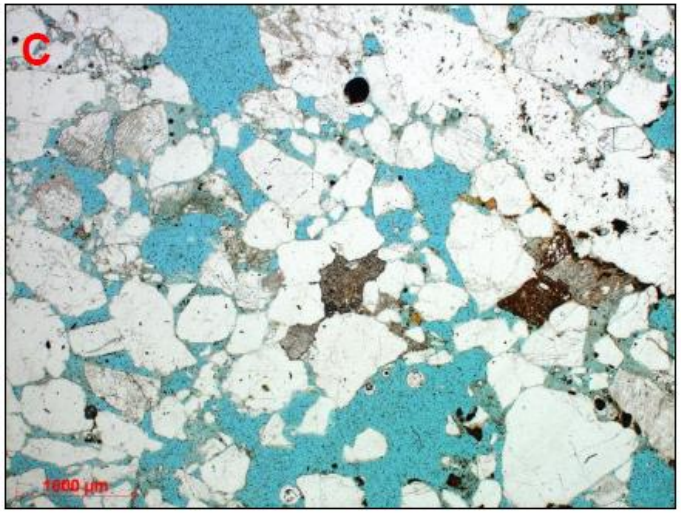

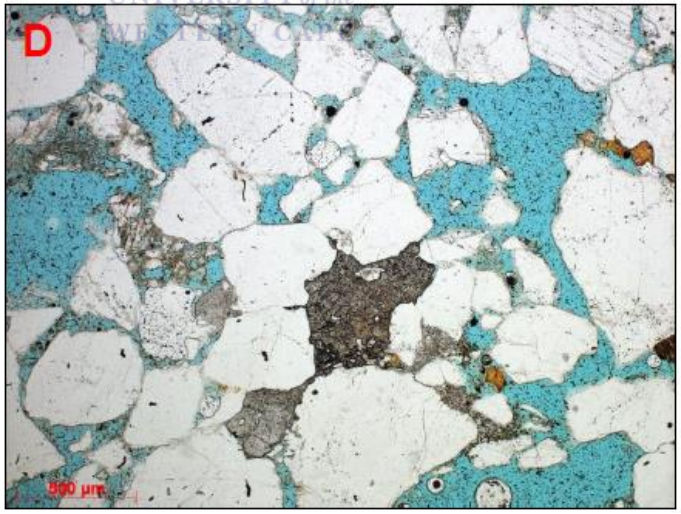

Lithology: Sandstone

Classification: Subfeldspathic arenite*

Texture:
Sample is poorly consolidated; a few consolidated/carbonate cemented grains are noted (centre of Image C). Coarse grained sand is dominant.

Detrital components:
- Predominant monocrystalline and polycrystalline quartz, with common K-feldspar and minor amounts of mica flakes, organic matter and heavy minerals (possible pyroxenes).

Matrix:
- Clays are scattered.

Authigenic phases:
- Scattered pore filling ferroan siderite and/or dolomite, minor pyrite and poorly developed quartz/feldspar overgrowths.

Pore system: Porosity is visually excellent, however, artificial pores are abundant.

Reservoir quality: Excellent by legacy core analysis data**

LEGACY CORE ANALYSIS DATA
Porosity: 23.1% at 1625.63m
Permeability: 2039mD at 1625.63m

Point Count Porosity: n/a

**Rock classification is based on visual estimation of mineralogical components.*

***It is suggested that legacy core analysis data be assessed with caution for this sample.*

Well: A-J1

Depth: 1627.87m

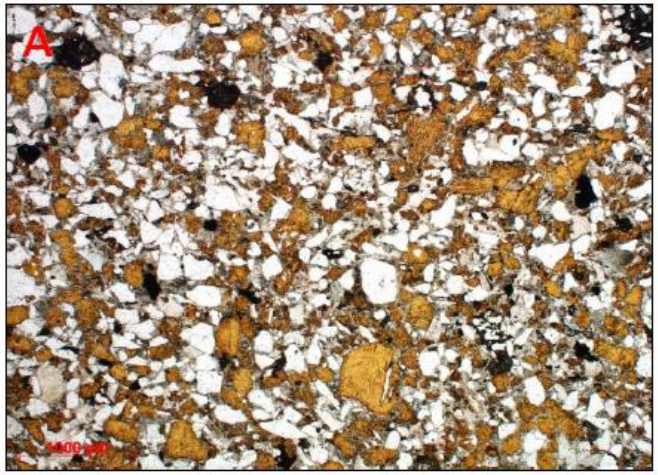

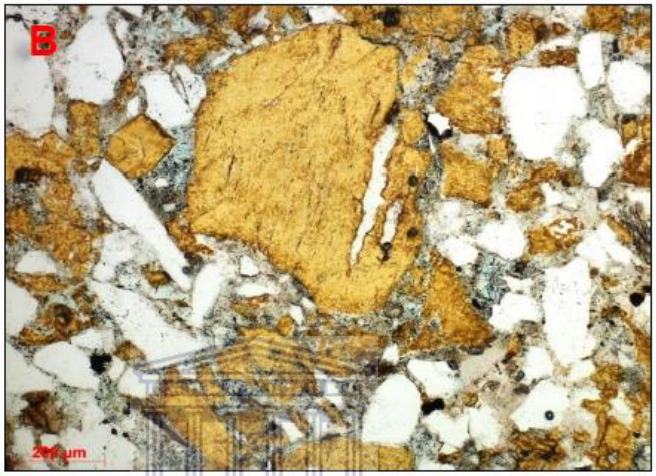

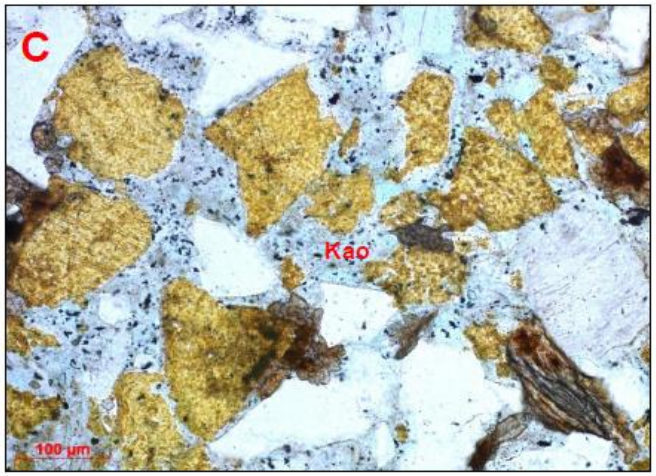

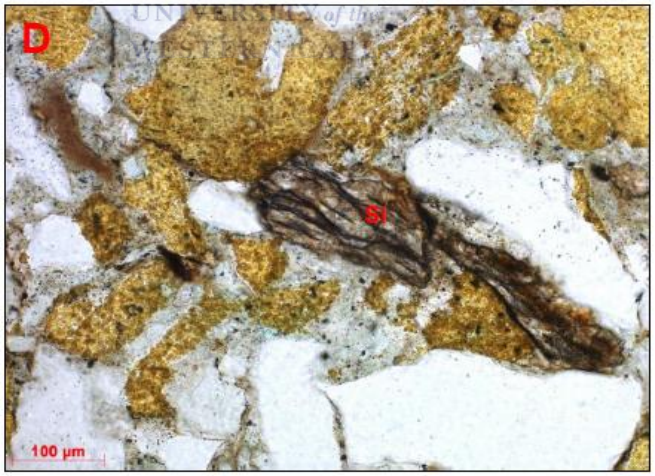

Lithology: Clayey sandstone

Classification: Feldspathic arenite*

Texture:
Grain size: Fine-grained sand is dominant.
Sorting: Moderately poorly sorted.
Grain contacts: Floating to long.
Grain shape: Angular to rounded.
Compaction: Moderate overall.

Detrital components:
- Predominant monocrystalline quartz and abundant K-feldspar;
- Common polycrystalline quartz and minor amounts of mudclasts, mica flakes, organic matter and heavy minerals (mainly zircon).

Matrix:
- Clays are common (orthomatrix).

Authigenic phases:
- Very finely crystalline pore filling kaolinite is common (Kao, Image C). Other clay types/platelets are inferred to be present, but they are optically irresolvable in thin section.
- Common pore filling to grain replacive siderite (Si, Image D).
- Lesser amounts of pore restricting quartz and feldspar overgrowths, and grain replacive pyrite are also noted.

Pore system: Macroporosity is poor. Micropores between clay platelets are optically irresolvable.

Reservoir quality: Very poor

LEGACY CORE ANALYSIS DATA
Porosity: n/a
Permeability: n/a

Point Count Porosity: n/a

**Rock classification is based on visual estimation of mineralogical components.*

Well: A-J1

Depth: 1627.87m

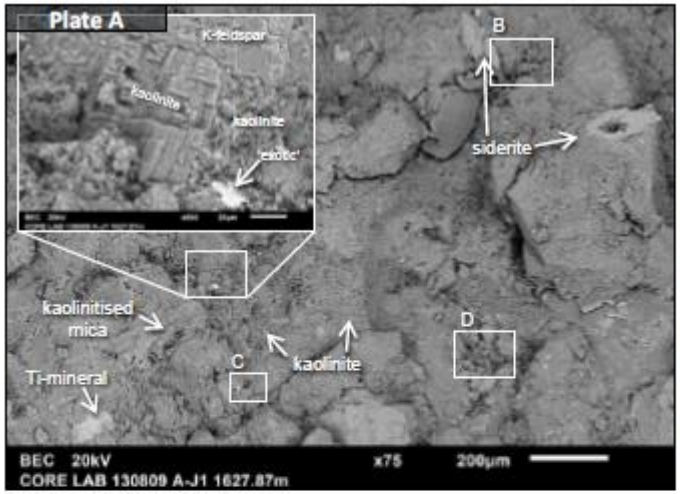

A moderately poorly sorted fine grained sandstone that appears massive at the scale of SEM (A). The sample is well compacted with long to weakly concavo-convex grain contacts observed.

Detrital grains are dominated by K-feldspar with abundant quartz. K-feldspar grains vary in preservation from fresh in appearance to weakly or highly leached (D). Accessory grains include Ti-minerals (A, C) and 'exotics' (A inset, Ca+Ce+Nd+La mineral).

The sample is characterised by abundant kaolinite, which is pore-lining, pore-filling and commonly grain-replacive. The kaolinite is very variable in form, observed mainly as very fine platy to blocky books and short verms, and in places is pseudomorphic after precursor grains (A, mica; and inset possibly after ?feldspar grain).

Quartz overgrowths are common, typically as thin developments (B, D). Possible overgrowths of K-feldspar are highly leached (D). Minor siderite (A, B) takes the form of fine lozenges, locally with leached cores visible (A). The siderite has a strong Mg component, with very low Ca and Mn detected by EDX analysis. A trace of barite was also observed (C).

Porosity appears moderate, and is dominated by microporosity associated with kaolinite and leached K-feldspar grains. Intergranular pores are typically small and lined with kaolinite or overgrowths. Pore throats are commonly constricted and pore connectivity appears to be commonly restricted to microporous networks. Permeability is expected to be moderate to poor.

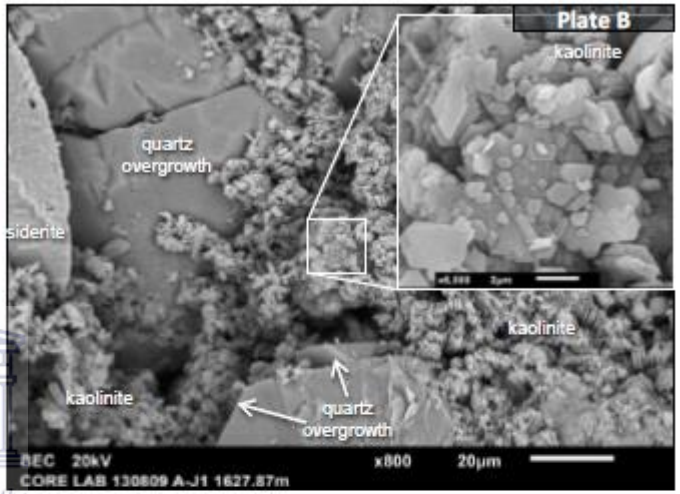

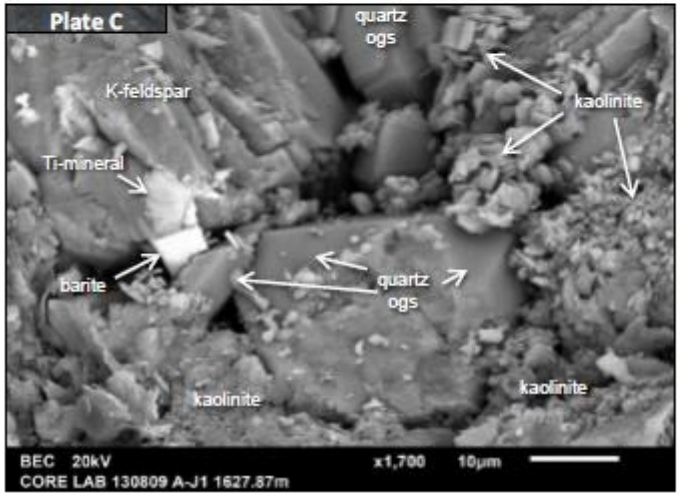

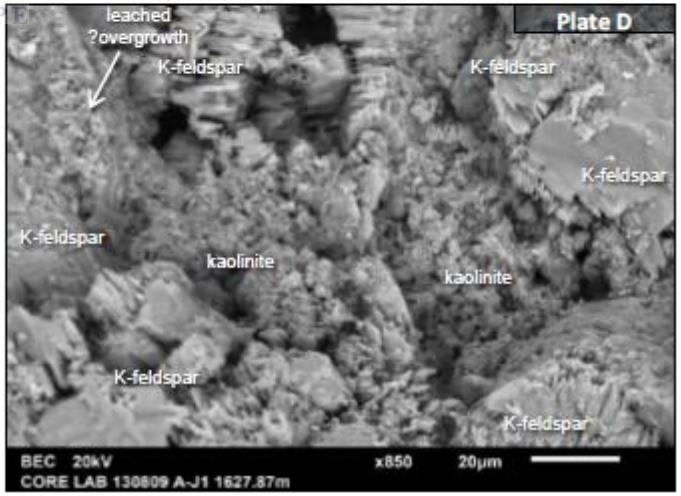

Well: A-J1

Depth: 1629.02m

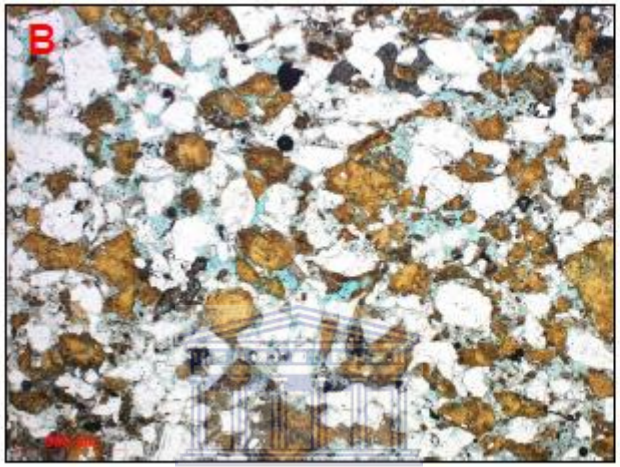

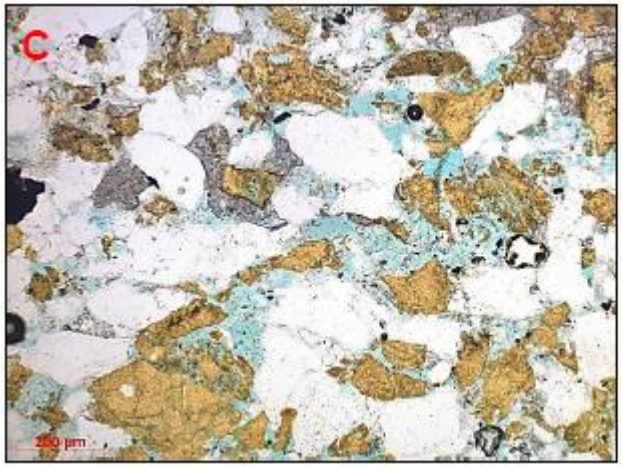

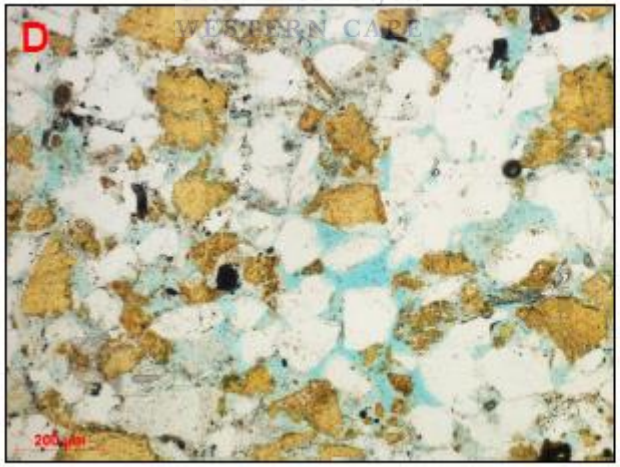

Lithology: Sandstone

Classification: Feldspathic arenite

Texture:
Grain size: Fine (upper)
Sorting: Moderately well sorted.
Grain contacts: Point to point to long.
Grain shape: Angular to rounded.
Compaction: Moderate.

Detrital components:
- Predominant monocrystalline quartz, abundant K-feldspar, common plagioclase and minor amounts of polycrystalline quartz, mica flakes, organic matter and heavy minerals (mainly zircon).

Matrix:
- Detrital clays are minor.

Authigenic phases:
- Sparse pore restricting quartz/feldspar overgrowths ;
- Scattered pore filling kaolinite and chlorite;
- Pore filling to grain replacive siderite/dolomite (also poikilotopic in structure) and calcite are noted;
- Minor pyrite framboids.

Pore system: Porosity is moderately good. Macropores are mainly secondary, the latter linked to the dissolution of K-feldspar grains.

Reservoir quality: Poor to locally moderate

LEGACY CORE ANALYSIS DATA
Porosity: 12.4% at 1629.07m
Permeability: 0.42mD at 1629.07m

Point Count Porosity: 14.3%

Well: A-J1

Depth: 1630.54m

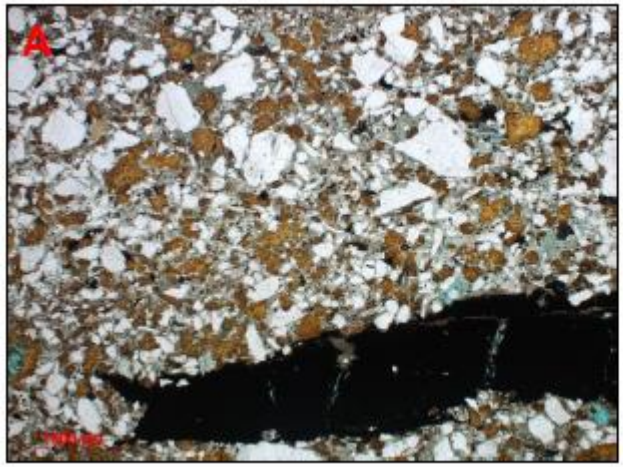

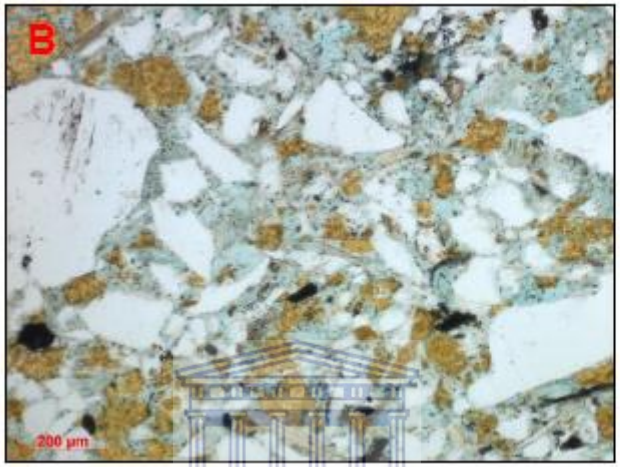

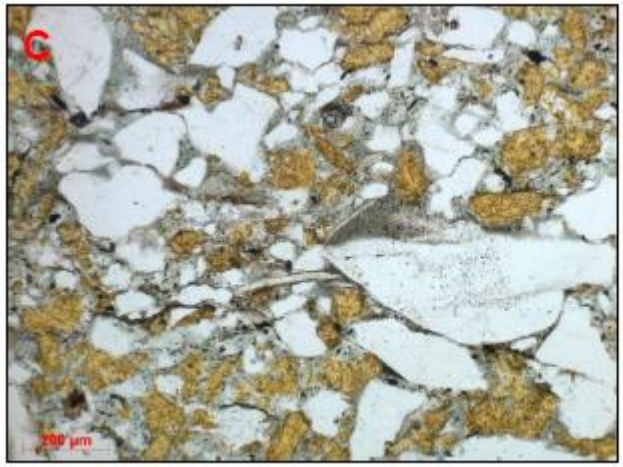

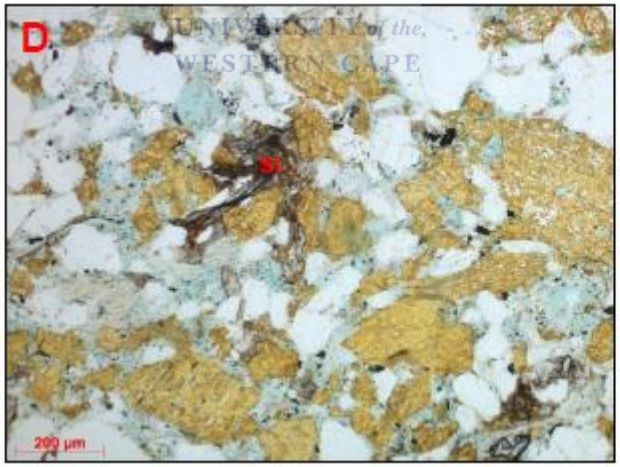

Lithology: Wackes

Classification: Feldspathic wacke*

Texture:
Grain size: Fine to very coarse.
Sorting: Poorly sorted.
Grain contacts: Floating to long.
Grain shape: Angular (locally shardy) to locally rounded.
Compaction: Moderately weak.

Detrital components:
- Predominant monocrystalline quartz, with abundant K-feldspar, common polycrystalline quartz and mica flakes. Organic matter/carbonaceous material and heavy minerals (mainly zircon) are sparse.

Matrix:
- Clays are common (orthomatrix).

Authigenic phases:
- Very finely crystalline pore filling kaolinite is common.
- Sparse pore filling to grain replacive siderite (Si, Image D).
- Lesser amounts of pore restricting quartz and feldspar overgrowths, and pyrite are also noted.

Pore system: Macroporosity is poor. Micropores between clay platelets are likely common, but optically irresolvable.

Reservoir quality: Very poor

LEGACY CORE ANALYSIS DATA
Porosity: 11.8% at 1630.61m
Permeability: 0.21mD at 1630.61m

Point Count Porosity: n/a

**Rock classification is based on visual estimation of mineralogical components.*

Well: A-J1

Depth: 1632.72m

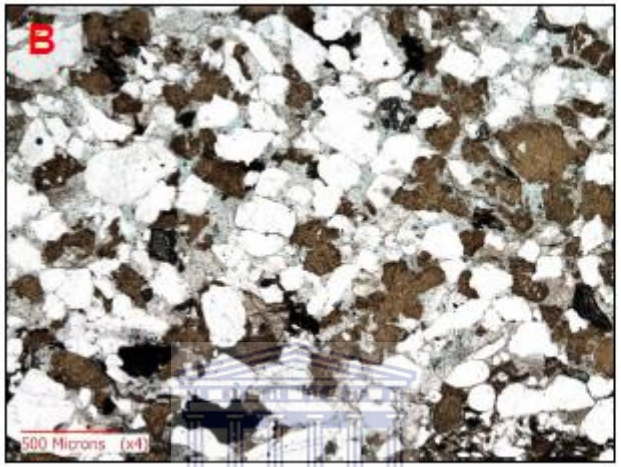

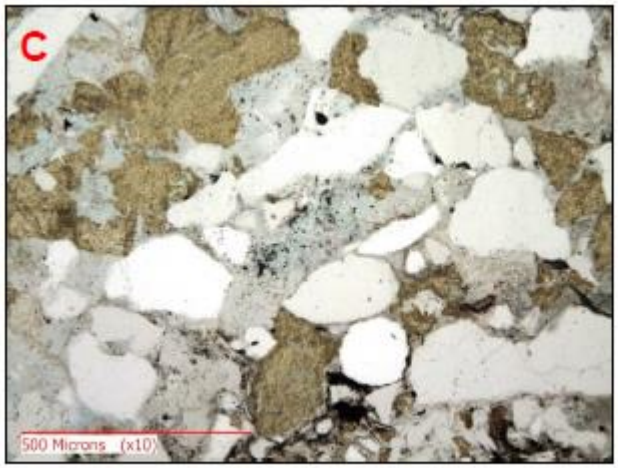

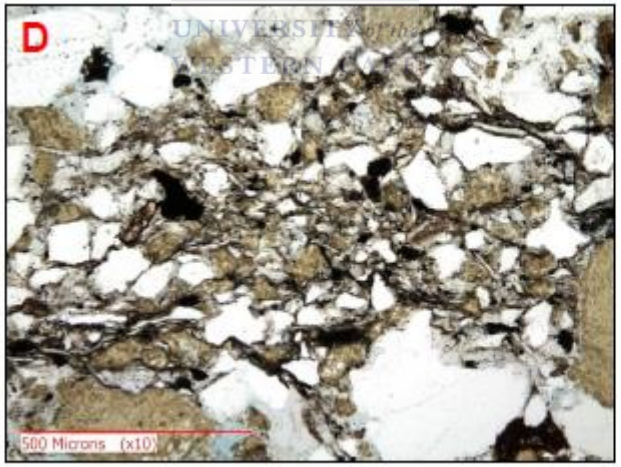

Lithology: Argillaceous sandstone

Classification: Feldspathic arenite*

Texture:
Grain size: Medium (lower) sand is dominant.
Sorting: Moderately poorly sorted.
Grain contacts: Long to concavo-convex.
Grain shape: Angular to well rounded.
Compaction: Moderate overall.

Detrital components:
- Predominant monocrystalline quartz, with abundant K-feldspar, common polycrystalline quartz, lithics (e.g. schistose metamorphic grains) and mica flakes. Organic matter/carbonaceous material and heavy minerals (mainly zircon) are also present.

Matrix:
- Clays are common and also associated with organic matter.

Authigenic phases:
- Common pore restricting quartz/feldspar overgrowths and very finely crystalline pore filling kaolinite;
- Sparse pore filling to grain replacive siderite and pyrite.

Pore system: Porosity is locally moderate. Pore effectiveness has been intensively reduced by detrital and authigenic clays.

Reservoir quality: Very poor

LEGACY CORE ANALYSIS DATA
Porosity: 8.7% at 1632.66m
Permeability: 0.67mD at 1632.66m

Point Count Porosity: n/a

**Rock classification is based on visual estimation of mineralogical components.*

Well: A-J1

Depth: 1633.1m

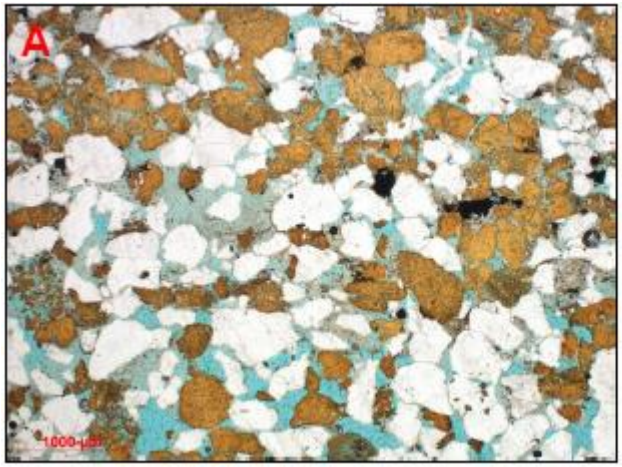

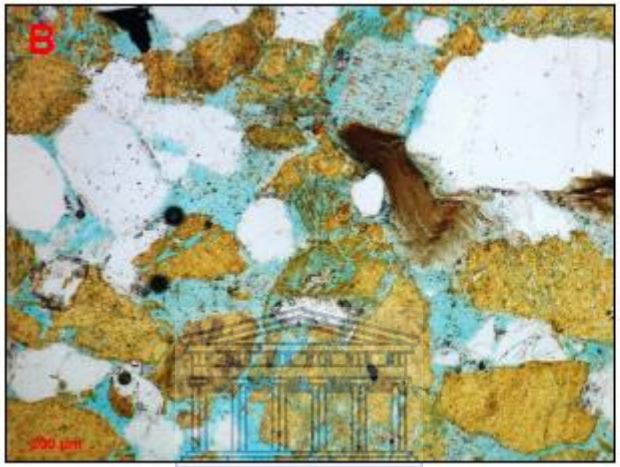

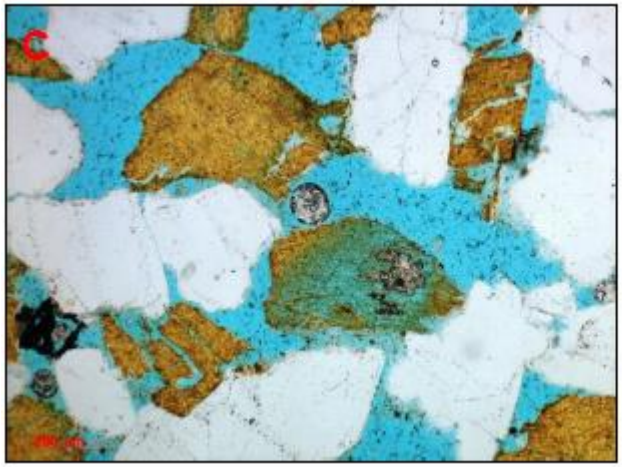

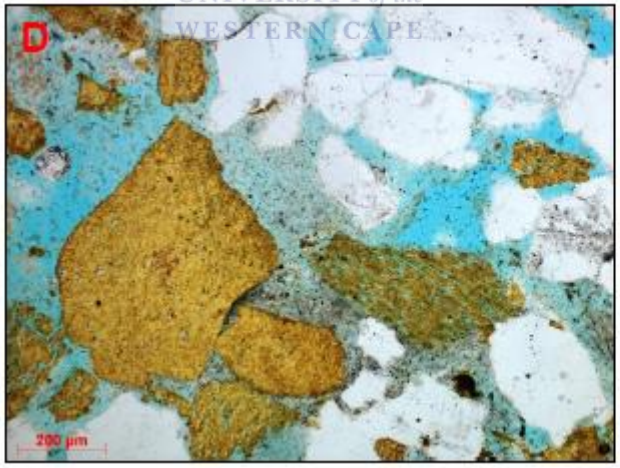

Lithology: Sandstone

Classification: Subfeldspathic arenite*

Texture:
Sample is slightly consolidated overall; coarse grained sand is dominant. Grain shape ranges from subangular to rounded.

Detrital components:
- Abundant monocrystalline and polycrystalline quartz, K-feldspar and minor amounts of mica flakes, organic matter and heavy minerals (zircon).

Matrix:
- Clays are scattered.

Authigenic phases:
- Sparse very finely crystalline pore filling kaolinite and quartz/feldspar overgrowths.
- Pore filling to grain replacive siderite and pyrite are also noted.

Pore system: Porosity is very good to excellent, although artificial pores are common.

Reservoir quality: Very good in the better consolidated areas of the sample; it cannot be assessed in areas with artificial pores.

LEGACY CORE ANALYSIS DATA
Porosity: 21.8% at 1632.92m
Permeability: 183mD at 1632.92m

Point Count Porosity: n/a

**Rock classification is based on visual estimation of mineralogical components.*

Well: A-J1

Depth: 1634.46m

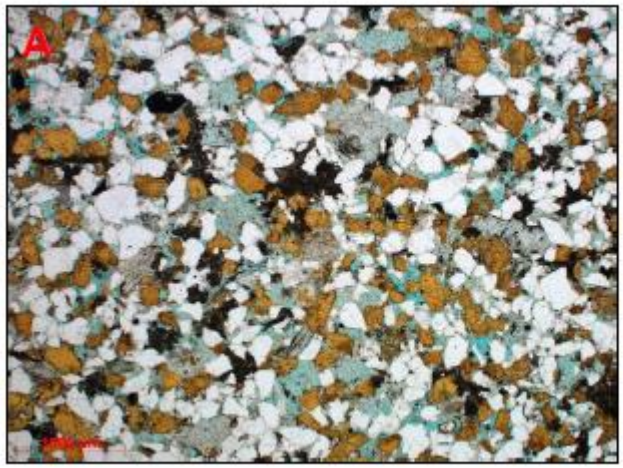

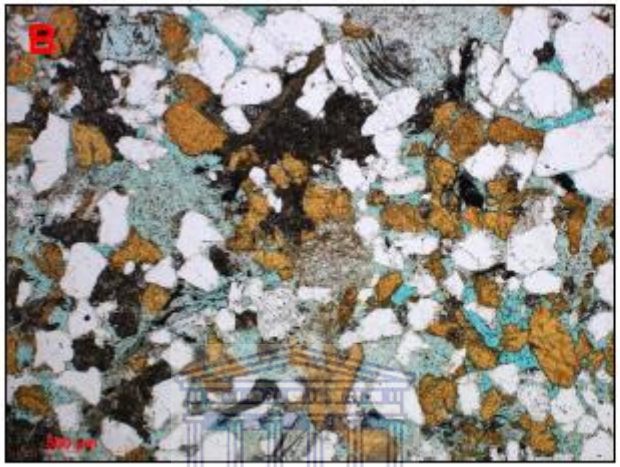

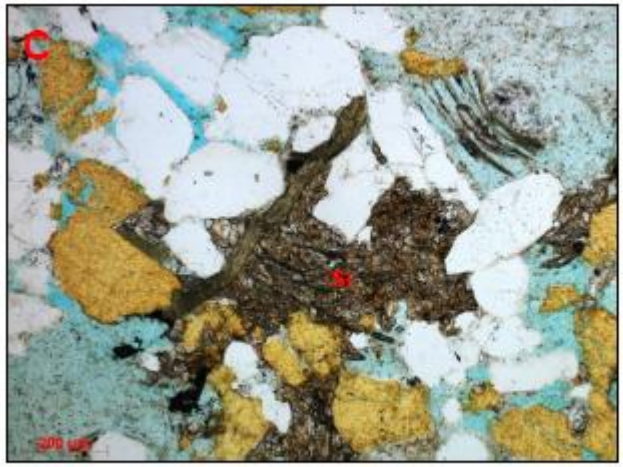

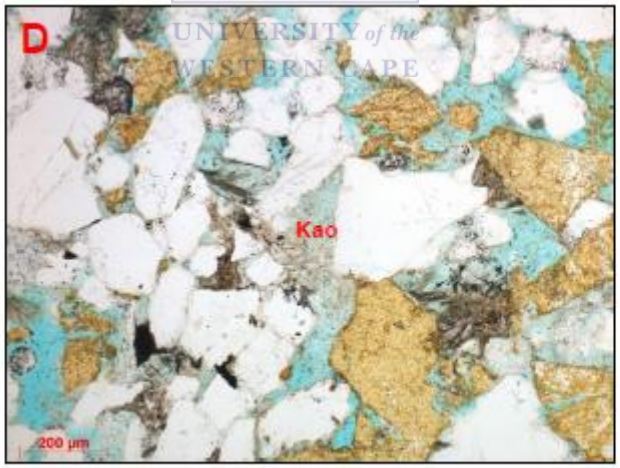

**Rock classification is based on visual estimation of mineralogical components.*

Lithology: Sandstone

Classification: Feldspathic arenite*

Texture:
Grain size: Fine (upper).
Sorting: Moderately well sorted.
Grain contacts: Point to point to long.
Grain shape: Angular to subrounded.
Compaction: Moderately weak overall.

Detrital components:
- Predominant monocrystalline quartz, abundant K-feldspar and lesser amounts of polycrystalline quartz, mica flakes, detrital chlorite, organic matter and heavy minerals (zircon).

Matrix:
- Detrital clays are minor.

Authigenic phases:
- Common pore filling to grain replacive siderite (Si, Image C) is mainly formed by clusters of crystals ranging from ~20µm to ~50µm in size.
- Common very finely to finely crystalline kaolinite (Kao, Image D) fills primary and secondary pores.
- Sparse pore restricting quartz/feldspar overgrowths and pyrite framboids are also noted.

Pore system: Macroporosity is moderate and represented by moderately connected primary and secondary pores. Micropores between kaolinite booklets are inferred to be common (mostly optically irresolvable).

Reservoir quality: Locally moderate

LEGACY CORE ANALYSIS DATA
Porosity: 16.1% at 1634.42m
Permeability: 6.9% at 1634.42m

Point Count Porosity: n/a

Well: A-J1

Depth: 3191.23m

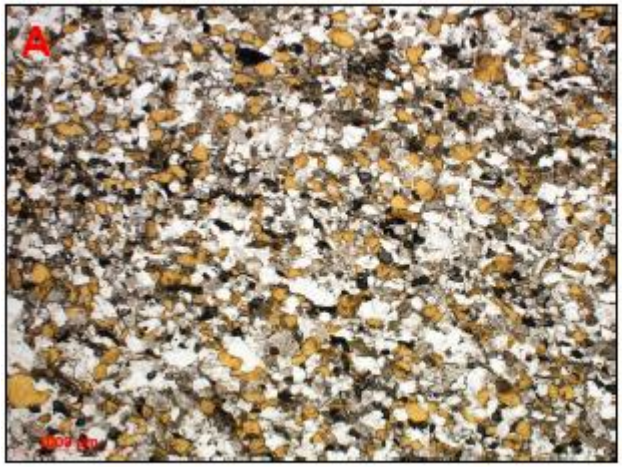

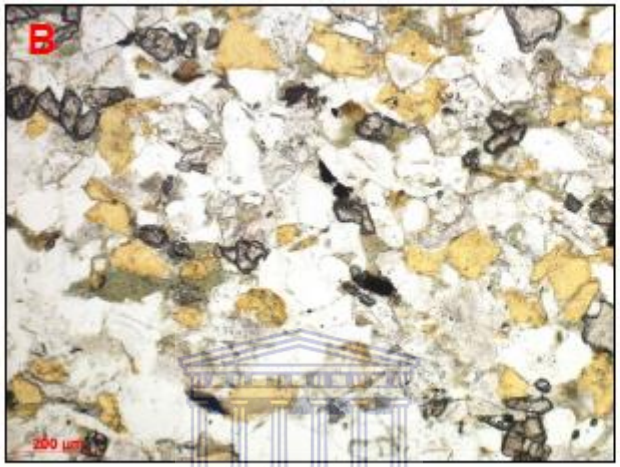

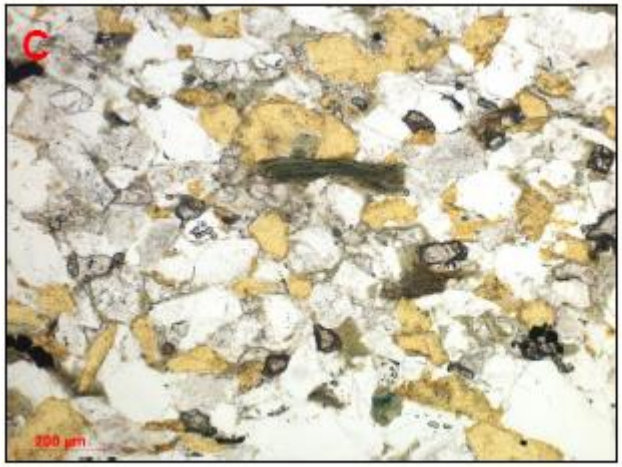

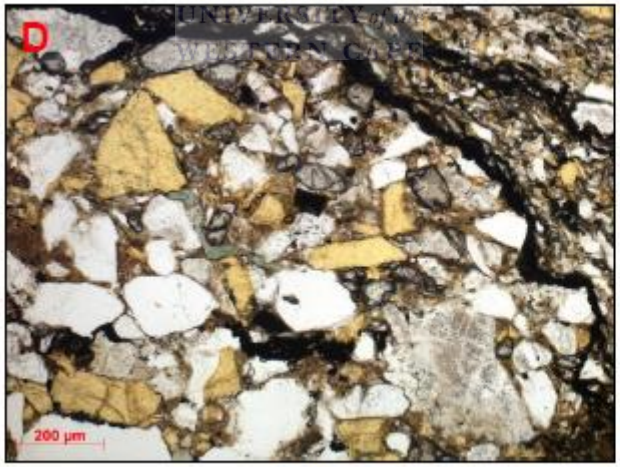

**Rock classification is based on visual estimation of mineralogical components.*

Lithology: Sandstone

Classification: Feldspathic arenite*

Texture:
Grain size: Very fine (upper).
Sorting: Moderately to poorly sorted.
Grain contacts: Point to point to concavo-convex.
Grain shape: Mainly angular to subrounded.
Compaction: Locally strong.

Detrital components:
- Predominant monocrystalline quartz, abundant K-feldspar, relatively common schistose metamorphic grains, mica flakes, detrital chlorite, and organic matter. Heavy minerals (zircon and tourmaline), peloidal grains, remnants of mollusks and possible greenish/brownish ?smectitic pellets.

Matrix:
- Detrital clays are locally abundant.

Authigenic phases:
- Abundant pore filling to replacement siderite, calcite and/or dolomite (also ?botryoidal in structure, see centre of Image E, next page).
- Common grain replacive chlorite and ?smectite ;
- Common pore restricting quartz/feldspar overgrowths;
- Sparse pyrite framboids/microcubes.

Pore system: Porosity is not noted.

Reservoir quality: Very poor

LEGACY CORE ANALYSIS DATA
Porosity: 0.2% at 3191.32m
Permeability: 0.01mD at 3191.32m

Point Count Porosity: n/a

Well: A-J1

Depth: 3191.23m

Well: A-J1

Depth: 3191.23m

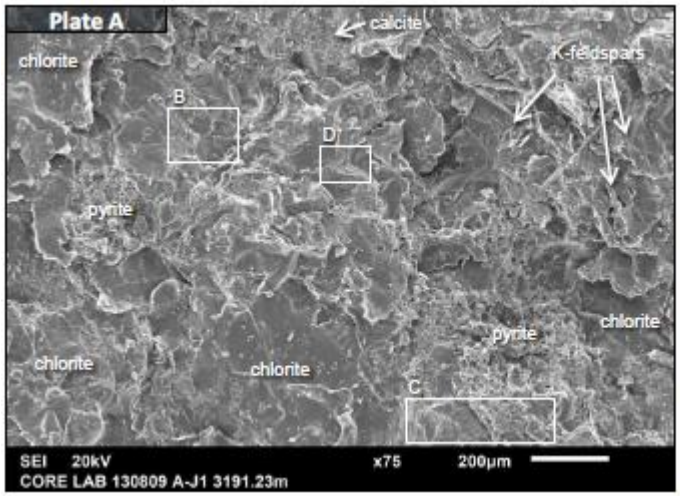

A moderately poorly sorted fine to locally medium grained sample that appears massive at the scale of SEM (A). The sample appears highly compacted with long to concavo-convex grain contacts abundant.

Detrital grains comprise a mix of quartz, K-feldspar (locally leached), plagioclase and chlorite. Abundant chlorite appears to be mainly in the form of compacted detrital flakes (all views), but may include ?matrix clays that could not be differentiated under SEM. (EDX analysis locally detected Ca associated with the chlorite. It is unclear if this is due to ?underlying calcite or is a component of chlorite (possibly ?smectitic).) Accessory grains include scattered Ti-minerals (including sphene) and zircon (D).

Authigenic cements are dominated by common calcite, which forms fine, patchy anhedral developments (B, C). Moderate patchy pyrite forms finely crystalline aggregates of cubes and octahedra (A, C). No overgrowths were identified. Straight and angular forms within K-feldspars (A, C) are thought to be due to breakage along cleavages, but could possibly include ?overgrowths.

Minor chloritic clays were identified as an intergranular phase (D). These are matted to weakly webbed, with K and Ca detected by EDX analysis indicating a probable smectitic composition.

Porosity appears to be very poor, consisting entirely of tight micropores within clays / micas and at grain / clay / cement interfaces. Due to the lack of any visible pore network permeability is expected to be negligible.

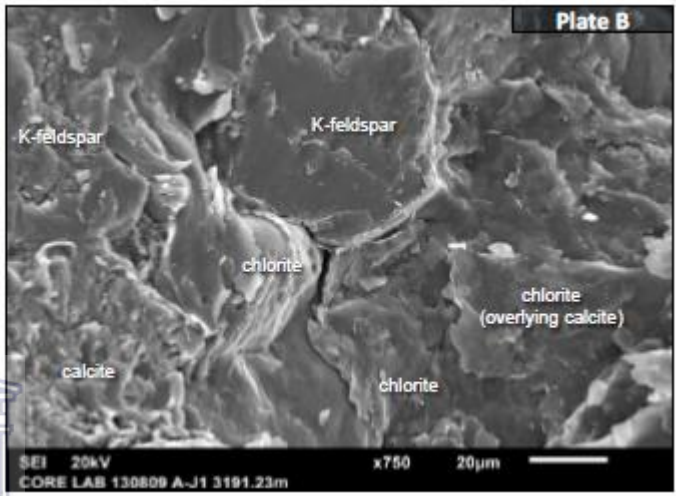

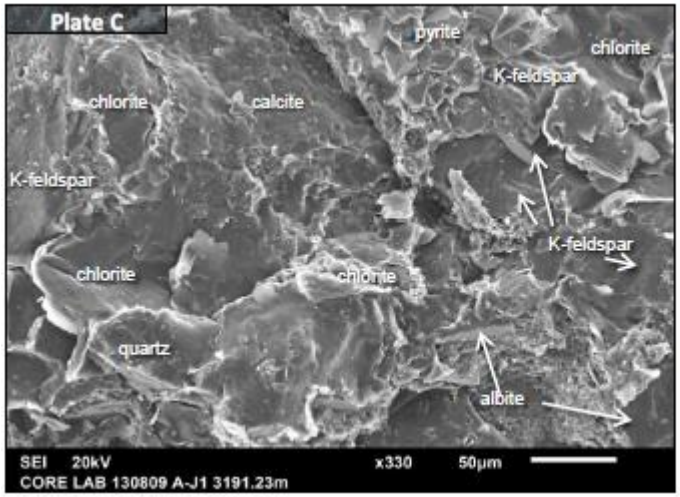

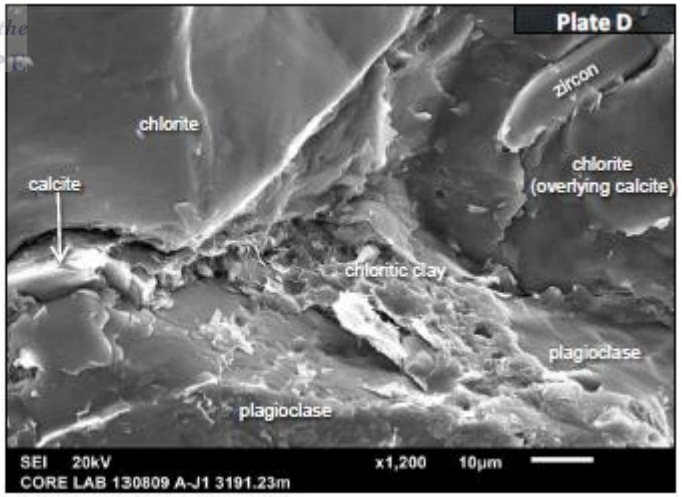

Well: A-J1

Depth: 3191.61m

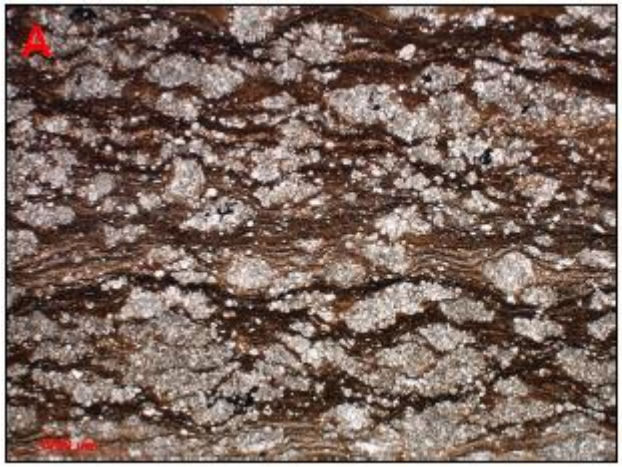

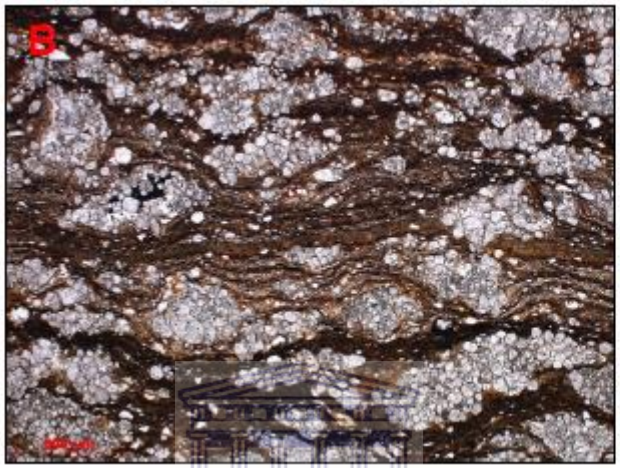

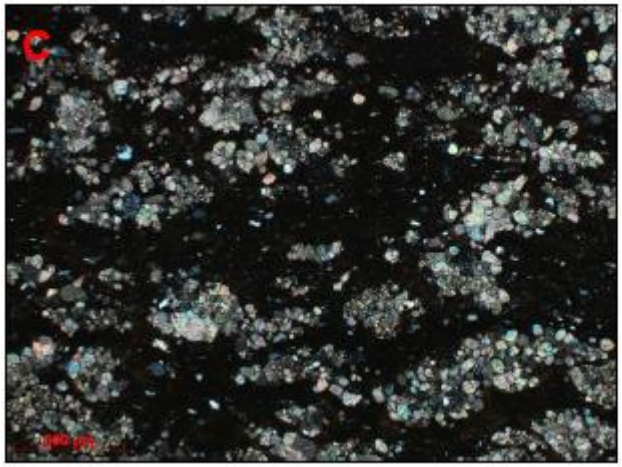

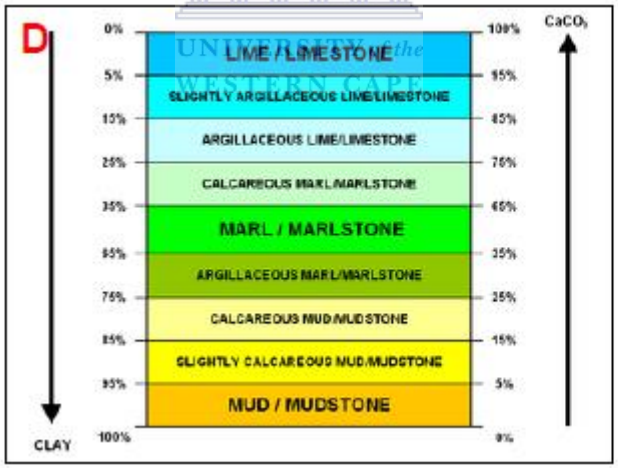

Lithology: Silty/sandy marlstone

Classification: Dolo-marlstone*

Texture:
Burrow-mottled fabric.

Detrital components:
- Silt-grade to medium grained quartz, K-feldspar, small mica flakes and organic matter.

Matrix:
- Abundant clays and dolomicrospar.

Authigenic phases:
- Dolomite filling burrows and replacive of clayey matrix.
- Relatively common pyrite framboids are disseminated within the matrix of this sample.

Pore system: Porosity is not noted.

Reservoir quality: Very poor

LEGACY CORE ANALYSIS DATA
Porosity: n/a
Permeability: n/a

Point Count Porosity: n/a

**Rock classification is based on visual estimation of mineralogical components.*

Well: A-J1

Depth: 3192.59m

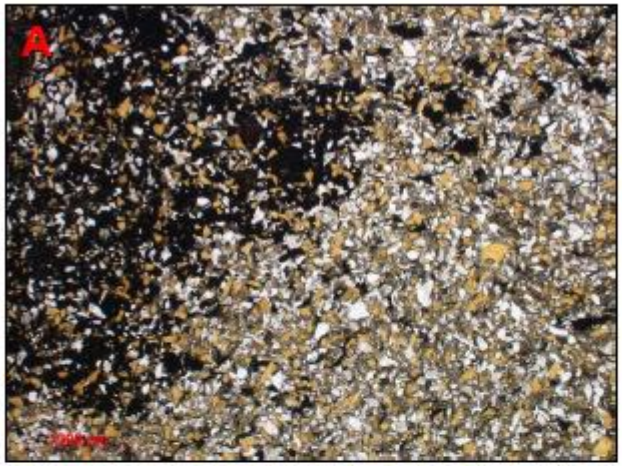

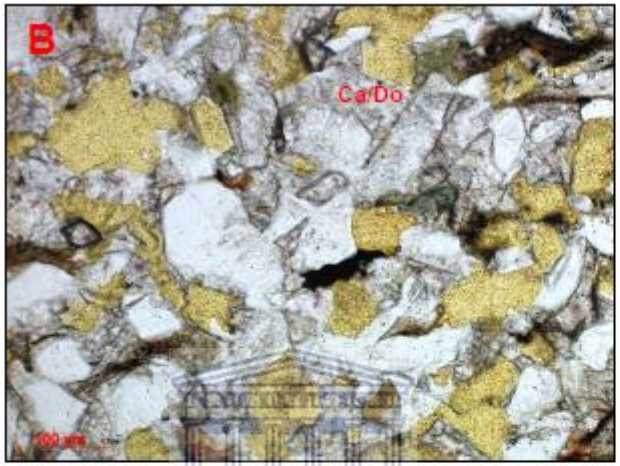

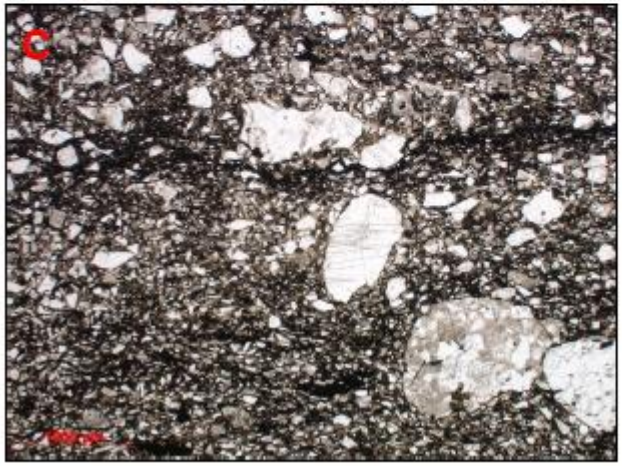

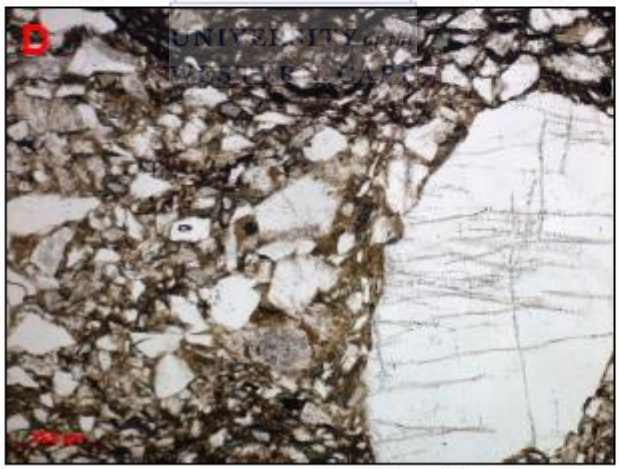

**Rock classification is based on visual estimation of mineralogical components.*

Lithology: Sandstone/argillaceous sandstone

Classification: Feldspathic arenite*

Texture:
Sample is likely at the boundary between two petrotypes (see Images A-B vs. C-D). Such petro-types mainly show substantial variations of clayey matrix and carbonate cement (e.g. Images A-B). Grain size ranges from very fine to granules. Sorting is variable.

Detrital components:
- Predominant monocrystalline quartz, with abundant K-feldspar, common mica flakes, organic matter/carbonaceous material and lesser amounts of plagioclase, polycrystalline quartz, metamorphic grains, detrital chlorite and heavy minerals (mainly zircon & tourmaline).

Matrix:
- Clays range from minor to abundant.

Authigenic phases:
- Pore filling calcite/dolomite is locally abundant (Ca/Do, Image B).
- Pyrite/pyro-bitumen is locally abundant (left side of Image A).
- Grain replacive, siderite, chlorite, ?smectite and pore restricting quartz/feldspar overgrowths are noted.

Pore system: Porosity is not noted.

Reservoir quality: Negligible

LEGACY CORE ANALYSIS DATA
Porosity: n/a
Permeability: n/a

Point Count Porosity: n/a

Well: A-J1

Depth: 3193.5m

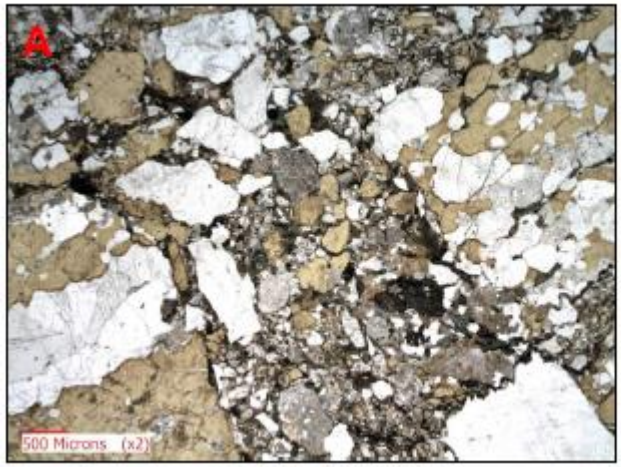

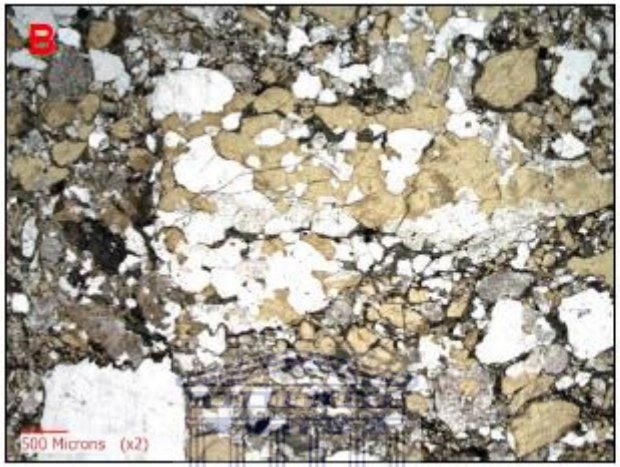

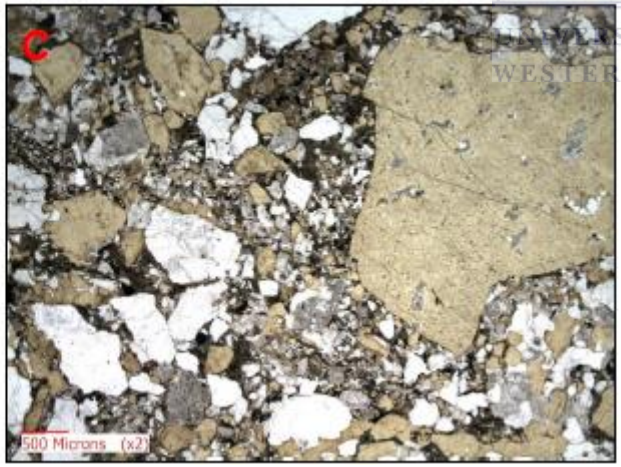

Lithology: Pebbly sandstone

Classification: (Pebbly) feldspathic arenite*

Texture:
Sample contains very fine grained sand to pebbles; sorting is very poor.

Detrital components:
- Predominant quartz, abundant feldspars (mainly K-feldspar), common mica flakes, quartzo-feldspathic metamorphic lithics, mudclasts, organic matter, detrital chlorite and heavy minerals (zircon).

Matrix:
- Sample is shaly.

Authigenic phases:
- Common siderite, pyrite and chlorite (mainly replacement phases); quartz/feldspar overgrowths are also noted.

Pore system: Porosity is poor overall. Micropores between clay platelets are optically irresolvable.

Reservoir quality: Very poor to poor.

LEGACY CORE ANALYSIS DATA
Porosity: 8.3% at 3193.54m
Permeability: 1.6mD at 3193.54m

Point Count Porosity: n/a

**Rock classification is based on visual estimation of mineralogical components.*

Well: A-J1

Depth: 3195.35m

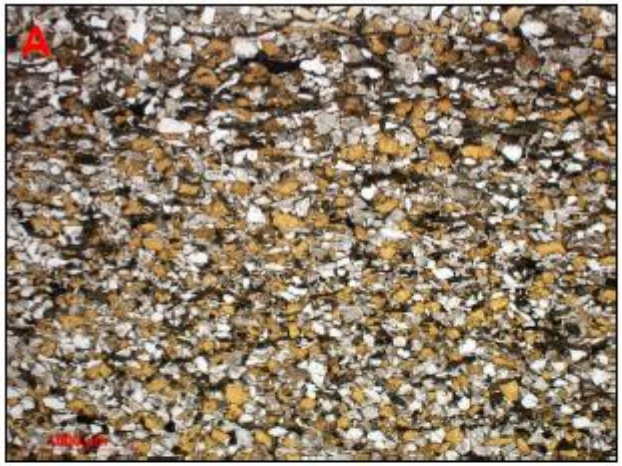

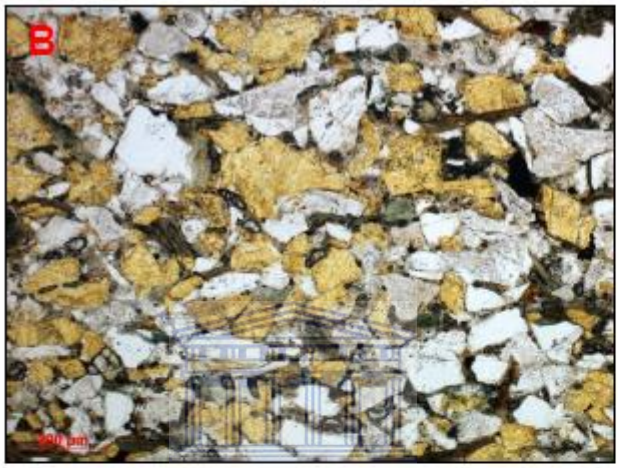

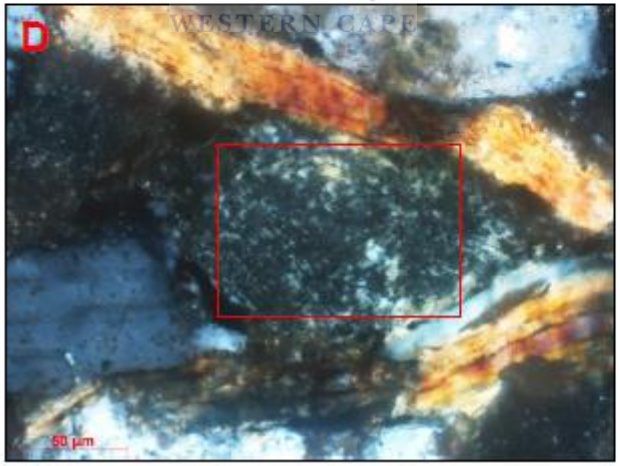

Lithology: Sandstone

Classification: (Micaceous-rich) feldspathic arenite*

Texture:
Grain size: Fine (lower).
Sorting: Moderately well sorted.
Grain contacts: Long to sutured.
Grain shape: Angular to subrounded.
Compaction: Strong.

Detrital components:
- Predominant monocrystalline quartz, abundant feldspars (mainly K-feldspar), common mica flakes and detrital chlorite, as well as organic matter/carbonaceous material.
- Lithics (e.g. chert), brownish/light greenish ?smectitic pellets (Images C-D) and heavy minerals (zircon & tourmaline) are also noted.

Matrix:
- Sample is moderately shaly overall.

Authigenic phases:
- Common pore restricting quartz/feldspar overgrowths;
- Grain replacive chlorite, siderite and pyrite are also present.

Pore system: Porosity is not noted, being occluded by compaction, clays and quartz/feldspar overgrowths.

Reservoir quality: Very poor

LEGACY CORE ANALYSIS DATA
Porosity: n/a
Permeability: n/a

Point Count Porosity: n/a

**Rock classification is based on visual estimation of mineralogical components.*

Well: A-J1

Depth: 3195.35m

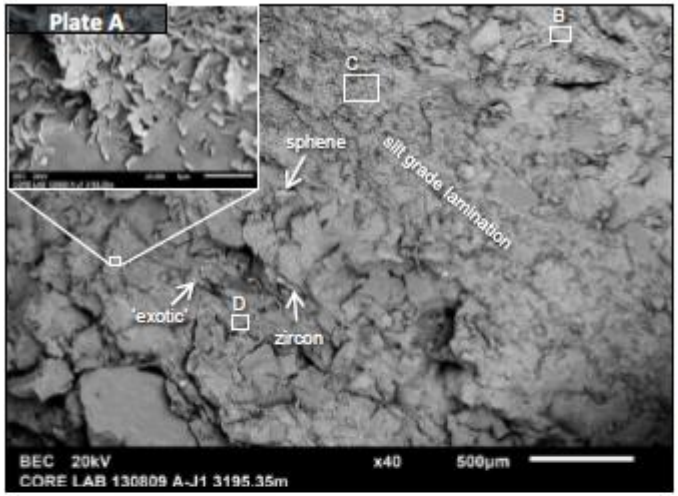

A mainly sandstone sample that is laminated by variations in grain size (A). The sample is mainly fine grained, with rare grains up to coarse; with very fine and silt dominated (C) laminae. The sample is well compacted with common long grain contacts observed.

Detrital grains are dominated by K-feldspar with abundant quartz and plagioclase. Detrital chlorite takes the form of fine flakes (C). Common Ti-minerals, concentrated within silt grade lamination are dominated by sphene (C, sph). Accessory grains include zircon, apatite and 'exotics' (A, 'exotic' is a Ca+La+Ce+Nd mineral).

Authigenic chlorite is abundant as a well developed authigenic phase within sand grade laminae. The chlorite is both grain-coating (B) and pore-filling (D). Intergranular chlorite also commonly takes the form of poorly developed matted to weakly platy matrix clays.

Overall porosity appears moderate to moderately poor, and is dominated by microporosity associated with clays and silt grade phases. Pore connectivity appears to be largely restricted to microporous pathways, so permeability is expected to be poor.

C annotation: KF = K-feldspar; sph = sphene

Note: sphene was not detected by XRD analysis, possibly due to sample heterogeneity / laminations

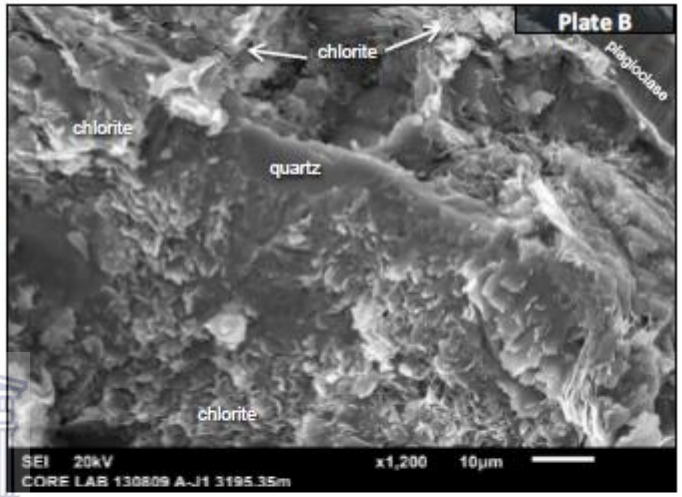

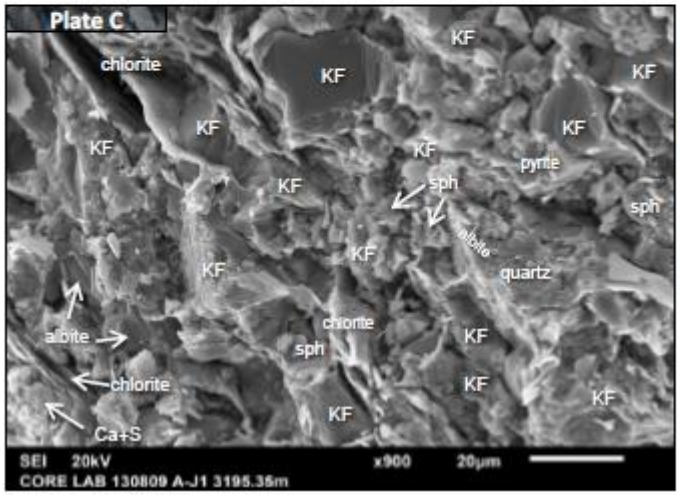

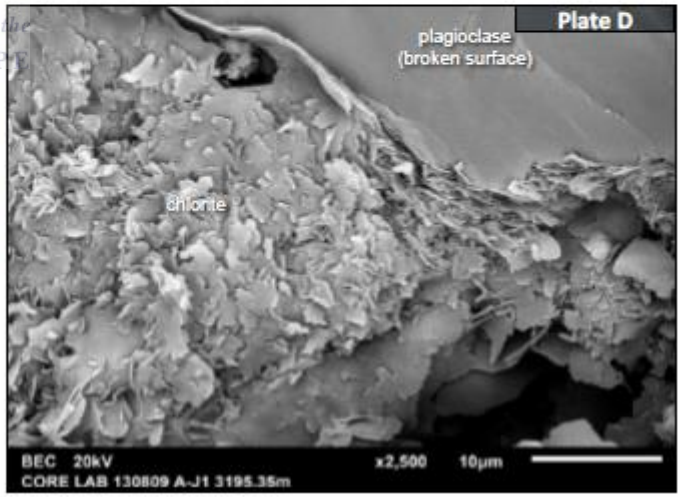

Well: A-J1

Depth: 3198.67m

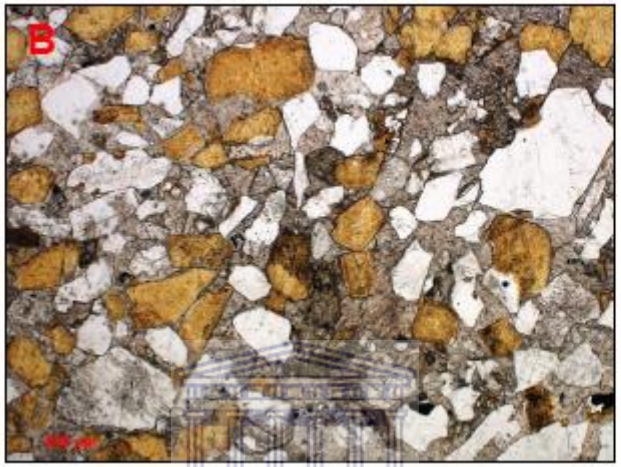

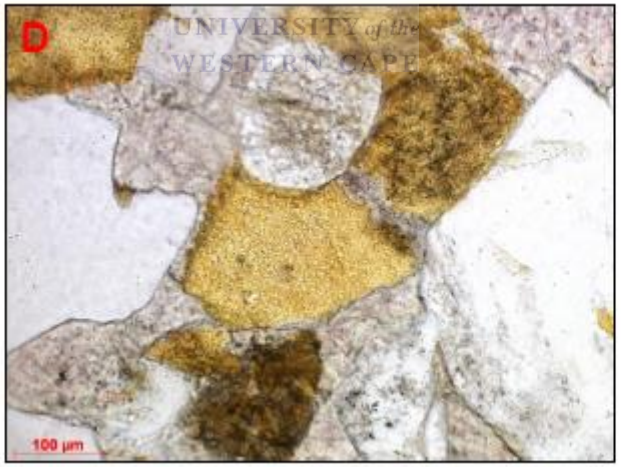

Lithology: Sandstone

Classification: Feldspathic arenite*

Texture:
Grain size: Fine (upper) sand is dominant; granules are also noted.
Sorting: Moderately poorly sorted.
Grain contacts: Floating (due to carbonate cementation) to point to point.
Grain shape: Angular to locally rounded.
Compaction: Weak

Detrital components:
- Predominant monocrystalline quartz, with abundant feldspars (mainly K-feldspar), common mica flakes and detrital chlorite, and lesser amounts of metamorphic lithics, organic matter and heavy minerals (e.g. zircon).

Matrix:
- Sample is clean.

Authigenic phases:
- Extensive non ferroan calcite (mainly poikilotopic in structure) occludes primary and secondary pores and replaces grains.
- Lesser amounts of pore restricting quartz/feldspar overgrowths, grain replacive chlorite, siderite and pyrite are also present.

Pore system: Porosity is not noted.

Reservoir quality: Negligible

LEGACY CORE ANALYSIS DATA
Porosity: 6.6% at 3198.74m
Permeability: 0.01mD at 3198.74m

Point Count Porosity: n/a

**Rock classification is based on visual estimation of mineralogical components.*

Well: A-J1

Depth: 3199.81m

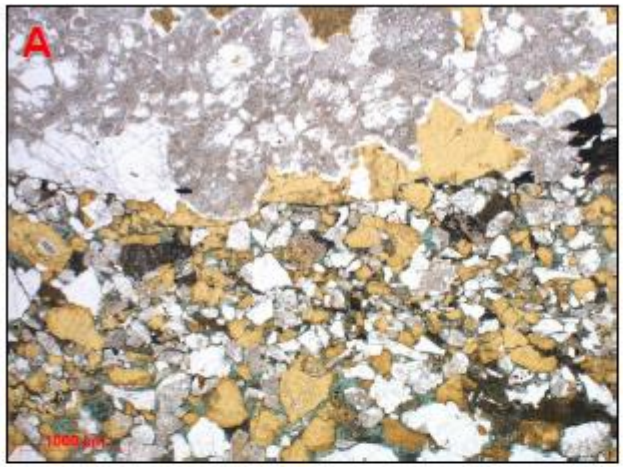

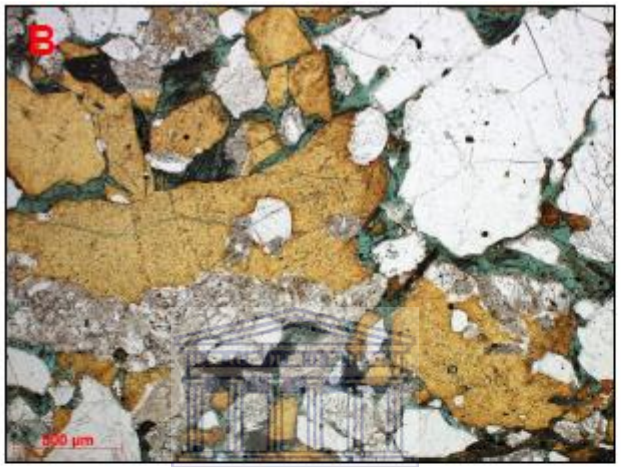

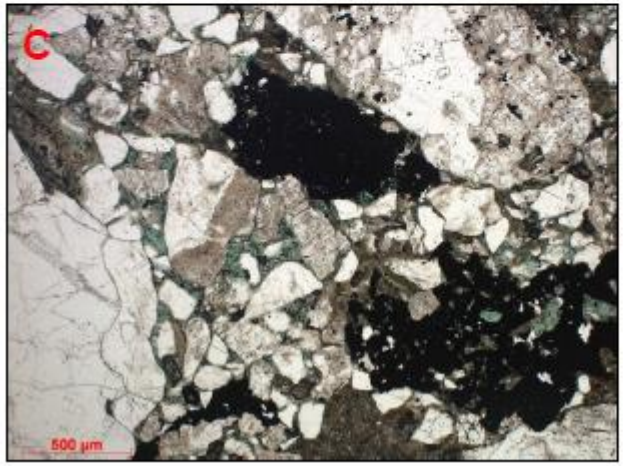

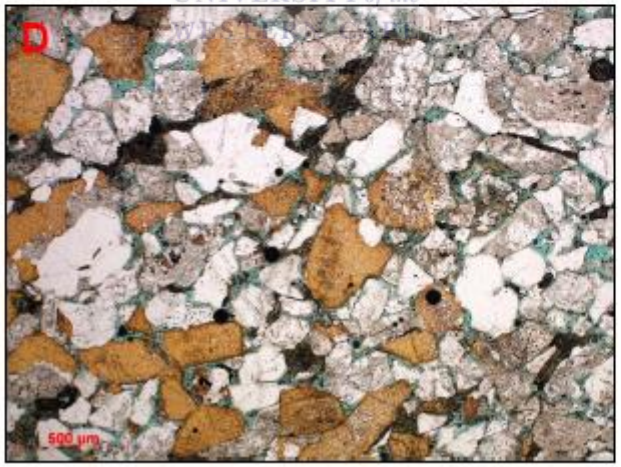

Lithology: Pebbly sandstone

Classification: Feldspathic arenite*

Texture:
Grain size: Up to pebbles.
Sorting: (Very) poorly sorted.
Grain contacts: Long to point to point.
Grain shape: Angular to subrounded.
Compaction: Moderate overall.

Detrital components:
- Predominant monocrystalline quartz and abundant K-feldspar, polycrystalline quartz and quartzo-feldspathic-rich lithics (likely fragments of gneiss).
- Mudclasts, plagioclase, granules of plagioclase-rich volcanic rocks, mica flakes and organic matter are also noted.

Matrix:
- Sample is moderately shaly overall.

Authigenic phases:
- Pore restricting quartz/feldspar overgrowths, authigenic clays (?chlorite), siderite and pyrite/?pyrobitumen.

Pore system: Porosity is locally moderate, however, macropores are poorly interconnected.

Reservoir quality: Poor

LEGACY CORE ANALYSIS DATA
Porosity: 9.4% at 3199.86m
Permeability: 2.7mD at 3199.86m

Point Count Porosity: n/a

**Rock classification is based on visual estimation of mineralogical components.*

Well: A-J1

Depth: 3200.9m

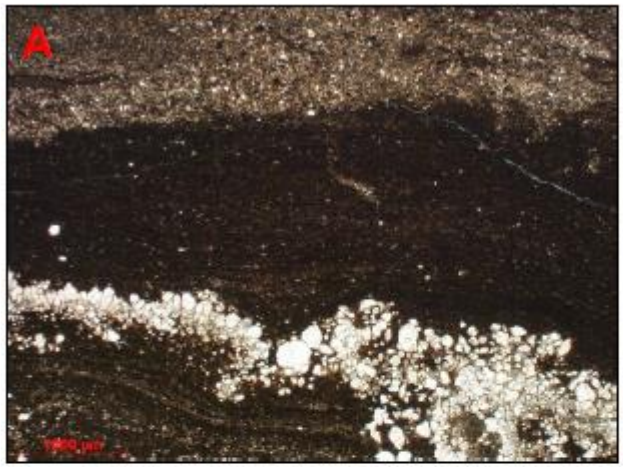

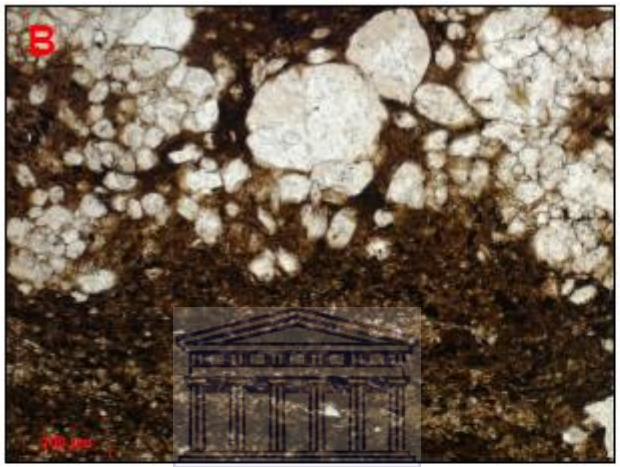

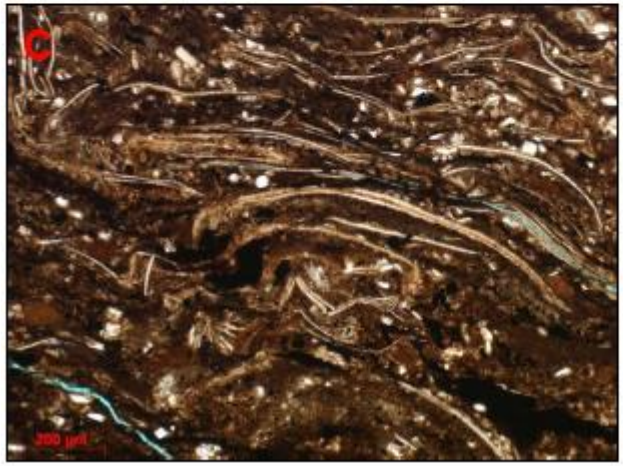

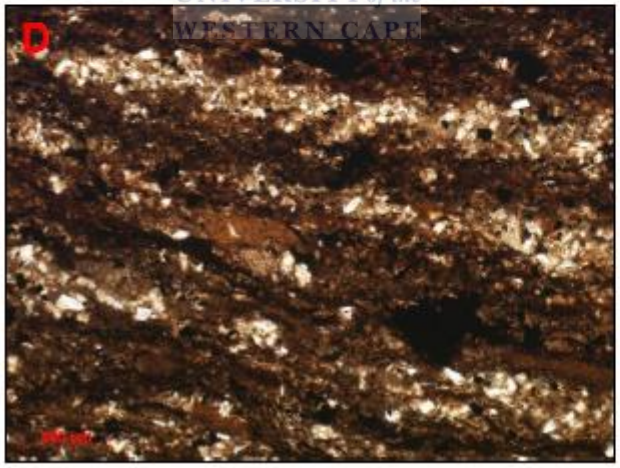

Lithology: Dolomitic claystone

Classification: Silty/sandy dolomitic claystone*

Texture:
Burrow-mottled fabric.

Detrital components:
- Silt-grade to fine grained quartz, K-feldspar, small mica flakes, phosphatic material and organic matter/carbonaceous material. Thin bivalves (Image C) are locally common.

Matrix:
- Abundant clays locally intermixed with dolomicrospar.

Authigenic phases:
- Dolomite filling burrows and replacive of clayey matrix.
- Relatively common pyrite framboids are disseminated within the matrix of this sample.

Pore system: Porosity is not noted.

Reservoir quality: Very poor

LEGACY CORE ANALYSIS DATA
Porosity: n/a
Permeability: n/a

Point Count Porosity: n/a

**Rock classification is based on visual estimation of mineralogical components.*

Well: A-J1

Depth: 3201.6m

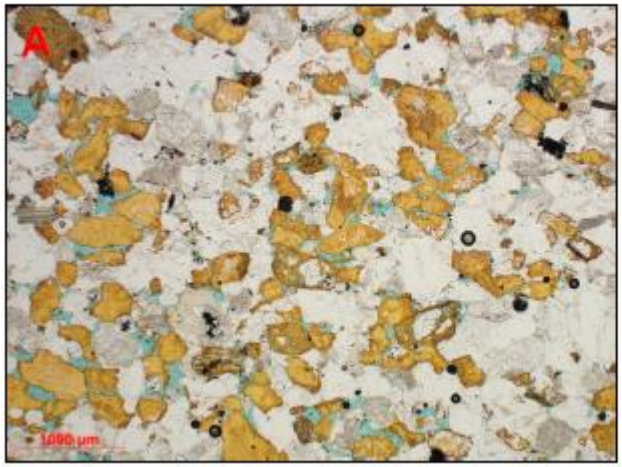

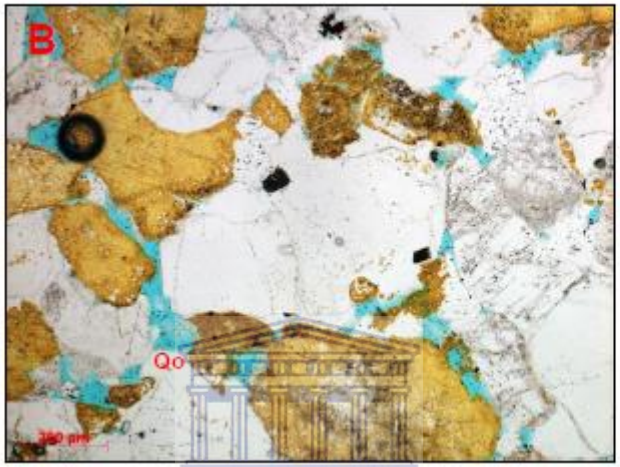

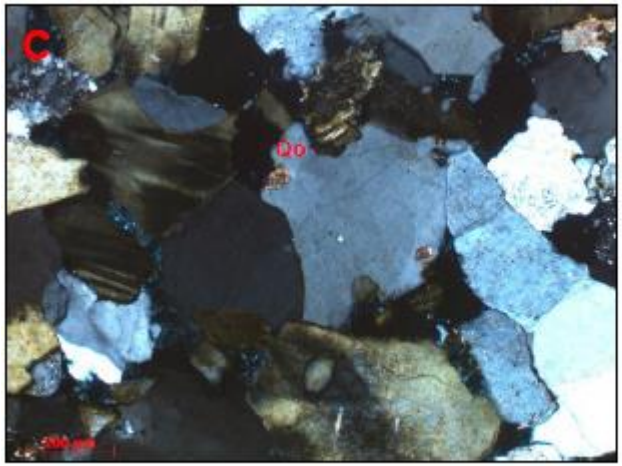

Lithology: Sandstone

Classification: Feldspathic arenite

Texture:
Grain size: Medium (lower) sand is dominant.
Sorting: Moderately well sorted.
Grain contacts: Long to sutured.
Grain shape: Angular to rounded.
Compaction: Moderately strong.

Detrital components:
- Predominant monocrystalline quartz and abundant feldspars (both plagioclase and K-feldspar), with lesser amounts of polycrystalline quartz, mica flakes, lithics, organic matter and zircon.

Matrix:
- Clays are minor.

Authigenic phases:
- Abundant tabular to prismatic quartz overgrowths (Qo, Images B-C, XPL) and common feldspar overgrowths restrict pores and pore throats;
- Scattered pore filling to grain replacive non ferroan calcite (Ca, Image D) and siderite are also present.
- Minor grain replacive chlorite, kaolinite and pyrite.

Pore system: Porosity is locally moderate. Pore effectiveness has been strongly downgraded by compaction and quartz/feldspar overgrowths, locally by carbonate cementation. Note that artificial pores and fractures are present.

Reservoir quality: Locally moderate

LEGACY CORE ANALYSIS DATA
Porosity: 9.6% at 3201.52m
Permeability: 41mD at 3201.52m

Point Count Porosity: 7.0%

Well: A-J1

Depth: 3205.42m

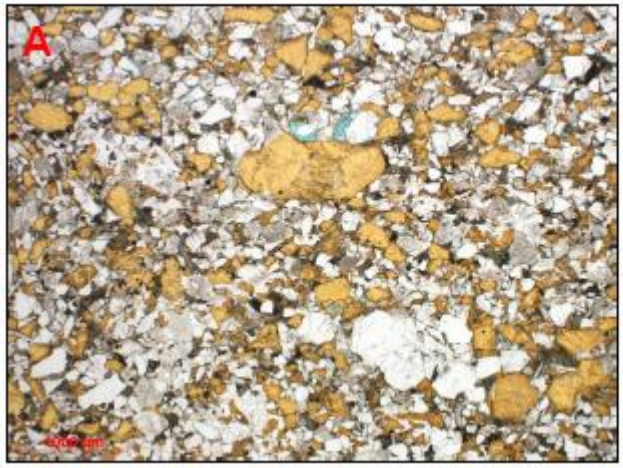

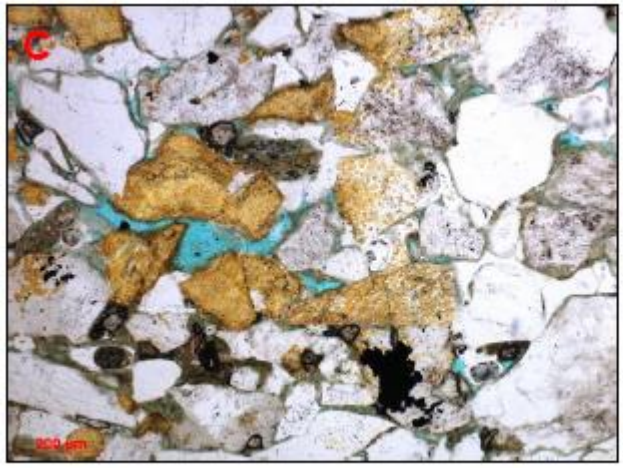

Lithology: Sandstone

Classification: Feldspathic arenite*

Texture:
Grain size: Fine and medium-grained sand are abundant.
Sorting: Moderately poorly sorted overall.
Grain contacts: Point to point to sutured.
Grain shape: Angular to rounded.
Compaction: Moderately strong.

Detrital components:
- Predominant monocrystalline quartz and abundant feldspars (mainly K-feldspar), common mica flakes (mainly biotite), polycrystalline quartz and detrital chlorite;
- Lithics (metamorphic and volcanic), organic matter and heavy minerals (e.g. zircon & tourmaline) are noted.

Matrix:
- Sample is moderately shaly overall.

Authigenic phases:
- Common quartz/feldspar overgrowths restrict pores and pore throats;
- Patchy pore occluding non ferroan calcite (Ca, Image B) is present;
- Grain rimming to grain replacive chlorite, siderite and pyrite framboids/microcubes are sparse.

Pore system: Macroporosity is poor, being significantly downgraded by compaction and cementation by quartz/feldspar overgrowths and calcite.

Reservoir quality: Very poor to poor

LEGACY CORE ANALYSIS DATA
Porosity: 12.1% at 3205.37m
Permeability: 0.141mD at 3205.37m

Point Count Porosity: n/a

**Rock classification is based on visual estimation of mineralogical components.*

Well: A-J1

Depth: 3210.2m

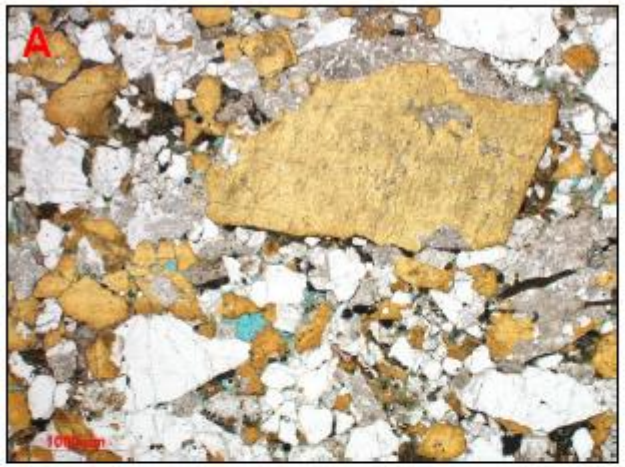

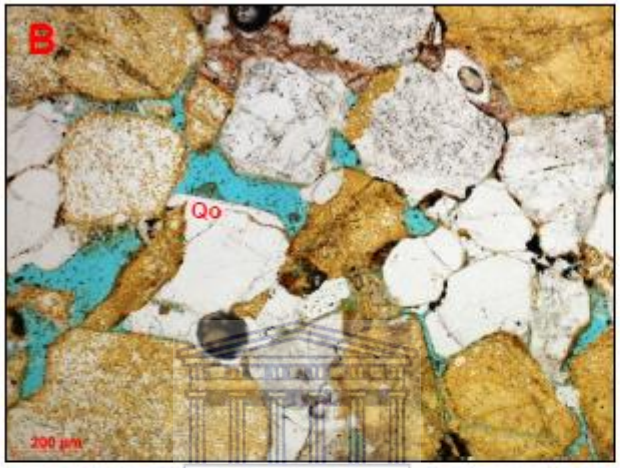

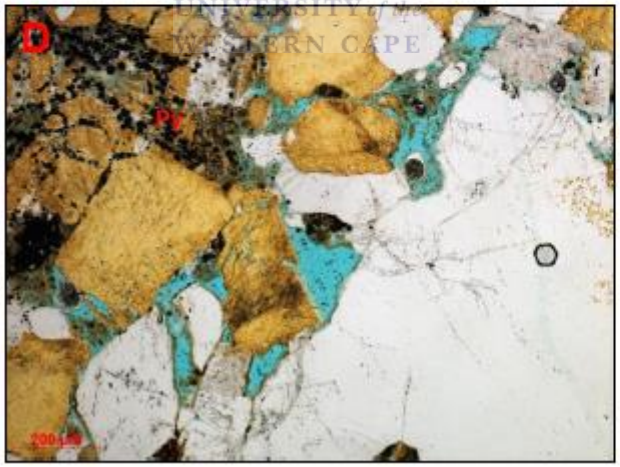

Lithology: Granular sandstone

Classification: Feldspathic arenite

Texture:
Grain size: Very fine to granules.
Sorting: Poorly sorted.
Grain contacts: Mainly long to concavo-convex.
Grain shape: Subangular to rounded.
Compaction: Moderately strong.

Detrital components:
- Predominant monocrystalline quartz, with abundant feldspars (mainly K-feldspar), sparse polycrystalline quartz, lithics (mainly metamorphic) mica flakes (mainly biotite), detrital chlorite, organic matter and heavy minerals (e.g. tourmaline).

Matrix:
- Sample is slightly shaly.

Authigenic phases:
- Common quartz overgrowths (Qo, Image B)/feldspar overgrowths restrict pores and pore throats;
- Patchy pore occluding non ferroan calcite (Ca, Image C) is present;
- Grain rimming to grain replacive chlorite, as well as grain replacive siderite and pyrite (Py, Image D) are sparse.

Pore system: Porosity is poor overall. Poorly connected macropores are primary and secondary, the latter being linked to the dissolution of feldspar grains.

Reservoir quality: Poor

LEGACY CORE ANALYSIS DATA
Porosity: 9.1% at 3210.29m
Permeability: 6.3% at 3210.29m

Point Count Porosity: 5.7%

Well: A-J1

Depth: 33113.47m

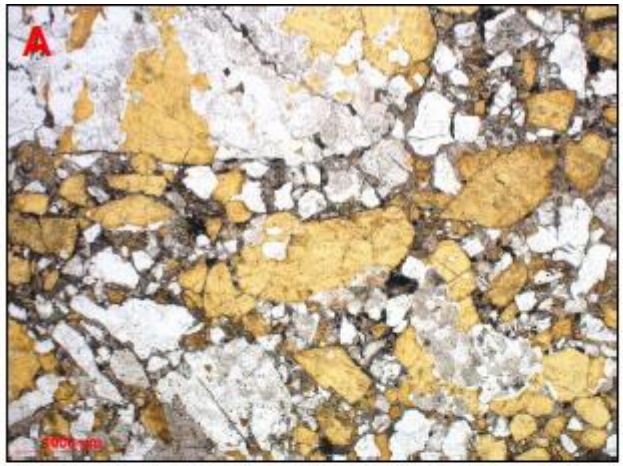

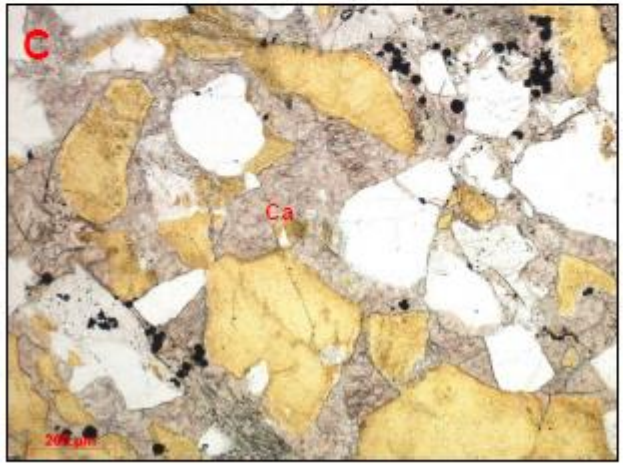

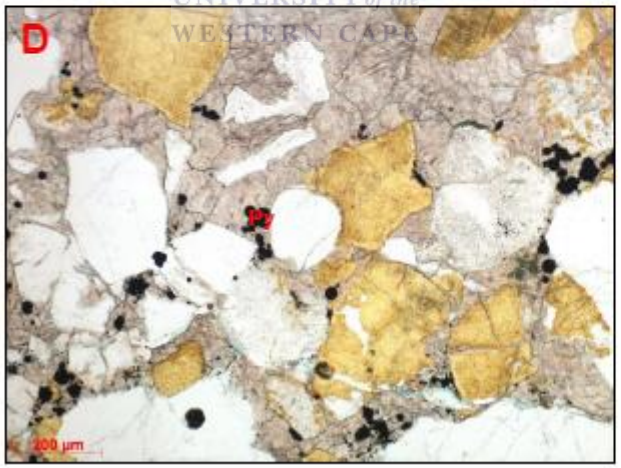

Lithology: Pebbly sandstone

Classification: Feldspathic arenite*

Texture:
Grain size: Very fine to pebbles.
Sorting: Very poorly sorted.
Grain contacts: Floating to point to point.
Grain shape: Angular to rounded.
Compaction: Moderately weak

Detrital components:
- Predominant monocrystalline quartz, with abundant feldspars (mainly K-feldspar), common polycrystalline quartz, common lithics (metamorphic) and sparse mica flakes (biotite), detrital chlorite, organic matter and heavy minerals (zircon & tourmaline).

Matrix:
- Detrital clays are sparse and locally intermixed with micrite/microspar.

Authigenic phases:
- Extensive non ferroan calcite (Ca, Image C) occludes primary and secondary pores, and replaces grains.
- Pore restricting quartz/feldspar overgrowths and pyrite framboids (Py, Image D) are also relatively common.

Pore system: Porosity is not noted. Thin fractures present in this sample are thought to be artificial.

Reservoir quality: Negligible

LEGACY CORE ANALYSIS DATA
Porosity: 6% at 3213.55m
Permeability: 0.05mD at 3213.55m

Point Count Porosity: n/a

**Rock classification is based on visual estimation of mineralogical components.*

Well: A-J1

Depth: 3213.88m

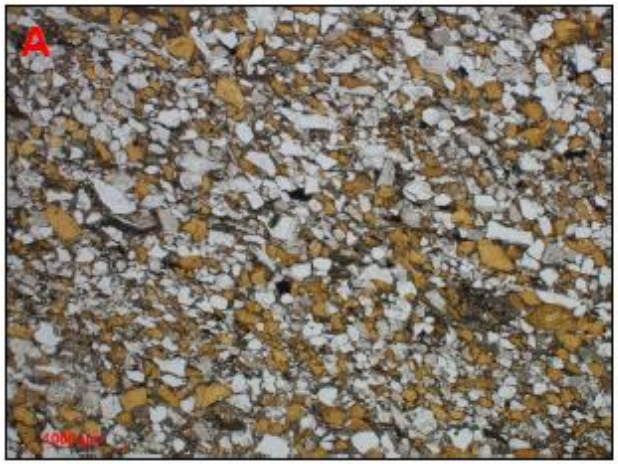

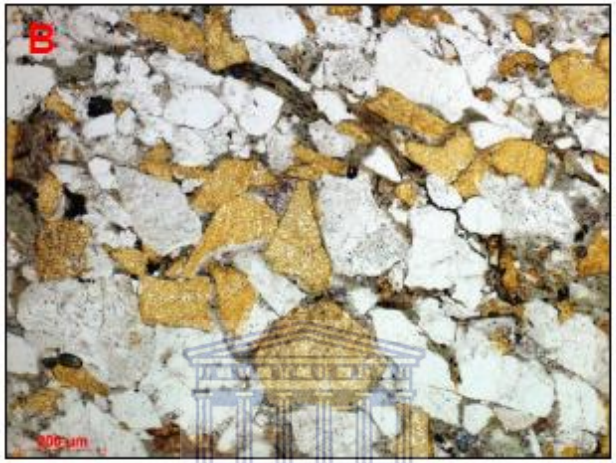

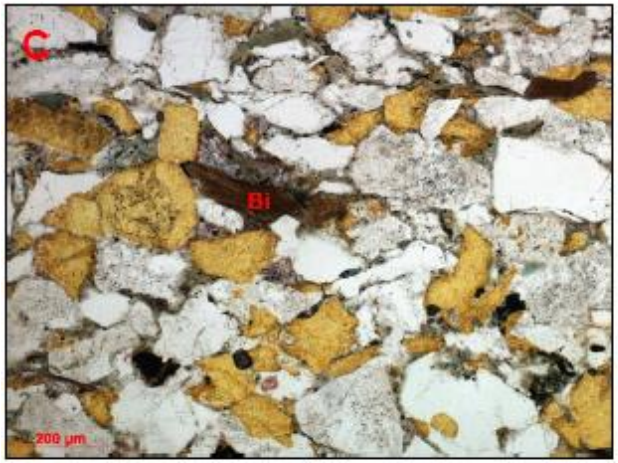

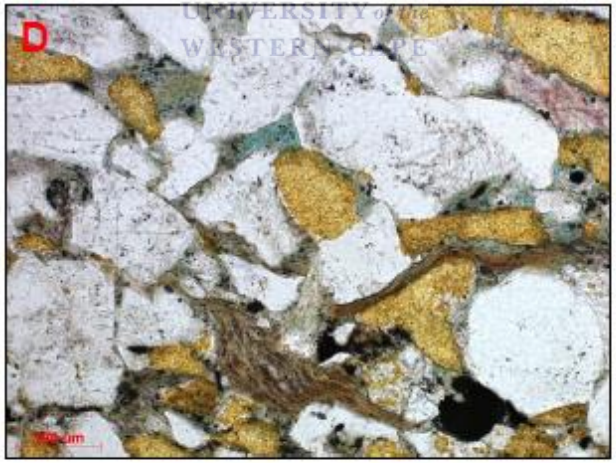

Lithology: Sandstone

Classification: Feldspathic arenite*

Texture:
Grain size: Very fine to fine. Sample is laminitic.
Sorting: Moderately sorted overall.
Grain contacts: Long to sutured.
Grain shape: Angular to rounded.
Compaction: Strong.

Detrital components:
- Predominant monocrystalline quartz, abundant K-feldspar, common plagioclase, biotite flakes (Bi, Image C), detrital chlorite and lesser amounts of lithics (volcanic and metamorphic grains), polycrystalline quartz, organic matter and heavy minerals (zircon).

Matrix:
- Clays are relatively common (pseudo & ortho-matrix).

Authigenic phases:
- Common pore restricting quartz/feldspar overgrowths and patchy pore occluding to grain replacive non ferroan calcite;
- Lesser amounts of pore filling kaolinite, pore lining to grain replacive chlorite, siderite and pyrite are also noted.

Pore system: Porosity is poor. Macropores are poorly interconnected. Micropores between clay platelets are optically irresolvable.

Reservoir quality: Poor

LEGACY CORE ANALYSIS DATA
Porosity: 9.7% at 3213.79m
Permeability: 0.98mD at 3213.79m

Point Count Porosity: n/a

**Rock classification is based on visual estimation of mineralogical components.*

Well: A-J1

Depth: 3215.37m

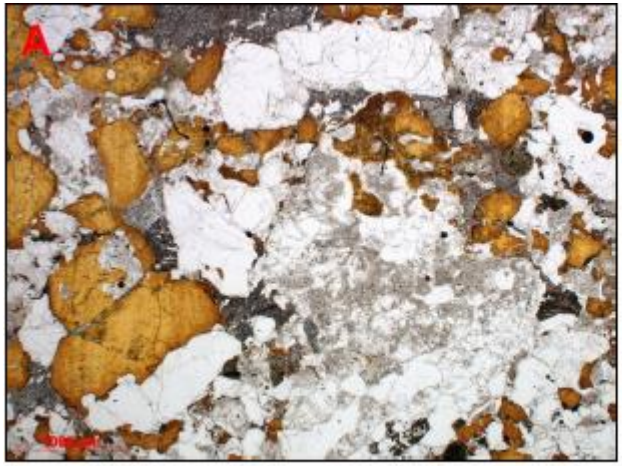

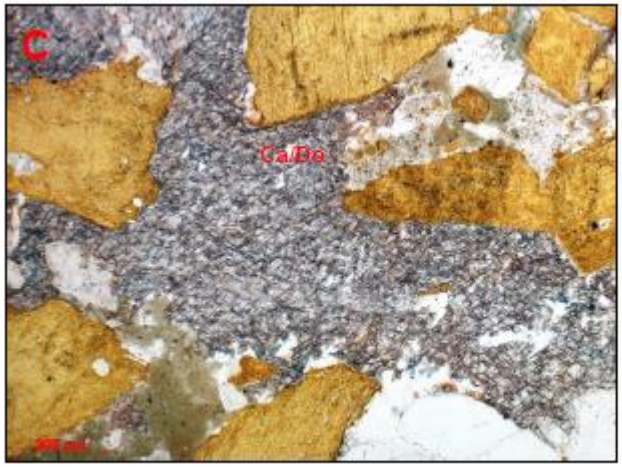

Lithology: Pebbly sandstone

Classification: Feldspathic arenite*

Texture:
Grain size: Very fine to pebbles.
Sorting: Very poorly sorted.
Grain contacts: Concavo-convex to sutured.
Grain shape: Angular to rounded.
Compaction: Strong.

Detrital components:
- Predominant monocrystalline quartz, with abundant feldspars (mainly K-feldspar), common polycrystalline quartz, common quartzo-feldspathic metamorphic lithics, sparse mica flakes (biotite), detrital chlorite and lesser amounts of organic matter.

Matrix:
- Detrital clays are sparse.

Authigenic phases:
- Patchy non ferroan to ferroan calcite/dolomite (Ca/Do, Images C-D) occludes primary and secondary pores, and replaces grains.
- Pore restricting quartz/feldspar overgrowths, grain replacive chlorite and pyrite framboids are also noted.

Pore system: Isolated macropores are locally noted.

Reservoir quality: Very poor

LEGACY CORE ANALYSIS DATA
Porosity: n/a
Permeability: n/a

Point Count Porosity: n/a

**Rock classification is based on visual estimation of mineralogical components.*

Well: A-J1

Depth: 3217.96m

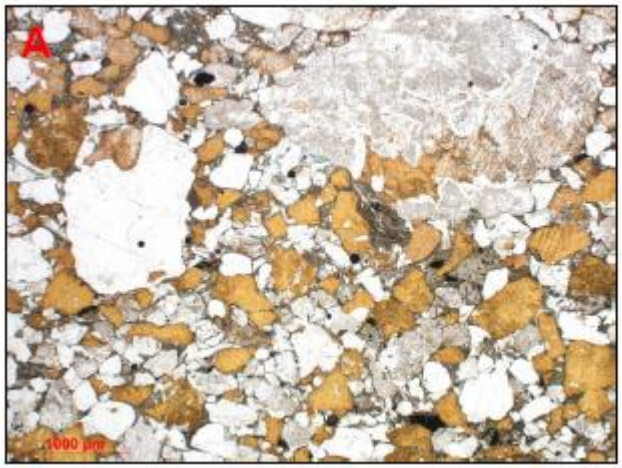

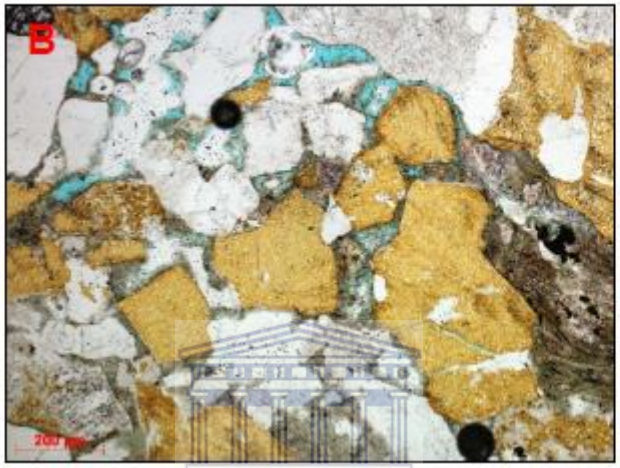

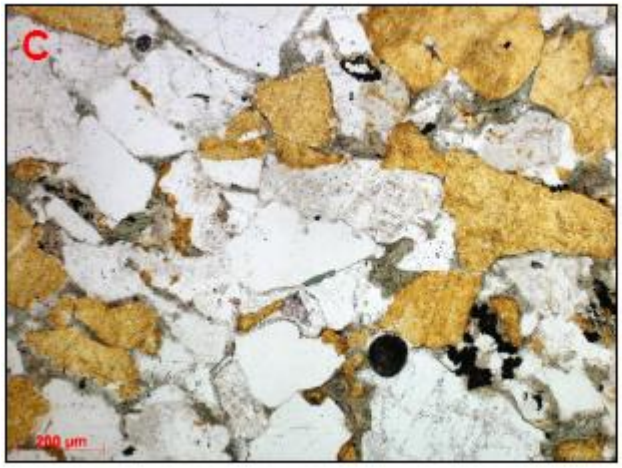

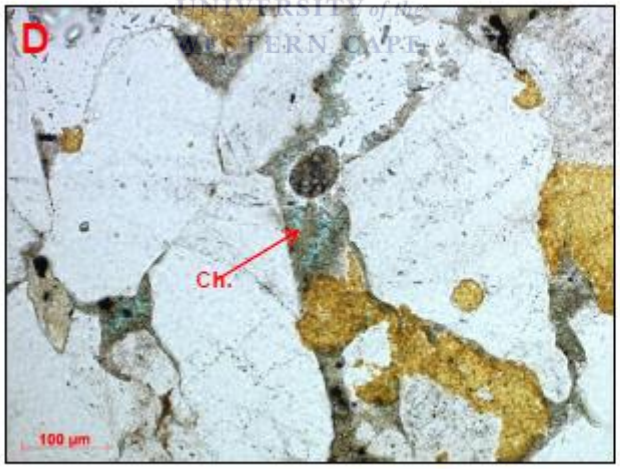

Lithology: Granular sandstone

Classification: Feldspathic arenite*

Texture:
Grain size: Very fine to granules.
Sorting: Poorly sorted.
Grain contacts: Concavo-convex to sutured.
Grain shape: Angular to rounded.
Compaction: Strong.

Detrital components:
- Predominant monocrystalline quartz, with abundant feldspars (mainly K-feldspar), common polycrystalline quartz, common quartzo-feldspathic metamorphic lithics, sparse biotite, detrital chlorite, organic matter and heavy minerals (zircon).

Matrix:
- Clays are relatively common (ortho/pseudo-matrix).

Authigenic phases:
- Common pore restricting quartz/feldspar overgrowths;
- Patchy non ferroan calcite occludes primary and secondary pores, and replaces grains.
- Grain replacive chlorite (also fibrous in habit, Ch, Image D), siderite and pyrite framboids are also present.

Pore system: Porosity is poor and mainly represented by isolated secondary pores.

Reservoir quality: Very poor

LEGACY CORE ANALYSIS DATA
Porosity: 4.1% at 3217.88m
Permeability: 0.018mD at 3217.88m

Point Count Porosity: n/a

**Rock classification is based on visual estimation of mineralogical components.*

Well: A-J1

Depth: 3219.62m

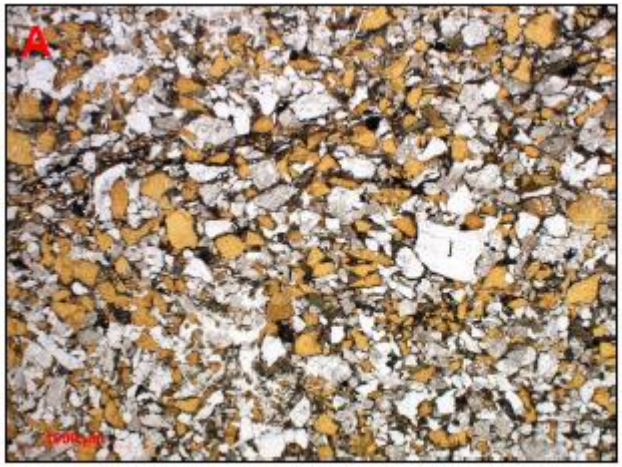

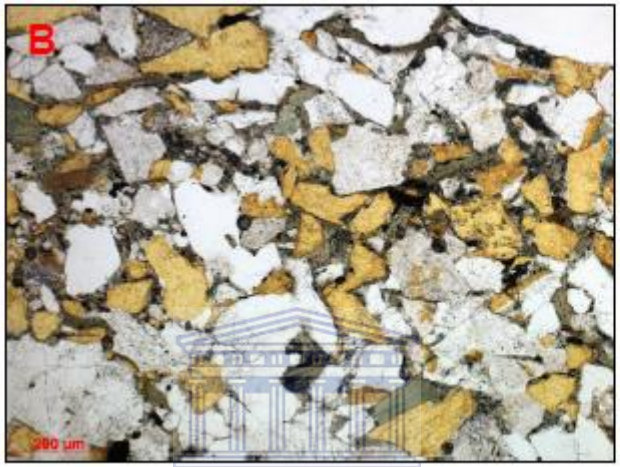

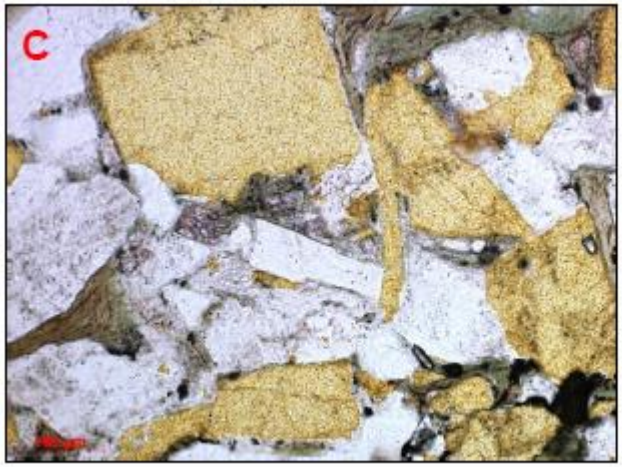

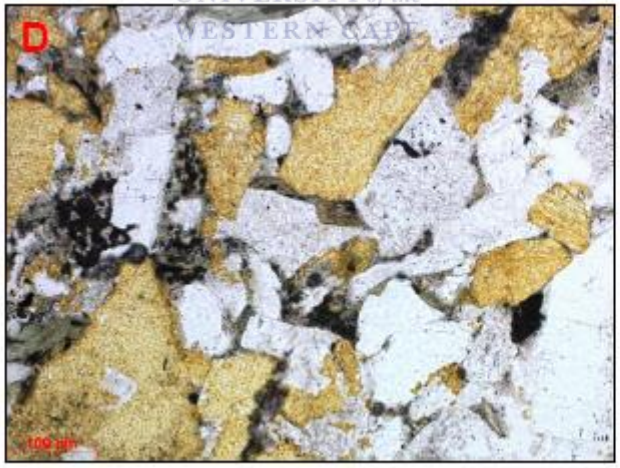

Lithology: Sandstone

Classification: Feldspathic arenite*

Texture:
Grain size: Fine (upper) sand is dominant.
Sorting: Moderately poorly sorted.
Grain contacts: Long to sutured.
Grain shape: Angular to rounded.
Compaction: Strong.

Detrital components:
- Predominant monocrystalline quartz, abundant K-feldspar, common plagioclase, polycrystalline quartz and mica flakes (mainly biotite), and lesser amounts of lithics (metamorphic), detrital chlorite, organic matter and zircon.

Matrix:
- Clays are mainly concentrated along stylo-laminae and also associated with organic matter.

Authigenic phases:
- Common pore restricting quartz/feldspar overgrowths;
- Grain replacive chlorite and ?smectite, pore filling to grain replacive calcite and pyrite (also framboidal in habit) are present.

Pore system: Porosity is poor and mainly represented by isolated secondary pores.

Reservoir quality: Very poor

LEGACY CORE ANALYSIS DATA
Porosity: 7.7% at 3219.64m
Permeability: 0.01mD at 3219.64m

Point Count Porosity: n/a

**Rock classification is based on visual estimation of mineralogical components.*

Well: A-J1

Depth: 3220.72m

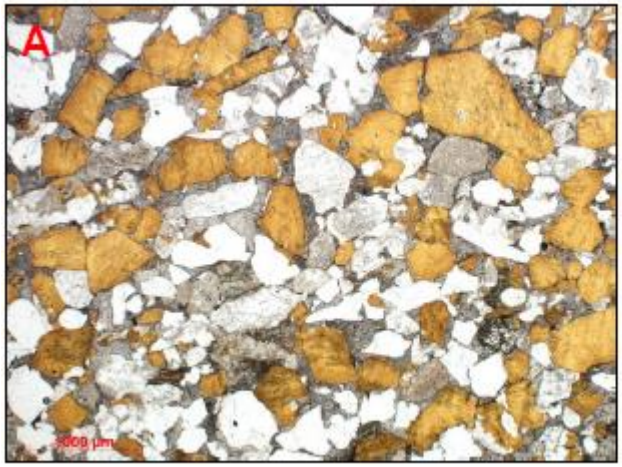

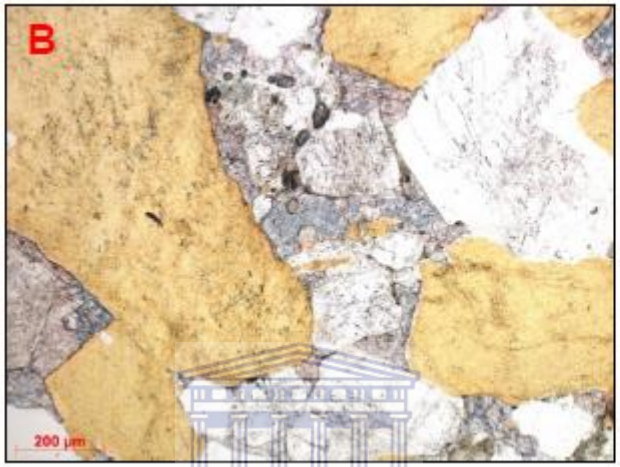

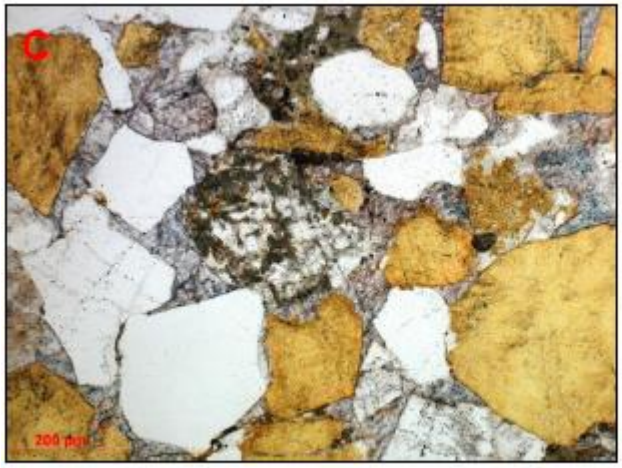

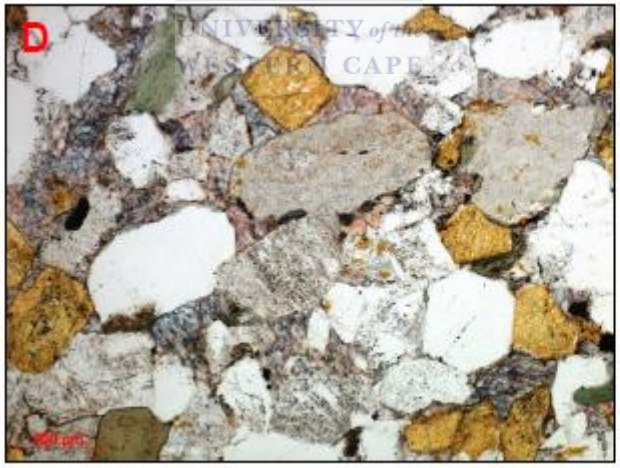

Lithology: Sandstone

Classification: Calcite/dolomite cemented feldspathic arenite*

Texture:
Grain size: Medium to coarse grains are dominant; granules are also present.
Sorting: Moderately poorly sorted.
Grain contacts: Point to point, long and locally sutured.
Grain shape: Angular to rounded.
Compaction: Moderate.

Detrital components:
- Predominant monocrystalline quartz, abundant K-feldspar and lesser amounts of plagioclase, polycrystalline quartz, metamorphic grains, mica flakes, detrital chlorite and organic matter.

Matrix:
- Detrital clays are scattered.

Authigenic phases:
- Extensive non ferroan to ferroan calcite/dolomite occludes primary and secondary pores, and replaces grains;
- Common pore restricting quartz/feldspar overgrowths are present;
- Grain replacive chlorite and pyrite are sparse.

Pore system: Porosity is not noted.

Reservoir quality: Negligible

LEGACY CORE ANALYSIS DATA
Porosity: 3.9% at 3220.64m
Permeability: 0.01mD at 3220.64m

Point Count Porosity: n/a

**Rock classification is based on visual estimation of mineralogical components.*

Well: A-J1

Depth: 3222.15m

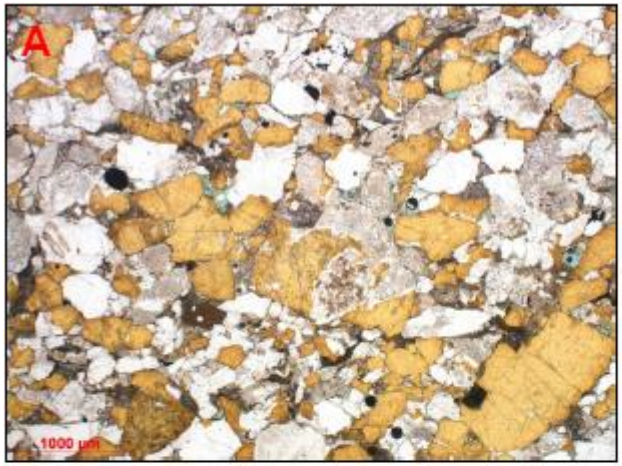

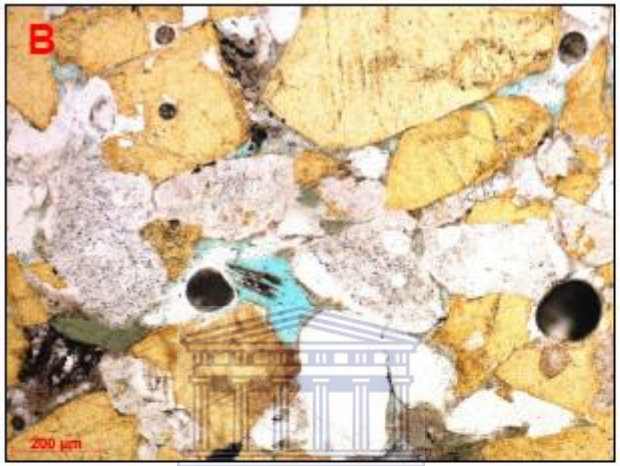

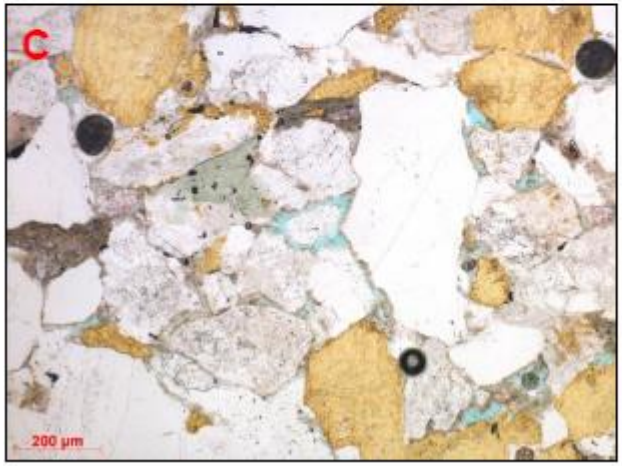

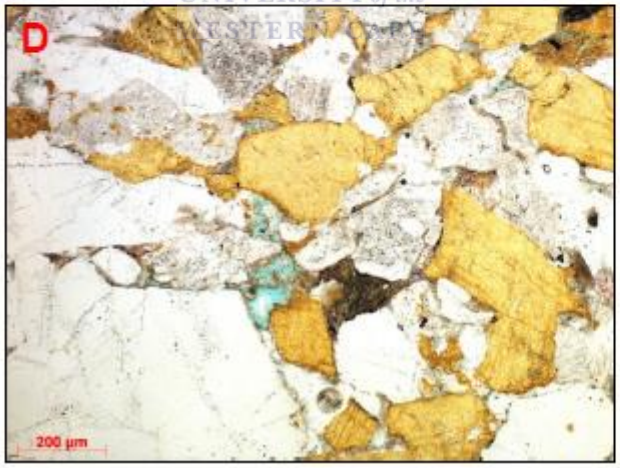

Lithology: Sandstone

Classification: Feldspathic arenite*

Texture:
Grain size: Medium.
Sorting: Moderately sorted overall.
Grain contacts: Long to sutured.
Grain shape: Subangular to rounded.
Compaction: Strong.

Detrital components:
- Predominant monocrystalline quartz, abundant K-feldspar and lesser amounts of plagioclase, polycrystalline quartz, metamorphic grains, biotite flakes, detrital chlorite and organic matter.

Matrix:
- Detrital clays are sparse.

Authigenic phases:
- Common pore restricting quartz/feldspar overgrowths;
- Patchy pore filling to grain replacive non ferroan to ferroan calcite;
- Sparse grain replacive to pore lining chlorite and minor pyrite.

Pore system: Porosity is locally moderate. Isolated macropores are primary and secondary, the latter linked to the dissolution of feldspar-rich detrital grains.

Reservoir quality: Very poor

LEGACY CORE ANALYSIS DATA
Porosity: 8.2% at 3222.20m
Permeability: 0.4% at 3222.20m

Point Count Porosity: n/a

**Rock classification is based on visual estimation of mineralogical components.*

Well: A-J1

Depth: 3222.88m

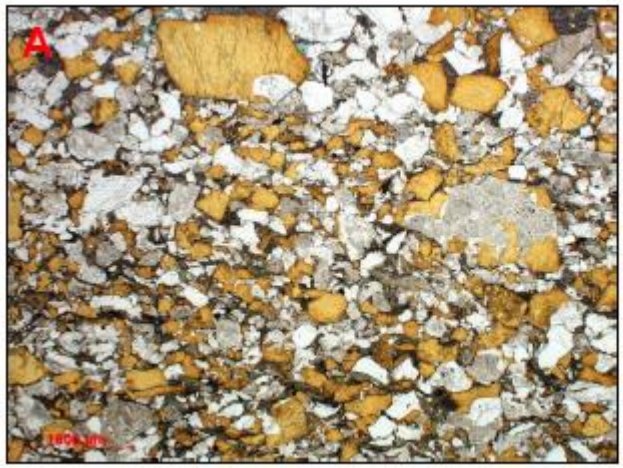

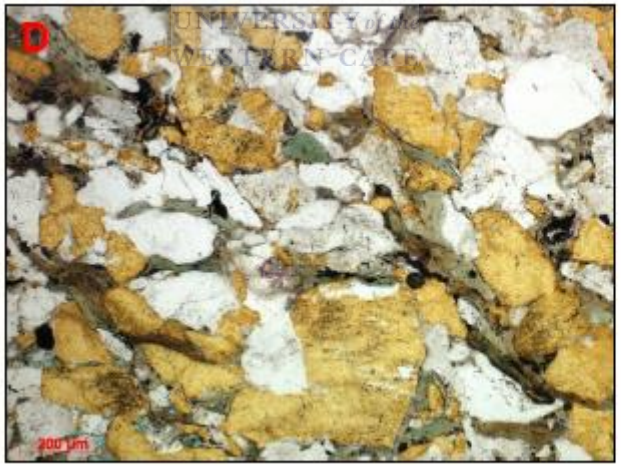

Lithology: Granular sandstone

Classification: Feldspathic arenite*

Texture:
Grain size: Fine to granules.
Sorting: Poorly sorted.
Grain contacts: Long to sutured.
Grain shape: Angular to rounded.
Compaction: Strong.

Detrital components:
- Predominant monocrystalline quartz, with abundant feldspars (mainly K-feldspar), common polycrystalline quartz, quartzo-feldspathic metamorphic lithics, biotite and detrital chlorite;
- Organic matter and heavy minerals (zircon) are scattered.

Matrix:
- Detrital clays are scattered.

Authigenic phases:
- Common pore restricting quartz/feldspar overgrowths;
- Patchy non ferroan to ferroan calcite (Ca, Image C) occlude primary and secondary pores, and replace grains.
- Common grain replacive to pore filling chlorite;
- Sparse siderite and pyrite framboids.

Pore system: Porosity is very poor and mainly represented by isolated secondary pores.

Reservoir quality: Very poor

LEGACY CORE ANALYSIS DATA
Porosity: 6.8% at 3222.93m
Permeability: 0.27mD at 3222.93m

Point Count Porosity: n/a

**Rock classification is based on visual estimation of mineralogical components.*

Well: A-J1

Depth: 3232.25m

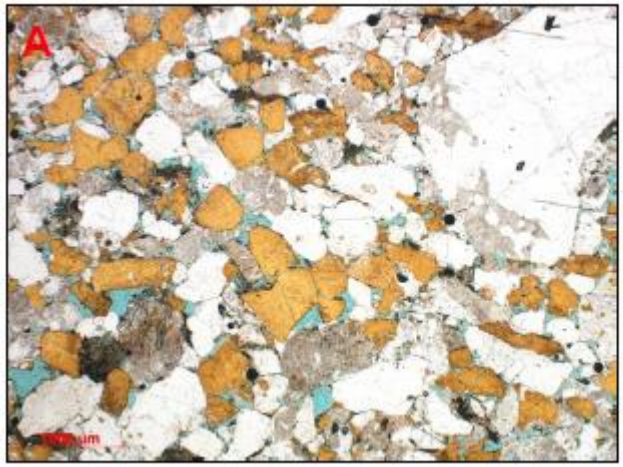

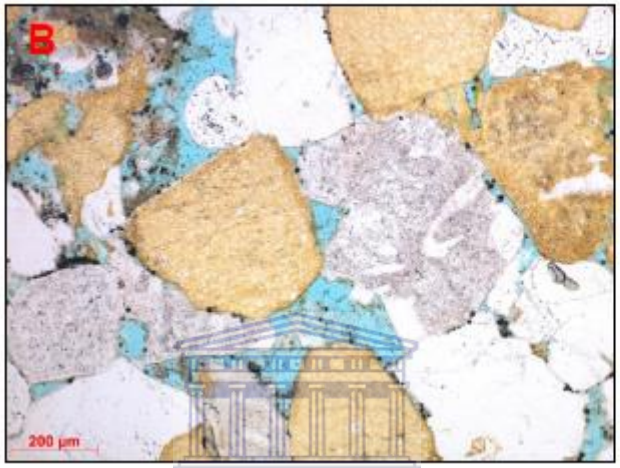

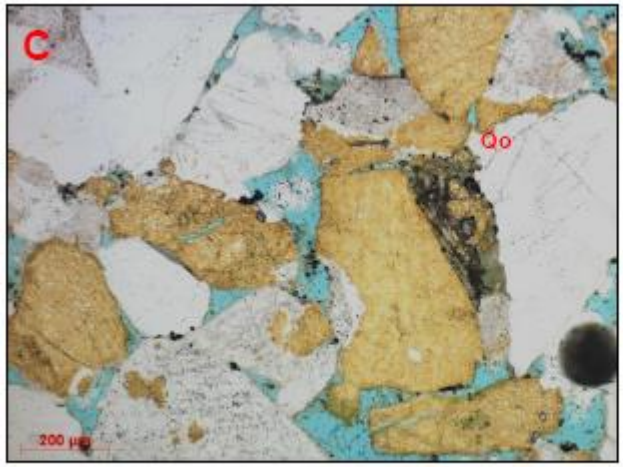

Lithology: Sandstone

Classification: Feldspathic arenite

Texture:
Grain size: Medium (upper).
Sorting: Moderately sorted.
Grain contacts: Mainly long.
Grain shape: Subangular to rounded.
Compaction: Moderate overall.

Detrital components:
- Predominant monocrystalline quartz, with abundant feldspars, relatively common polycrystalline quartz, lithics (mainly metamorphic grains), mica flakes (mainly biotite) and detrital chlorite;
- Organic matter and heavy minerals (e.g. zircon) are also locally noted.

Matrix:
- Detrital clays and carbonate matrix are minor.

Authigenic phases:
- Common pore restricting quartz overgrowths (Qo, Image C) and sparse feldspar overgrowths;
- Minor pore filling to grain replacive calcite (Ca, Image D);
- Grain replacive chlorite, ?smectite and pore filling to grain replacive pyrite framboids and siderite are also present.

Pore system: Porosity is moderate. Moderately connected macropores are primary and secondary; pore effectiveness has been mainly downgraded by quartz/feldspar overgrowths.

Reservoir quality: Moderate overall

LEGACY CORE ANALYSIS DATA
Porosity: 13.4% at 3232.16m
Permeability: 40mD at 3232.16m

Point Count Porosity: 14.0%

Well: A-J1

Depth: 3235.42m

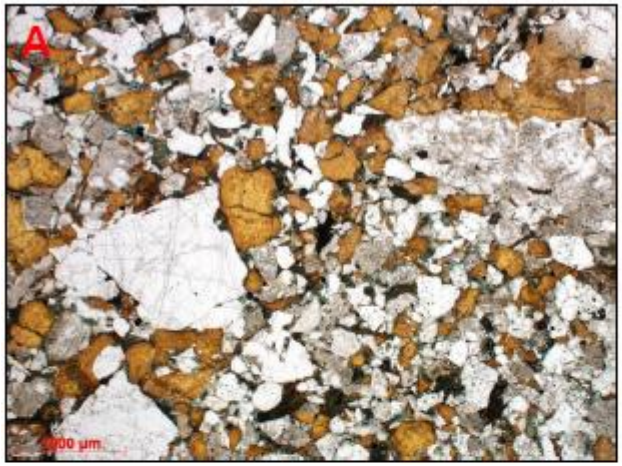

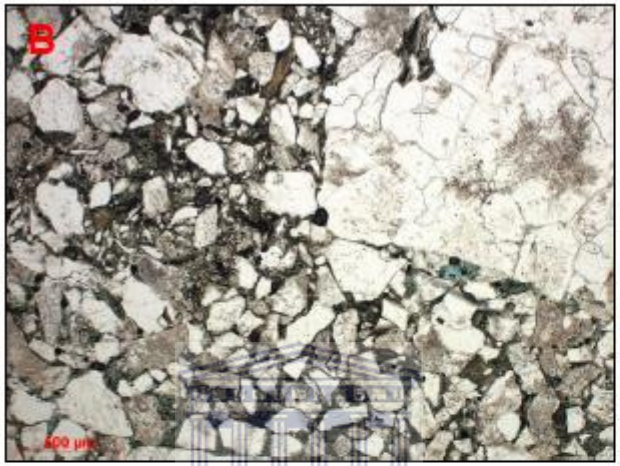

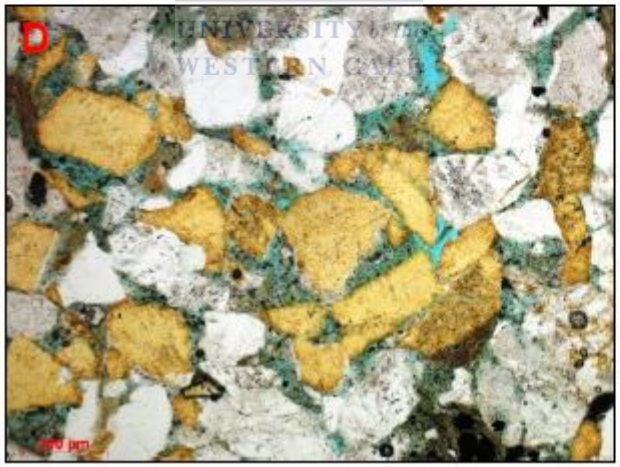

Lithology: Granular/pebbly sandstone

Classification: Feldspathic arenite*

Texture:
Grain size: Very fine to pebbles.
Sorting: Poorly sorted.
Grain contacts: Point to point to concavo-convex.
Grain shape: Angular to rounded.
Compaction: Moderately strong overall.

Detrital components:
- Predominant monocrystalline quartz, abundant feldspars (mainly K-feldspar), common polycrystalline quartz, lithics (mainly metamorphic), mica flakes and detrital chlorite;
- Organic matter and heavy minerals (tourmaline and zircon) are sparse.

Matrix:
- Sample is moderately shaly.

Authigenic phases:
- Common pore restricting quartz/feldspar overgrowths;
- Common grain replacive to pore filling clays (mainly chlorite);
- Sparse grain replacive pyrite and siderite.

Pore system: Porosity is locally moderate. Primary and secondary macropores are downgraded to micropores by clays.

Reservoir quality: Poor

LEGACY CORE ANALYSIS DATA
Porosity: 11.3% at 3235.36m
Permeability: 0.29mD at 3235.36m

Point Count Porosity: n/a

**Rock classification is based on visual estimation of mineralogical components.*

Well: A-J1

Depth: 3237.29m

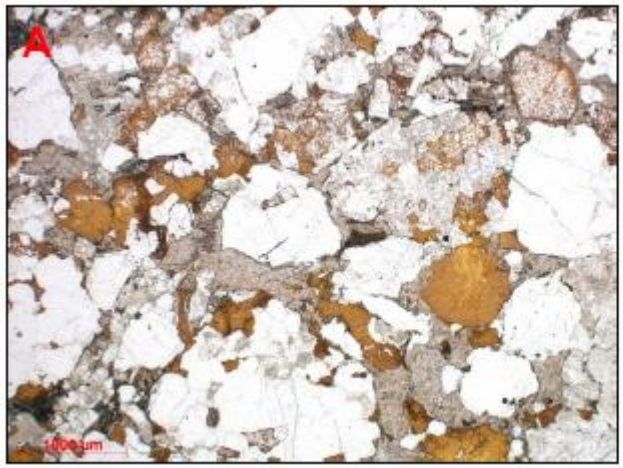

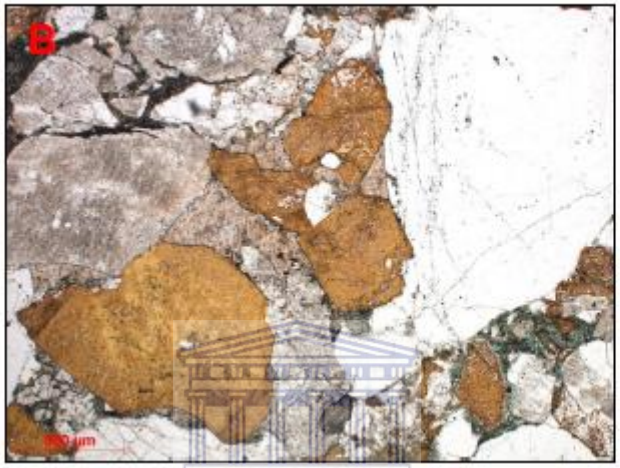

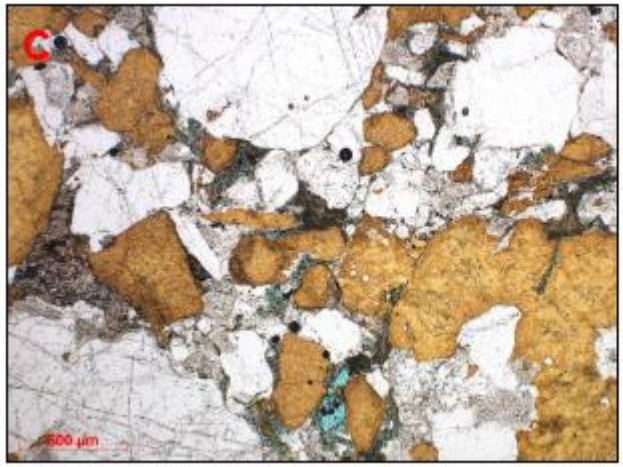

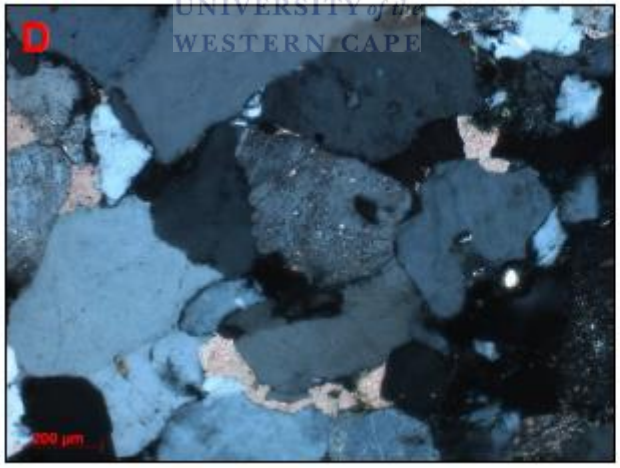

Lithology: Pebbly sandstone

Classification: Feldspathic arenite*

Texture:
Grain size: Up to pebbles.
Sorting: Poorly sorted.
Grain contacts: Point to point to concavo-convex.
Grain shape: Subangular to rounded.
Compaction: Moderately strong overall.

Detrital components:
- Predominant monocrystalline quartz and abundant feldspars (mainly K-feldspar);
- Common lithics (mainly metamorphic), polycrystalline quartz and mica flakes, and lesser amounts of detrital chlorite, organic matter and zircon.

Matrix:
- Sample is slightly shaly.

Authigenic phases:
- Common pore occluding to grain replacive non ferroan calcite and pore restricting quartz/feldspar overgrowths;
- Sparse grain replacive to pore filling chlorite and scattered grain replacive pyrite.

Pore system: Porosity is poor, being significantly downgraded by calcite and quartz/feldspar overgrowths.

Reservoir quality: Poor

LEGACY CORE ANALYSIS DATA
Porosity: 8.5% at 3237.18m
Permeability: 1mD at 3237.18m

Point Count Porosity: n/a

**Rock classification is based on visual estimation of mineralogical components.*

Well: A-J1

Depth: 3238.54m

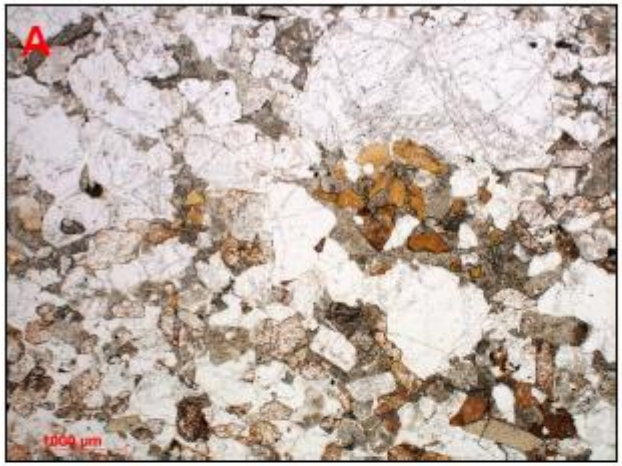

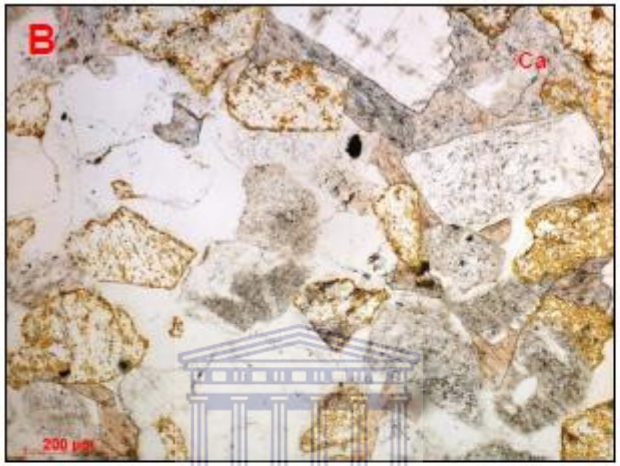

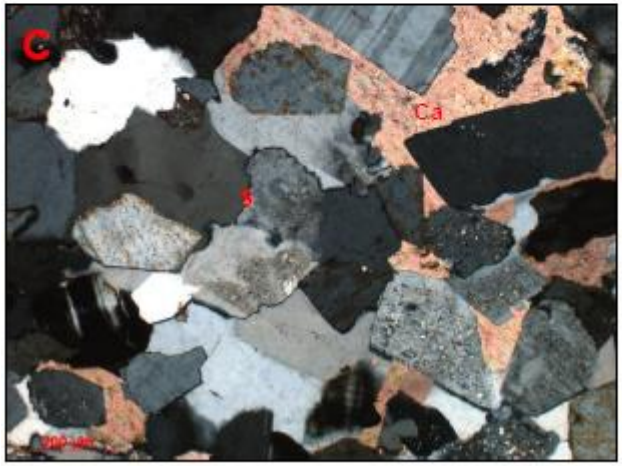

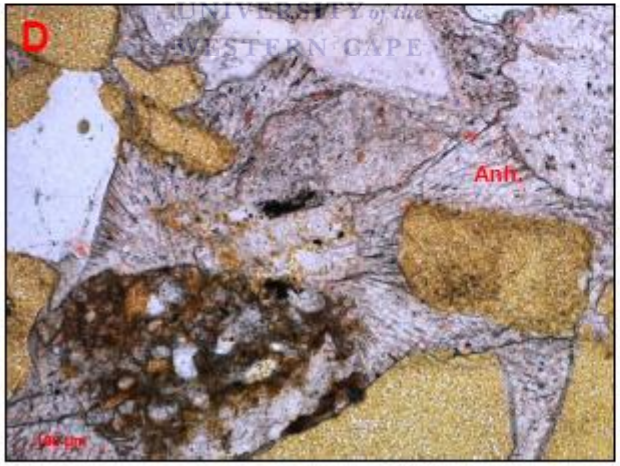

**Rock classification is based on visual estimation of mineralogical components.*

Lithology: Sandstone

Classification: Feldspathic arenite

Texture:
Grain size: Very fine to granules.
Sorting: Poorly sorted.
Grain contacts: Sutured contacts are common (S, Image C).
Grain shape: Angular to rounded.
Compaction: Strong.

Detrital components:
- Predominant monocrystalline quartz, abundant feldspars (both K-feldspar and plagioclase) and lesser amounts of polycrystalline quartz, metamorphic grains, mica flakes, detrital chlorite, organic matter/carbonaceous material and heavy minerals (also ?apatite).

Matrix:
- Minor detrital clays and carbonate matrix.

Authigenic phases:
- Extensive pore filling to grain replacive non ferroan to ferroan calcite (Ca, Images B-C, XPL) locally grades into bluish ferroan dolomite.
- Common pore restricting quartz/feldspar overgrowths;
- Sparse anhydrite (Anh., Image D & E, XPL, next page) shows fibrous radial structure and occludes primary and secondary pores.
- Minor pyrite and siderite.

Pore system: Porosity is not noted.

Reservoir quality: Negligible

LEGACY CORE ANALYSIS DATA
Porosity: 1% at 3238.59m
Permeability: 0.01mD at 3238.59m

Point Count Porosity: n/a

Well: A-J1

Depth: 3238.54m

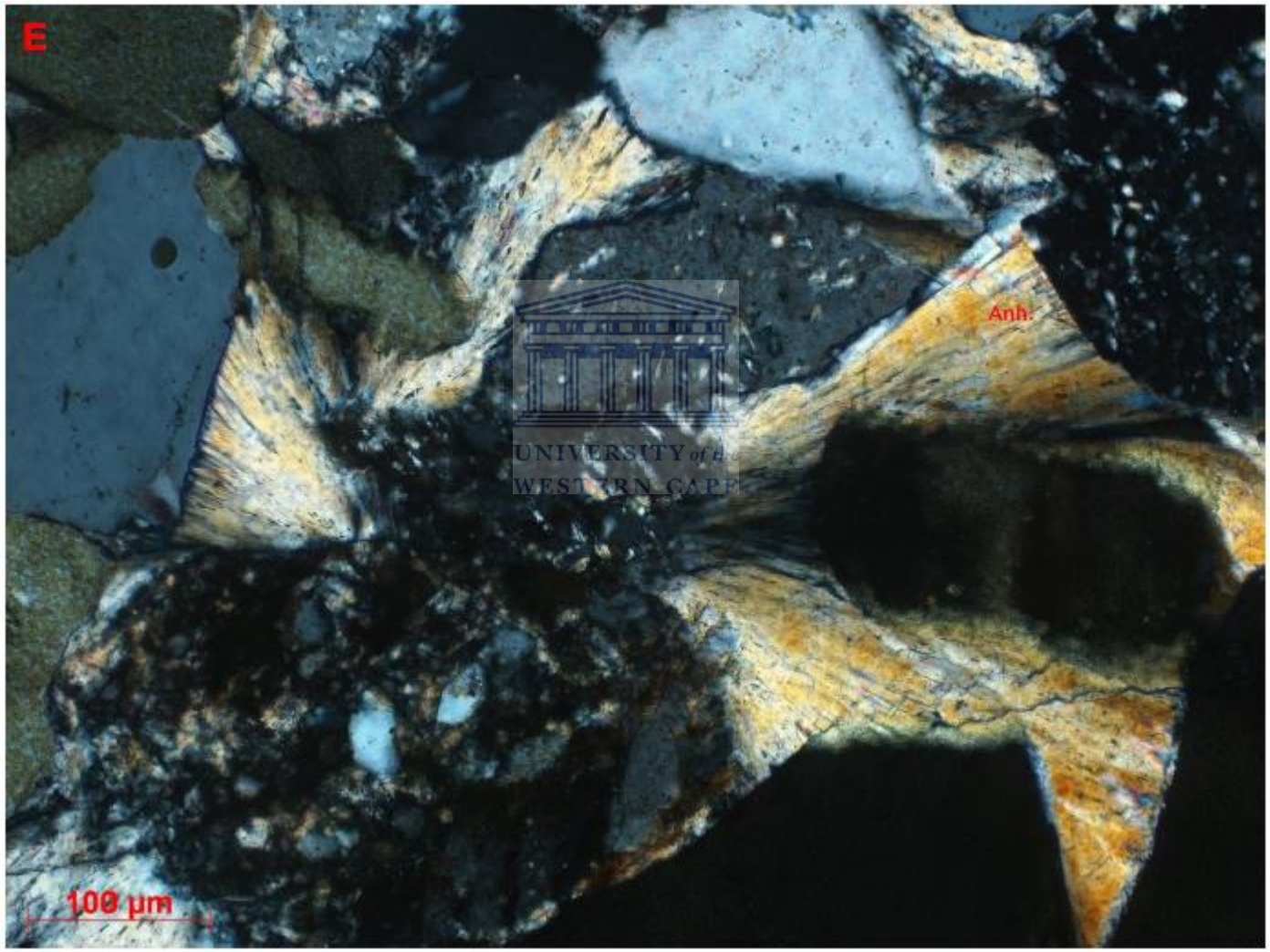

Well: A-J1

Depth: 3245.03m

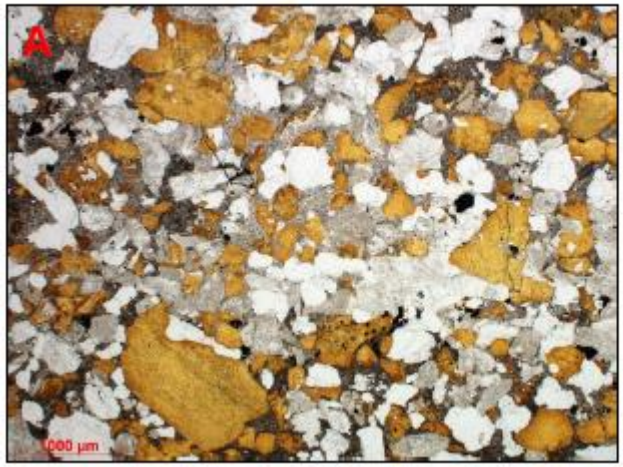

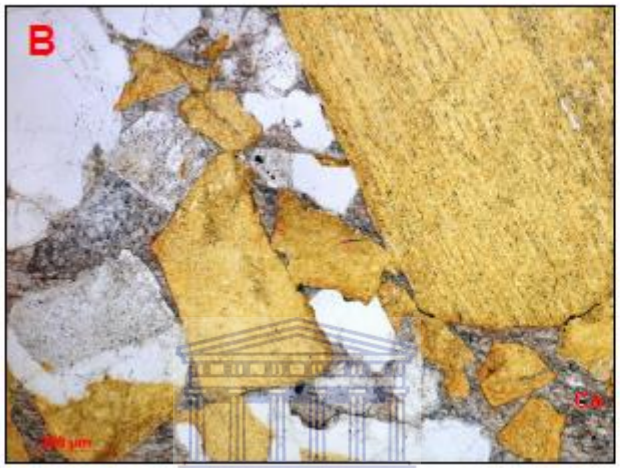

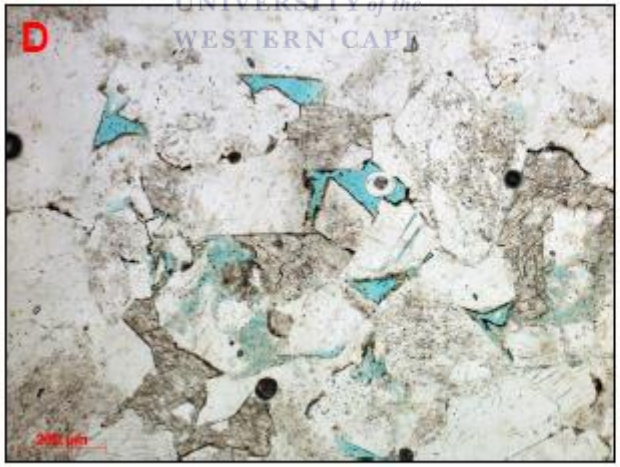

Lithology: Sandstone

Classification: Feldspathic arenite*

Texture:
Grain size: Very fine to granules (predominantly medium).
Sorting: Poorly sorted.
Grain contacts: Point to point to sutured.
Grain shape: Angular to rounded.
Compaction: Moderately strong overall.

Detrital components:
- Predominant monocrystalline quartz, abundant feldspars (both K-feldspar and plagioclase) and lesser amounts of polycrystalline quartz, lithics (metamorphic grains and minor mudclasts), mica flakes and organic matter.

Matrix:
- Sample is clean.

Authigenic phases:
- Extensive pore filling to grain replacive non ferroan to ferroan calcite (Ca, Image B) locally grades into bluish ferroan dolomite (Do, Image C);
- Common pore restricting quartz/feldspar overgrowths;
- Minor grain replacive chlorite and pyrite.

Pore system: Porosity is very poor to poor and represented by isolated primary and secondary pores.

Reservoir quality: Very poor

LEGACY CORE ANALYSIS DATA
Porosity: 7.3% at 3244.98m
Permeability: 3.6mD at 3244.96m

Point Count Porosity: n/a

**Rock classification is based on visual estimation of mineralogical components.*

Well: A-J1

Depth: 3248.95m

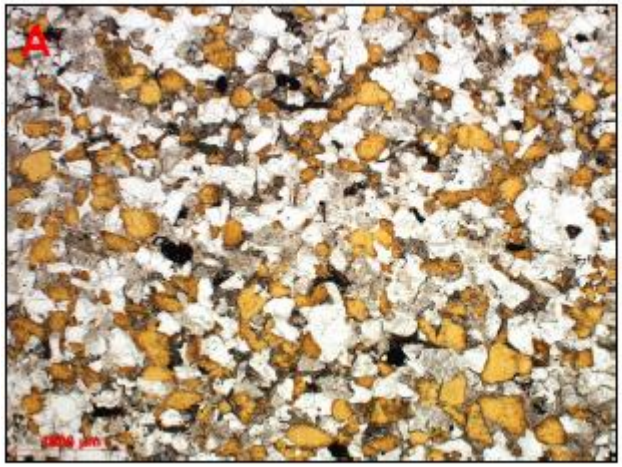

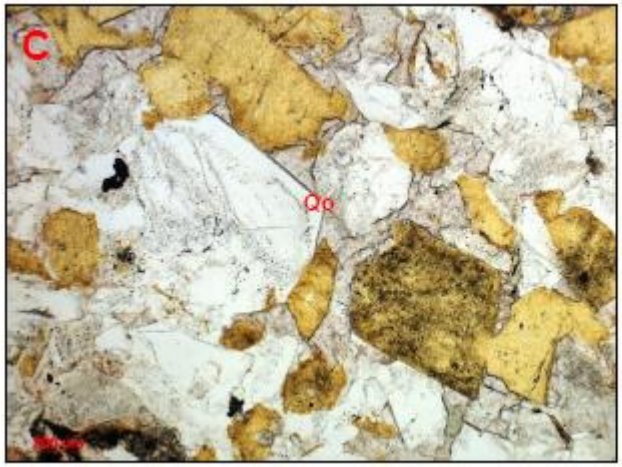

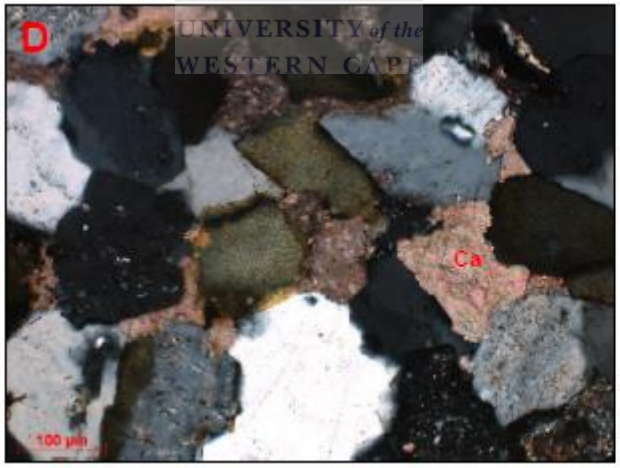

Lithology: Sandstone

Classification: Feldspathic arenite*

Texture:
Grain size: Fine (upper).
Sorting: Moderately well sorted.
Grain contacts: Point to point to sutured.
Grain shape: Angular to rounded.
Compaction: Moderately strong overall.

Detrital components:
- Predominant monocrystalline quartz, abundant K-feldspar, common plagioclase, polycrystalline quartz and mica flakes;
- Metamorphic grains, peloids, detrital chlorite and organic matter/carbonaceous material are also locally noted.

Matrix:
- Clays and carbonate matrix are minor.

Authigenic phases:
- Extensive pore filling to grain replacive non ferroan to ?ferroan calcite (Ca, Image D, XPL);
- Common pore restricting quartz overgrowths (Qo, Image C)/feldspar overgrowths;
- Scattered grain replacive chlorite and pyrite/?pyro-bitumen.

Pore system: Porosity is not noted.

Reservoir quality: Negligible

LEGACY CORE ANALYSIS DATA
Porosity: n/a
Permeability: n/a

Point Count Porosity: n/a

**Rock classification is based on visual estimation of mineralogical components.*

Well: A-J1

Depth: 3251.1m

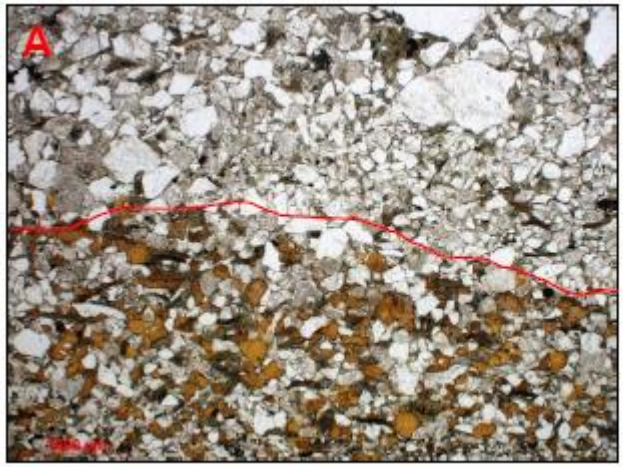

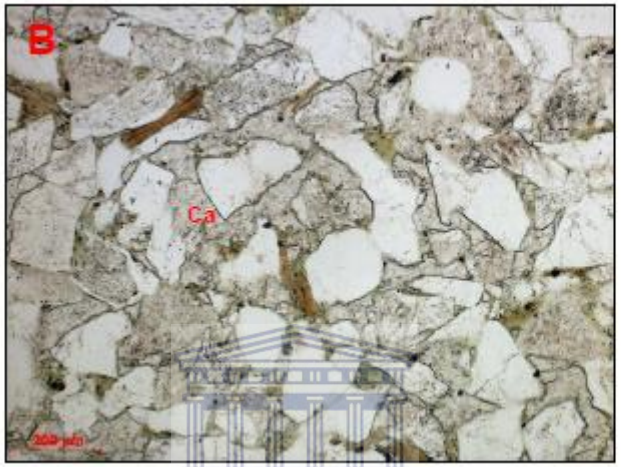

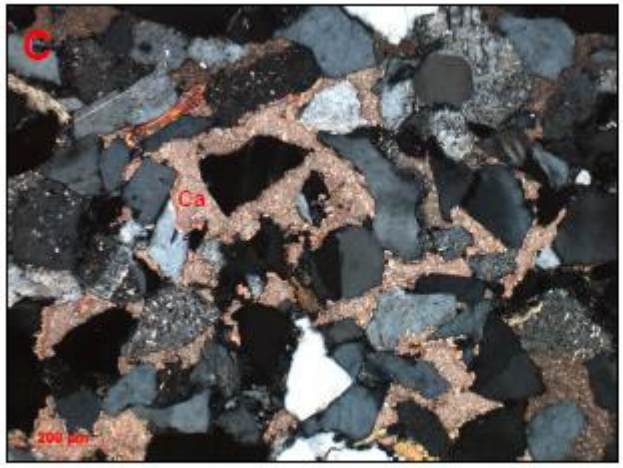

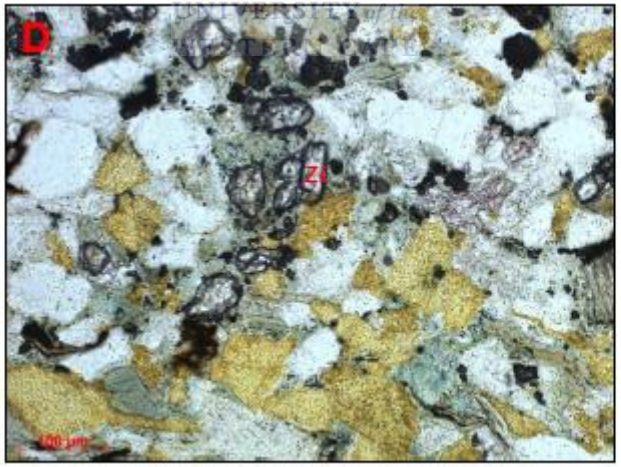

Lithology: Sandstone

Classification: Feldspathic arenite

Texture:
Sample is likely at the boundary between two petro-types: an extensive carbonate cemented arenite (above red line, Image A) and a micaceous, partially calcite cemented arenite (below red line, Image A). Very fine to fine grained sand is dominant, although medium to very coarse sand is also common.

Detrital components:
- Predominant monocrystalline quartz, abundant feldspars and mica flakes, common detrital chlorite and zircon (Zi, Image D), as well as lesser amounts of polycrystalline quartz, lithics (metamorphic grains) and organic matter.

Matrix:
- Minor detrital clays.

Authigenic phases:
- Extensive pore filling to grain replacive non ferroan to ferroan calcite (Ca, Images B-C, XPL);
- Common pore restricting quartz/feldspar overgrowths;
- Sparse grain replacive to pore filling chlorite, pyrite and siderite.

Pore system: Macroporosity is very poor. Micropores between clay platelets are optically irresolvable.

Reservoir quality: Very poor

LEGACY CORE ANALYSIS DATA
Porosity: 4.2% at 3251.09m
Permeability: 0.01mD at 3251.09m

Point Count Porosity: n/a

**Rock classification is based on visual estimation of mineralogical components.*

Well: A-J1

Depth: 3252.73m

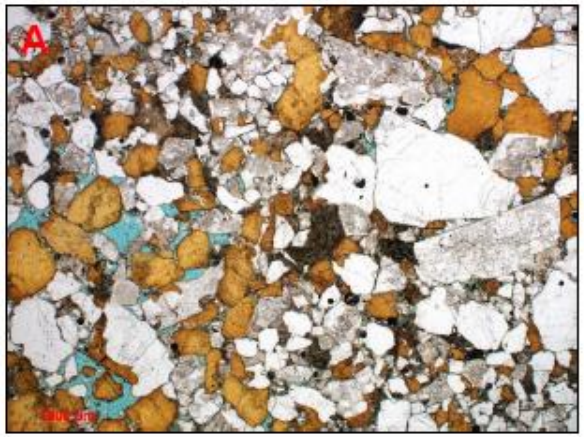

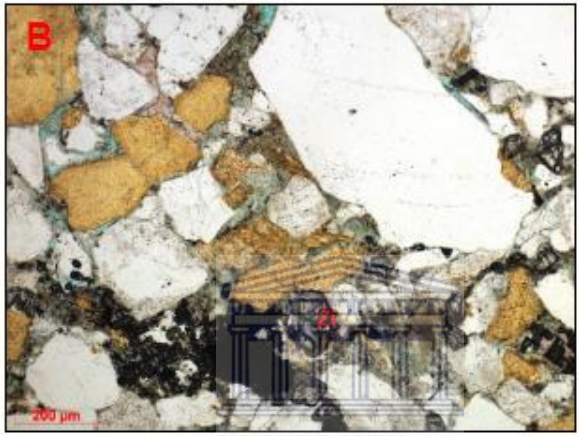

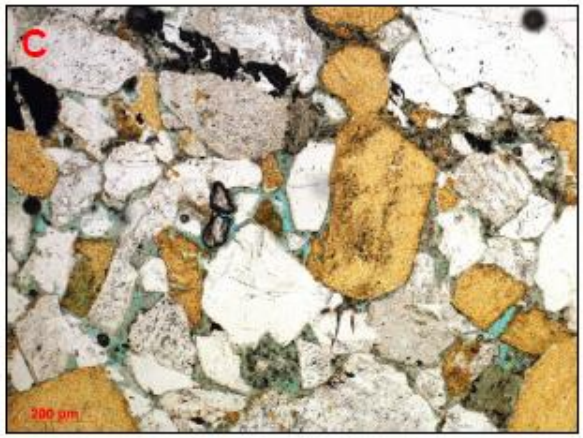

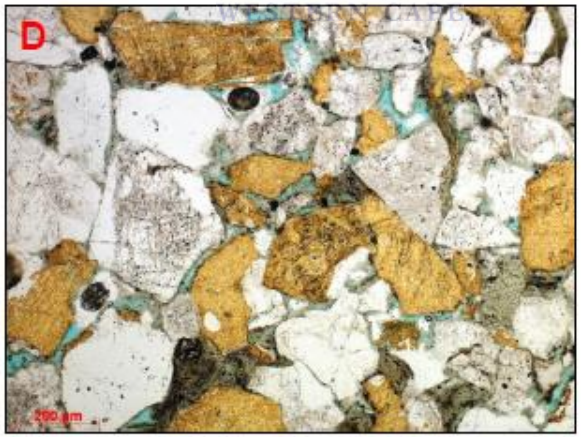

Lithology: Sandstone

Classification: Feldspathic arenite

Texture:
Grain size: Medium (lower). Granules and pebbles are locally noted.
Sorting: Poorly sorted.
Grain contacts: Long to concavo-convex.
Grain shape: Subangular to rounded.
Compaction: Moderately strong overall.

Detrital components:
- Predominant monocrystalline quartz, abundant feldspars, common mica flakes, sparse detrital chlorite and zircon (Zi, Image B), and lesser amounts of polycrystalline quartz, lithics (metamorphic) and organic matter.

Matrix:
- Scattered detrital clays.

Authigenic phases:
- Common grain replacive, grain rimming to pore filling chlorite; ?smectite, illite/sericite and very finely crystalline ?kaolinite are also noted;
- Relatively common pore restricting quartz/feldspar overgrowths;
- Patchy pore filling to grain replacive non ferroan calcite, siderite and pyrite.

Pore system: Porosity is moderately poor: it has been enhanced by the dissolution of unstable detrital grains (e.g. feldspars). Pore effectiveness has been strongly downgraded by compaction and cementation by quartz/feldspar overgrowths and also calcite.

Reservoir quality: Poor

LEGACY CORE ANALYSIS DATA
Porosity: 6.9% at 3252.62m
Permeability: 0.1mD at 3252.62m

Point Count Porosity: 7.0%

Well: A-J1

Depth: 3254.19m

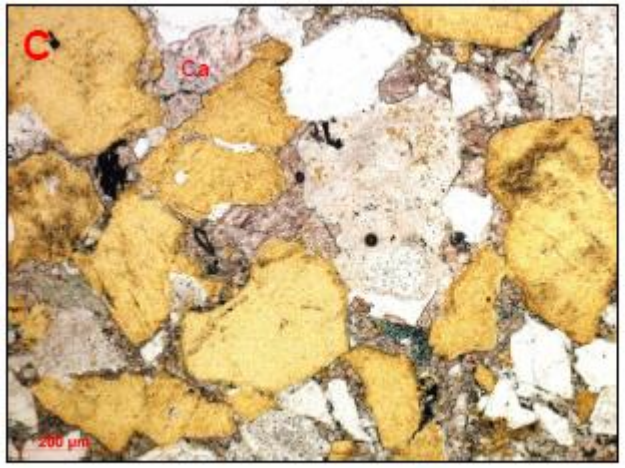

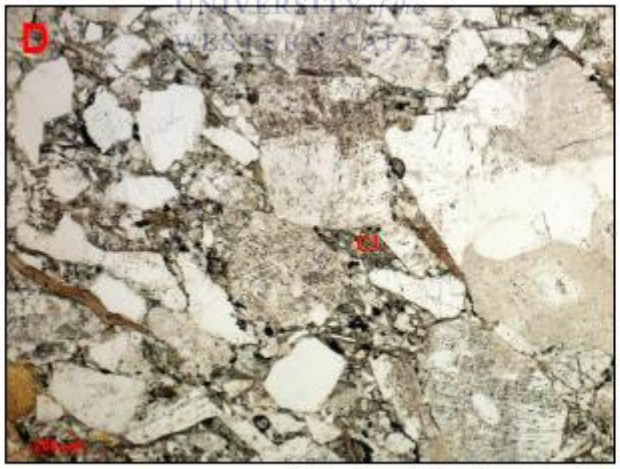

**Rock classification is based on visual estimation of mineralogical components.*

Lithology: Pebbly sandstone

Classification: Feldspathic arenite*

Texture:
Grain size: Up to pebbles.
Sorting: Poorly sorted.
Grain contacts: Point to point to concavo-convex.
Grain shape: Subangular to rounded.
Compaction: Moderately strong overall. Note that sample also shows heterogeneous distribution of clays vs. calcite (matrix and cement).

Detrital components:
- Predominant monocrystalline quartz and abundant feldspars (mainly K-feldspar);
- Common lithics (mainly metamorphic), polycrystalline quartz and mica flakes, with lesser amounts of detrital chlorite, organic matter and zircon.

Matrix:
- Detrital clays (Cl, Image D) range from scattered to common and are also intermixed with micrite/microspar.

Authigenic phases:
- Common pore occluding to grain replacive non ferroan calcite (Ca, Image C) and pore restricting quartz/feldspar overgrowths;
- Grain replacive to pore filling chlorite, ?illite/sericite, siderite and grain replacive pyrite are also noted.

Pore system: Macroporosity is not noted.

Reservoir quality: Very poor

LEGACY CORE ANALYSIS DATA
Porosity: n/a
Permeability: n/a

Point Count Porosity: n/a

Well: A-J1

Depth: 3255.42m

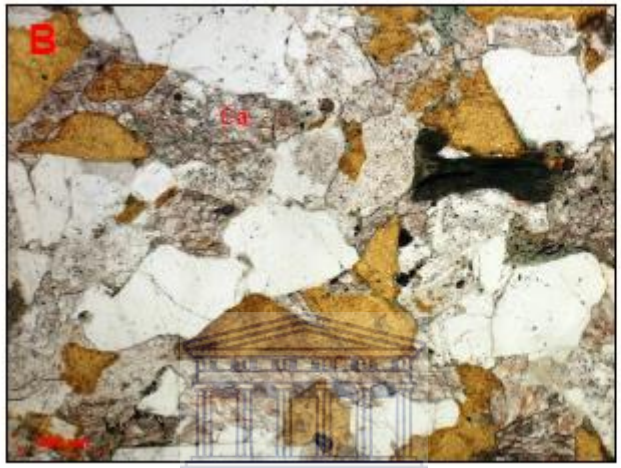

Lithology: Sandstone

Classification: Feldspathic arenite*

Texture:
Grain size: Very fine (upper).
Sorting: Moderately sorted.
Grain contacts: Long to sutured.
Grain shape: Subangular to rounded.
Compaction: Strong.

Detrital components:
- Predominant monocrystalline quartz, abundant feldspars (mainly K-feldspar) and relatively lesser amounts of lithics (e.g. metamorphic), mica flakes, detrital chlorite, zircon and organic matter.

Matrix:
- Detrital clays are scattered and associated with stylo-laminae and organic matter.

Authigenic phases:
- Common pore restricting quartz/feldspar overgrowths;
- Patchy pore occluding to grain replacive non ferroan calcite (Ca, Image B).
- Sparse grain replacive to pore filling authigenic clays (chlorite), siderite and pyrite.

Pore system: Porosity is poor. Poorly connected macropores are primary and secondary, the latter linked to the dissolution of feldspar grains.

Reservoir quality: Very poor

LEGACY CORE ANALYSIS DATA
Porosity: 9.8% at 3255.39m
Permeability: 0.28mD at 3255.39m

Point Count Porosity: n/a

**Rock classification is based on visual estimation of mineralogical components.*

Well: A-J1

Depth: 3256m

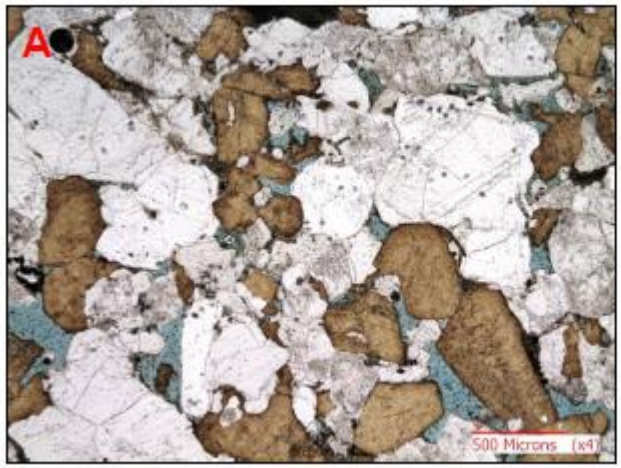

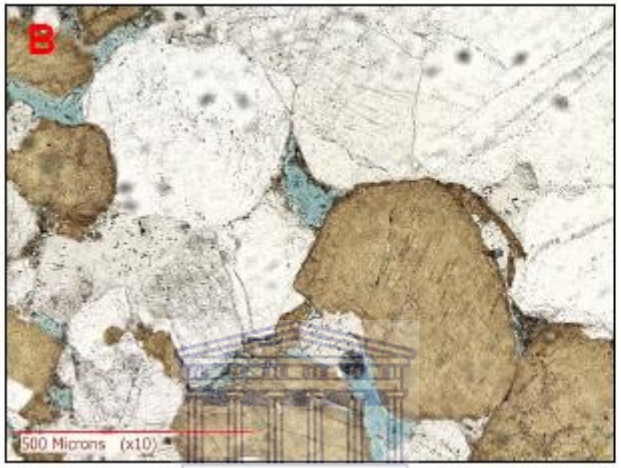

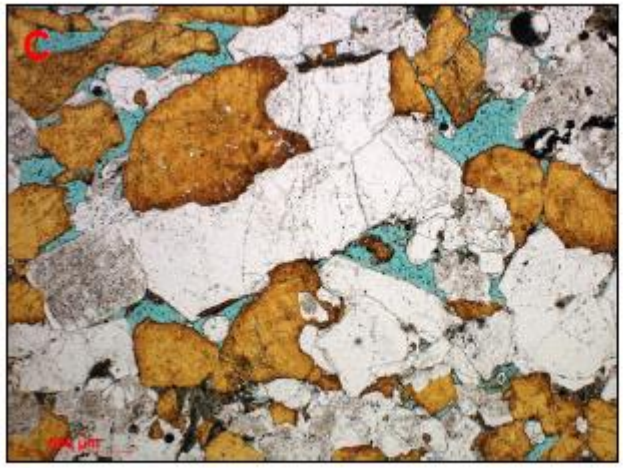

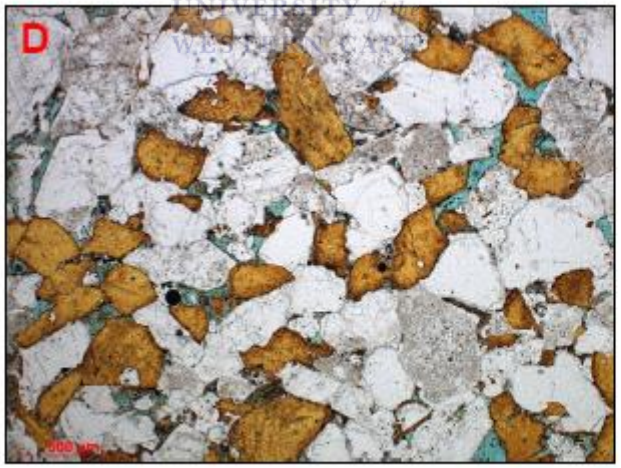

Lithology: Sandstone

Classification: Feldspathic arenite

Texture:
Grain size: Coarse.
Sorting: Moderate overall (granules and pebbles are present, not shown).
Grain contacts: Long to concavo-convex.
Grain shape: Subangular to well rounded.
Compaction: Moderately strong.

Detrital components:
- Predominant monocrystalline quartz and abundant feldspars (mainly K-feldspar);
- Metamorphic lithics, mica flakes and detrital chlorite are sparse.

Matrix:
- Detrital clays are scattered.

Authigenic phases:
- Common pore restricting quartz overgrowths and sparse feldspar overgrowths;
- Scattered pore filling calcite/dolomite, grain replacive chlorite, minor siderite and pyrite.

Pore system: Porosity is visually good. although artificial pores are thought to be common. Pore effectiveness has been mainly downgraded by compaction and quartz/feldspar overgrowths.

Reservoir quality: Permeability is thought to be locally moderate (see also legacy core analysis data).

LEGACY CORE ANALYSIS DATA
Porosity: 8.1% at 3256.06m
Permeability: 54mD at 3256.06m

Point Count Porosity: 6%*

* Note that artificial pores have been disregarded during point count analysis.

Well: K-A2 – Petrographic Analyses
Depth: 3982.77m

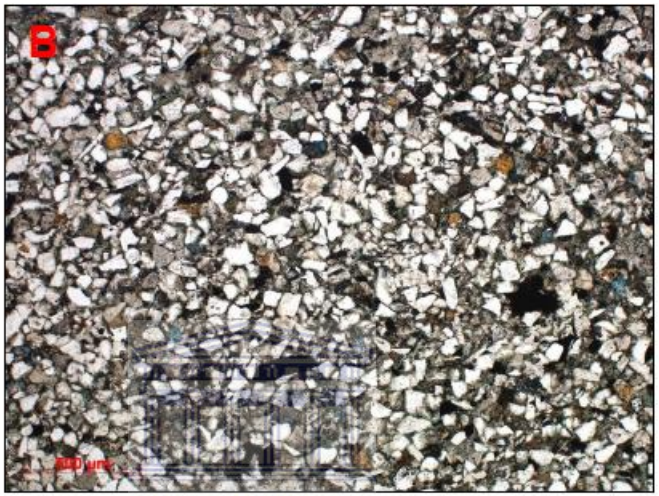

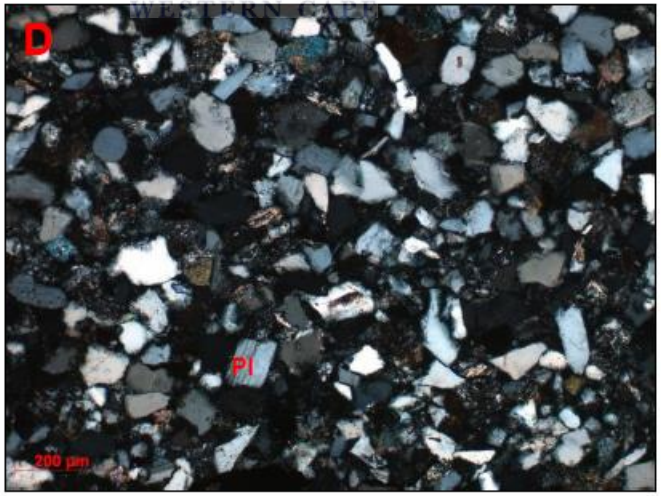

Lithology: Silty sandstone

Classification: Subfeldspathic arenite*

Texture:
Grain size: Very fine (lower).
Sorting: Well sorted.
Grain contacts: Long to concavo-convex.
Grain shape: Angular to well rounded.
Compaction: Moderately strong.

Detrital components:
- Predominant monocrystalline quartz;
- Common K-feldspar, plagioclase (Pl, Image D, XPL), lithics (mudclasts, volcanic and metamorphic grains);
- Sparse mica flakes, zircon and organic matter.

Matrix:
- Relatively common clays.

Authigenic phases:
- Common clays (likely chlorite/smectite);
- Sparse poorly developed quartz overgrowths, patchy ferroan dolomite and pyrite.

Pore system: Porosity is poor overall (visually ~5%); microporosity between clay platelets is optically irresolvable.

Reservoir quality: Permeability of this rock is inferred to be very poor.

LEGACY CORE ANALYSIS DATA
Porosity: n/a
Permeability: n/a

Point Count Porosity: n/a

**Rock classification is based on visual estimation of mineralogical components.*

Well: K-A2

Depth: 3982.77m

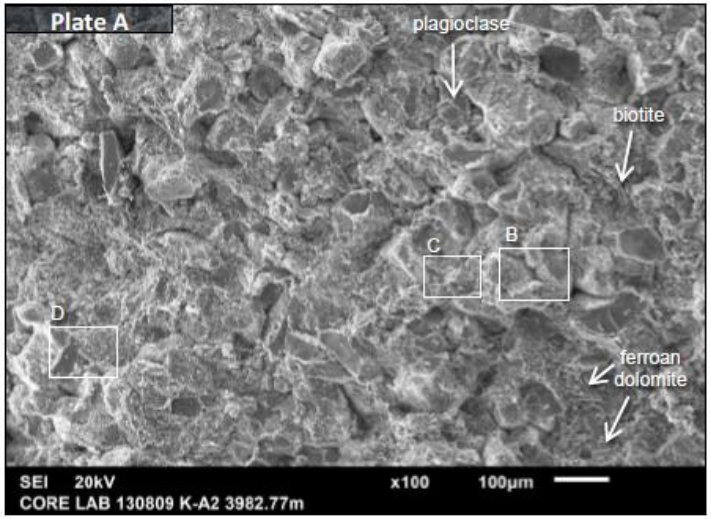

A well sorted very fine (upper) grained sandstone that appears massive at the scale of SEM (A). The sample is well compacted and long grain contacts dominate (B).

Detrital grains include quartz; abundant feldspars (plagioclase with rare K-feldspar) that are commonly leached; lithic grains (mainly clay-rich, with microquartz-rich varieties); micaceous minerals (including biotite and chlorite); and minor scattered Ti-minerals.

The authigenic mineralogy is dominated by abundant grain-coating chlorite, which forms isopachous platy rims on grains (B, C, D). Platy aggregates of chlorite also appear to be intergranular / ?matrix-replacive in places (difficult to clearly differentiate potential pore-filling clays from compacted clay-rich lithic grains). The development of overgrowths has been inhibited by the chloritic clays. Rare small isolated quartz overgrowths were observed (C). Authigenic albite forms very fine blocky developments associated with leached feldspar grains (C). Moderate calcite (C) forms fine subhedral developments, that may be ?replacive as well as pore-filling. Rare ferroan dolomite takes the form of fine rhombic developments (A, C), and is a microcrystalline replacive phase within some clay-rich lithics.

Traces of NaCl are thought to be a drying precipitate.

Porosity appears to be moderately poor, dominated by microporosity associated with clays and leached framework grains. Intergranular pores (B) are small, having been significantly reduced by compaction and grain-coating clay development. Pore connectivity appears to be restricted to microporous / highly tortuous pathways. Permeability is expected to be poor to very poor.

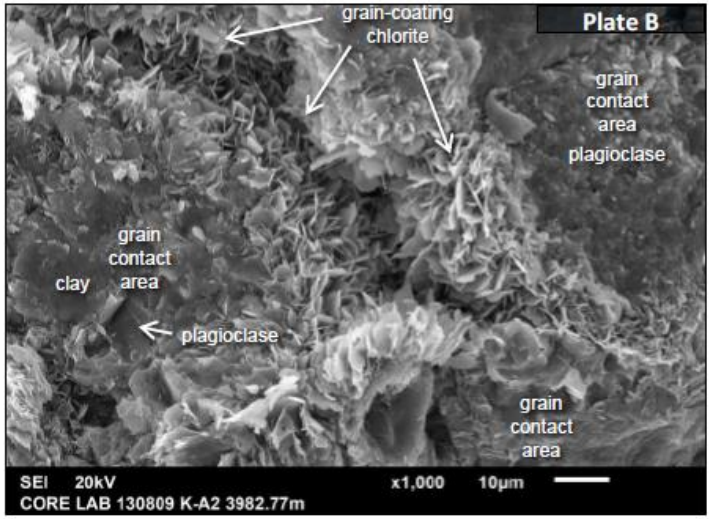

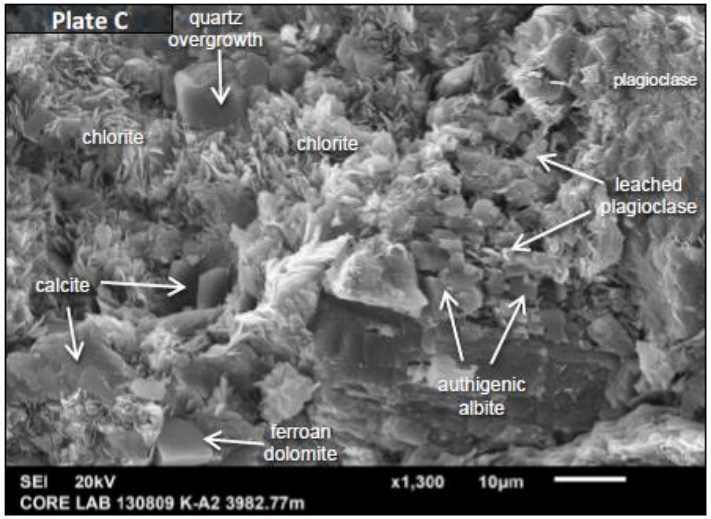

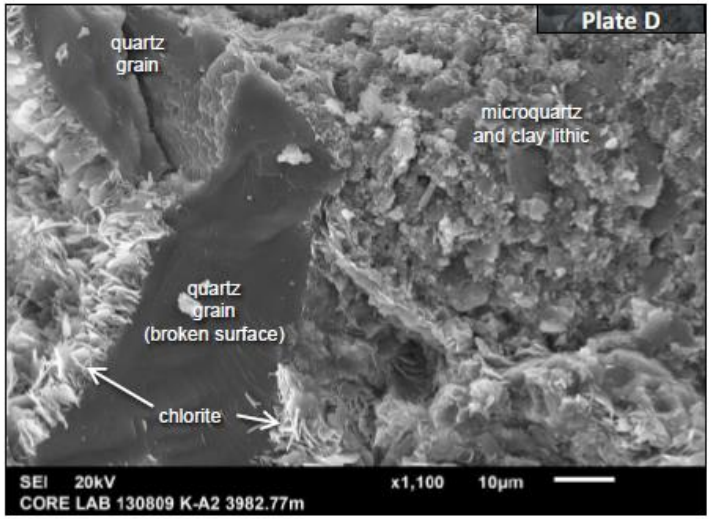

Well: K-A2

Depth: 3984.64m

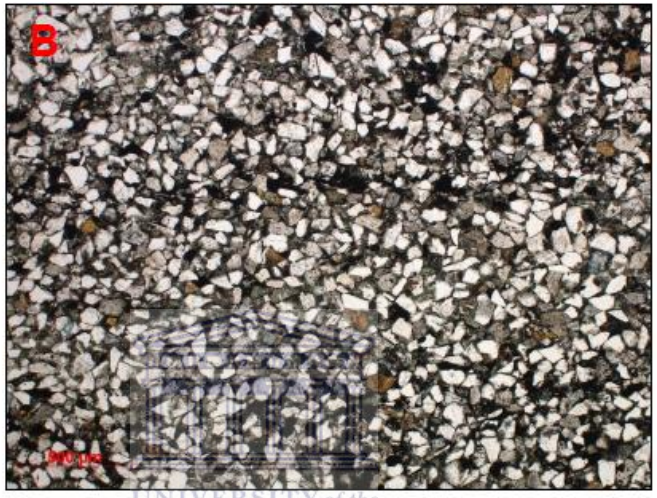

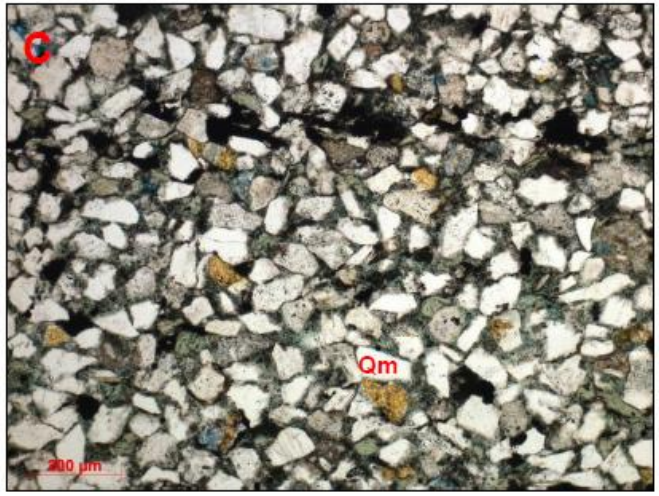

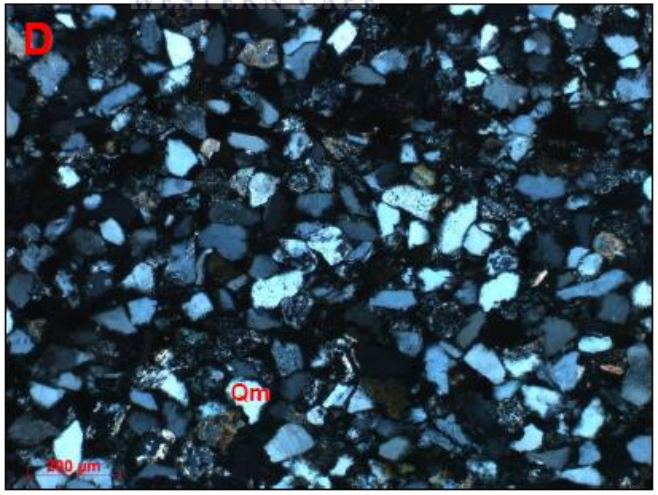

Lithology: Argillaceous sandy siltstone

Classification: Sandy feldspathic siltstone*

Texture:
Grain size: Silt to very fine grained sand.
Sorting: Well sorted.
Grain contacts: Long to concavo-convex.
Grain shape: Angular to rounded.
Compaction: Moderately strong.

Detrital components:
- Predominant monocrystalline quartz (Qm, Images C-D, XPL);
- Common K-feldspar, plagioclase, lithics (mudclasts, volcanic and schistose metamorphic grains);
- Sparse mica flakes, zircon and organic matter.

Matrix:
- Common clays.

Authigenic phases:
- Common clays (likely chlorite/smectite);
- Thin quartz overgrowths, patchy ferroan dolomite and pyrite.

Pore system: Porosity is poor overall (visually ~5%); microporosity between clay platelets is optically irresolvable.

Reservoir quality: Very poor

LEGACY CORE ANALYSIS DATA
Porosity: n/a
Permeability: n/a

Point Count Porosity: n/a

**Rock classification is based on visual estimation of mineralogical components.*

Well: K-A2

Depth: 3986.72m

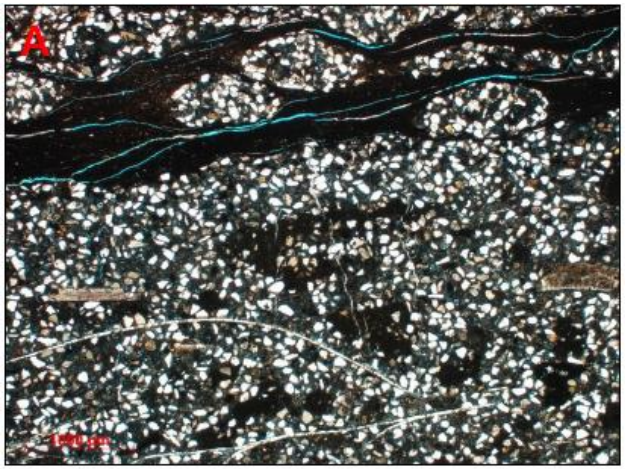

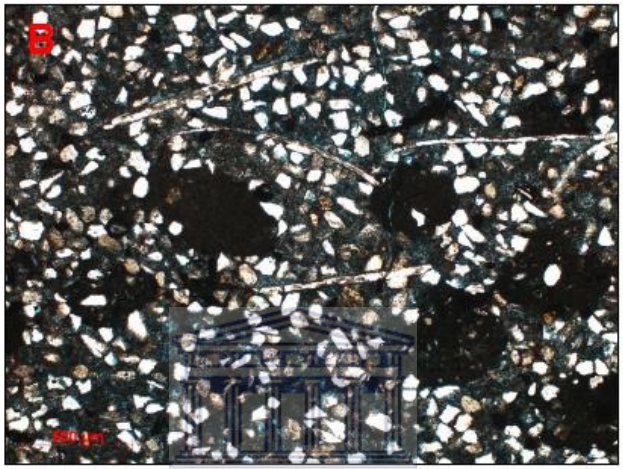

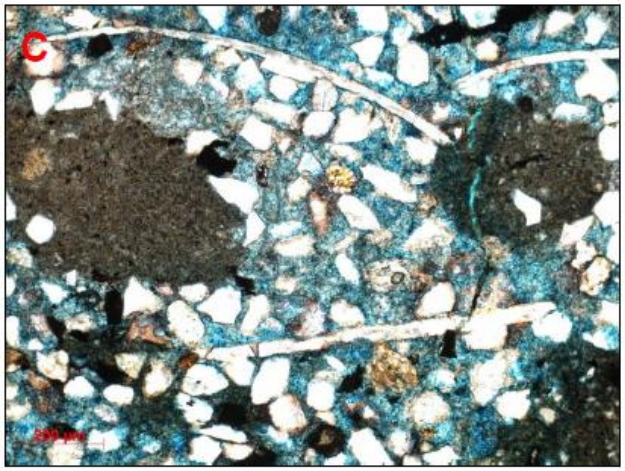

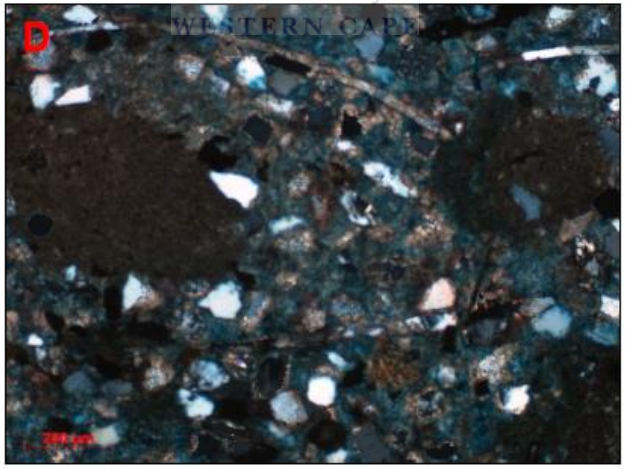

Lithology: Sandy siltstone

Classification: Dolomitic & bioclastic sandy siltstone*

Texture:
Sample is composed of silt-grade to very fine grained siliciclastic components, clay laminae and bioclasts; grain contacts are floating to point to point. Quartz grains are angular to rounded in shape.

Detrital components:
- Predominant monocrystalline quartz;
- Common K-feldspar, plagioclase, mudclasts, volcanic grains, schistose metamorphic grains, glauconite and mollusks;
- Sparse mica flakes, zircon and organic matter.

Matrix:
- Common clayey and dolomitic matrix.

Authigenic phases:
- Abundant ferroan dolomite occluding pores and fractures;
- Sparse grain replacive to pore filling pyrite framboids.

Pore system: Porosity is not noted, except for the presence of artificial fractures

Reservoir quality: Negligible

LEGACY CORE ANALYSIS DATA
Porosity: n/a
Permeability: n/a

Point Count Porosity: n/a

**Rock classification is based on visual estimation of mineralogical components.*

Well: K-A2

Depth: 3987.63m

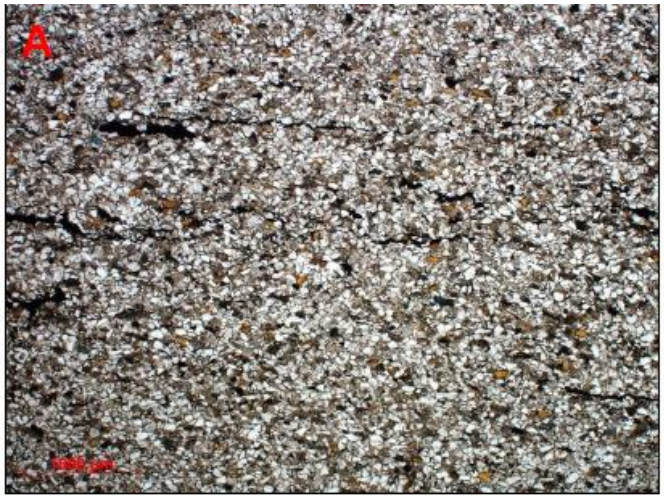

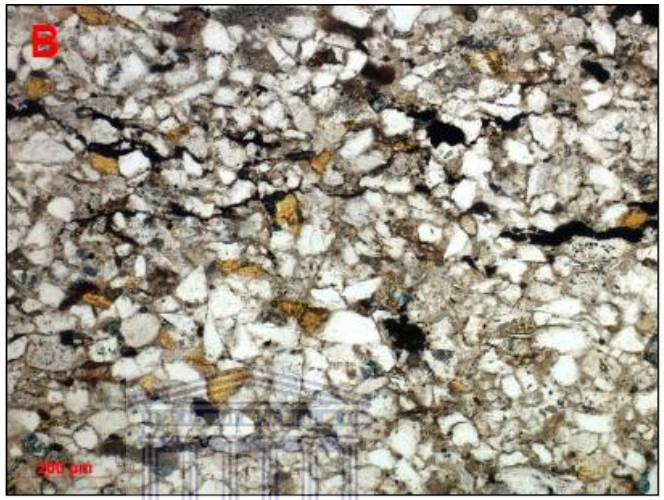

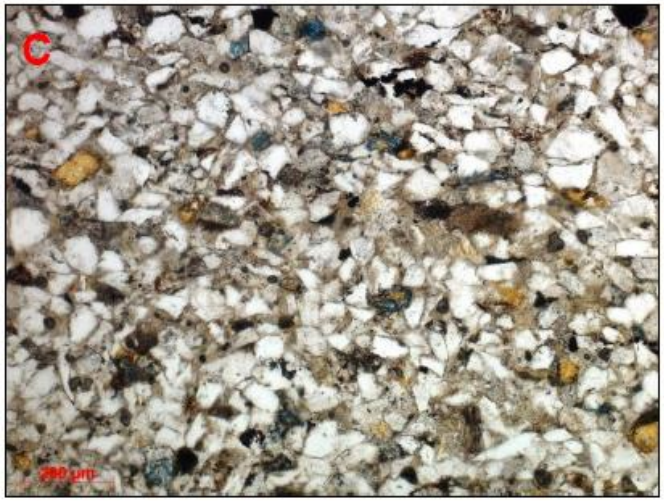

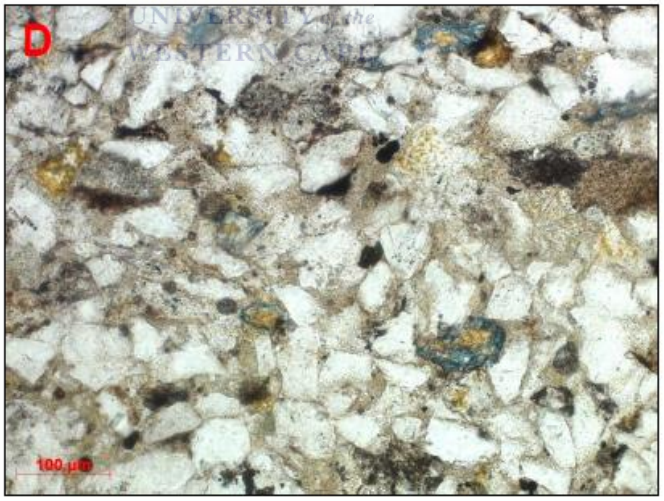

Lithology: Sandy siltstone

Classification: Argillaceous feldspathic sandy siltstone*

Texture:
Sample is composed of silt-grade to very fine grained siliciclastic components and detrital clays. Grain contacts are long to concavo-convex. Quartz grains are angular to rounded.

Detrital components:
- Predominant monocrystalline quartz;
- Common K-feldspar, plagioclase, lithics (mudclasts, volcanic & schistose metamorphic grains);
- Mica flakes, organic matter/carbonaceous material, glauconite and heavy minerals (zircon) are present.

Matrix:
- Abundant clays and minor dolomicrospar.

Authigenic phases:
- Sparse ferroan dolomite (mainly replacement phase) and grain replacive pyrite. Thin protrusions of quartz overgrowths and siderite crystals are also noted.

Pore system: Porosity is not noted.

Reservoir quality: Negligible

LEGACY CORE ANALYSIS DATA
Porosity: n/a
Permeability: n/a

Point Count Porosity: n/a

**Rock classification is based on visual estimation of mineralogical components.*

Well: K-A2

Depth: 3989.7m

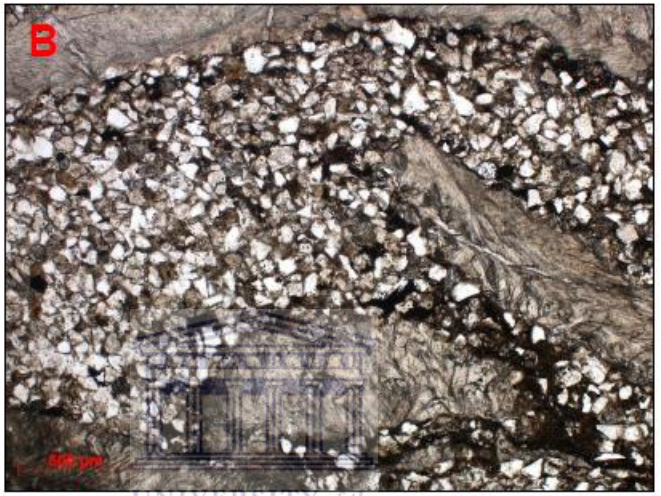

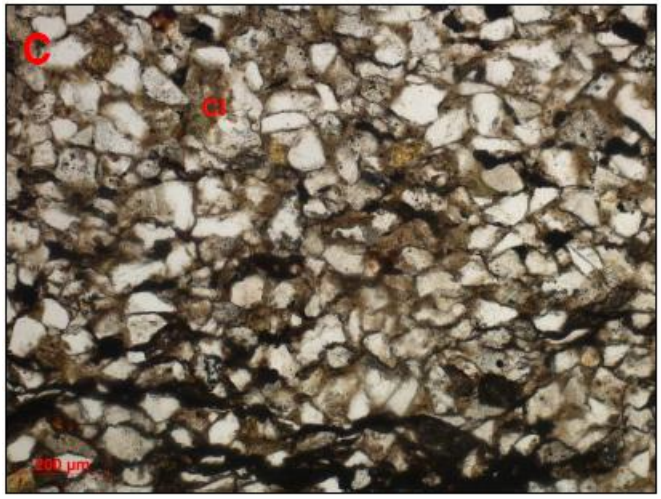

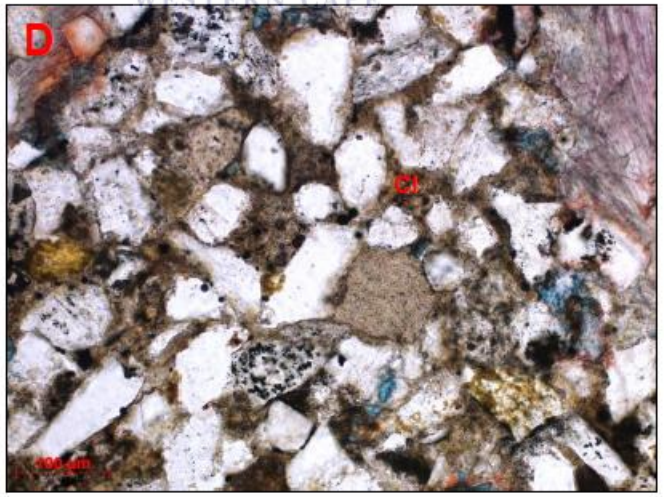

Lithology: Argillaceous silty sandstone

Classification: (Bioclastic/argillaceous) subfeldspathic arenite*

Texture:
Abundant silt-grade to very fine grained siliciclastic detritus and carbonate allochems are intermixed with clays (grain contacts are floating to long). Quartz grains are angular to rounded in shape.

Detrital components:
- Abundant monocrystalline quartz, feldspars & molluscan debris;
- Common mudclasts, igneous grains, metamorphic grains and organic matter/ carbonaceous material;
- Sparse glauconite, ?foraminifera, mica flakes and zircon.

Matrix:
- Abundant brownish detrital clays (Cl, Images C-D).

Authigenic phases:
- Common grain replacive to pore filling illite/sericite, non ferroan calcite, ferroan dolomite, pyrite and hematite.

Pore system: Porosity is not noted. Artificial fractures are present.

Reservoir quality: Negligible.

LEGACY CORE ANALYSIS DATA
Porosity: n/a
Permeability: n/a

Point Count Porosity: n/a

**Rock classification is based on visual estimation of mineralogical components.*

Well: K-A2

Depth: 3991.4m

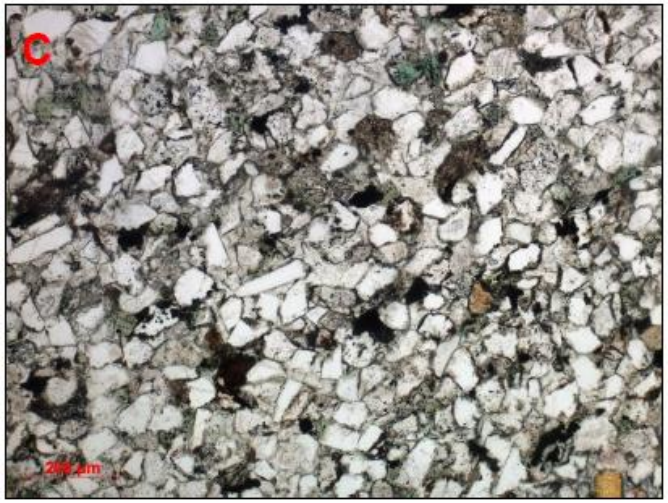

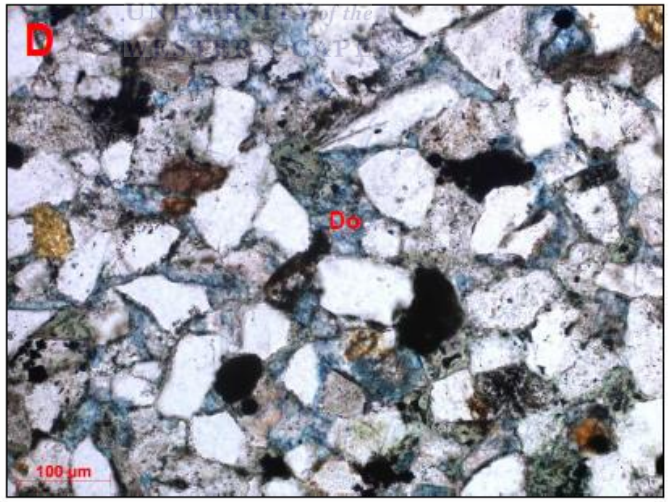

Lithology: Sandy siltstone

Classification: Dolomitic/feldspathic sandy siltstone*

Texture:
Abundant silt-grade to very fine grained siliciclastic detritus with long contacts and angular to rounded shape.

Detrital components:
- Predominant monocrystalline quartz;
- Common K-feldspar, plagioclase, lithics (mudclasts, volcanic and schistose metamorphic grains);
- Sparse mica flakes, zircon and organic matter.

Matrix:
- Sparse detrital clays.

Authigenic phases:
- Abundant pore filling ferroan dolomite (Do, Image D);
- Sparse chlorite/?smectite, thin quartz overgrowths and pyrite.

Pore system: Porosity is rare; microporosity between clay platelets is optically irresolvable.

Reservoir quality: Very poor

LEGACY CORE ANALYSIS DATA
Porosity: n/a
Permeability: n/a

Point Count Porosity: n/a

**Rock classification is based on visual estimation of mineralogical components.*

Well: K-A2

Depth: 4076.6m

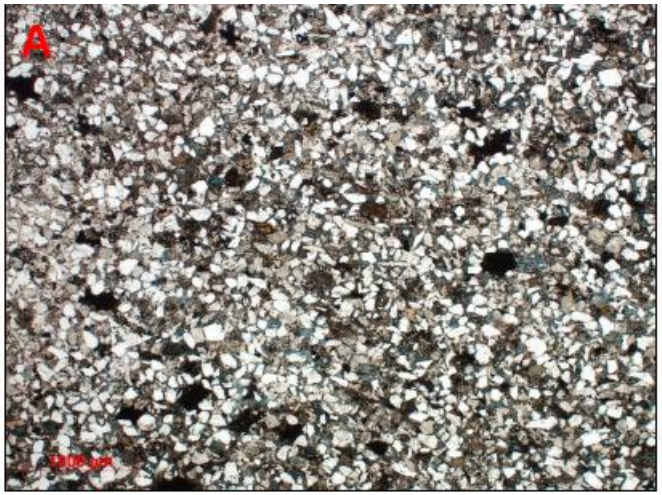

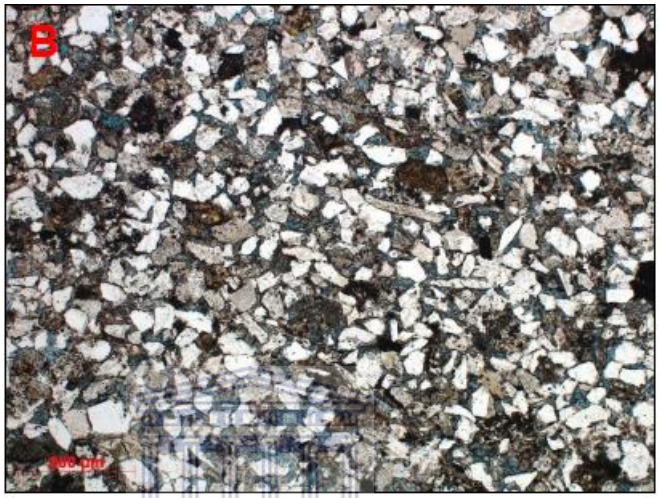

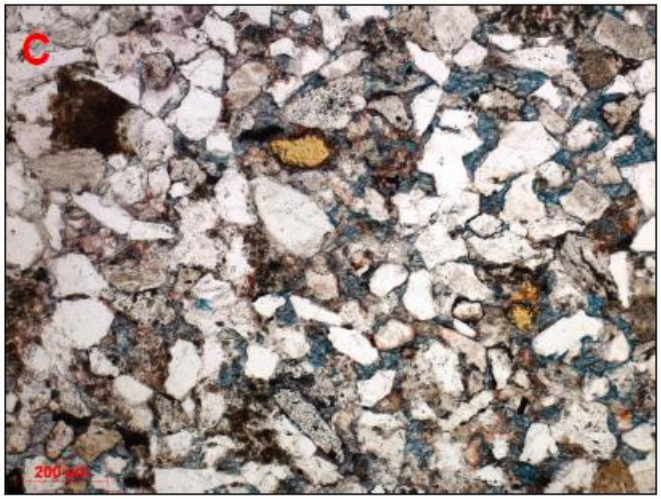

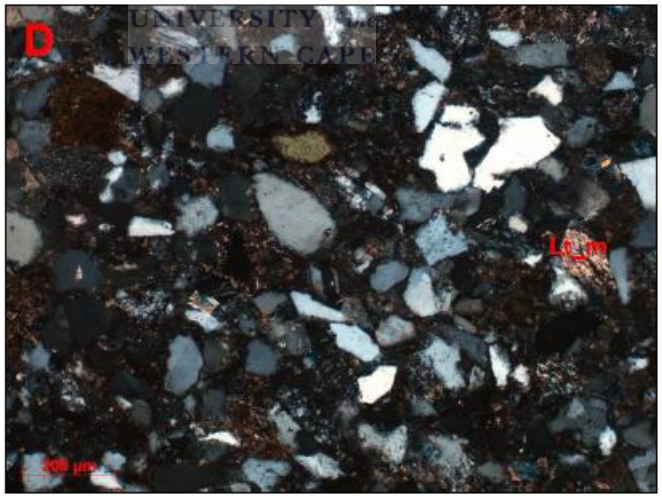

Lithology: Silty sandstone

Classification: Subfeldspathic-sublithic arenite*

Texture:
Grain size: Very fine.
Sorting: Well sorted.
Grain contacts: Floating (due to carbonate cementation) to concavo-convex.
Grain shape: Angular to subrounded.
Compaction: Moderate overall.

Detrital components:
- Abundant monocrystalline quartz;
- Common K-feldspar, plagioclase, volcanic grains, schistose metamorphic grains (Lt_m, Image D, XPL), sideritic mudclasts and chert grains;
- Sparse muscovite flakes and blebs of organic matter.

Matrix:
- Sparse detrital clays.

Authigenic phases:
- Abundant pore filling ferroan dolomite;
- Sparse non ferroan calcite, thin quartz overgrowths, grain replacive siderite and pyrite.

Pore system: Porosity is not noted.

Reservoir quality: Negligible.

LEGACY CORE ANALYSIS DATA
Porosity: n/a
Permeability: n/a

Point Count Porosity: n/a

**Rock classification is based on visual estimation of mineralogical components.*

Well: K-A2

Depth: 4078.4m

Lithology: Sandy siltstone/silty sandstone

Classification: Sandy siltstone/subfeldspathic-sublithic arenite*

Texture:
Sample is laminitic. It is composed of laminae with predominant silt and others with relatively more abundant very fine grained sand. Grains are angular to sub-rounded, locally rounded; compaction is strong.

Detrital components:
- Predominant monocrystalline quartz;
- Common feldspars, volcanic grains, mudclasts, chert, metamorphic grains and organic matter/carbonaceous material;
- Sparse mica flakes and heavy minerals (zircon).

Matrix:
- Grain rimming to pore filling clays (also pseudomatrix).

Authigenic phases:
- Quartz overgrowths, ferroan dolomite, uncertain clays, hematite and pyrite.

Pore system: Porosity is not noted. Artificial fractures are present.

Reservoir quality: Negligible

LEGACY CORE ANALYSIS DATA
Porosity: n/a
Permeability: n/a

Point Count Porosity: n/a

**Rock classification is based on visual estimation of mineralogical components.*

Well: K-A2

Depth:4078.4m

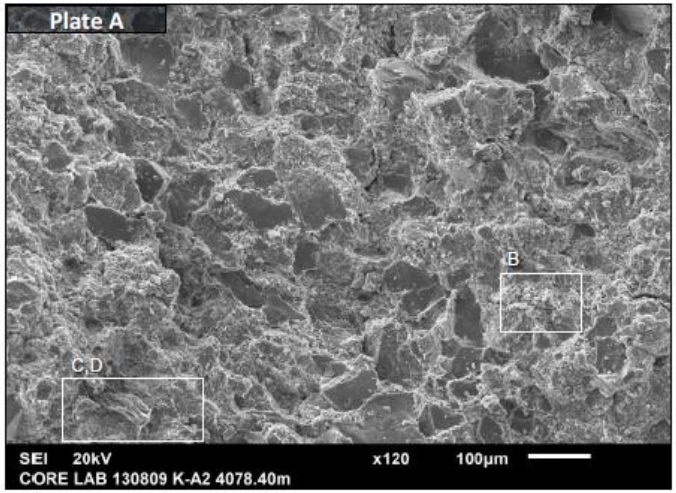

A well sorted very fine (lower-upper) grained sandstone that appears mainly massive, with some alignment of elongate grains (A). The sample appears well compacted, with long grain contacts observed (B), although grain contacts are commonly obscured by matrix clays.

Detrital grains include quartz; abundant feldspars (plagioclase with rare K-feldspar) that are locally leached; lithic grains (mainly clay-rich, with quartz-mica varieties); micaceous minerals (including biotite and muscovite); and accessory grains (Ti-minerals and traces of apatite). It is difficult to fully differentiate some compacted lithic grains from matrix material.

Matrix clays are abundant. EDX analysis indicates these are likely to be dominated by chlorite, with some mixed compositions. Matrix clays are matted / morphologically indeterminate in form. Well developed platy chlorite is locally common, coating grains and lining pores, associated mainly with small open intergranular pores (B) and probable altered lithic grains, and appears to also be partially matrix replacive.

Due to the abundance of clays, authigenic mineral cements are present in minor amounts only. Small isolated overgrowths of quartz and plagioclase are rare (B). Very fine / microcrystalline developments of quartz and albite may also be associated with altered ?lithic grains (D). Minor to moderate patchy calcite (D) forms finely crystalline developments, that are possibly replacive as well as pore-filling. EDX analysis indicates the calcite has minor Fe and Mn components. Rare ferroan dolomite forms very finely crystalline rhombs and subhedra. Porosity appears to be poor. Rare, small intergranular pores appear effectively isolated (B). Overall porosity is dominated by microporosity associated with matrix and authigenic clays and leached framework grains. Pore connectivity is restricted to microporous networks. Permeability is expected to be very poor.

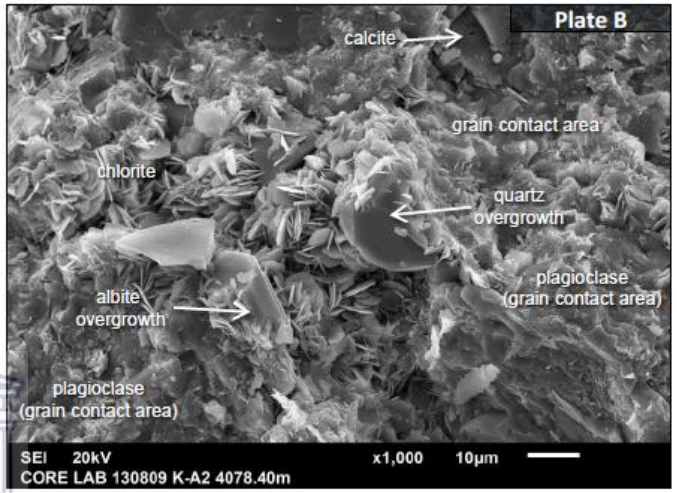

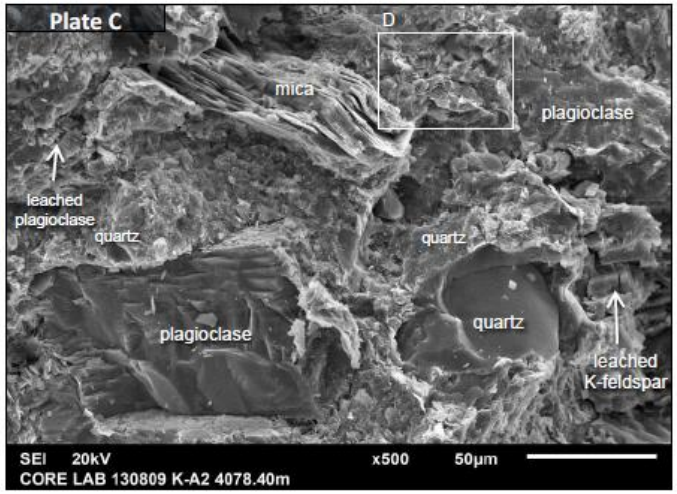

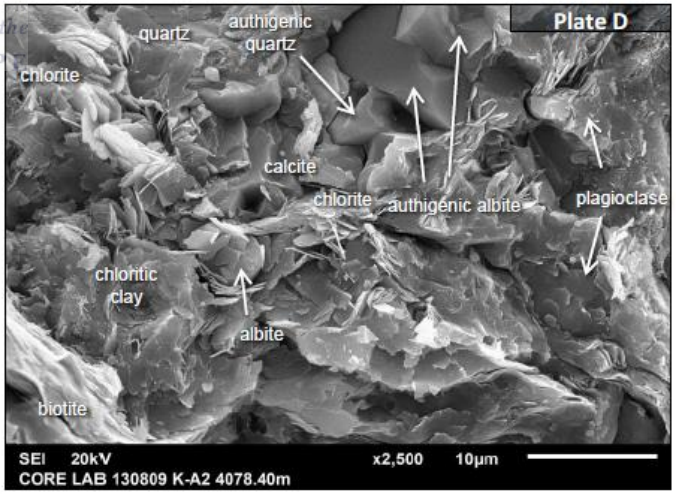

Well: K-A2

Depth: 4079.42m

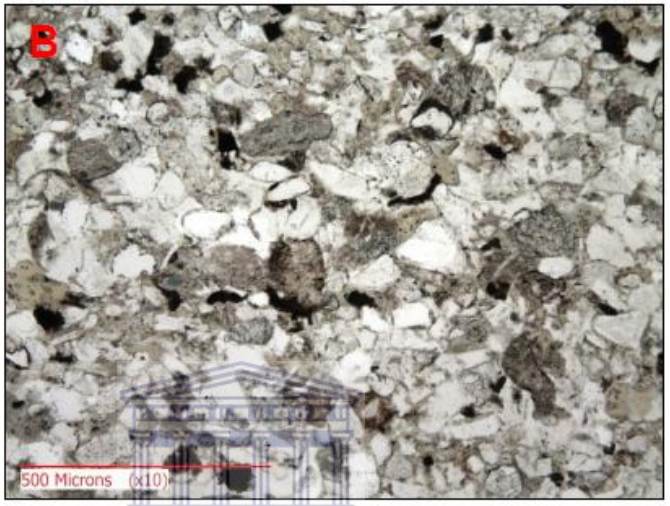

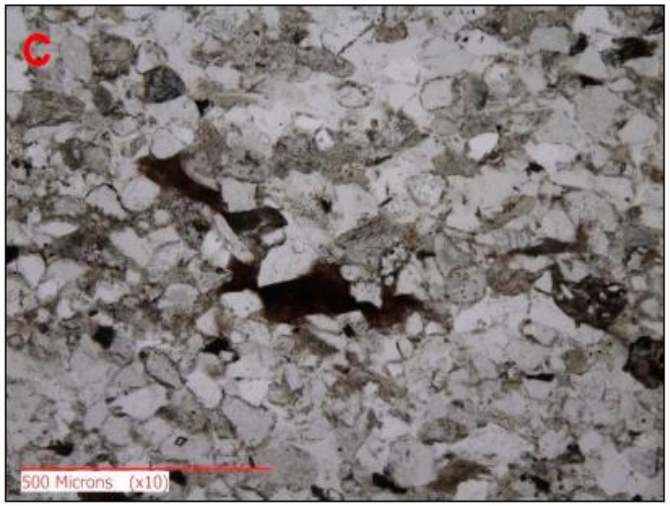

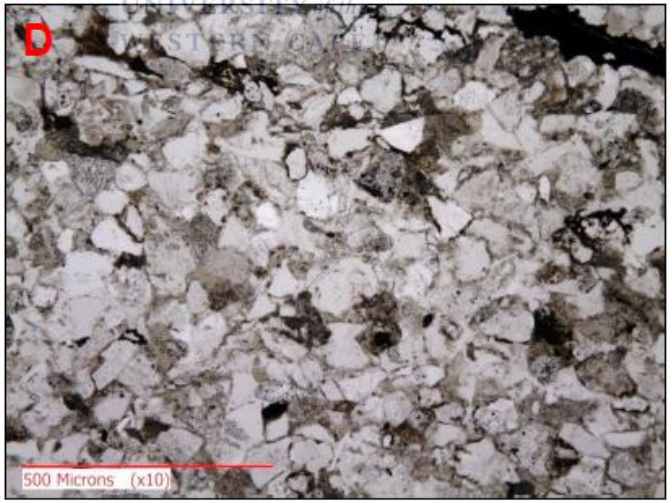

Lithology: Silty sandstone

Classification: Sublithic arenite*

Texture:
Sample is composed of laminae with predominant silt and others with relatively more abundant very fine grained sand. Grains are angular to rounded; compaction is strong (sutured contacts are common).

Detrital components:
- Predominant monocrystalline quartz;
- Common mudclasts (also sideritic), volcanic grains, chert, metamorphic grains and relatively lesser amounts of feldspars, mica flakes, organic matter/carbonaceous material and heavy minerals (zircon).

Matrix:
- Common clays (also pseudomatrix).

Authigenic phases:
- Quartz overgrowths, dolomite, siderite, ?chlorite and pyrite.

Pore system: Porosity is not noted.

Reservoir quality: Negligible

LEGACY CORE ANALYSIS DATA
Porosity: n/a
Permeability: n/a

Point Count Porosity: n/a

**Rock classification is based on visual estimation of mineralogical components.*

Well: A-H1 – Petrographic Analyses
Depth:3023.75m

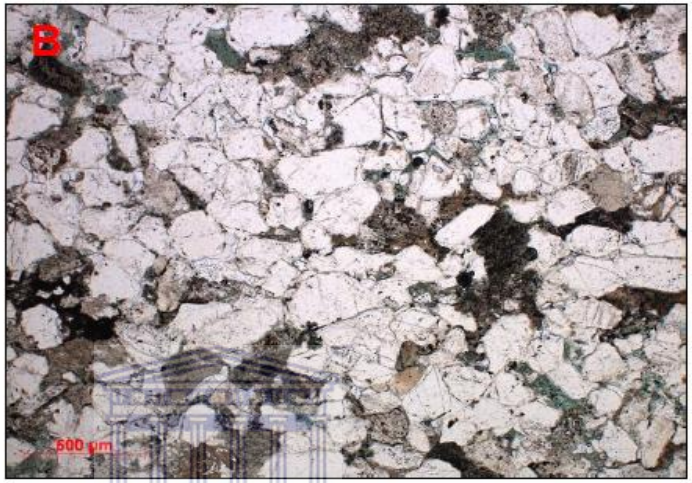

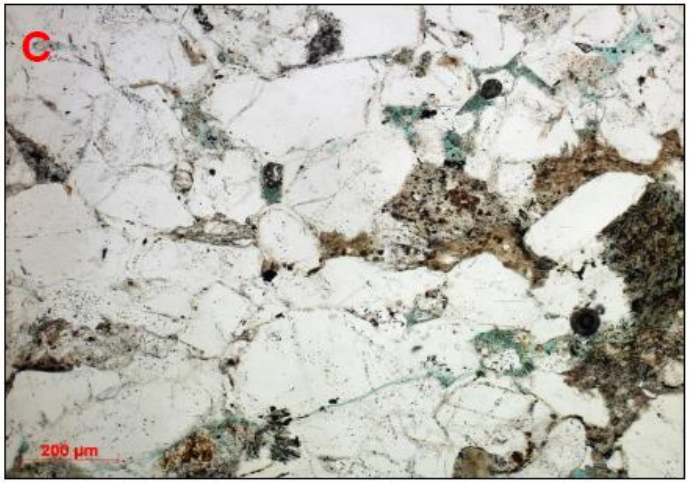

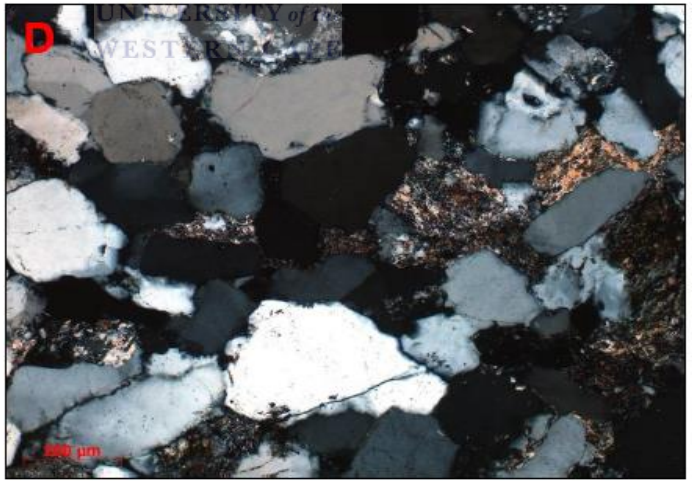

Lithology: Sandstone

Classification: Subfeldspathic-sublithic arenite

Texture:
Grain size: Fine (upper).
Sorting: Moderately well sorted.
Grain contacts: Long to sutured.
Grain shape: Subangular to rounded.
Compaction: Strong.

Detrital components:
- Abundant monocrystalline and polycrystalline quartz;
- Feldspars, mudclasts, chert, metamorphic grains and volcanic grains;
- Mica flakes, heavy minerals (tourmaline, zircon and garnet) and traces of organic matter.

Matrix:
- Detrital clays (mainly a pseudomatrix) are also locally noted.

Authigenic phases:
- Common quartz overgrowths restrict pores and pore throats;
- Grain replacive illite/sericite, pore filling kaolinite, grain replacive chlorite, siderite, ferroan dolomite and pyrite are also present.

Pore system: Porosity is poor to locally moderate and mainly represented by isolated secondary pores (mesopores). Micropores (~10µm) noted within partially dissolved grains, are also present.

Reservoir quality: Poor

LEGACY CORE ANALYSIS DATA
Porosity: n/a
Permeability: 3.6mD at 3023.85m

Point Count Porosity: 9.0%

Well: A-H1
Depth: 3024.2m

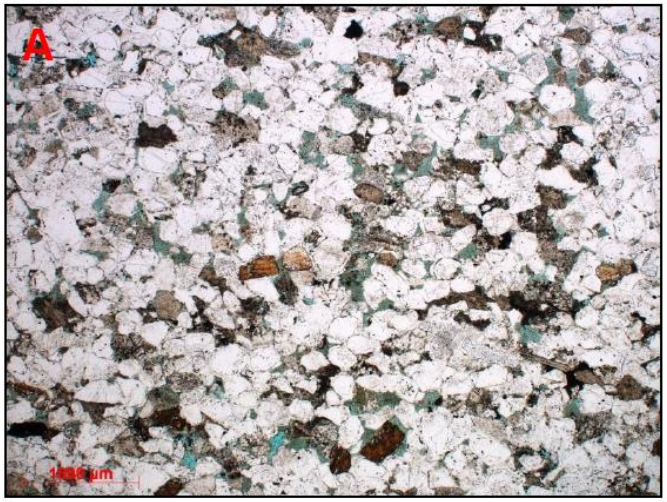

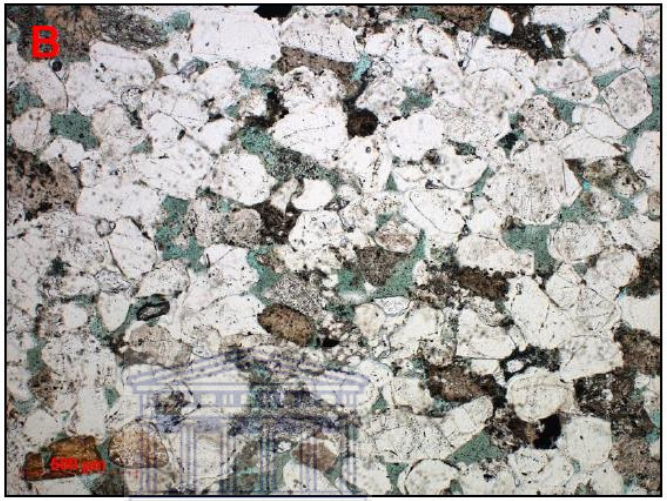

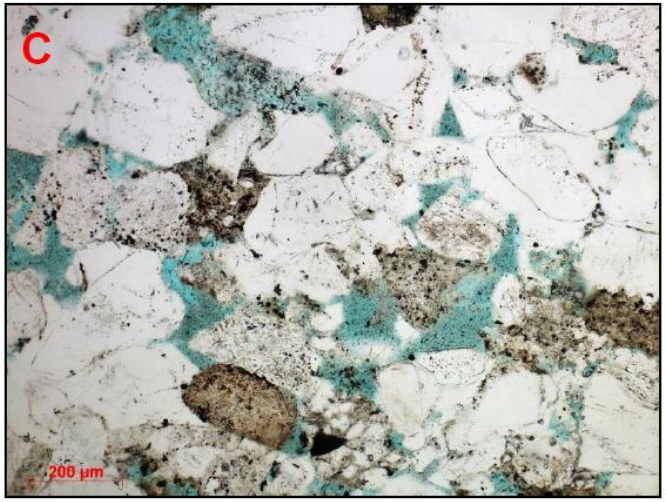

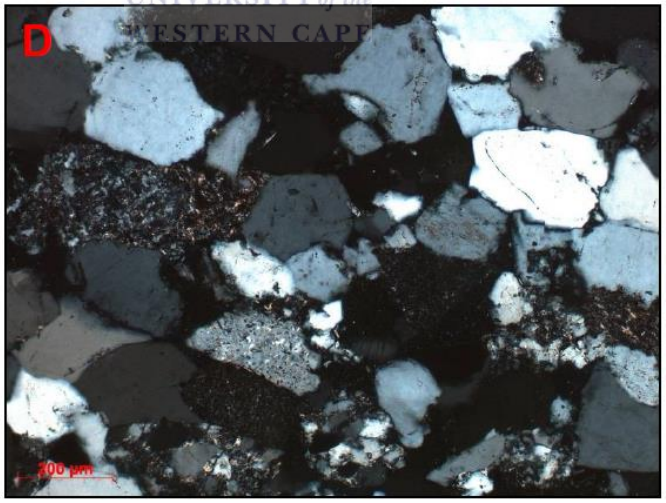

Lithology: Sandstone

Classification: Sublithic arenite

Texture:
Grain size: Fine (upper).
Sorting: Moderately well sorted.
Grain contacts: Long to sutured.
Grain shape: Subangular to rounded.
Compaction: Strong overall.

Detrital components:
- Predominant monocrystalline and polycrystalline quartz;
- Common feldspars, mudclasts, chert, metamorphic grains and volcanic grains;
- Sparse mica flakes, heavy minerals (tourmaline, zircon and garnet) and organic matter.

Matrix:
- Detrital clays (mainly a pseudomatrix) are scattered.

Authigenic phases:
- Common quartz overgrowths restrict pores and pore throats;
- Grain replacive illite/sericite, pore filling kaolinite, grain replacive chlorite, siderite, ferroan dolomite and pyrite are also present.

Pore system: Porosity is moderate. Macropores are primary and secondary, the latter linked to the dissolution of unstable feldspars and lithics. Micropores between clay platelets are optically irresolvable.

Reservoir quality: Poor to locally moderate.

LEGACY CORE ANALYSIS DATA
Porosity: 15.6% at 3024.24m
Permeability: 12mD at 3024.24m

Point Count Porosity: 10%

Well: A-H1
Depth: 3026.4m

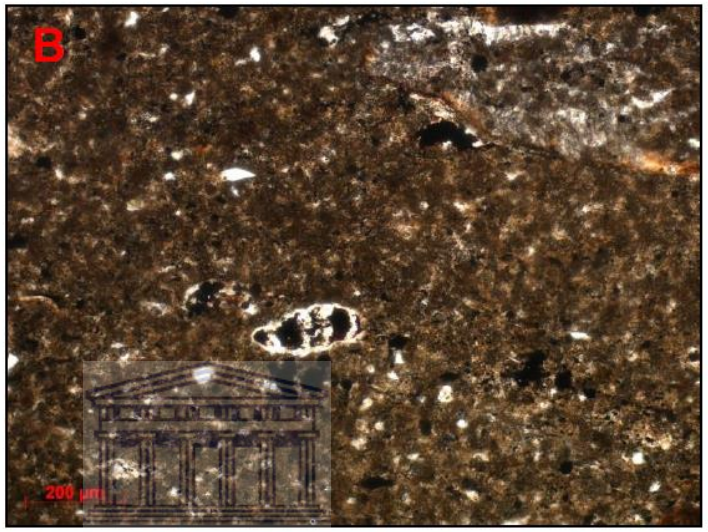

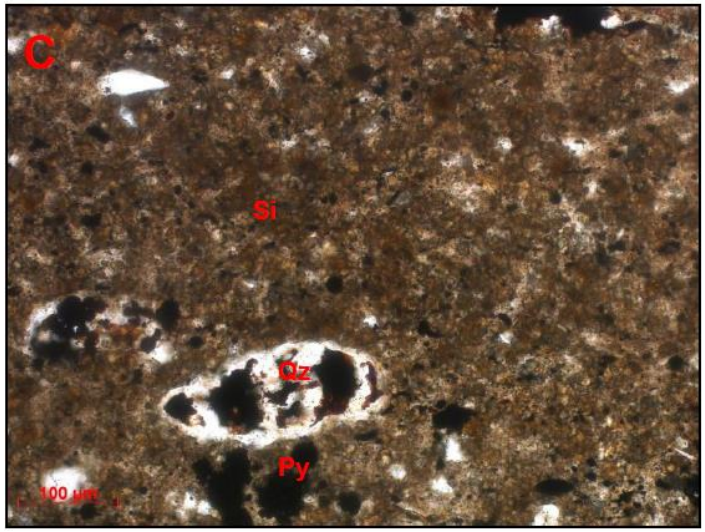

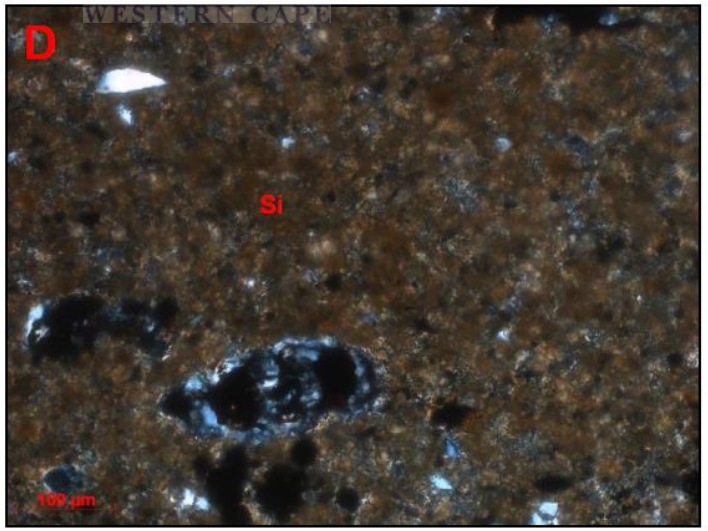

Lithology: Ironstone

Classification: Sideritic wackestone*

Texture:
Matrix supported: Large bioclasts float into a carbonate-rich (sideritic) matrix.

Detrital components:
Detrital quartz, large mollusks and silicified carbonate allochems (possible foraminifera).

Matrix:
- Predominant very finely crystalline siderite (Si, Images C & D, XPL) and relatively lesser amounts of micrite/dolomicrite and clays.

Authigenic phases:
- Pore filling dolomitized botryoidal calcite (likely initially aragonite);
- Replacement to pore filling dolomite (e.g. Do, Image A);
- Replacement microcrystalline quartz (Qz, Image C);
- Pyrite framboids (Py, Image C) disseminated within the matrix of this sample.

Pore system: Porosity is not noted. Fractures are relatively common, a part of which may represent a natural feature of this rock.

Reservoir quality: Negligible

LEGACY CORE ANALYSIS DATA
Porosity: n/a
Permeability: n/a

Point Count Porosity: n/a

**Rock classification is based on visual estimation of mineralogical components.*

Well: A-H1
Depth: 3029.32m

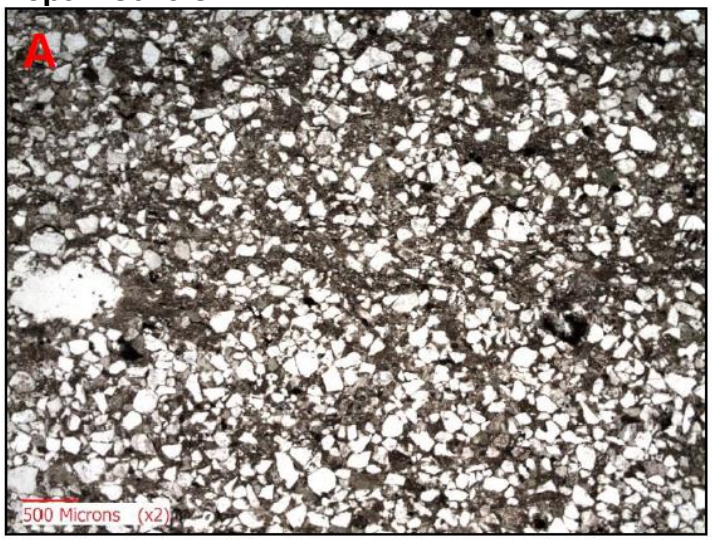

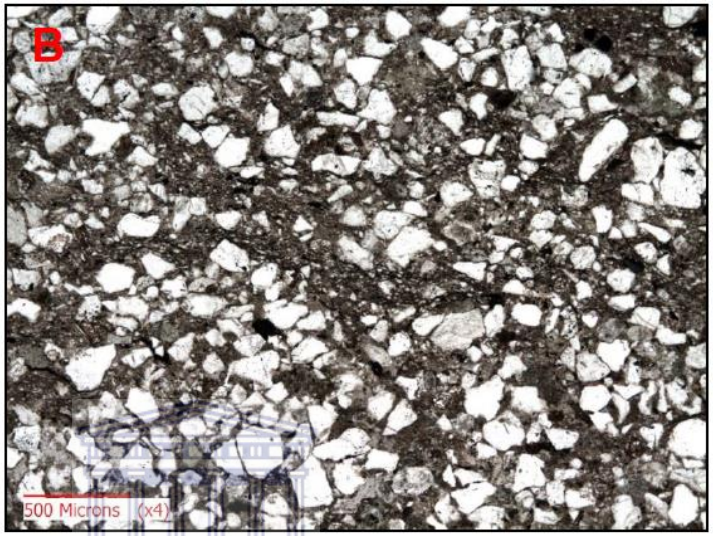

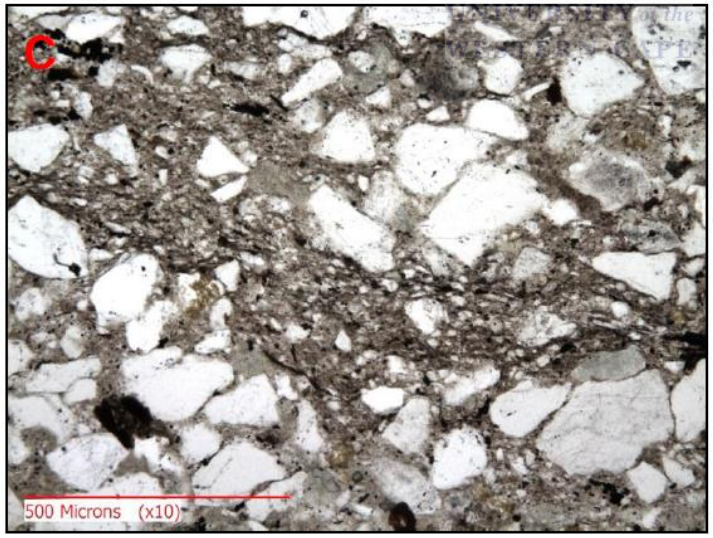

Lithology: Wackes

Classification: Quartz-feldspathic wacke*

Texture:
Matrix supported. Grains are angular to rounded.

Detrital components:
Detrital quartz, feldspars, chert, volcanic grains, metamorphic grains, mica flakes, detrital chlorite, organic matter, phosphatic material, tourmaline and glauconite.

Matrix:
- Predominant detrital clays.

Authigenic phases:
- Illite/sericite is likely abundant; ferroan dolomite, pyrite, quartz cement and siderite are also noted.

Pore system: Porosity is not noted.

Reservoir quality: Negligible

LEGACY CORE ANALYSIS DATA
Porosity: n/a
Permeability: 0.3mD at 3029.5m

Point Count Porosity: n/a

**Rock classification is based on visual estimation of mineralogical components.*

Well: A-H1
Depth: 3030.77m

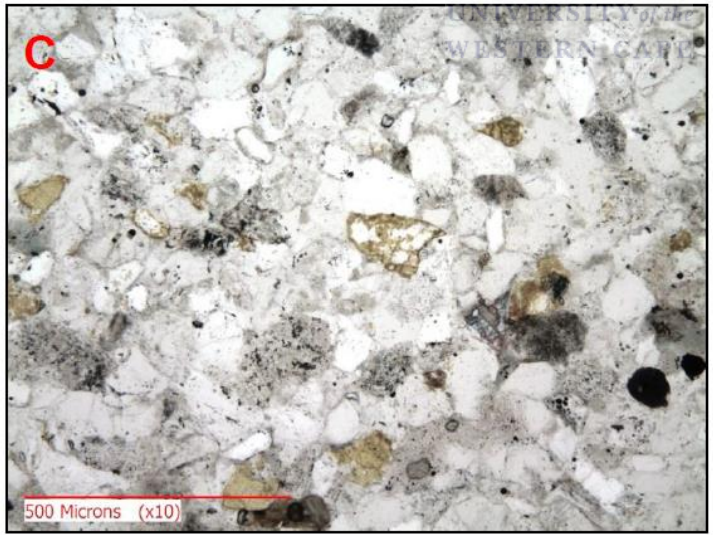

Lithology: Sandy siltstone

Classification: Feldspathic sandy siltstone*

Texture:
Grain size: Silt to very fine grade sand.
Sorting: Well sorted.
Grain contacts: Sutured.
Grain shape: Angular to rounded.
Compaction: Strong. Stylolites are noted.

Detrital components:
Detrital quartz, feldspars, chert, volcanic grains, metamorphic grains, mudclasts, mica flakes, organic matter, tourmaline and glauconite.

Matrix:
- Sample is moderately shaly.

Authigenic phases:
- Quartz overgrowths, illite/sericite, chlorite, ferroan dolomite, pyrite and siderite are the main phases noted in this sample.

Pore system: Porosity is very poor. Isolated primary and secondary pores are present.

Reservoir quality: Very poor

LEGACY CORE ANALYSIS DATA
Porosity: n/a
Permeability: 1.3mD at 3030.64m

Point Count Porosity: n/a

**Rock classification is based on visual estimation of mineralogical components.*

Well: A-H1
Depth: 3032.64m

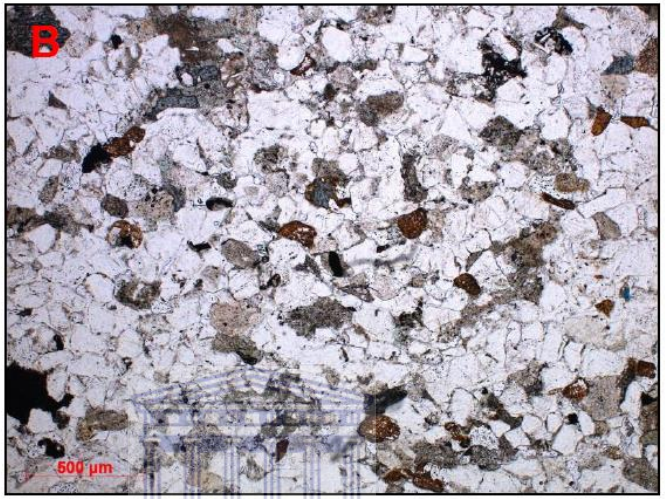

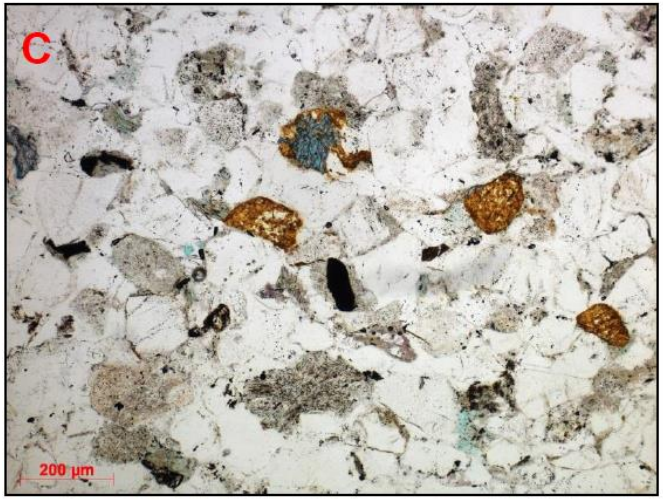

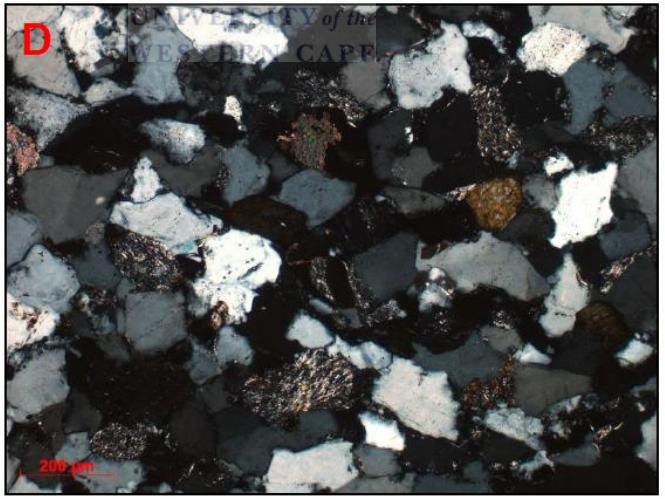

Lithology: Sandstone

Classification: Subfeldspathic-sublithic arenite*

Texture:
Grain size: Fine (lower).
Sorting: Well sorted.
Grain contacts: Long to sutured.
Grain shape: Subangular to rounded.
Compaction: Strong.

Detrital components:
- Predominant monocrystalline and polycrystalline quartz;
- Common feldspars, mudclasts, chert, metamorphic grains and volcanic grains;
- Sparse mica flakes (mainly muscovite) and organic matter.

Matrix:
- Sparse detrital clays (mainly a pseudomatrix) also associated with very finely crystalline siderite.

Authigenic phases:
- Quartz overgrowths restrict pores and pore throats. Pore filling chalcedony is also locally noted;
- Authigenic clays (illite/sericite & chlorite), carbonates (replacement siderite, pore filling to replacement ferroan calcite/dolomite) and pyrite framboids are also present.

Pore system: Porosity is rare (isolated secondary pores).

Reservoir quality: Very poor

LEGACY CORE ANALYSIS DATA
Porosity: n/a
Permeability: n/a

Point Count Porosity: n/a

**Rock classification is based on visual estimation of mineralogical components.*

Well: A-H1
Depth: 3033.26m

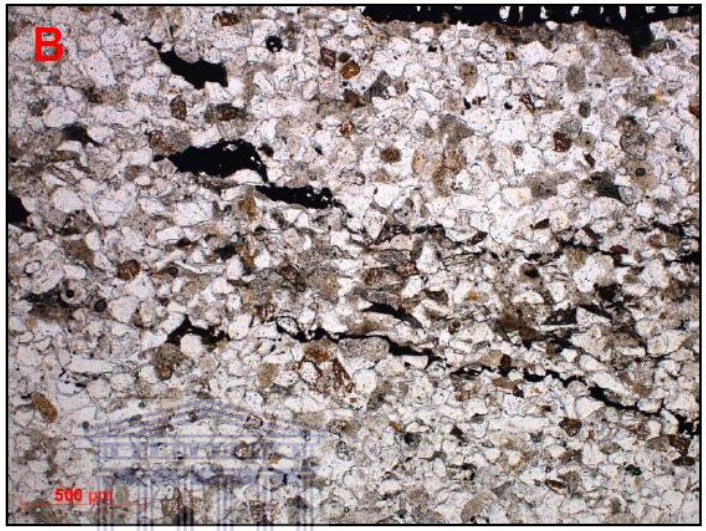

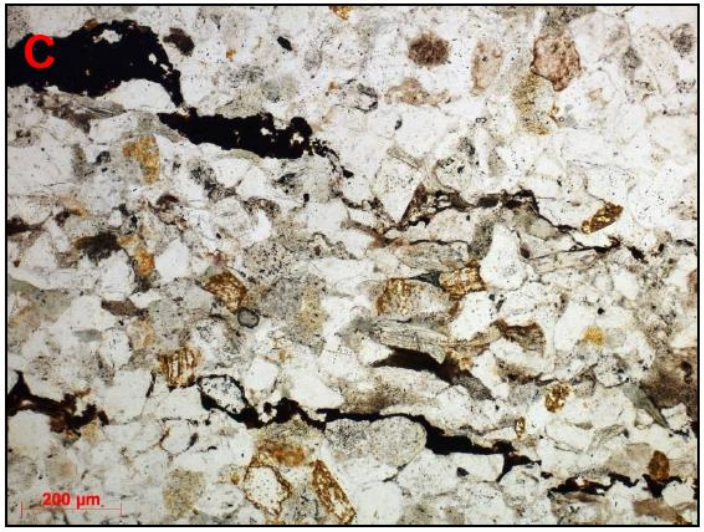

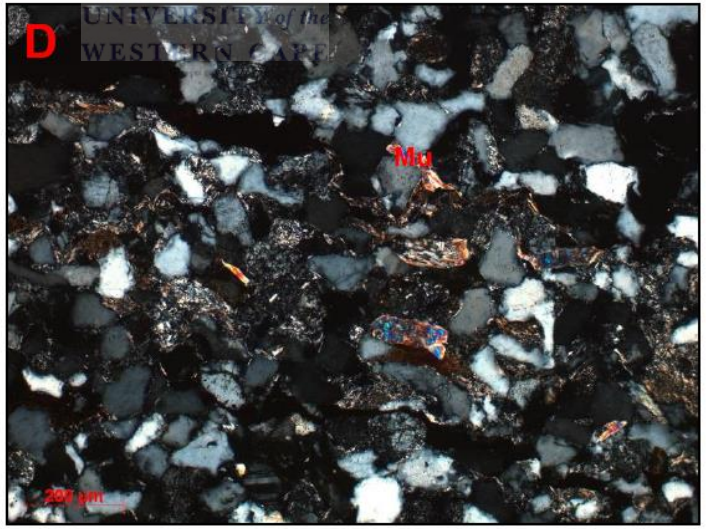

Lithology: Sandstone

Classification: Subfeldspathic-sublithic arenite*

Texture:
Grain size: Very fine
Sorting: Well sorted.
Grain contacts: Long to sutured.
Grain shape: Angular to rounded.
Compaction: Strong.

Detrital components:
- Predominant monocrystalline quartz;
- Common feldspars, mudclasts, chert, metamorphic grains, volcanic grains and organic matter/carbonaceous material;
- Compacted mica flakes (mainly muscovite, Mu, Image D) and heavy minerals (tourmaline and zircon).

Matrix:
- Sample is moderately shaly. Detrital clays are also associated with organic matter.

Authigenic phases:
- Common pore restricting quartz overgrowths;
- Grain replacive illite/sericite, ?chlorite, siderite and pyrite/?pyrobitumen.

Pore system: Porosity is not noted.

Reservoir quality: Negligible

LEGACY CORE ANALYSIS DATA
Porosity: n/a
Permeability: n/a

Point Count Porosity: n/a

**Rock classification is based on visual estimation of mineralogical components.*

Well: A-H1
Depth: 3033.26m

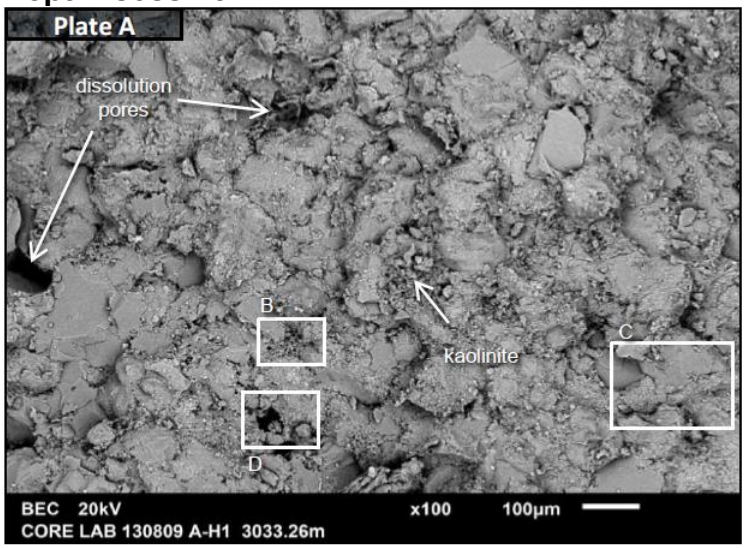

A moderately well sorted very fine (lower - upper) grained sandstone that appears massive at the scale of SEM (A). The sample is well compacted, with common long grain contacts observed.

Detrital grains include quartz (including microquartz, C); common feldspars (plagioclase with rare K-feldspar, locally leached or albitised). Some indeterminate grains are leached to leave dissolution pores (A).

Pore-lining / ?matrix clays appear to be widespread, and of mixed composition. Matted clays are observed adjacent to grain contact areas. Authigenic grain-coating clays comprise a mix of platy chlorite and very finely webbed to wispy clays (?illite / ?illite-smectite) (B, D). Kaolinite is a common patchy phase that appears to be an intergranular as well as a replacive phase, typically forming short blocky verms (B). Quartz overgrowths were observed as mainly isolated projections, and are rarely interlocking (C). Rare authigenic albite is present within dissolution pores / replacive of leached feldspar grains (D). Traces of ferroan dolomite were also observed within dissolution pores (D).

Porosity appears to be moderate to moderately poor. Small intergranular and scattered dissolution pores appear largely isolated. Overall porosity may be dominated by microporosity mainly associated with clay mineral aggregates. Pore connectivity appears to be largely restricted to microporous networks. Permeability is expected to be poor.

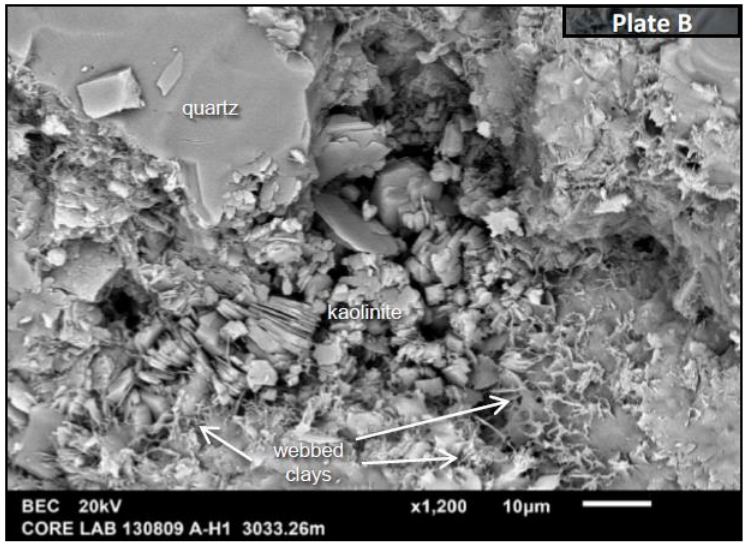

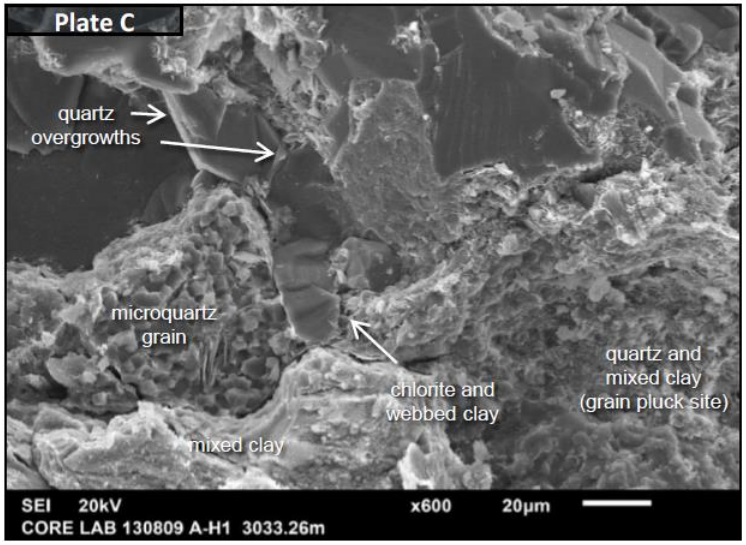

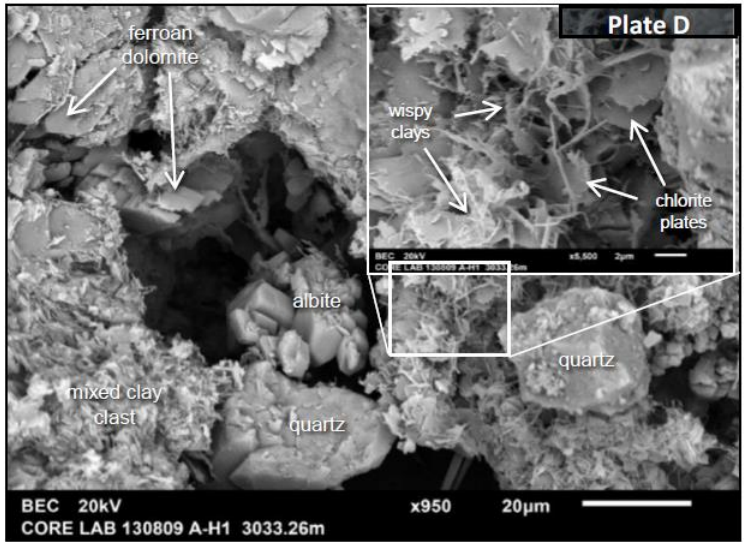

Well: A-H1
Depth: 3035.2m

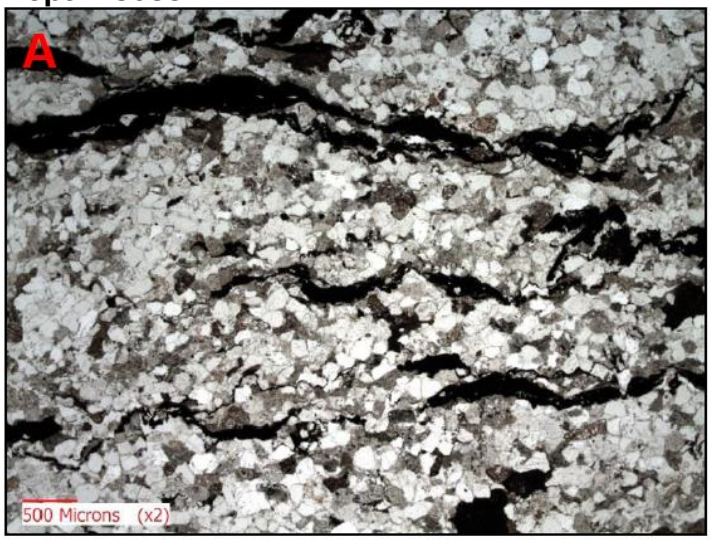

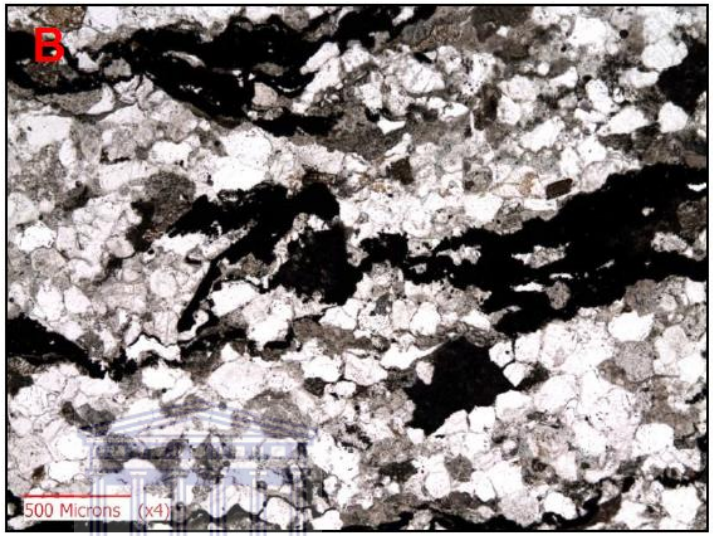

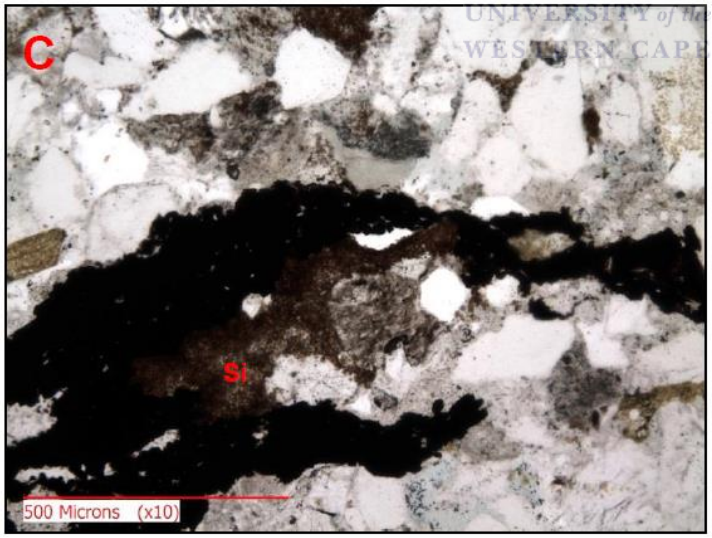

Lithology: Sandstone

Classification: Subfeldspathic-sublithic arenite*

Texture:
Grain size: Fine grained sand is dominant.
Sorting: Well sorted.
Grain contacts: Mainly sutured.
Grain shape: Angular to rounded.
Compaction: Strong.

Detrital components:
- Predominant monocrystalline quartz, with common feldspars, mudclasts, chert, metamorphic grains, volcanic grains, mica flakes and organic matter/carbonaceous material.

Matrix:
- Sample is moderately shaly overall.

Authigenic phases:
- Common pore restricting quartz overgrowths, with relatively lesser amounts of grain replacive illite/sericite, ?chlorite, ferroan dolomite, siderite (Si, Image C) and pyrite/?pyrobitumen.

Pore system: Porosity is very poor and represented by isolated secondary pores.

Reservoir quality: Very poor

LEGACY CORE ANALYSIS DATA
Porosity: 13.8% at 3035m
Permeability: 0.3mD at 3035m

Point Count Porosity: n/a

**Rock classification is based on visual estimation of mineralogical components.*

Well:A-H1
Depth: 3037.8m

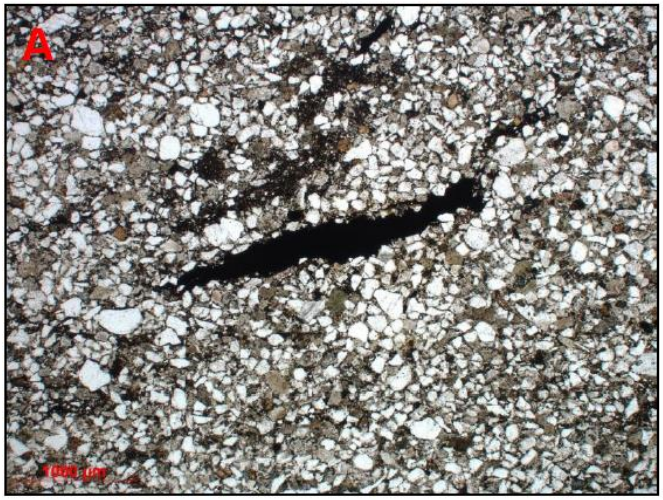

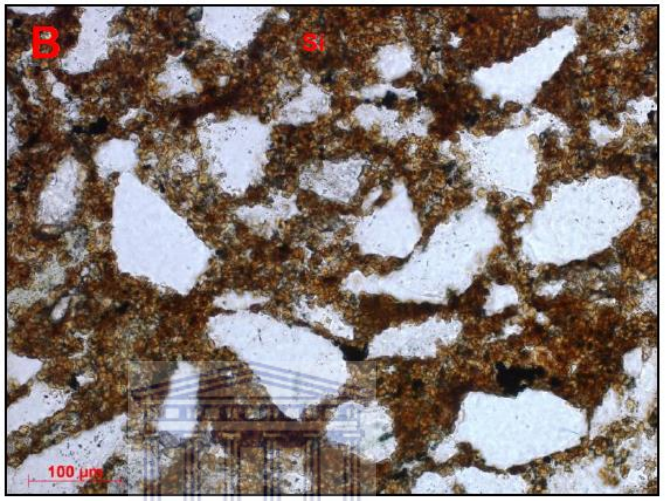

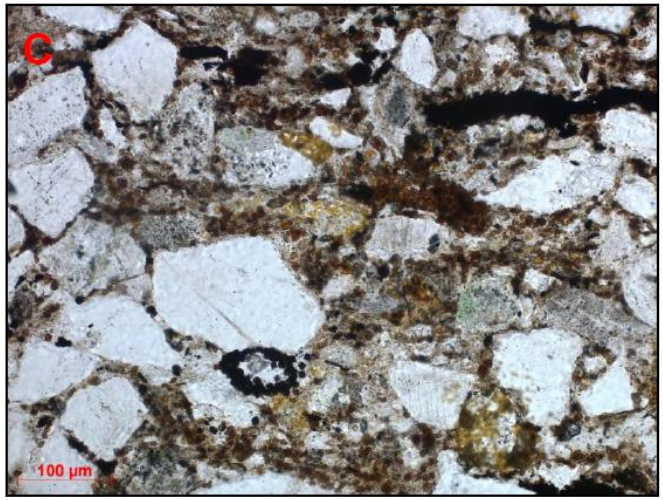

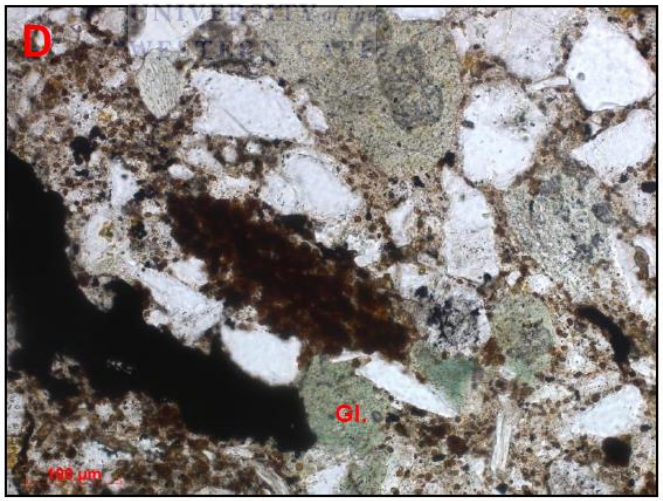

** Berner, R.A. (1981)-New geochemical classification of sedimentary environments. Journal of Sedimentary Petrology, 51, 359-365

Lithology: Sideritic wacke

Classification: Lithic wacke*

Texture:
Very fine to medium (upper) sand is locally embedded into a clayey and sideritic matrix.

Detrital components:
- Predominant monocrystalline quartz;
- Common feldspars, mudclasts, chert, schistose metamorphic grains, volcanic grains and organic matter/carbonaceous material;
- Sparse mica flakes, detrital chlorite, glauconite (Gl, Image D) and a large mollusk with foliated wall structure (not in photomicrographs).

Matrix:
- Common detrital clays intermixed with siderite (Si, Image B).

Authigenic phases:
- Common pore filling to replacement siderite, grain replacive illite/sericite, chlorite and ?smectite/glauconite;
- Sparse pore restricting quartz overgrowths, pore filling ferroan dolomite and grain replacive pyrite.

Note that the combined presence of glauconite and siderite points to the presence of a slightly reducing, anoxic, non sulphidic, post-oxic diagenetic environment (*sensu* Berner**, 1981).

Pore system: Porosity is not noted.

Reservoir quality: Negligible

LEGACY CORE ANALYSIS DATA
Porosity: n/a
Permeability: 0.4mD at 3037.83m

Point Count Porosity: n/a

**Rock classification is based on visual estimation of mineralogical components.*

Well: A-H1
Depth: 3038m

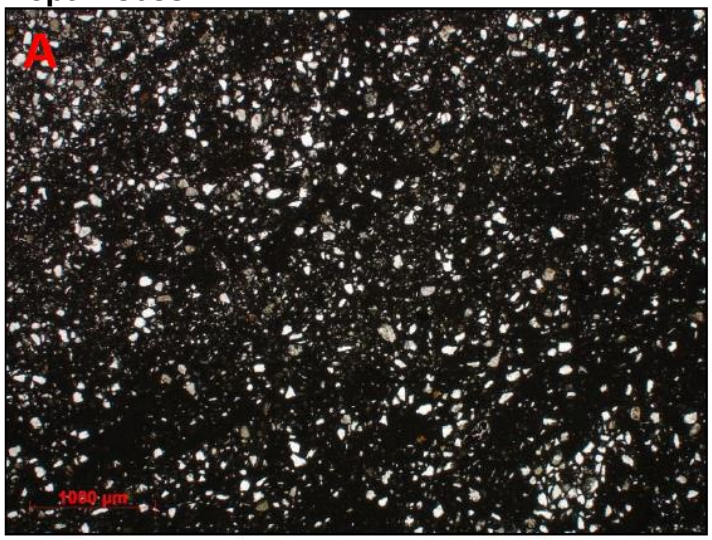

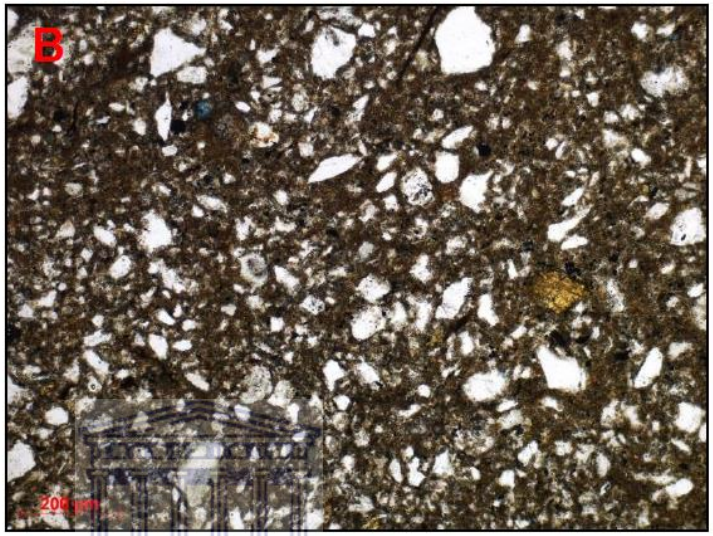

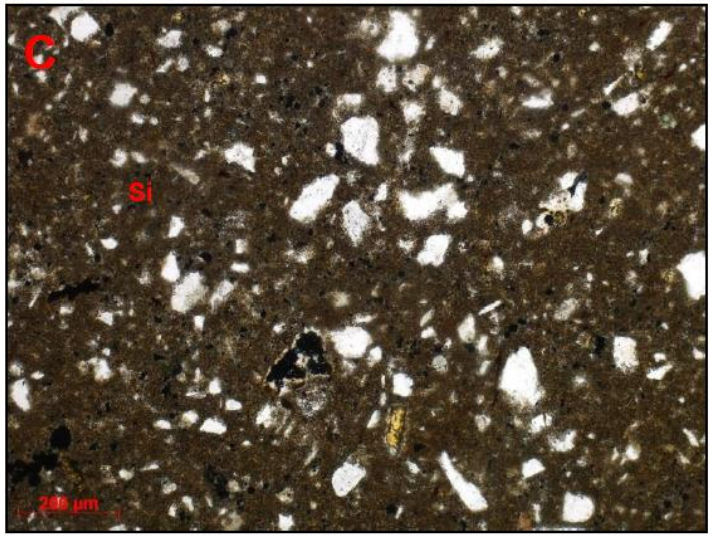

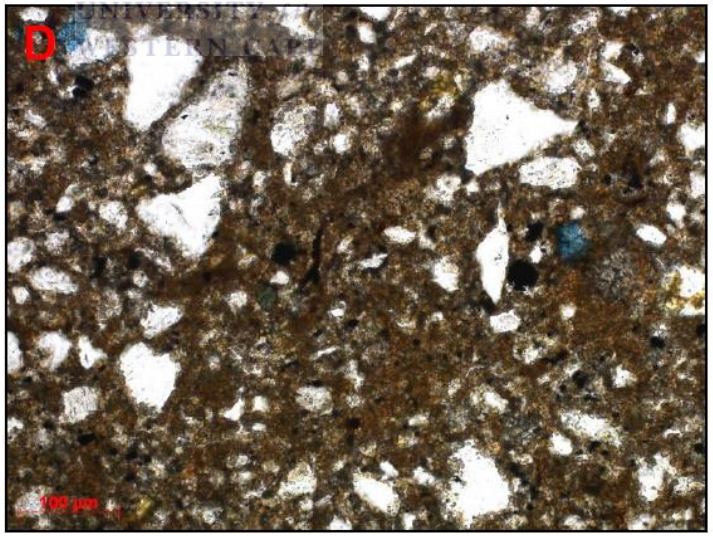

Lithology: Sandy ironstone

Classification: Sandy sideritic wackestone*

Texture:
Very fine to medium sand is locally embedded into a dominant sideritic matrix.

Detrital components:
- Abundant monocrystalline quartz;
- Common feldspars, chert, schistose metamorphic grains and volcanic grains;
- Sparse mica flakes, organic matter, glauconite, mollusks and ?foraminifera.

Matrix:
- Predominant microcrystalline siderite (Si, Image C).

Authigenic phases:
- Abundant pore filling to ?replacement siderite.
- ?Chlorite, ?smectite/glauconite, quartz overgrowths, ferroan dolomite and pyrite framboids are noted in lesser amounts.

Pore system: Porosity is not noted.

Reservoir quality: Negligible

LEGACY CORE ANALYSIS DATA
Porosity: n/a
Permeability: n/a

Point Count Porosity: n/a

**Rock classification is based on visual estimation of mineralogical components.*

Well: A-K1 – Petrographic Analyses
Depth:3236.46m

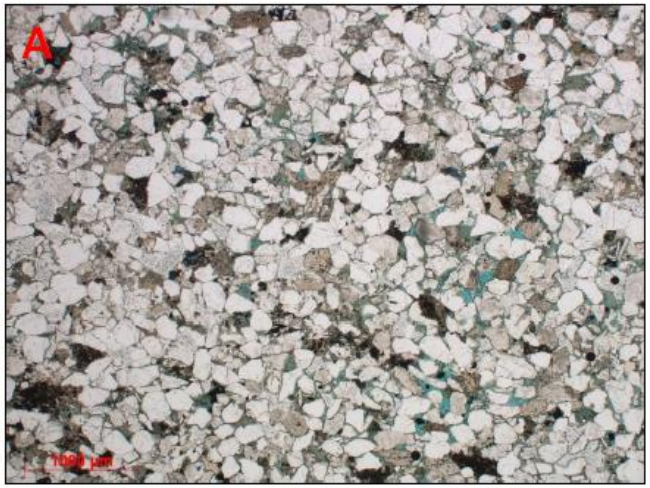

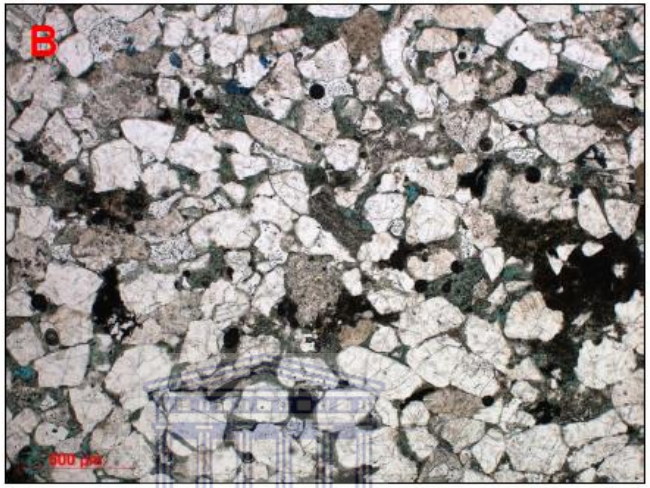

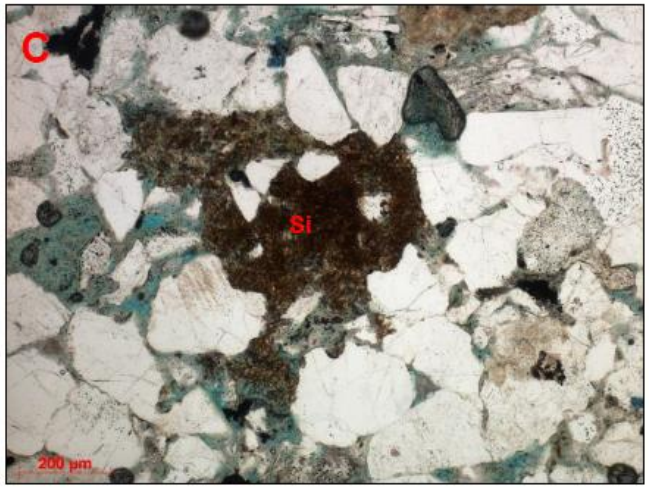

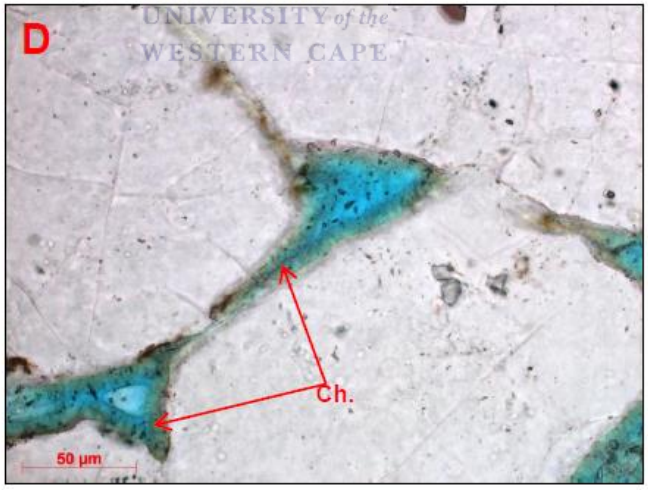

Lithology: Sandstone

Classification: Sublithic arenite

Texture:
Grain size: Fine (upper).
Sorting: Well sorted.
Grain contacts: Mainly long.
Grain shape: Subangular to subrounded.
Compaction: Moderate overall.

Detrital components:
- Predominant monocrystalline quartz;
- Common lithics (chert, mudclasts, igneous and metamorphic grains) and plagioclase;
- Sparse mica flakes, organic matter and heavy minerals (zircon).

Matrix:
- Scattered detrital clays (also a pseudomatrix).

Authigenic phases:
- Common authigenic clays (mainly pore filling/grain rimming chlorite, Ch., Image D);
- Common pore filling quartz overgrowths, grain replacive siderite (Si, Image C) and lesser amounts of pore filling dolomite, grain replacive pyrite and non ferroan calcite.

Pore system: Porosity is moderate (primary and secondary); micropores ~10µm in size are locally noted.

Reservoir quality: Poor overall; permeability is downgraded by clays and quartz overgrowths.

LEGACY CORE ANALYSIS DATA
Porosity: n/a
Permeability: n/a

Point Count Porosity: 10.9%

Well: A-K1
Depth: 3238.57m

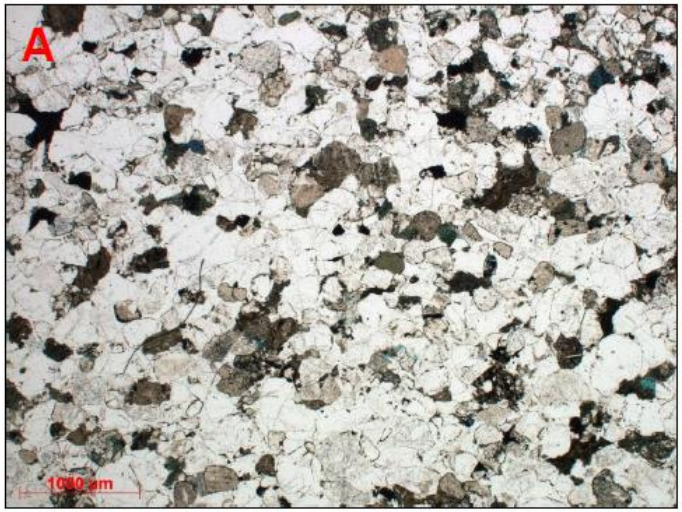

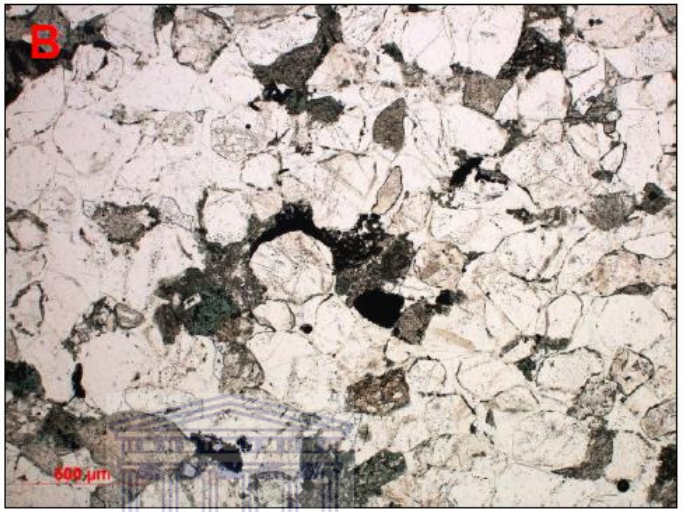

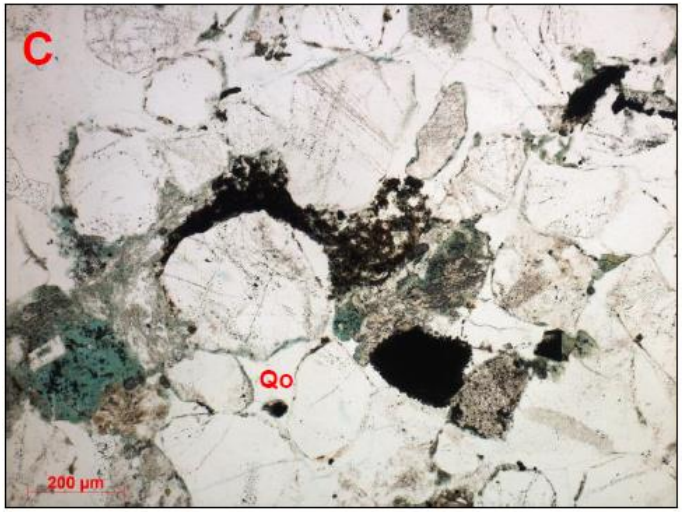

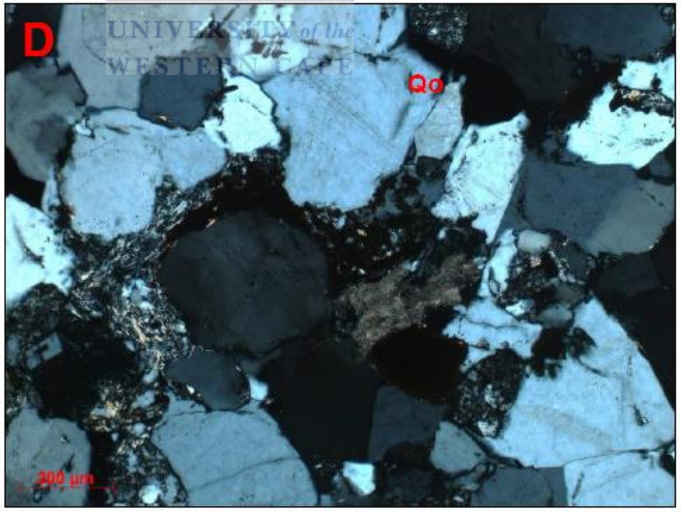

Lithology: Sandstone

Classification: Sublithic arenite*

Texture:
Grain size: Medium (lower)
Sorting: Well sorted.
Grain contacts: Long to sutured.
Grain shape: Subangular to rounded.
Compaction: Moderately strong overall.

Detrital components:
- Predominant monocrystalline quartz;
- Lithics [chert, mudclasts, igneous (e.g. plagioclase-rich) and metamorphic grains], plagioclase and polycrystalline quartz;
- Mica flakes and organic matter.

Matrix:
- Sparse detrital clays (?pseudomatrix).

Authigenic phases:
- Extensive pores and pore throats restricting tabular to prismatic quartz overgrowths (Qo, Images C-D);
- Common pore filling/grain rimming chlorite;
- Sparse pore filling ferroan dolomite and grain replacive pyrite.

Pore system: Porosity is very poor (mainly secondary, ~3% visually); pore effectiveness is significantly downgraded by quartz cementation (likely also linked to pressure solution processes).

Reservoir quality: Very poor

LEGACY CORE ANALYSIS DATA
Porosity: 6.6% at 3238.75m
Permeability: 0.14mD at 3238.75m

Point Count Porosity: n/a

**Rock classification is based on visual estimation of mineralogical components.*

Well: A-K1
Depth: 3239.2m

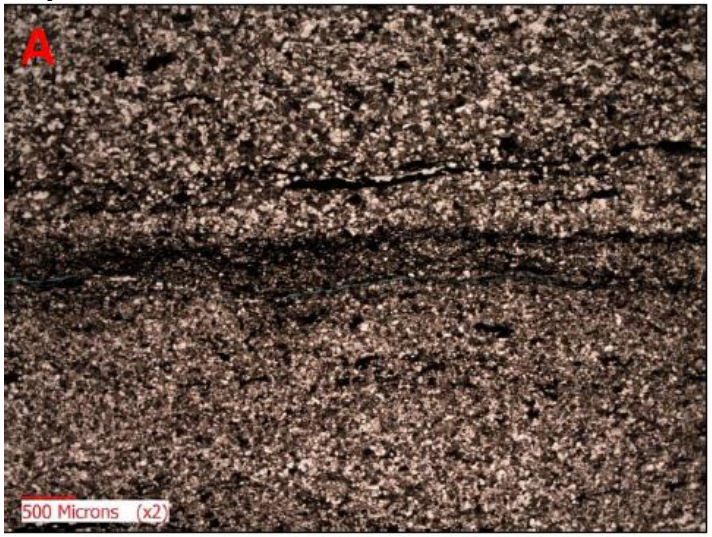

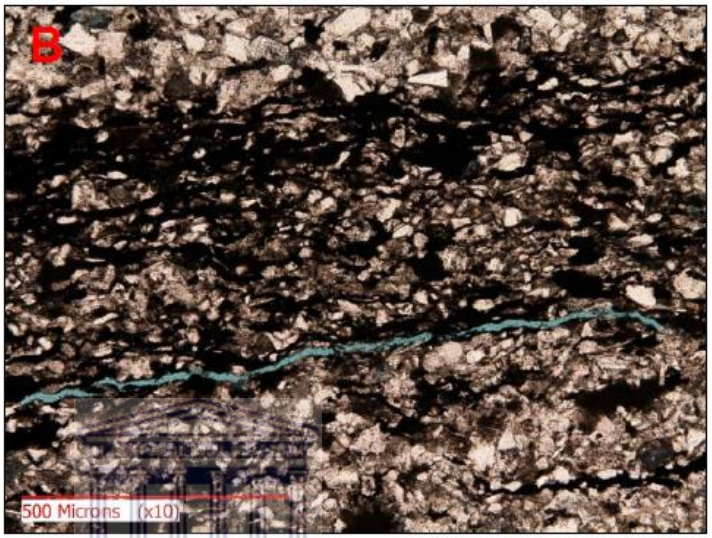

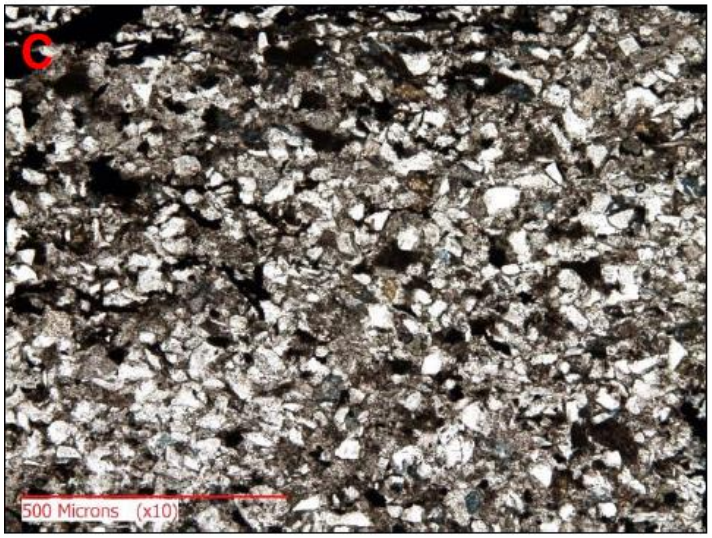

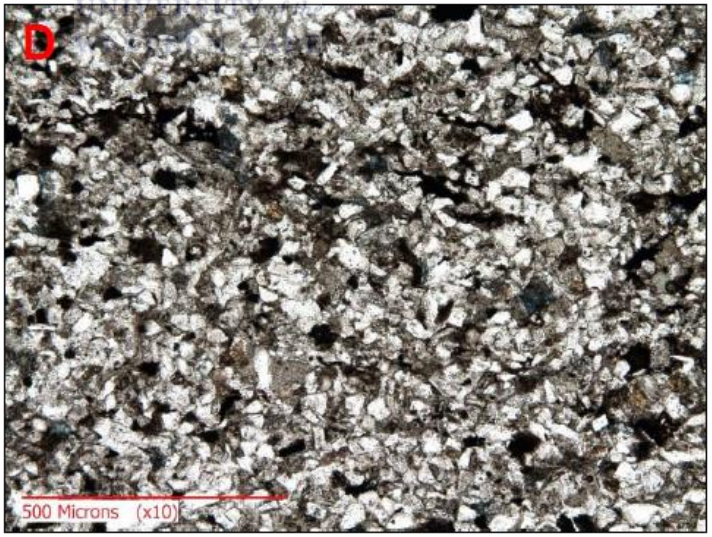

Lithology: Sandy siltstone

Classification: Argillaceous/organic matter-rich siltstone*

Texture:
Sample is composed of silt-grade to very fine grained siliciclastic detritus associated with organic matter and clay laminae.

Detrital components:
- Abundant monocrystalline quartz;
- Common feldspars, lithics, micas flakes, detrital chlorite and organic matter/carbonaceous material.
- Sparse heavy minerals (zircon).

Matrix:
- Abundant clays associated with organic matter.

Authigenic phases:
- Common illite/sericite, pyrite, ferroan dolomite and siderite (also spherosiderite with maltese cross extinction).

Pore system: Porosity is not noted.

Reservoir quality: Negligible

LEGACY CORE ANALYSIS DATA
Porosity: n/a
Permeability: n/a

Point Count Porosity: n/a

**Rock classification is based on visual estimation of mineralogical components.*

Well: A-K1
Depth: 3243.58m

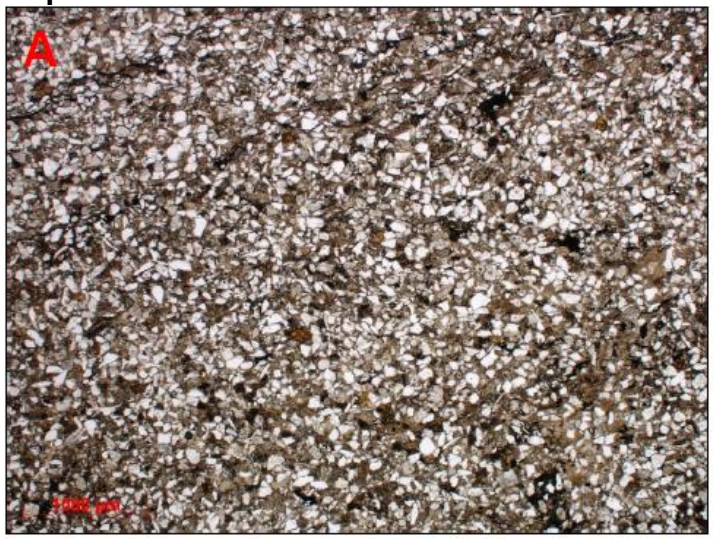

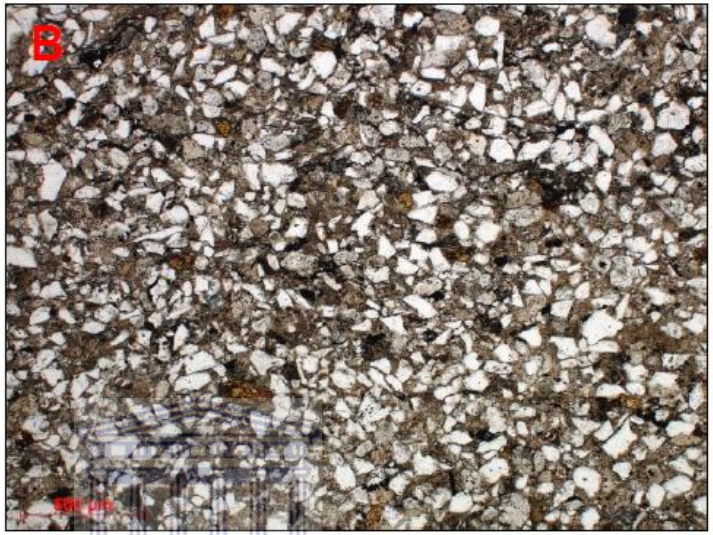

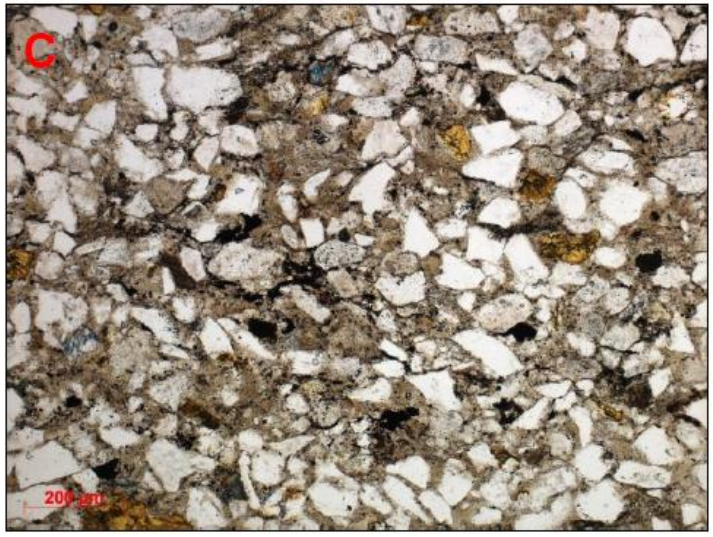

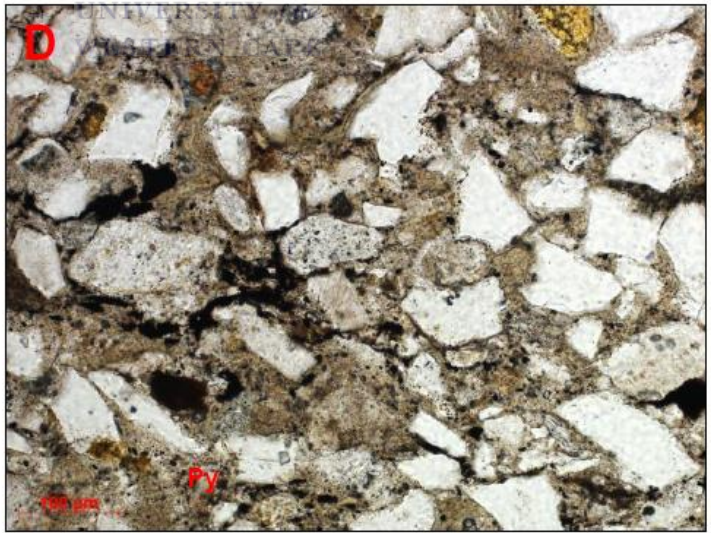

Lithology: Wackes

Classification: Feldspathic/lithic wacke*

Texture:
Siliciclastic grains are noted floating into an argillaceous-rich matrix. Grains are angular to subrounded.

Detrital components:
- Abundant monocrystalline quartz;
- Common feldspars, lithics (e.g. chert, ?volcanic and metamorphic grains), micas and organic matter/carbonaceous material.
- Sparse heavy minerals (tourmaline and zircon).

Matrix:
- Abundant clays (orthomatrix).

Authigenic phases:
- Common illite/sericite and pyrite (also as framboids disseminated within the matrix, e.g. Py, Image D).

Pore system: Porosity is not noted.

Reservoir quality: Negligible

LEGACY CORE ANALYSIS DATA
Porosity: n/a
Permeability: n/a

Point Count Porosity: n/a

**Rock classification is based on visual estimation of mineralogical components.*

Well: A-K1
Depth: 3284.41m

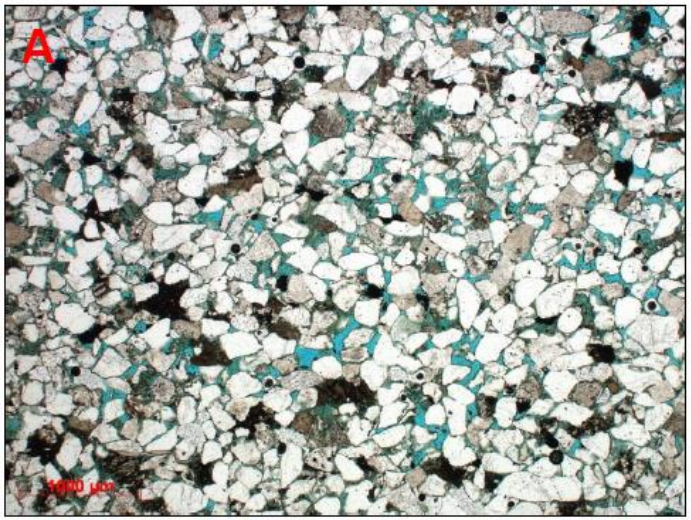

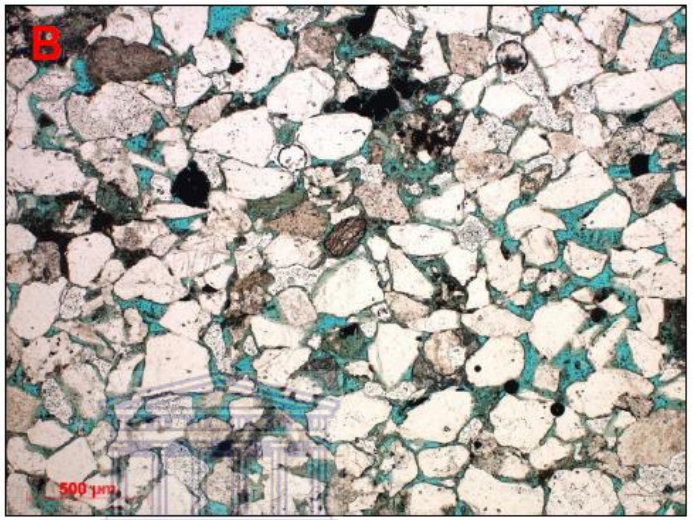

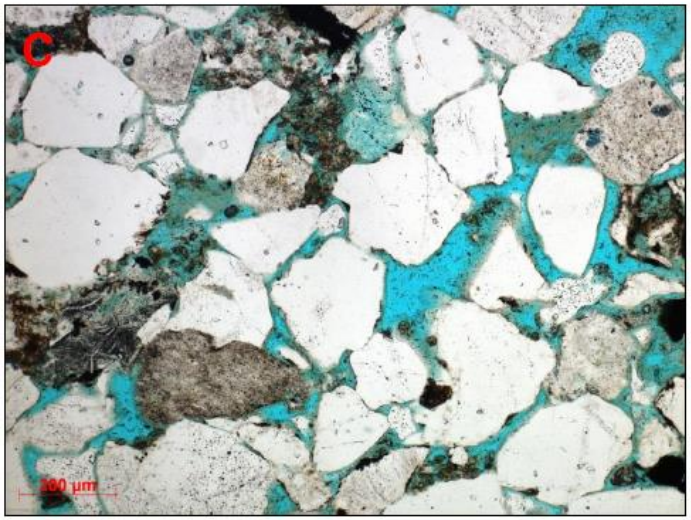

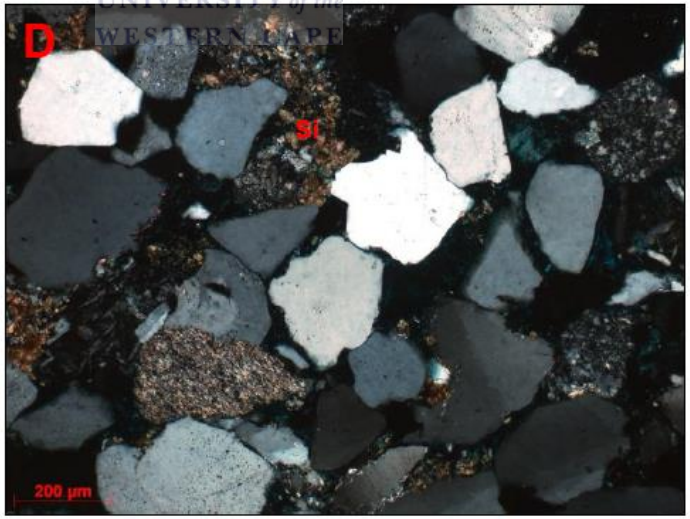

Lithology: Sandstone

Classification: Sublithic arenite

Texture:
Grain size: Fine (upper).
Sorting: Well sorted.
Grain contacts: Mainly long to point to point.
Grain shape: Angular to rounded.
Compaction: Moderate overall.

Detrital components:
- Predominant monocrystalline quartz;
- Common lithics (chert, igneous and metamorphic grains) and plagioclase;
- Sparse organic matter, mica flakes and heavy minerals (tourmaline).

Matrix:
- Sample is slightly shaly overall.

Authigenic phases:
- Common quartz overgrowths and authigenic clays (e.g. chlorite and kaolinite);
- Sparse pore filling to grain replacive siderite (Si, Image D, XPL) and ferroan dolomite;
- Minor hematite.

Pore system: Porosity is good. Pores are primary and secondary, the latter resulting from the dissolution of unstable lithics and feldspars. Pore effectiveness is downgraded by quartz overgrowths and authigenic clays. Micropores between clay platelets are optically irresolvable.

Reservoir quality: Good.

LEGACY CORE ANALYSIS DATA
Porosity: 22.4% at 3284.3m
Permeability: 30mD at 3284.3m

Point Count Porosity: 15%

Well: A-K1
Depth: 3285.9m

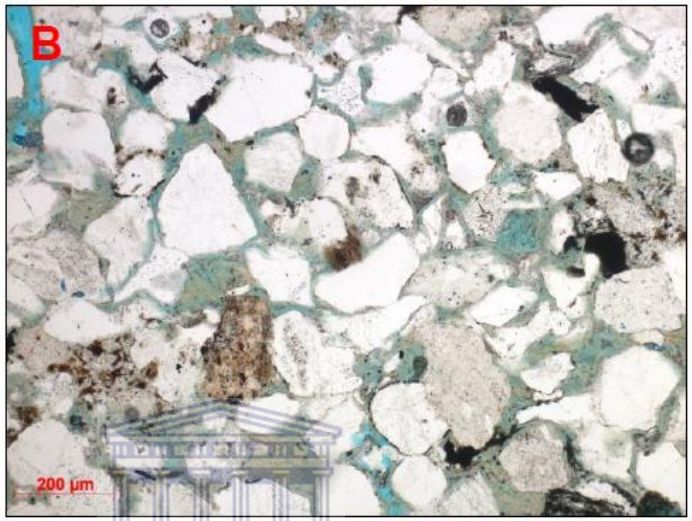

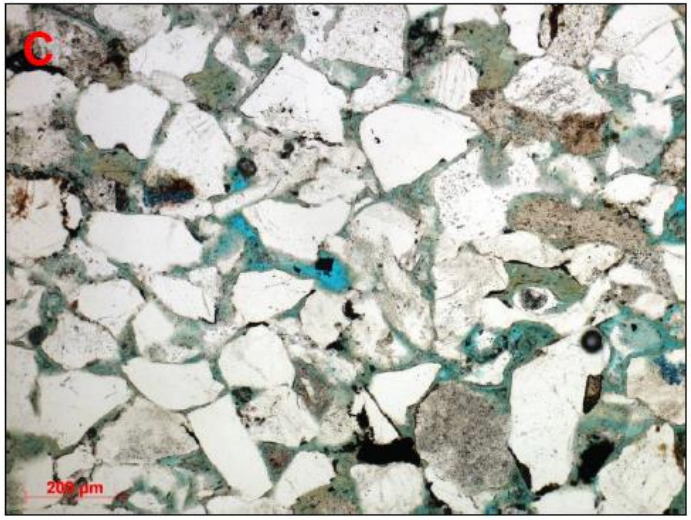

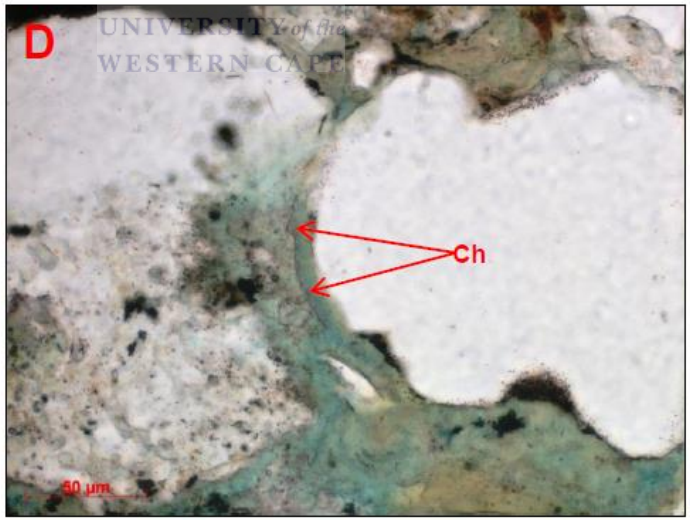

Lithology: Argillaceous sandstone

Classification: Sublithic arenite*

Texture:
Grain size: Fine (upper).
Sorting: Well sorted.
Grain contacts: Point to point to long.
Grain shape: Subangular to well rounded.
Compaction: Moderate overall.

Detrital components:
- Predominant monocrystalline quartz;
- Common lithics (chert, igneous and metamorphic grains), plagioclase and polycrystalline quartz;
- Sparse organic matter, mica flakes, heavy minerals (zircon) and ?glauconite.

Matrix:
- Sample is shaly.

Authigenic phases:
- Abundant authigenic clays are composed of grain rimming to pore filling chlorite (e.g. Ch, Image D) and also ?smectite;
- Pore restricting quartz overgrowths;
- Minor dolomite and pyrite.

Pore system: Macroporosity is relatively poor (~5% visually). Micropores between clay platelets are inferred to be abundant, but they are optically irresolvable.

Reservoir quality: Poor to moderate.

LEGACY CORE ANALYSIS DATA
Porosity: 18.4% at 3286.04m
Permeability: 6.6mD at 3286.04m

Point Count Porosity: n/a

**Rock classification is based on visual estimation of mineralogical components.*

Well: A-K1
Depth: 3285.9m

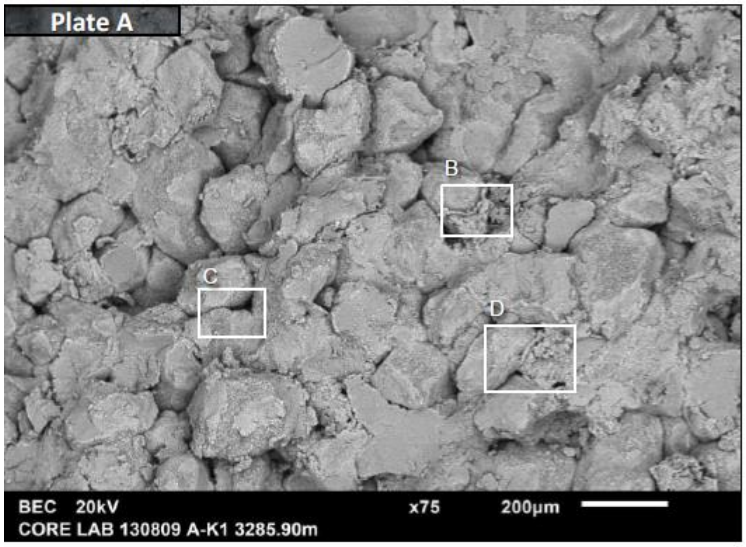

A moderately well sorted very fine to fine grained sandstone that appears mainly massive at the scale of SEM, with some alignment of elongate grains (A). The sample is well compacted and long grain contacts are common (C, D).

Detrital grains are dominated by quartz. Common feldspar grains (plagioclase and minor K-feldspar) are locally leached or albitised (B). Lithic grains include clay-rich, quartz-mica and Ti-rich varieties. Scattered Ti-minerals are typically corroded (B). Traces of apatite are also present.

The authigenic mineralogy is dominated by abundant grain-coating chlorite, which forms isopachous platy rims on grains (B, C, D). The development of overgrowths has been inhibited by the chloritic clays. Rare small isolated quartz and albite overgrowths were observed (C). Authigenic albite more commonly forms fine blocky developments associated with leached feldspar grains / dissolution pores (B). Traces of ferroan dolomite were observed within dissolution pores (B, possibly ?pre-dating authigenic albite).

Porosity appears to be moderately good, comprising a mix of intergranular pores, dissolution pores and microporosity associated with chloritic clays and leached framework grains. Abundant grain-coating chlorite means pore walls typically have very high surface areas, and pore throats are constricted / made tortuous. Overall pore connectivity and permeability are expected to be moderate.

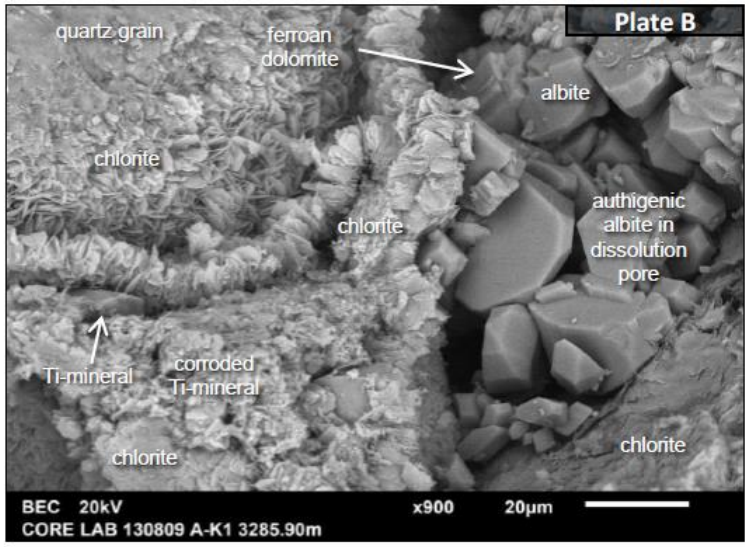

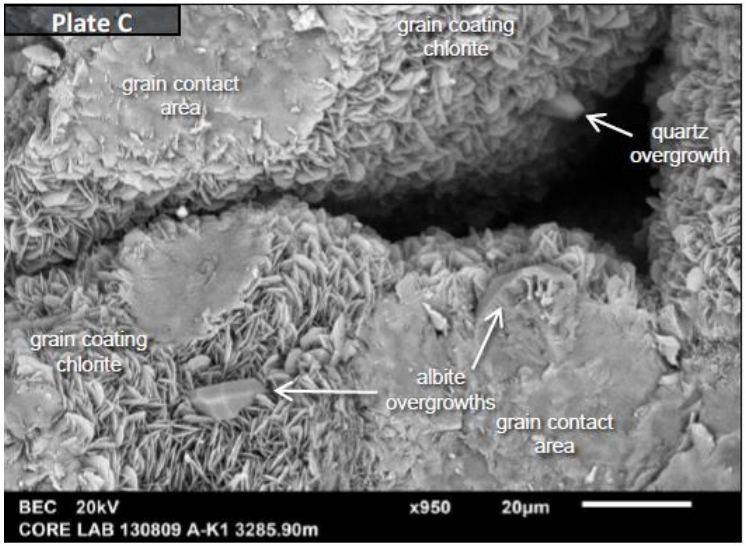

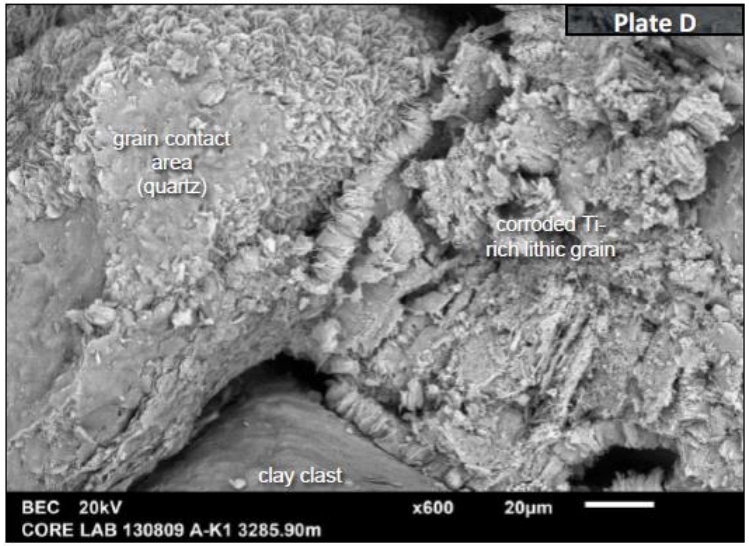

Well: A-K1
Depth: 3287.33m

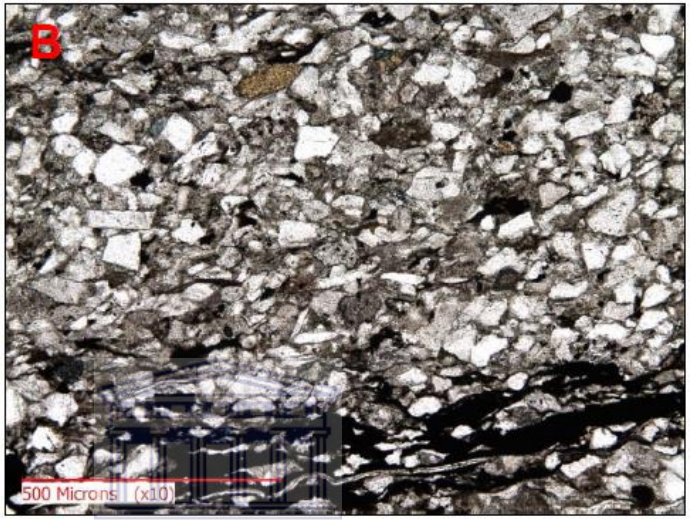

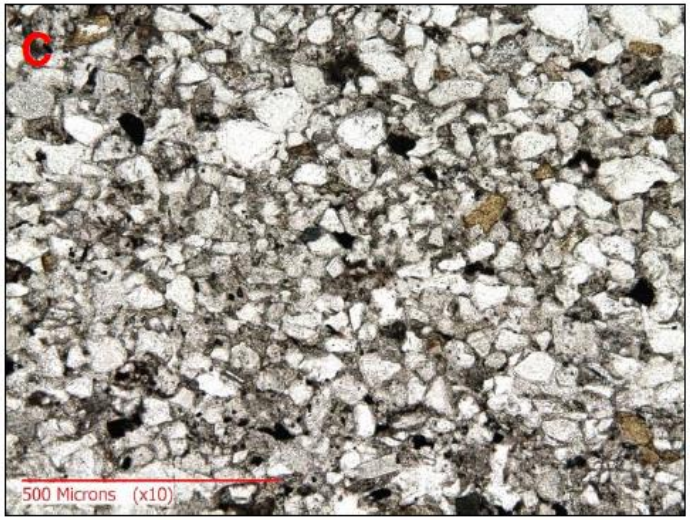

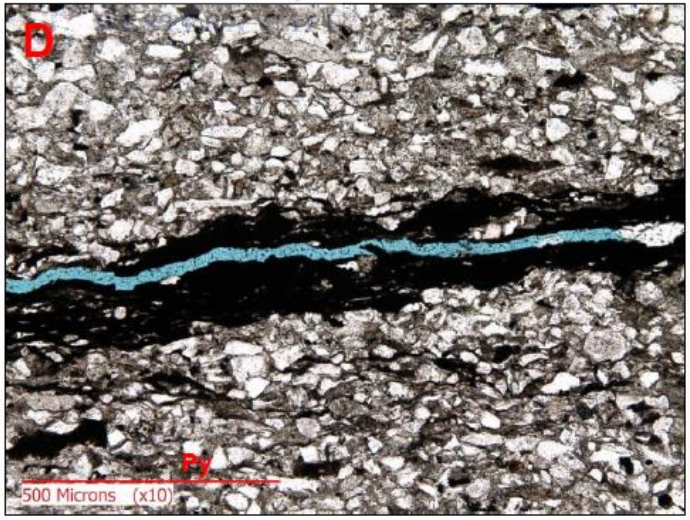

Lithology: Sandy siltstone

Classification: Argillaceous feldspathic siltstone*

Texture:
Sample is composed of silt-grade to fine grained siliciclastic detritus associated with organic matter and detrital clays. Grains are angular to rounded.

Detrital components:
- Abundant monocrystalline quartz;
- Common feldspars, lithics (e.g. mudclasts), micas flakes, detrital chlorite and organic matter/carbonaceous material.
- Heavy minerals (e.g. zircon) and dolomitised ?forams are locally noted.

Matrix:
- Abundant clays also associated with organic matter.

Authigenic phases:
- Common illite/sericite, pyrite, ?chlorite, ferroan dolomite and siderite (also locally spherosiderite).

Pore system: Porosity is not noted; artificial fractures are present.

Reservoir quality: Negligible

LEGACY CORE ANALYSIS DATA
Porosity: 18.9% at 3287.26m
Permeability: 13mD at 3287.26m

Point Count Porosity: n/a

**Rock classification is based on visual estimation of mineralogical components.*

APPENDIX III – CORE SAMPLES AND WELL LOG INTEGRATION

Well: A-J1 Integration of core data with well log

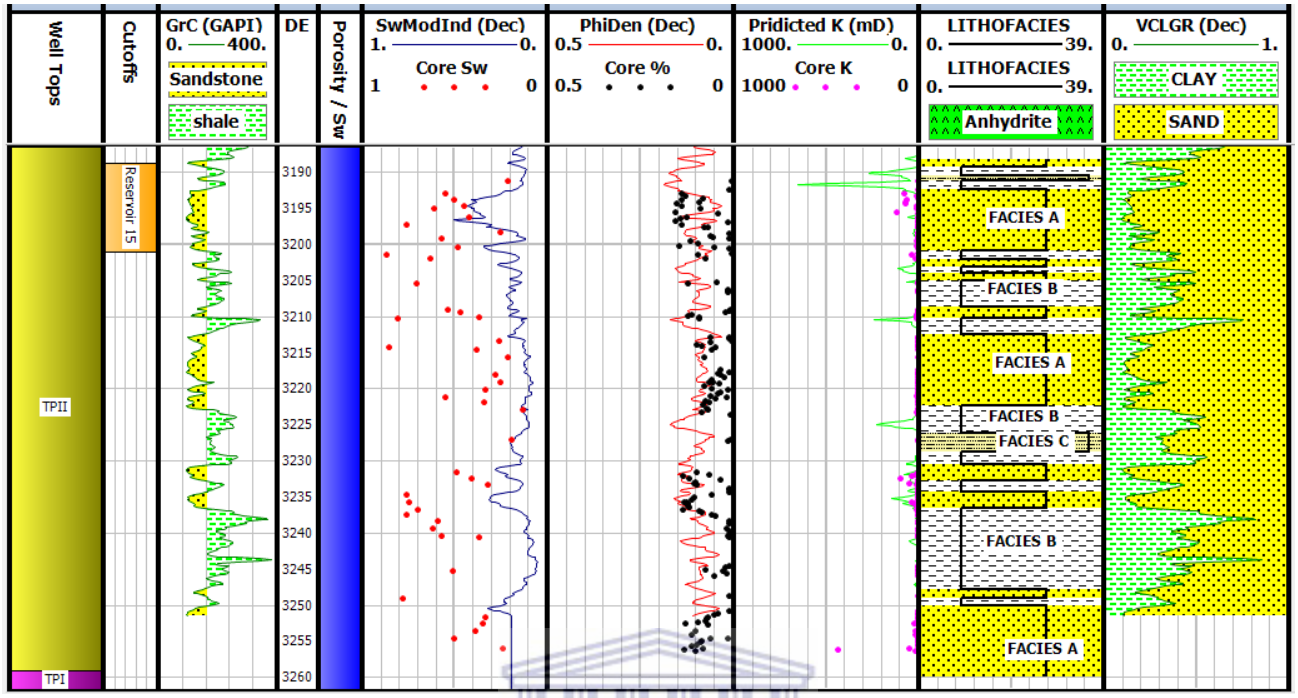

Well: A-D1 Integration of core data with well log

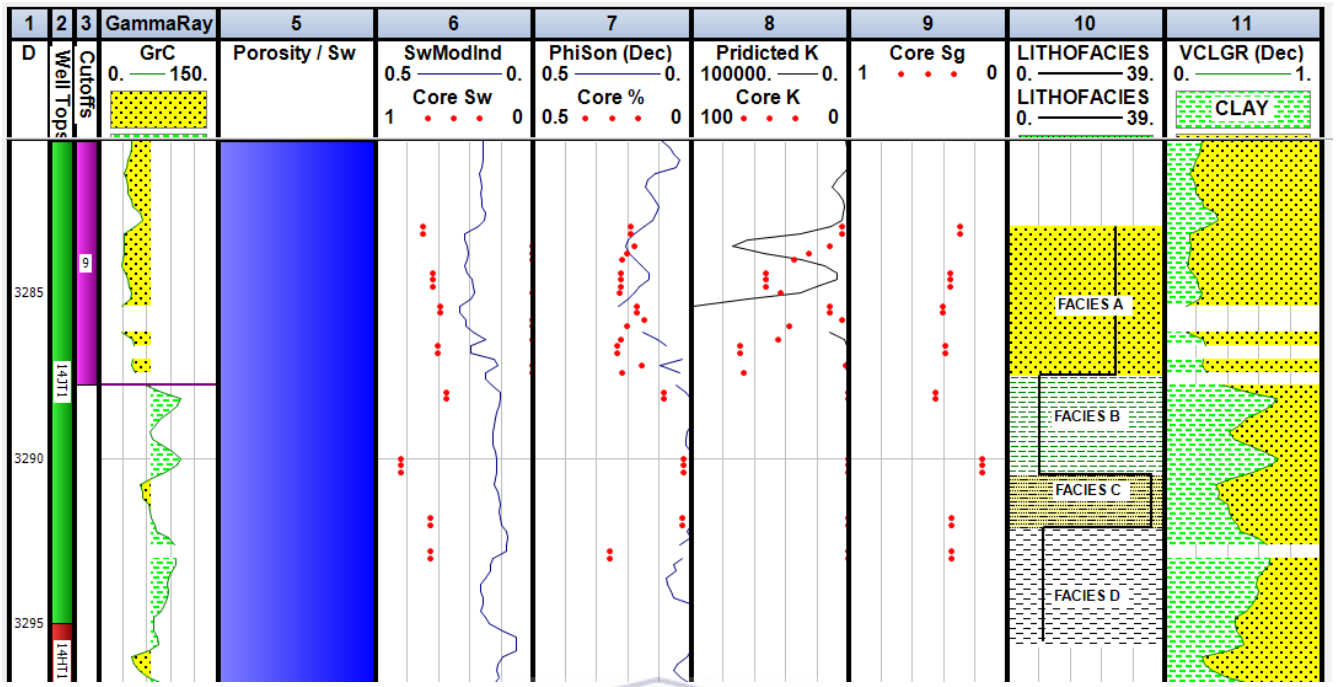

Well: A-H1 Integration of core data with well log

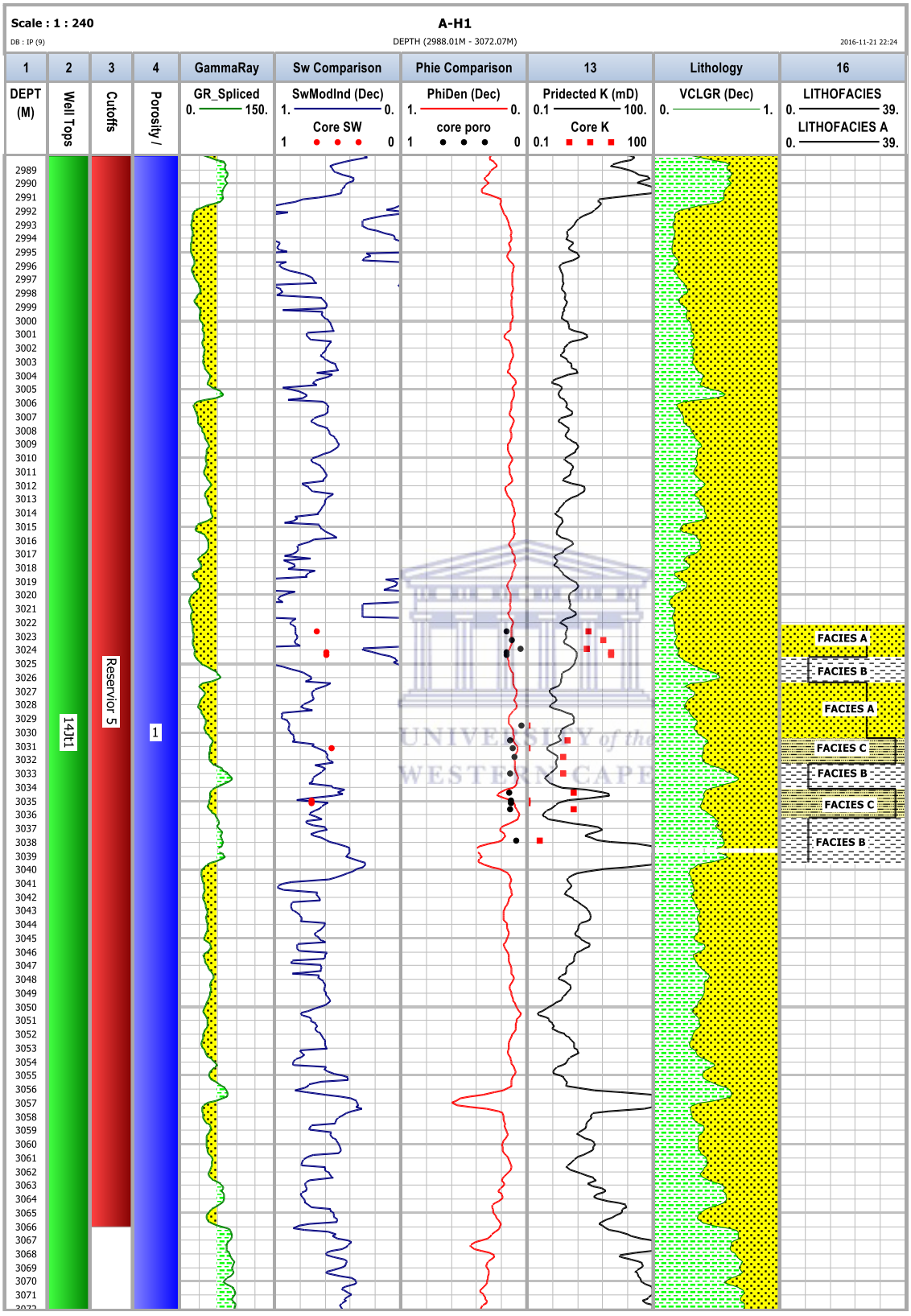

Well: A-K1 Integration of core data with well log

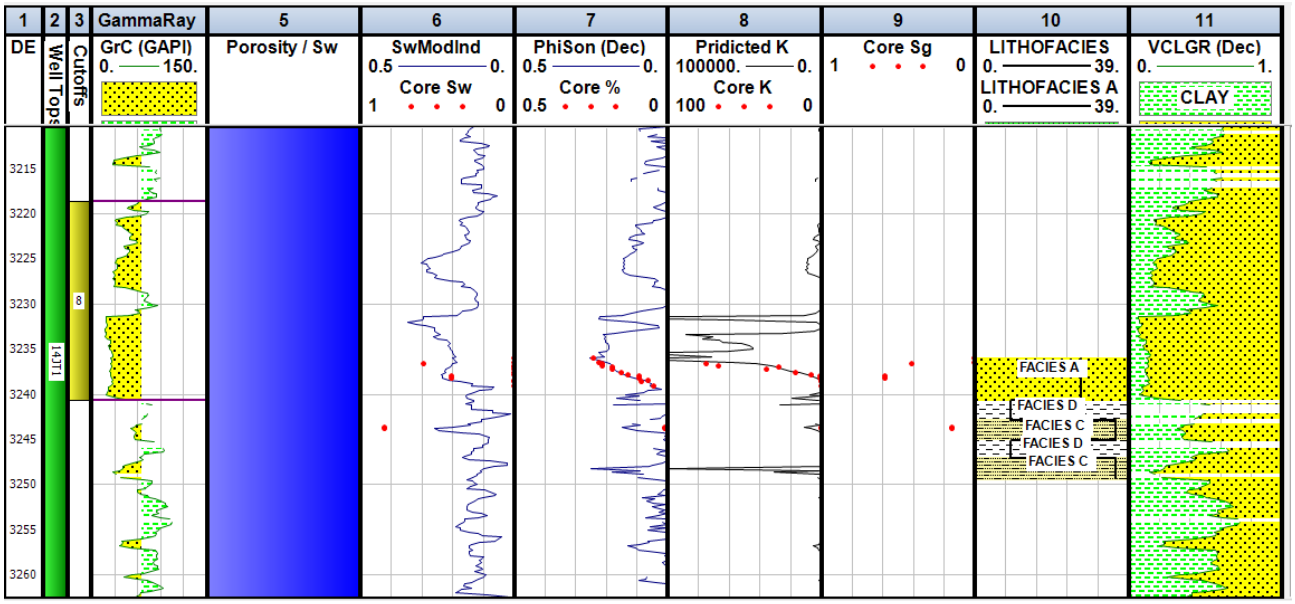

Well: K-A2 Integration of core data with well log

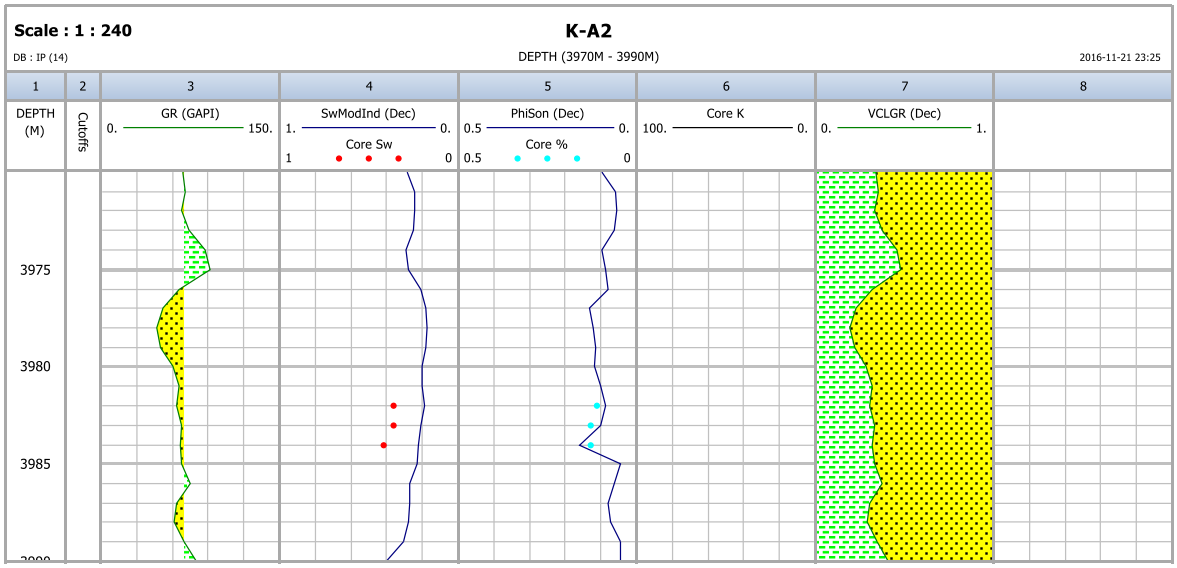

APPENDIX IV – WIRELINE LOG INTERPRETATION

Well: A-J1 – wireline log interpretation

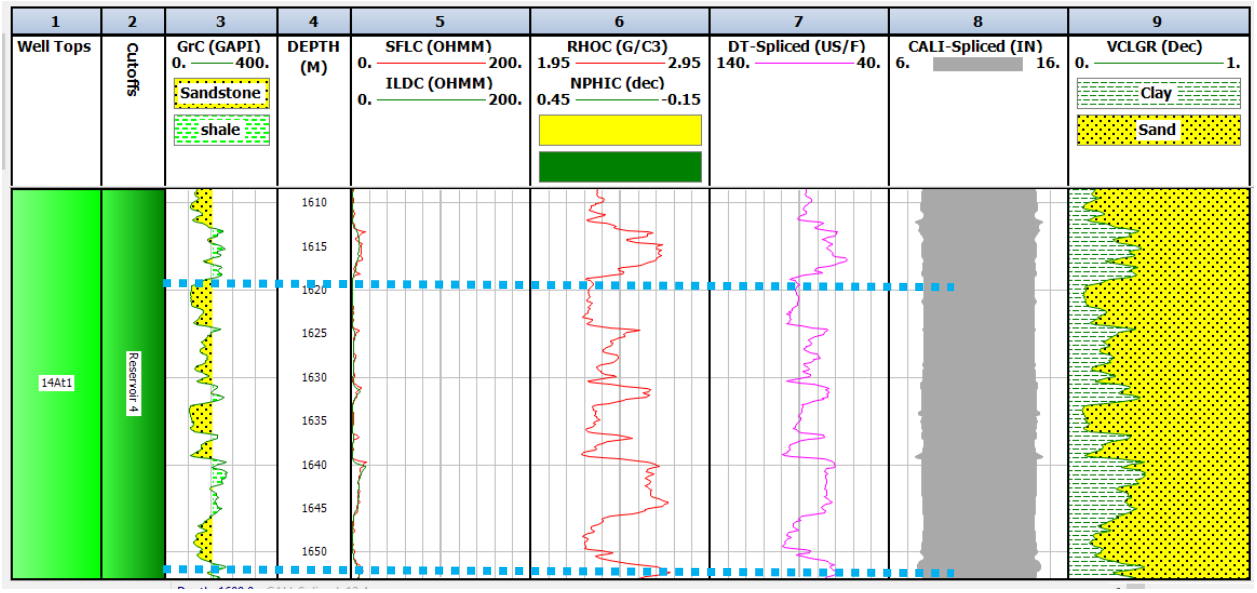

Figure 1: A-J1 selected reservoir interval between 1618 – 1651 m in the post-rift (Albian age) sequence.

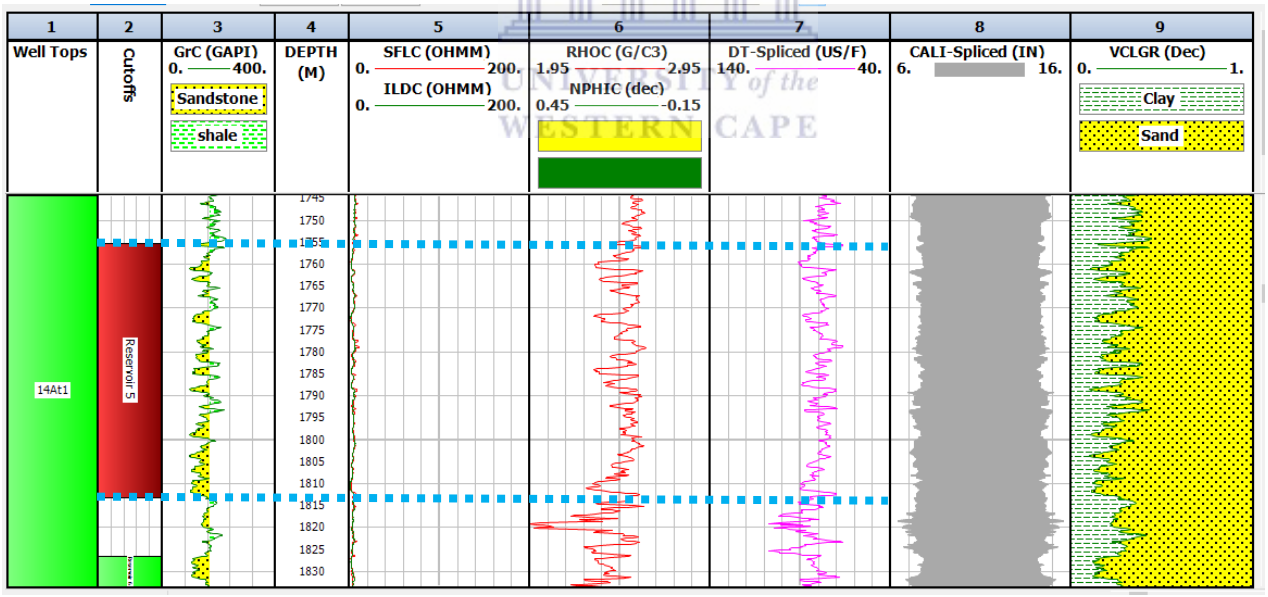

Figure 2: A-J1 selected reservoir interval between 1755 – 1810 m in the post-rift (Albian age) Sequence.

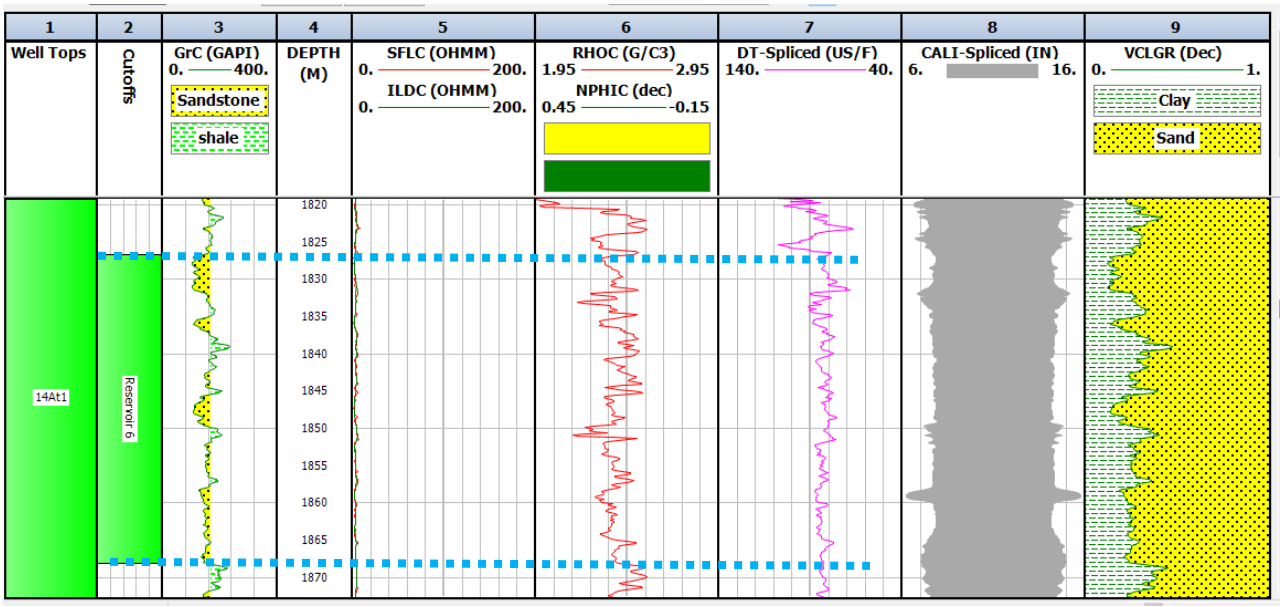

Figure 3: A-J1 selected reservoir interval between 2047 – 2078 m in the post-rift (Albian age) Sequence.

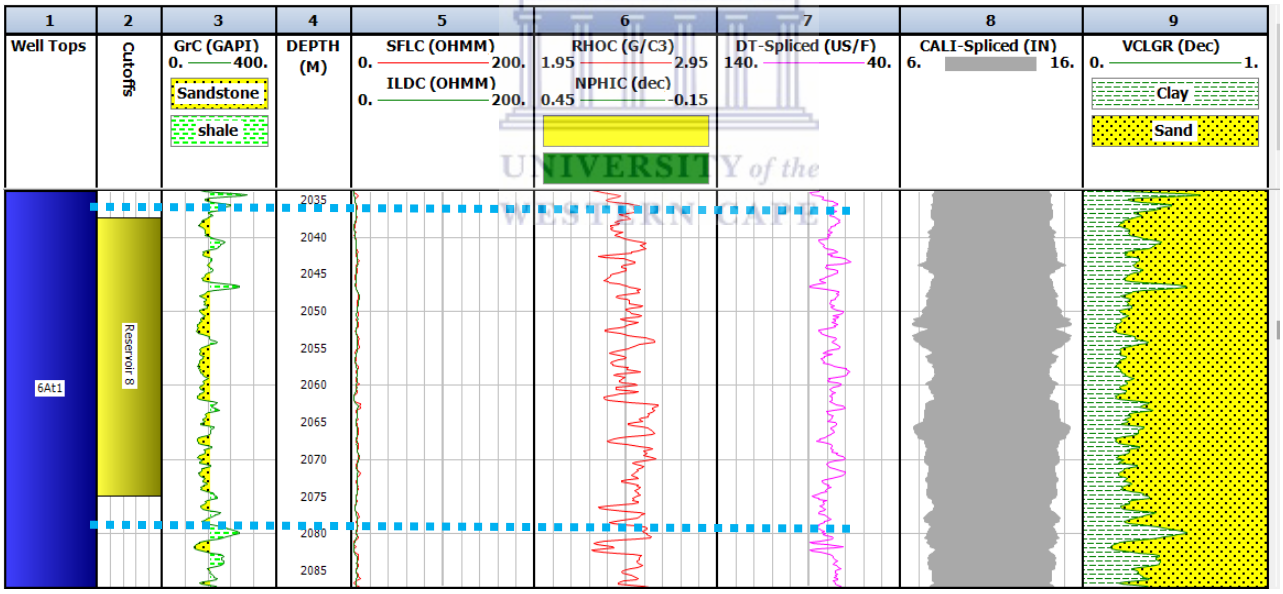

Figure 4: A-J1 selected reservoir interval between 2047 – 2078m in the syn-rift (Hauterevian age) Sequence.

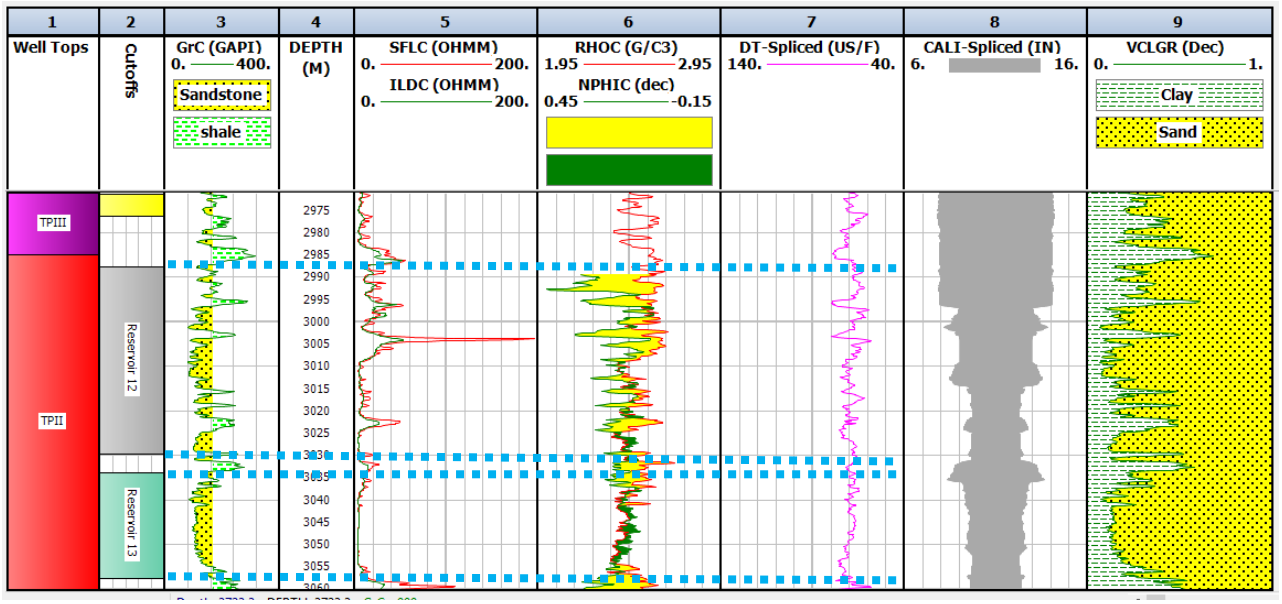

Figure 5: A-J1 selected reservoir intervals between 2987 – 3030 m and 3035 – 3055m in the syn-rift (Hauterevian age) Sequence.

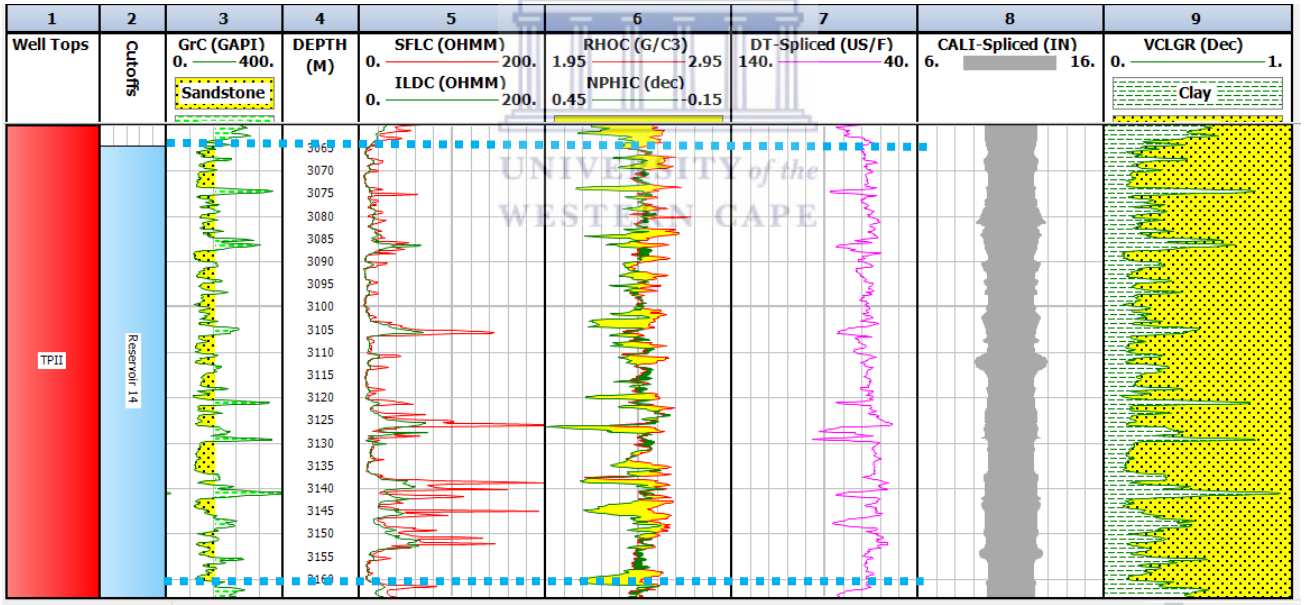

Figure 6: A-J1 selected reservoir interval between 3065 – 3160m in the syn-rift (Hauterevian age) Sequence.

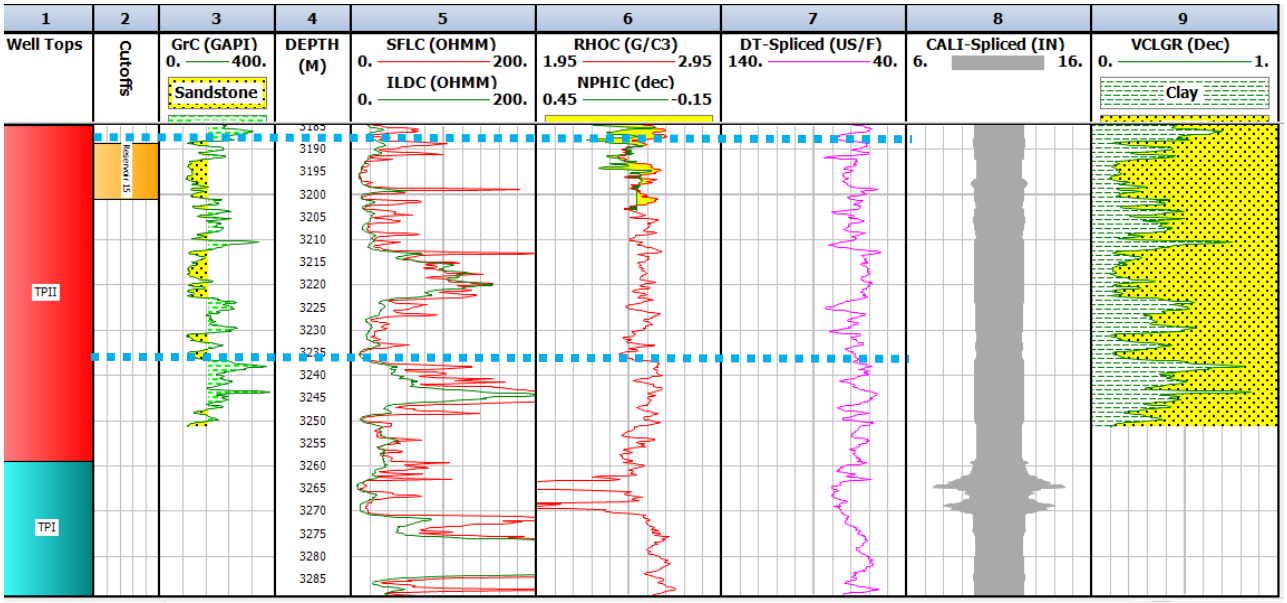

Figure 7: A-J1 selected reservoir interval between 3188 – 3235m in the syn-rift (Hauterevian age) Sequence.

Well: A-D1 – wireline log interpretation

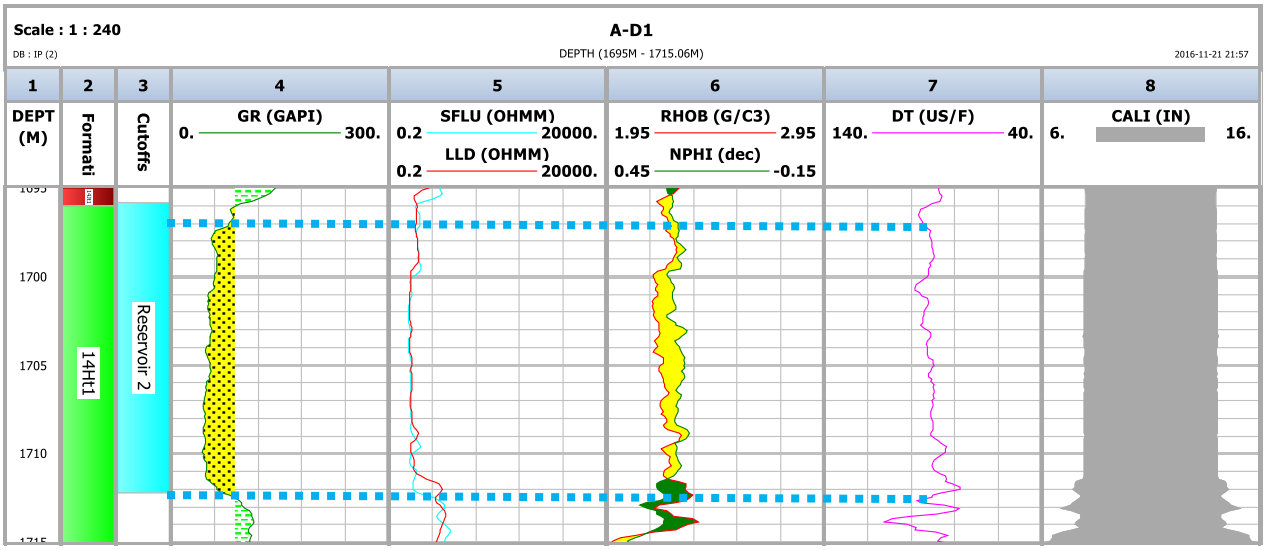

Figure 8: A-D1 selected reservoir interval between 1696 – 1712 m in the post-rift (Albian age) sequence.

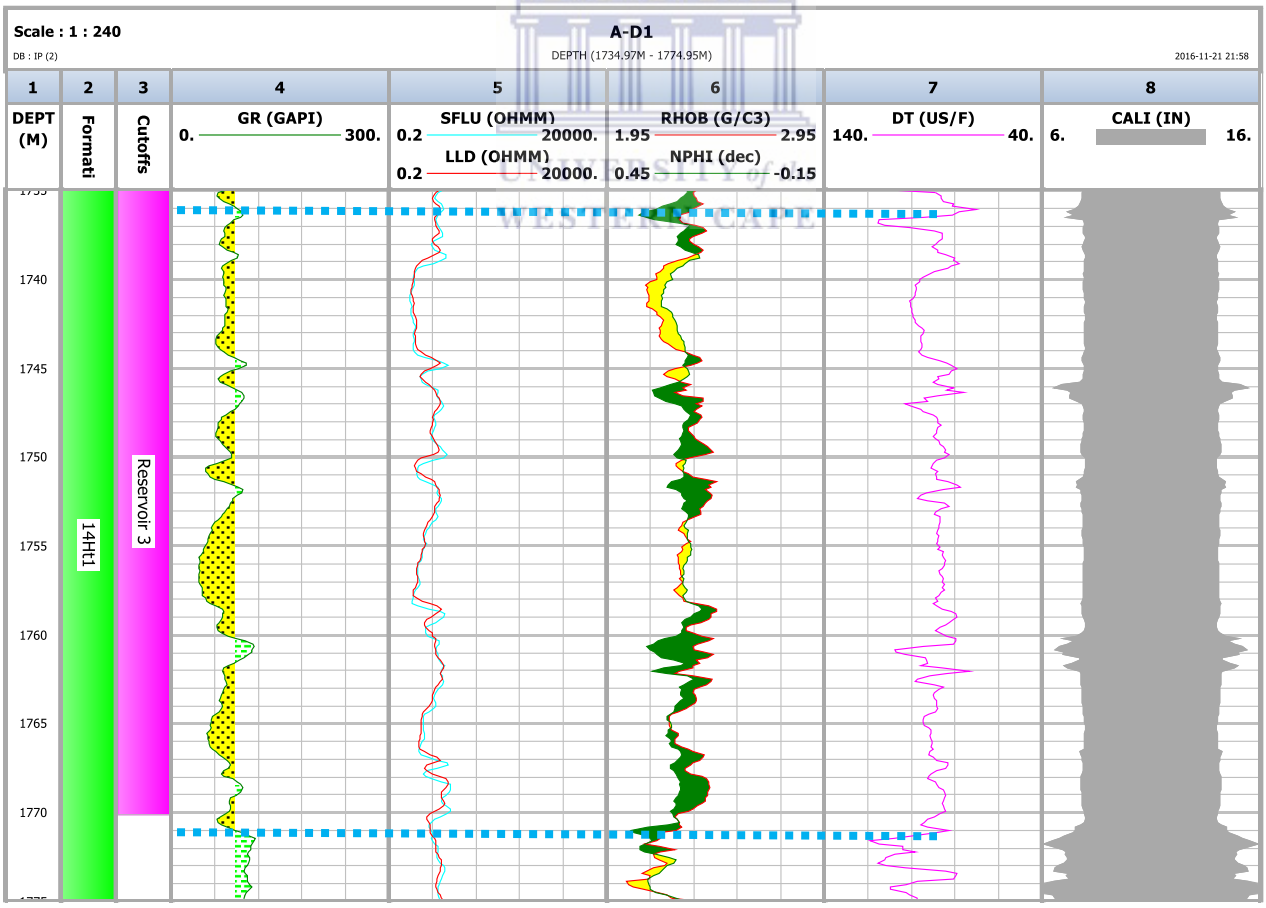

Figure 9: A-D1 selected reservoir interval between 1734 – 1774 m in the post-rift (Albian age) sequence.

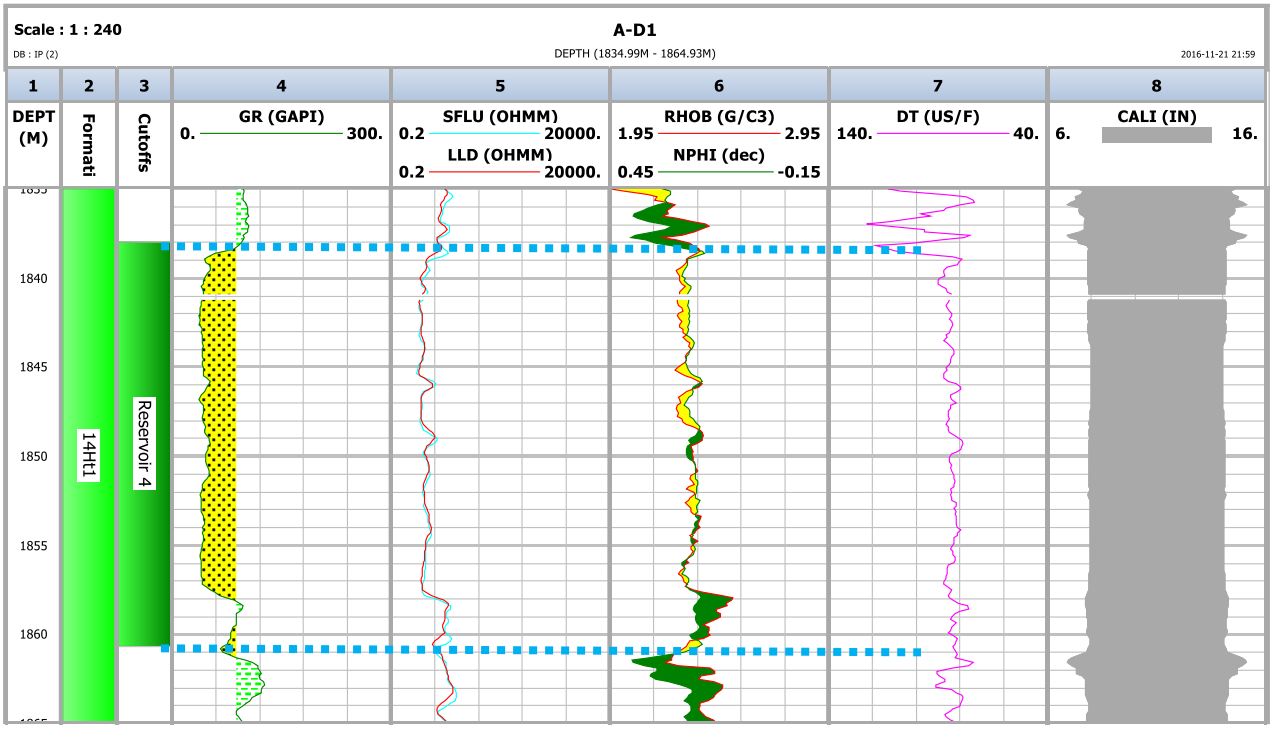

Figure 10: A-D1 selected reservoir interval between 1837 – 1865 m in the post-rift (Albian age) sequence.

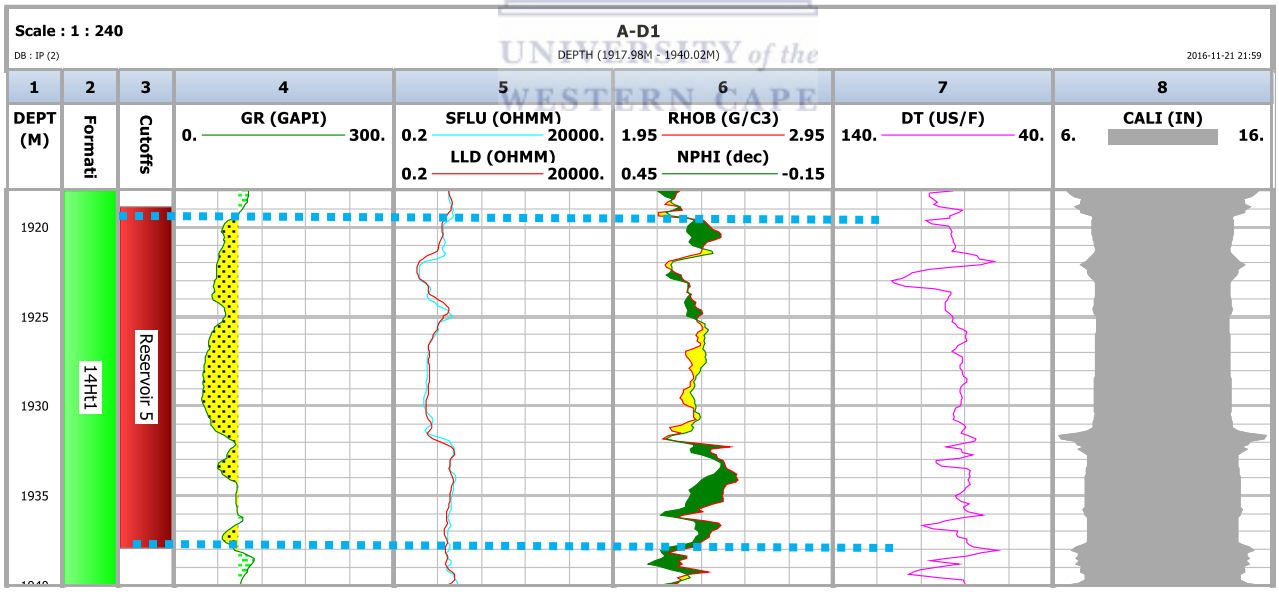

Figure 11: A-D1 selected reservoir interval between 1917 – 1940 m in the post-rift (Albian age) sequence.

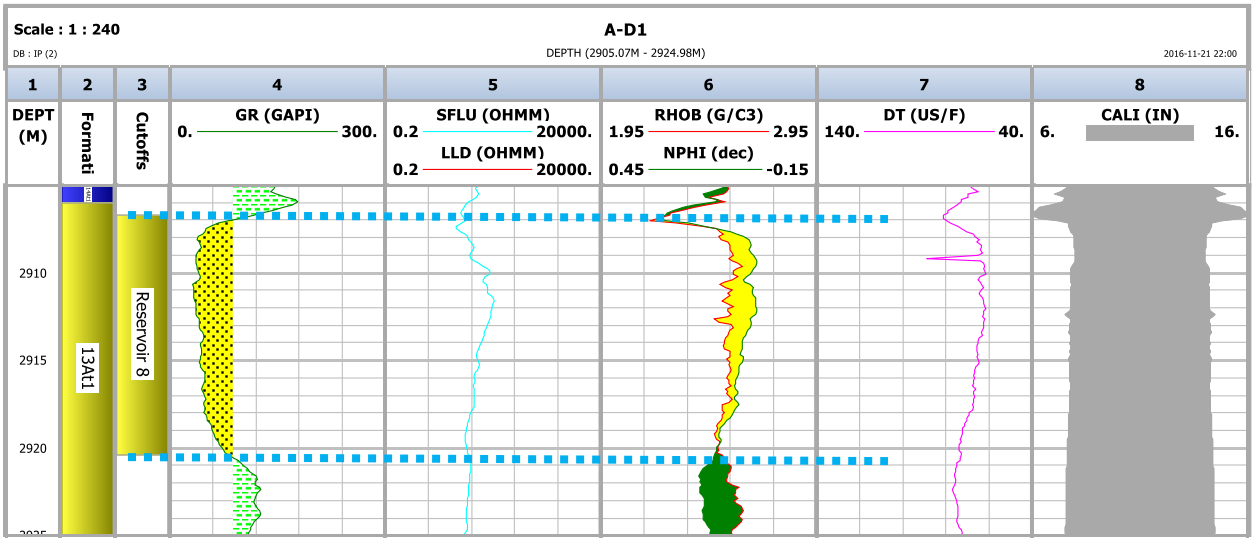

Figure 12: A-D1 selected reservoir interval between 2907 – 2921 m in the post-rift (Aptian age) sequence.

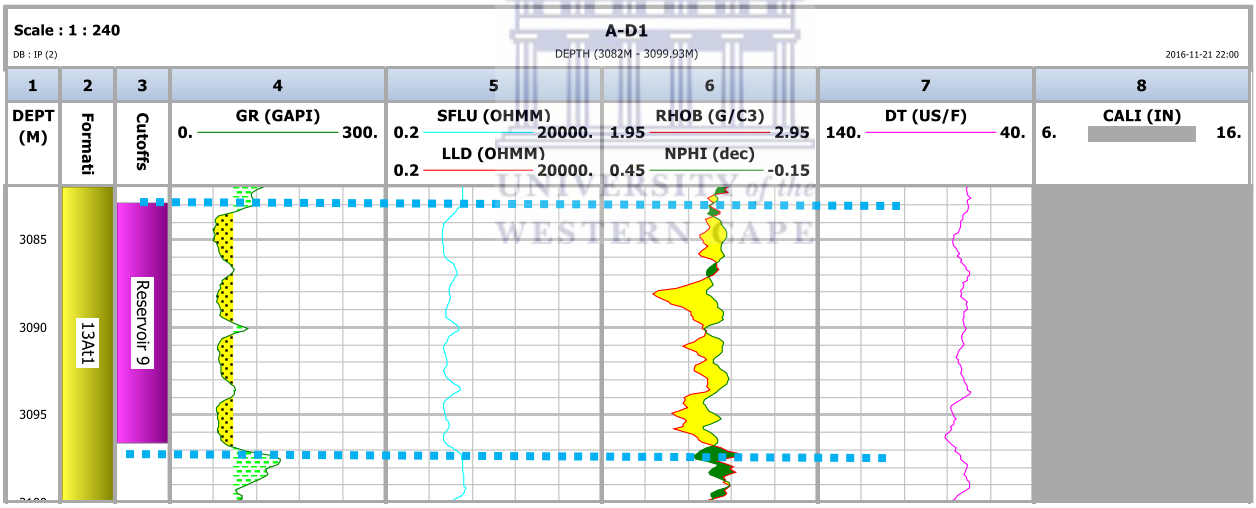

Figure 13: A-D1 selected reservoir interval between 3084 – 3097 m in the post-rift (Aptian age) sequence.

Well: A-H1 – wireline log interpretation

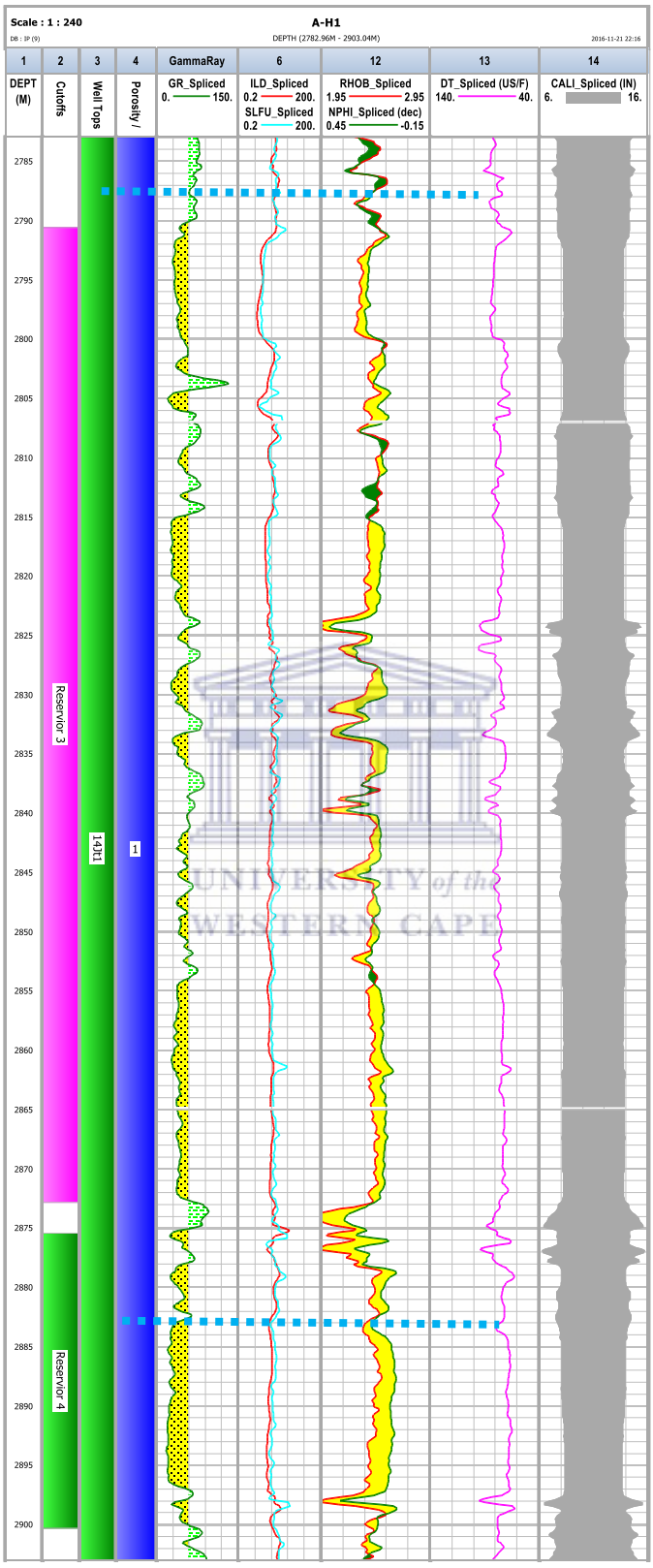

Figure 14: A-H1 selected reservoir interval between 2790 – 2900 m in the post-rift (Albian age) sequence.

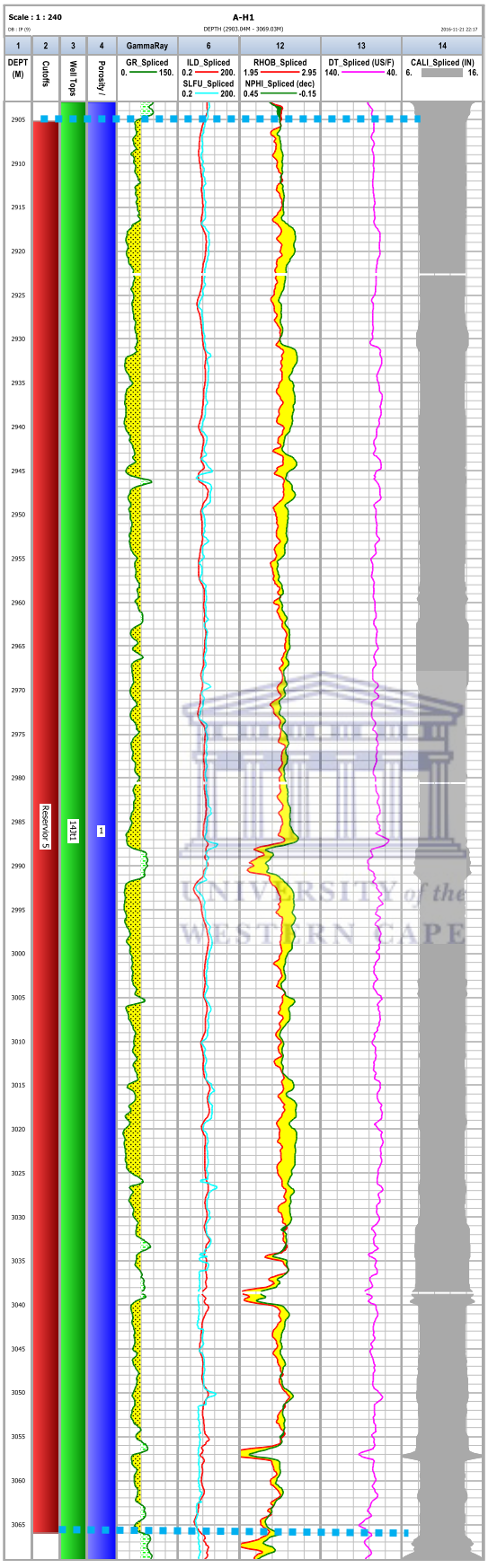

Figure 15: A-H1 selected reservoir interval between 2905 – 3066 m in the post-rift (Albian age) sequence.

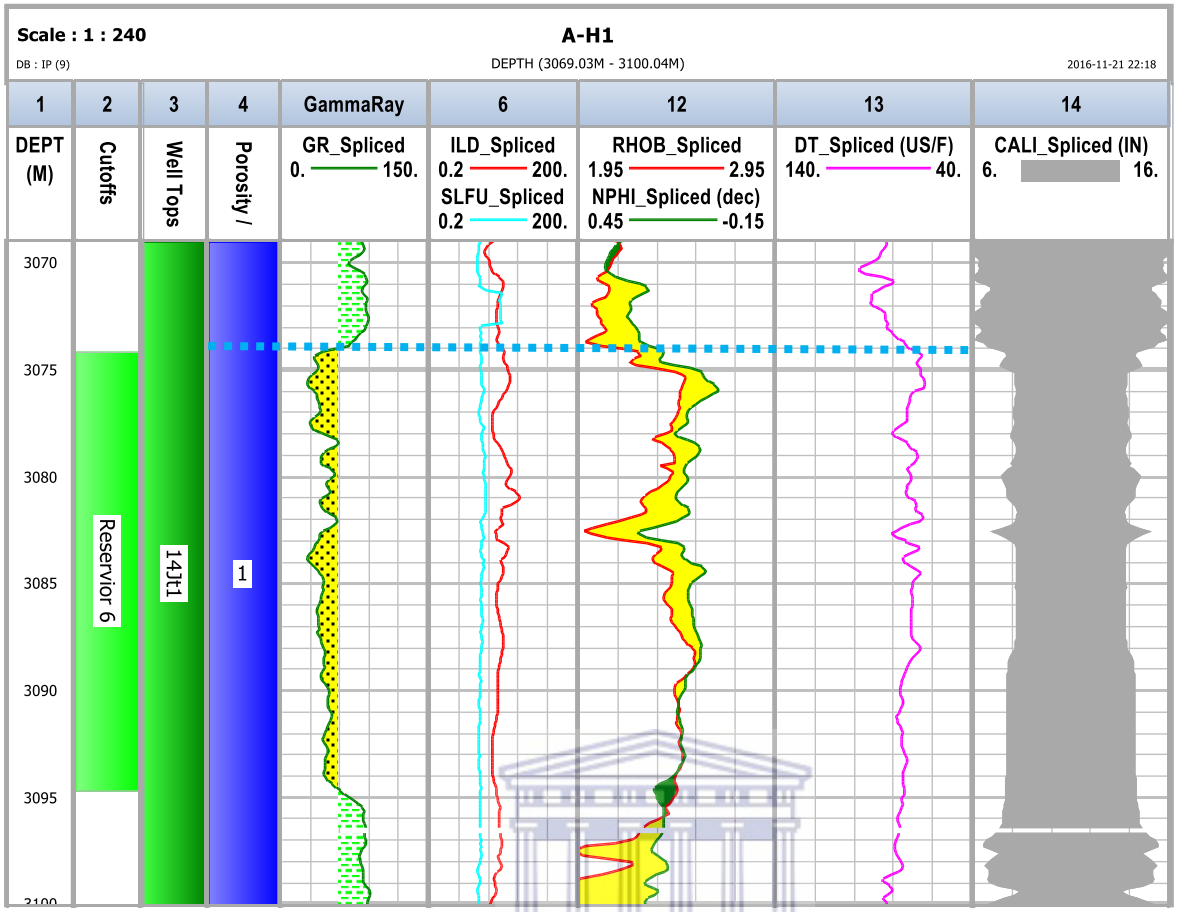

Figure 16: A-H1 selected reservoir interval between 3074 – 3096 m in the post-rift (Albian age) sequence.

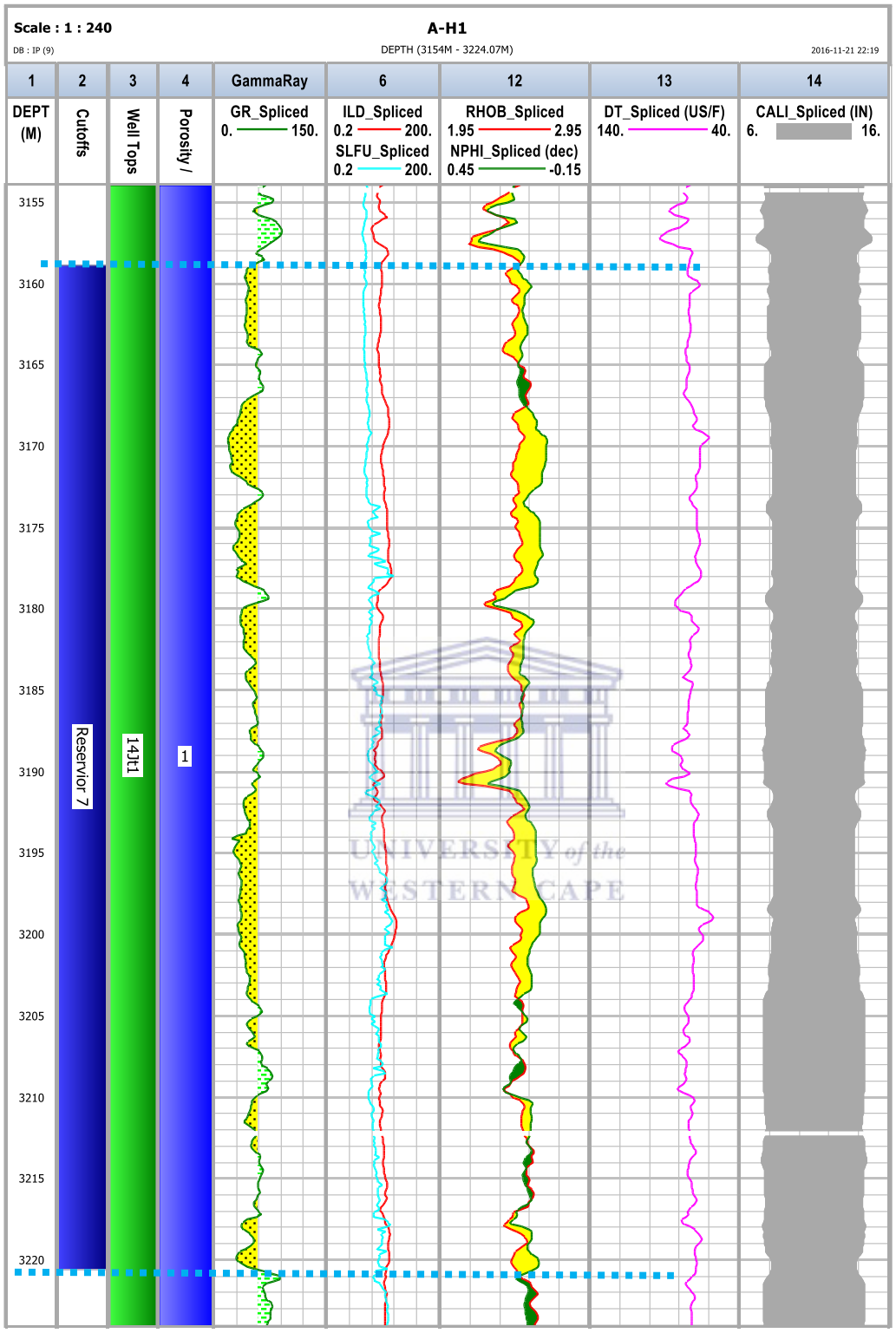

Figure 17: A-H1 selected reservoir interval between 3159 – 3221 m in the post-rift (Albian age) sequence.

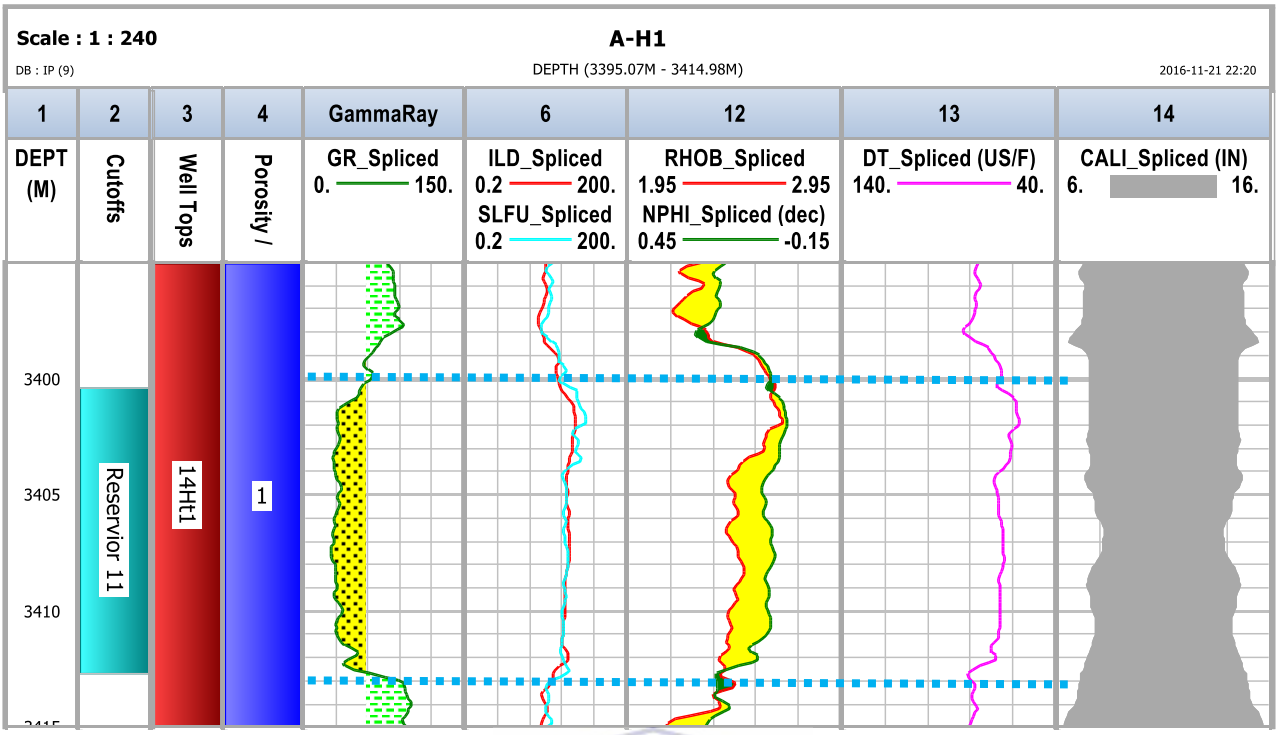

Figure 18: A-H1 selected reservoir interval between 3400 – 3413 m in the post-rift (Albian age) sequence.

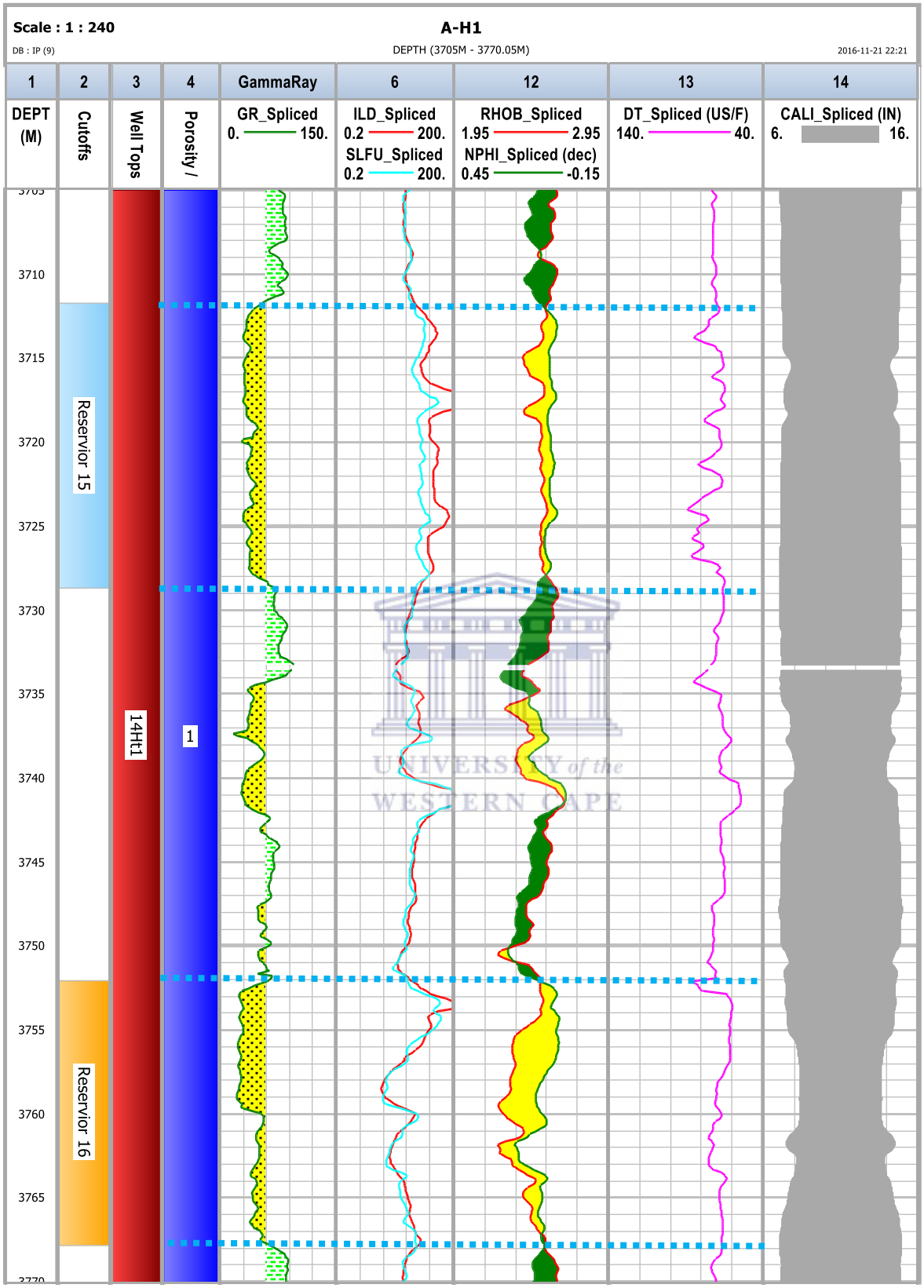

Figure 19: A-H1 selected reservoir interval between 3711 – 3768 m in the post-rift (Albian age) sequence.

Well: A-K1 – wireline log interpretation

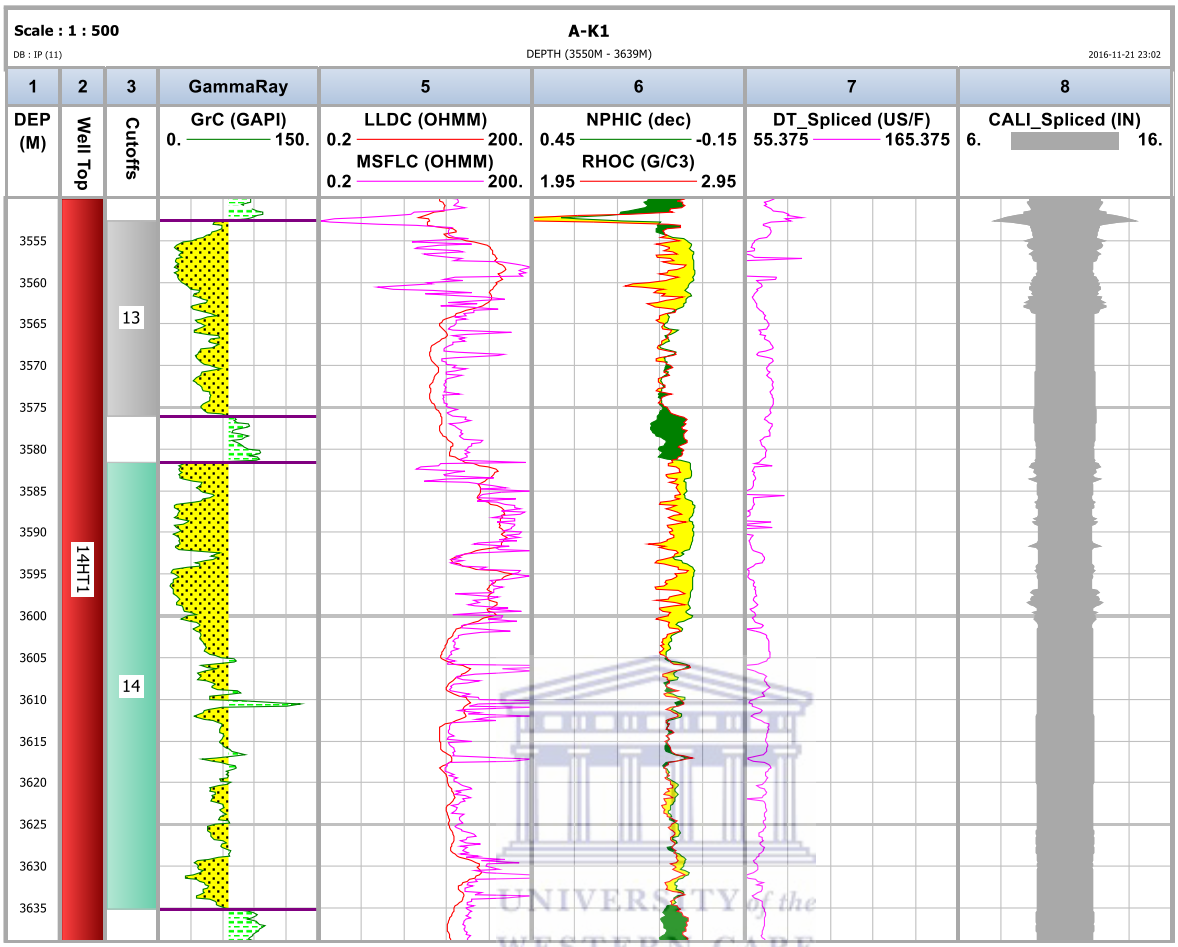

Figure 20: A-K1 selected reservoir interval between 3556 – 3635 m in the post-rift (Albian age) sequence.

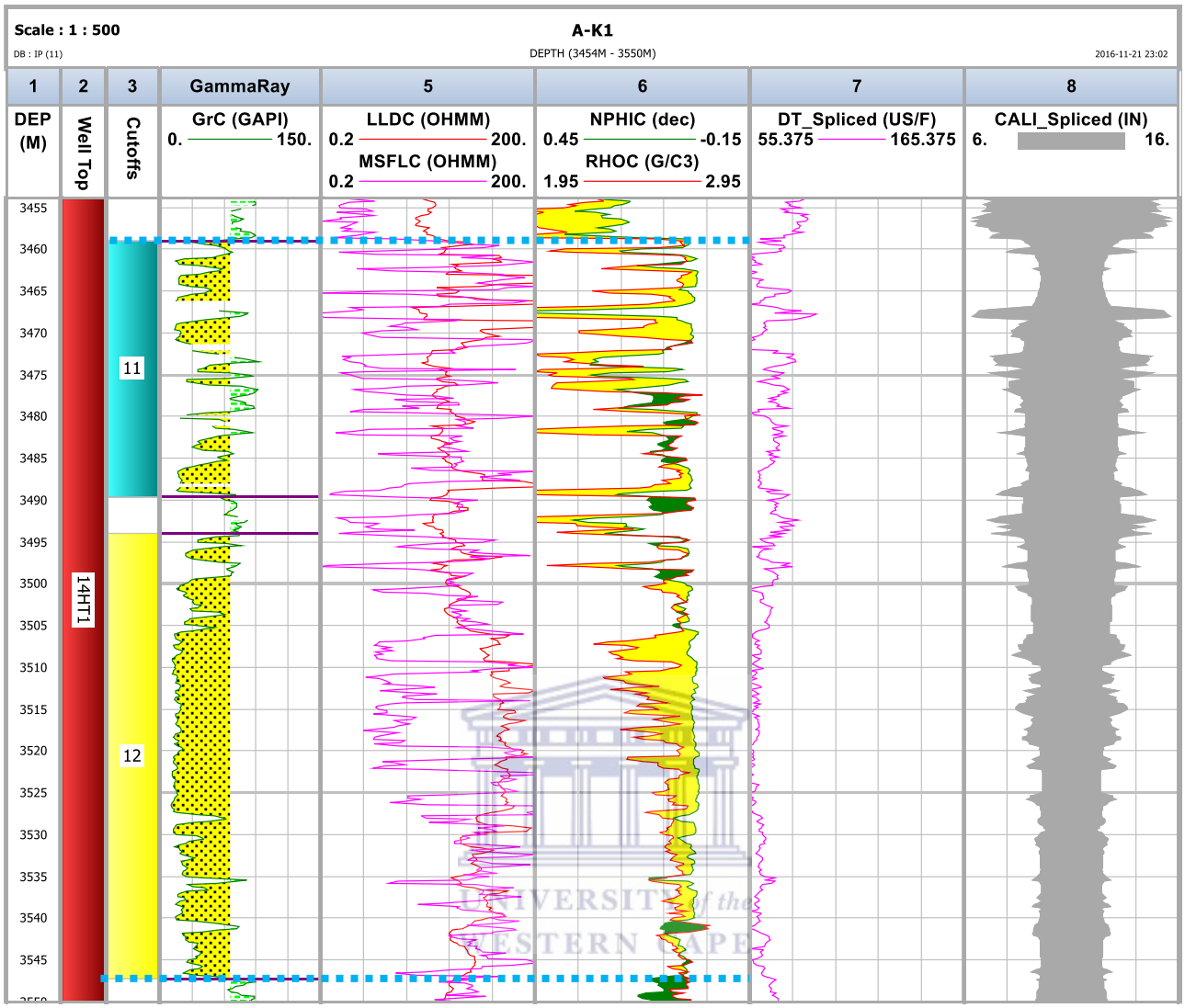

Figure 21: A-K1 selected reservoir interval between 3460 – 3545 m in the post-rift (Albian age) sequence.

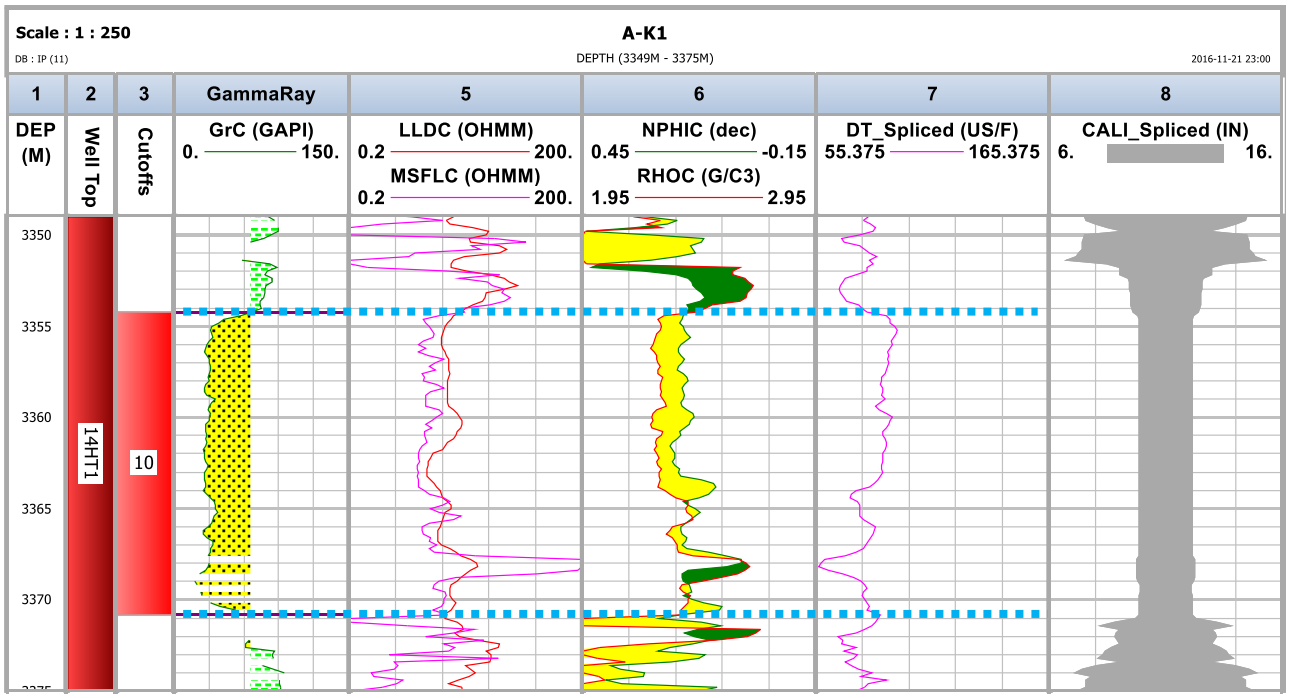

Figure 22: A-K1 selected reservoir interval between 3355 – 3371 m in the post-rift (Albian age) sequence.

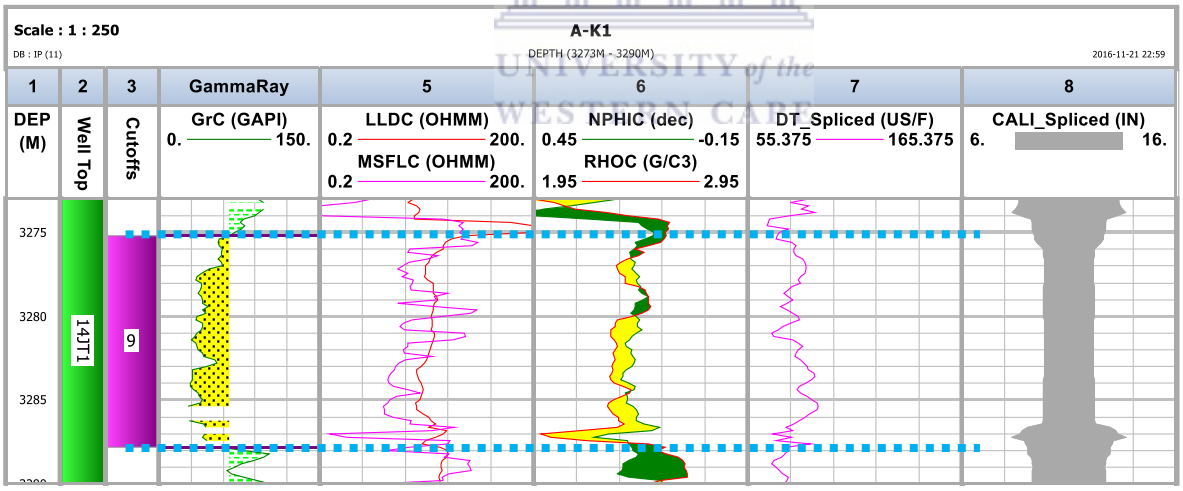

Figure 23: A-K1 selected reservoir interval between 3276 – 3288 m in the post-rift (Albian age) sequence.

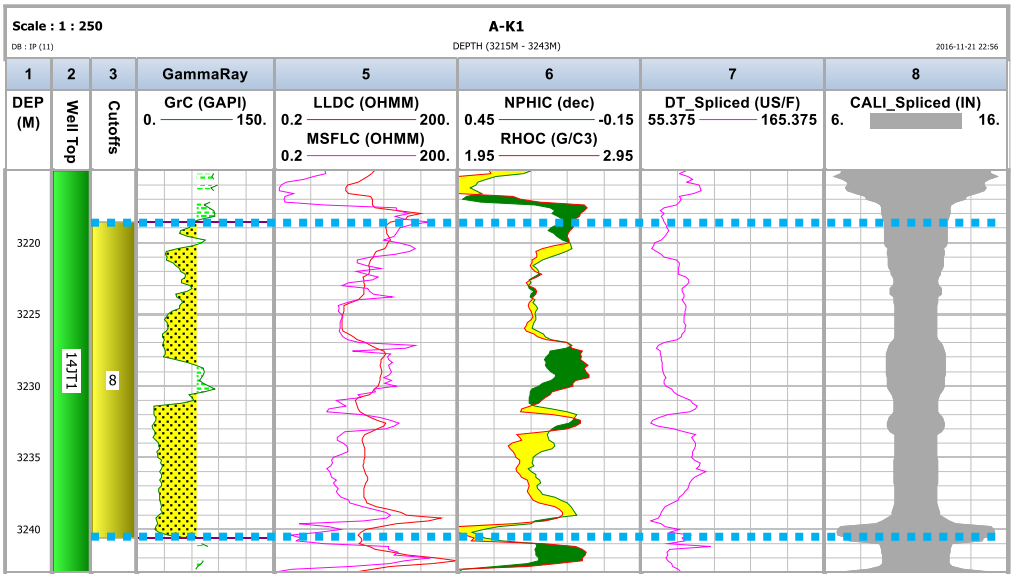

Figure 24: A-K1 selected reservoir interval between 3219 – 3241 m in the post-rift (Albian age) sequence.

Well: K-A2 – wireline log interpretation

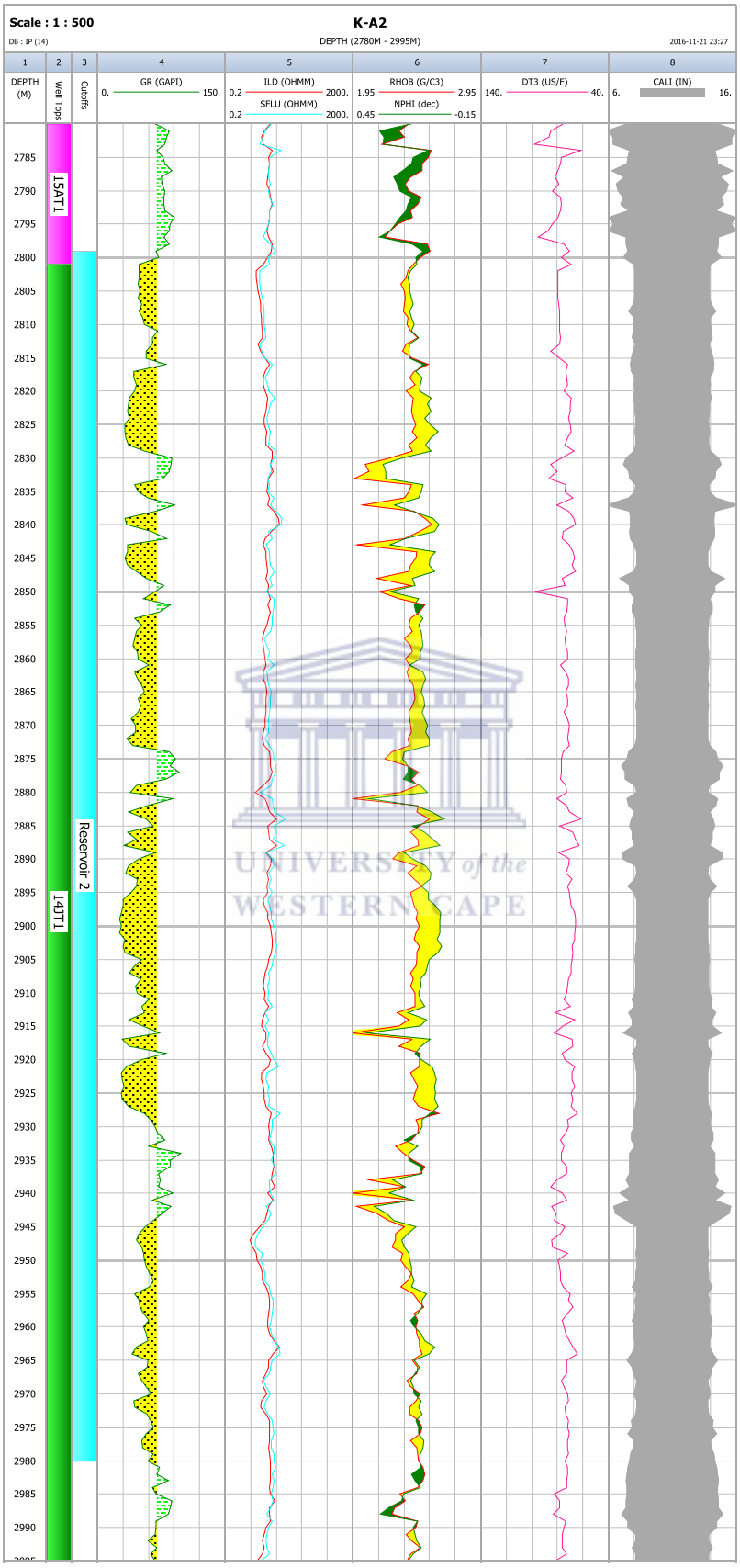

Figure 25: K-A2 selected reservoir interval between 3084 – 3097 m in the post-rift (Albian age) sequence.

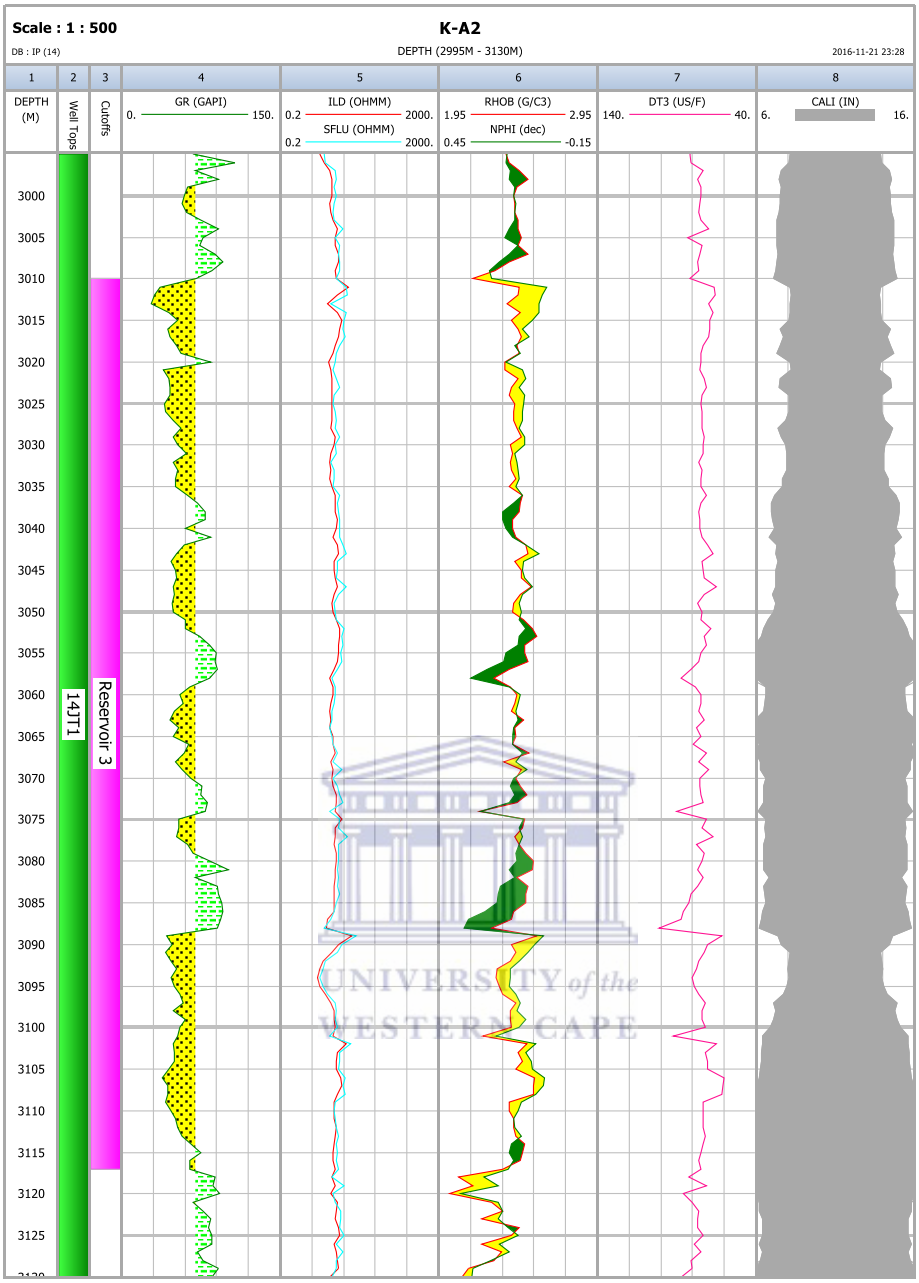

Figure 26: K-A2 selected reservoir interval between 3010 – 3117 m in the post-rift (Albian age) sequence.

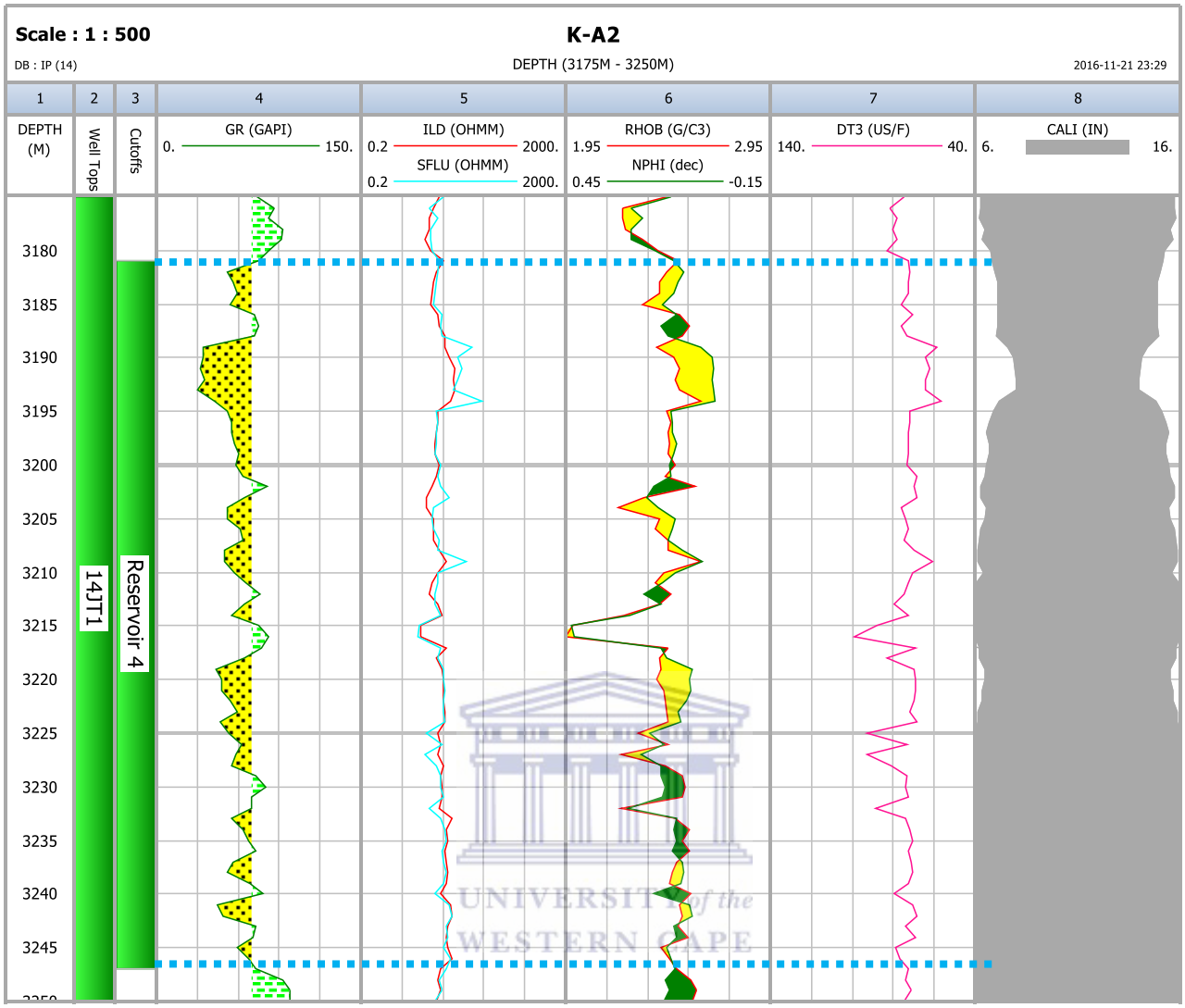

Figure 27: K-A2 selected reservoir interval between 3182 – 3247 m in the post-rift (Albian age) sequence.

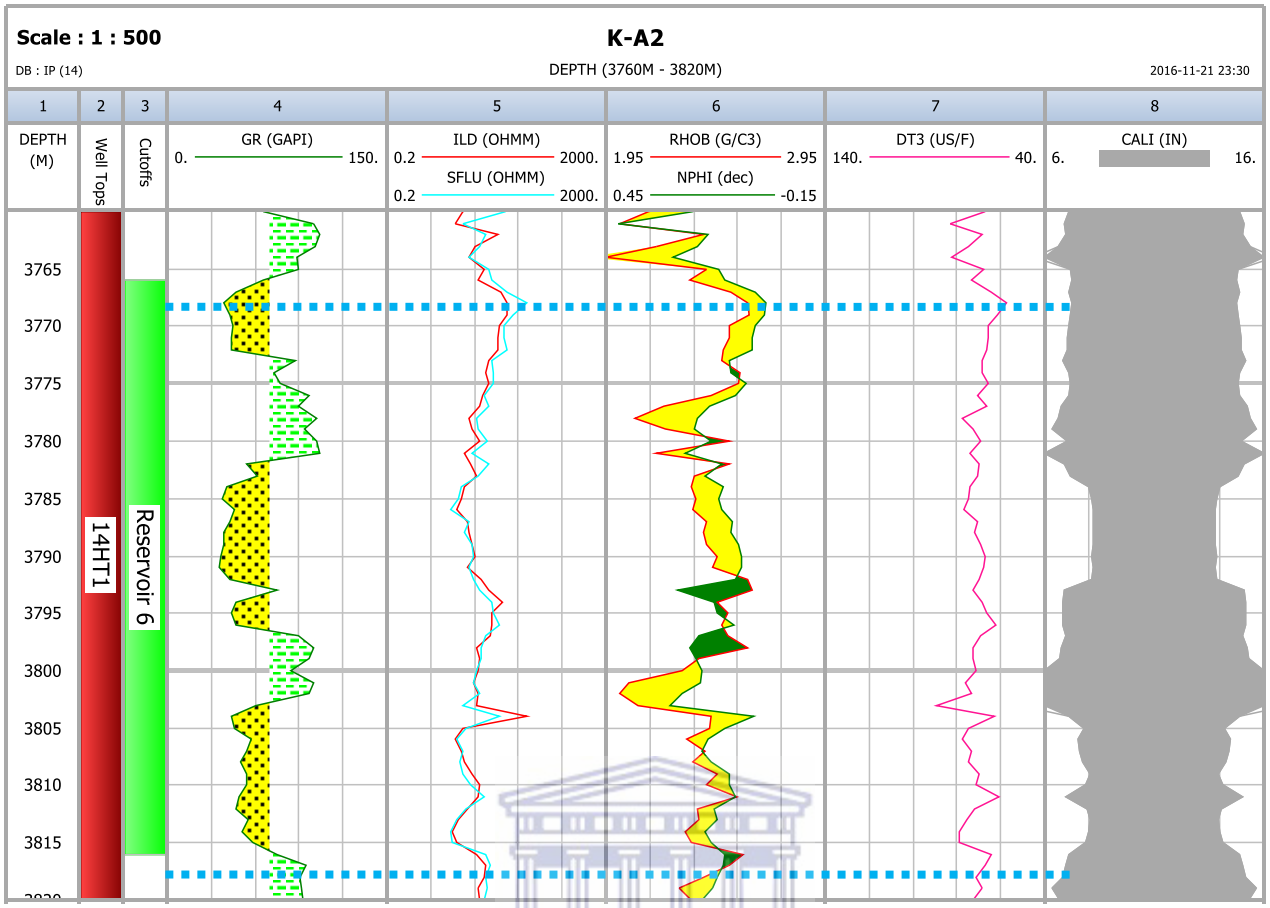

Figure 28: K-A2 selected reservoir interval between 3765 – 3815 m in the post-rift (Albian age) sequence.

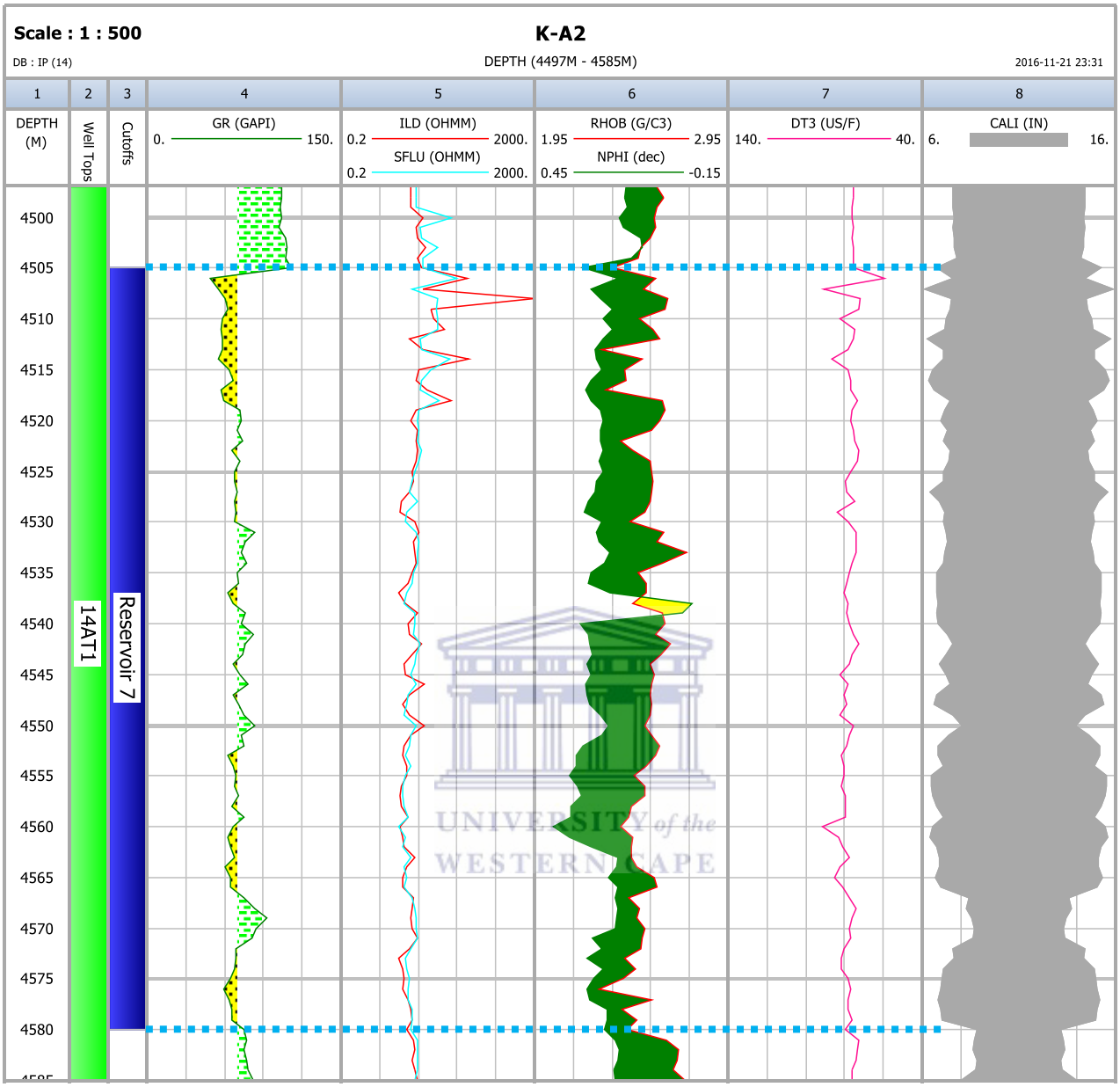

Figure 29: K-A2 selected reservoir interval between 4505 – 4580 m in the post-rift (Albian age) sequence.

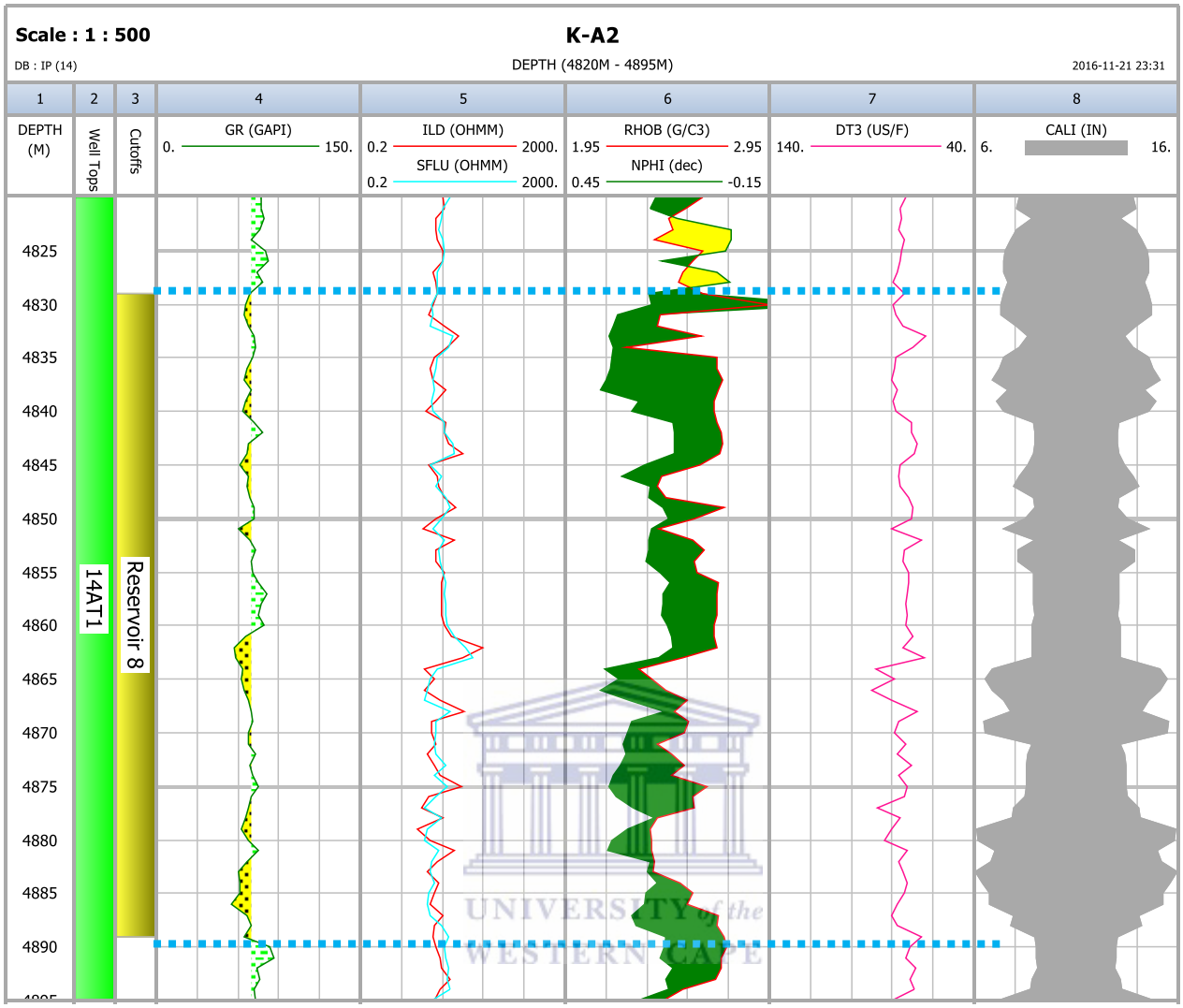

Figure 30: K-A2 selected reservoir interval between 4829 – 4890 m in the post-rift (Albian age) sequence.

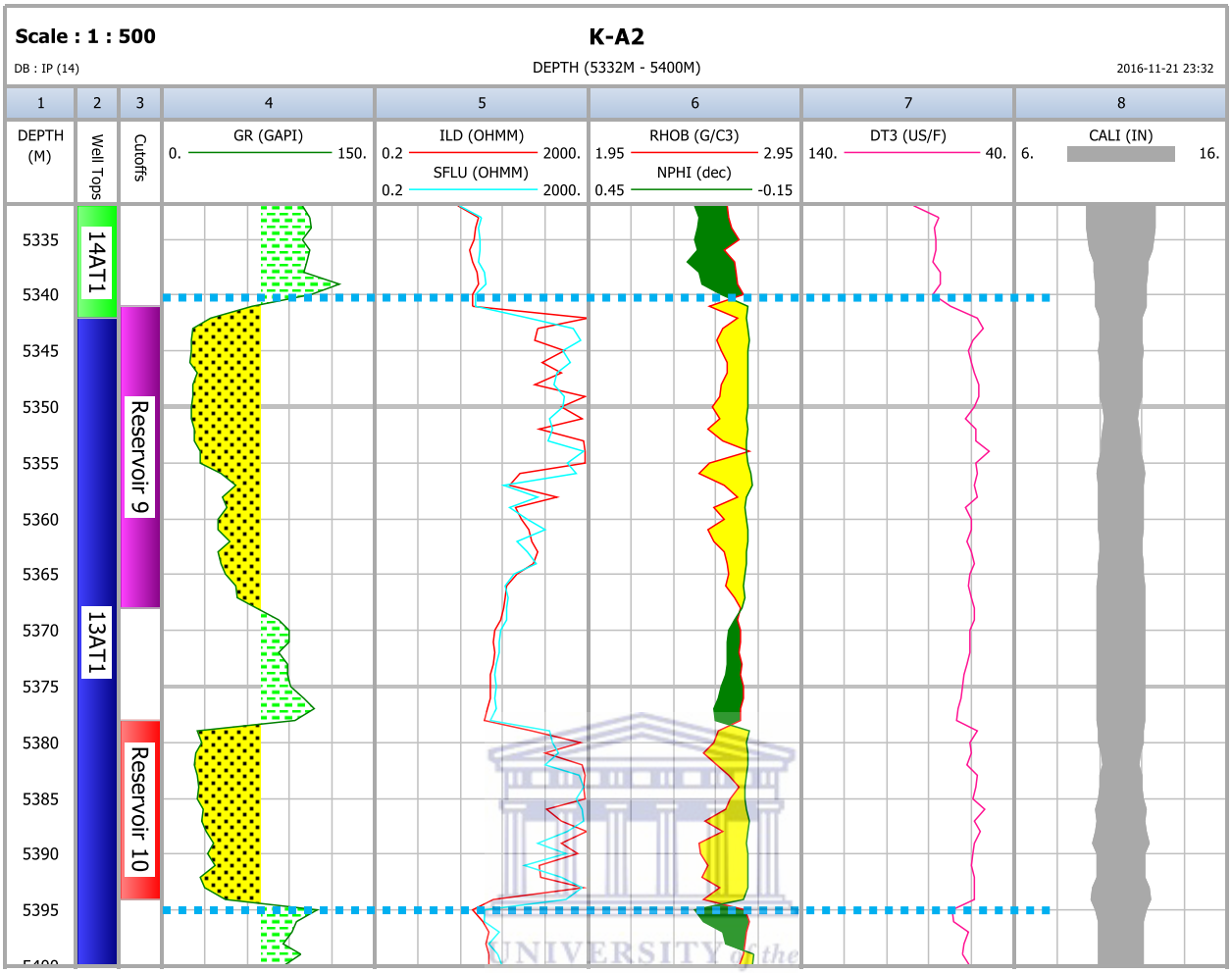

Figure 31: K-A2 selected reservoir interval between 5340 – 5395 m in the post-rift (Aptian - Albian age) sequence.

APPENDIX V – CUTOFFS

Well: A-J1 – wireline log interpretation

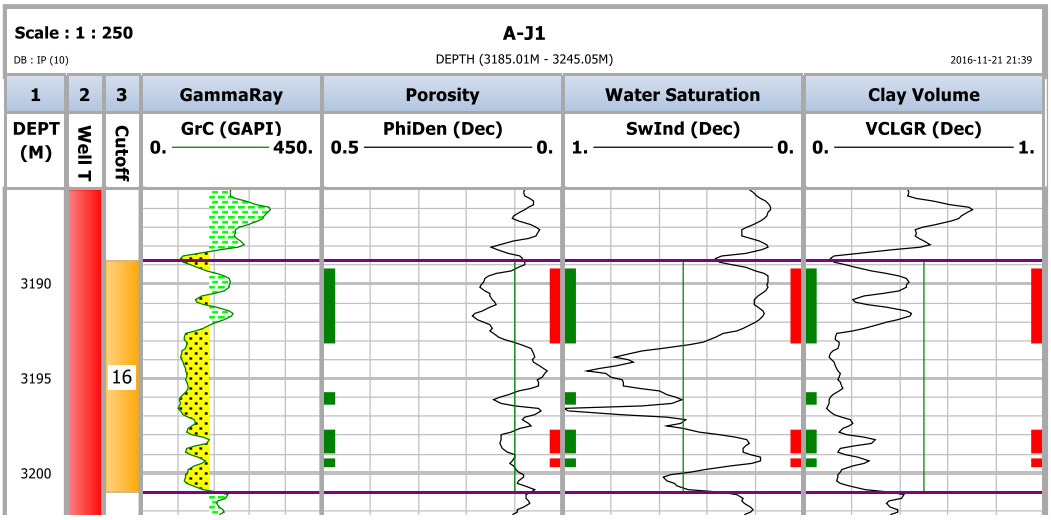

Figure 1: Well A-J1 showing calculated reservoir and pay flags of reservoir 16

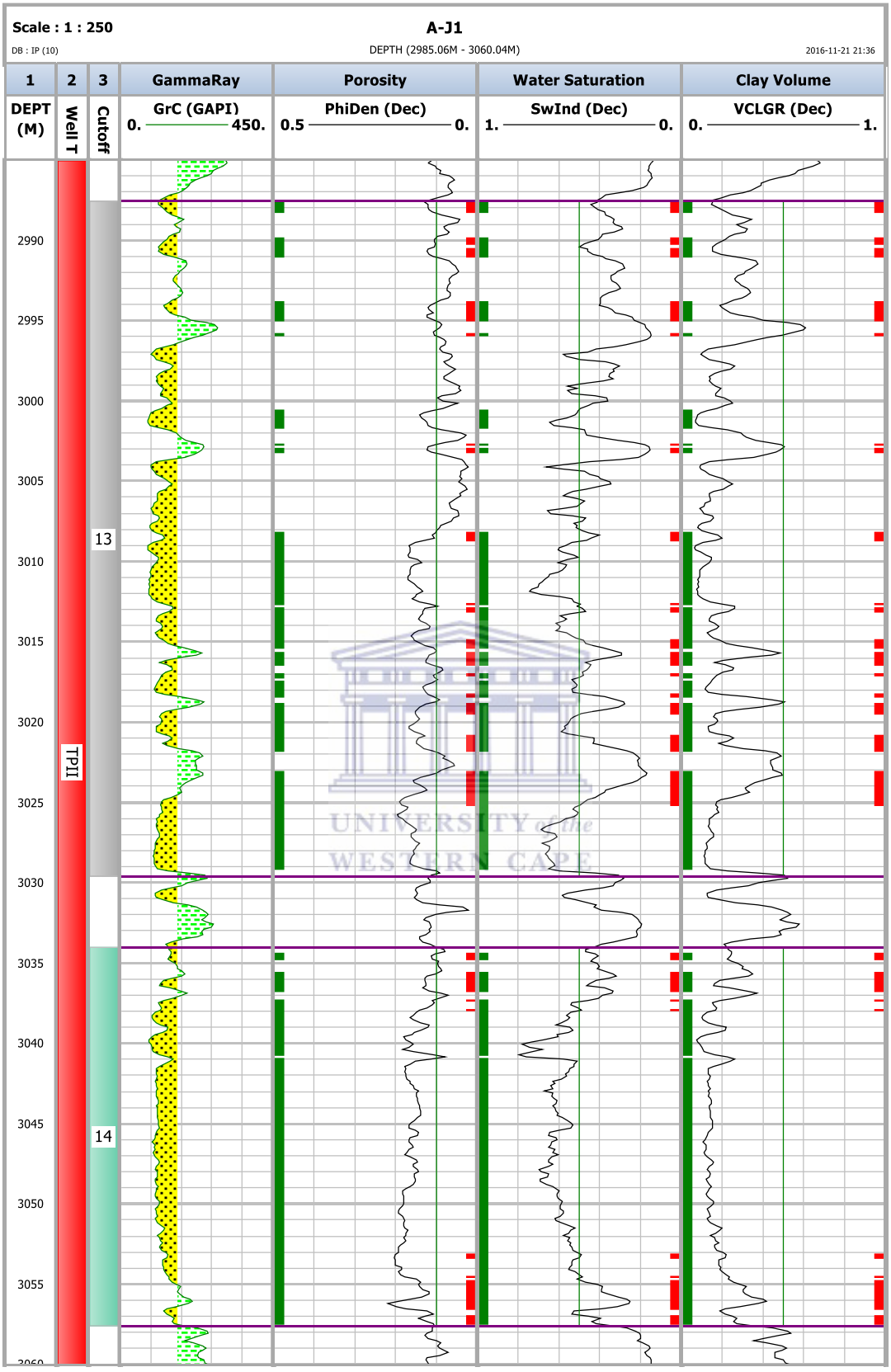

Figure 2: Well A-J1 showing calculated reservoir and pay flags of reservoir 14 and reservoir 13

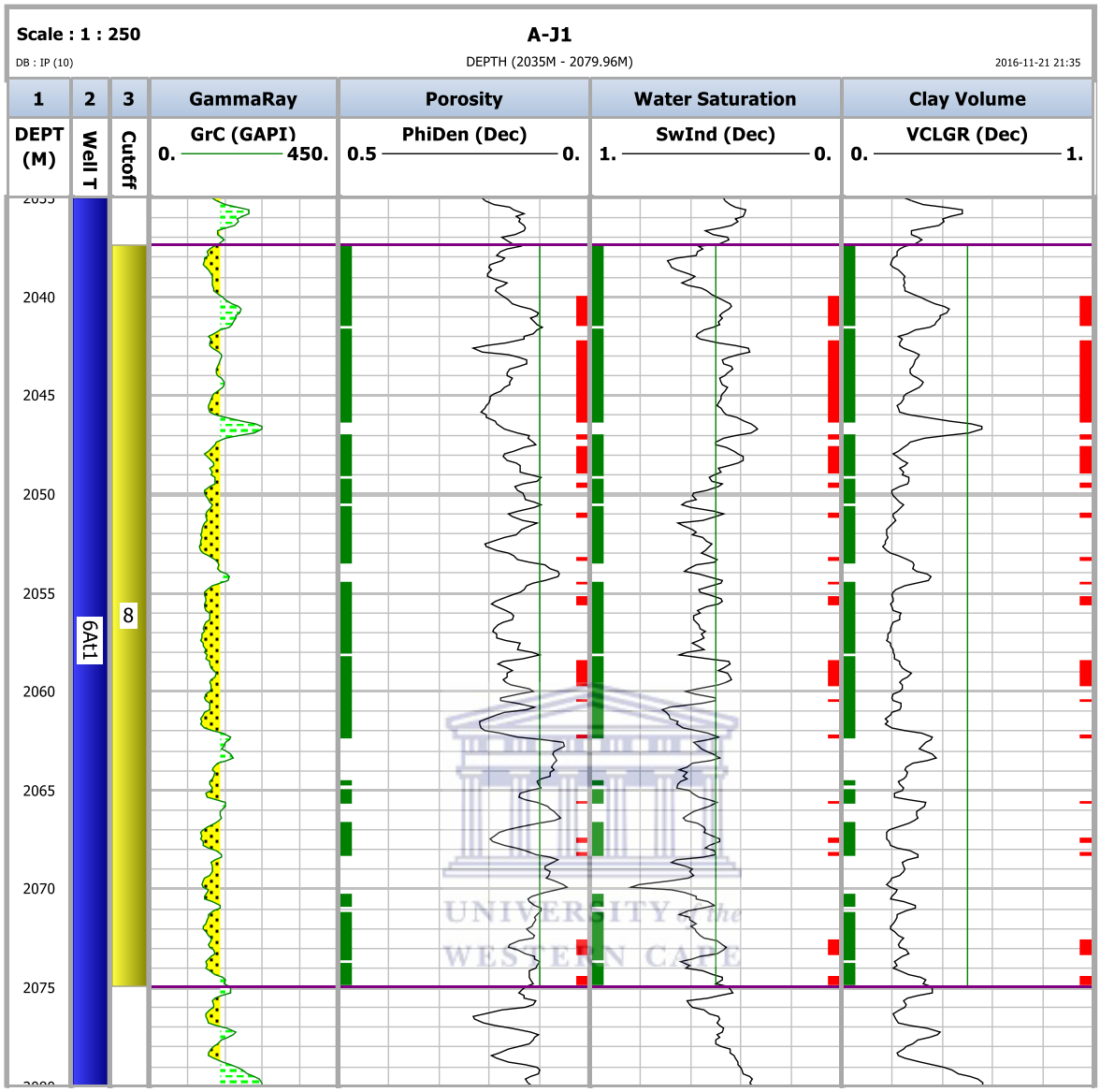

Figure 3: Well A-J1 showing calculated reservoir and pay flags of reservoir 8

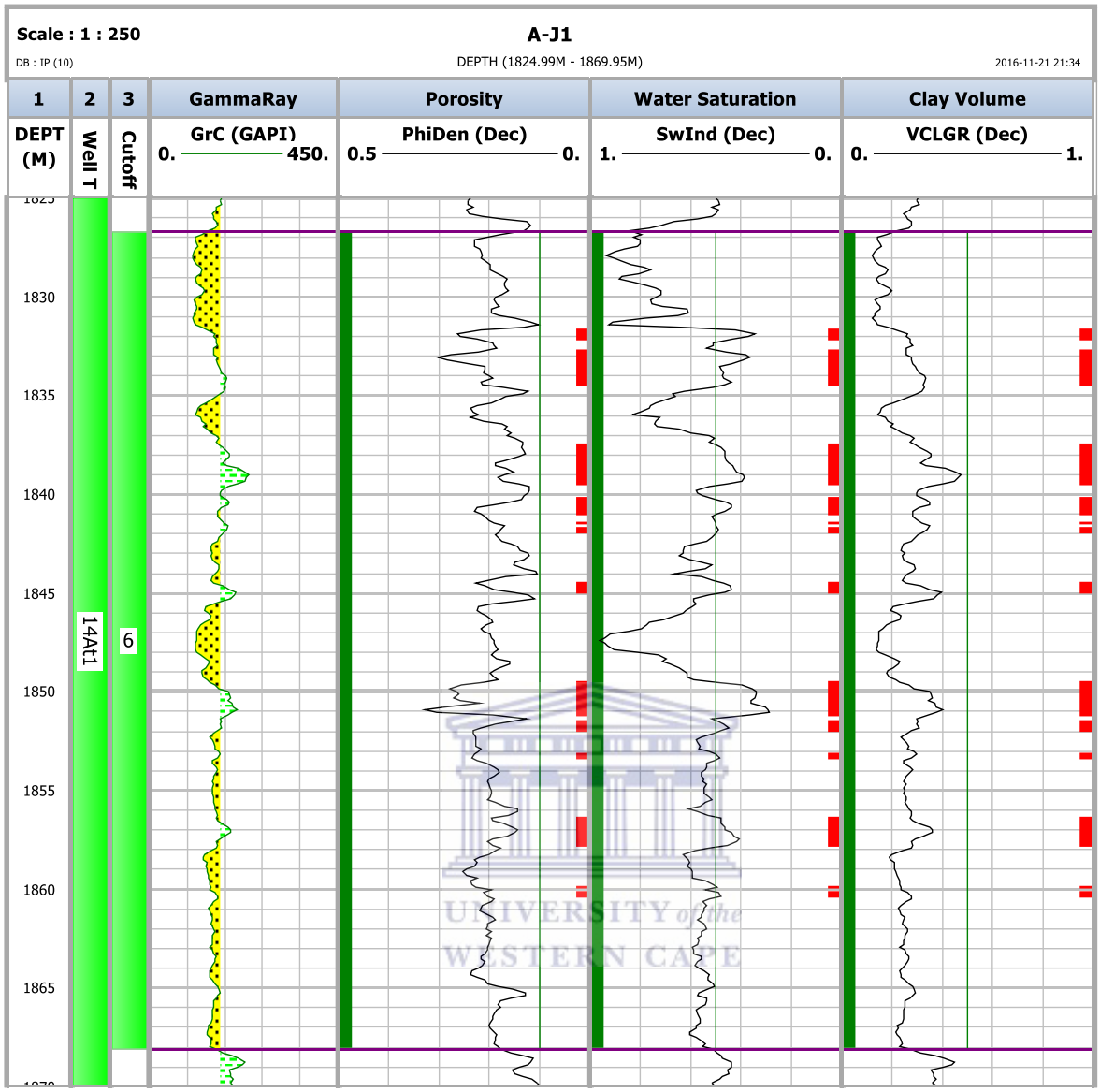

Figure 4: Well A-J1 showing calculated reservoir and pay flags of reservoir 6

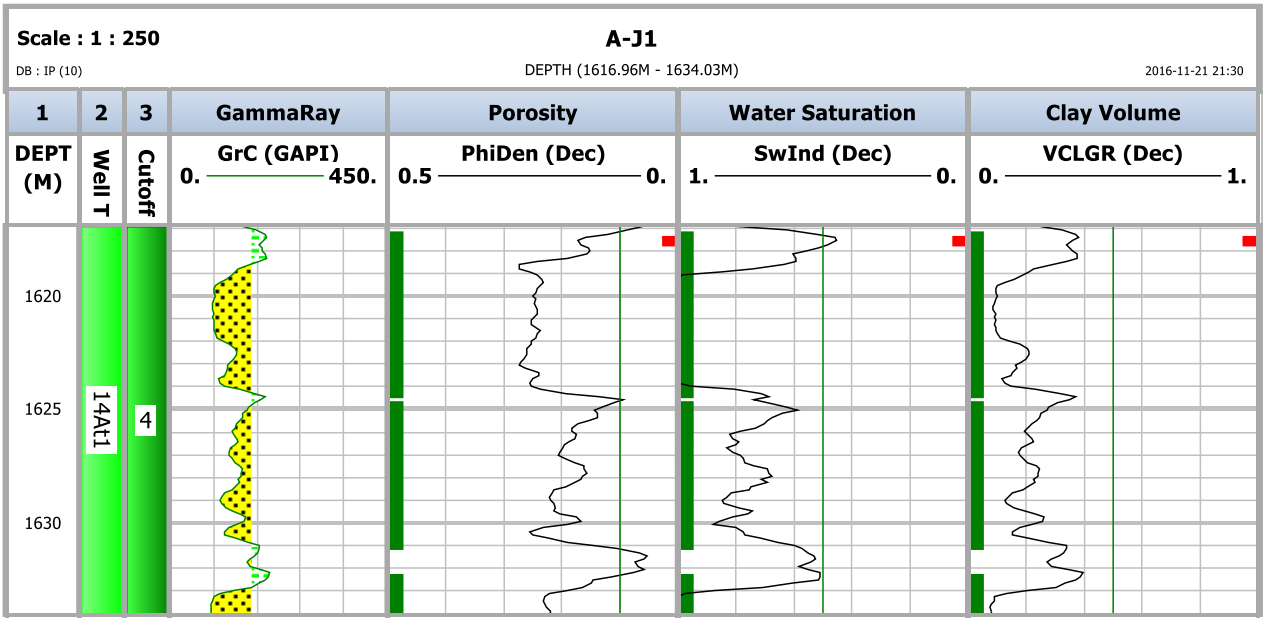

Figure 5: Well A-J1 showing calculated reservoir and pay flags of reservoir 6

Well: A-D1 – wireline log interpretation

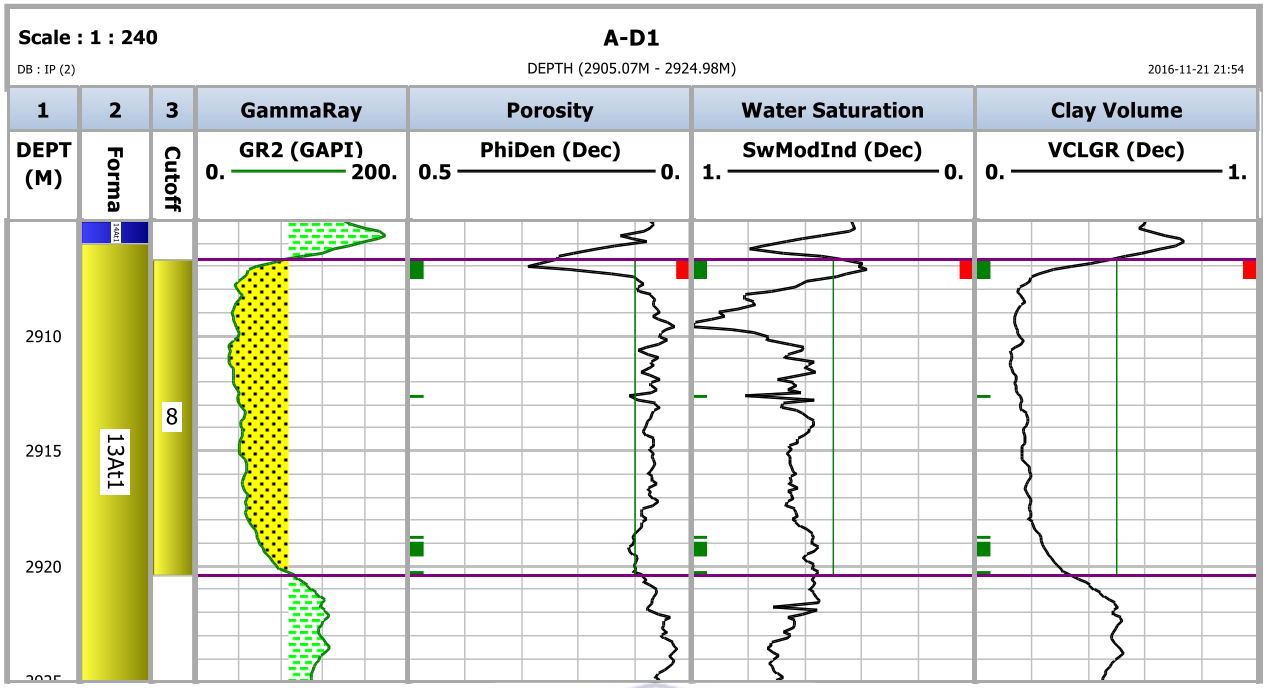

Figure 6: Well A-D1 showing calculated reservoir and pay flags of reservoir 8

Well: A-H1 – wireline log interpretation

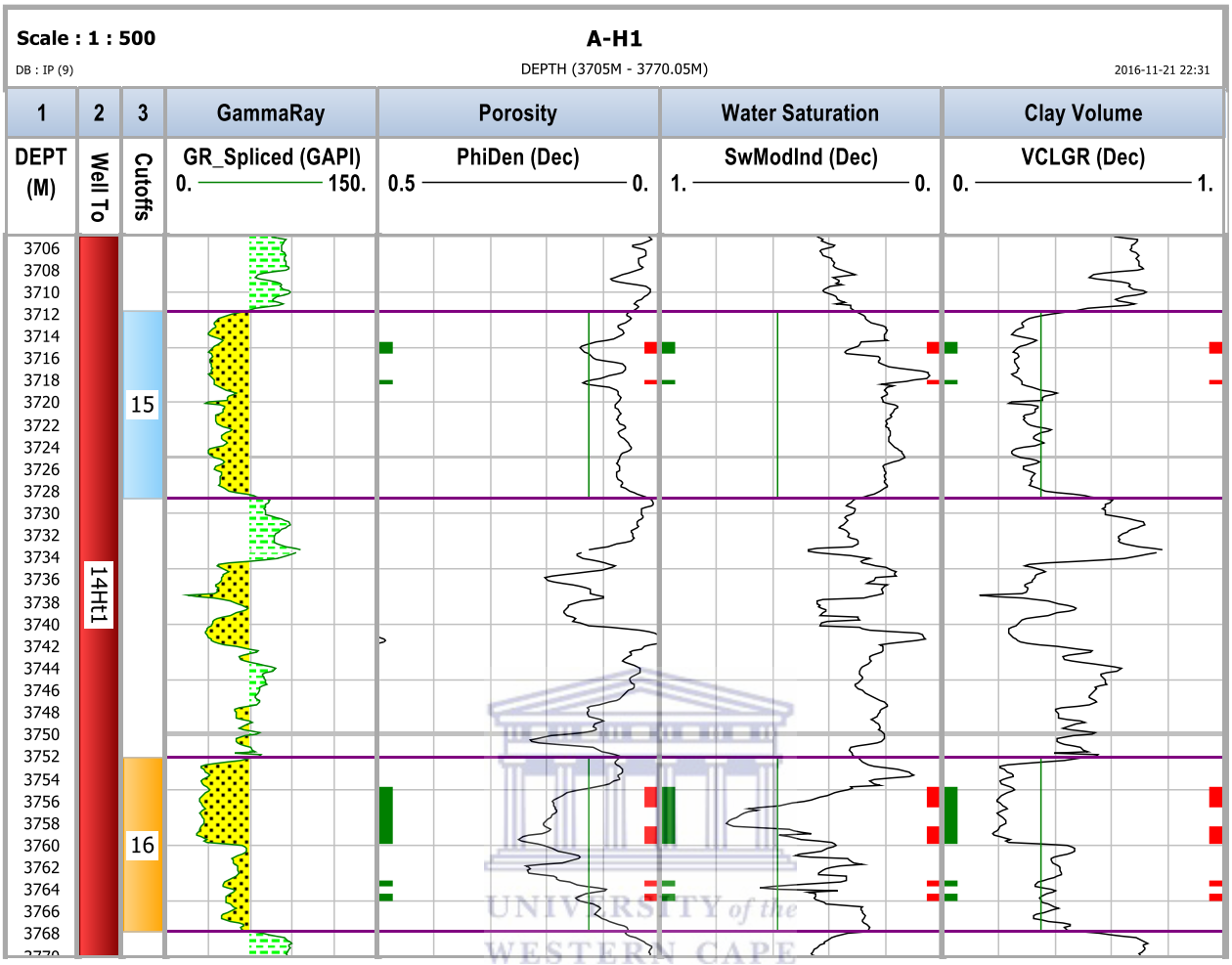

Figure 7: Well A-H1 showing calculated reservoir and pay flags of reservoir 16 and 15

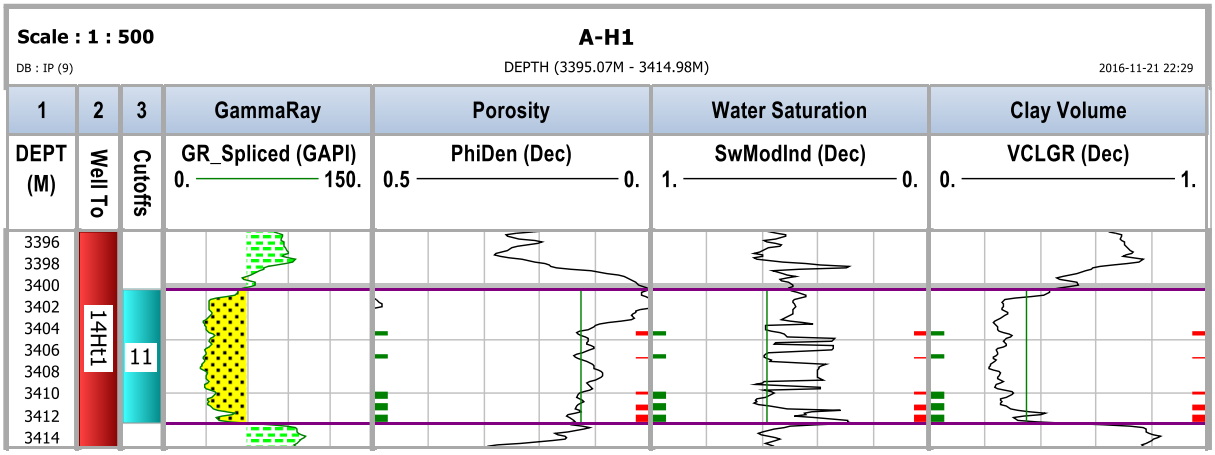

Figure 8: Well A-H1 showing calculated reservoir and pay flags of reservoir 11

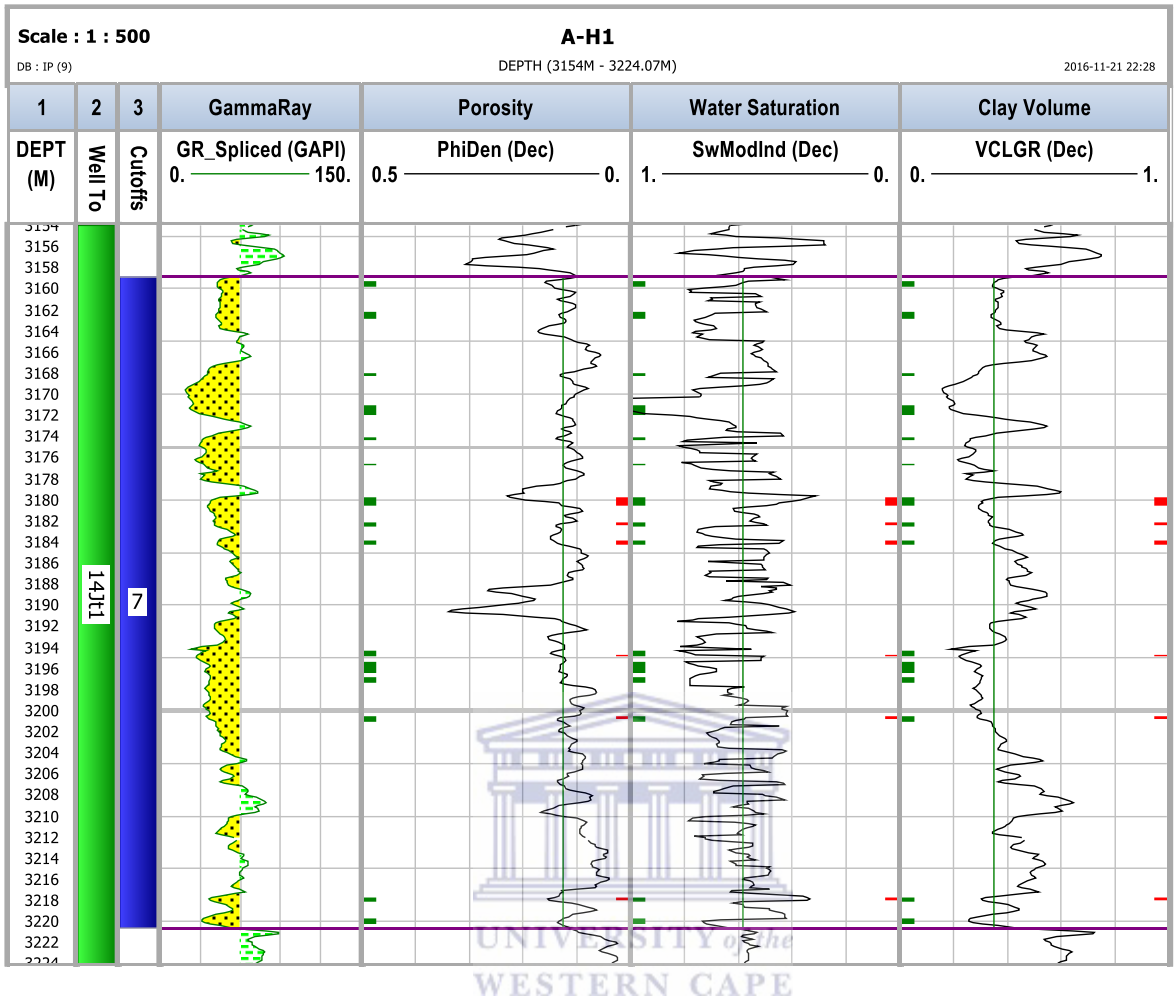

Figure 9: Well A-H1 showing calculated reservoir and pay flags of reservoir 7

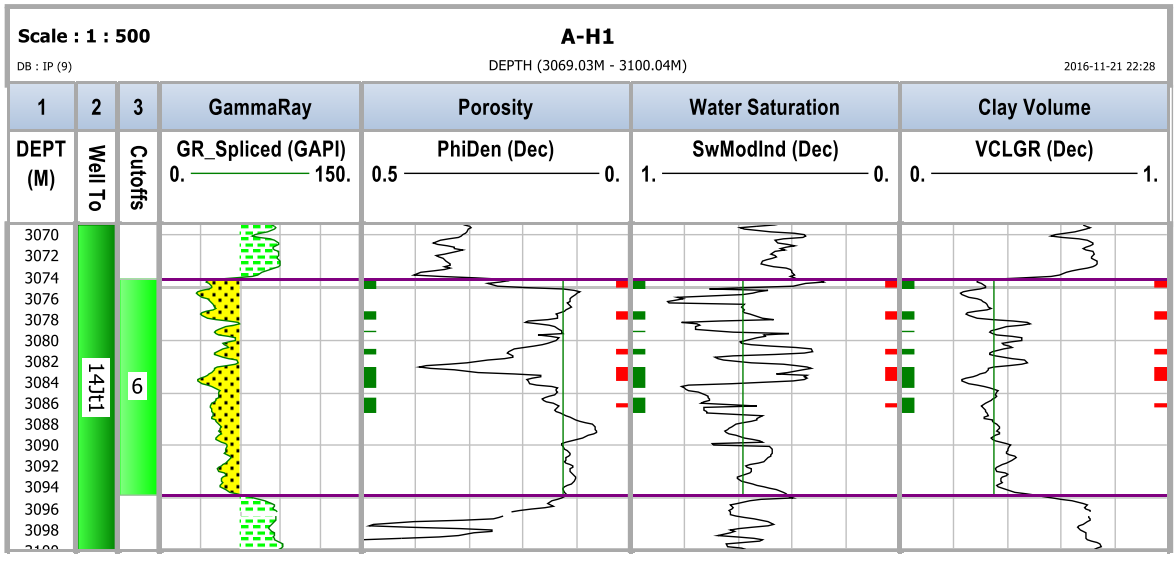

Figure 10: Well A-H1 showing calculated reservoir and pay flags of reservoir 6

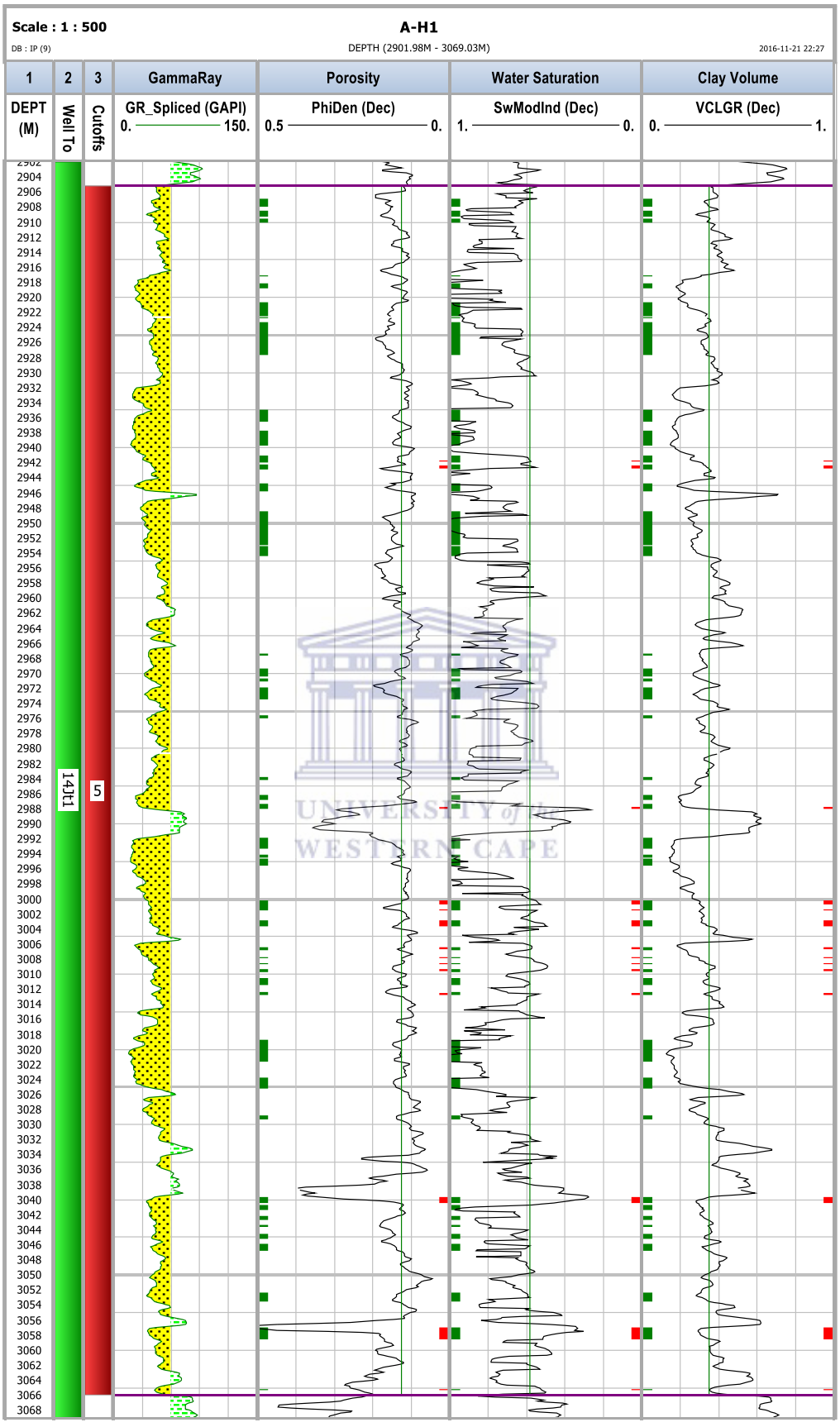

Figure 11: Well A-H1 showing calculated reservoir and pay flags of reservoir 5

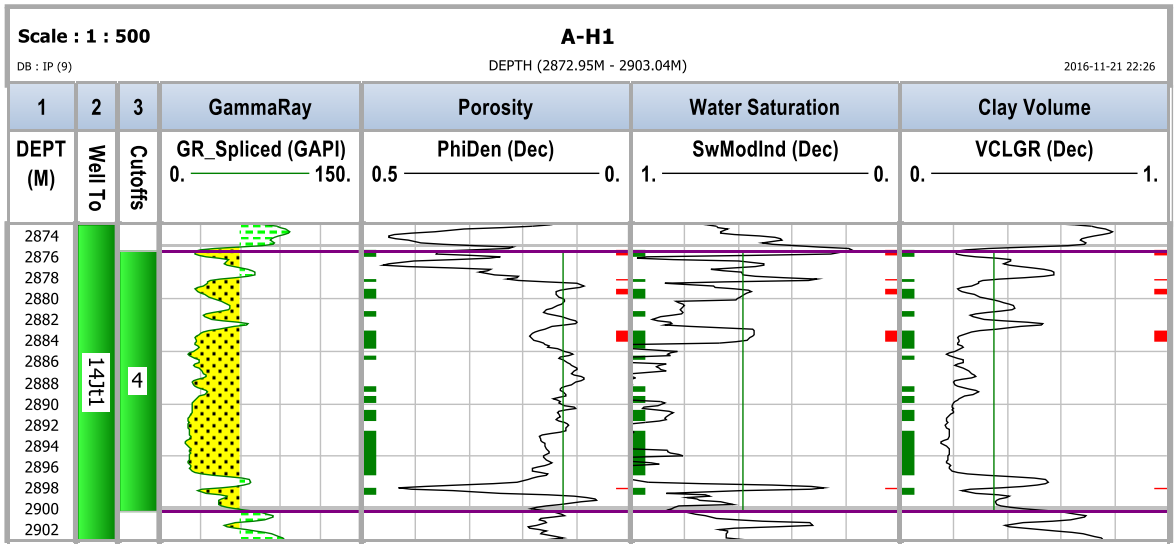

Figure 12: Well A-H1 showing calculated reservoir and pay flags of reservoir 4

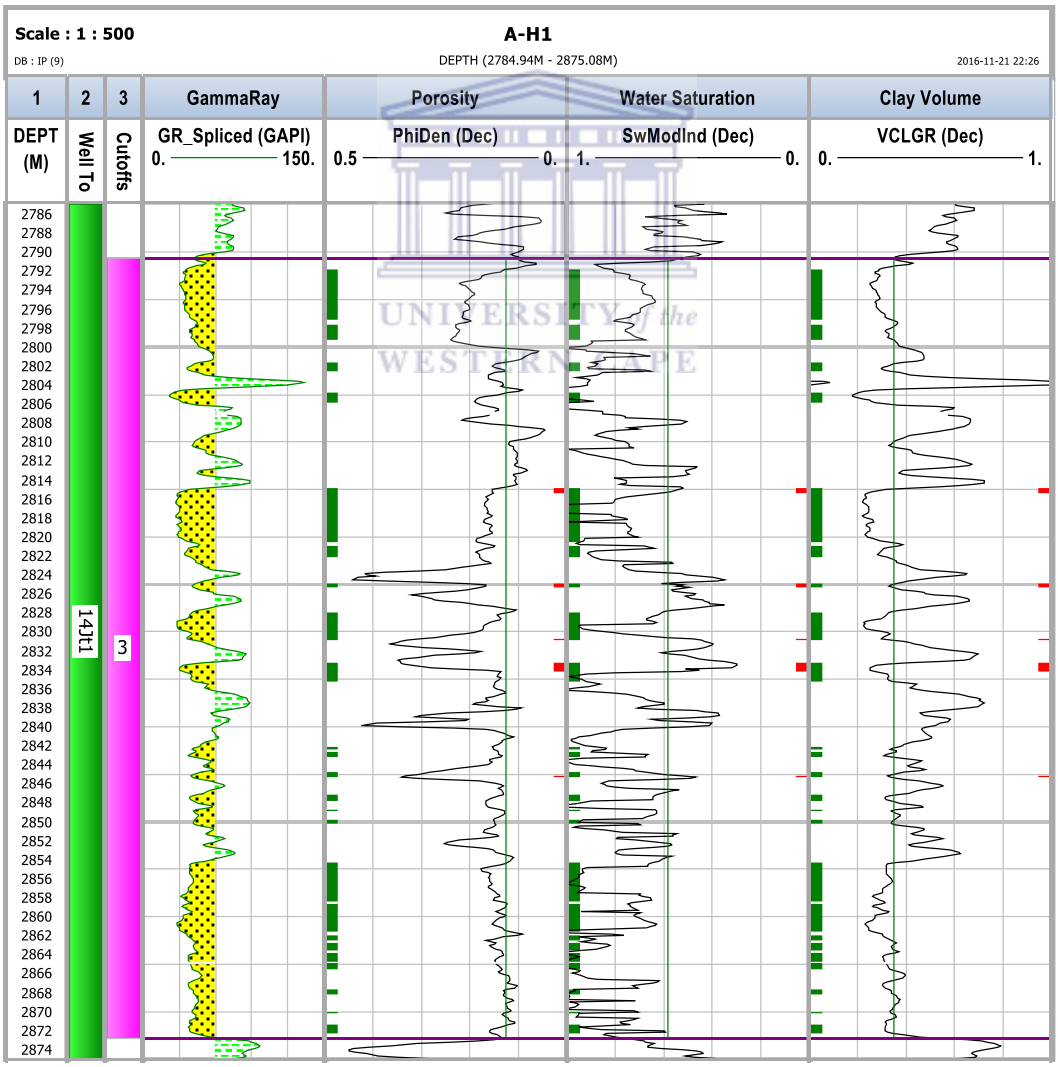

Figure 13: Well A-H1 showing calculated reservoir and pay flags of reservoir 3

Well: A-K1 – wireline log interpretation

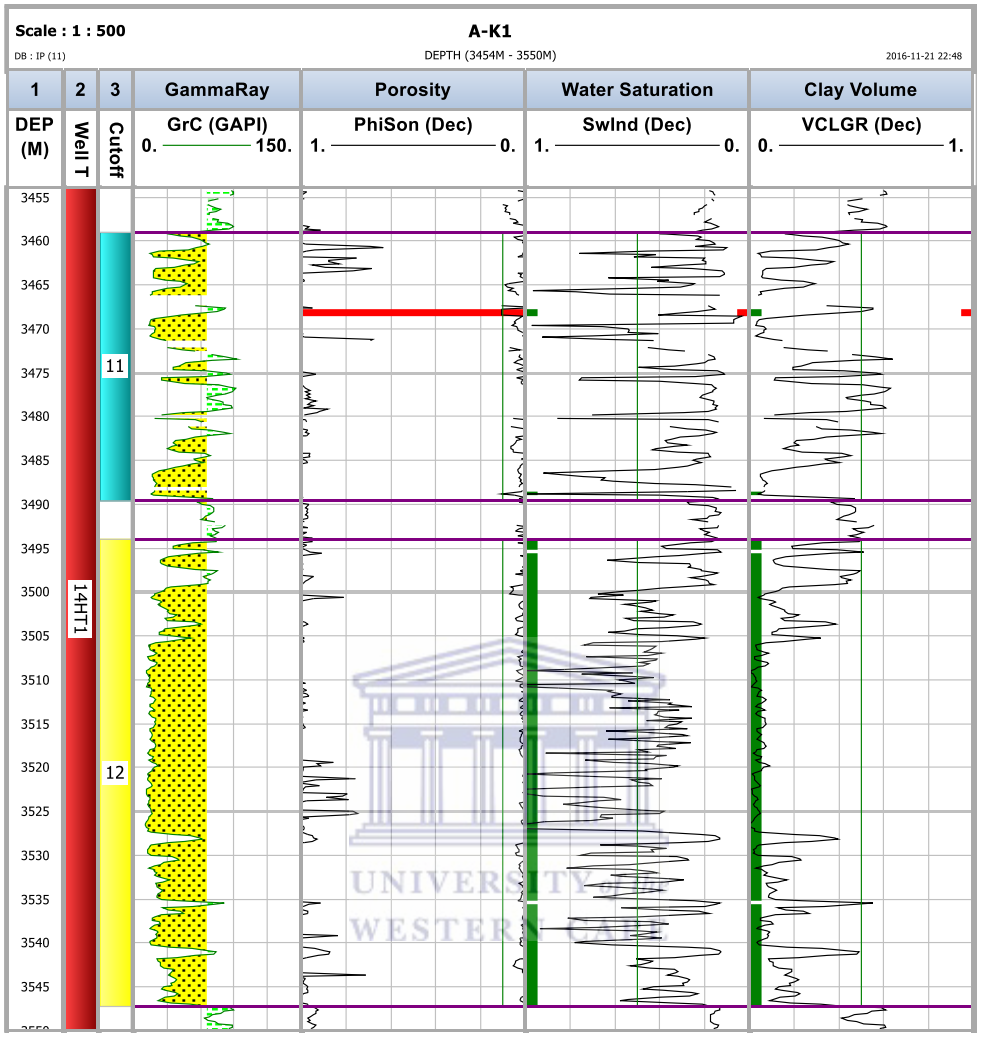

Figure 14: Well A-K1 showing calculated reservoir and pay flags of reservoir 12 & 11

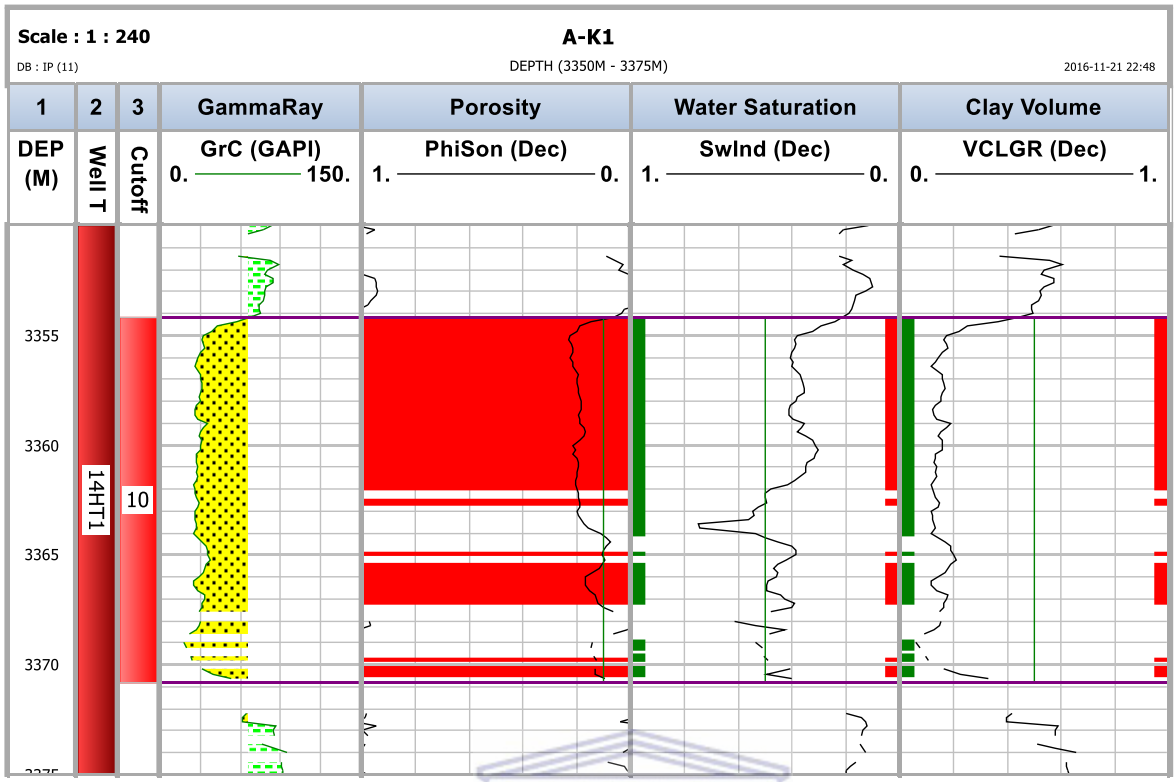

Figure 15: Well A-K1 showing calculated reservoir and pay flags of reservoir 10

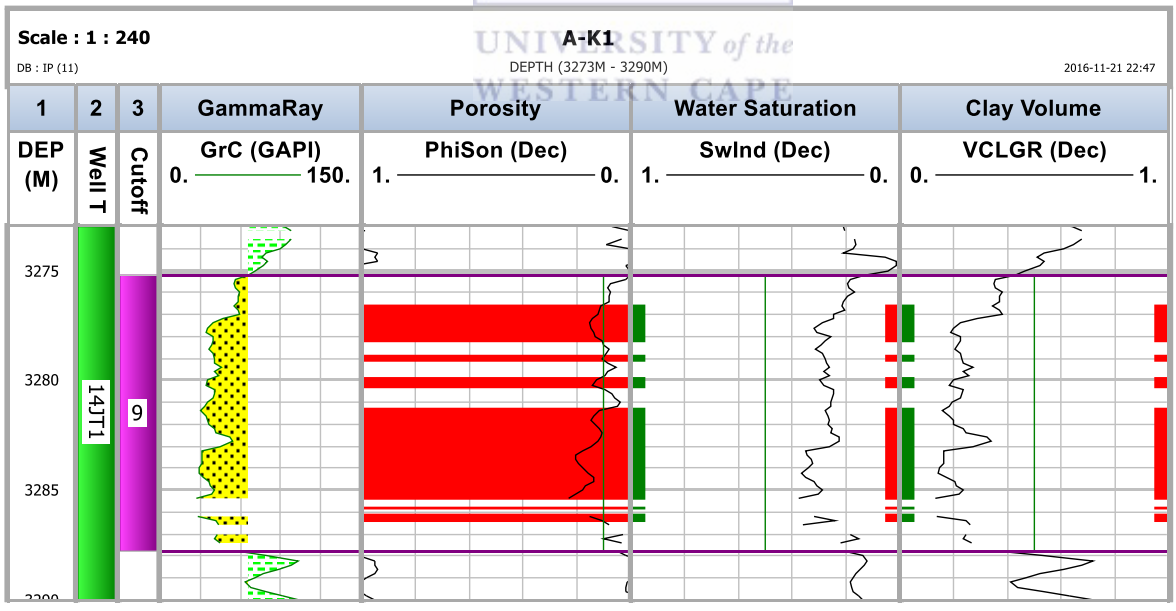

Figure 16: Well A-K1 showing calculated reservoir and pay flags of reservoir 9

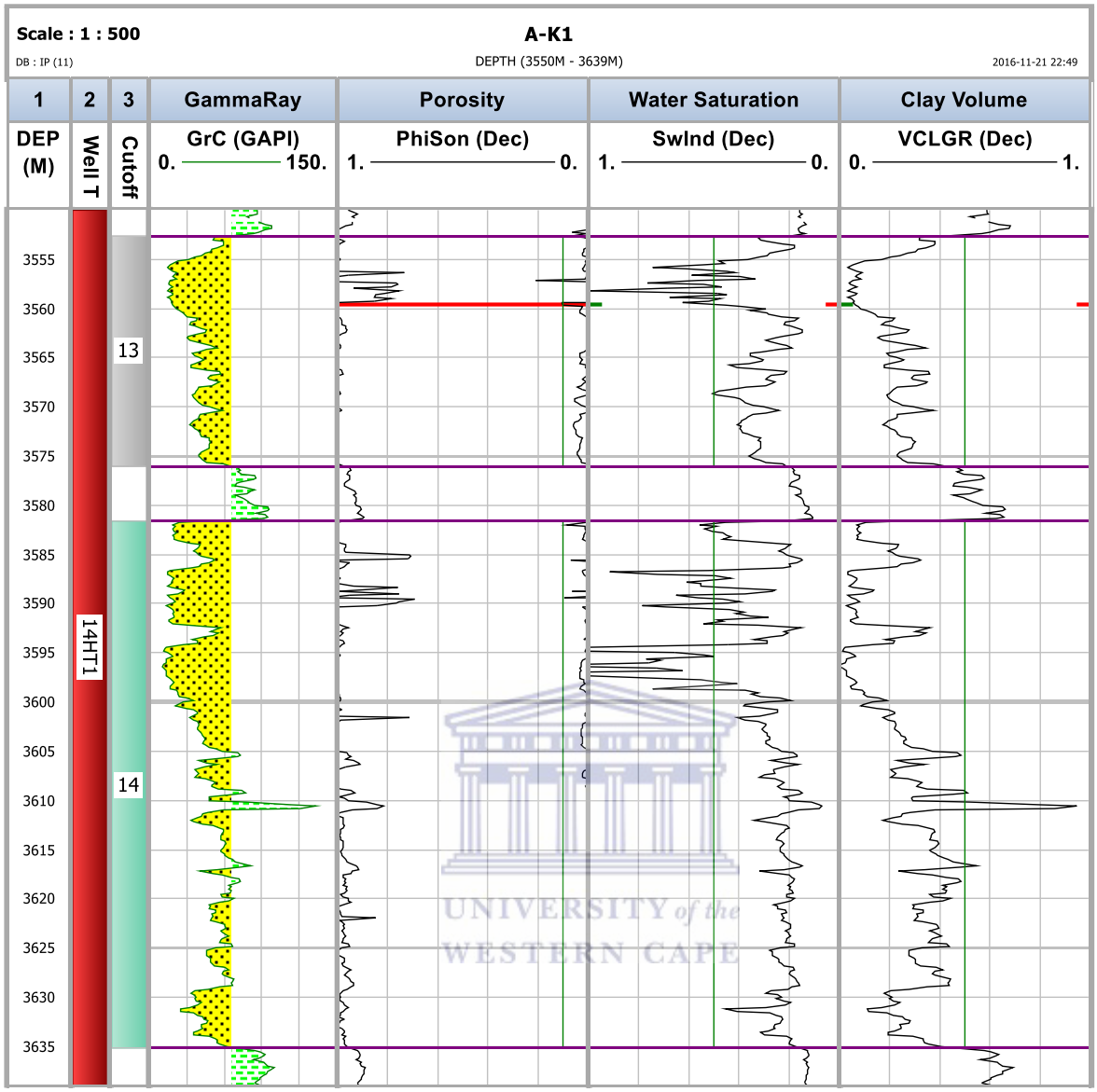

Figure 17: Well A-K1 showing calculated reservoir and pay flags of reservoir 14 & 13